AD-A085 480 ROYAL AIRCRAFT ESTABLISHMENT FARNBOROUGH (ENGLAND) F/G 17/7
CONTRIBUTIONS TO THE UK MICROWAVE LANDING SYSTEM RESEARCH AND D--ETC(U)
MAY 79 J M JONES
UNCLASSIFIED RAE-TR-79052-VOL-3 DRIC-BR-73763 NL

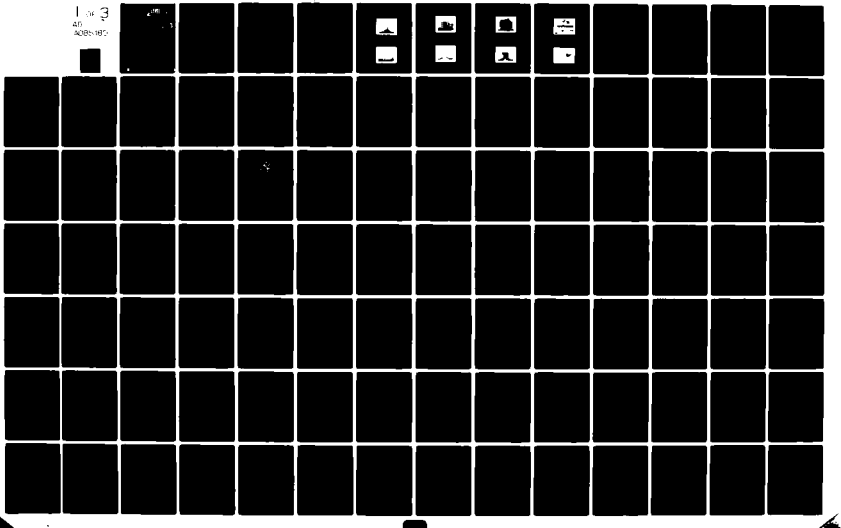

ROYAL AIRCRAFT ESTABLISHMENT

*

(9) Technical Report 79052

(11) May 1979

(6) CONTRIBUTIONS TO THE UK MICROWAVE LANDING SYSTEM RESEARCH AND DEVELOPMENT PROGRAMME 1974 TO 1978.

Volume 3.

(12) 238

by

(10) J.M. Jones

(14) RAE-TR-79052-VOL-3

VOLUME 3

*

(18) DRIC

(19) BR-73763

Procurement Executive, Ministry of Defence

Farnborough, Hants

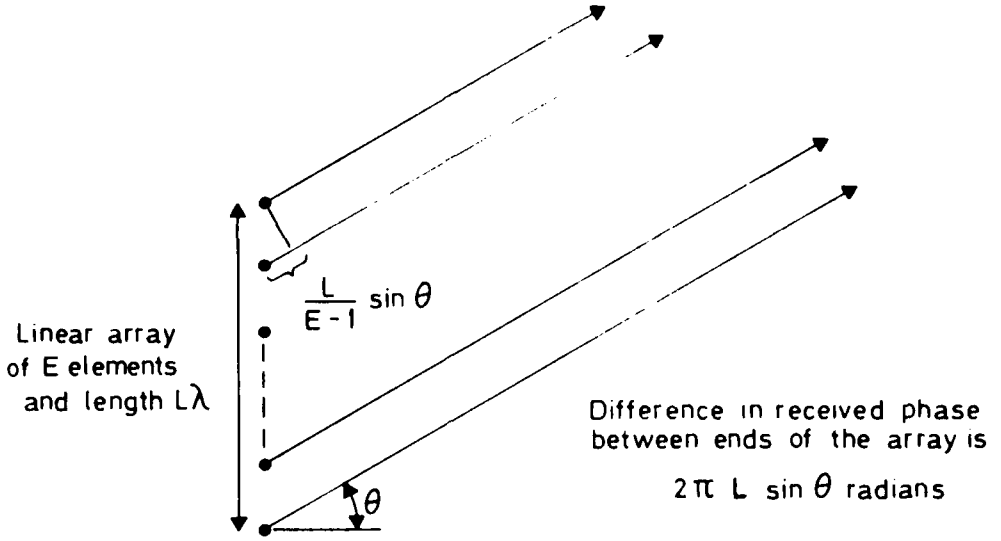

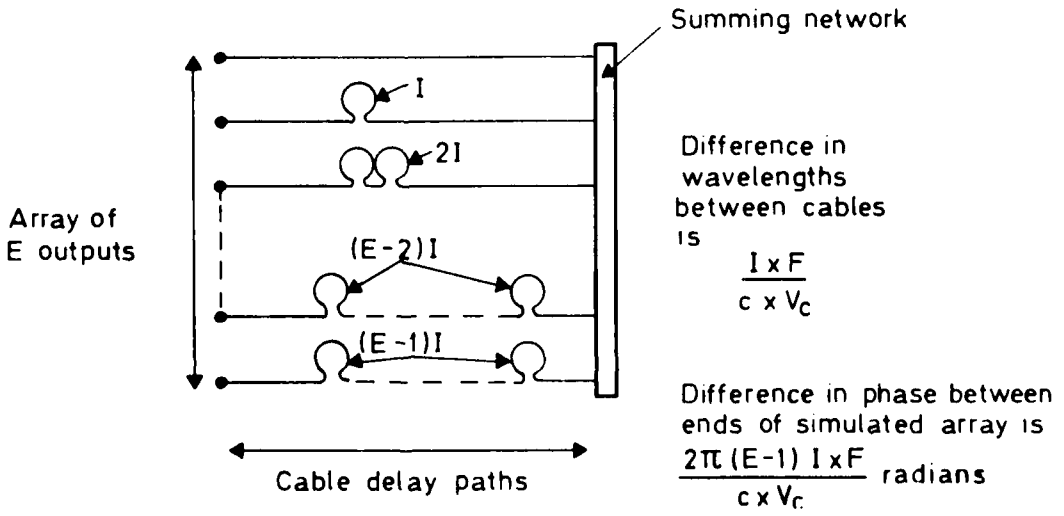

Fig 6.1 Comparison of Doppler antenna and cable transmission simulation

Fig 6.2

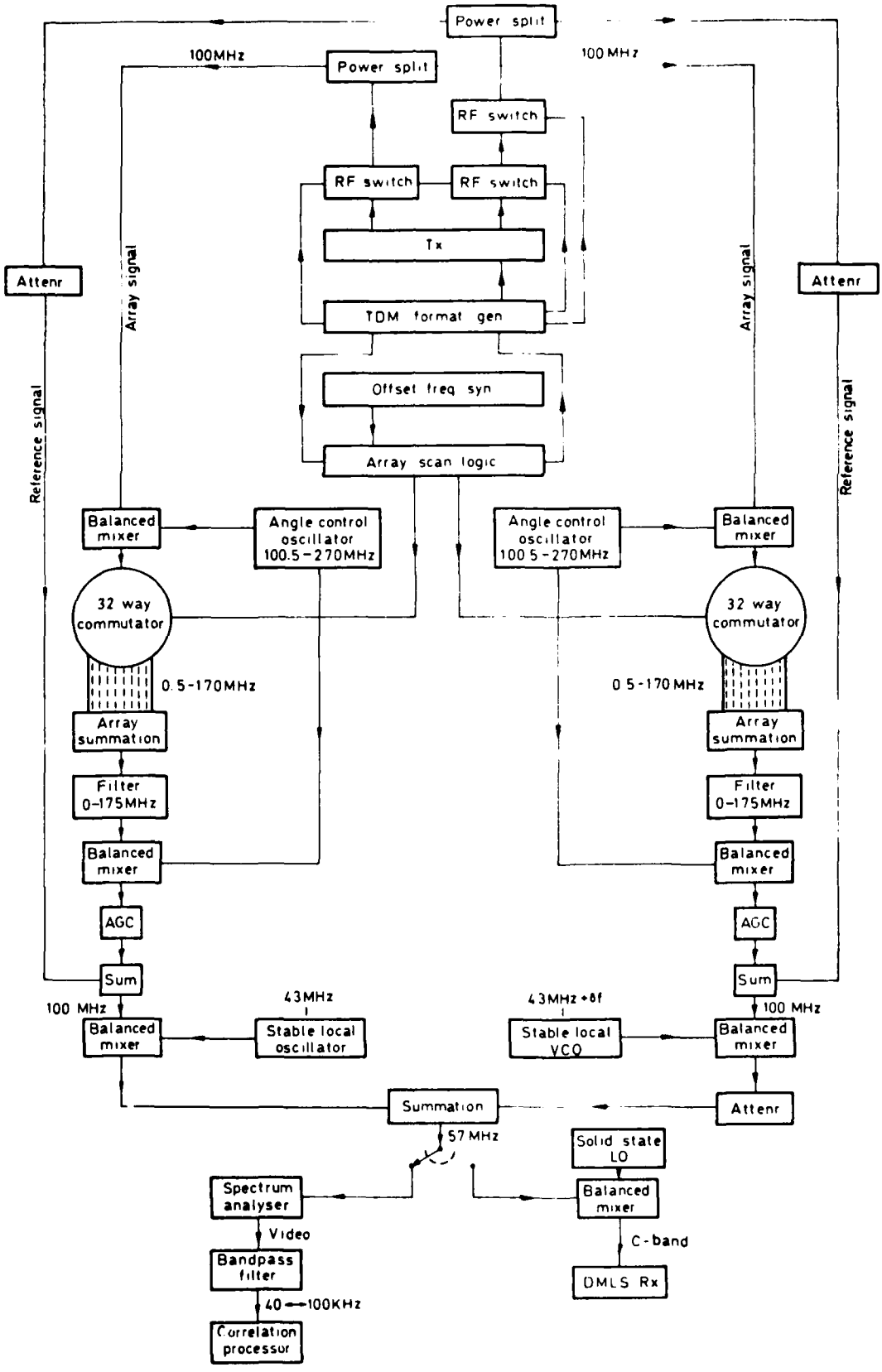

Fig 6.2 Simulator block diagram

Fig 6.3

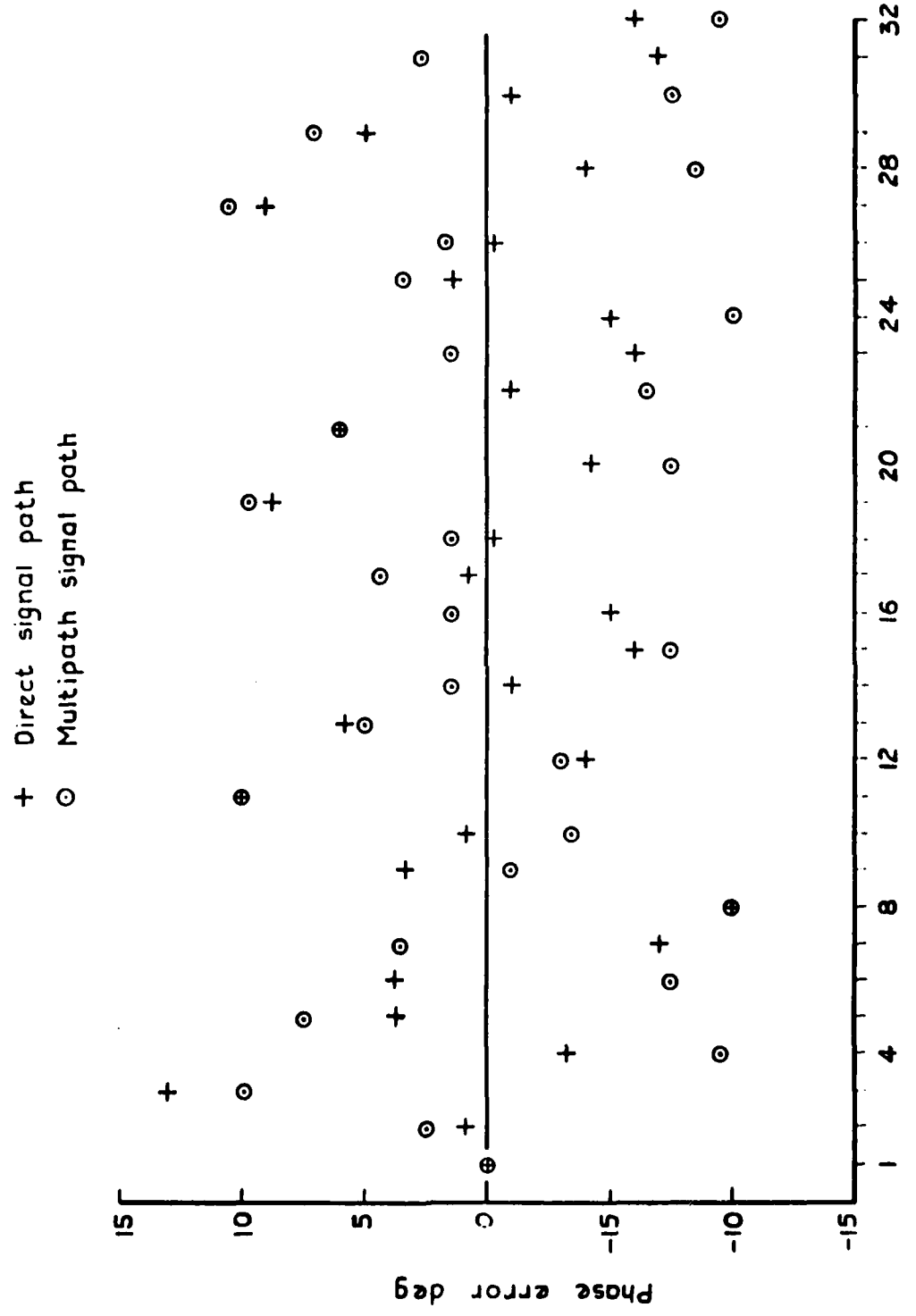

Fig 6.3 Simulator array phase errors at 170 MHz

IF bandwidth: 300 Hz
Spectrum width: 100 kHz/division
Amplitude: 10 dB/division

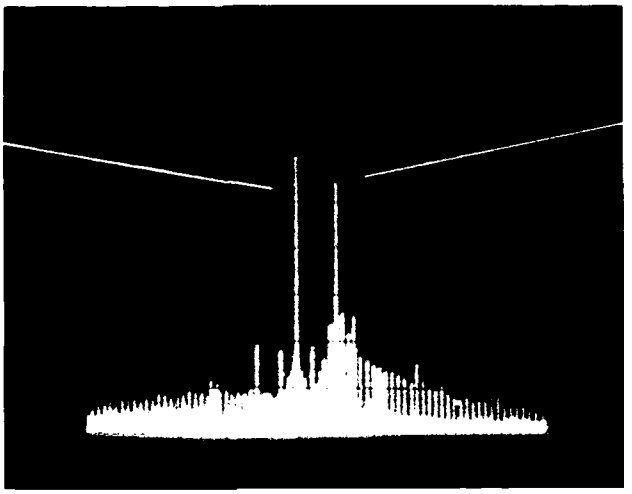

Fig 6.4 Simulator output spectrum – no multipath

IF bandwidth: 300 Hz
Spectrum width: 10 kHz/division
Amplitude: 10 dB/division

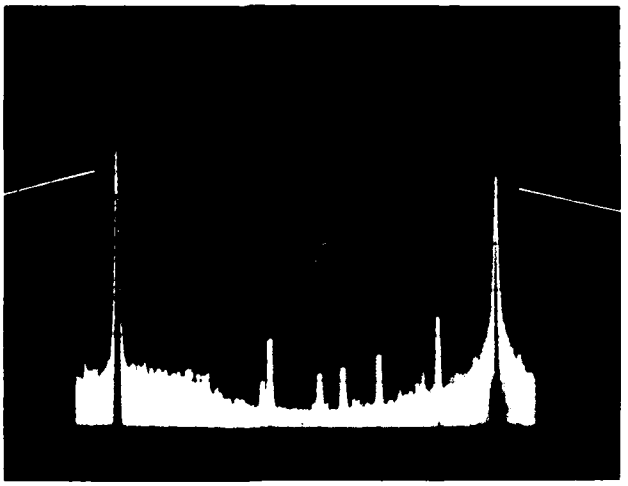

Fig 6.5 Simulator output spectrum – no multipath, expanded frequency scale

IF bandwidth: 300 Hz
Spectrum width: 10 kHz/division
Amplitude: 10 dB/division

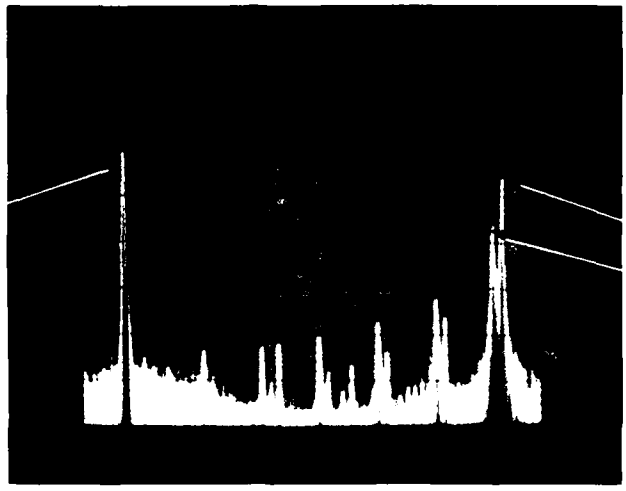

Fig 6.6 Simulator output spectrum with multipath signal

IF bandwidth: 300 Hz
Spectrum width: 2 kHz/division
Amplitude: 10 dB/division
Multipath -5° with respect to wanted signal

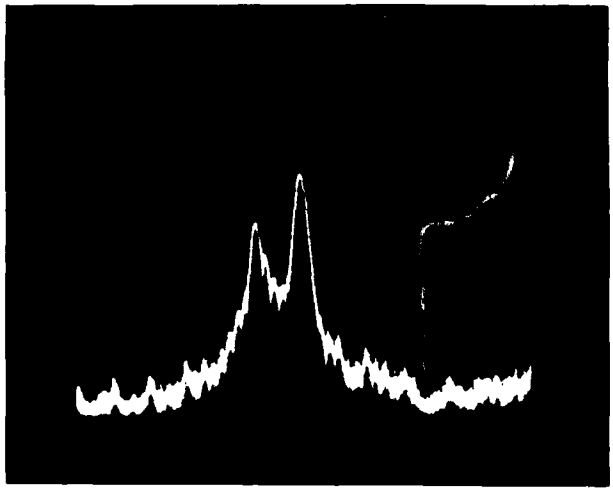

Fig 6.7 Simulator output spectrum with multipath signal. Expansion of Fig 6.6 around array signal

IF bandwidth: 300 Hz
Spectrum width: 2 kHz/division
Amplitude: 10 dB/division

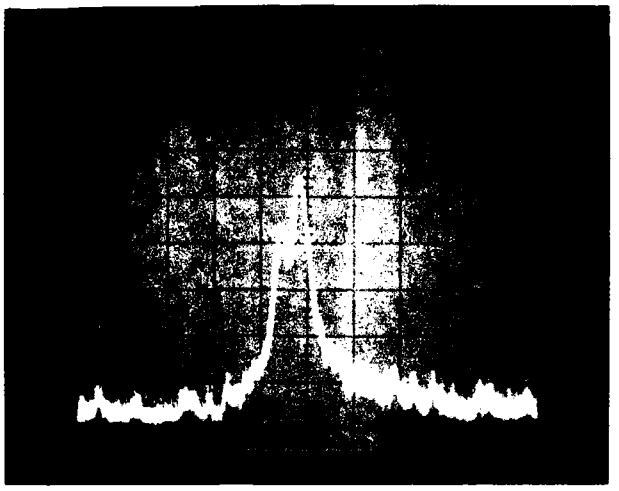

Fig 6.8 Expanded simulator output spectrum, multipath at −2 degrees separation

IF bandwidth: 300 Hz
Spectrum width: 2 kHz/division
Amplitude: 10 dB/division

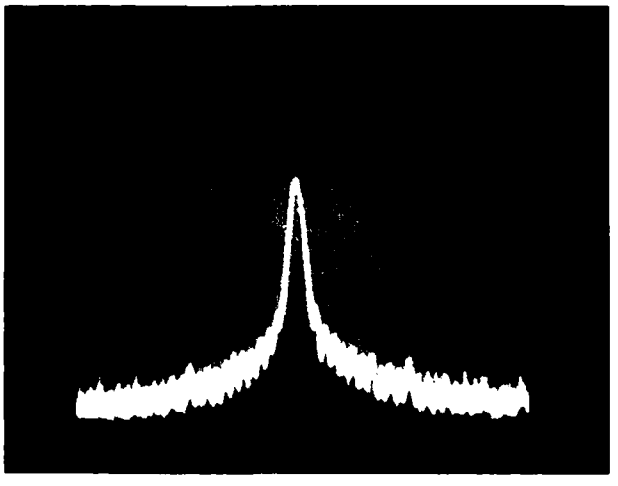

Fig 6.9 Expanded simulator array signal, no multipath

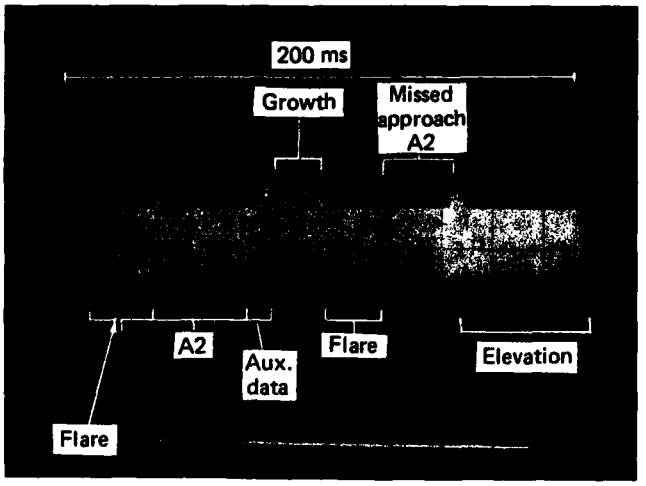

Fig 6.10 Receiver video output for a 200ms frame containing azimuth, elevation, missed approach azimuth flare and auxiliary data signals

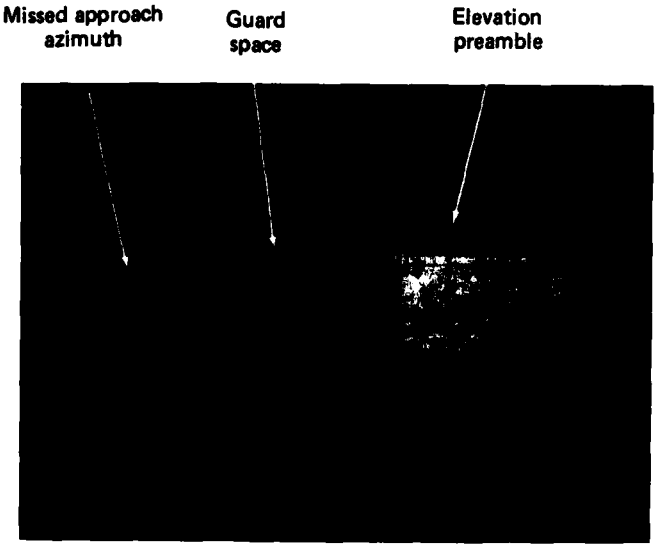

Fig 6.11 Part of Fig 6.10, expanded time scale

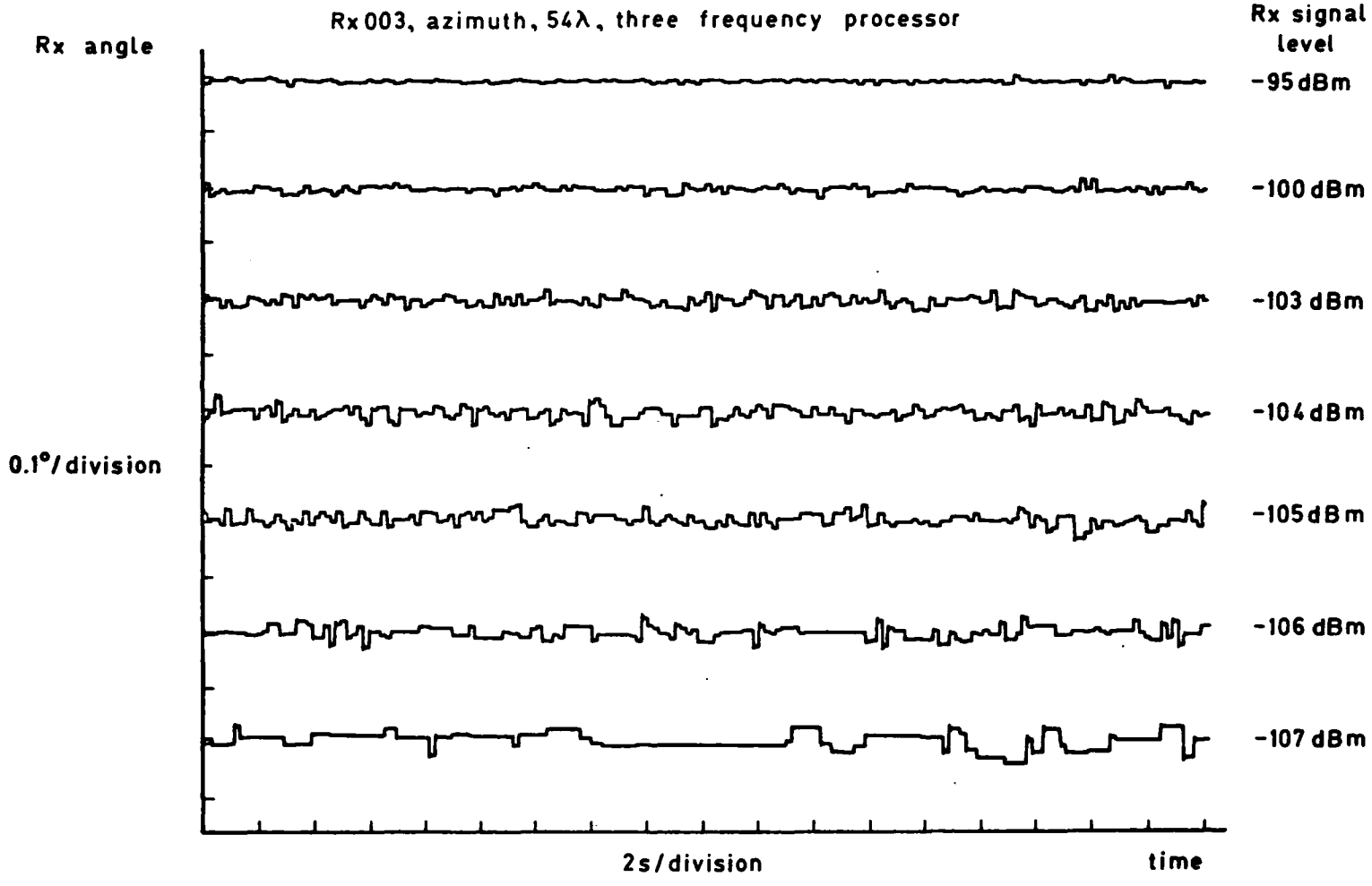

Fig 6.12a Azimuth angle noise as function of signal level (full system)

Fig 6.12a

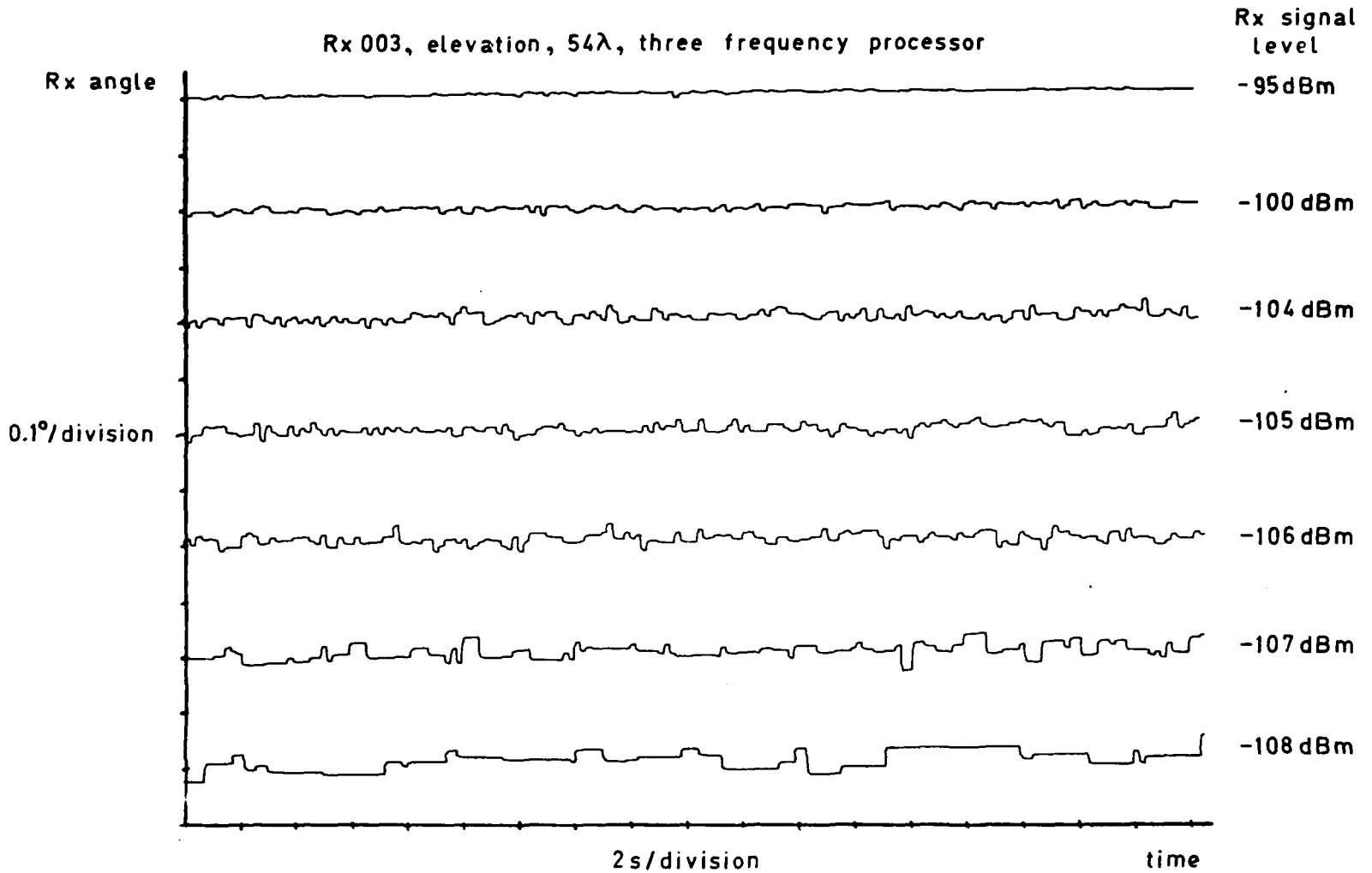

Fig 6.12b

Fig 6.12b Elevation angle noise as function of signal level (full system)

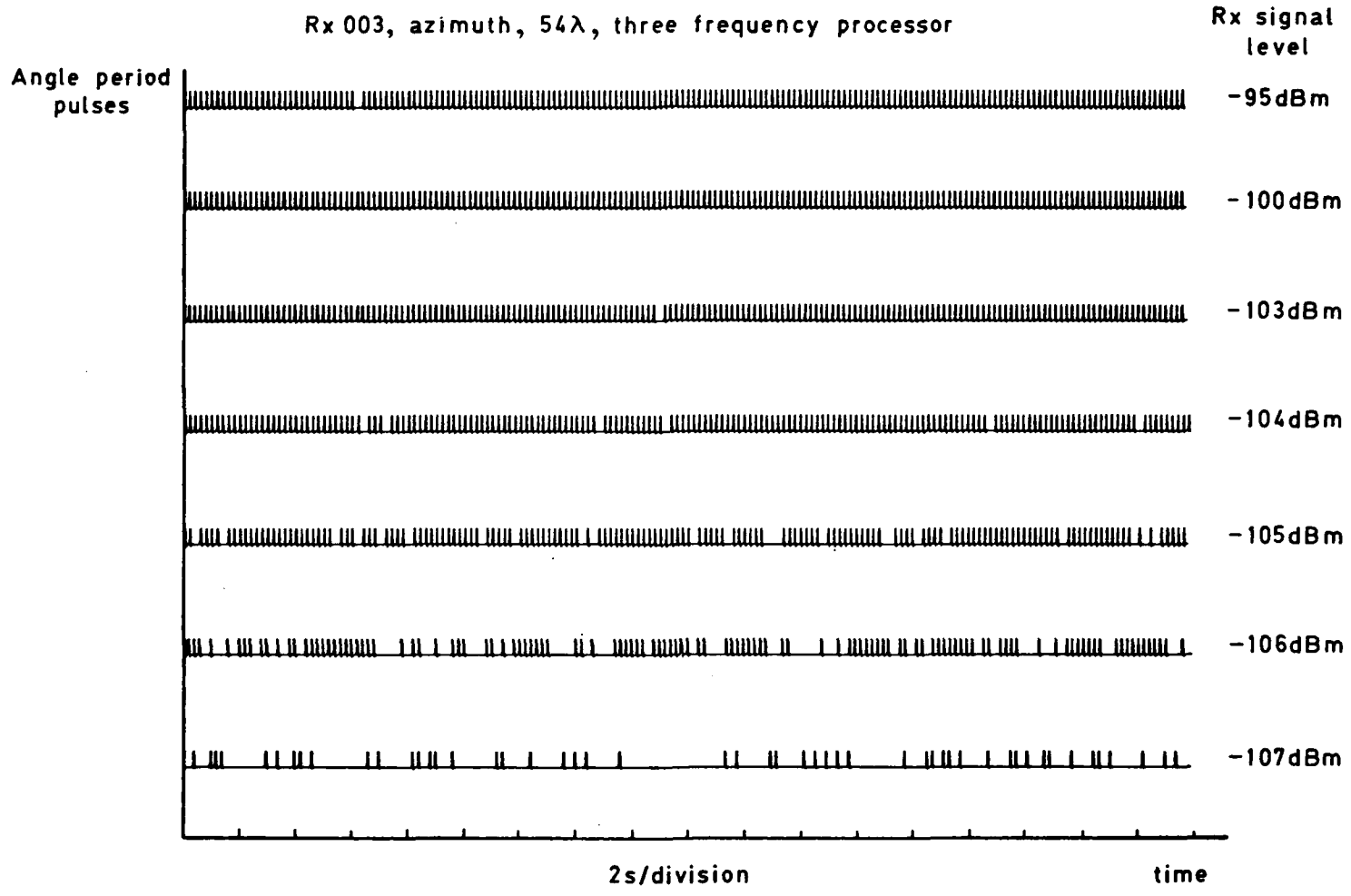

Fig 6.13a Azimuth function identity decode success

Fig 6.13a

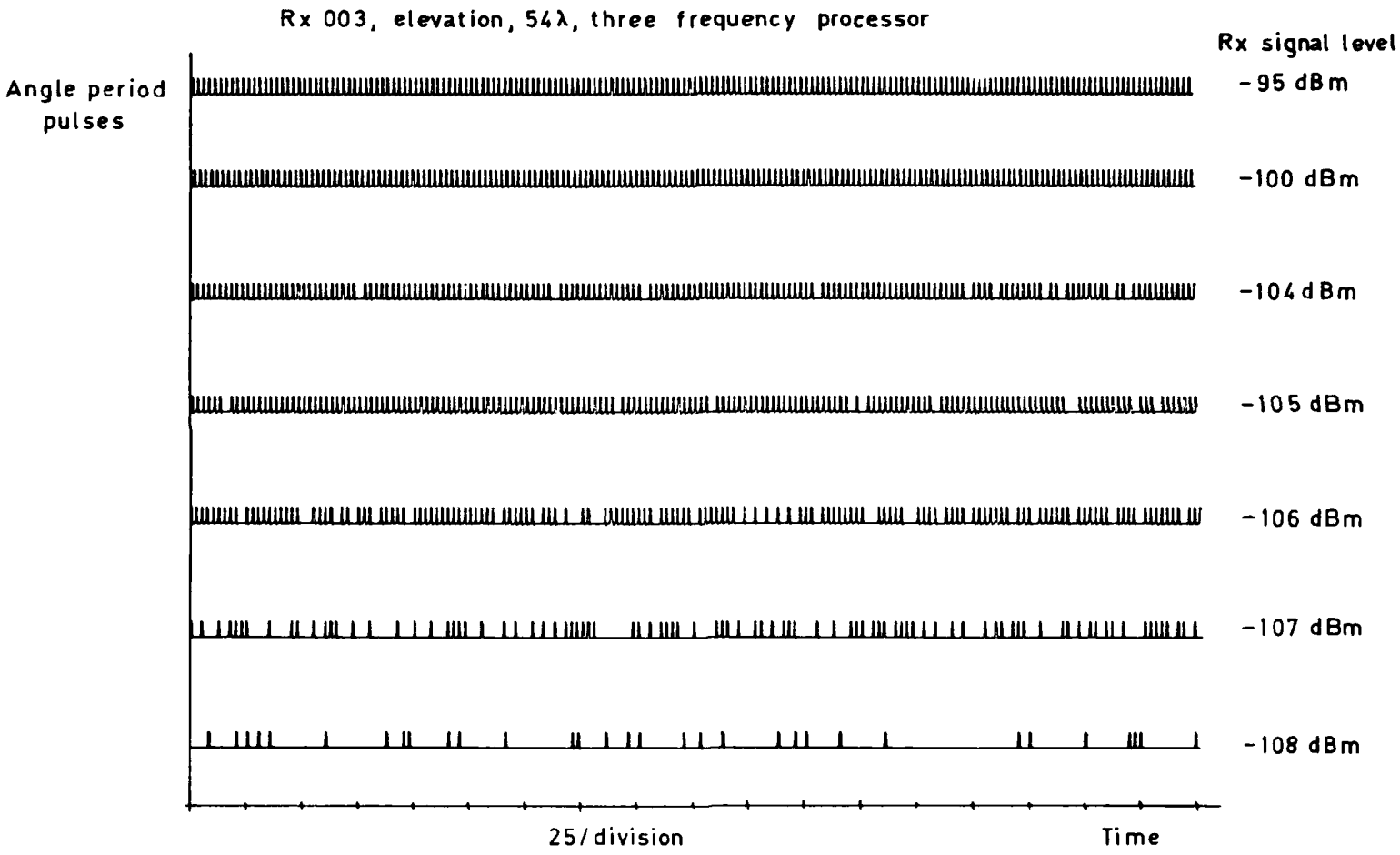

Fig 6.13b Elevation function identity decode success

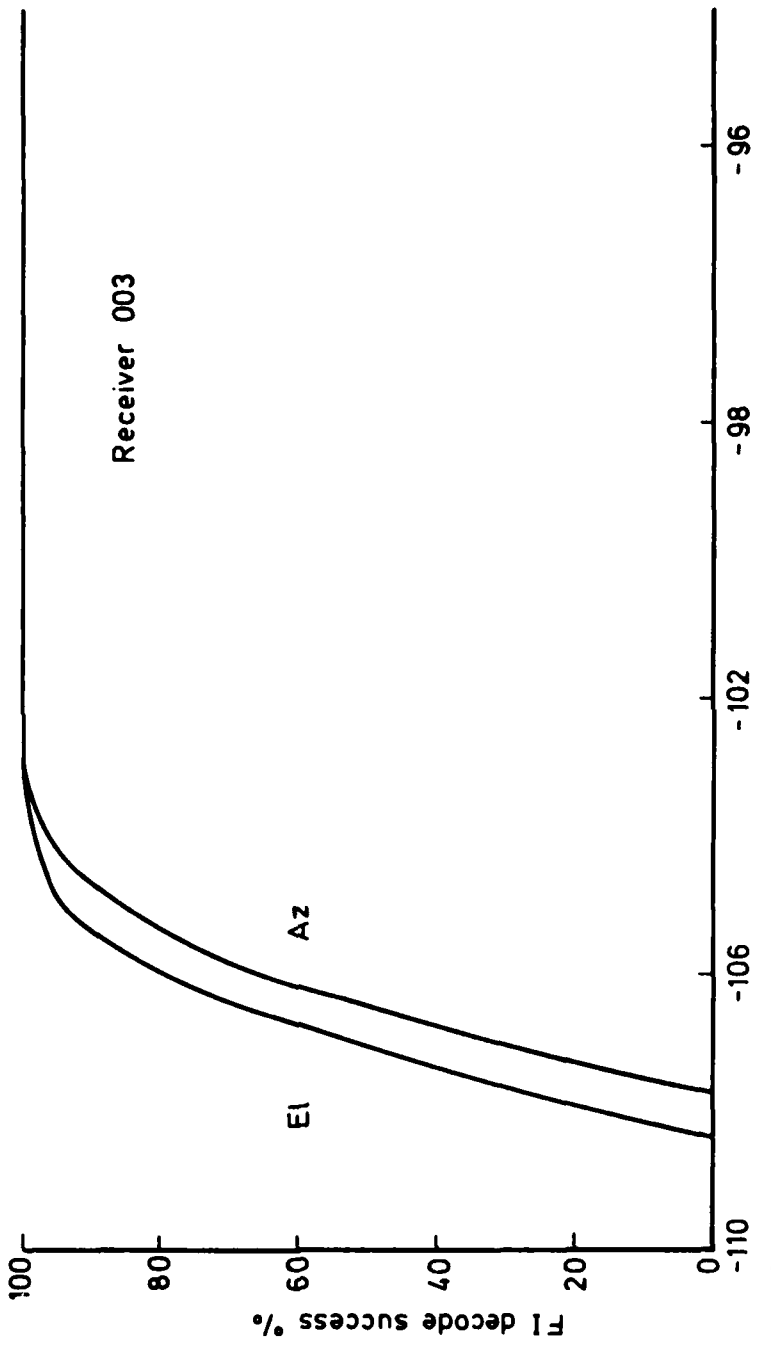

TR 79062

Fig 6.14 Receiver performance at low signal level

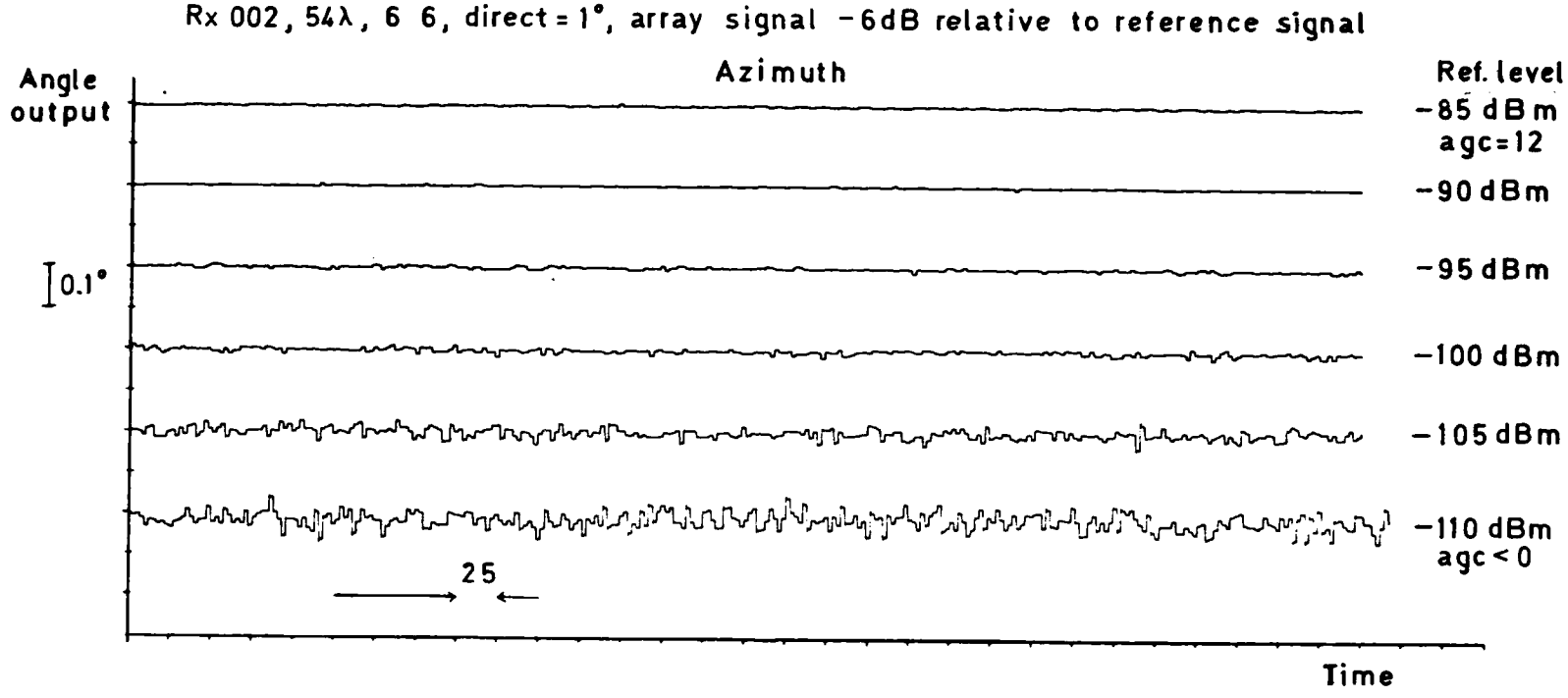

Fig 6.15 Azimuth receiver noise as a function signal input level (FI preamble hard wired)

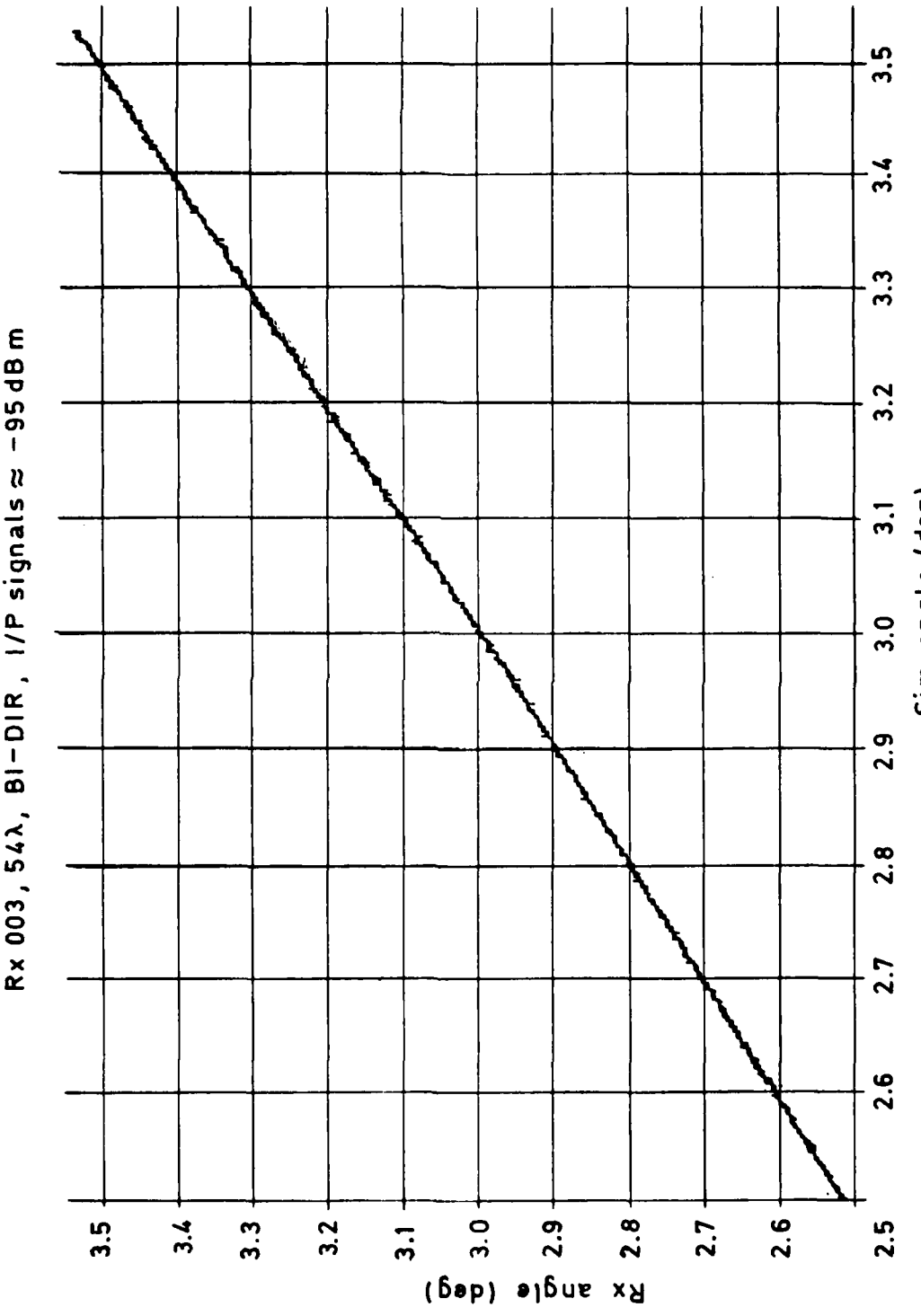

TR 79052

Fig 6.16 Azimuth angle output as a function of simulator angle

Fig 6.17a

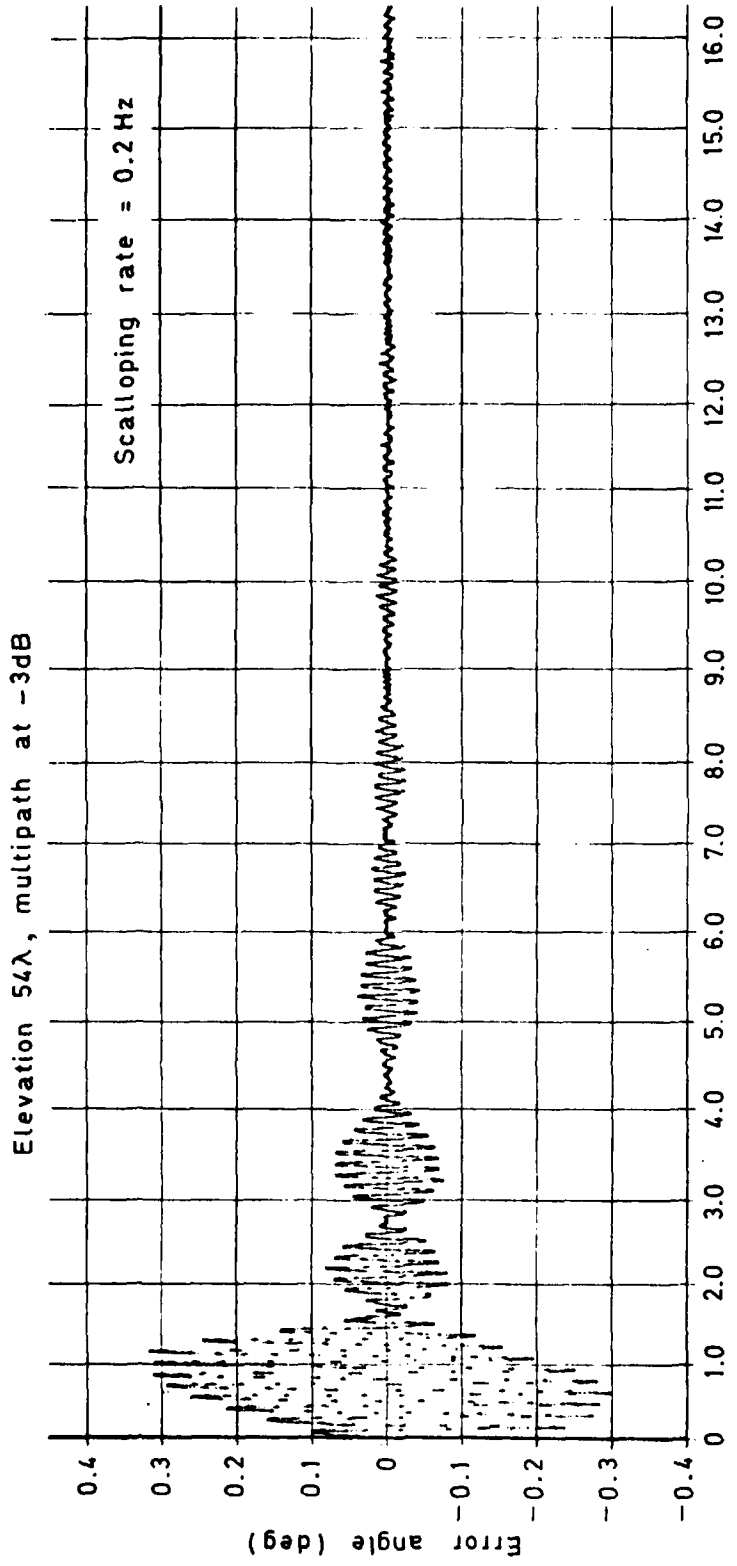

Fig 6.17a Elevation error as a function of separation angle – single frequency processor

TR 79052

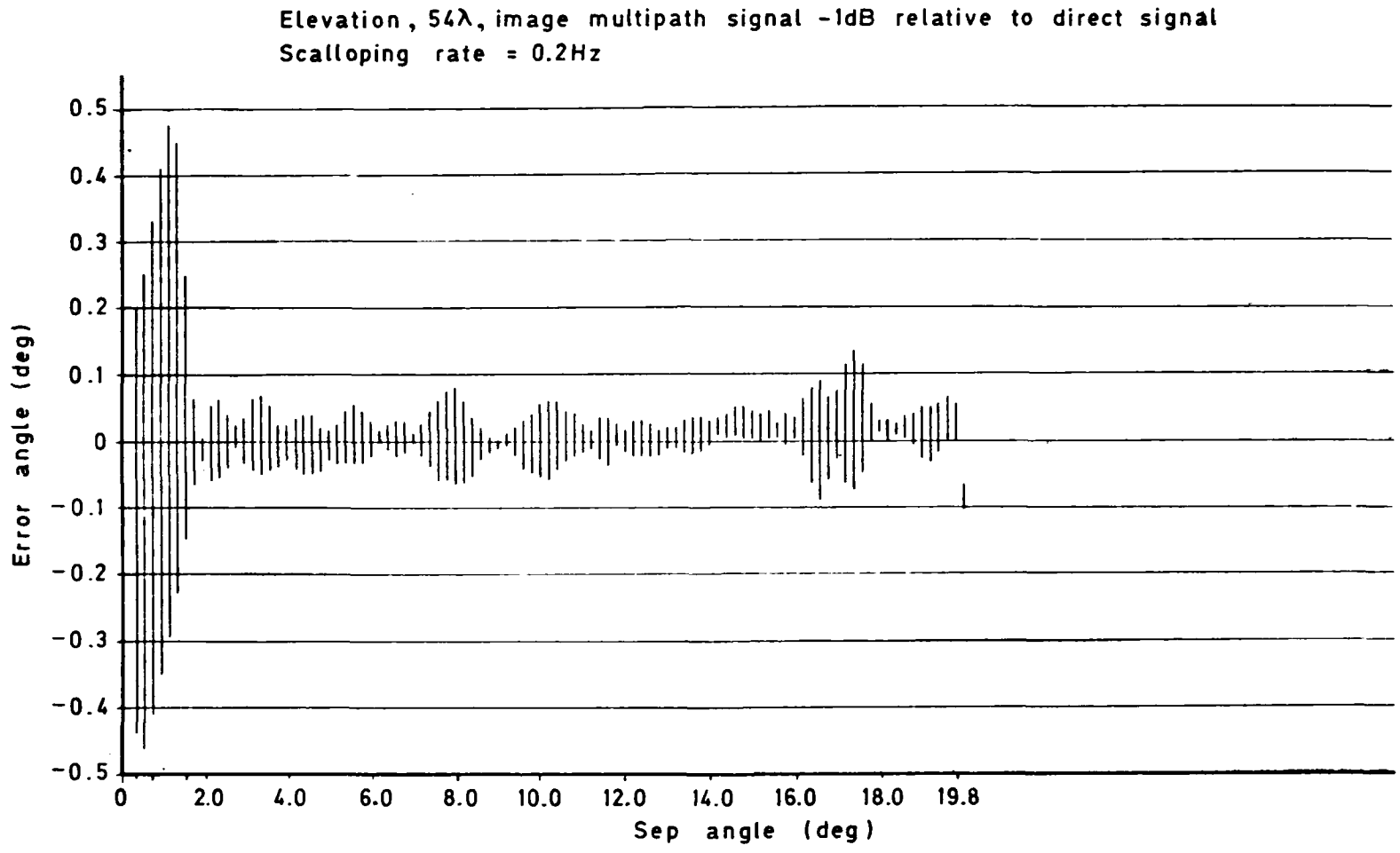

Fig 6.17b Elevation error as a function of separation angle – Taylor taper processor

Fig 6.17b

Fig 6.17c

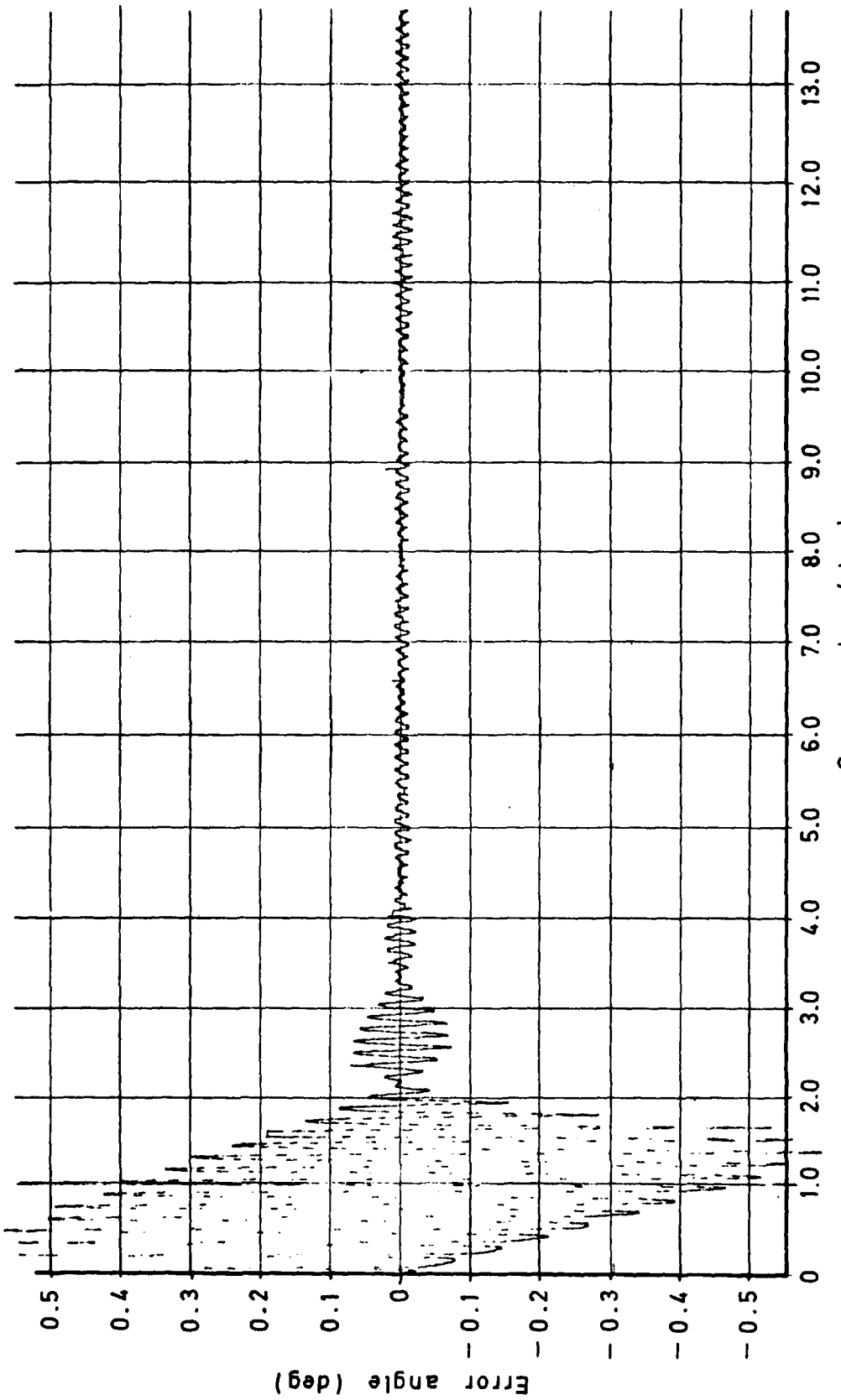

Fig 6.17c Elevation error as a function of separation angle – three frequency processor

TR 79062

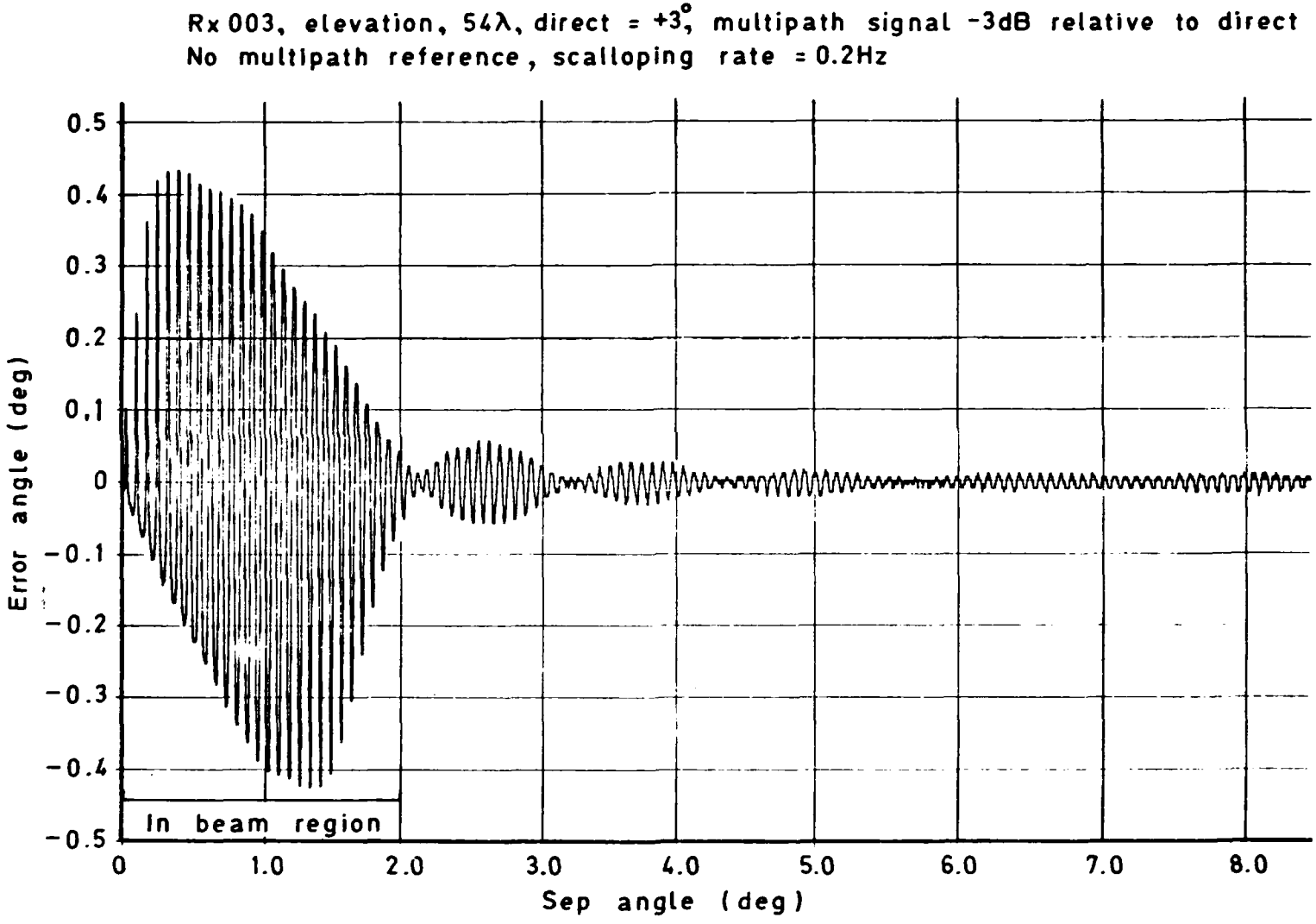

Fig 6.18a Elevation error as a function of separation angle — three frequency processor — 54λ

Fig 6.18a

Fig 6.18b

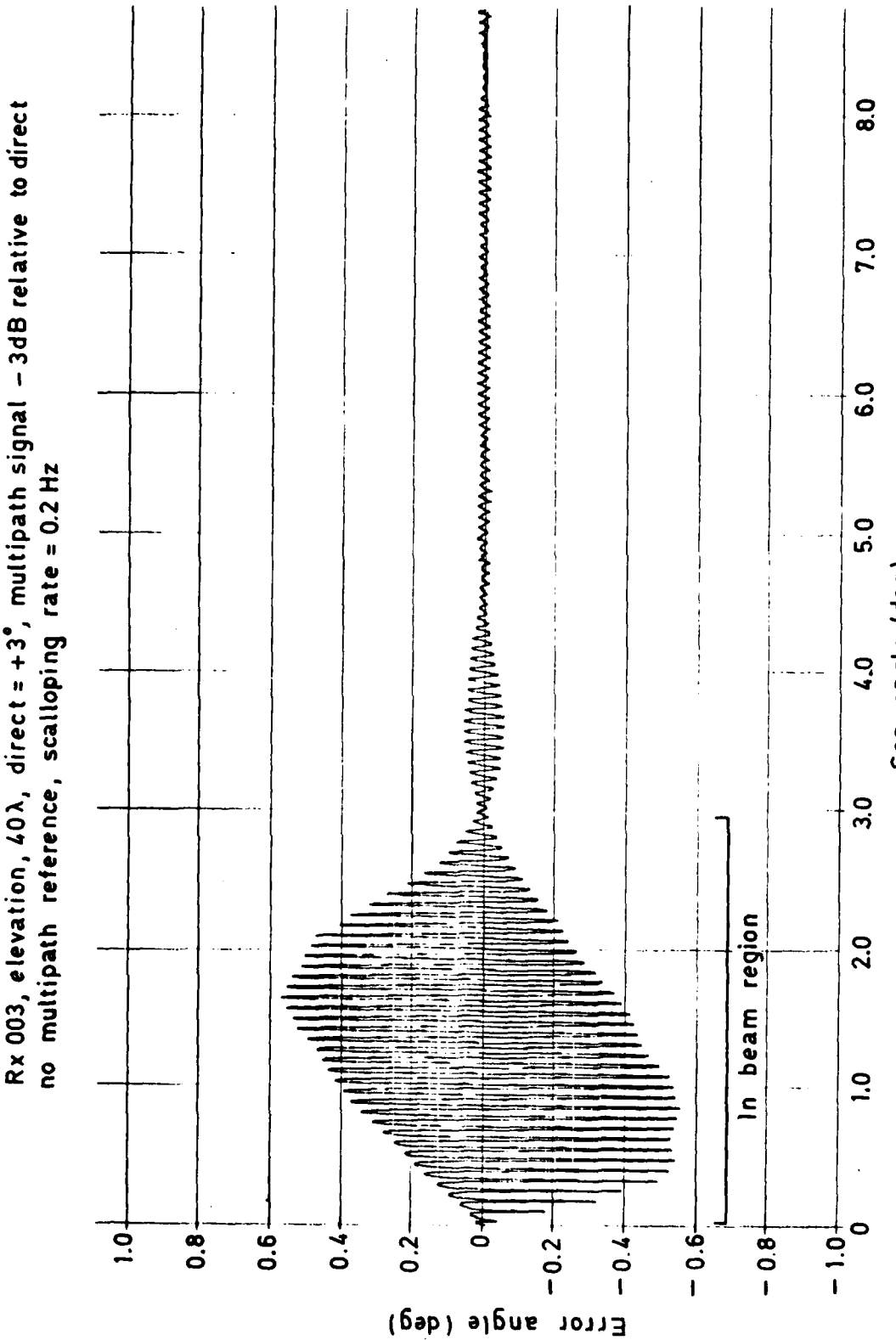

Fig 6.18b Elevation angle as a function of separation angle — three frequency processor — 40λ

TR 79052

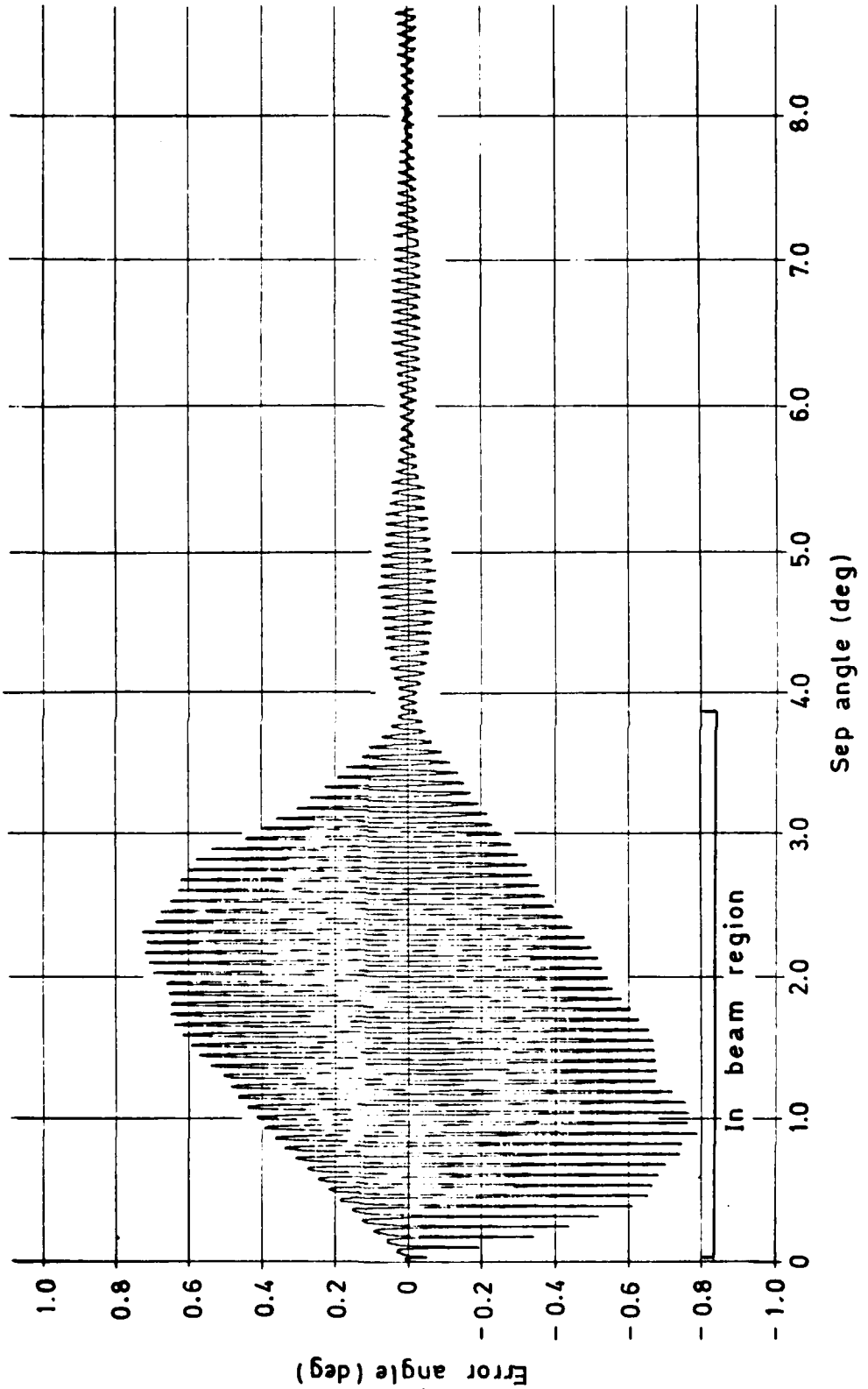

TR 79052

Fig 6.18c Elevation error as a function of separation angle – three frequency processor – 30λ

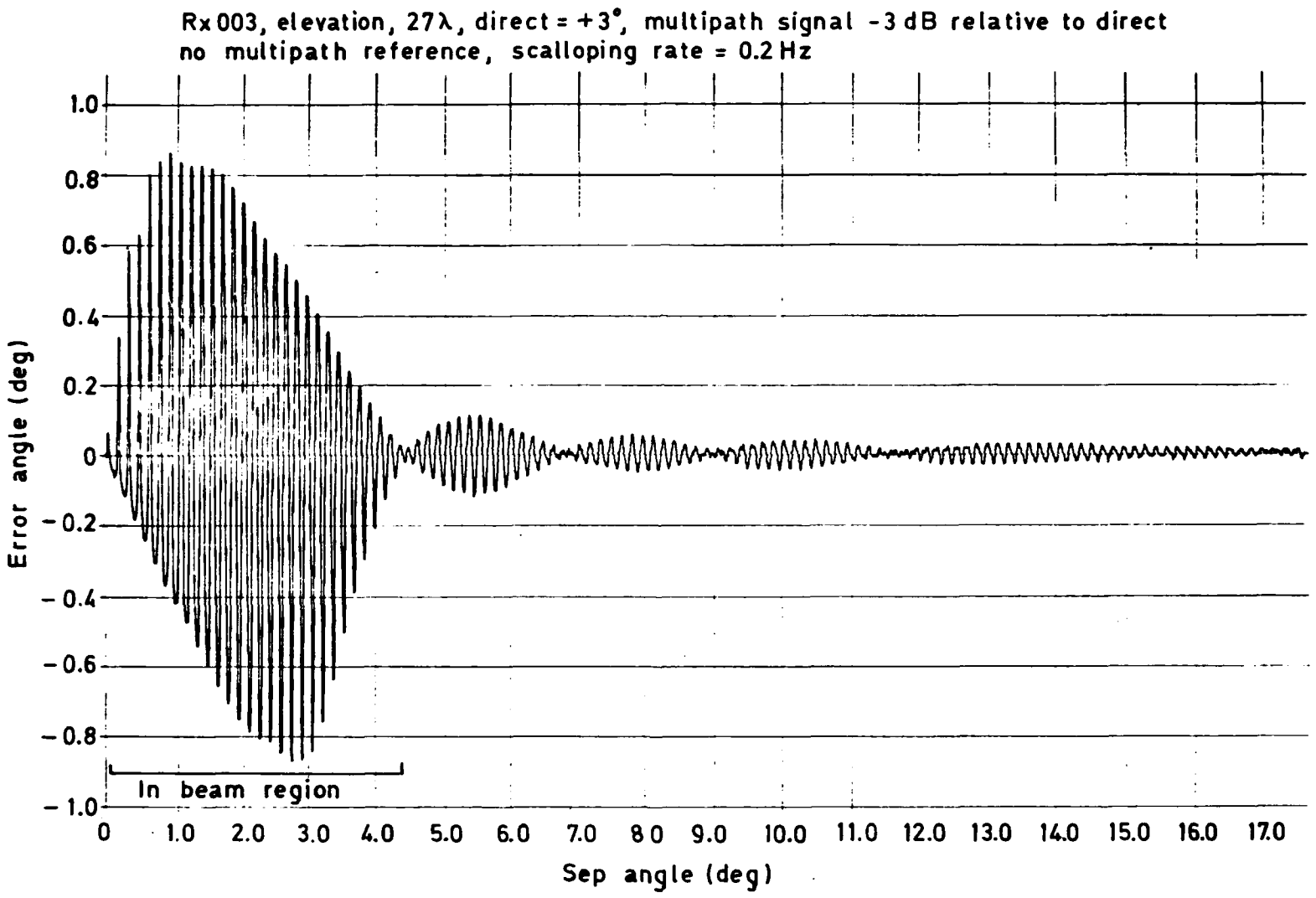

Fig 6.19 Elevation error as a function of separation angle — three frequency processor — 27λ

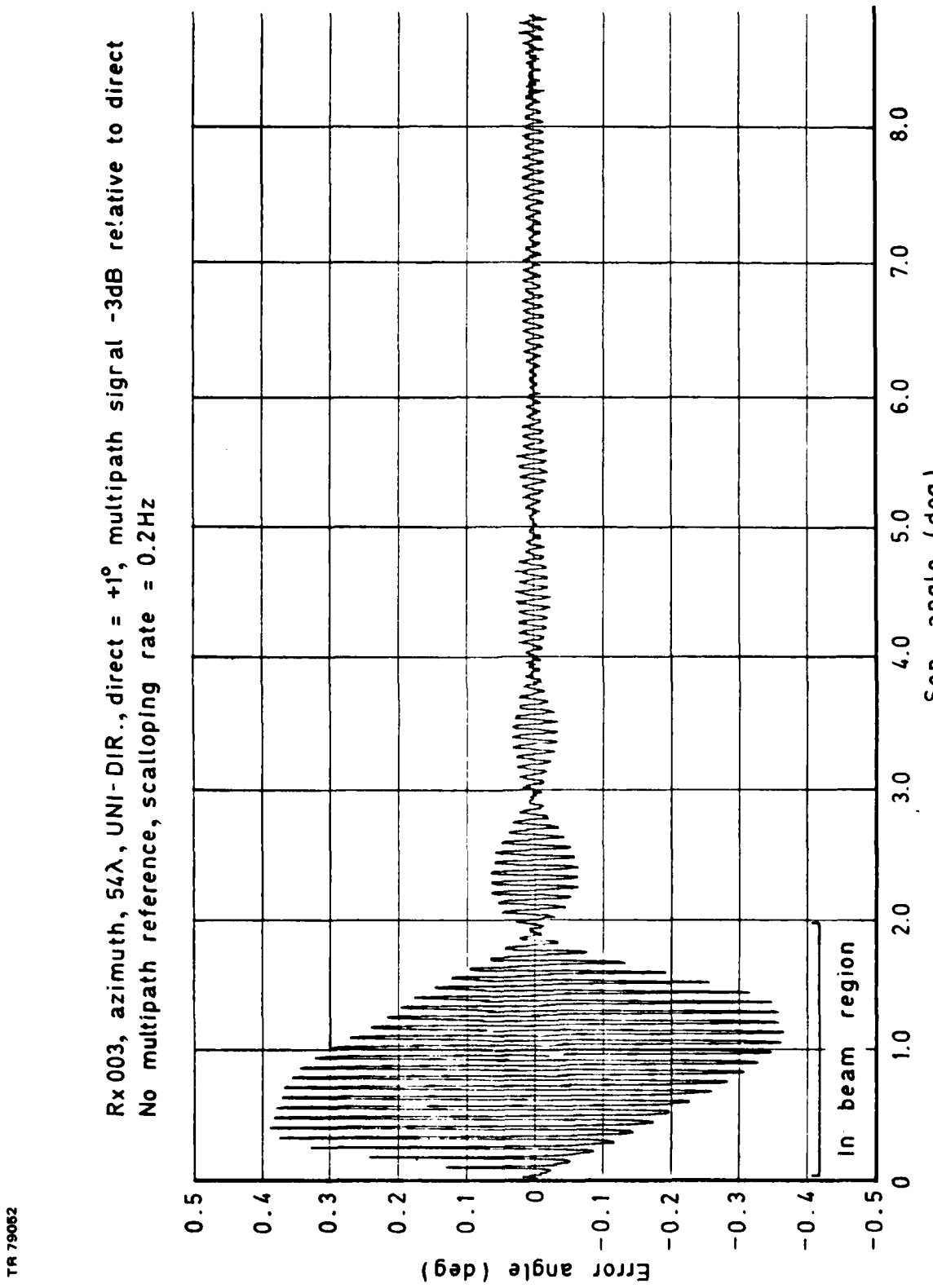

Fig 6.20a Azimuth error as a function of separation angle – three frequency processor – 54λ

Fig 6.20b

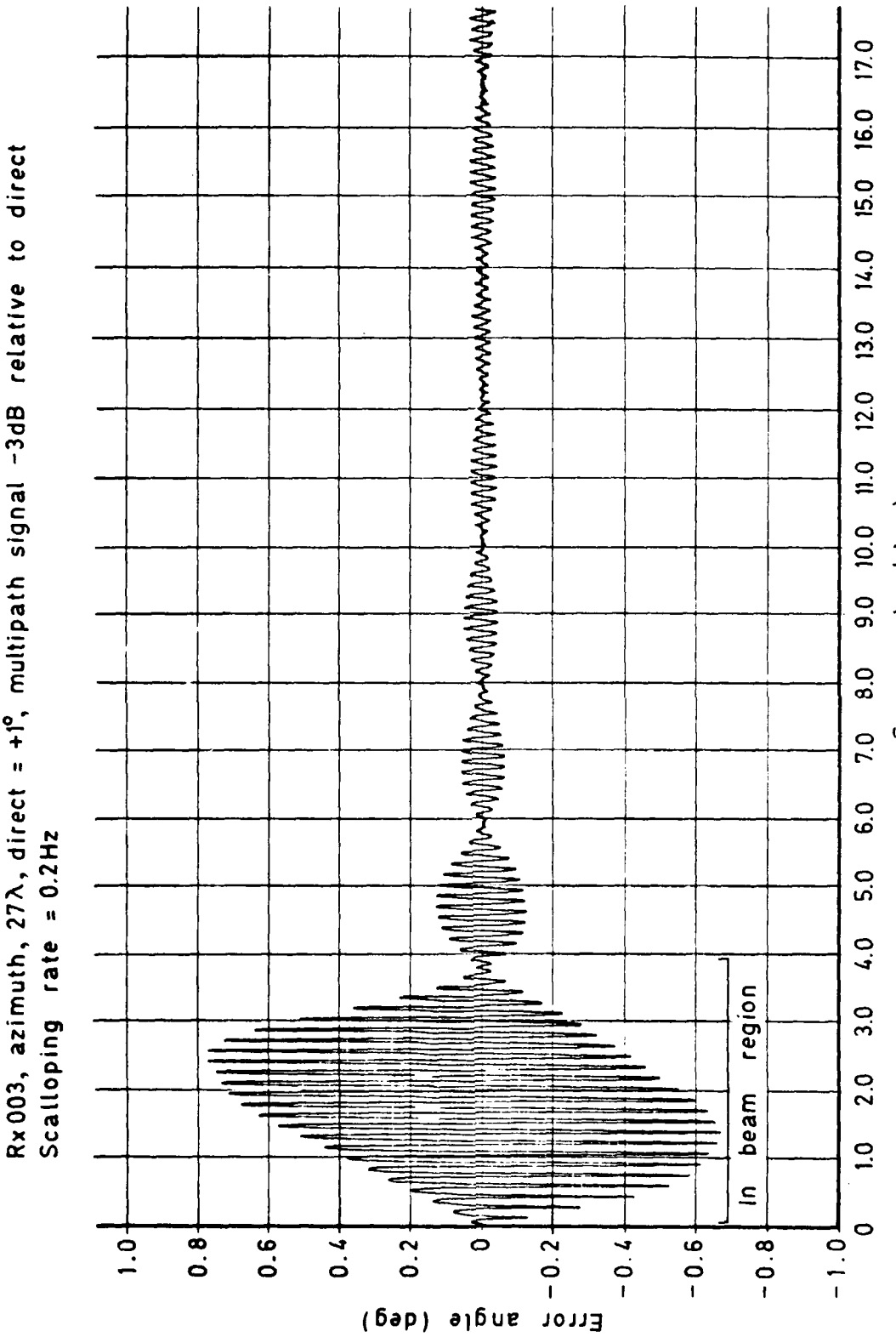

Fig 6.20b Azimuth error as a function of separation angle – three frequency processor – 27λ

TR 79062

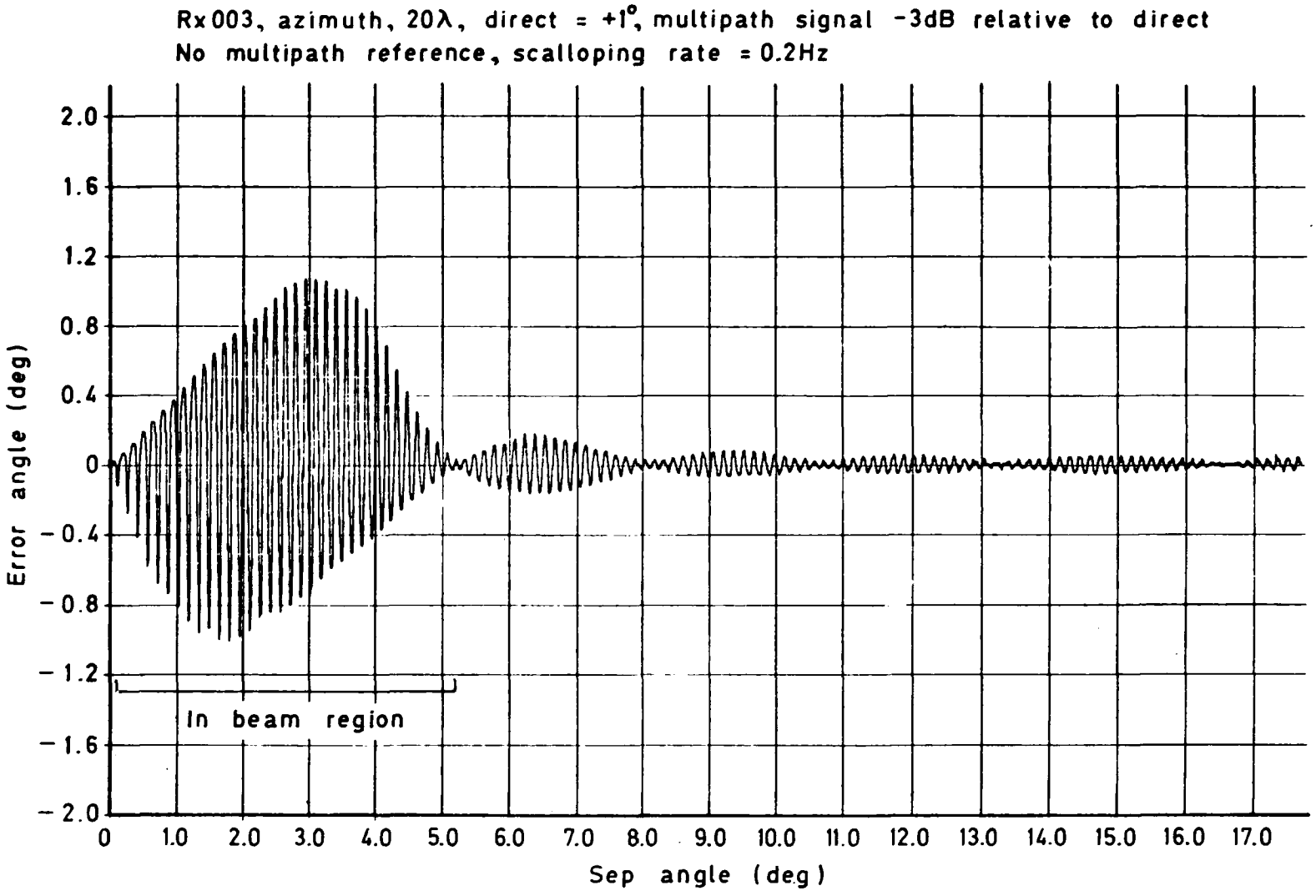

Fig 6.20c Azimuth error as a function of separation angle – three frequency processor – 20λ

Fig 6.20d

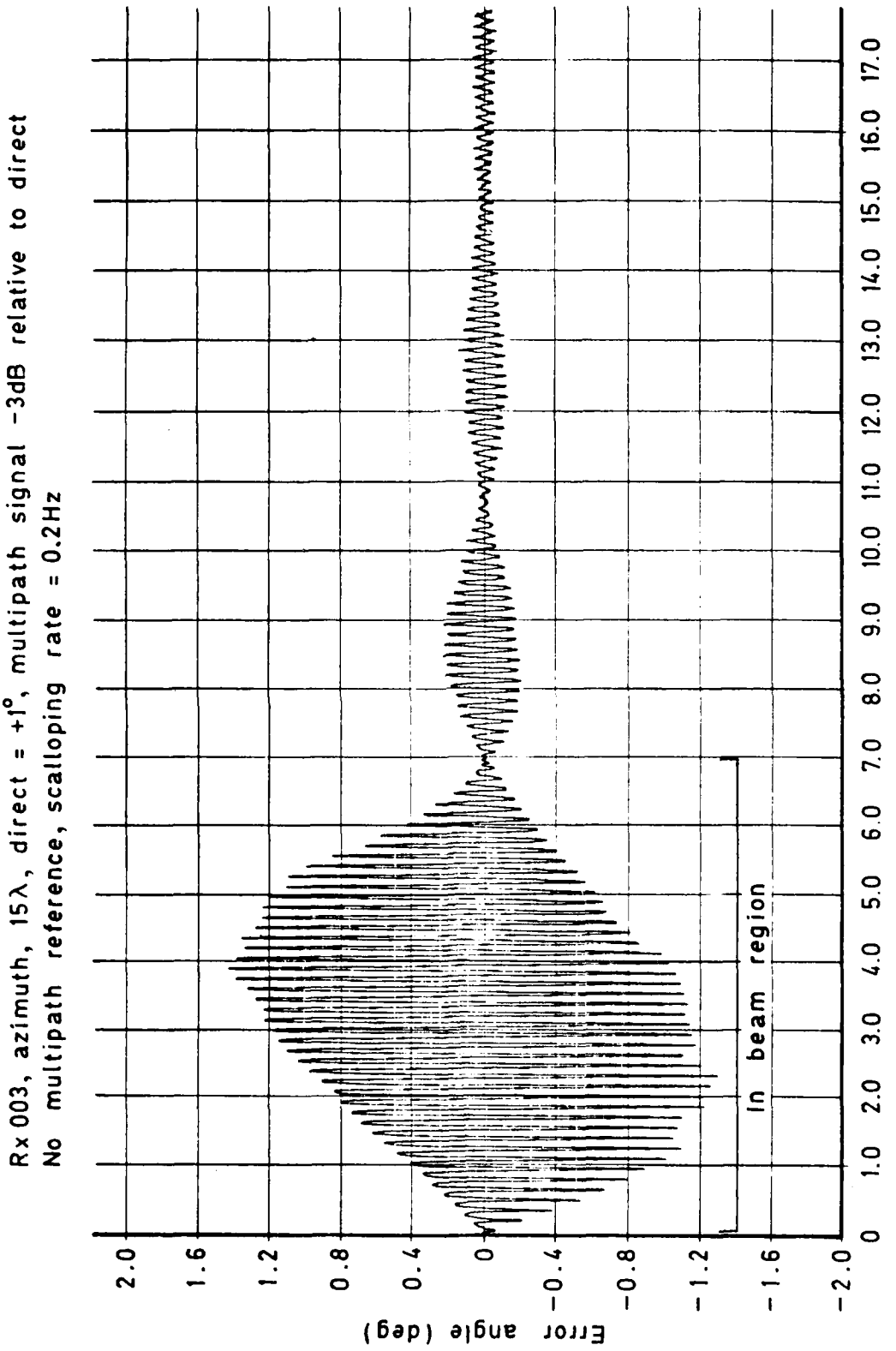

Fig 6.20d Azimuth error as a function of separation angle – three frequency processor – 15λ

TR 79052

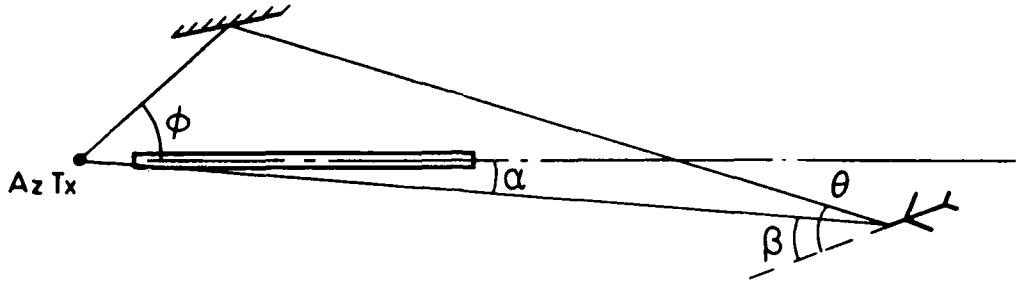

Direct signal code angle = α

Multipath code angle = ϕ

Differential fading rate = $\frac{v}{\lambda}(\cos\beta - \cos\theta)$

a Azimuth systems

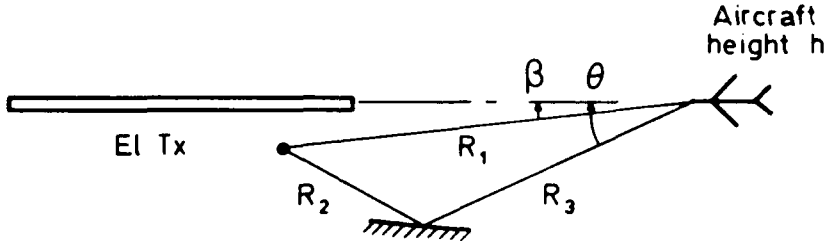

Direct signal code angle = $\alpha = \text{Tan}^{-1}\frac{h}{R_1}$

Multipath code angle = $\phi = \text{Tan}^{-}\frac{h}{R_2+R_3}$

Differential fading rate = $\frac{v}{\lambda}(\cos\beta - \cos\theta)$

b Elevation system

TR 79052

Fig 6.21 Typical multipath geometries

Fig 6.22

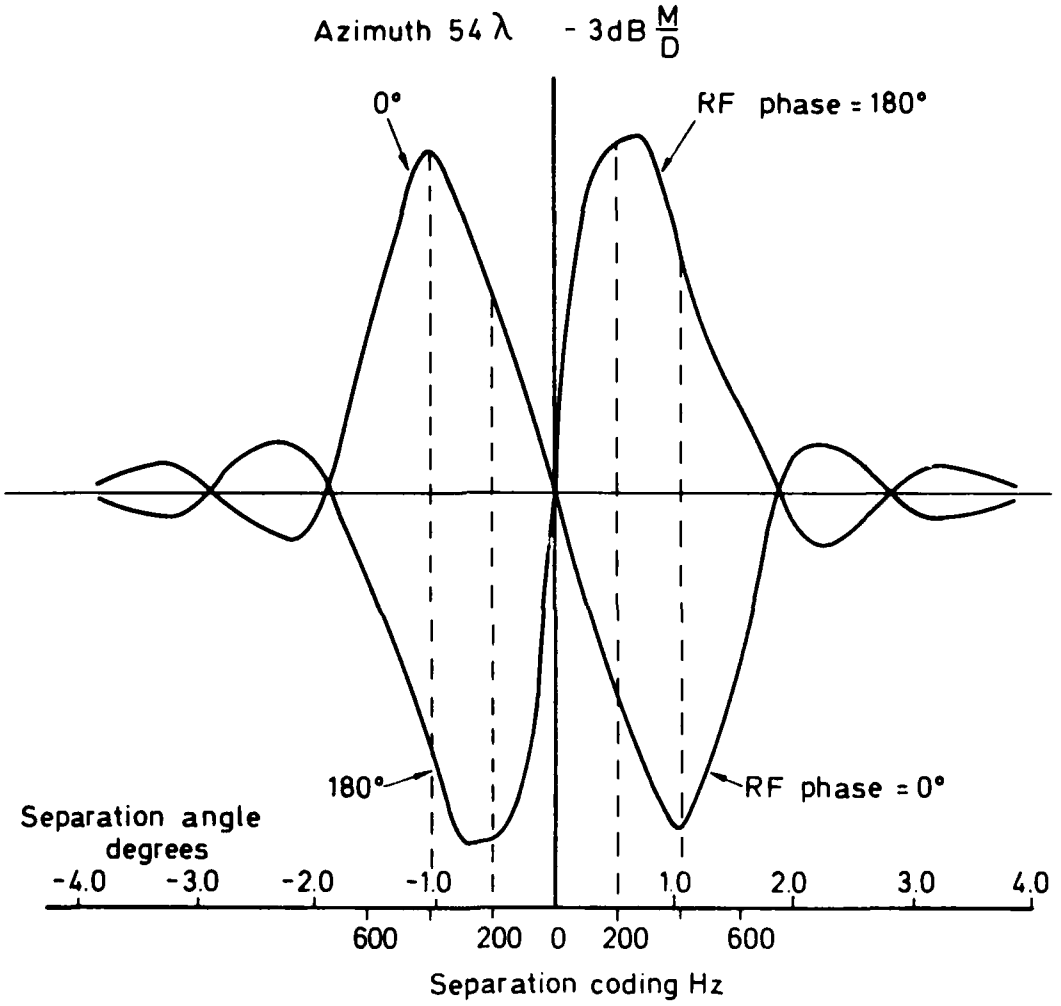

TR 79062

Fig 6.22 Multipath curves, worst case phase

Fig 6.23a

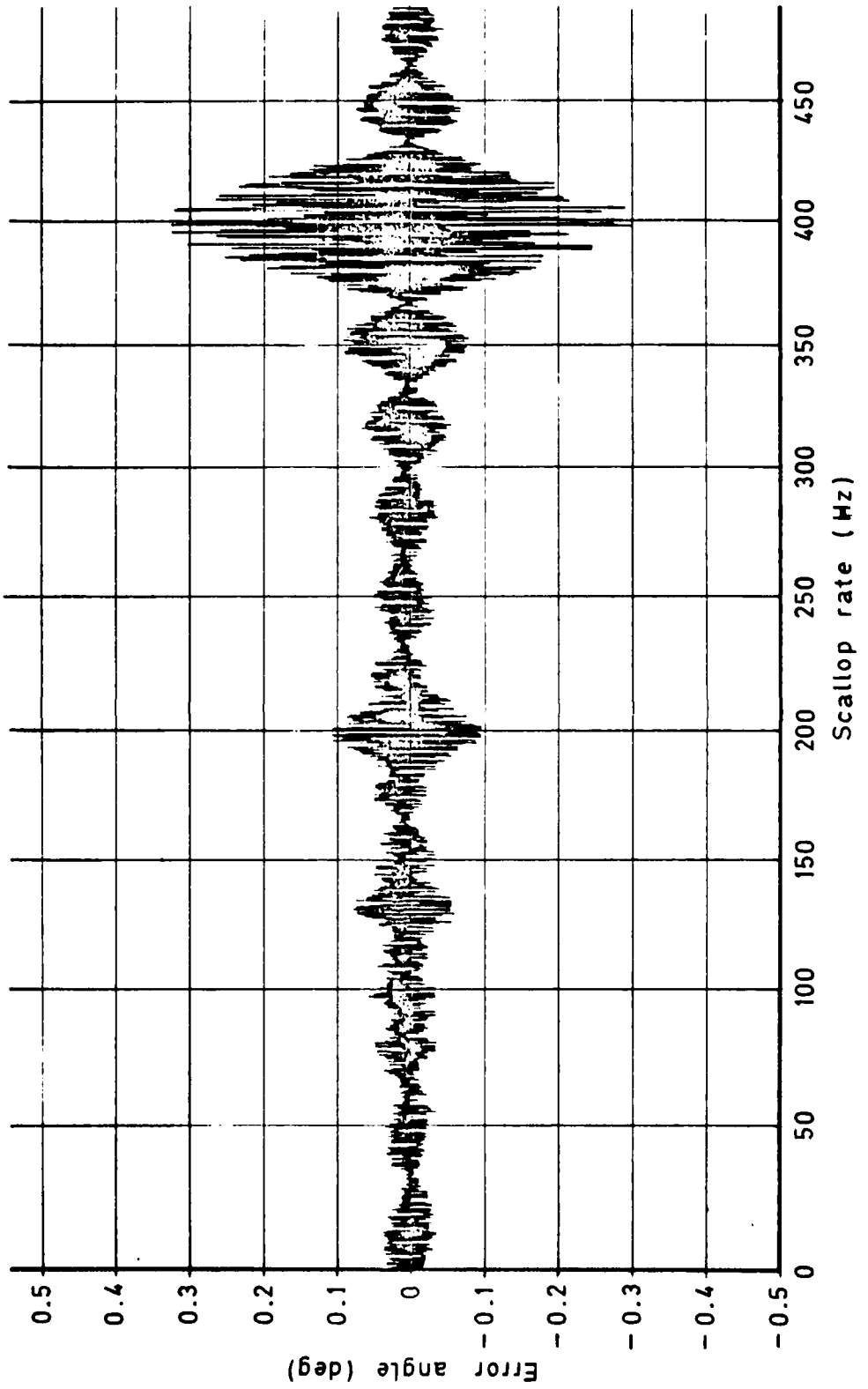

TR 79052

Fig 6.23a Azimuth error as a function of scalloping rate – 54λ, unidirectional scan

Fig 6.23b

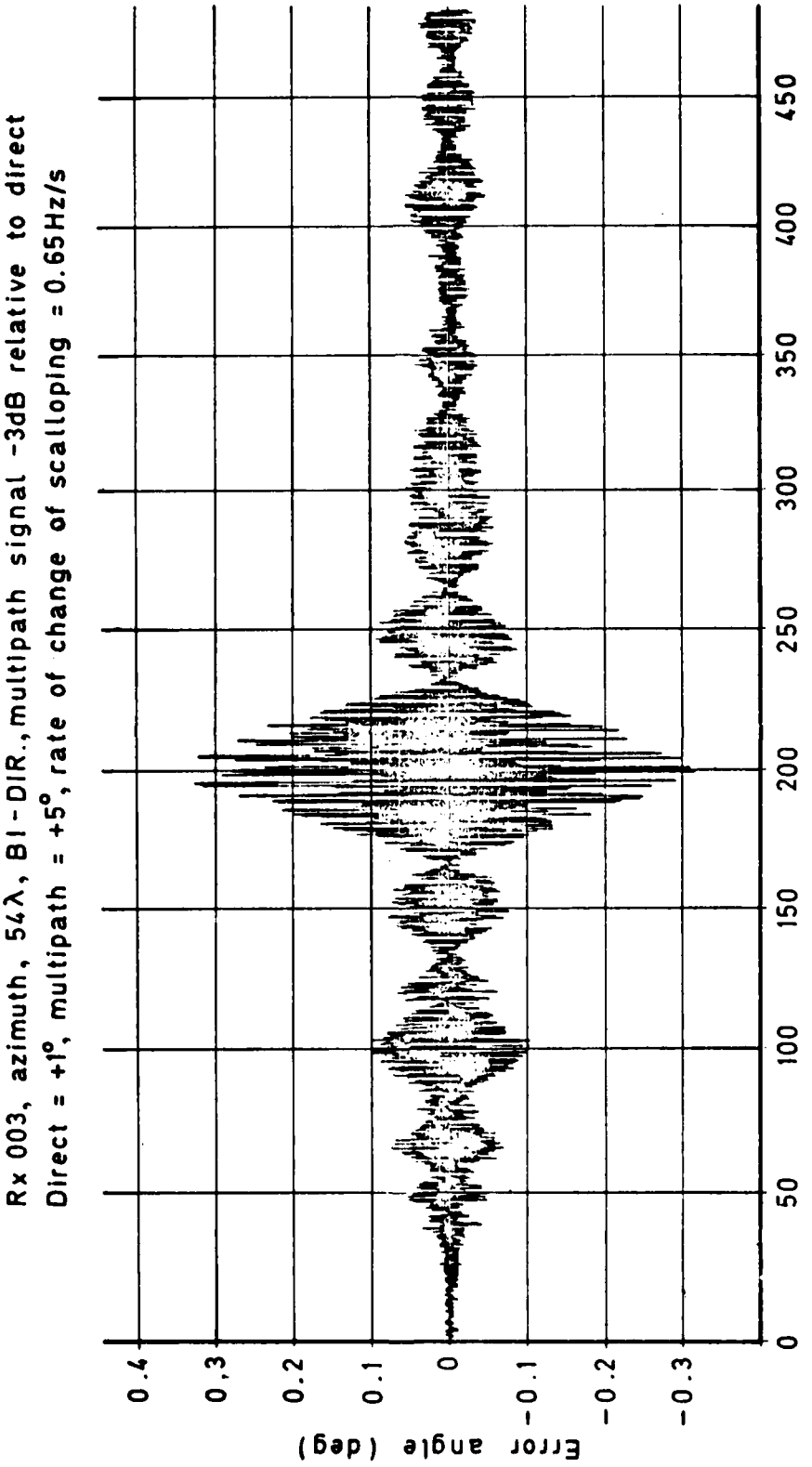

Fig 6.23b Azimuth error as a function of scalloping rate – 54λ, bidirectional scan

TR 79052

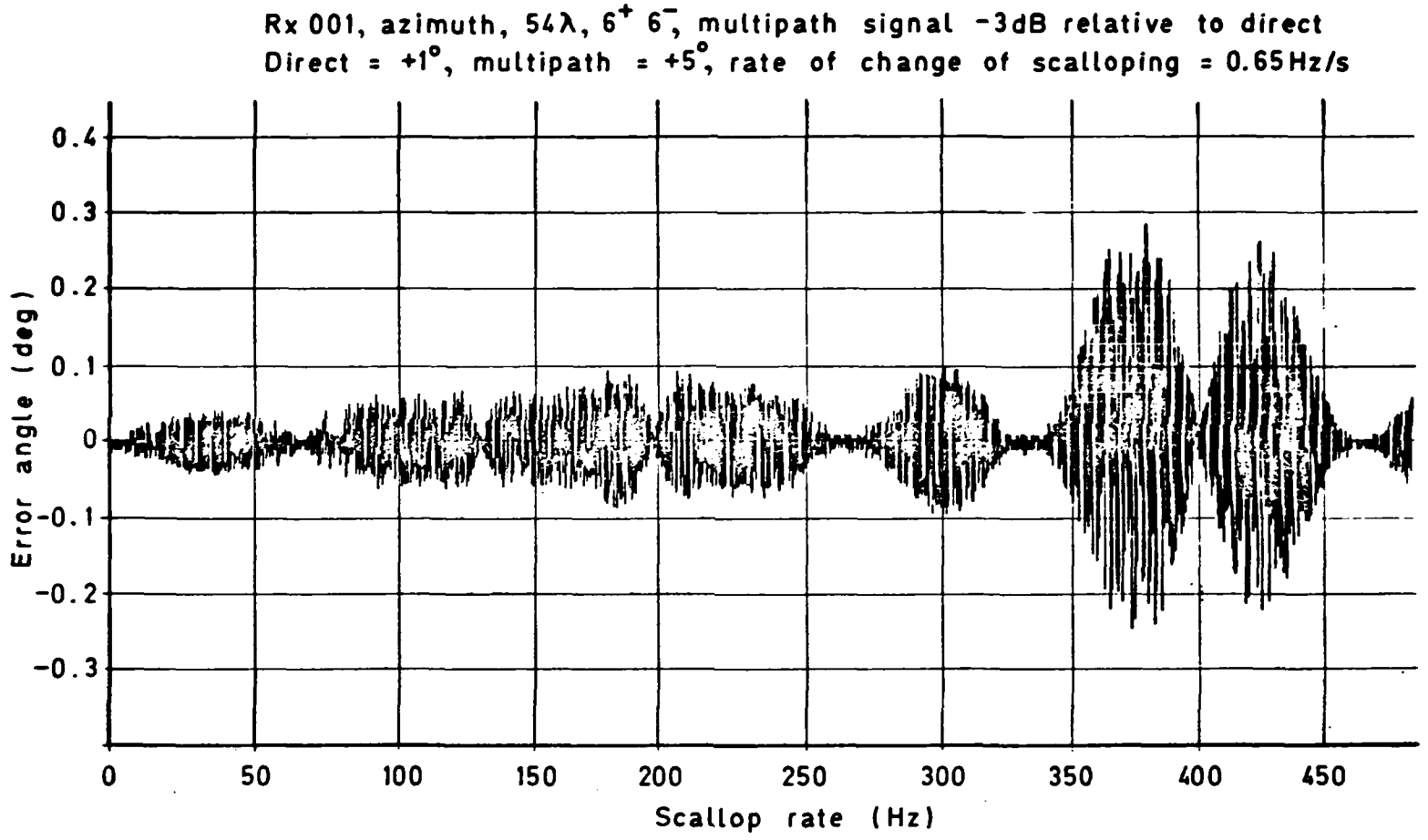

Fig 6.23c Azimuth error as a function of scalloping rate – 54λ, block scan (6^{+-})

Fig 6.23c

Fig 6.24

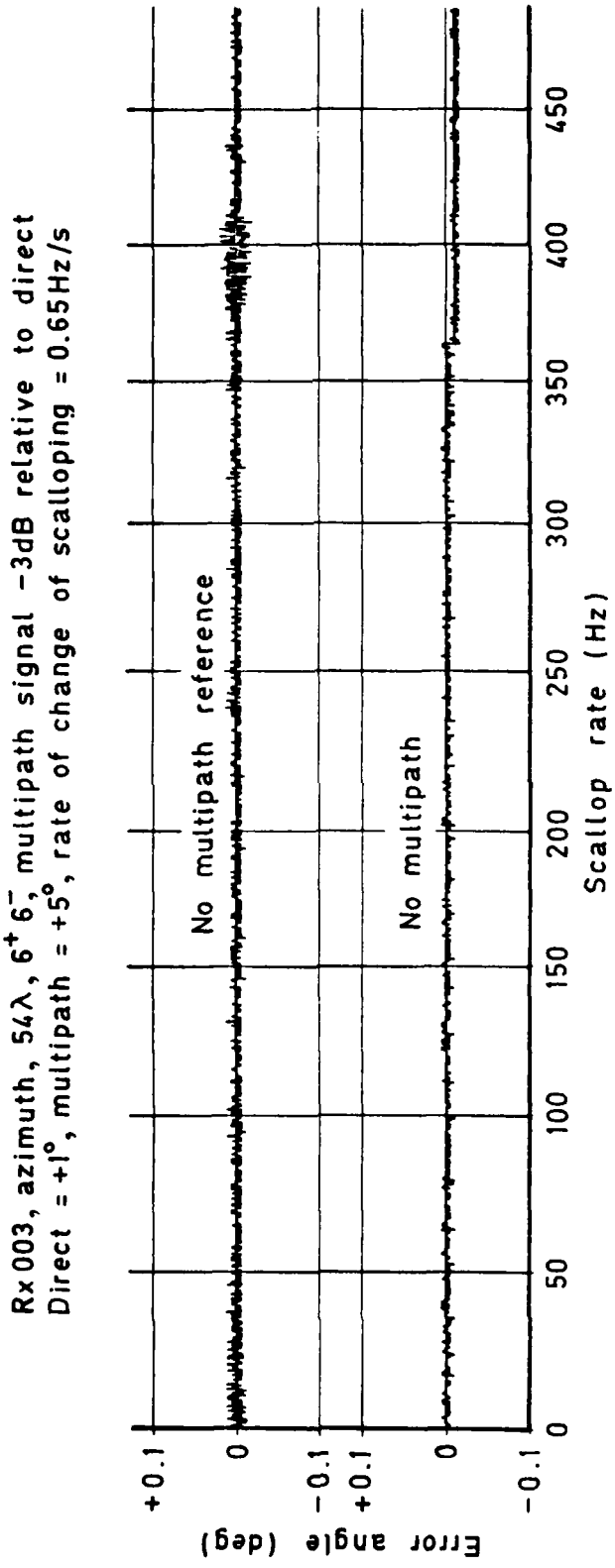

Fig 6.24 Azimuth error as a function of scalloping rate – 54λ, block scan

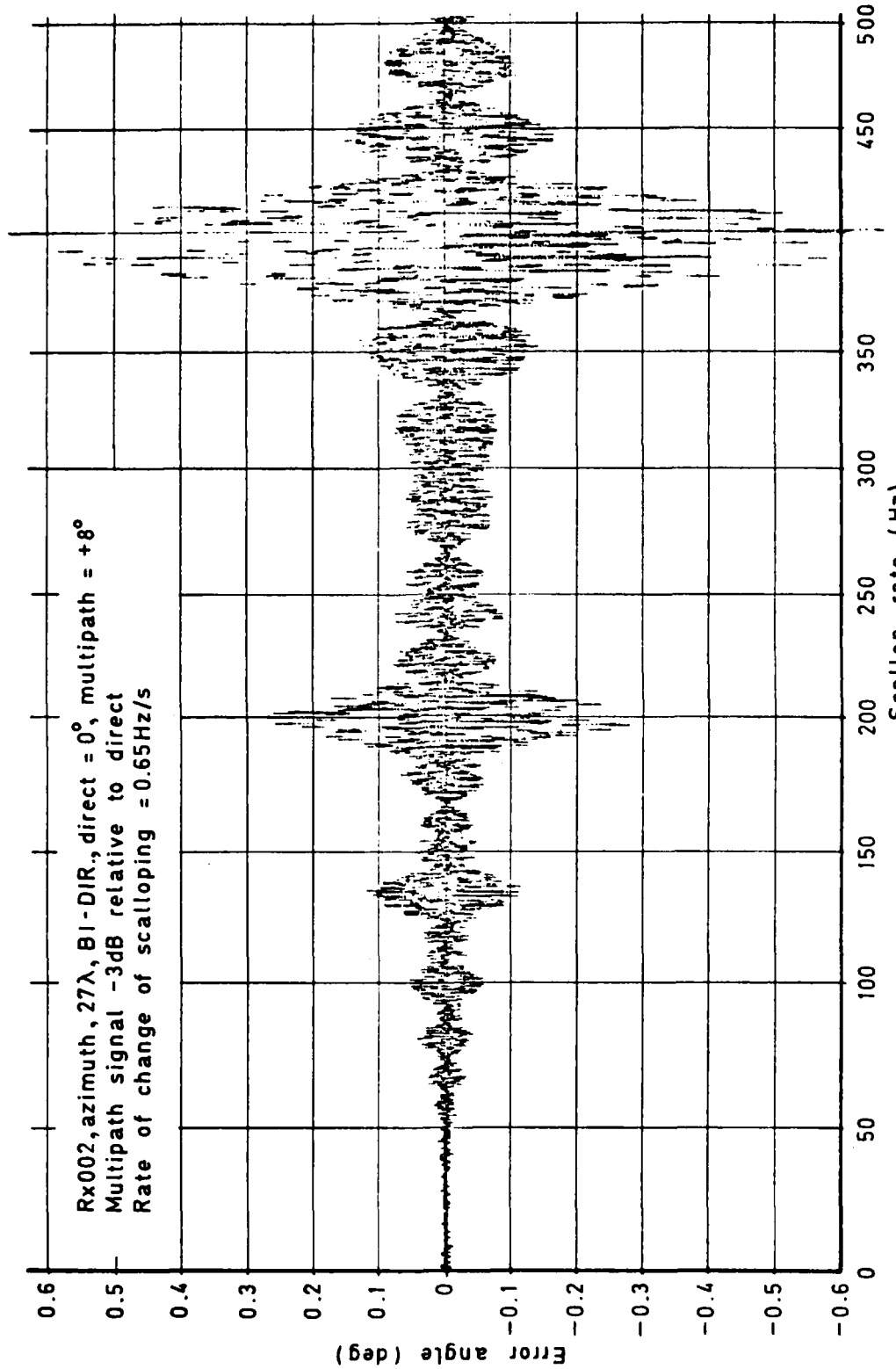

TR 79052

Fig 6.25a Azimuth error as a function of scalloping rate — 27λ, bidirectional scan

Fig 6.25b

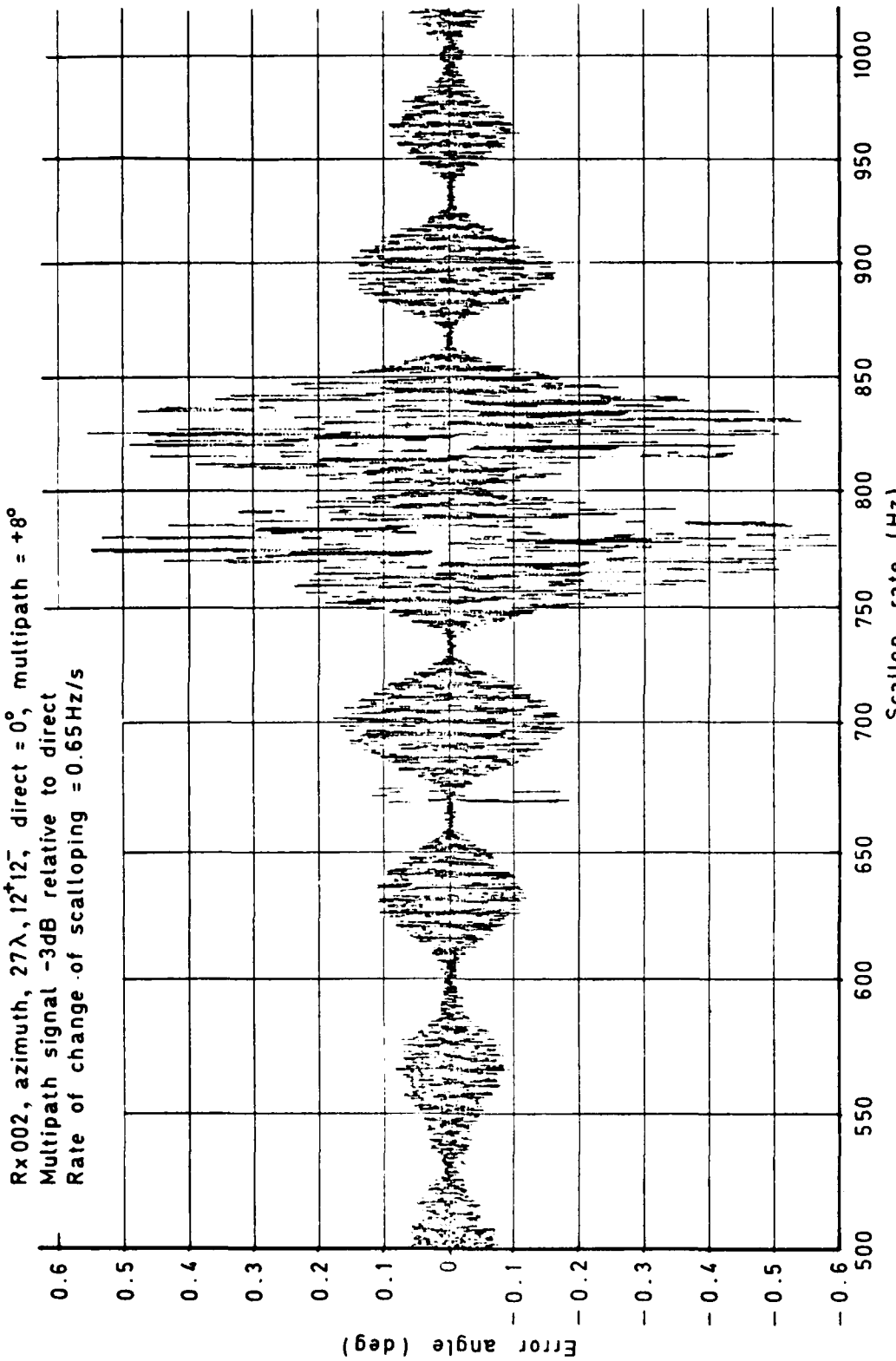

Fig 6.25b Azimuth error as a function of scalloping rate – 27λ, block scan (12^{+-})

TR 79052

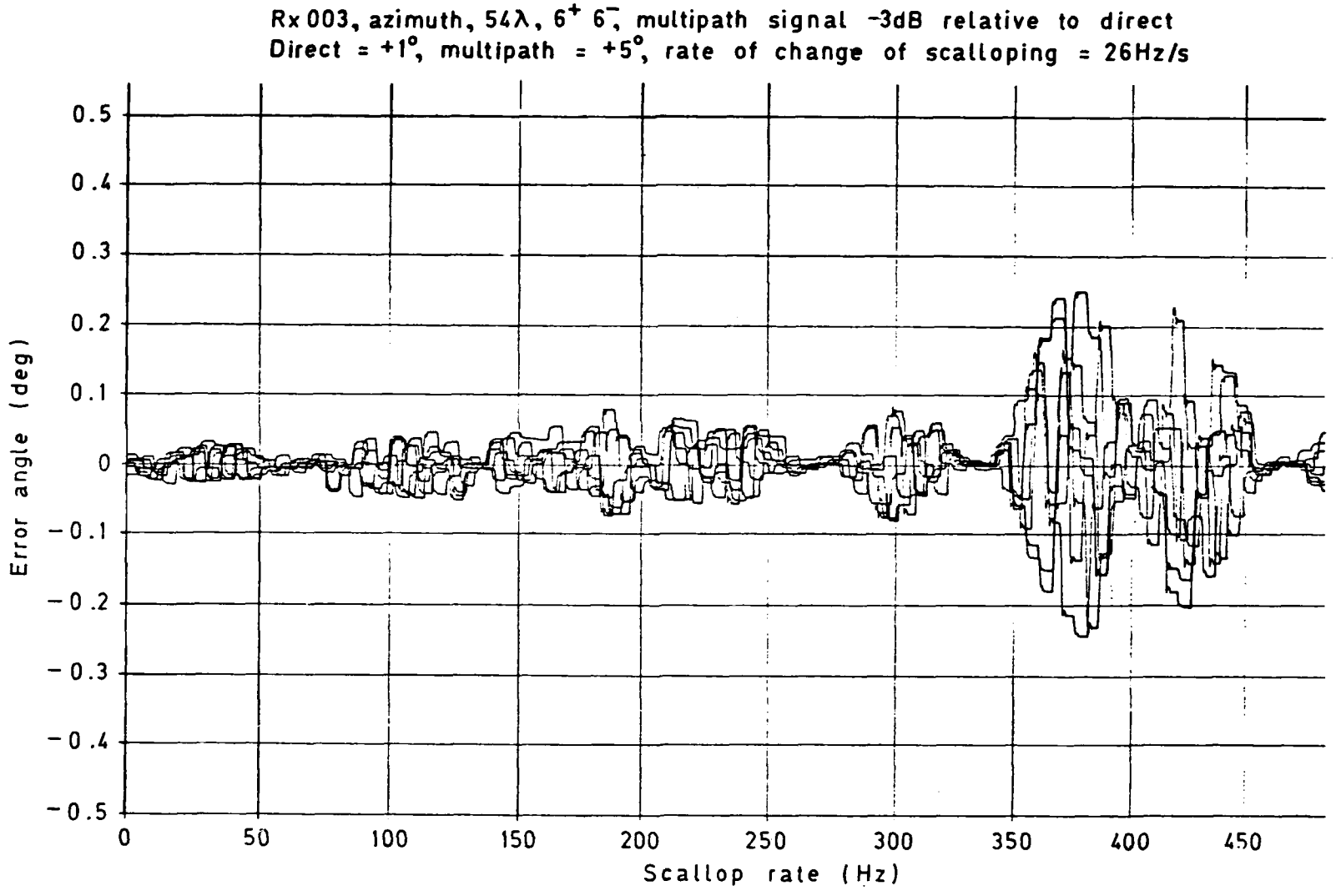

Fig 6.26 Azimuth error as a function of scalloping rate — 54λ, 6^{+-} scan, high rate of change

Fig 6.26

Fig 6.27a

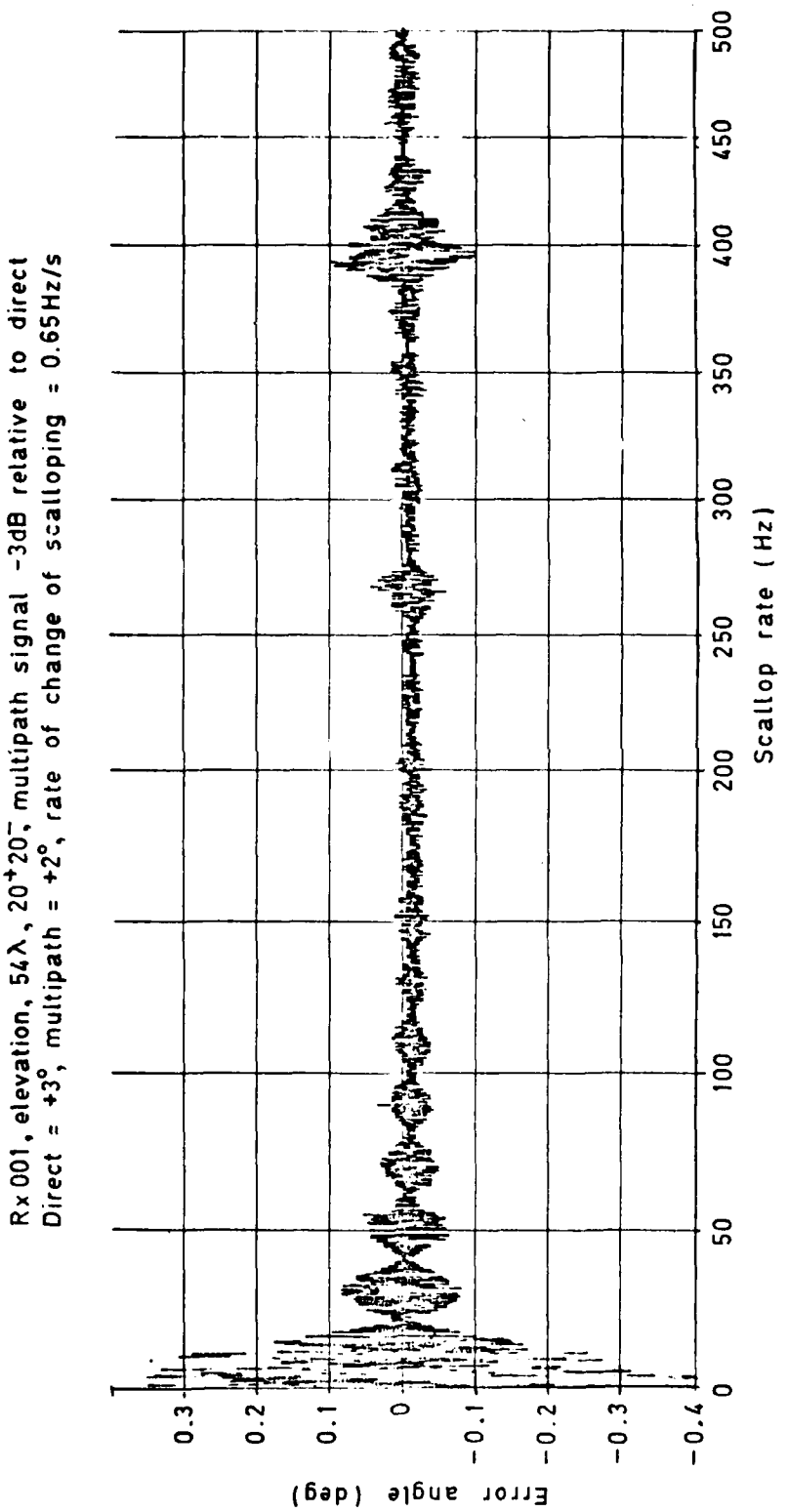

Fig 6.27a Elevation error as a function of scalloping rate – 54λ, block scan (20^{+}_{-})

TR 79052

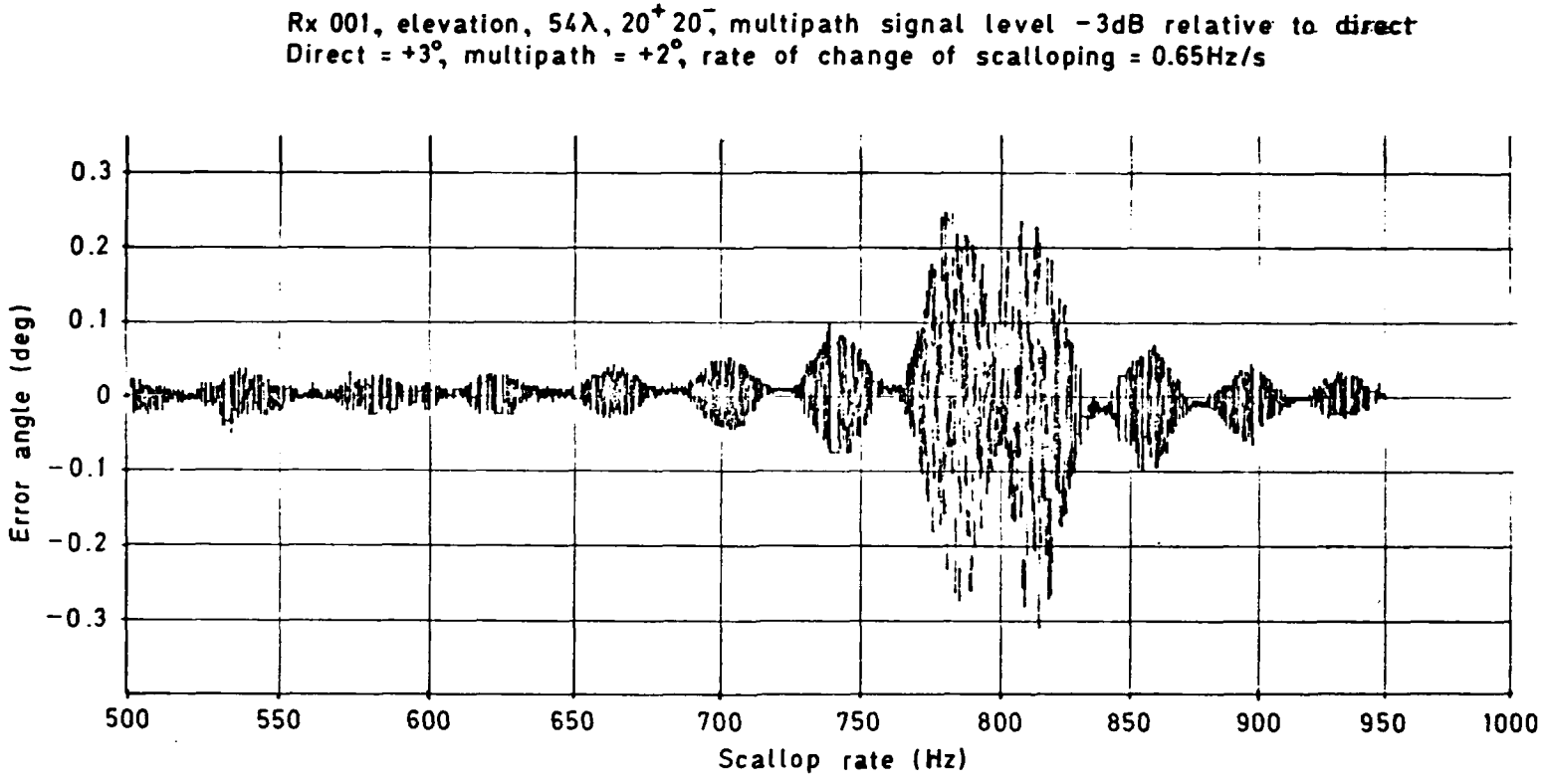

Fig 6.27b Elevation error as a function of scalloping rate — 54λ, block scan (20^{+-})

Fig 6.28a

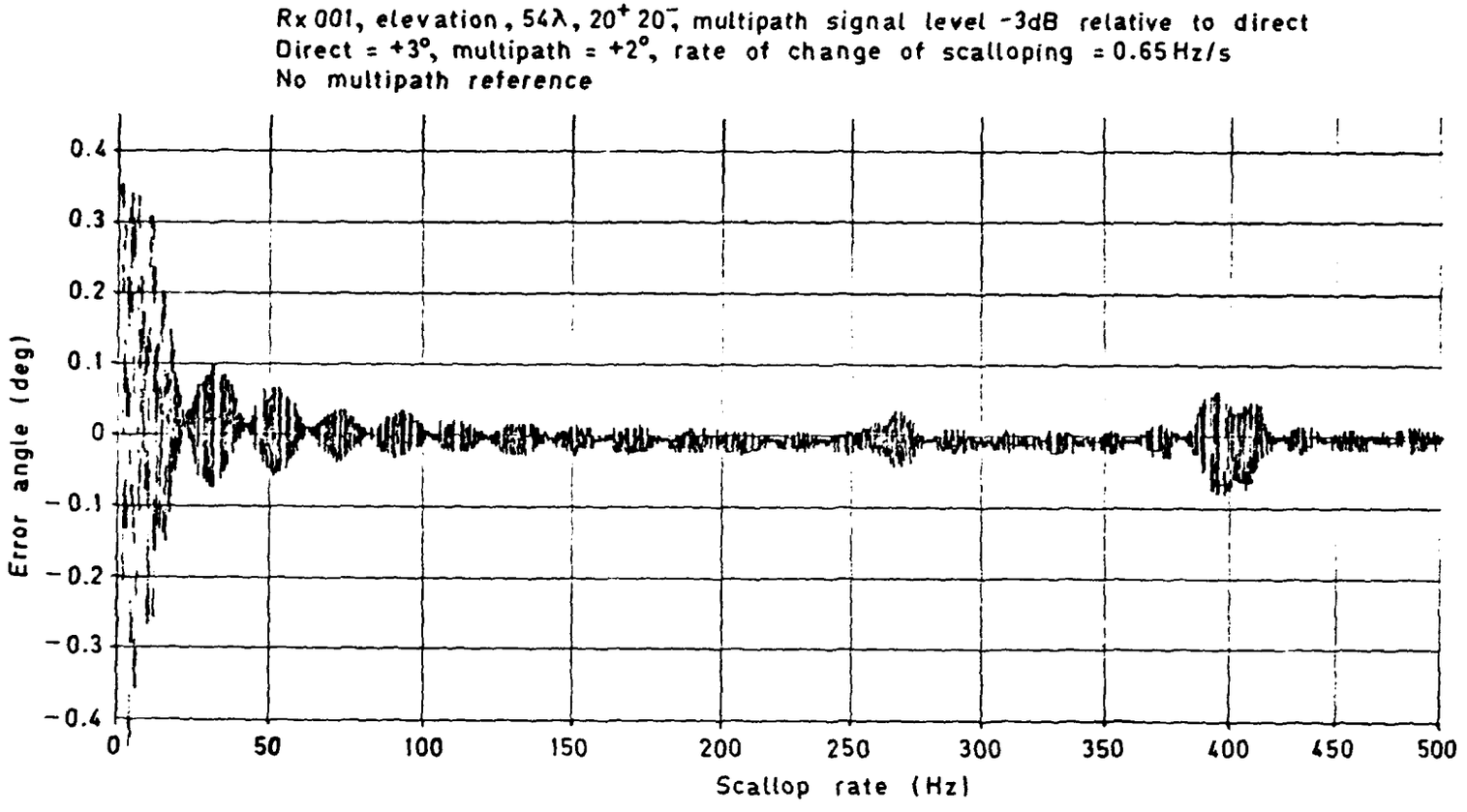

Fig 6.28a Elevation error as a function of scalloping rate — 54λ, block scan (20^{+-}), *no multipath reference*

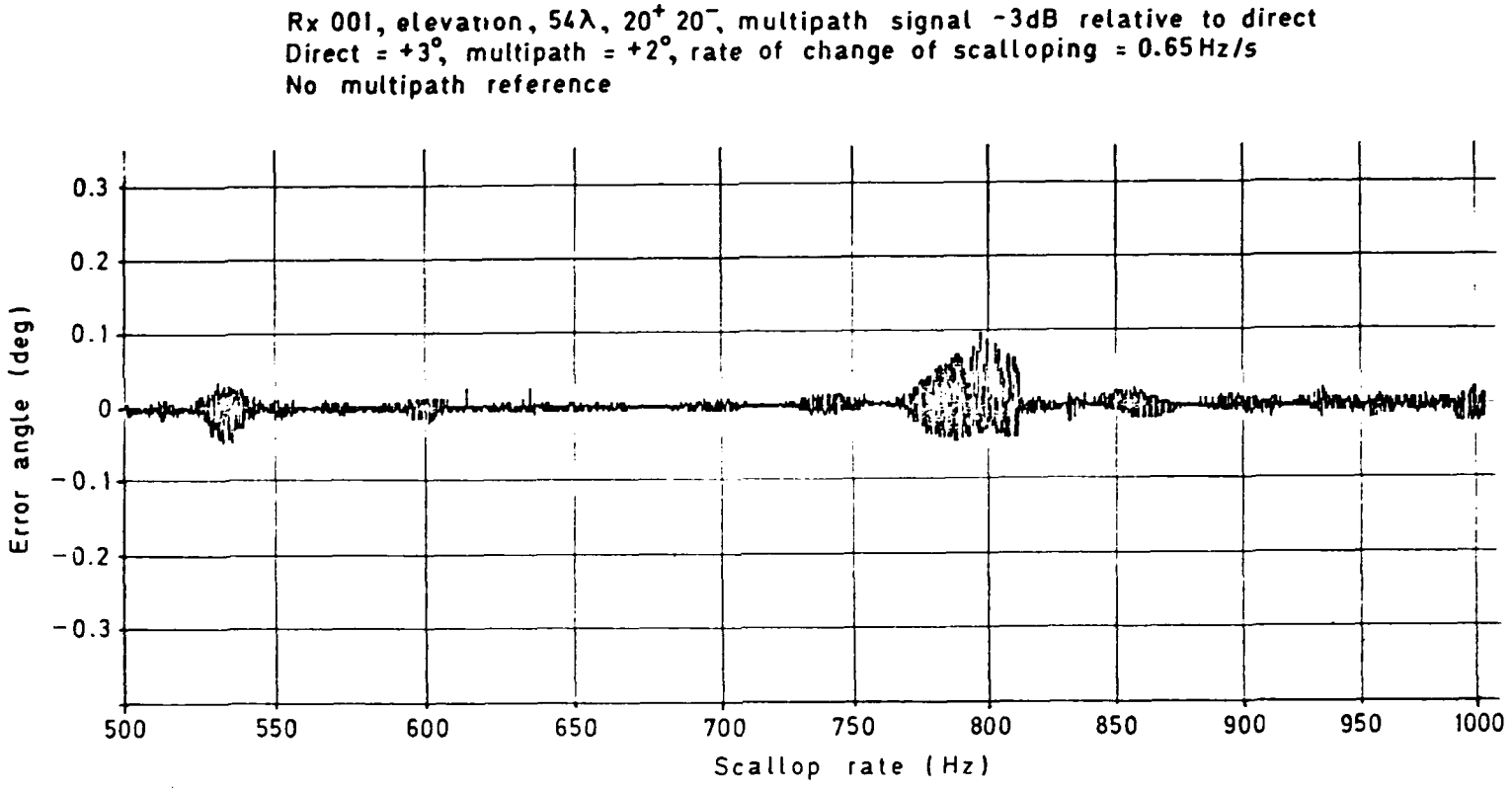

Fig 6.28b Elevation error as a function of scalloping rate — 54λ, block scan (20^{+-}), no multipath reference

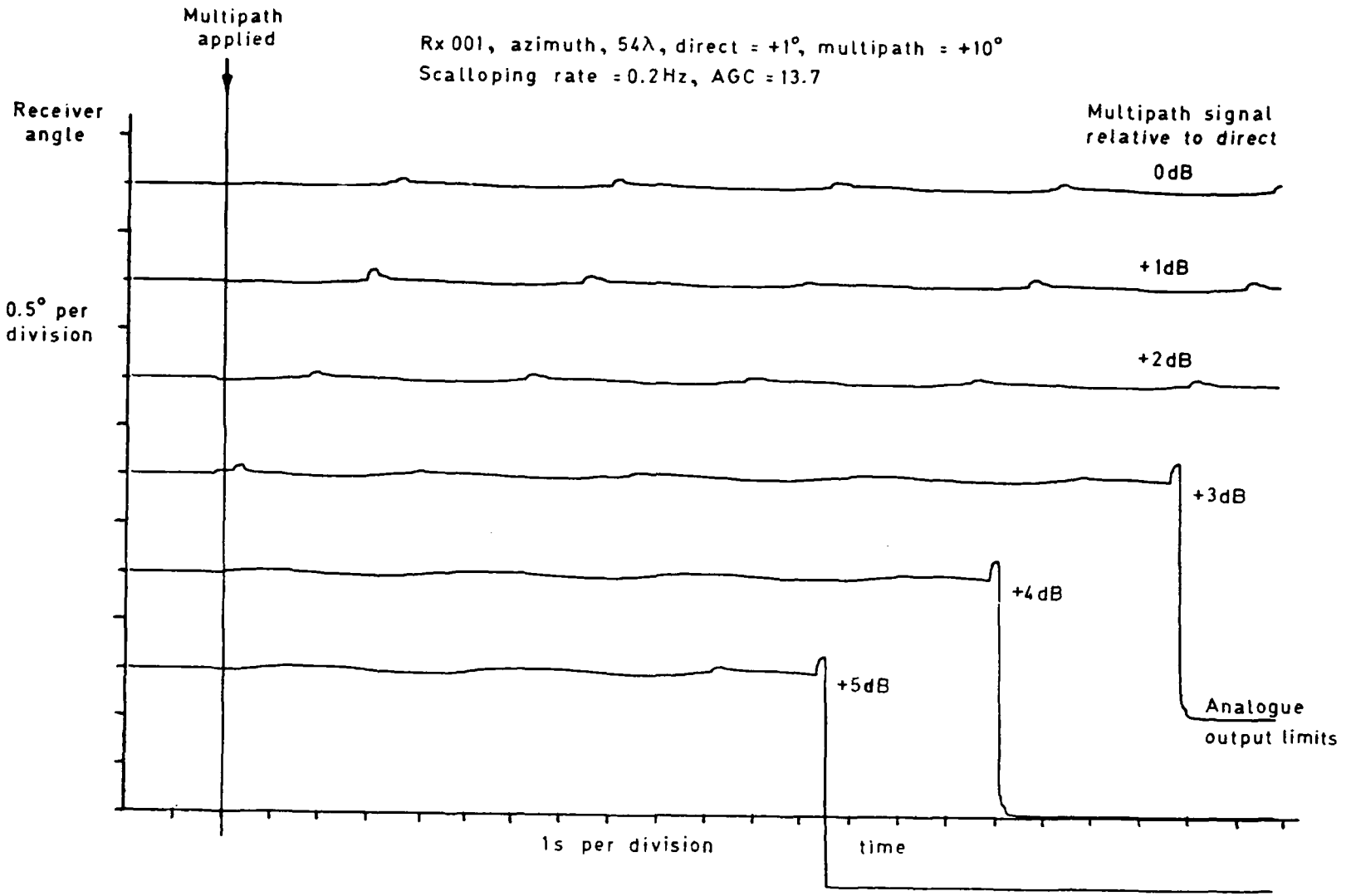

Fig 6.29 Multipath acquisition as a function of relative signal level — low scallop rate

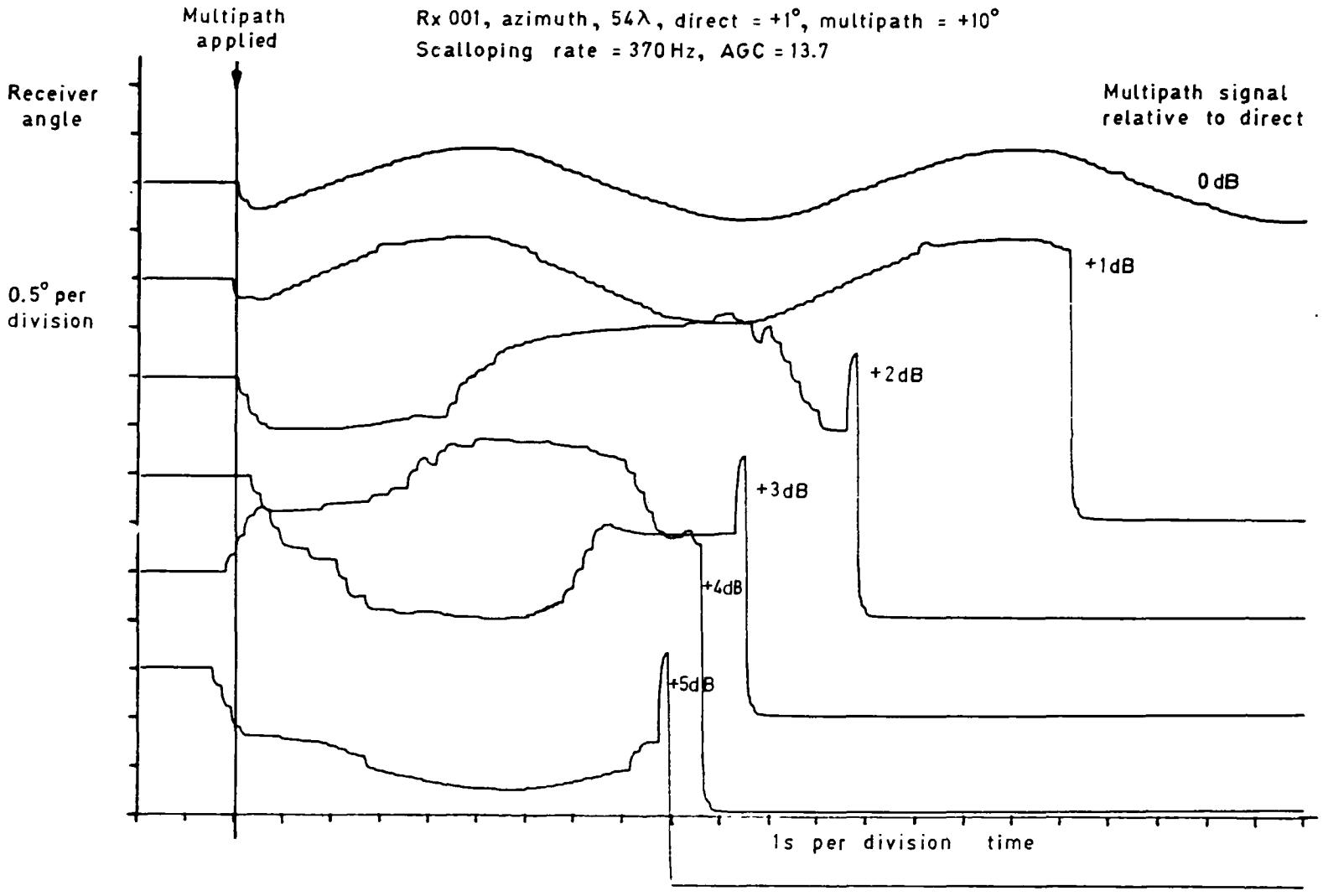

Fig 6.30 Multipath acquisition as a function of relative signal level — high scallop rate

Fig 6.30

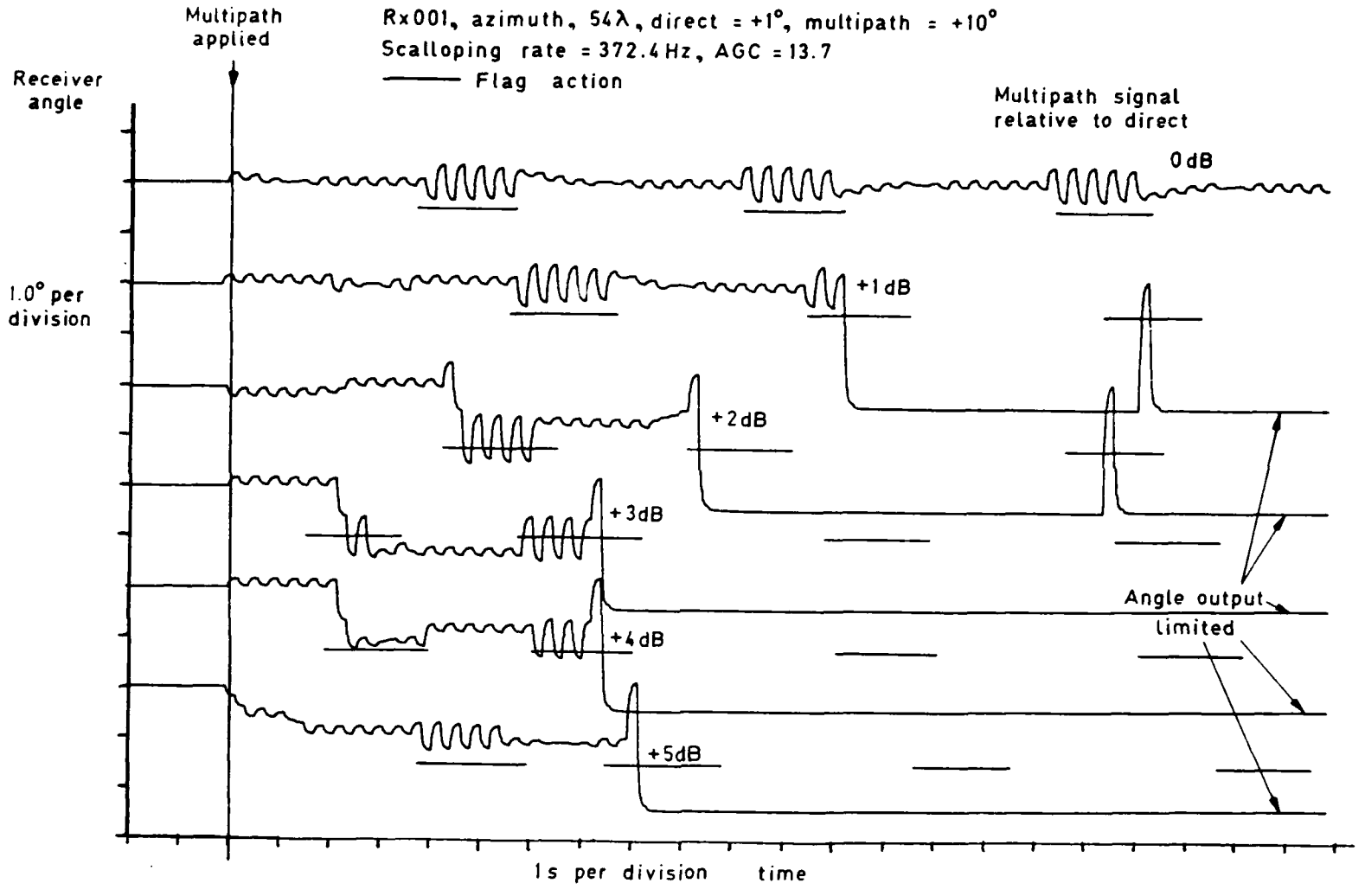

Fig 6.31

Fig 6.31 Multipath acquisition as a function of relative signal level — high scallop rate

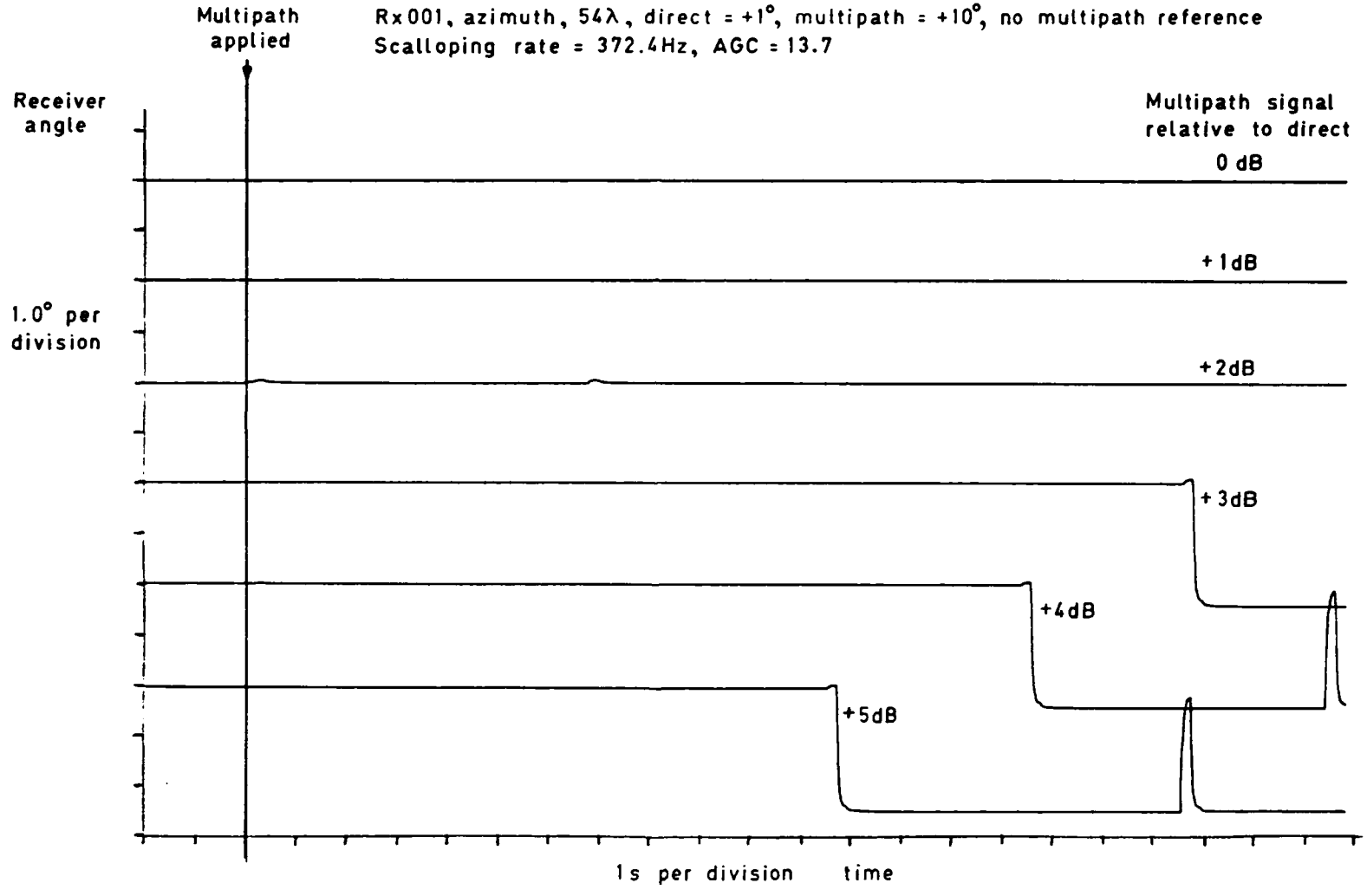

Fig 6.32 Multipath acquisition as a function of relative signal level — high scallop rate, no multipath reference

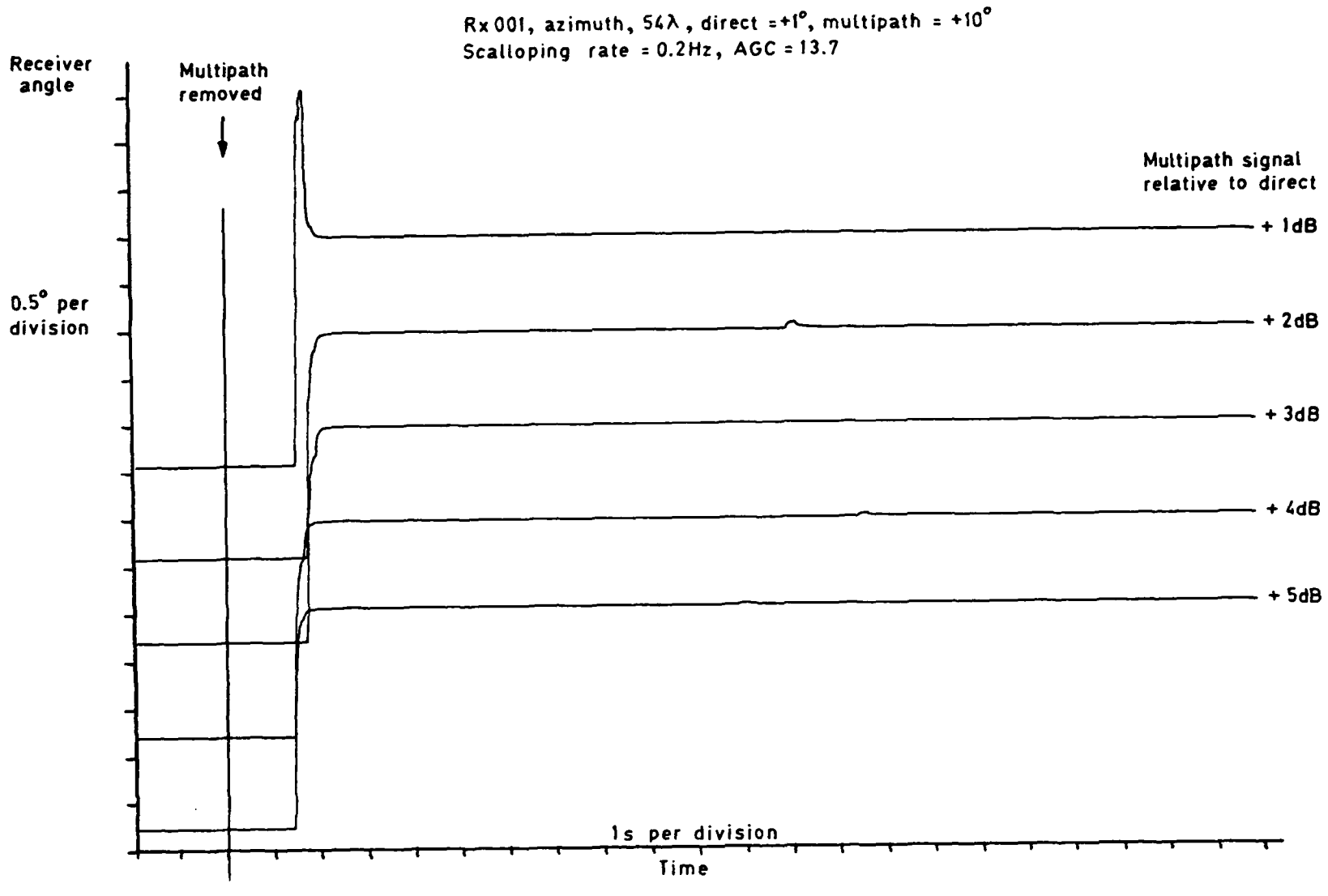

Fig 6.33 Signal reacquisition as a function of relative multipath level

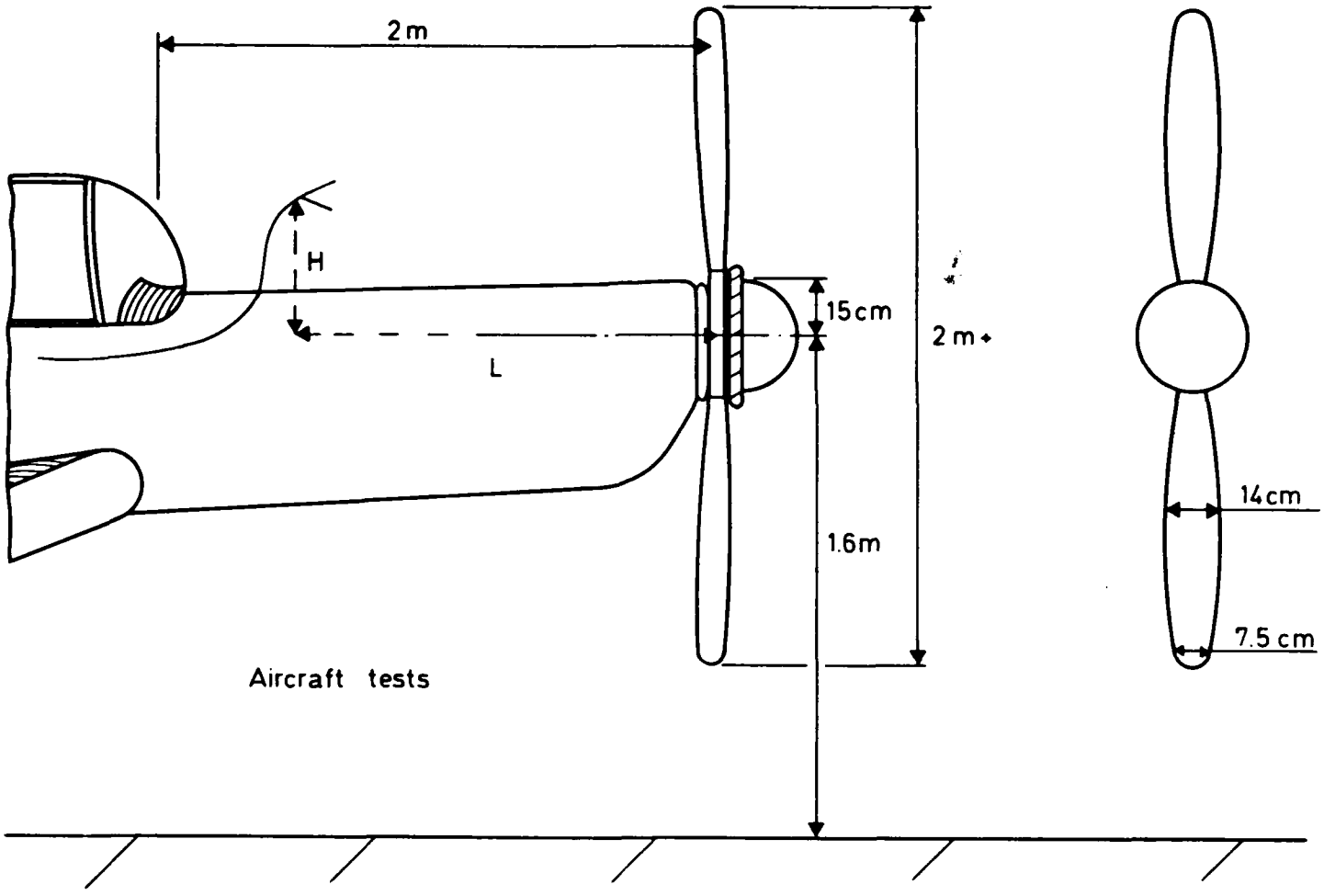

Fig 6.34 Geometry of aircraft propeller tests

Fig 6.34

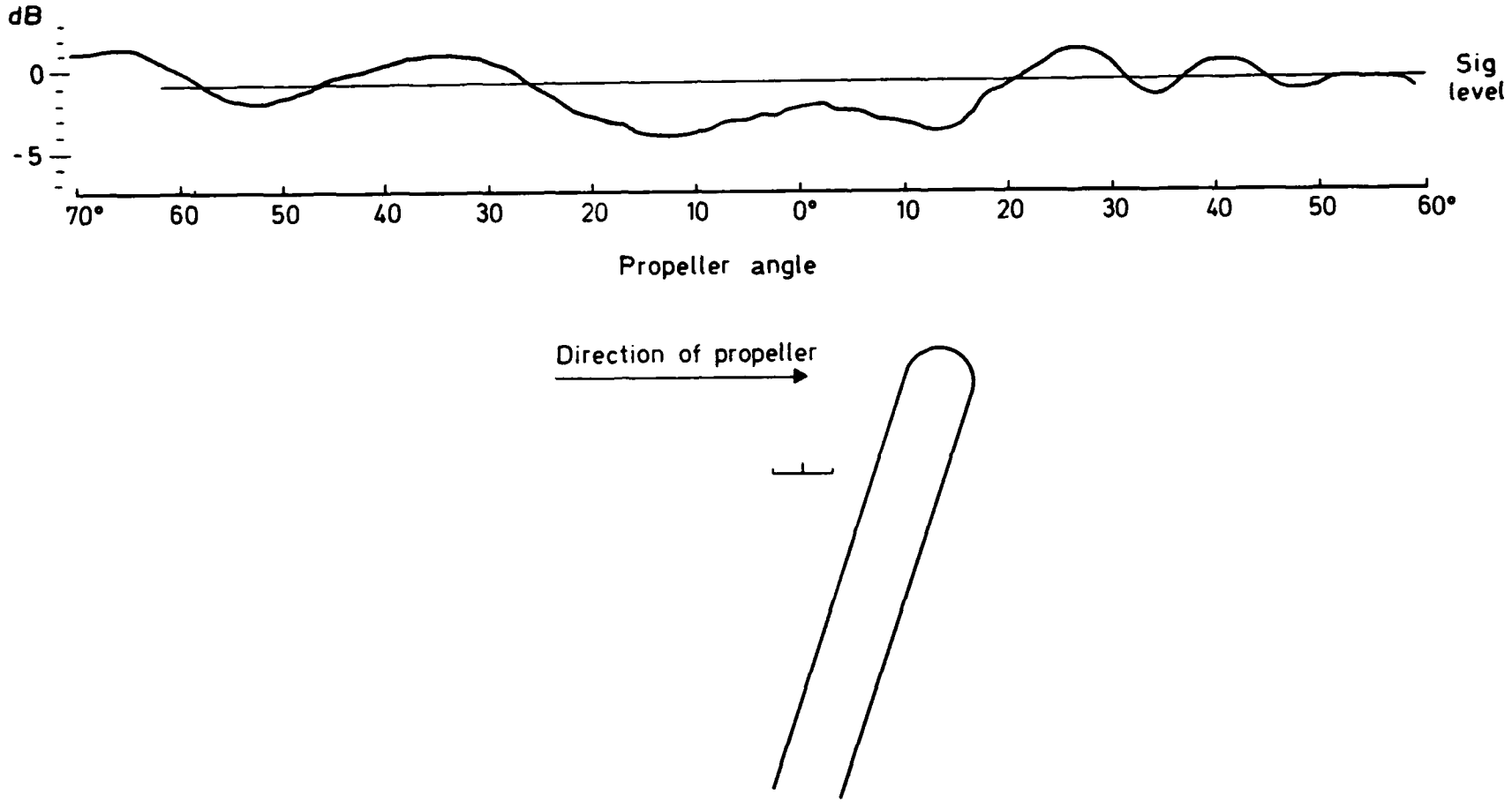

Fig 6.35 Aircraft propeller effects – monopole antenna, L = 28.3λ, H = 10λ

TR 79052

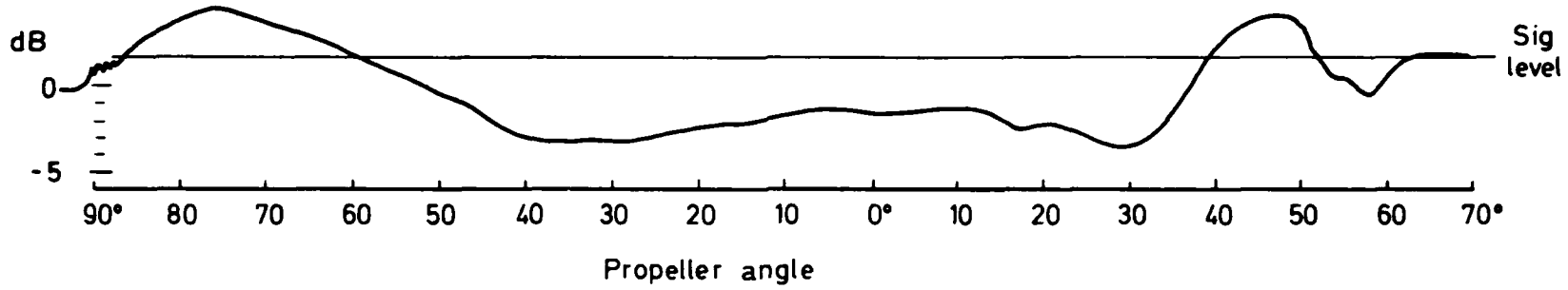

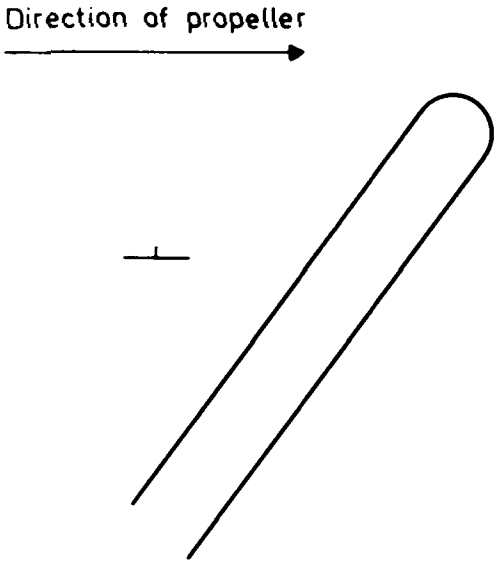

Fig 6.36 Aircraft propeller effects — monopole antenna, L = 28.3λ, H = 5λ

Fig 6.36

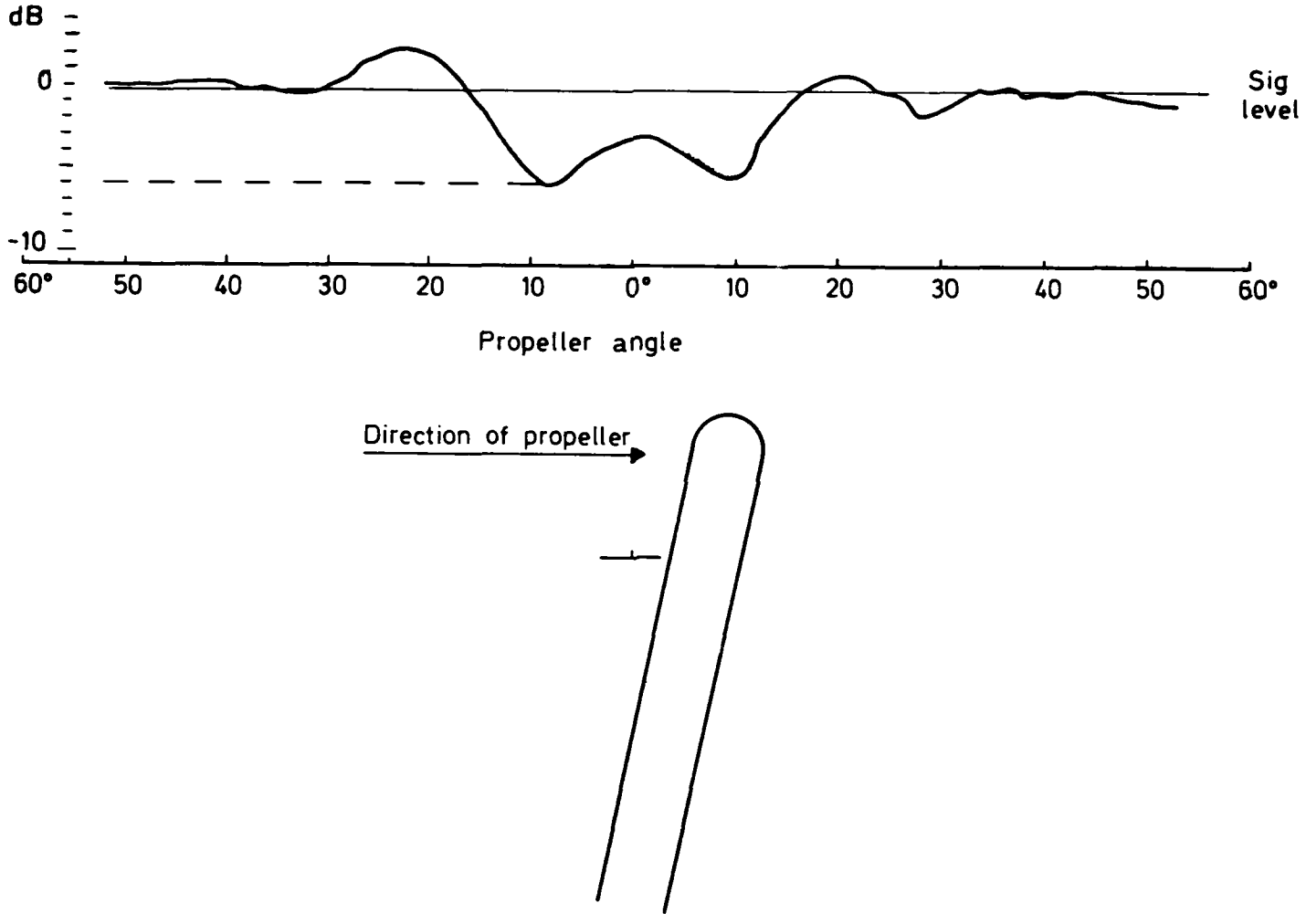

Fig 6.37 Aircraft propeller effects — monopole antenna, L = 16.6λ, H = 10λ

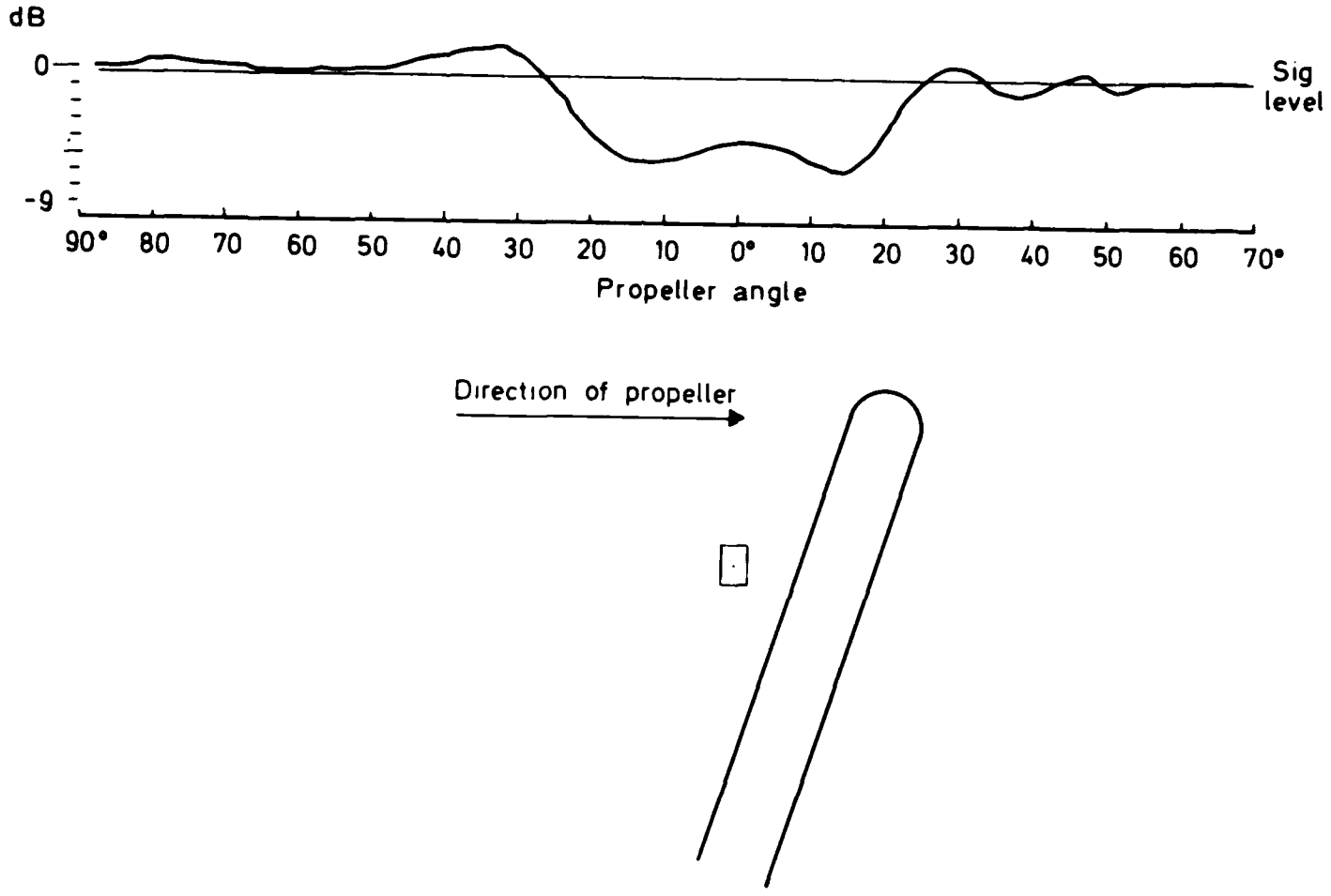

Fig 6.38 Aircraft propeller effects – small horn antenna, L = 16.6λ, H = 10λ

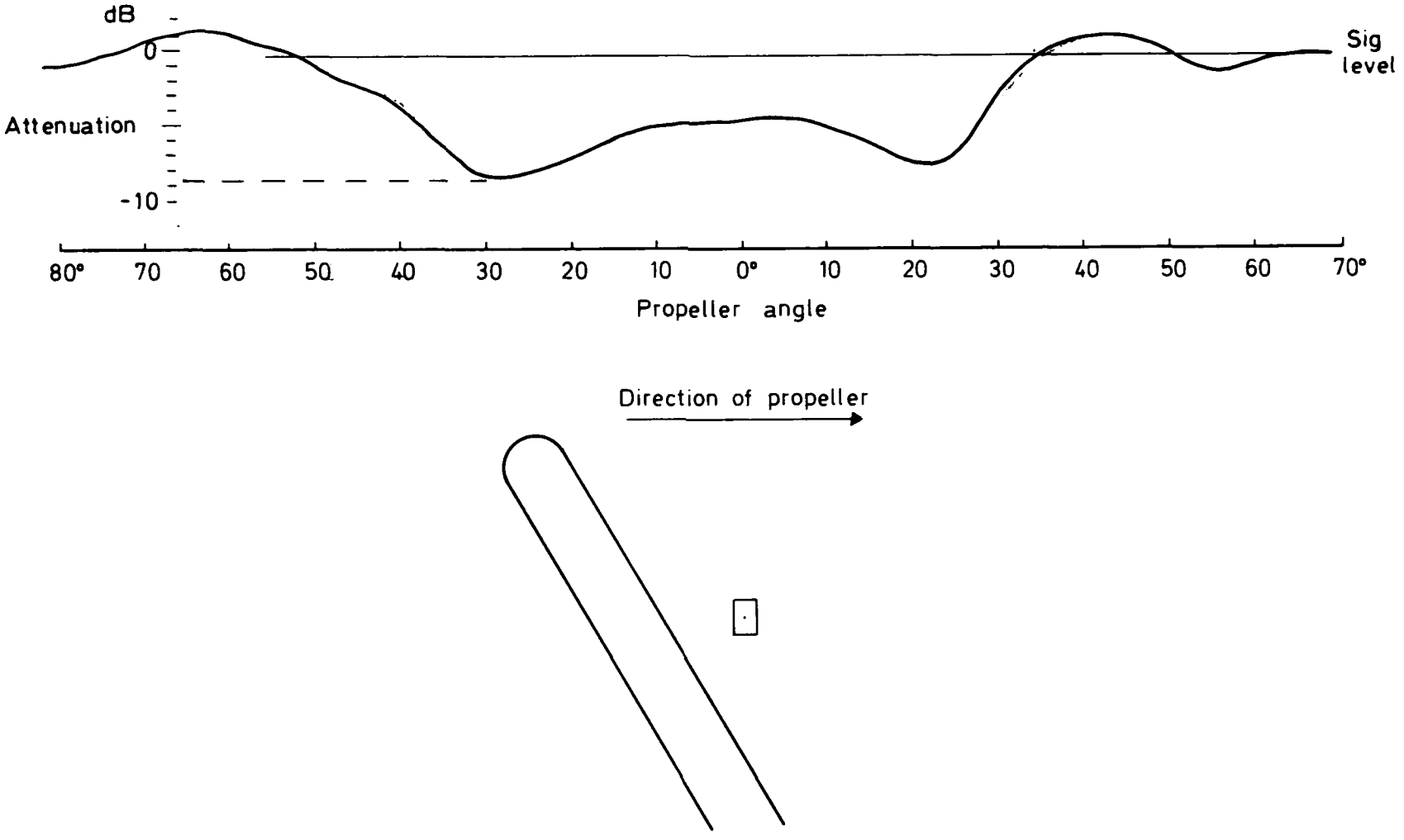

Fig 6.39

Fig 6.39 Aircraft propeller effects — small horn antenna, L = 16.6λ, H = 5λ

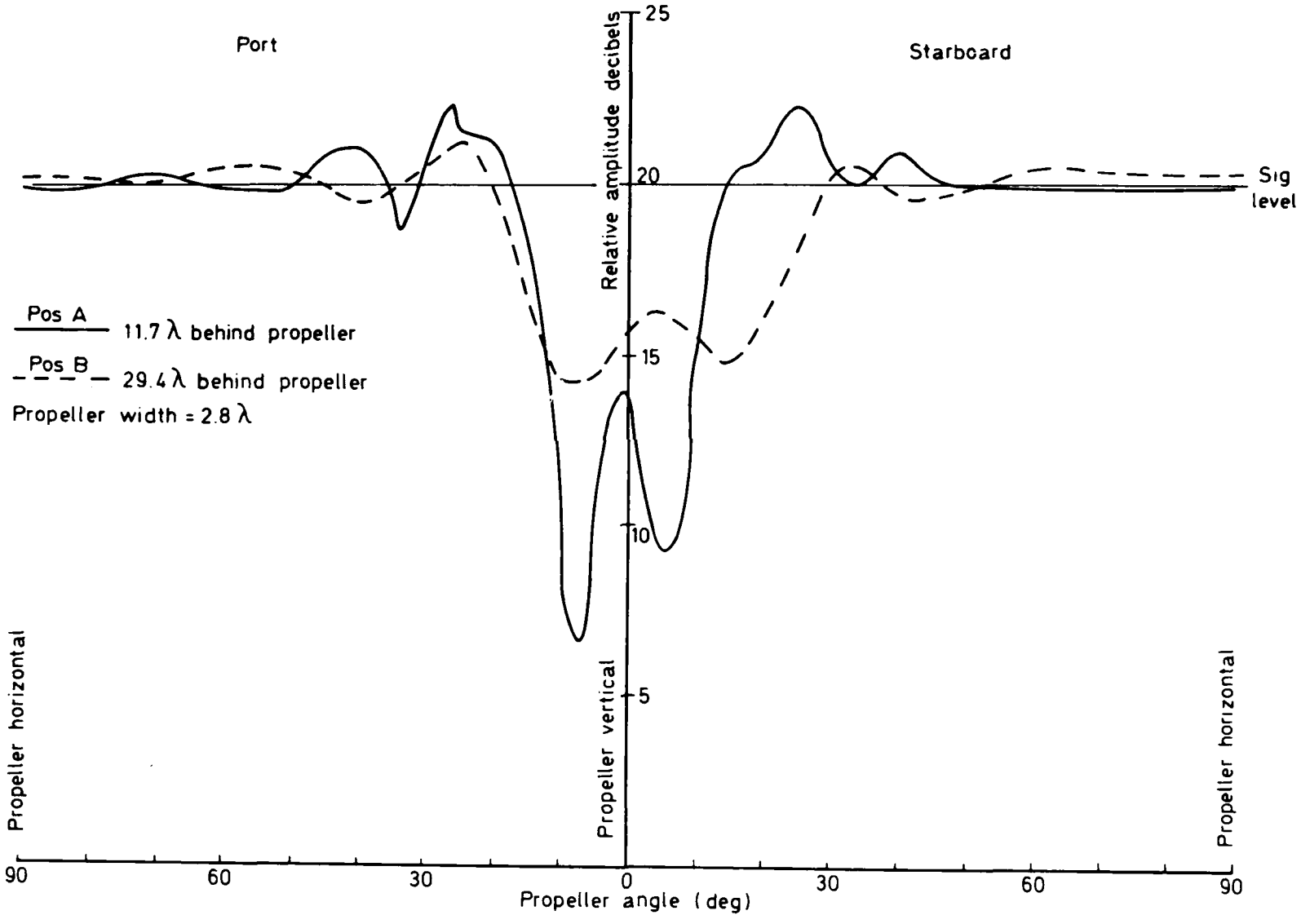

Fig 6.40 Aircraft propeller effects – FAA data

Fig 6.40

Fig 6.41

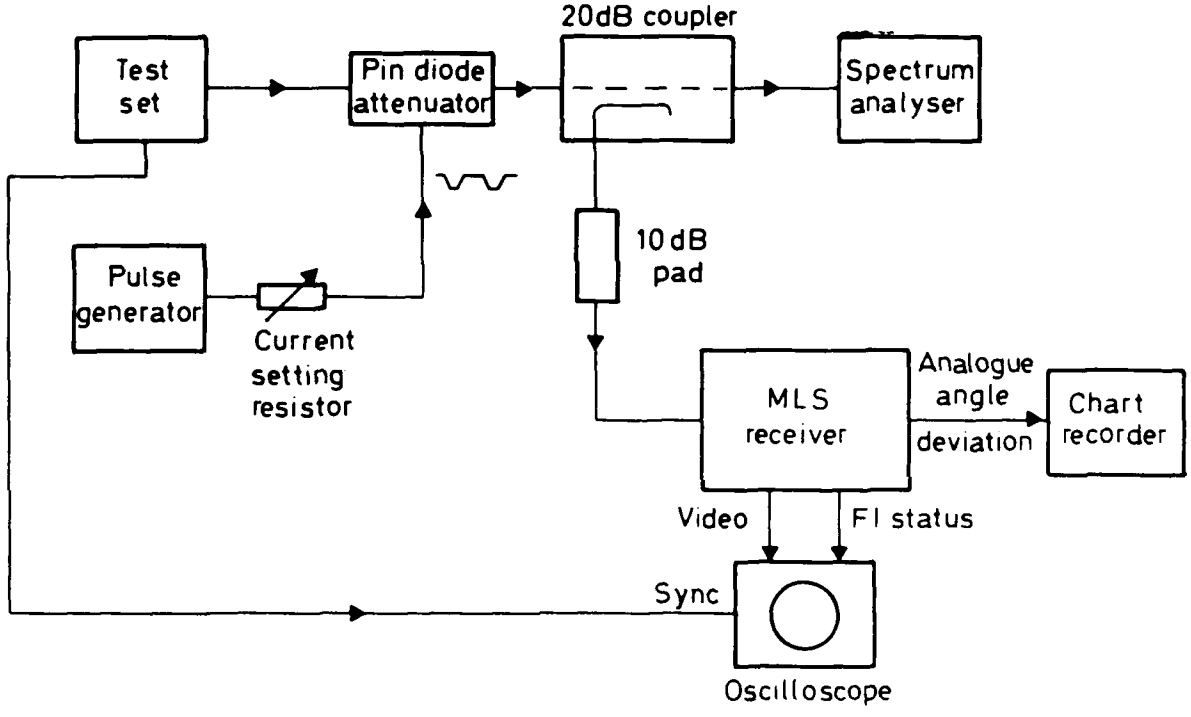

TR 79052

Fig 6.41 Experimental arrangement for propeller modulation simulation

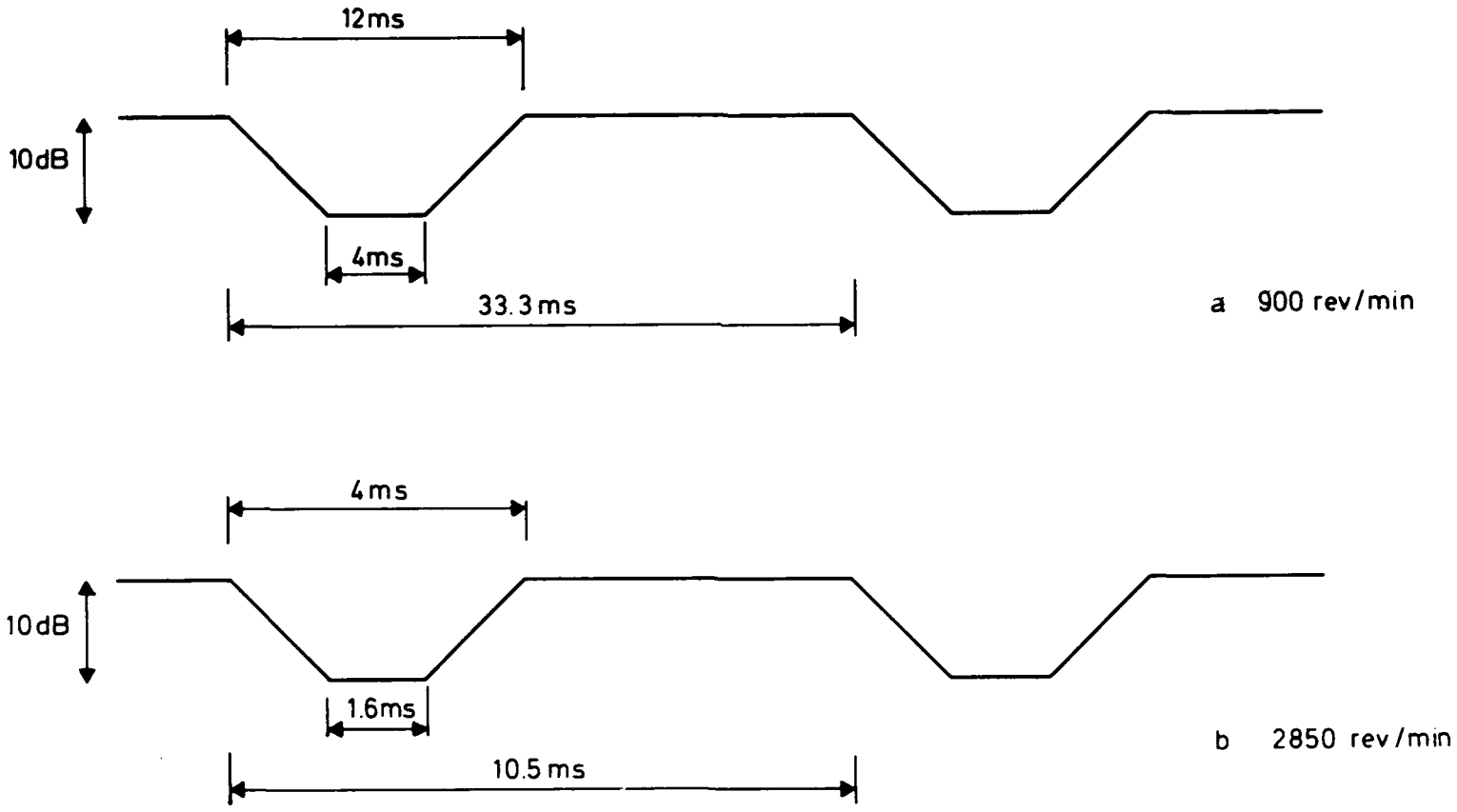

Fig 6.42 Propeller modulation waveforms – simulated two blade propeller

Fig 6.42

Fig 6.43

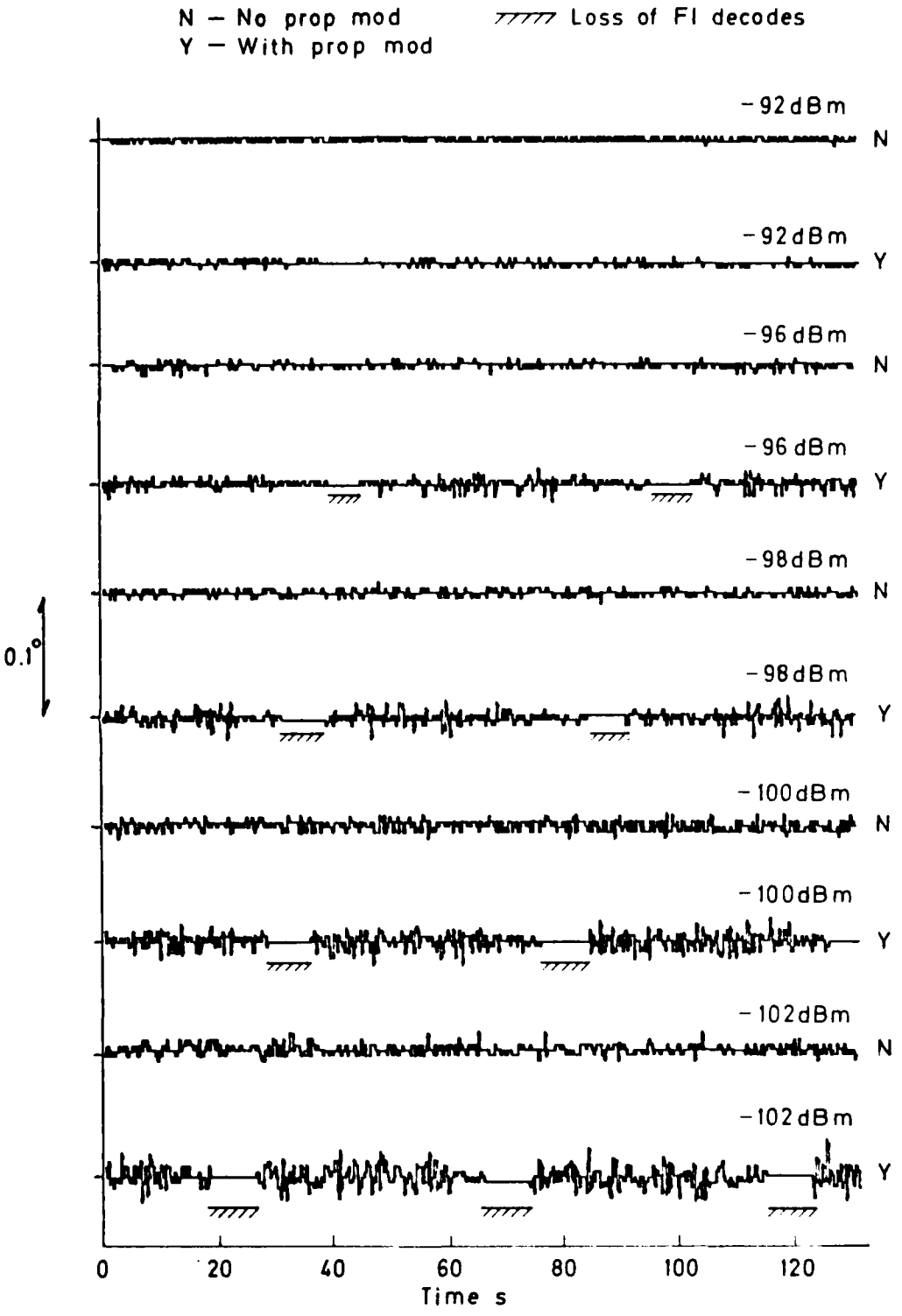

TR 79062

Fig 6.43 Typical effects of propeller modulation with max attenuation of −10 dB

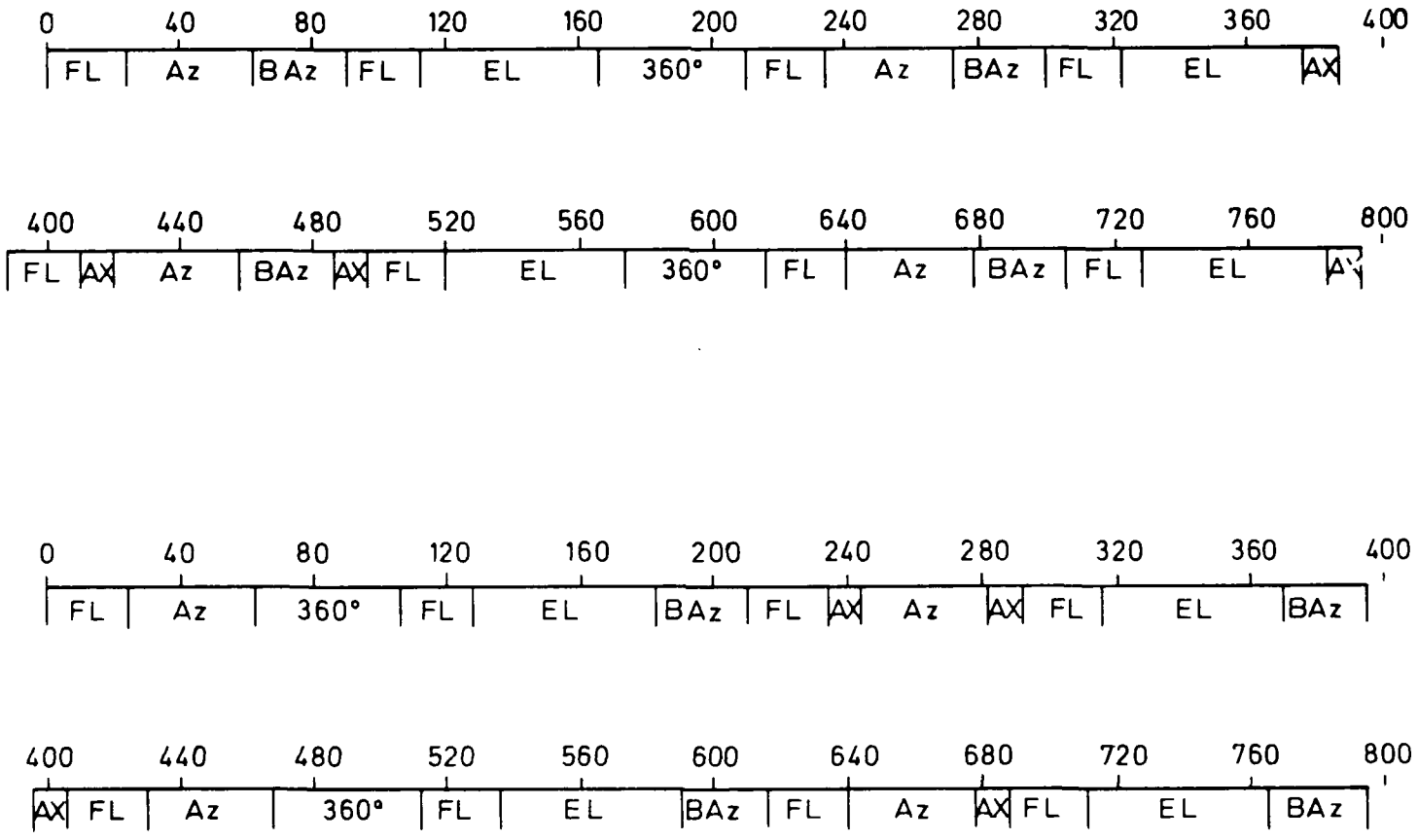

Fig 6.44 Typical DMLS formats with 360° azimuth and jitter

Fig 6.44

A STAN 38 glide path
B Doppler elevation (FDM)
C Doppler azimuth (FDM)
D STAN 37 localizer
E Kinetheodolite
F Doppler back azimuth (FDM)
G Colocated doppler TDM site — Site 3
H Doppler azimuth TDM — Site 1 and 2
J TDM elevation Site 2
K TDM elevation Site 1
L Crash barrier

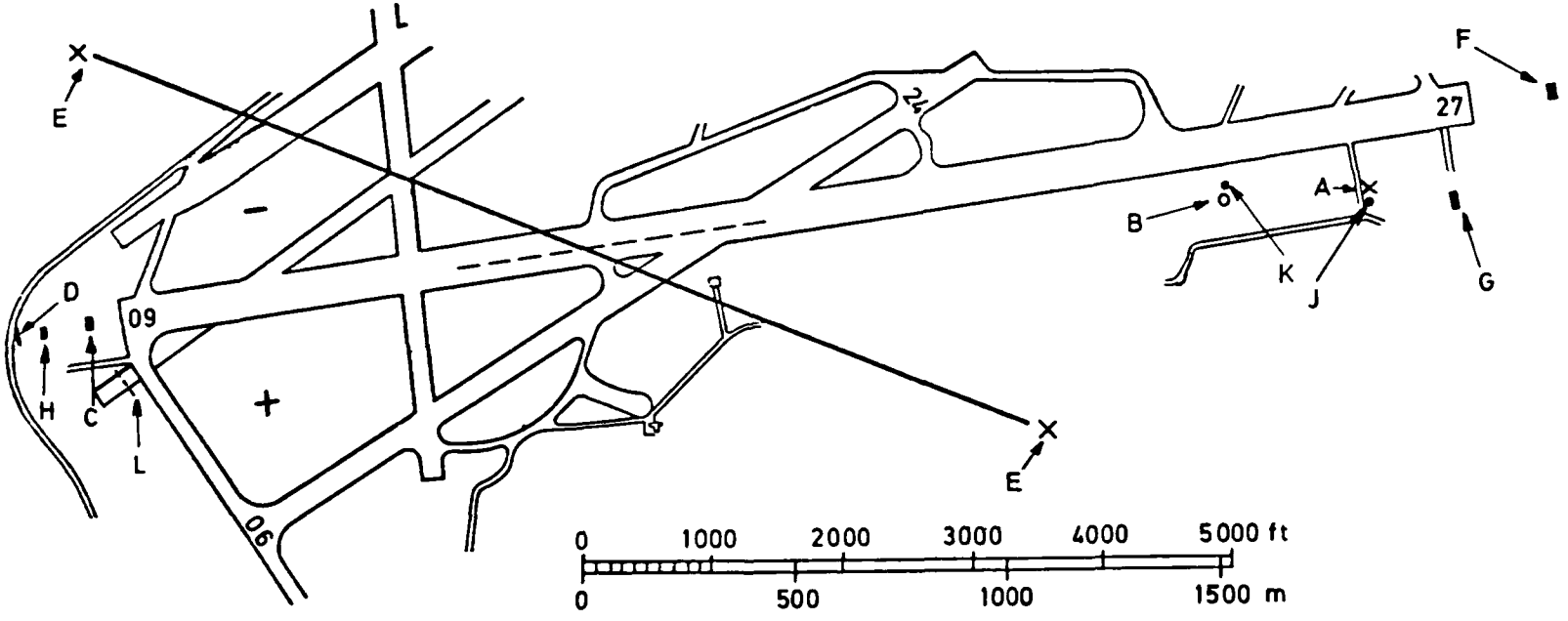

Fig 7.1 TDM equipment positions — Bedford airfield

Fig 7.1

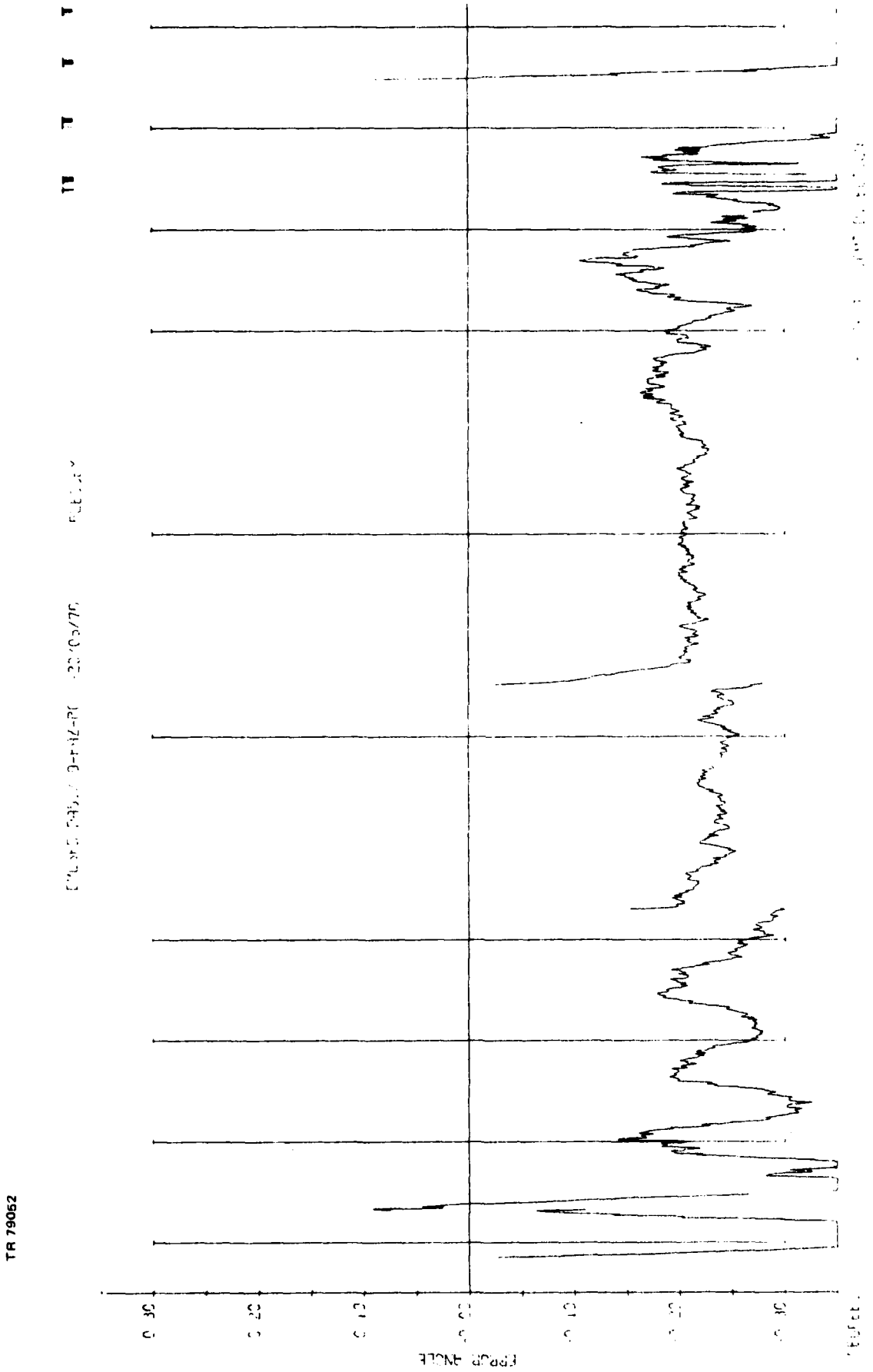

Fig 7.2 Azimuth part orbit at 4.4 n mile and 1900 ft (Site 3)

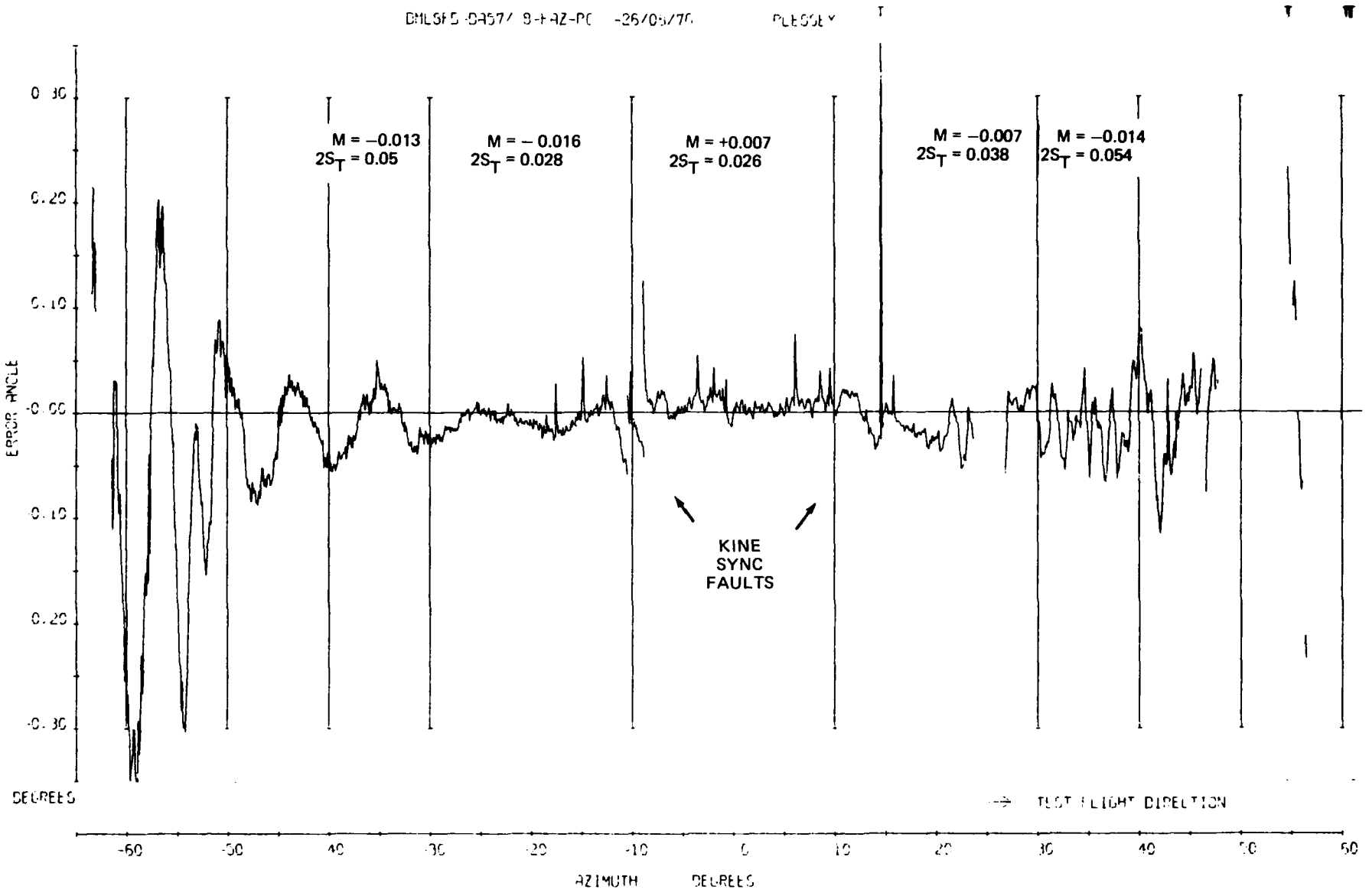

Fig 7.3

Fig 7.3 Azimuth part orbit at 5.8 n mile and 2000 ft (Site 3)

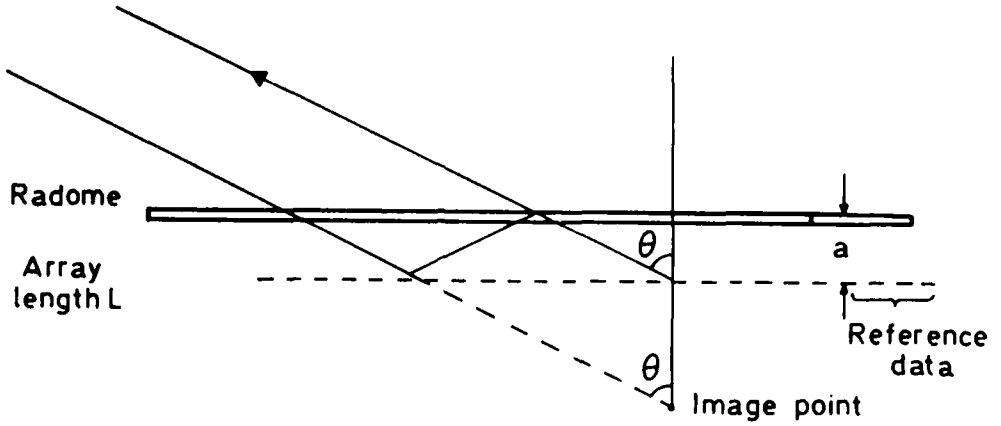

Effective image length $L - 2a \tan\theta$

Delay of reflected signal $\frac{2a\cos\theta 2\pi}{\lambda}$ radians

Relative level of reflected signal is ρ

Received signals

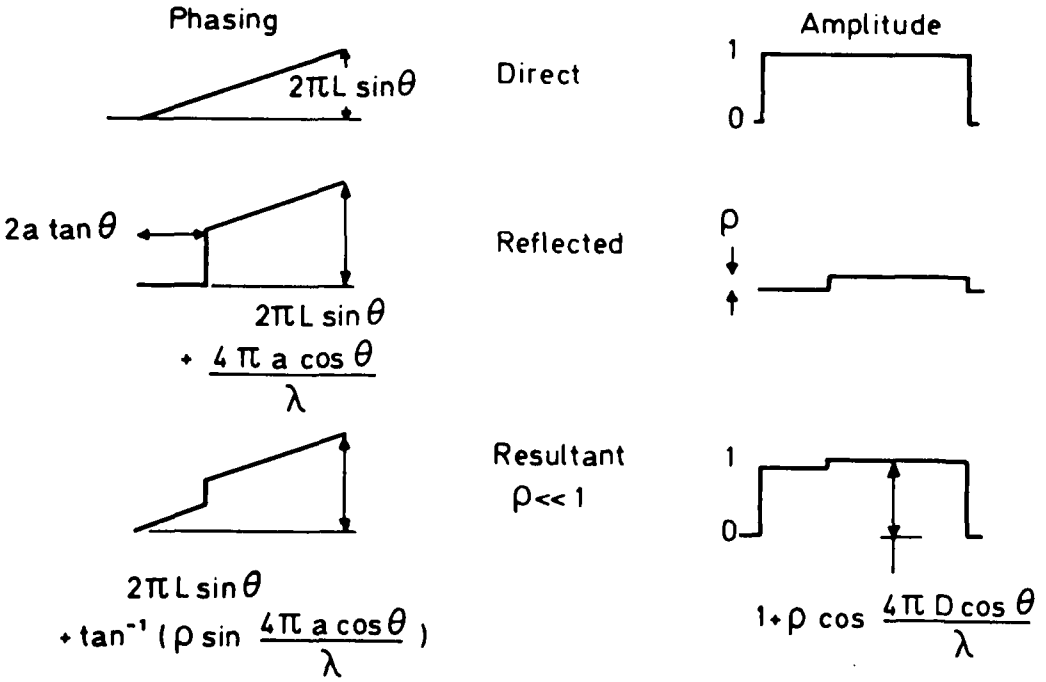

Error maxima occur at $\frac{4\pi a\cos\theta}{\lambda} = (2n+1)\frac{\pi}{2}$

TR 79052

Fig 7.4 Effect of radome mismatch

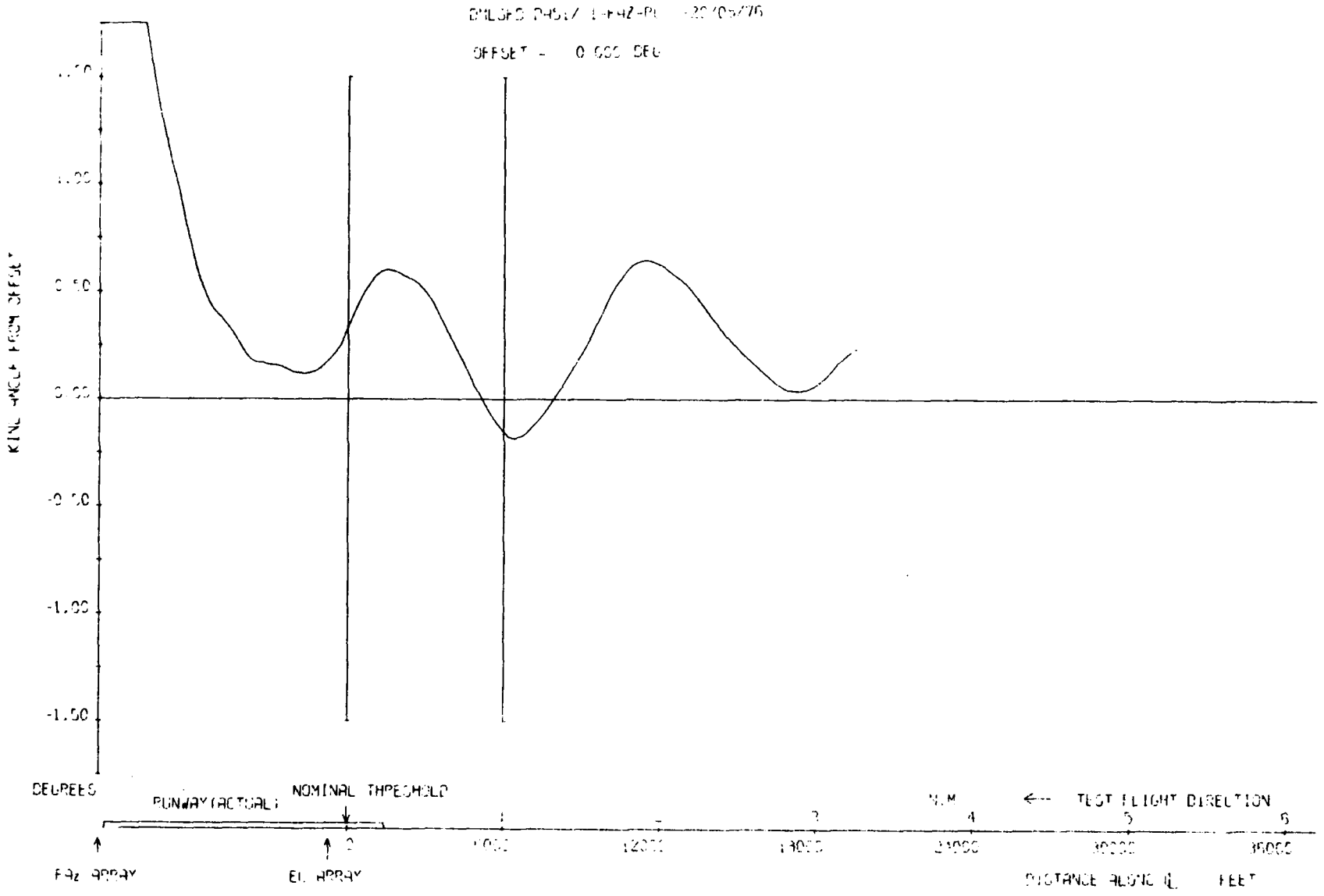

Fig 7.5a Azimuth 3 degree approach to low overshoot

Fig 7.5a

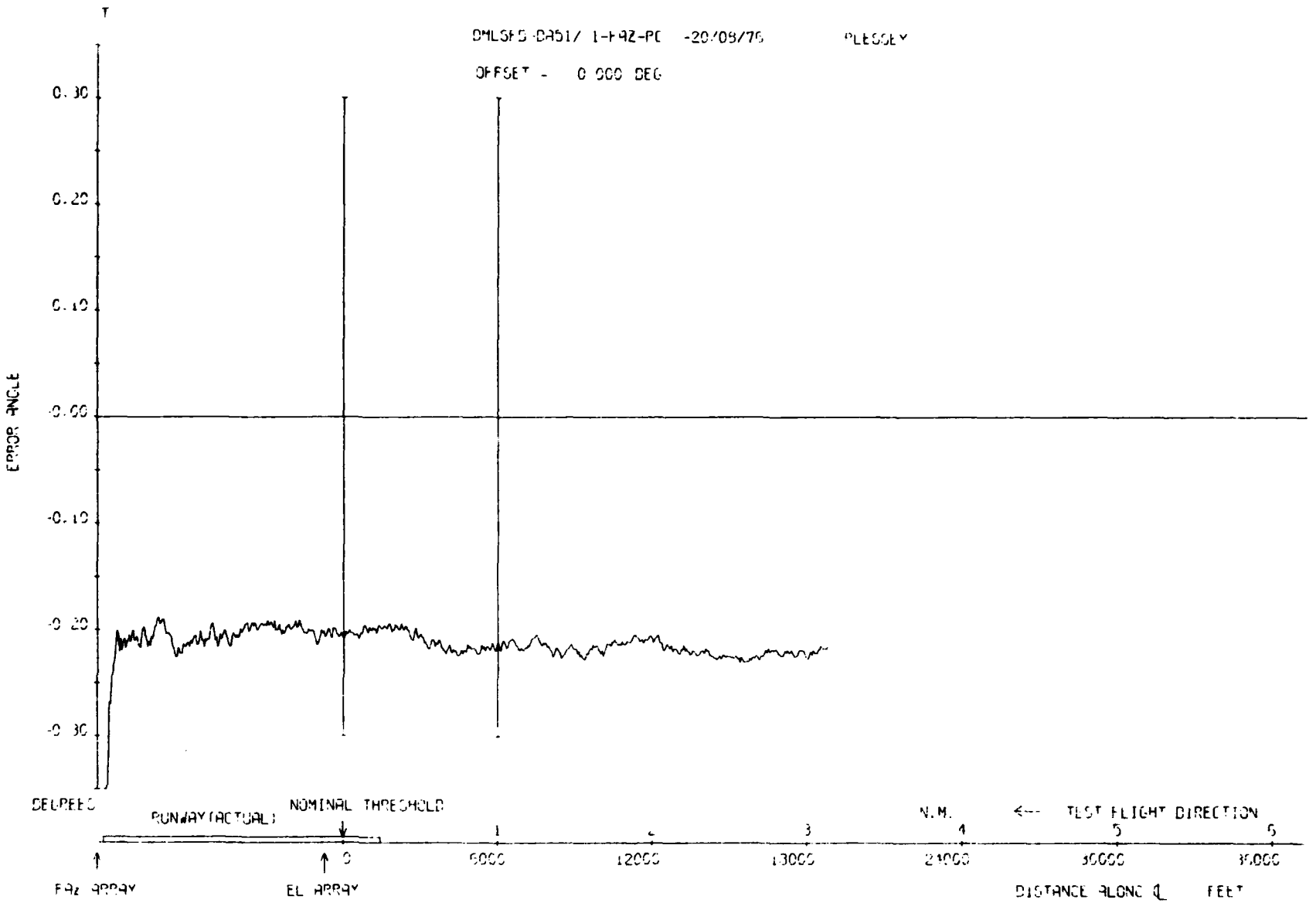

Fig 7.5b Azimuth 3 degree approach to low overshoot

Fig 7.5b

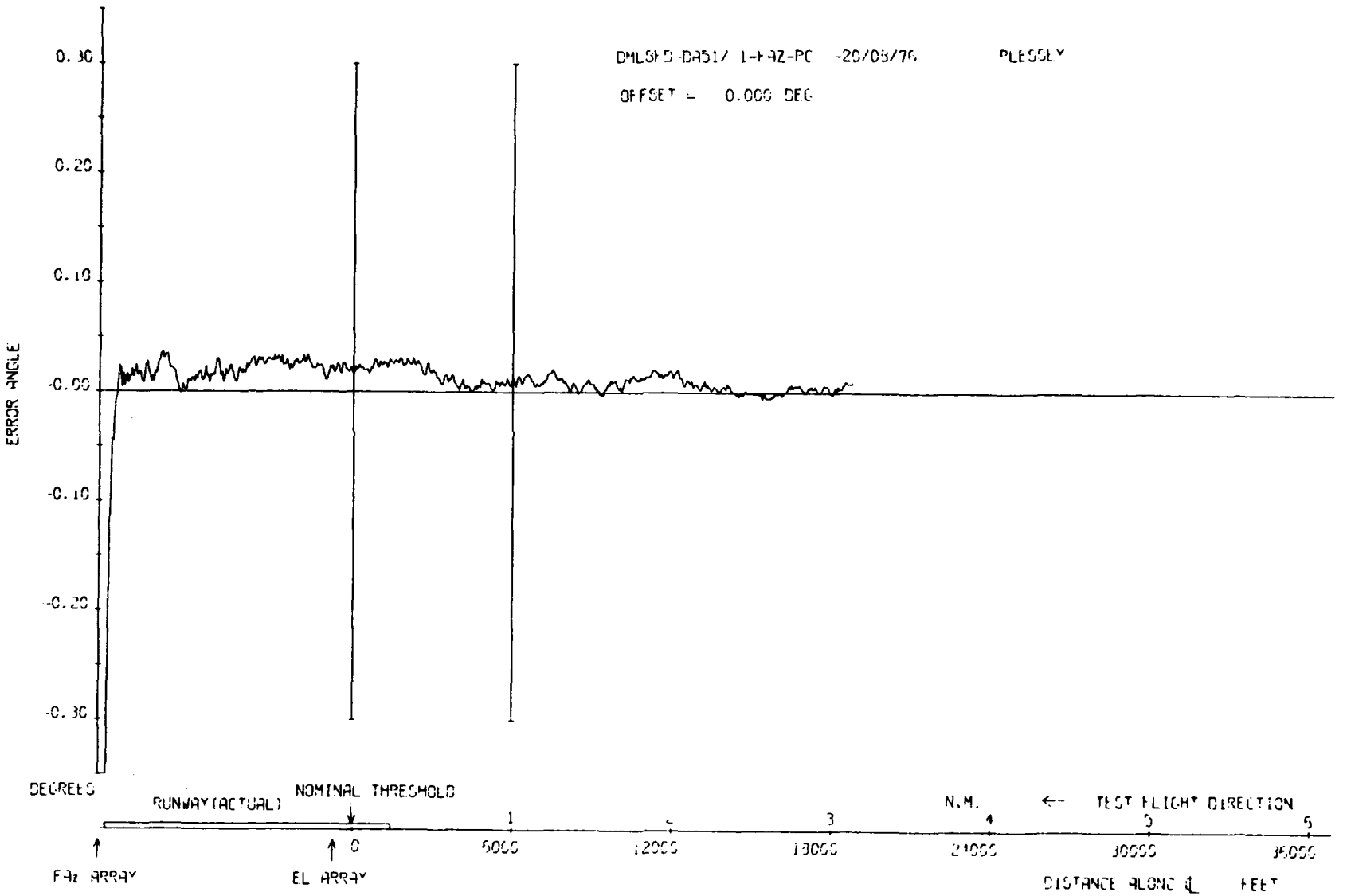

Fig 7.5c Azimuth 3 degree approach to low overshoot (bias removed)

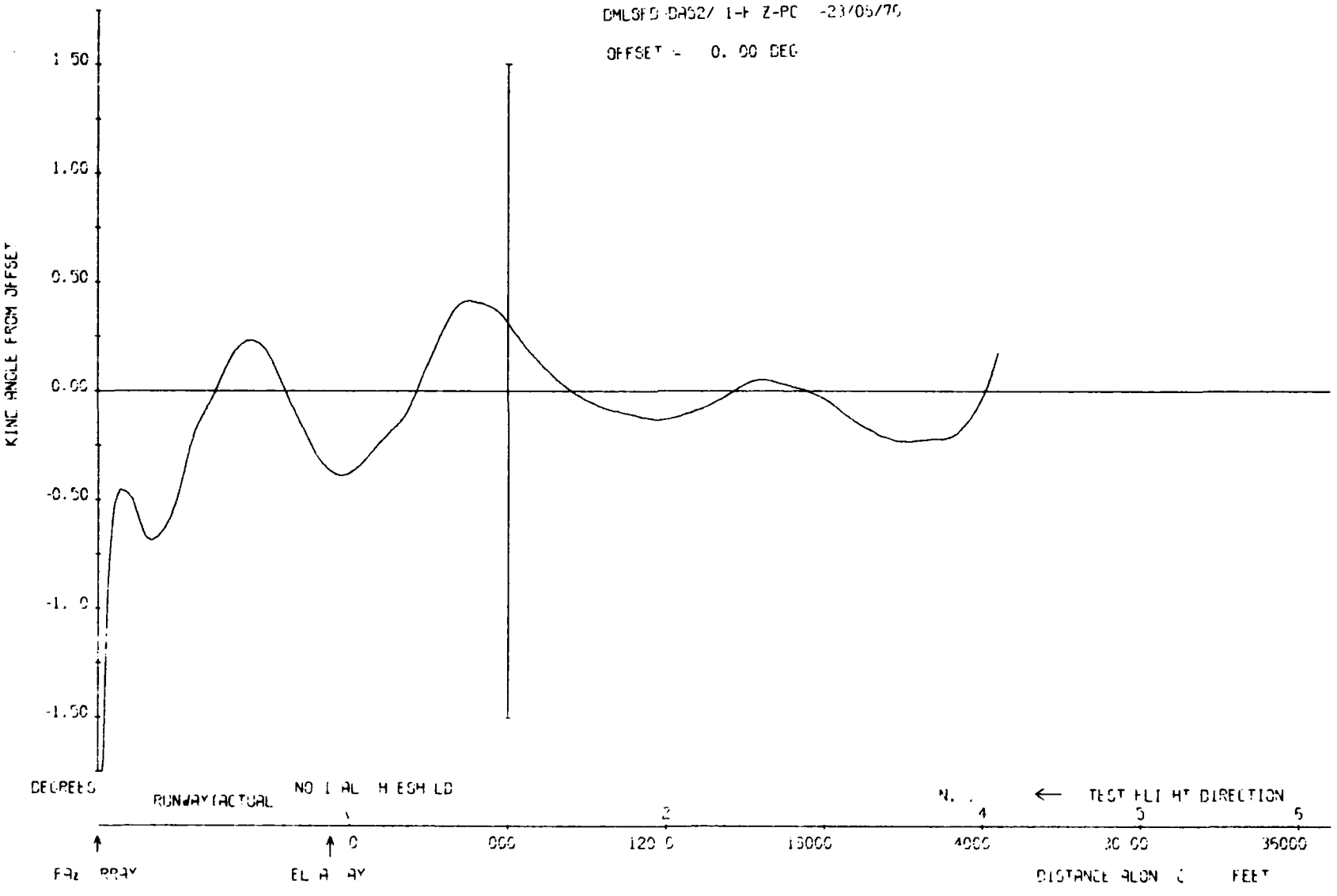

Fig 7.6a Azimuth 3 degree approach to low overshoot

Fig 7.6a

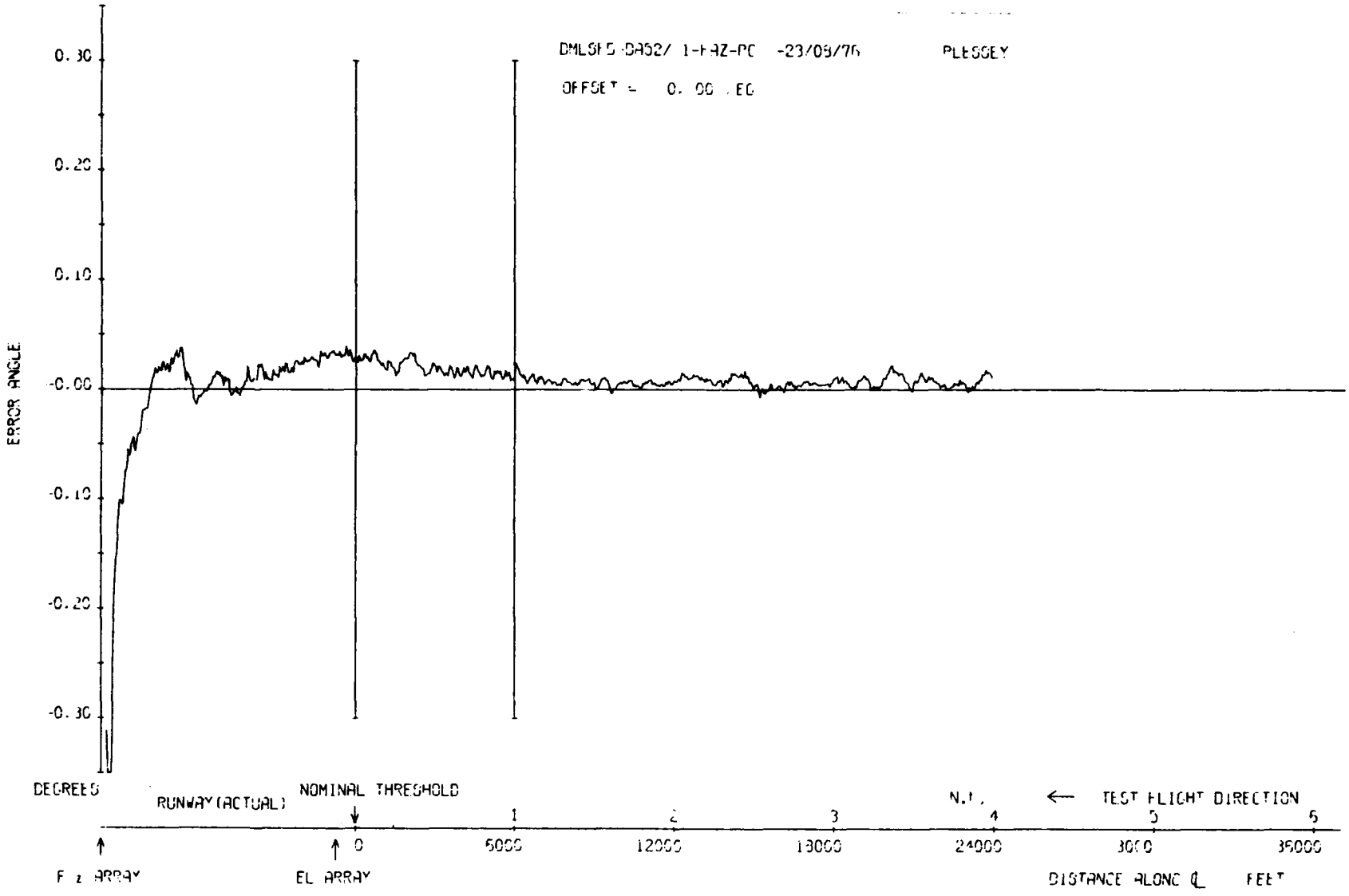

Fig 7.6b

Fig 7.6b Azimuth 3 degree approach to low overshoot

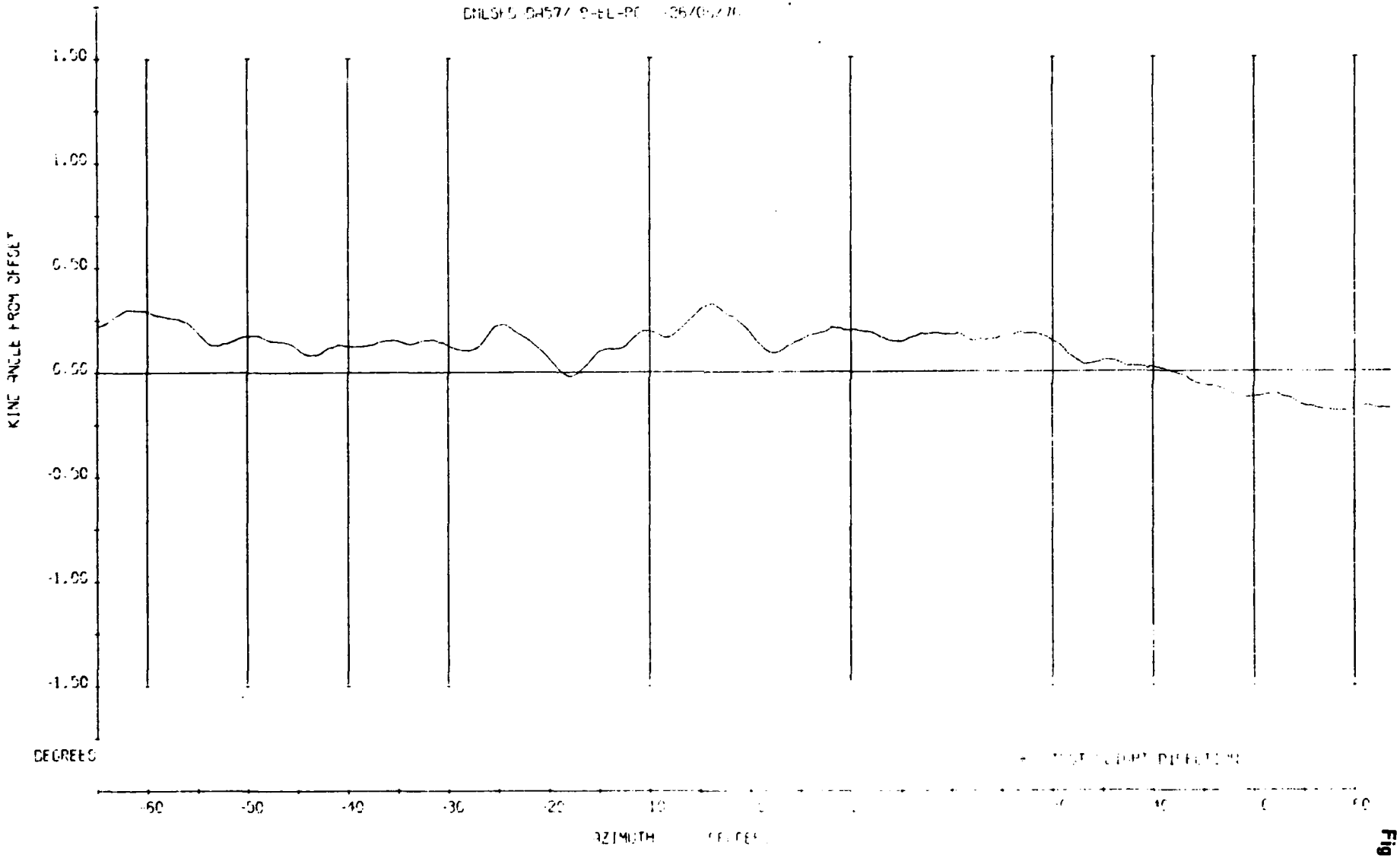

Fig 7.7a

Fig 7.7a Elevation orbit at 5.8 n mile and 2000 ft

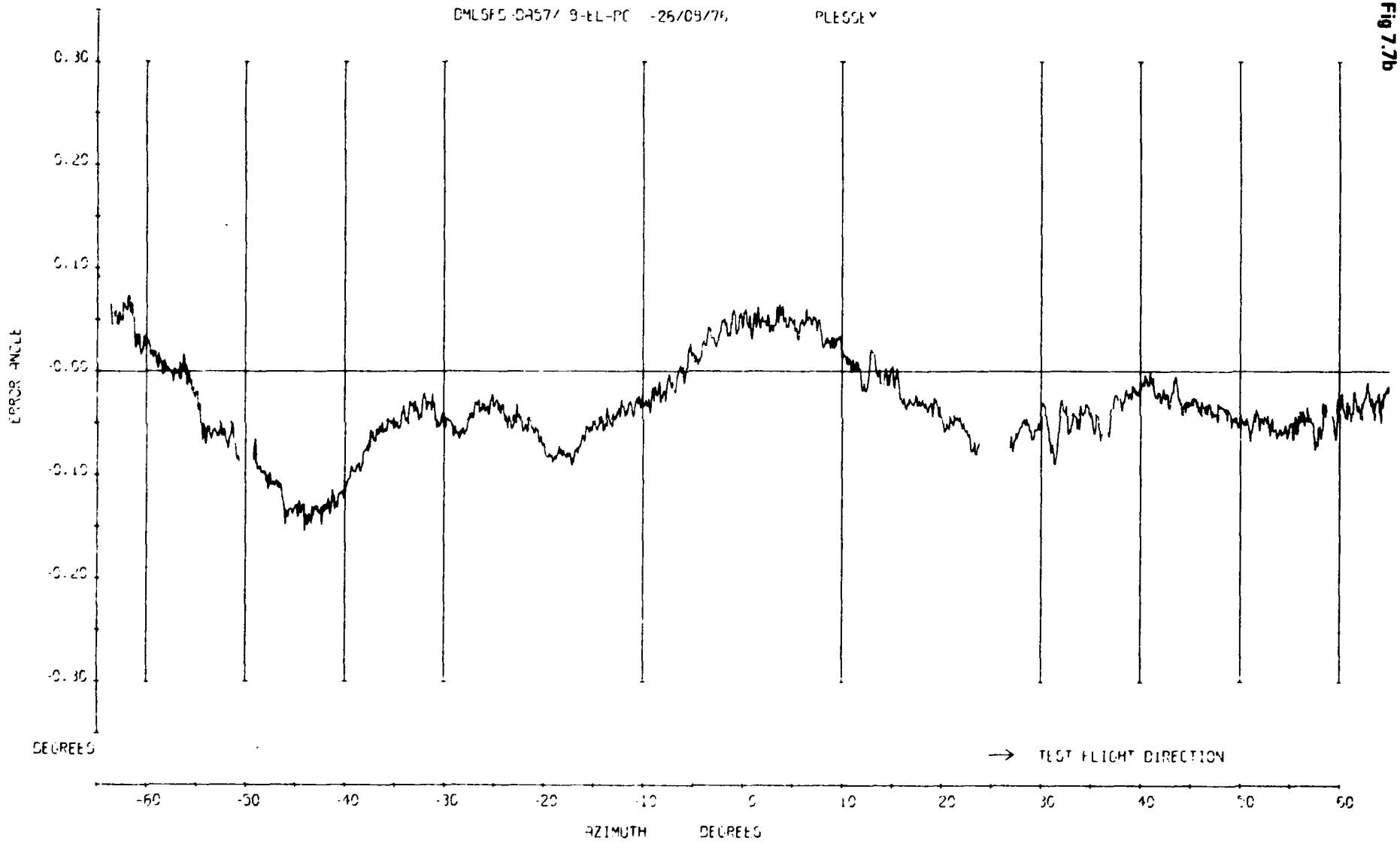

Fig 7.7b

Fig 7.7b Elevation orbit at 5.8 n mile and 2000 ft

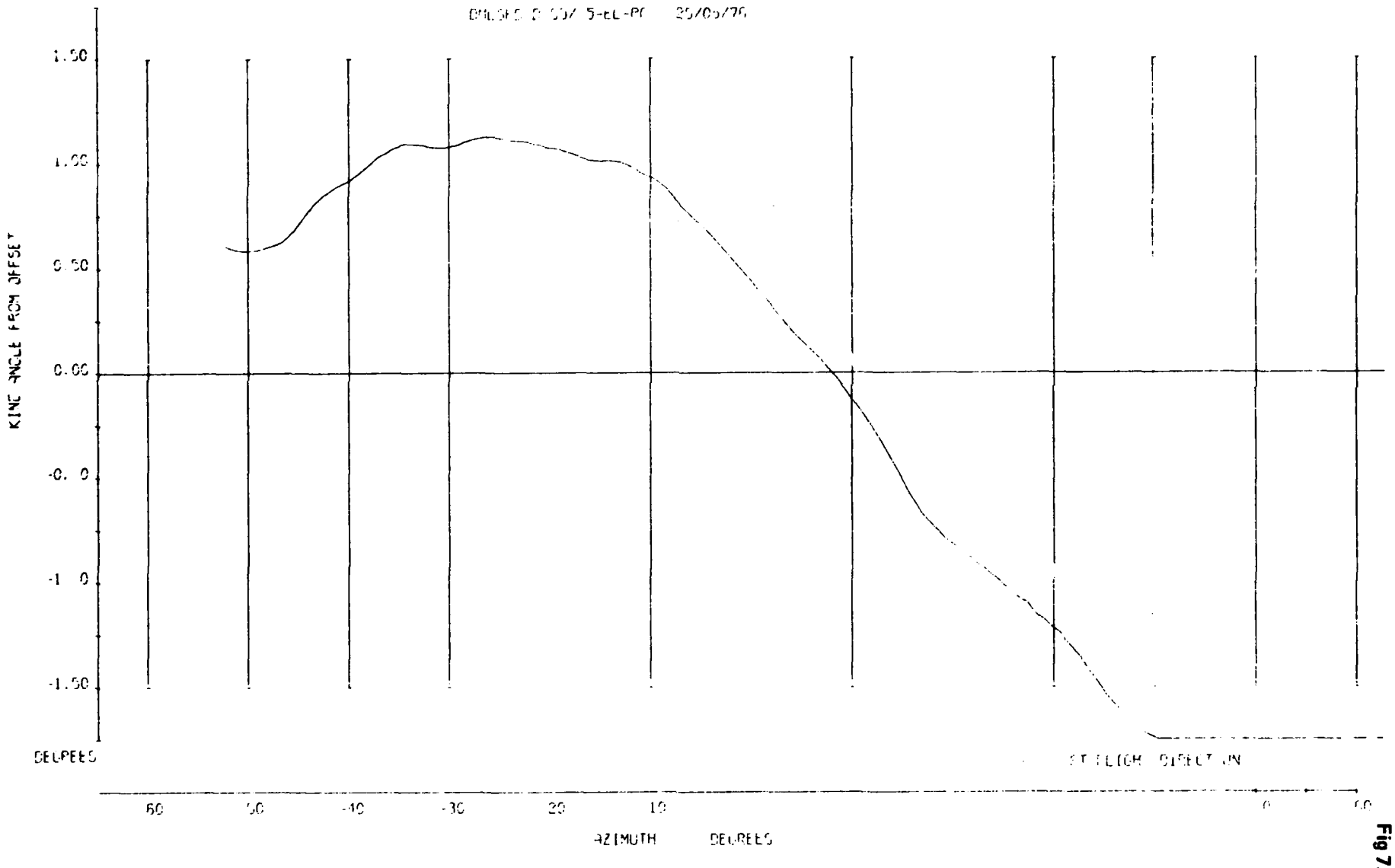

Fig 7.8a

Fig 7.8a Elevation orbit at 3.4 n mile and 3900 ft

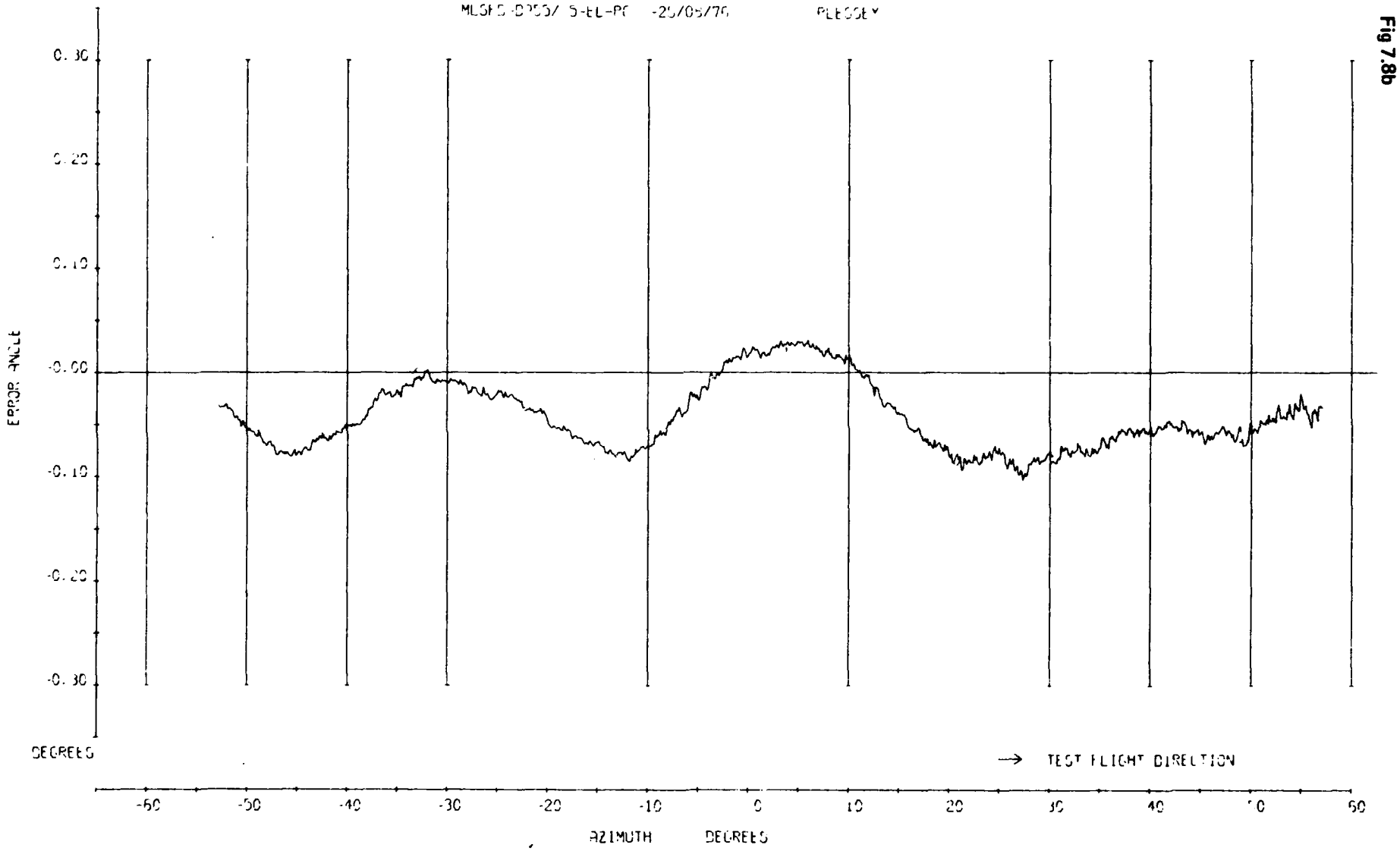

Fig 7.8b

Fig 7.8b Elevation orbit at 3.4 n mile and 3900 ft

Elevation array plan view

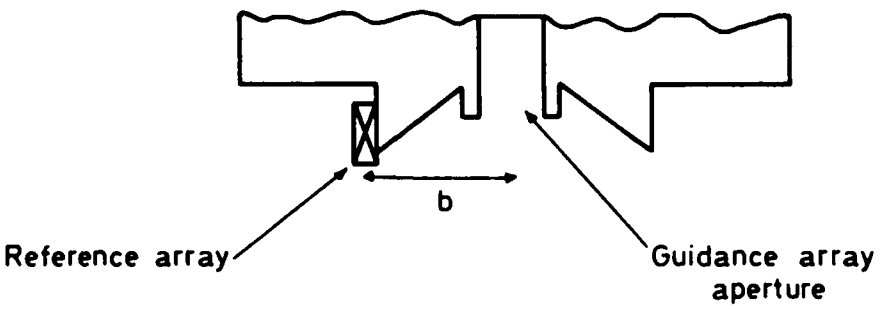

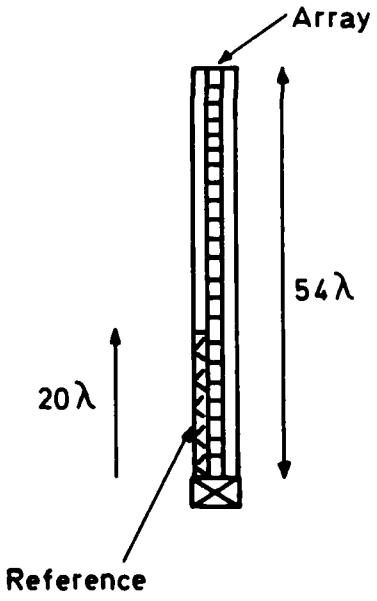

To a first approximation error peaks occur at

$$\frac{2\pi b}{\lambda} + \frac{2\pi b}{\lambda} \sin\theta = (2n+1)\frac{\pi}{2}$$

TR 79052

Fig 7.9 Geometry of elevation antenna

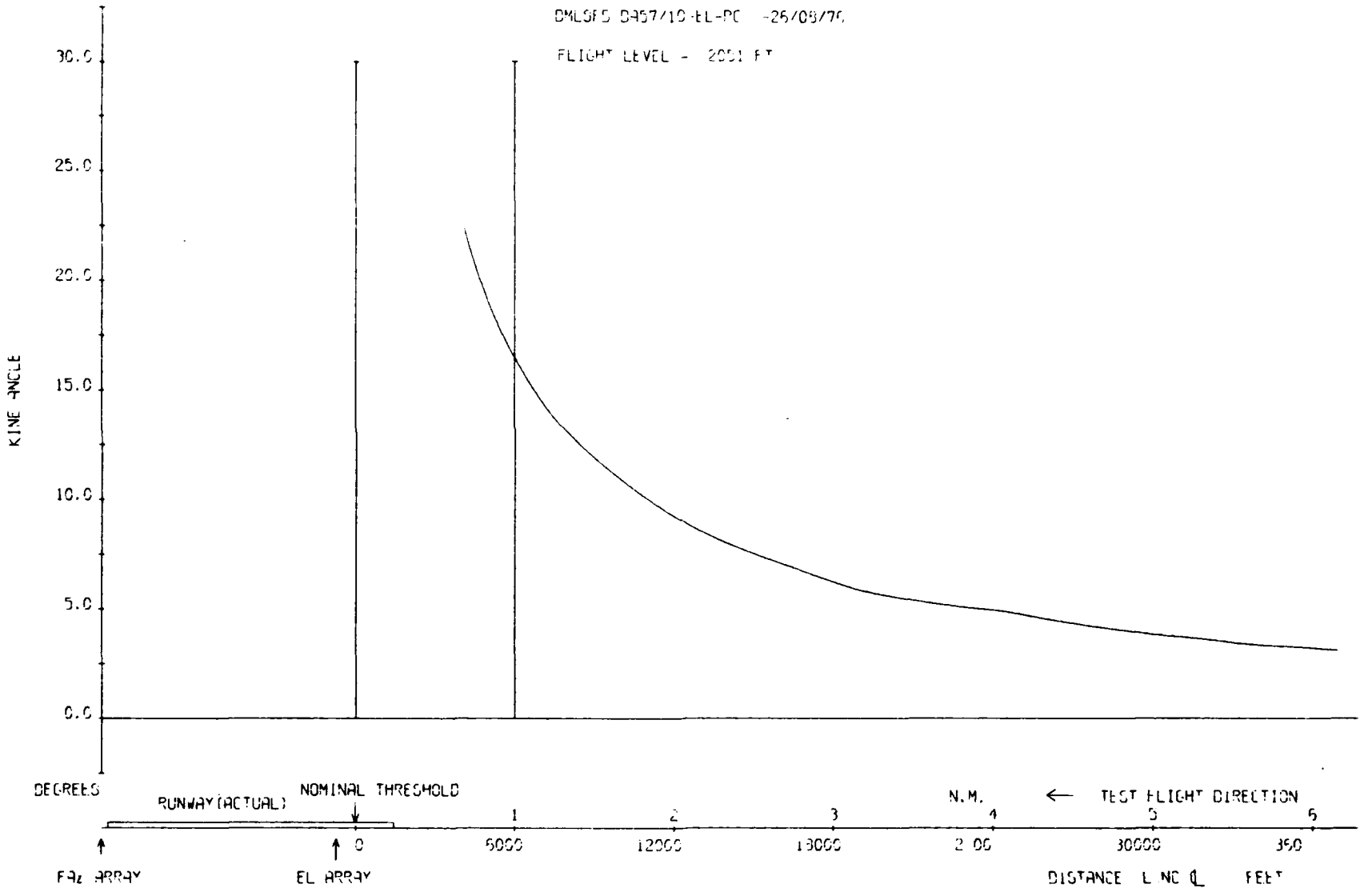

Fig 7.10a

Fig 7.10a Elevation radial at 2051 ft and zero azimuth

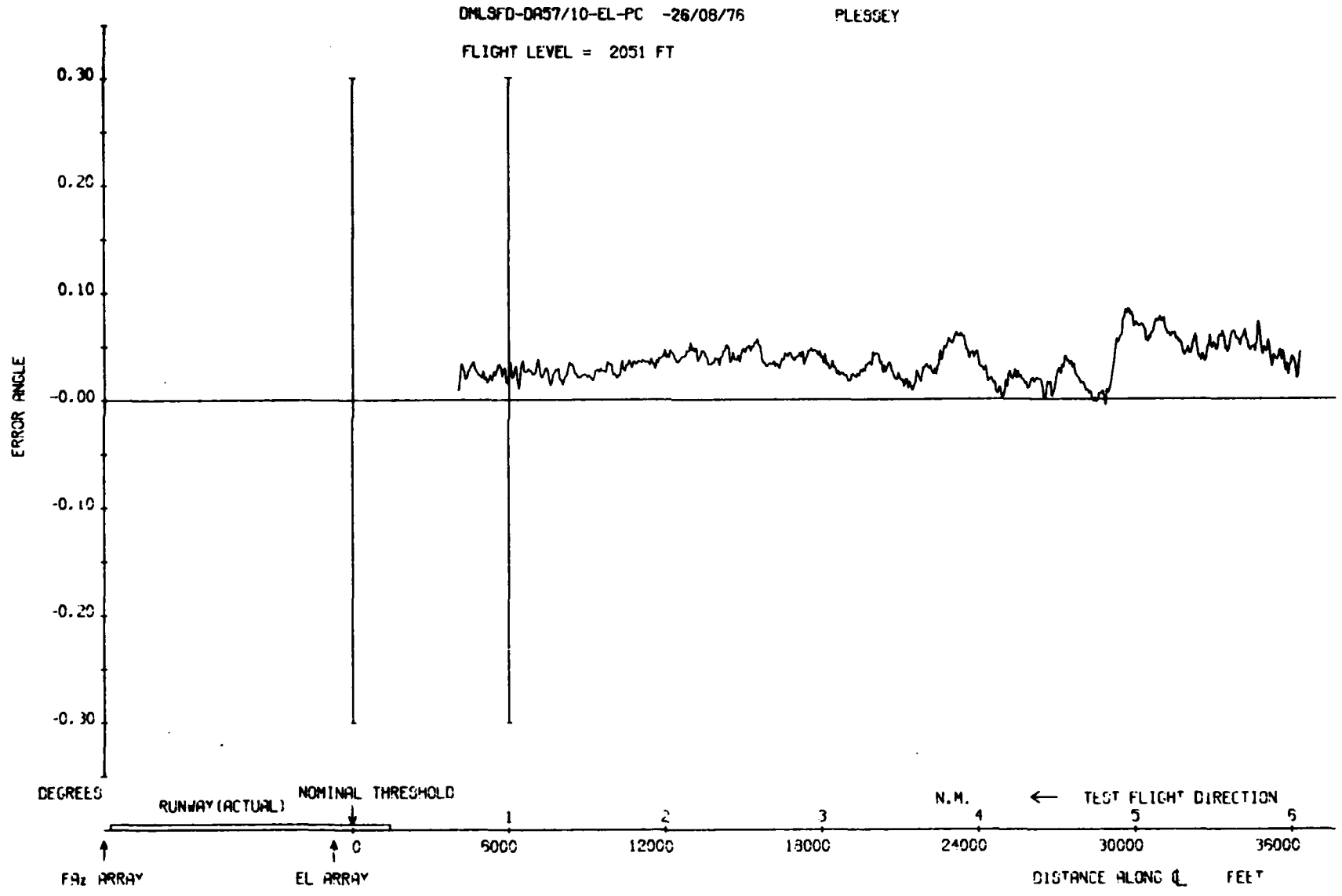

Fig 7.10b Elevation radial at 2051 ft and zero azimuth

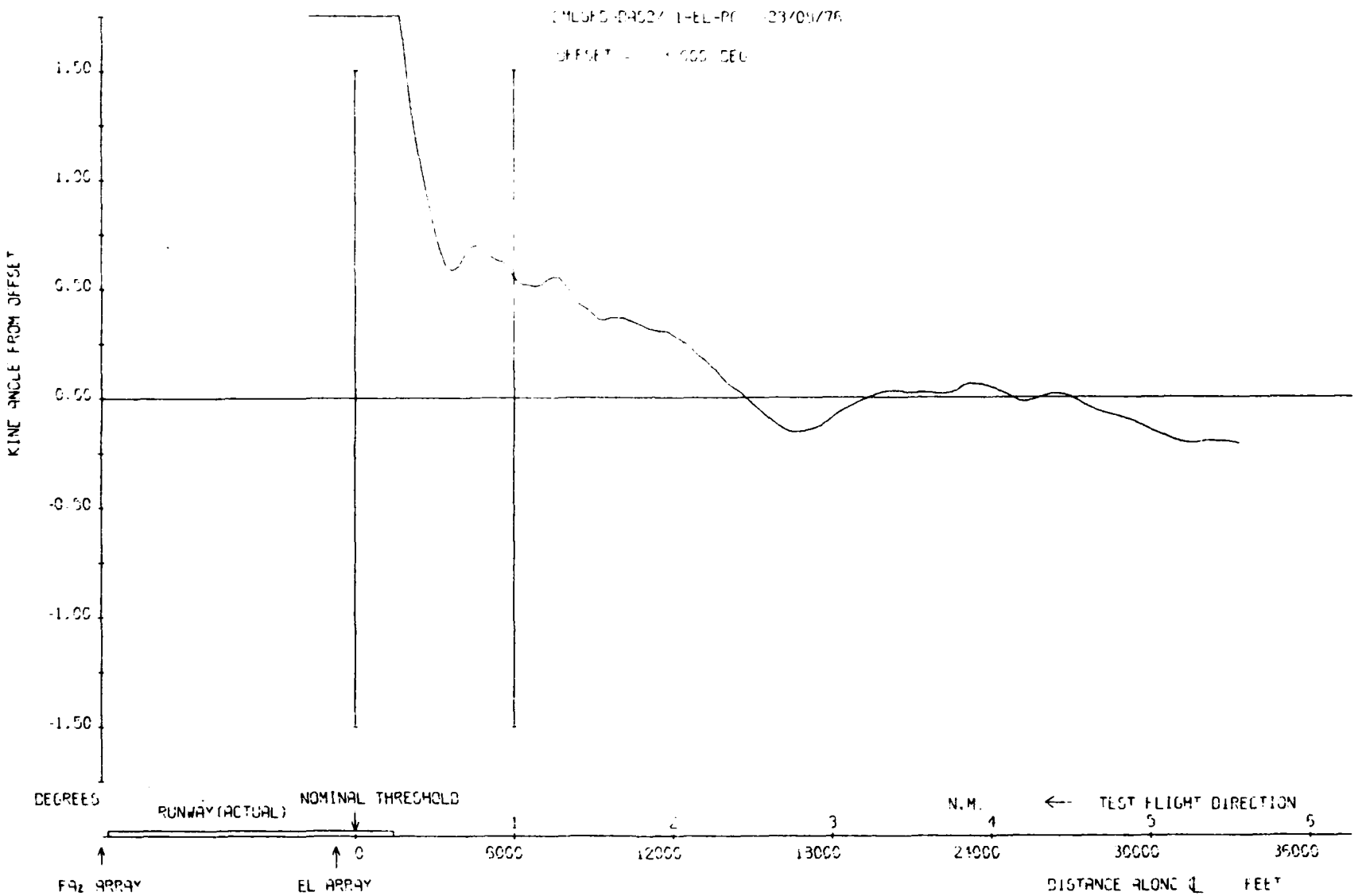

Fig 7.11a

Fig 7.11a Elevation 3 degree approach to low overshoot

TR 79052

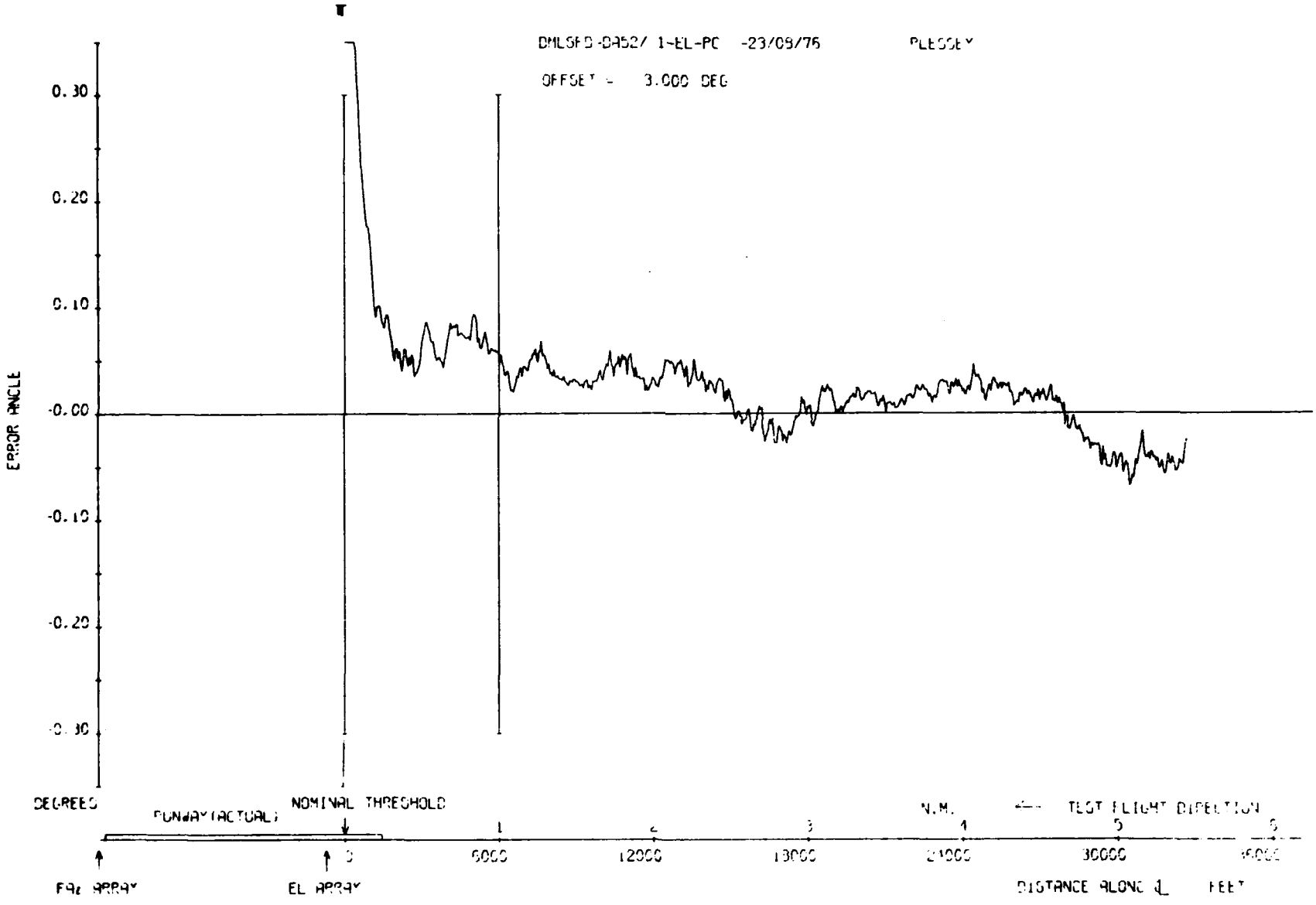

Fig 7.11b Elevation 3 degree approach to low overshoot

Fig 7.11b

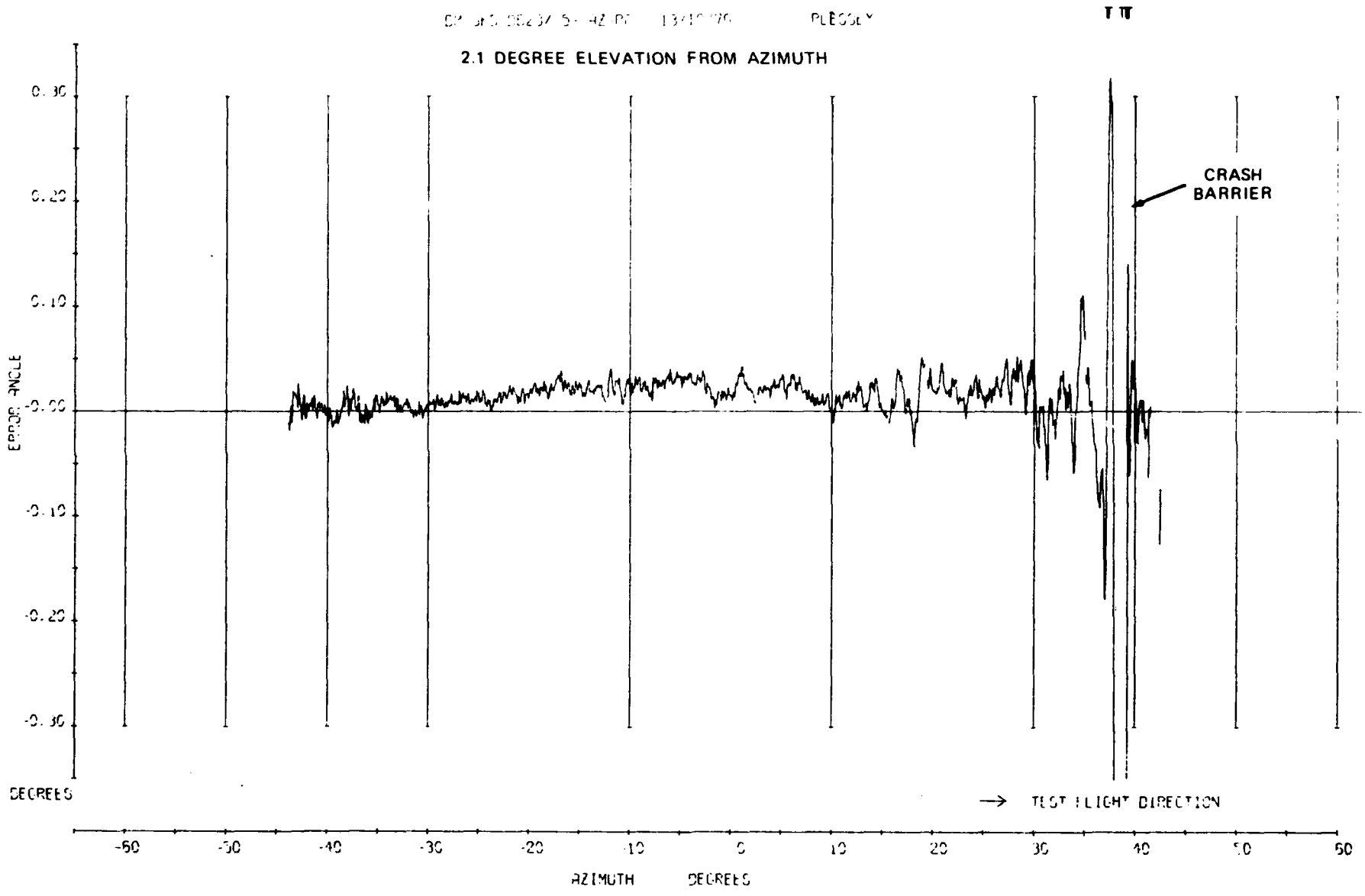

Fig 7.12

Fig 7.12 Azimuth part orbit at 8.8 n mile and 1950 ft height

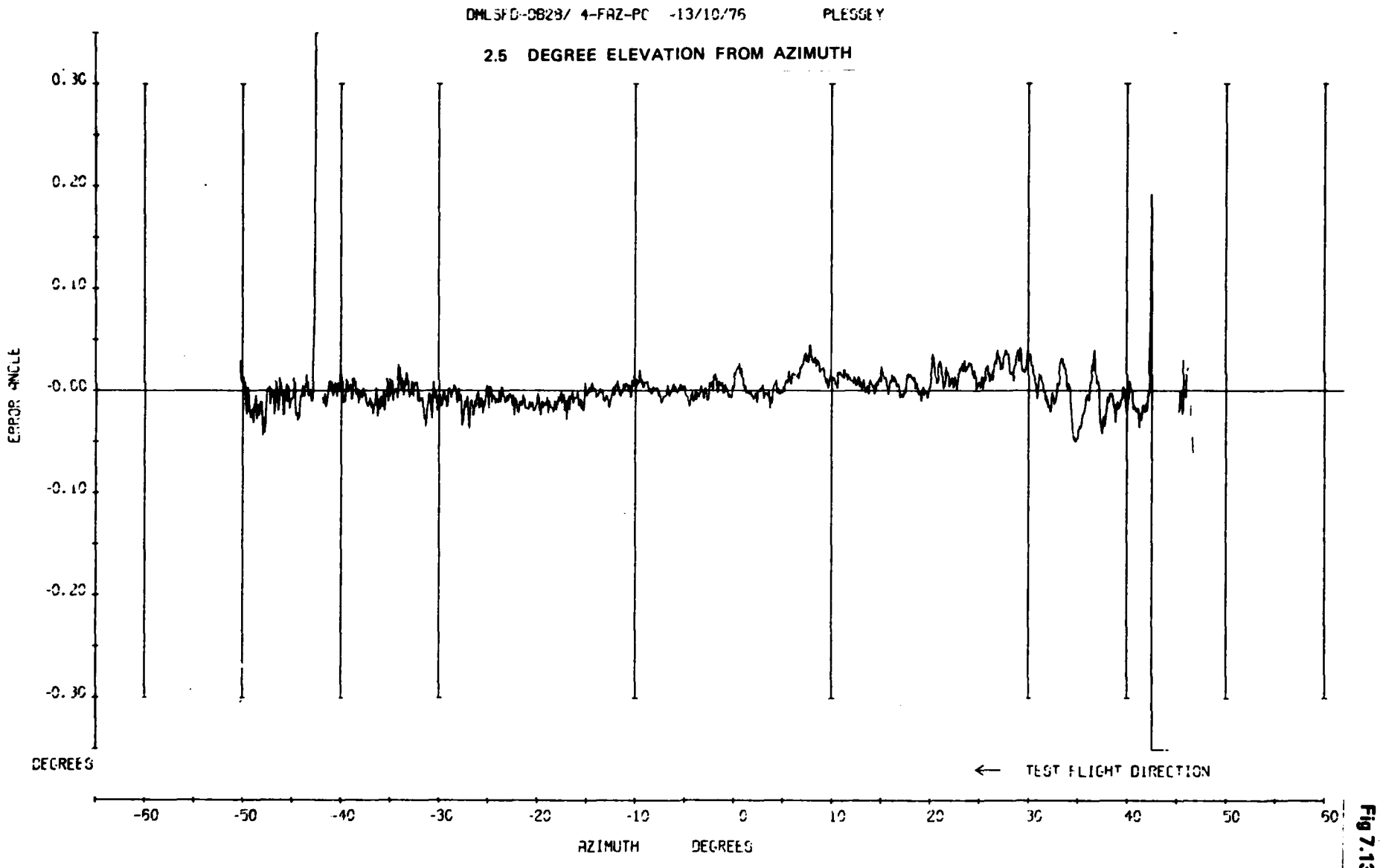

Fig 7.13

Fig 7.13 Azimuth part orbit at 7.5 n mile and 1950 ft height

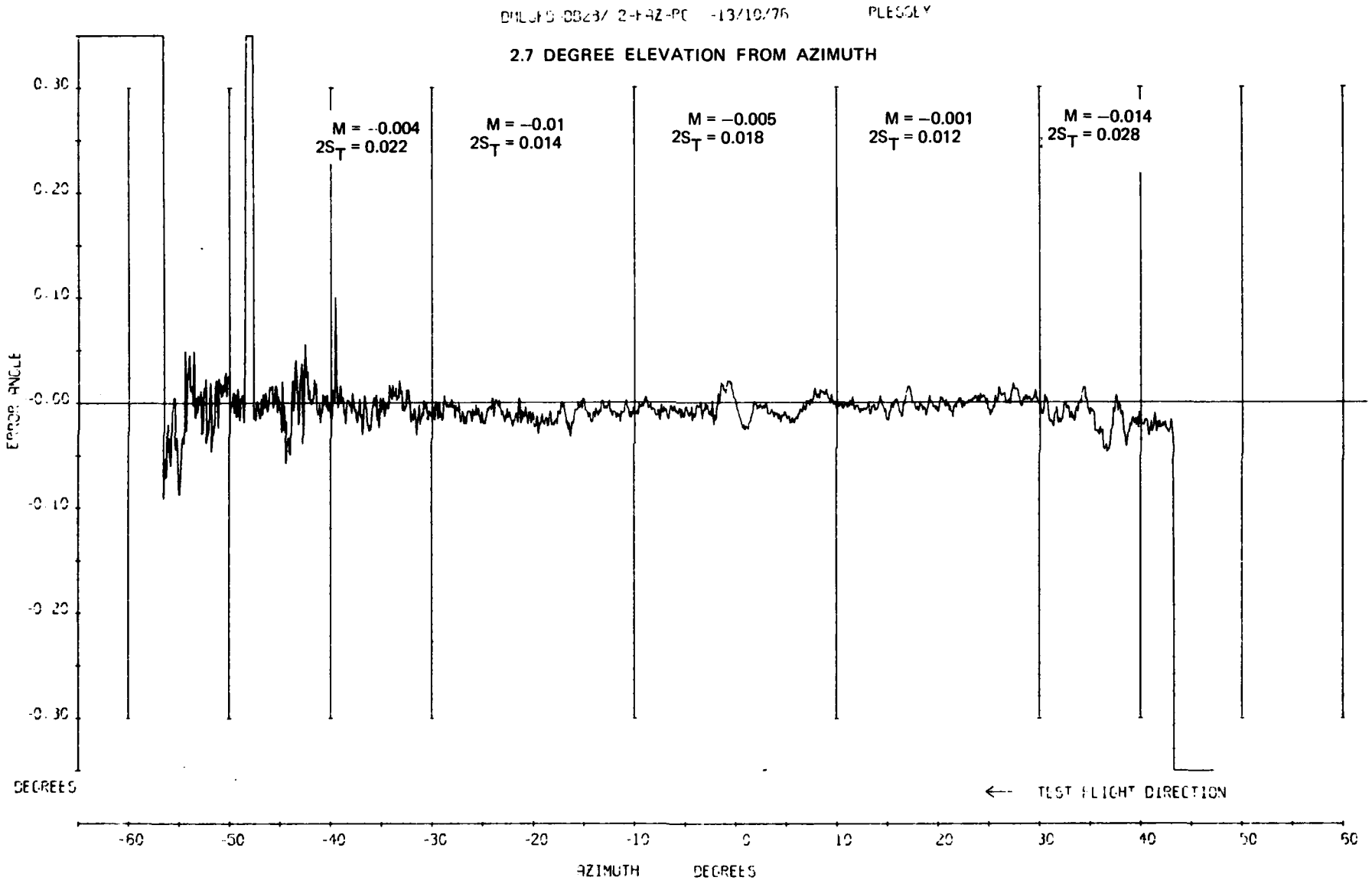

Fig 7.14

Fig 7.14 Azimuth part orbit at 6.8 n mile and 1930 ft height

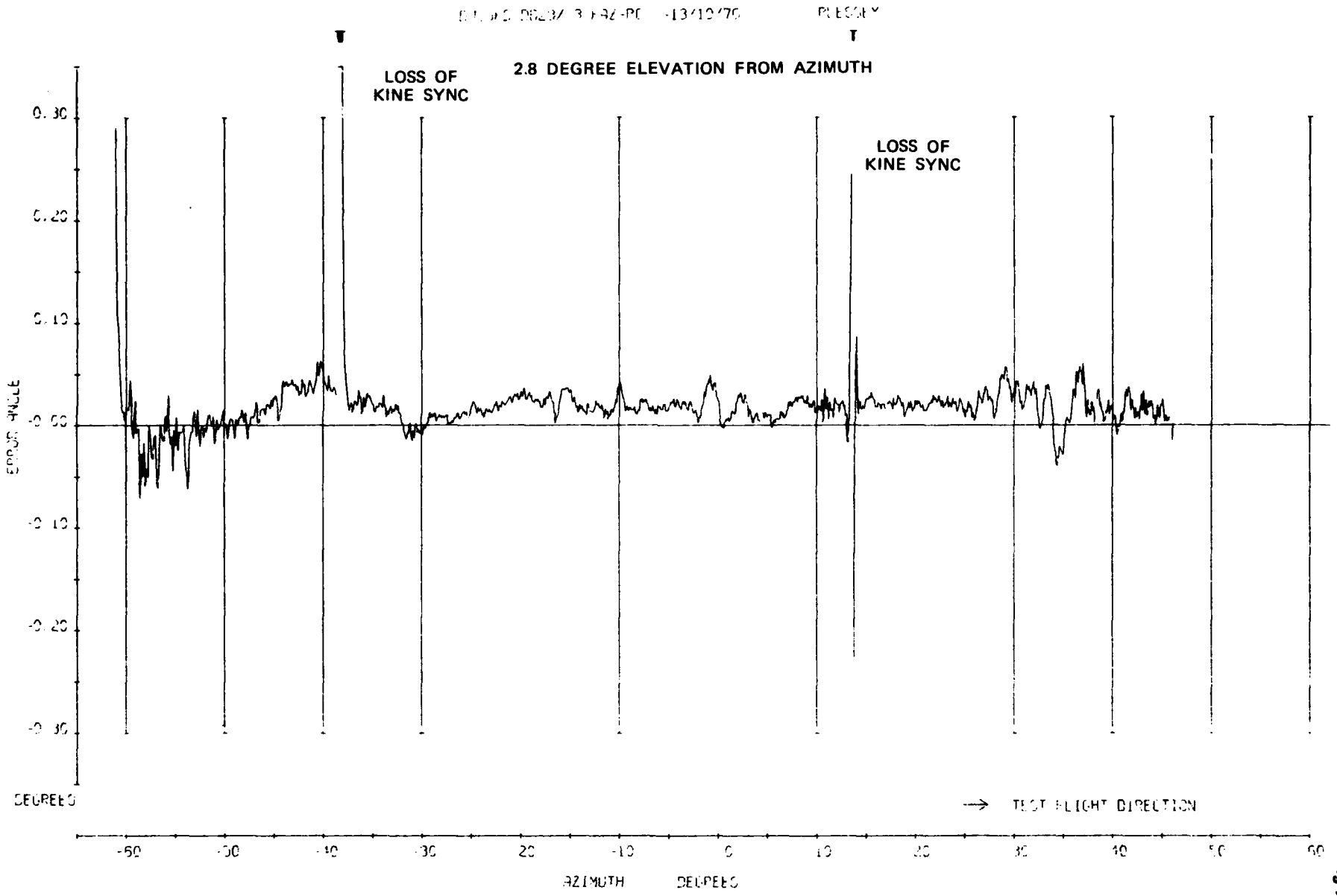

Fig 7.15

Fig 7.15 Azimuth part orbit at 6.6 n mile and 1950 ft height

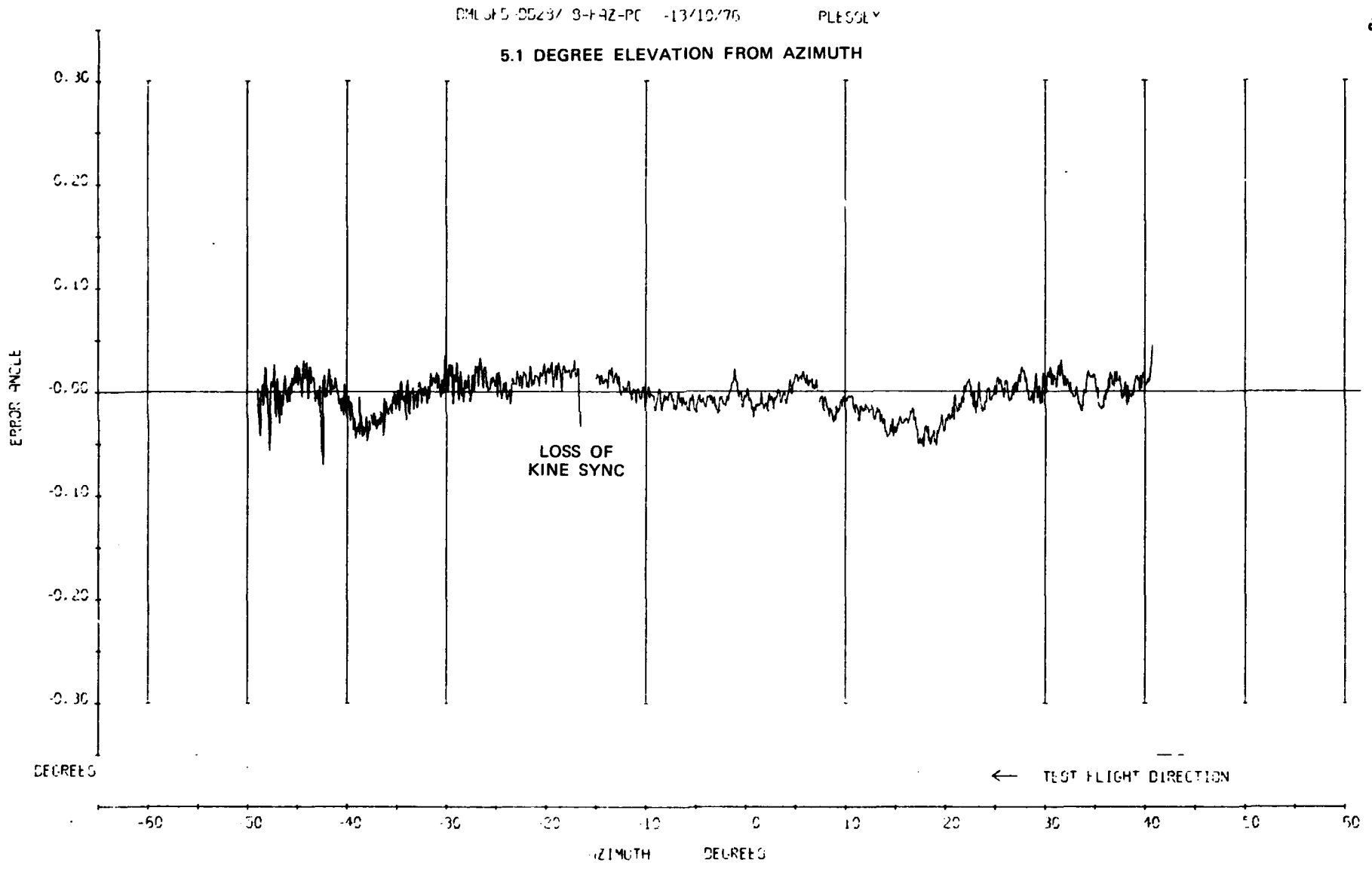

Fig 7.16c

Fig 7.16c Azimuth part orbit at 7.5 n mile and 4020 ft height

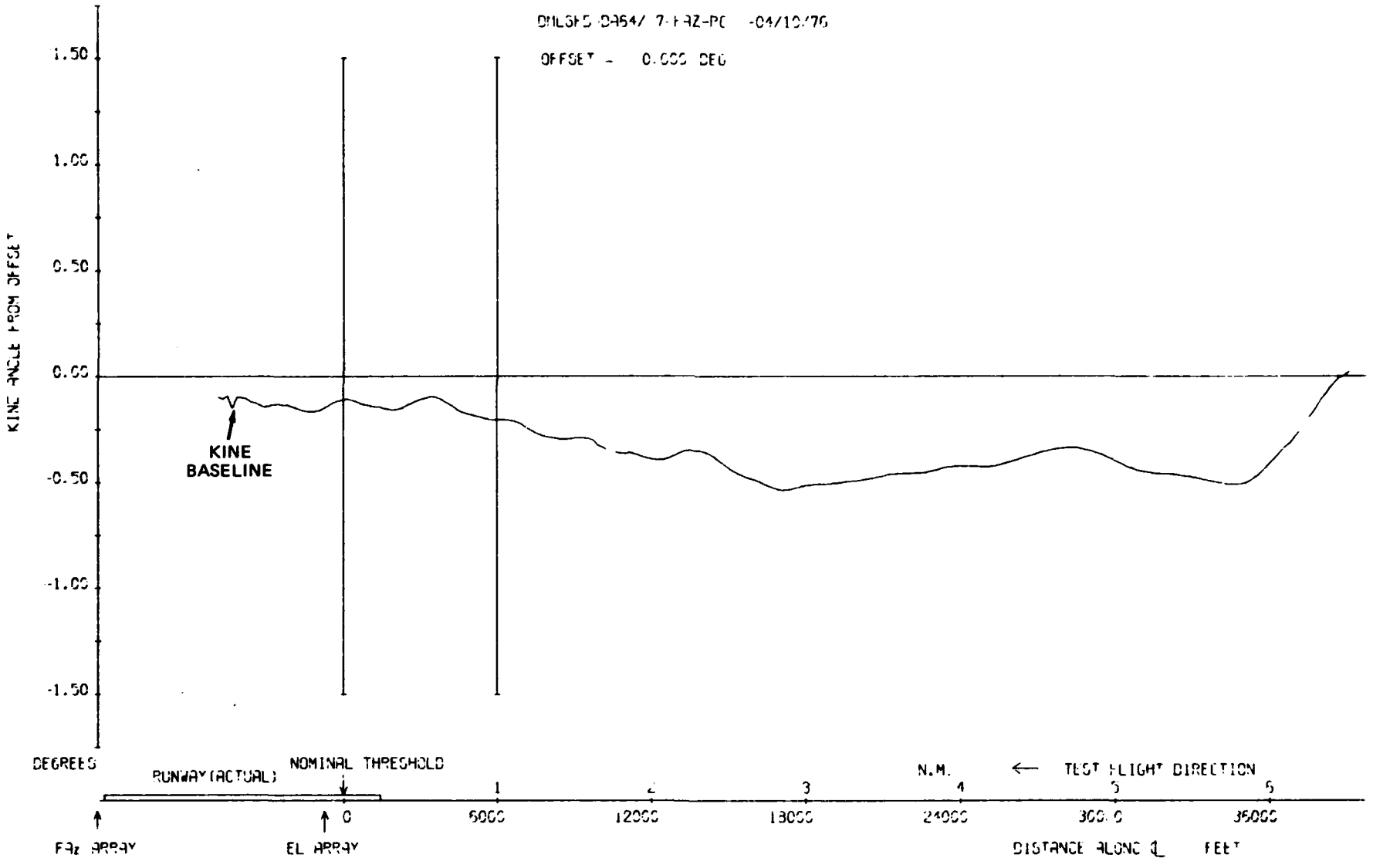

Fig 7.17a

Fig 7.17a Azimuth 3 degree approach to low overshoot

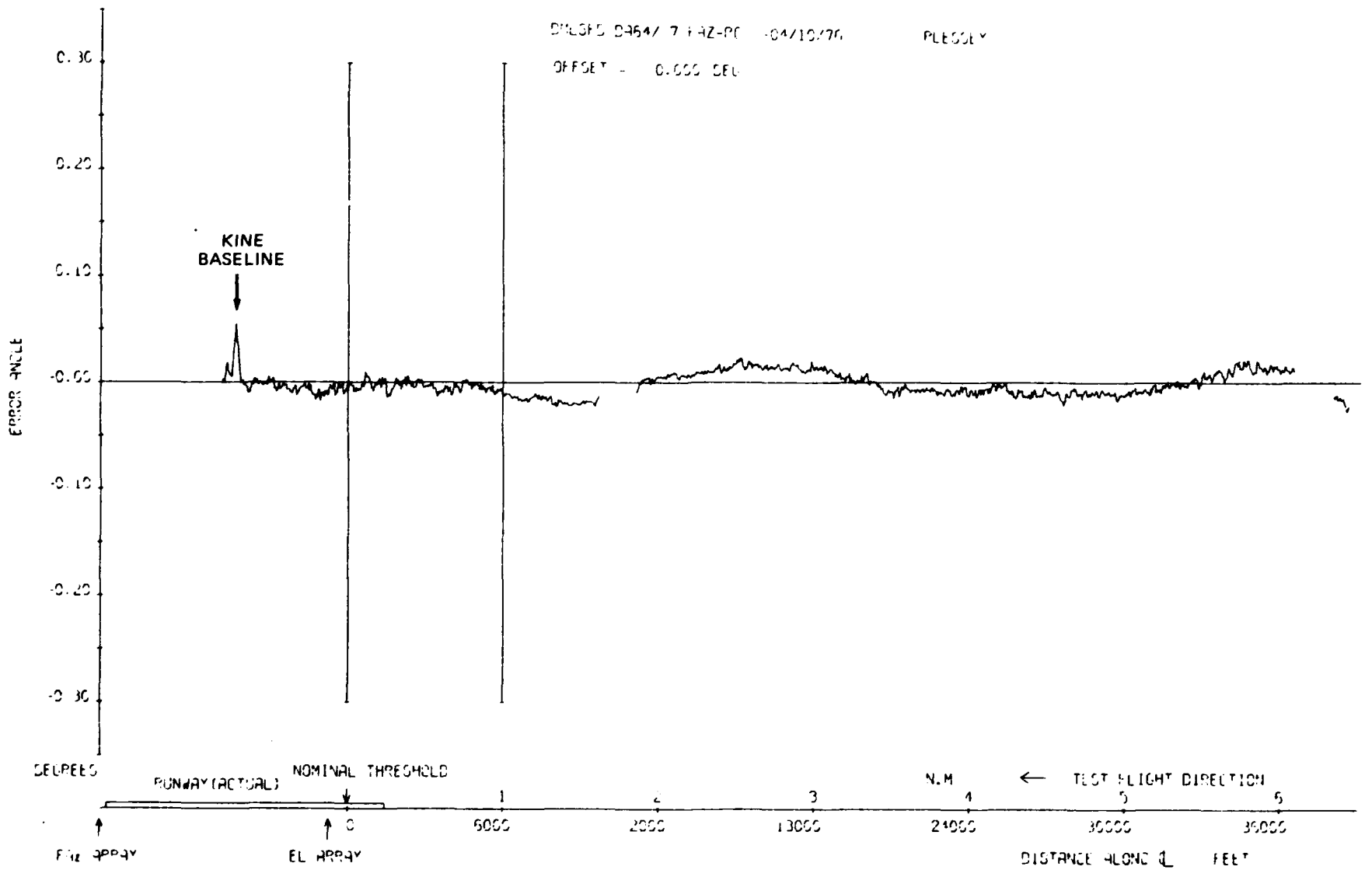

Fig 7.17b

Fig 7.17b Azimuth 3 degree approach to low overshoot

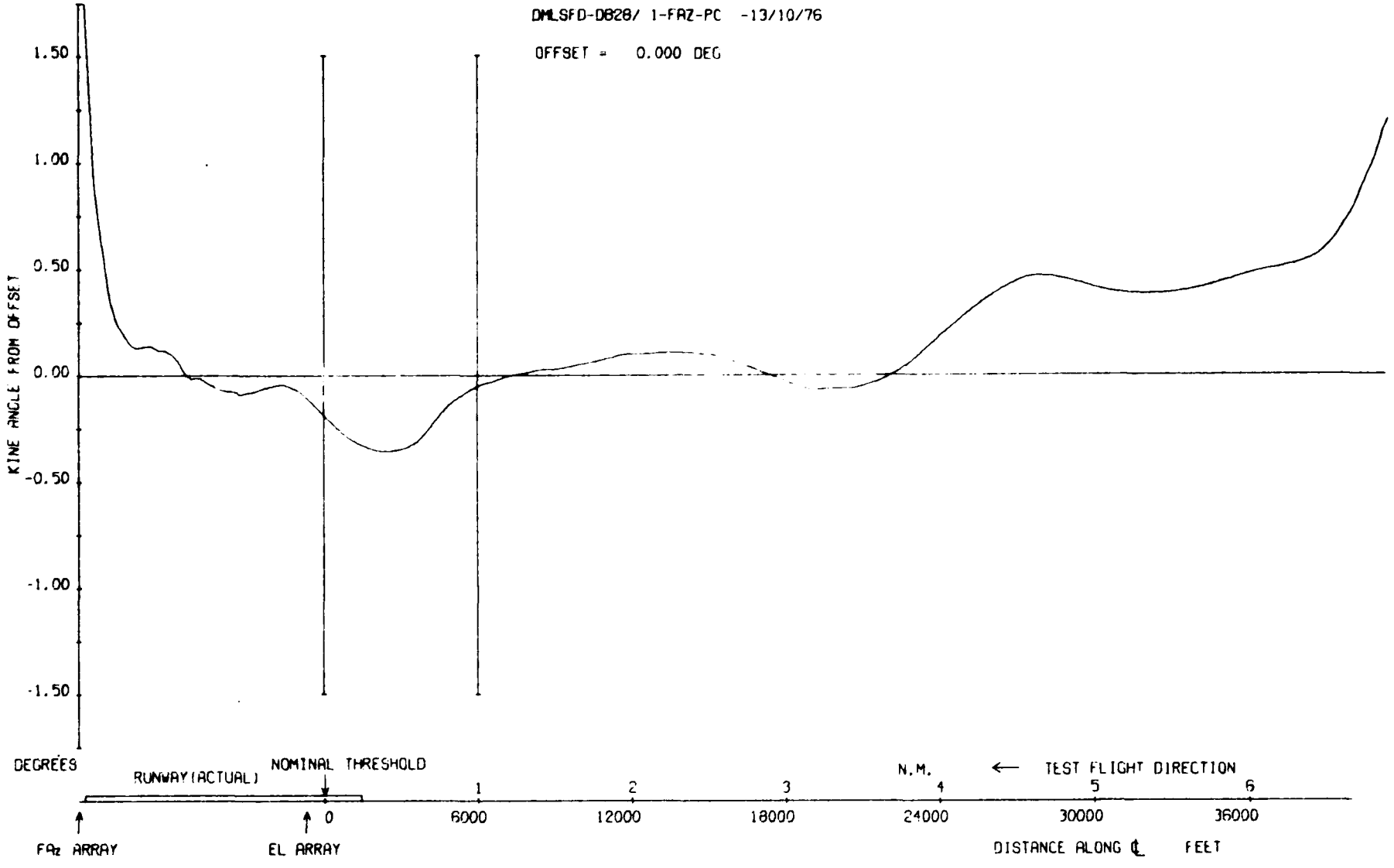

Fig 7.18a

Fig 7.18a Azimuth 3 degree approach to low overshoot

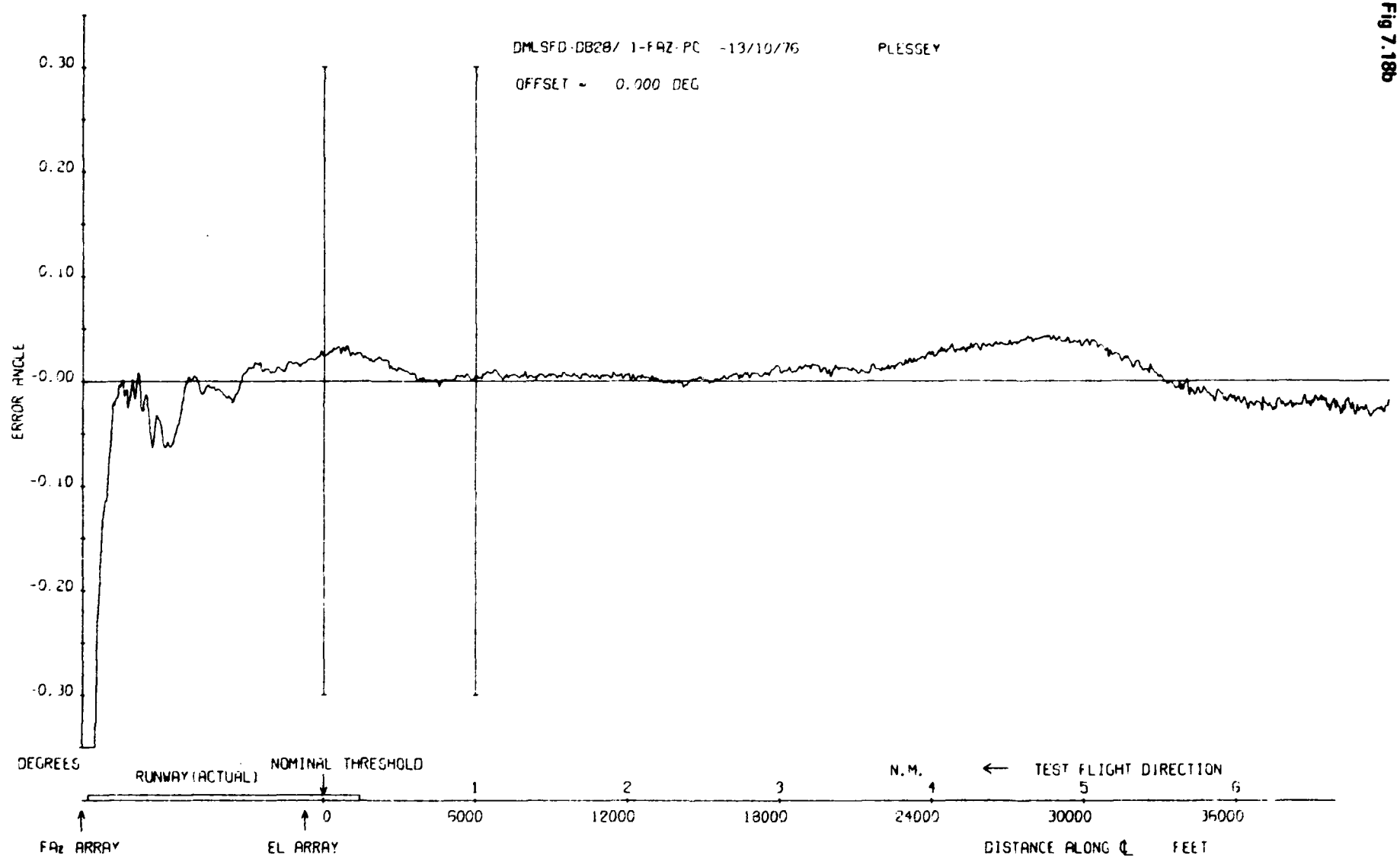

Fig 7.18b

Fig 7.18b Azimuth 3 degree approach to low overshoot

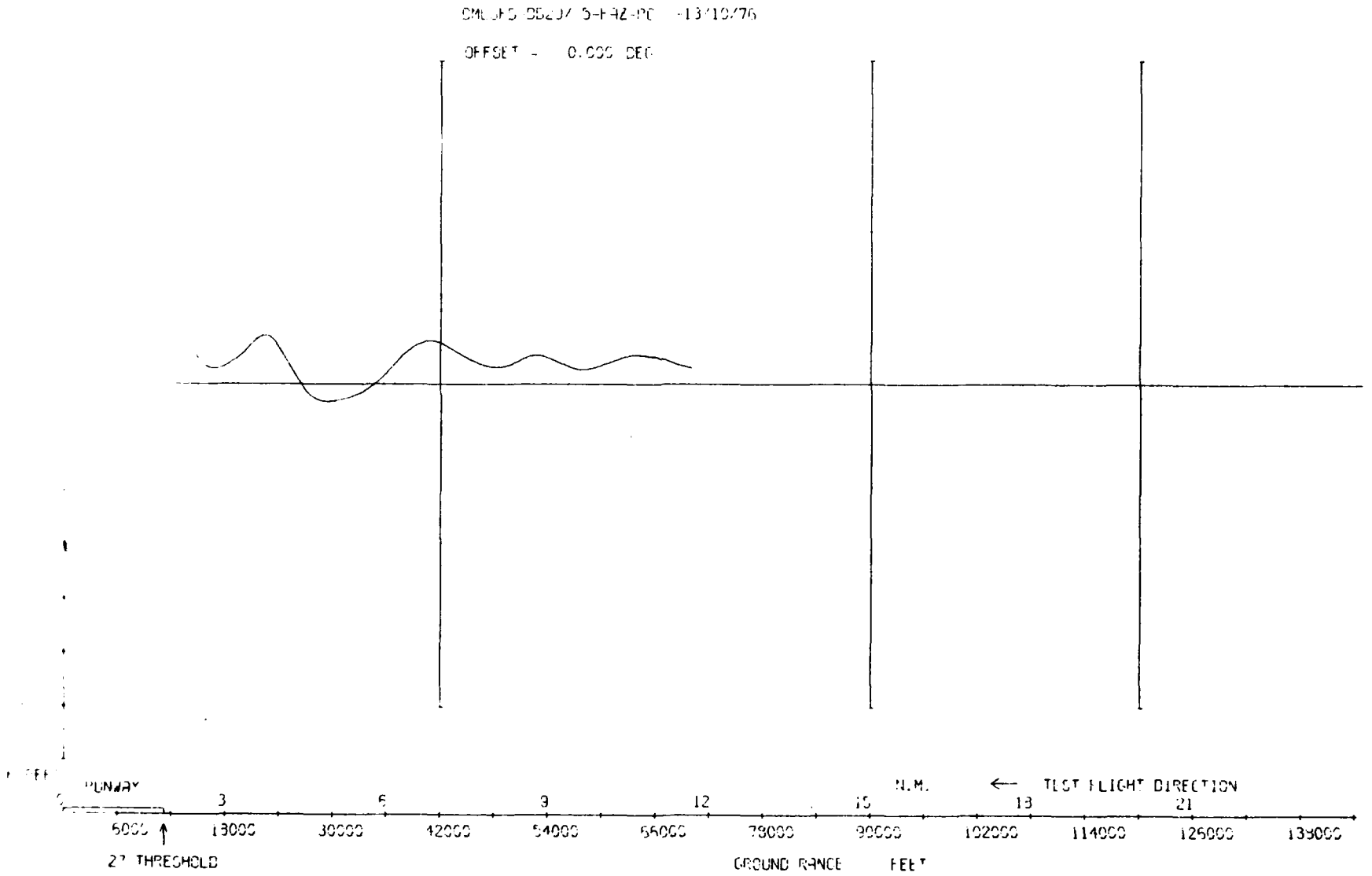

Fig 7.19a

Fig 7.19a Azimuth radial at 5000 ft

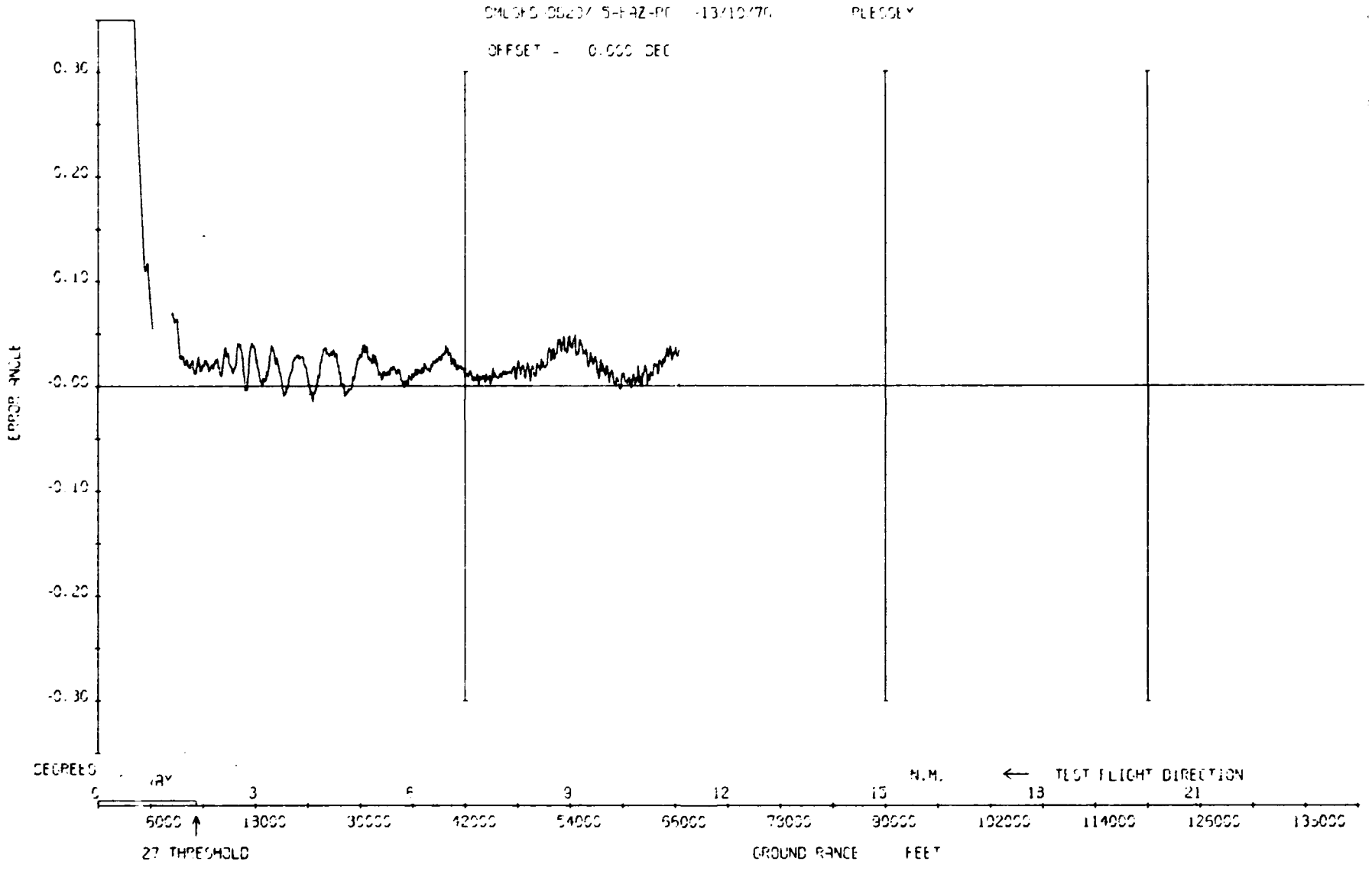

Fig 7.19b

Fig 7.19b Azimuth radial at 5000 ft

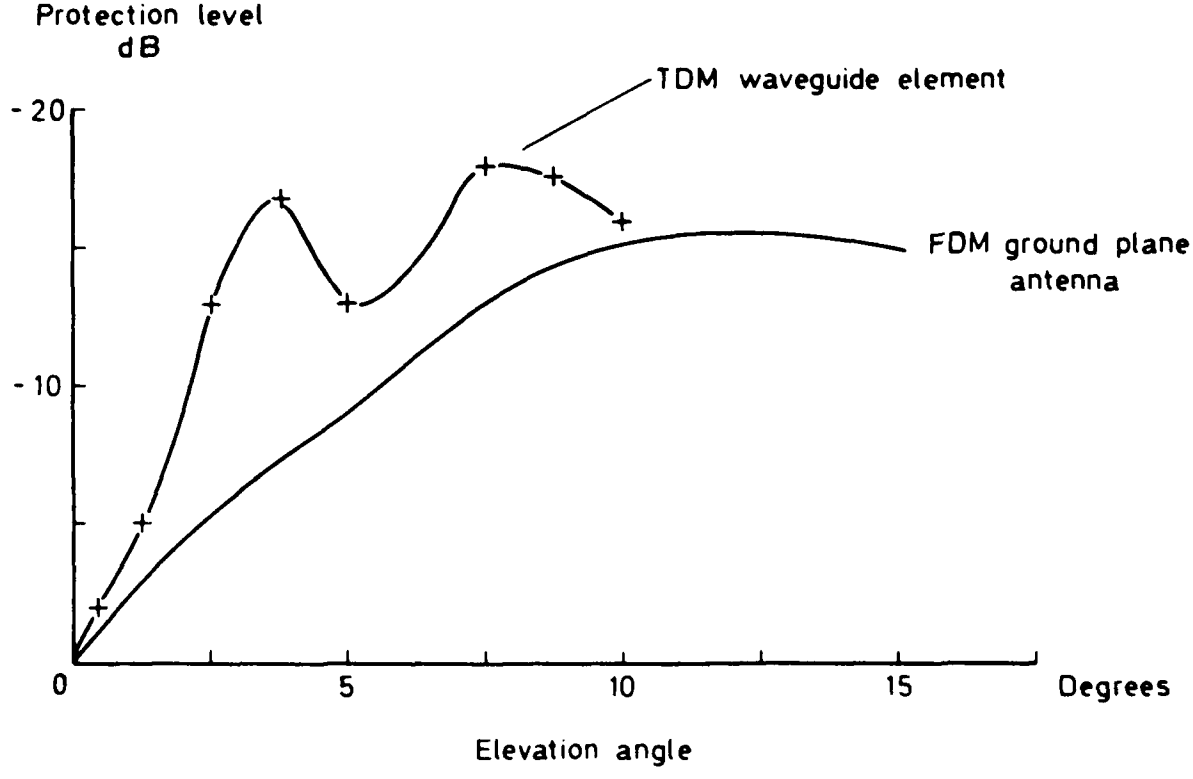

TR 79052

Fig 7.20 Azimuth antenna ground reflection attenuation factors

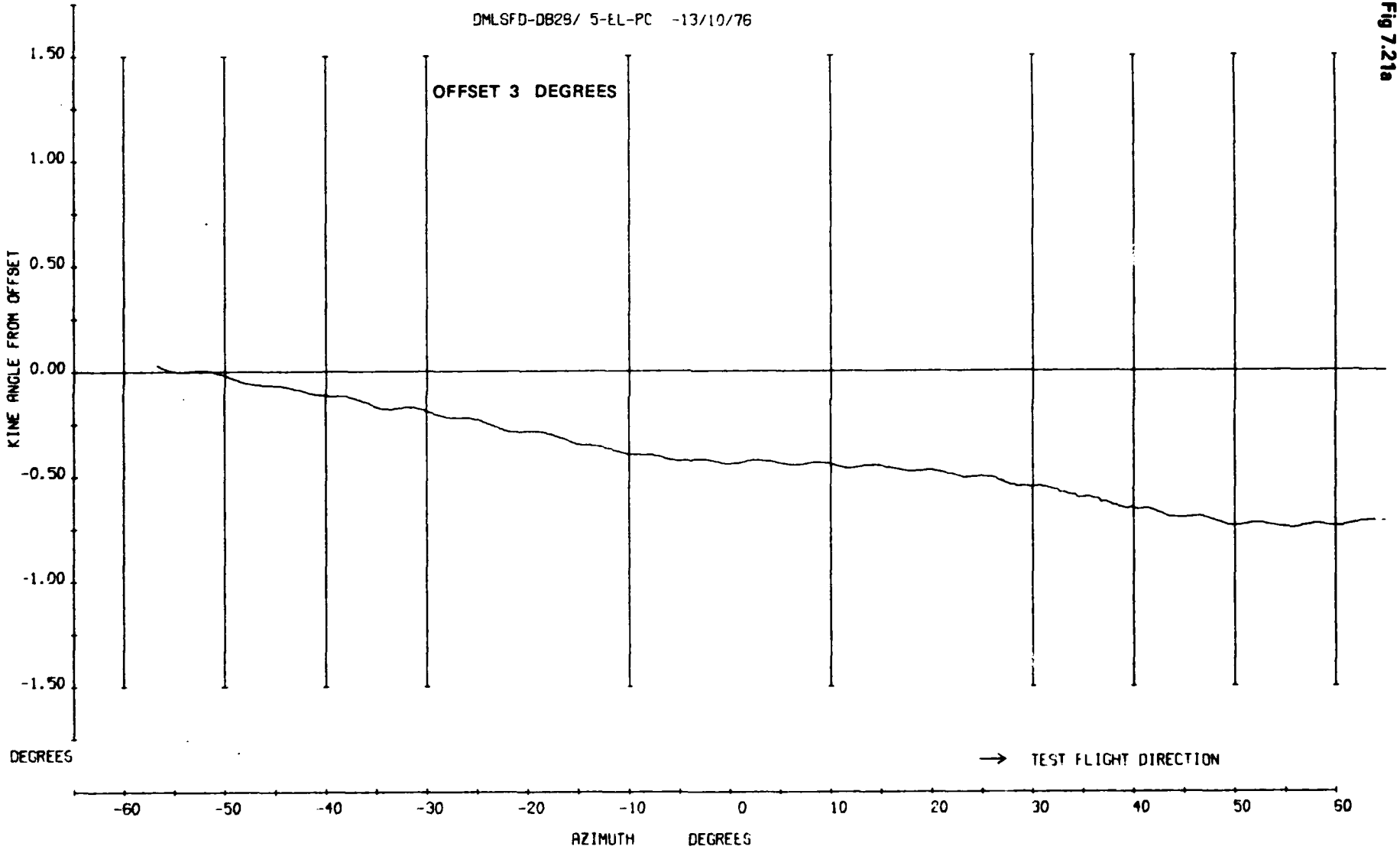

Fig 7.21a

Fig 7.21a Elevation part orbit at 2.6 degrees elevation

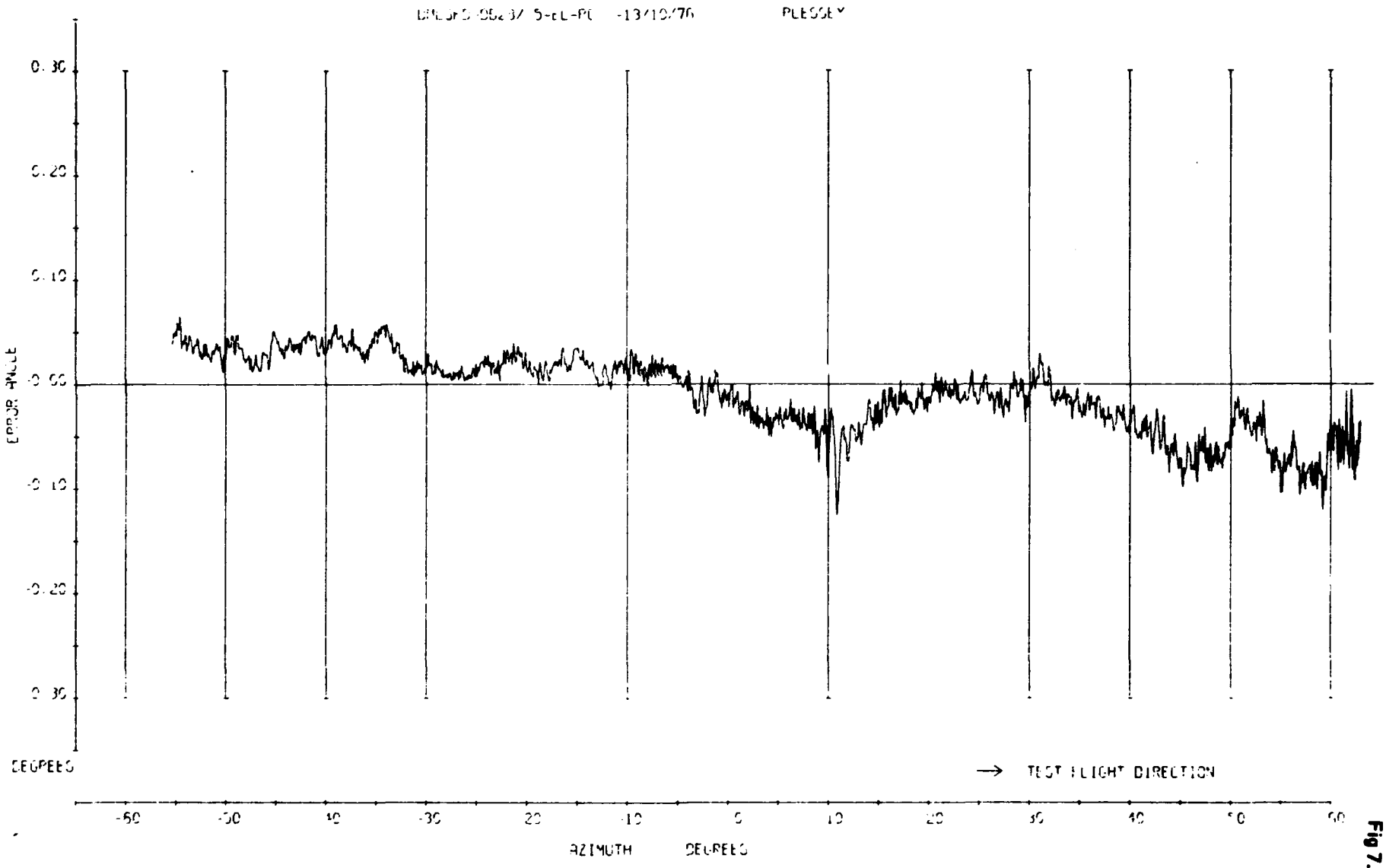

Fig 7.21b

Fig 7.21b Elevation part orbit at 2.6 degrees elevation

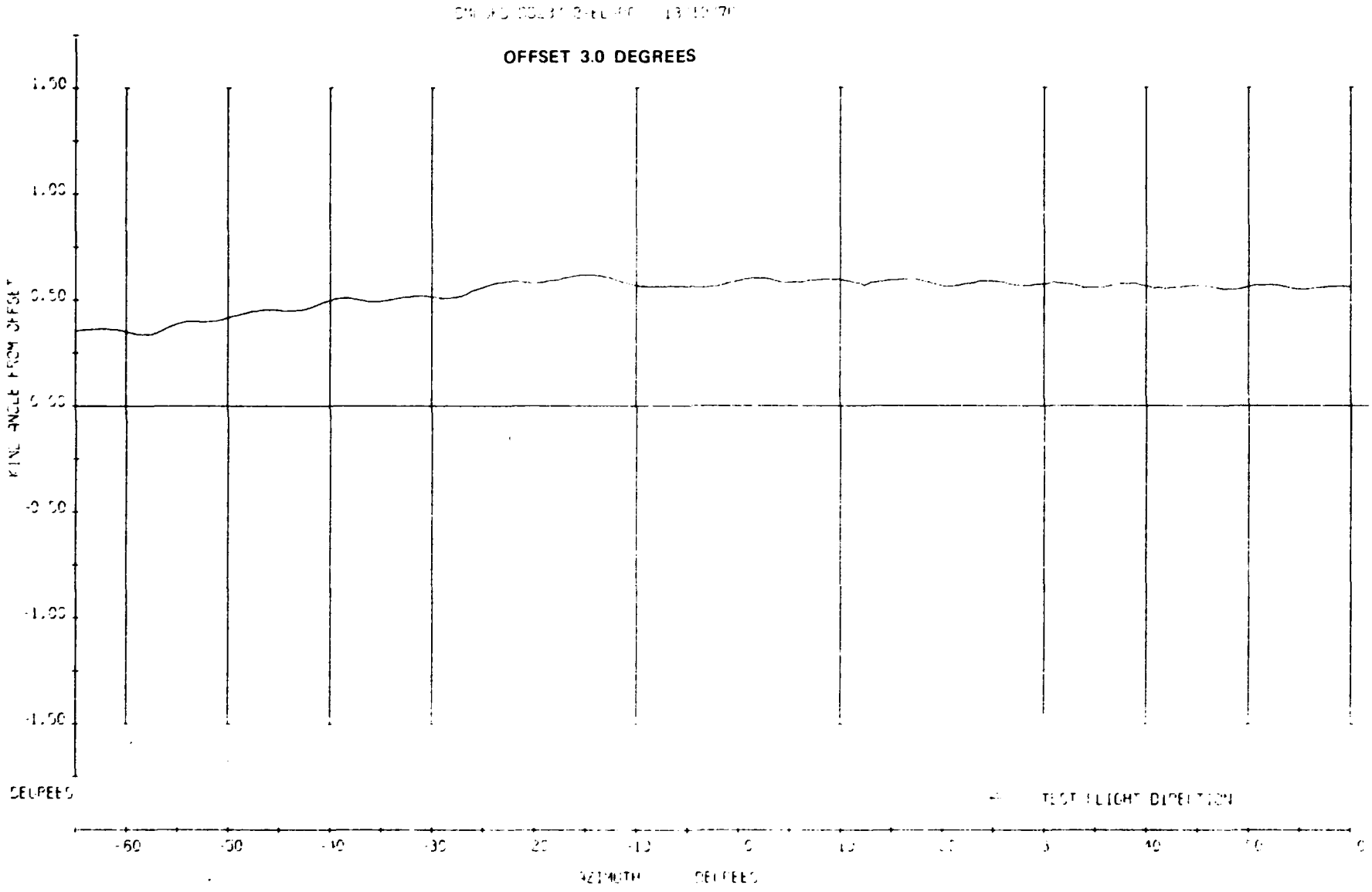

Fig 7.22a

Fig 7.22a Elevation part orbit at 3.5 degrees elevation

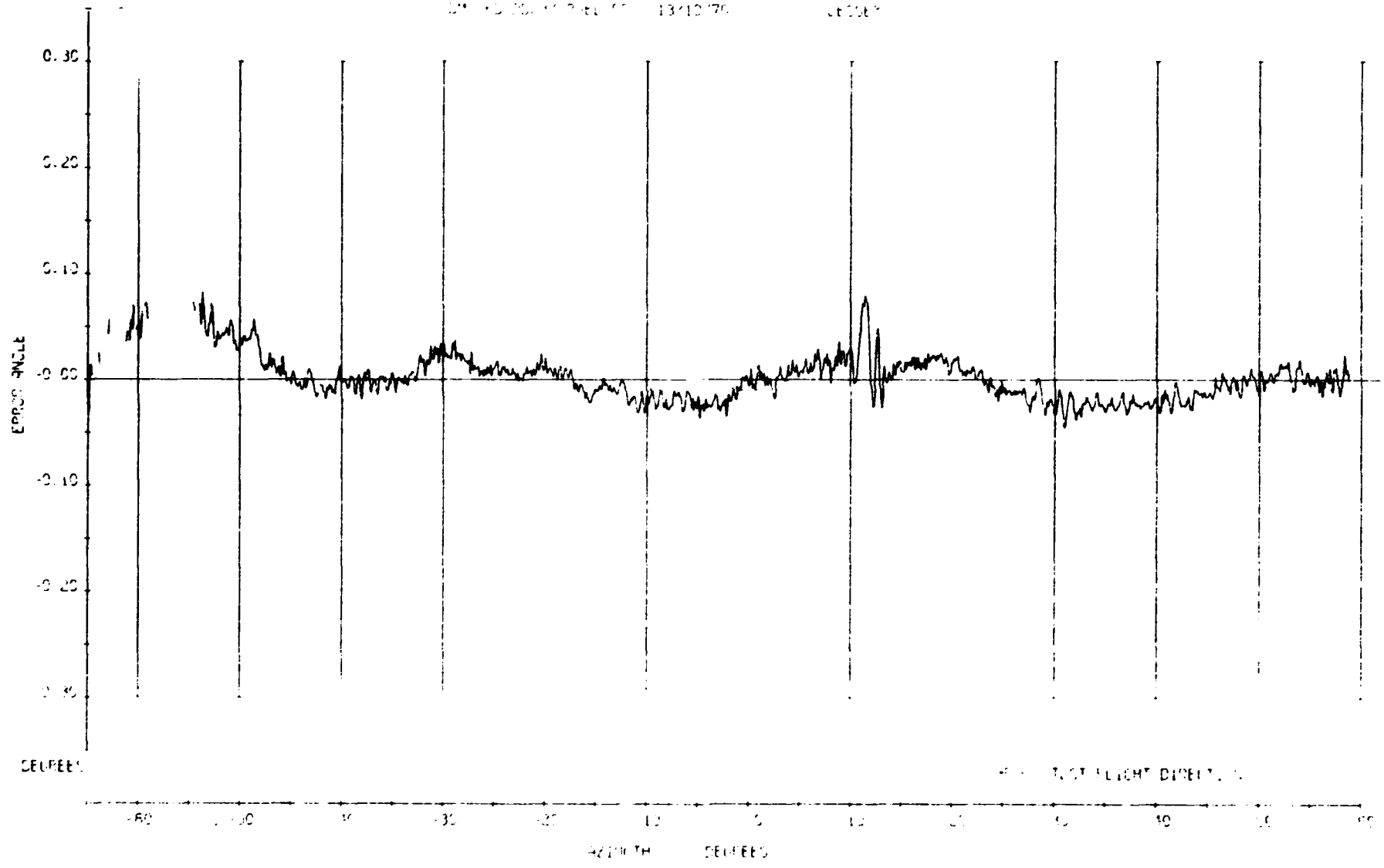

Fig 7.22b

Fig 7.22b Elevation part orbit at 3.5 degrees elevation

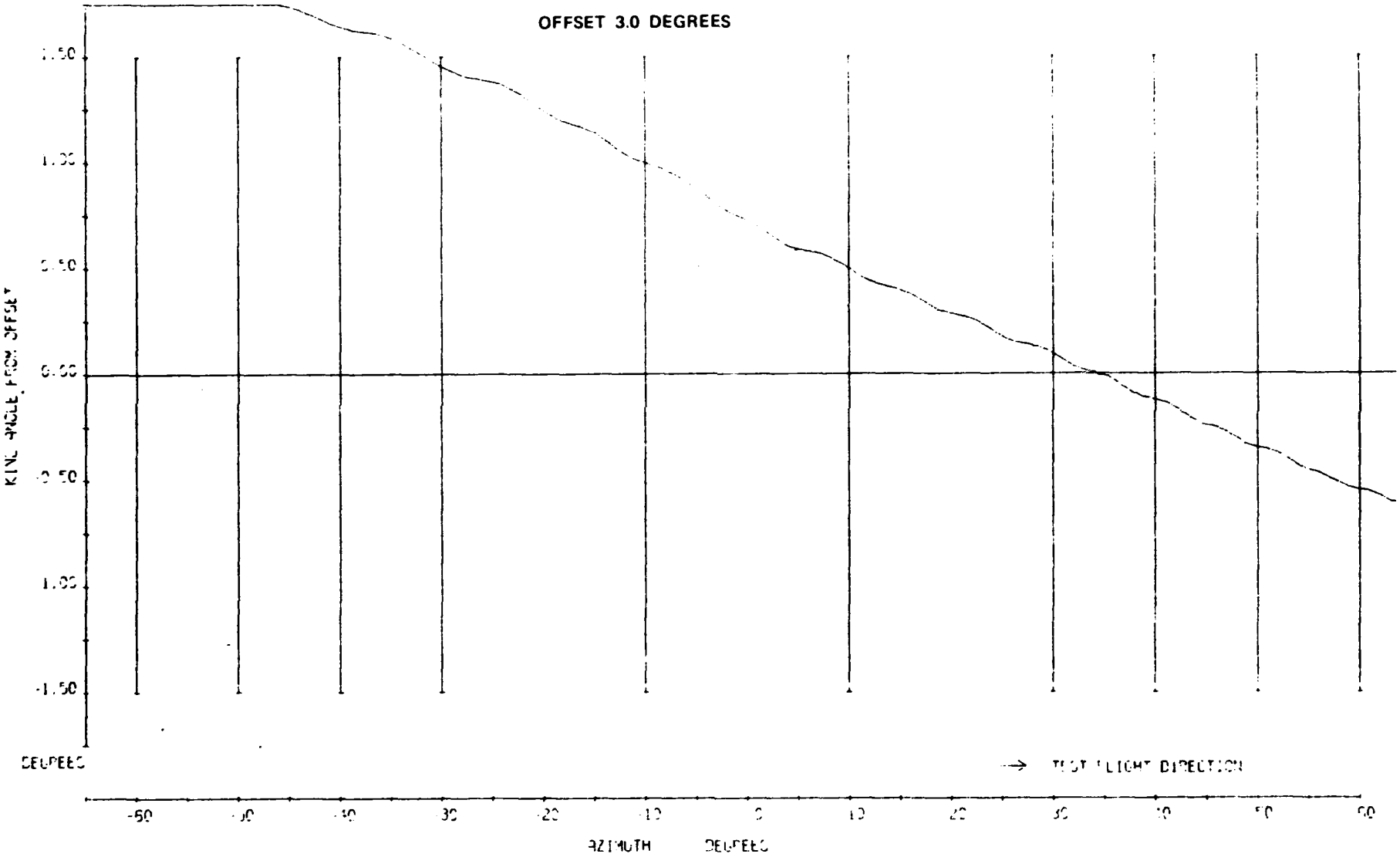

Fig 7.23a Elevation part orbit at 3.75 degrees elevation

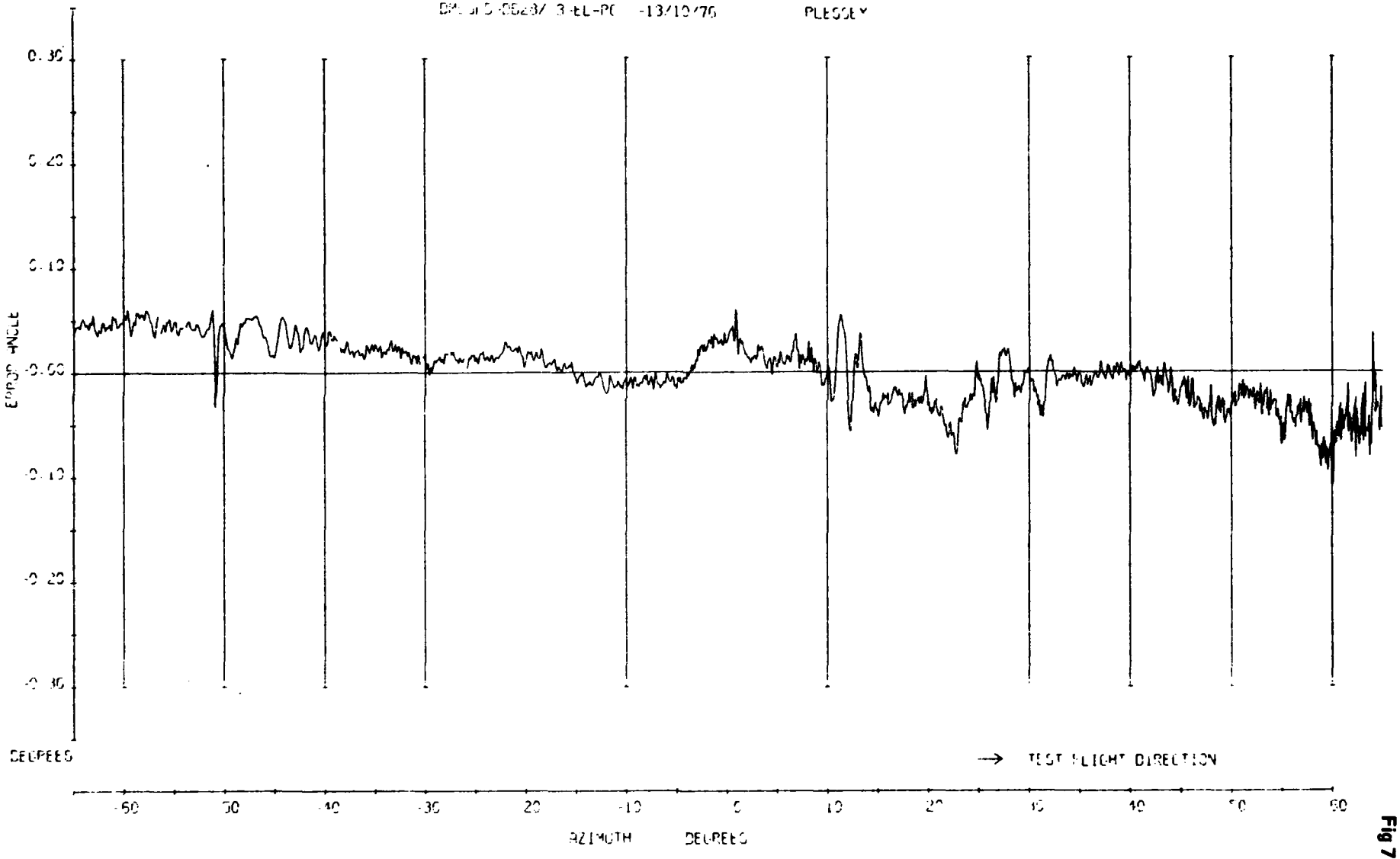

Fig 7.23b

Fig 7.23b Elevation part orbit at 3.75 degrees elevation

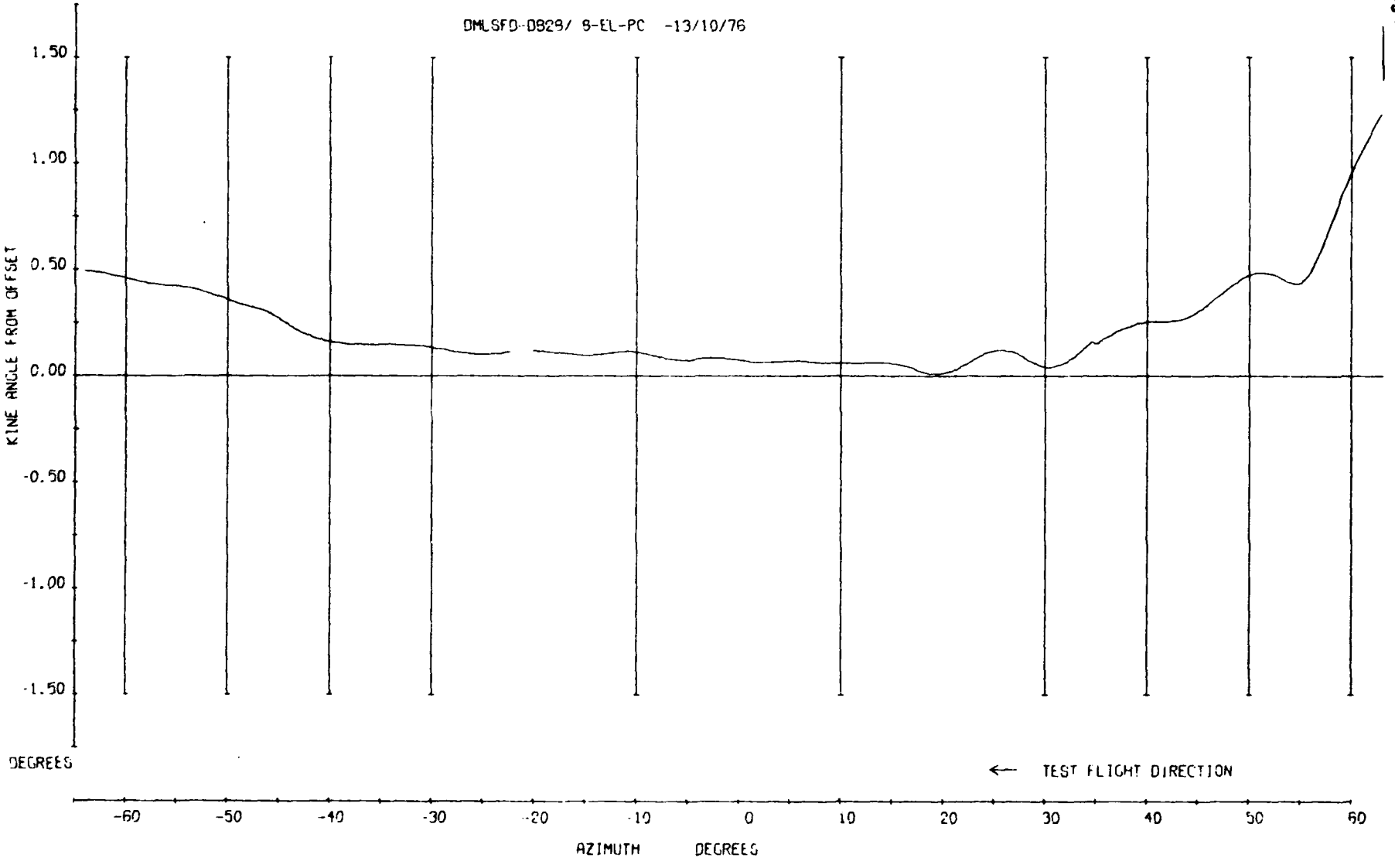

Fig 7.24a

Fig 7.24a Elevation part orbit at 6.5 degrees elevation

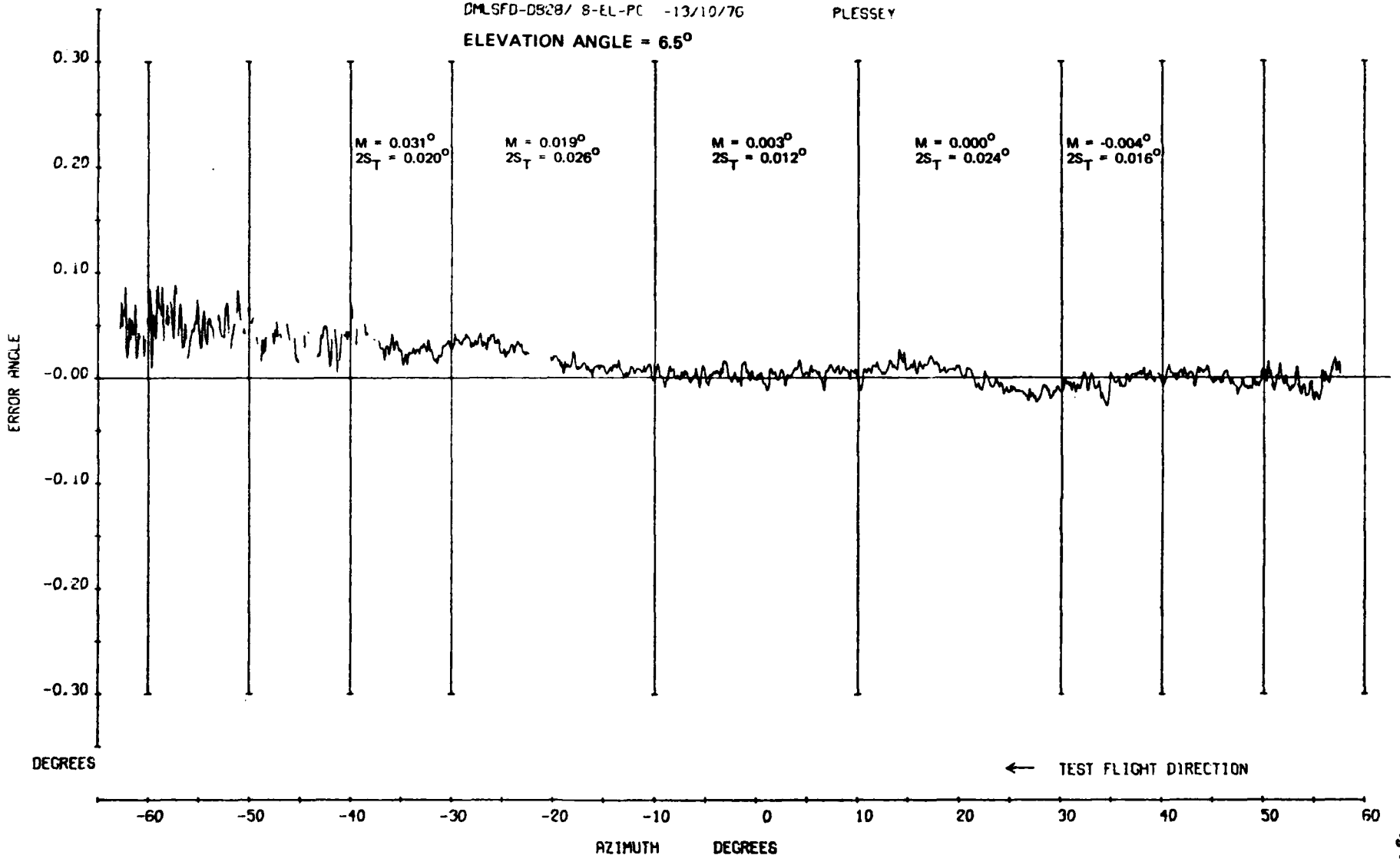

Fig 7.24b

Fig 7.24b Elevation part orbit at 6.5 degrees elevation

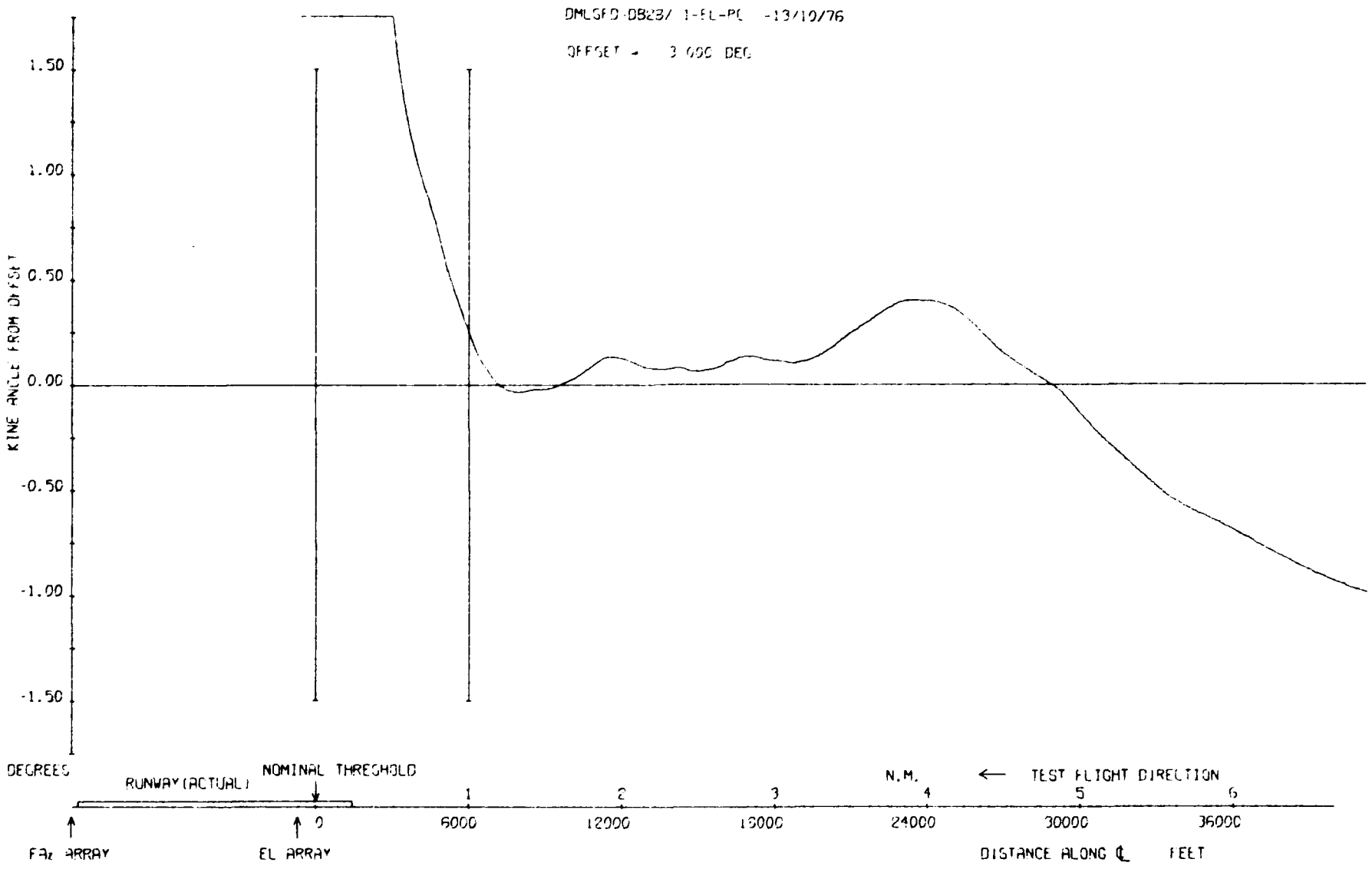

Fig 7.25a

Fig 7.25a Elevation 3 degree approach

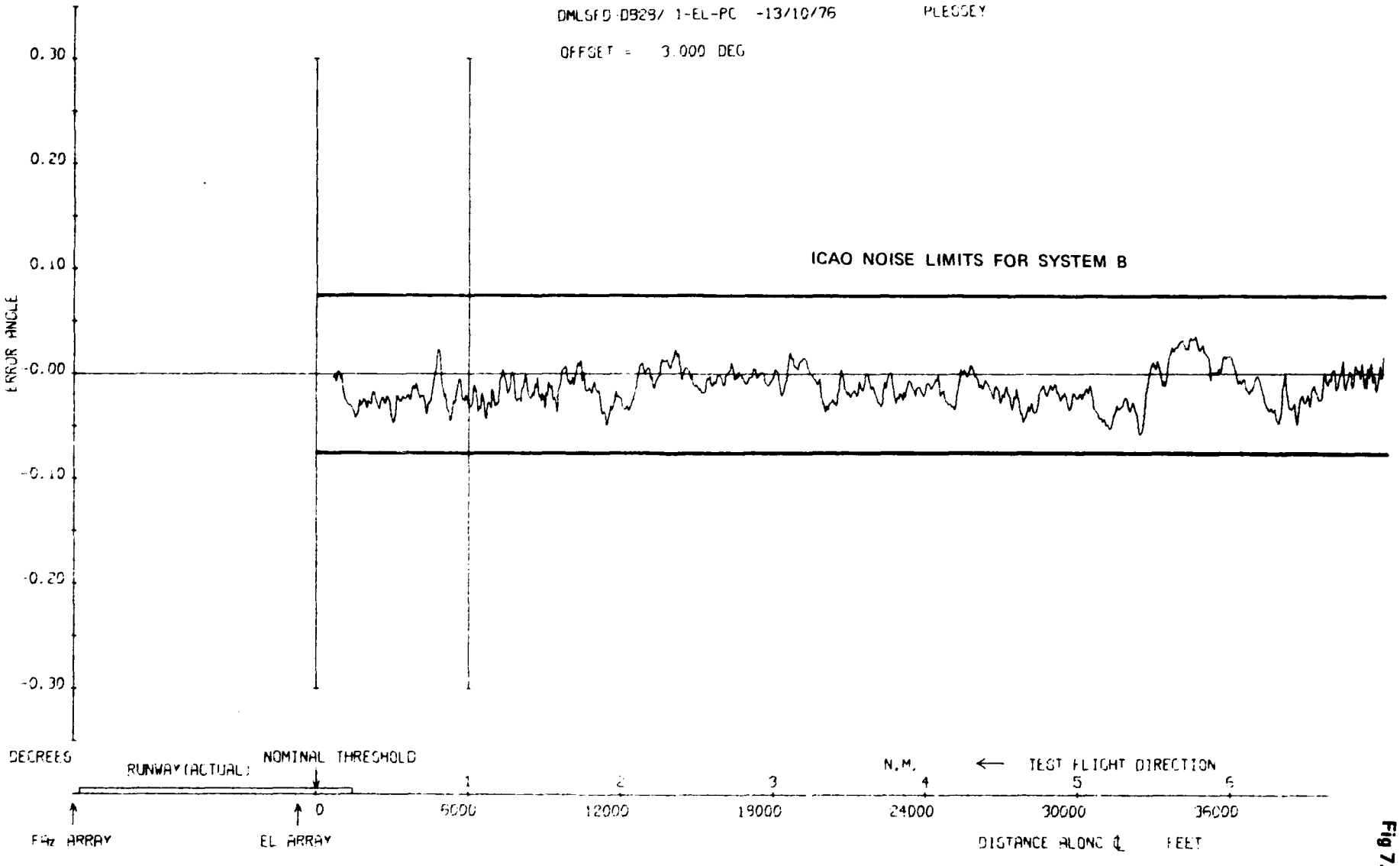

Fig 7.25b Elevation 3 degree approach

Fig 7.25b

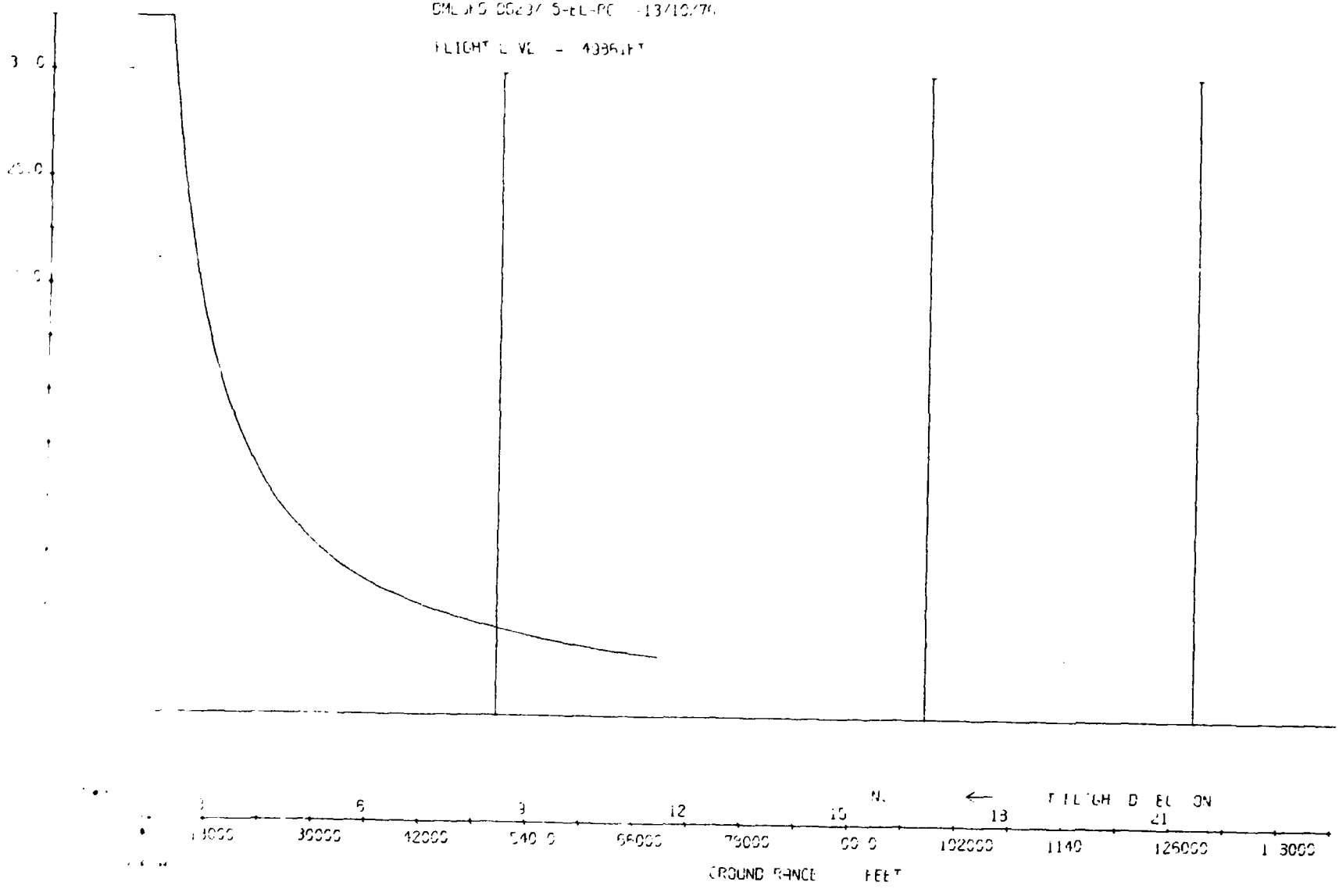

Fig 7.26a

Fig 7.26a Elevation radial at 5000 ft

AD-A085 480 ROYAL AIRCRAFT ESTABLISHMENT FARNBOROUGH (ENGLAND) F/6 17/7
CONTRIBUTIONS TO THE UK MICROWAVE LANDING SYSTEM RESEARCH AND D--ETC(U)
MAY 79 J M JONES
UNCLASSIFIED RAE-TR-79052-VOL-3 DRIC-BR-73763 NL

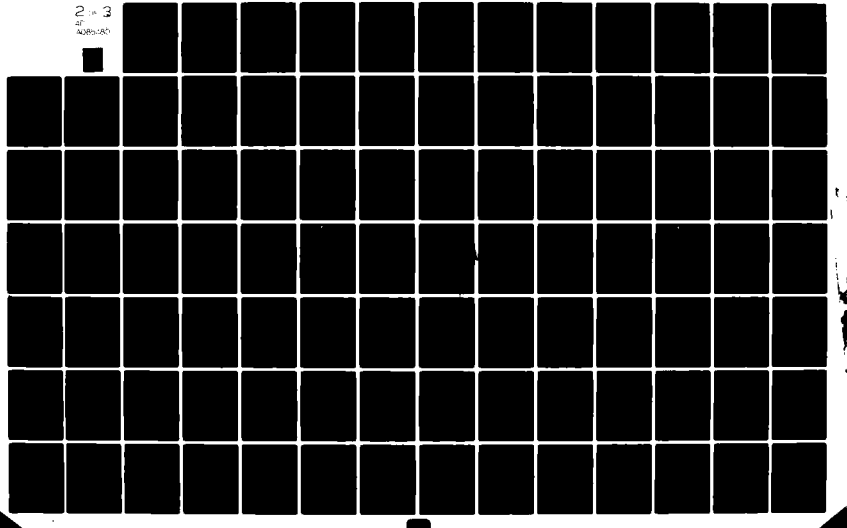

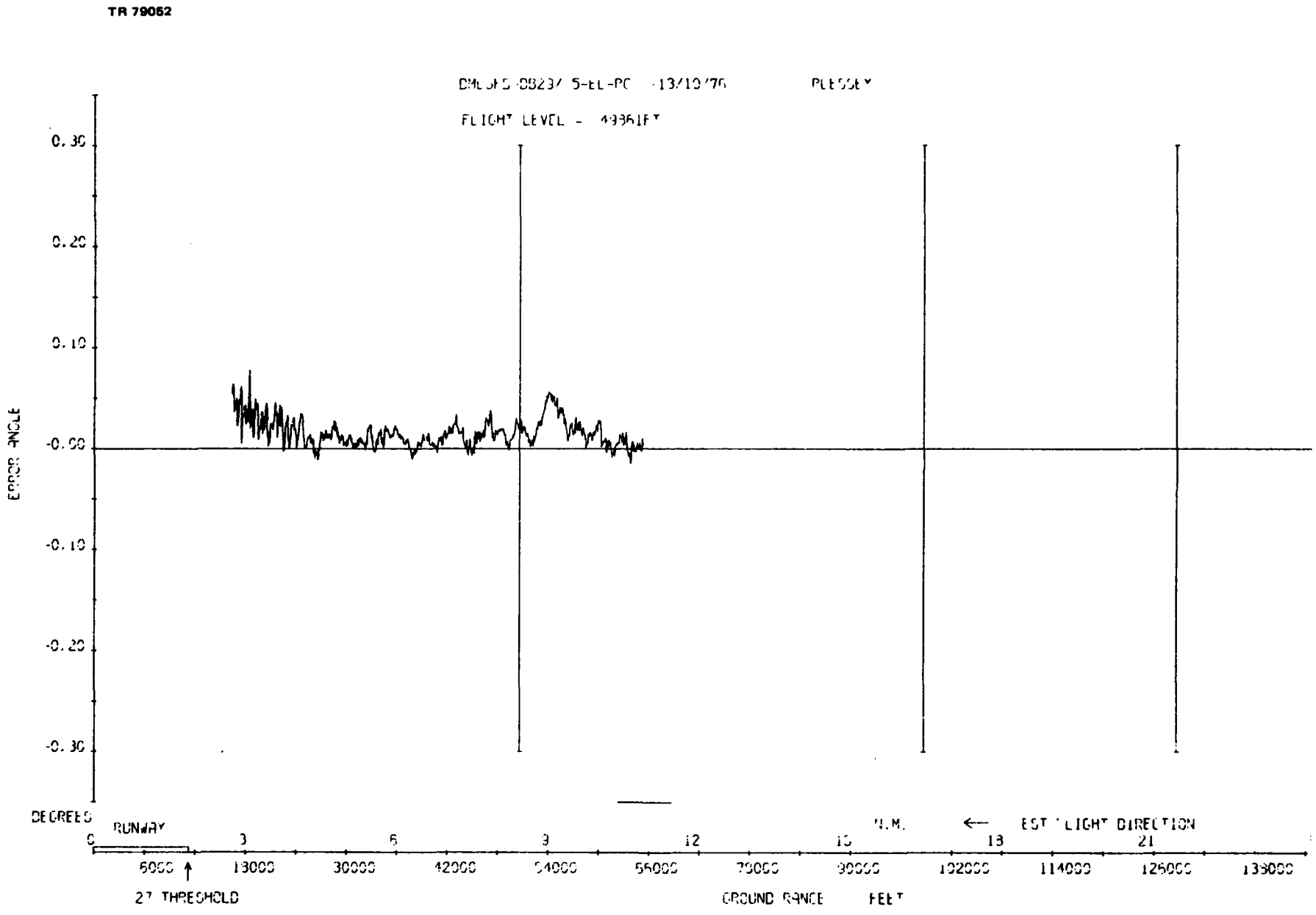

Fig 7.26b

Fig 7.26b Elevation radial at 5000 ft

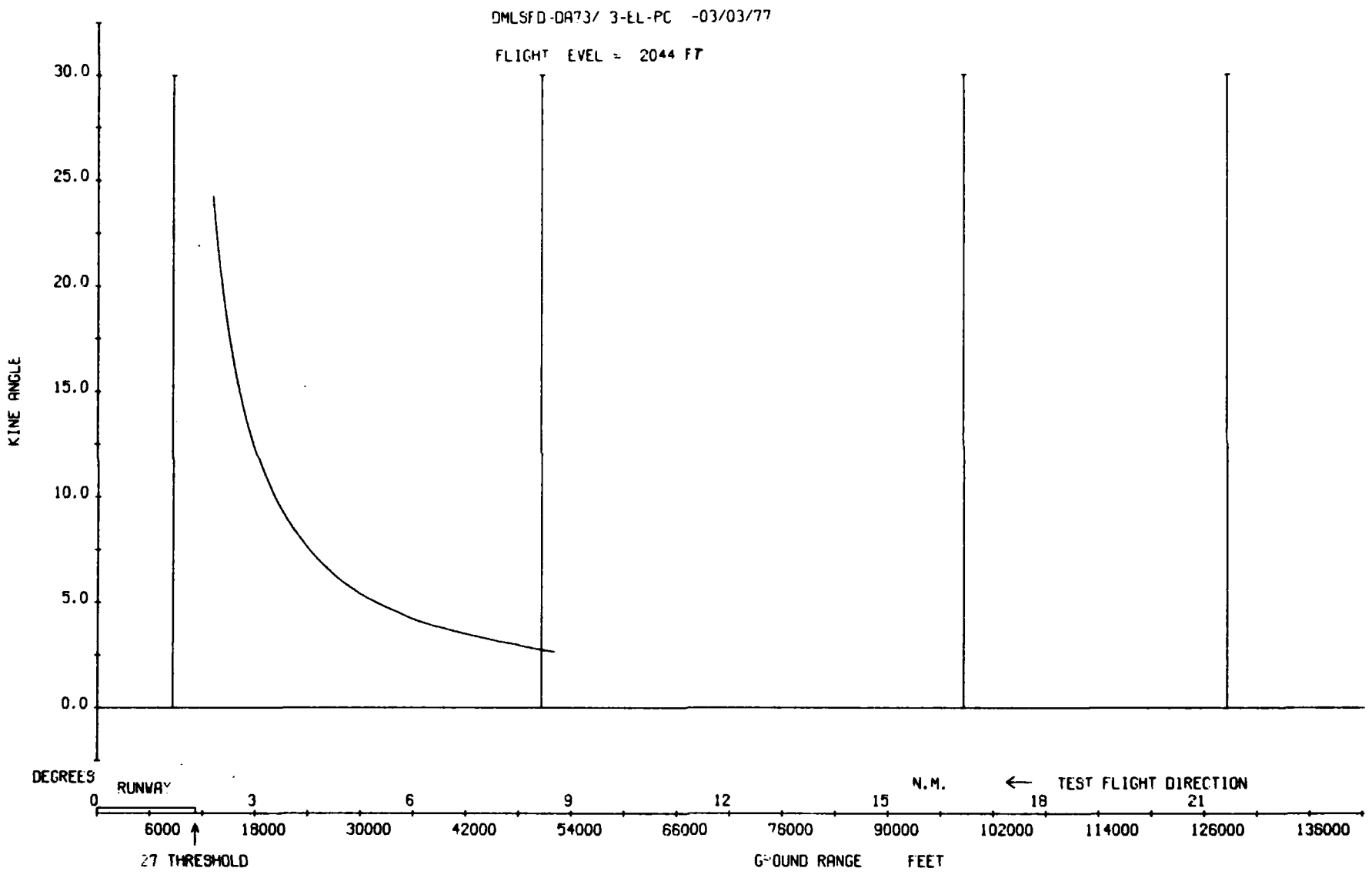

Fig 7.27a

Fig 7.27a Elevation 54λ, constant height radial at 2044 ft

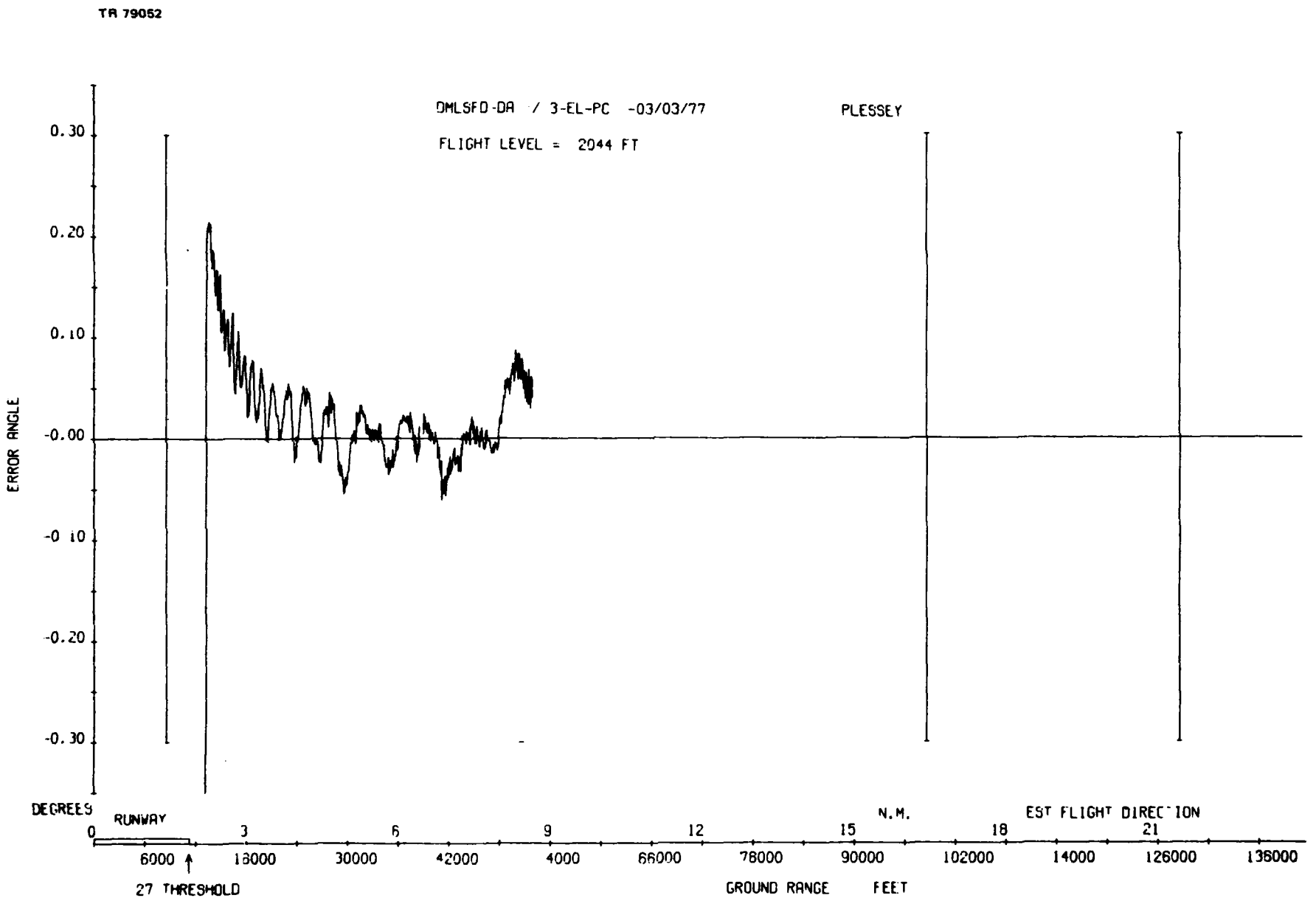

Fig 7.27b Elevation 54λ, constant height radial at 2044 ft

Fig 7.27b

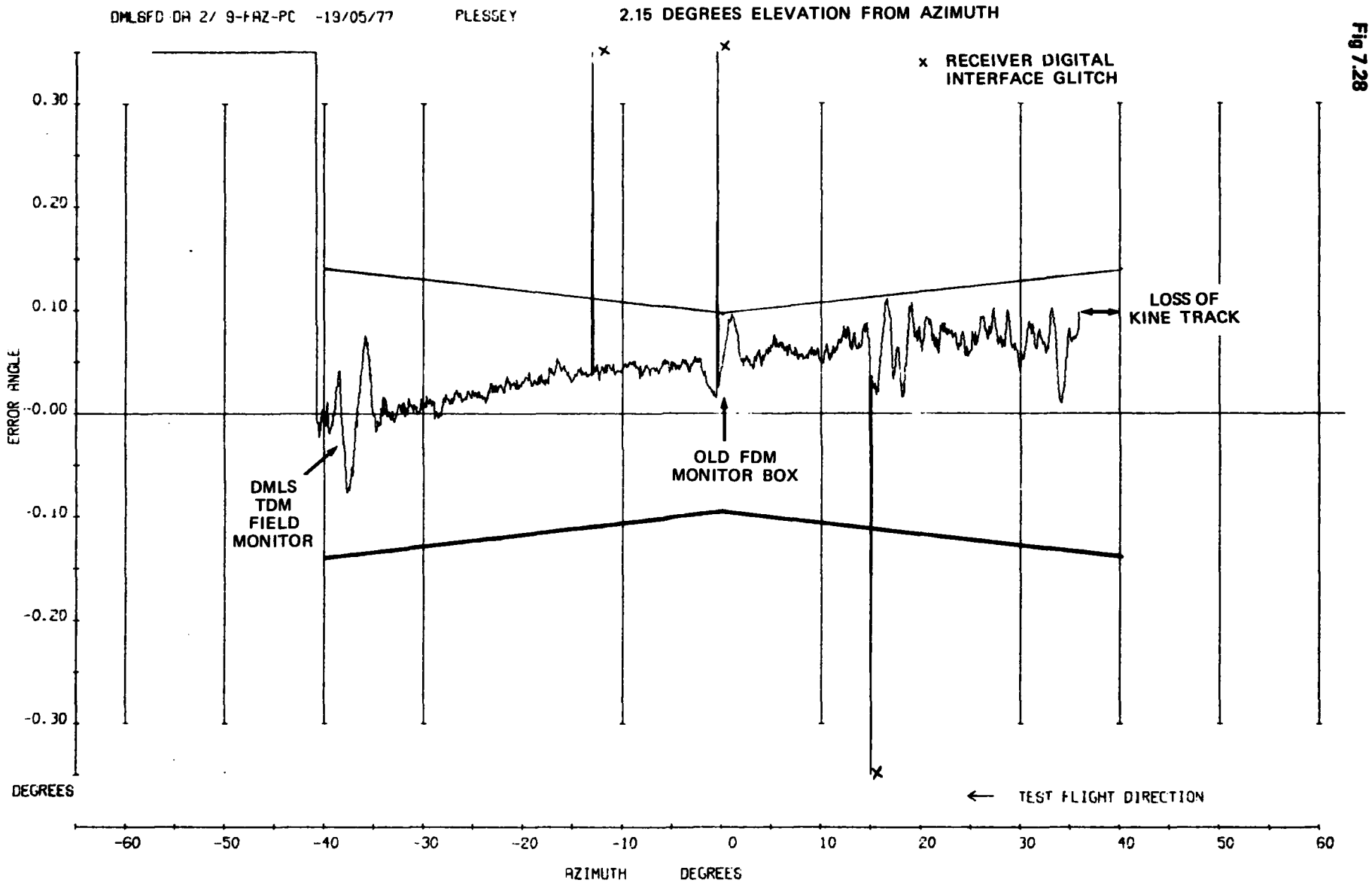

Fig 7.28

Fig 7.28 Azimuth 54λ, part orbit at 6.8 n mile and height 1540 ft

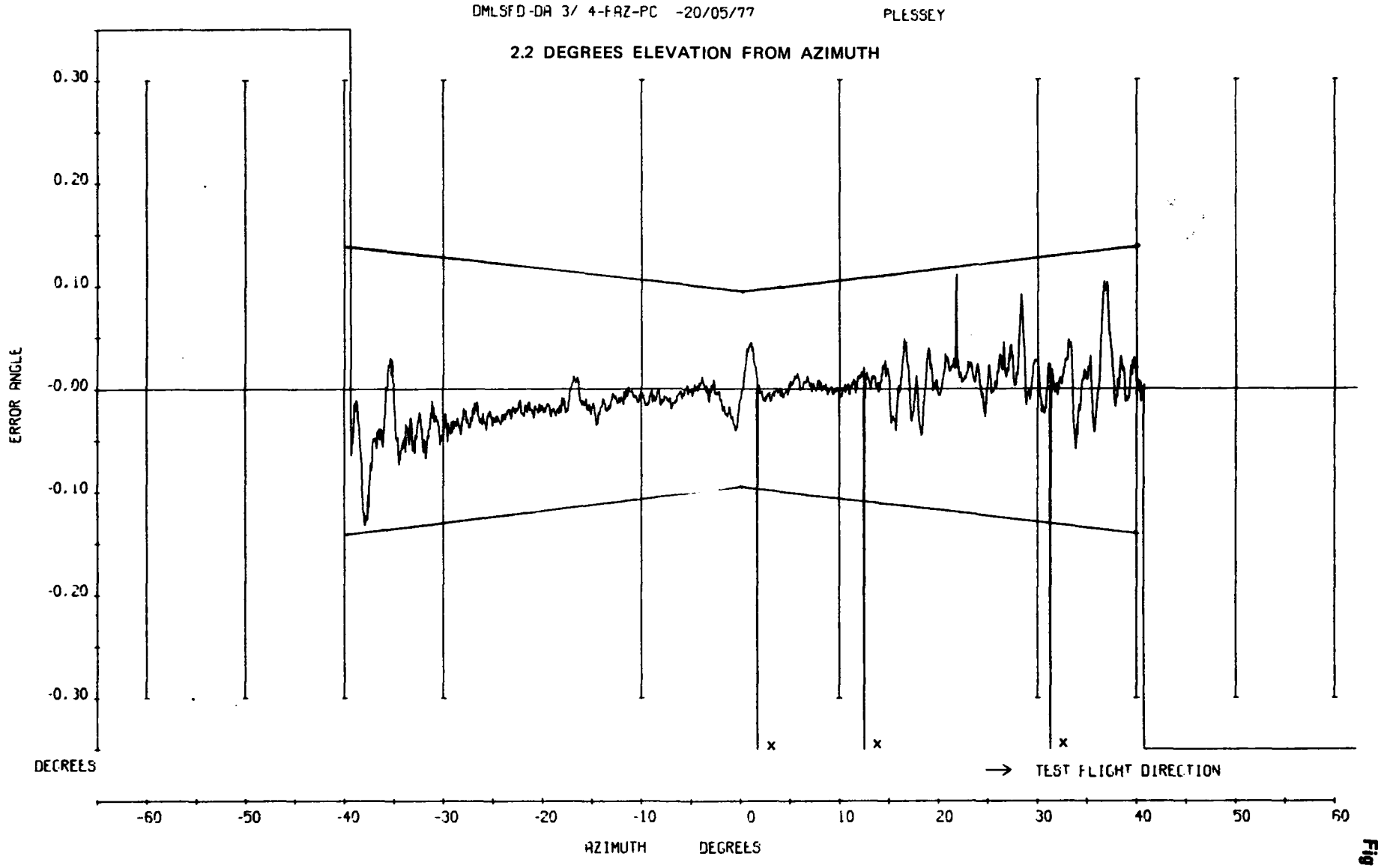

Fig 7.29

Fig 7.29 Azimuth 54λ, part orbit at 6.7 n mile and height 1554 ft

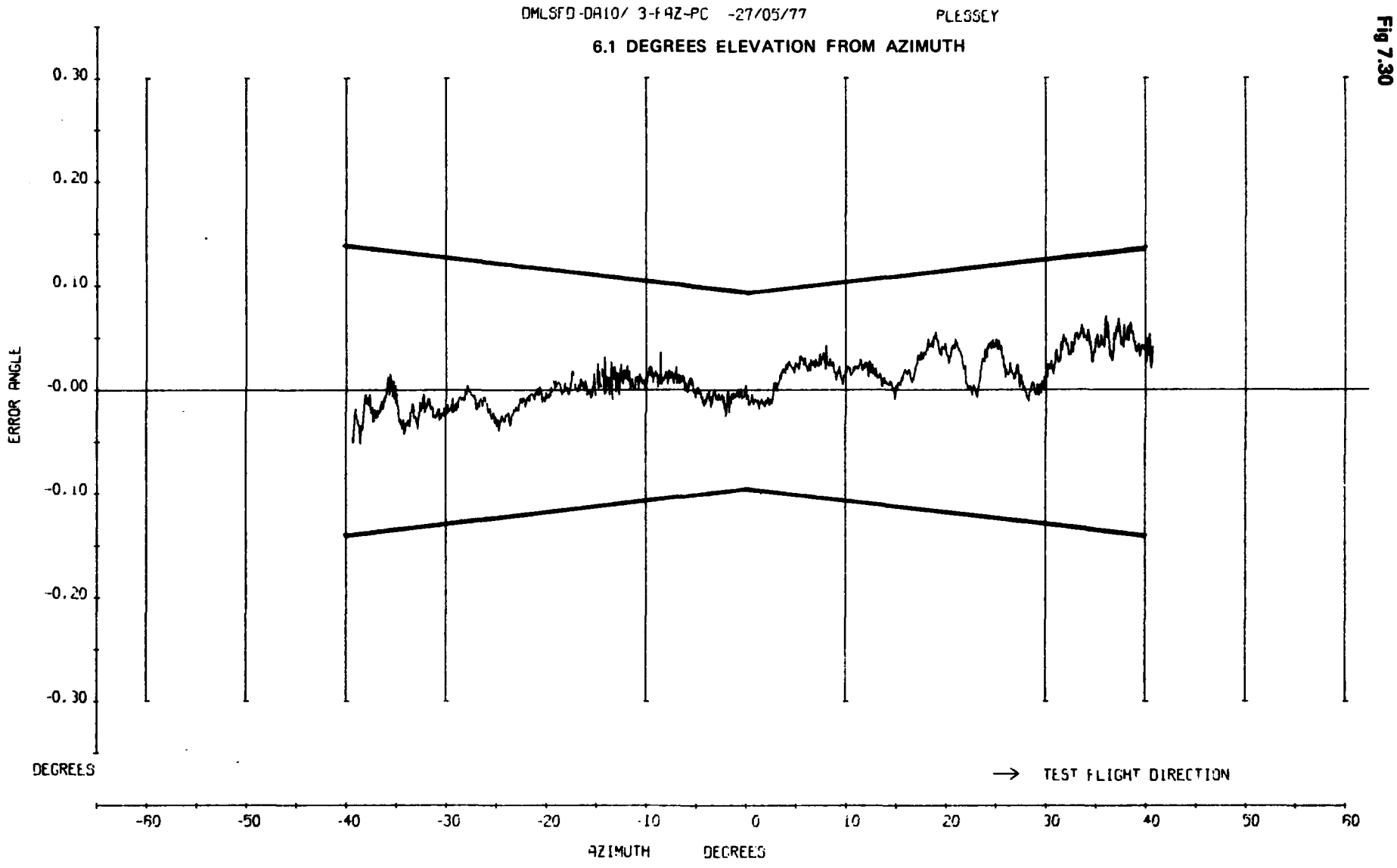

Fig 7.30

Fig 7.30 Azimuth 54λ,part orbit at 6.4 n mile height 4088 ft

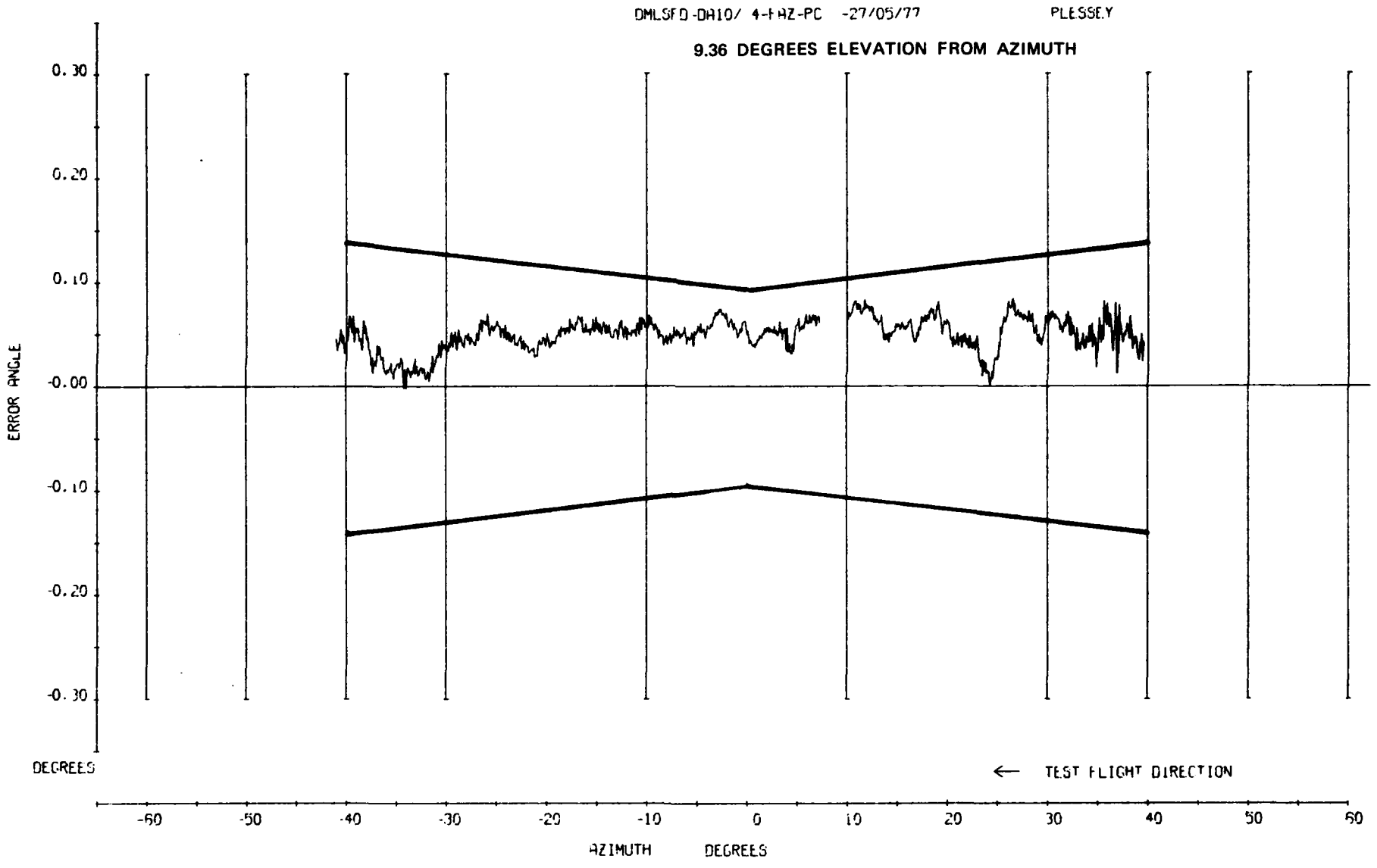

Fig 7.31

Fig 7.31 Azimuth part orbit at 6.5 n mile height 6498 ft

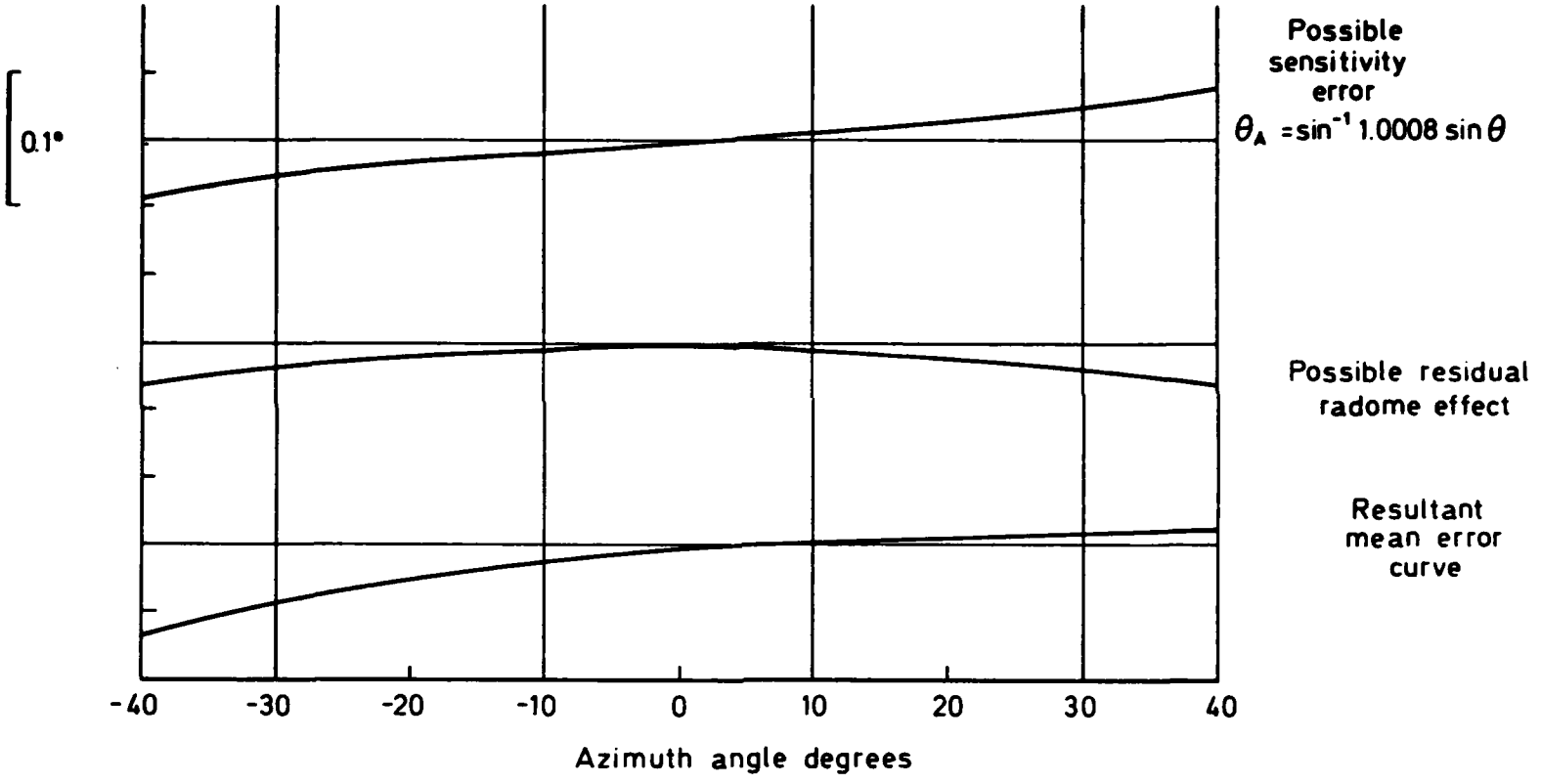

Fig 7.32 Probable source of orbital bias

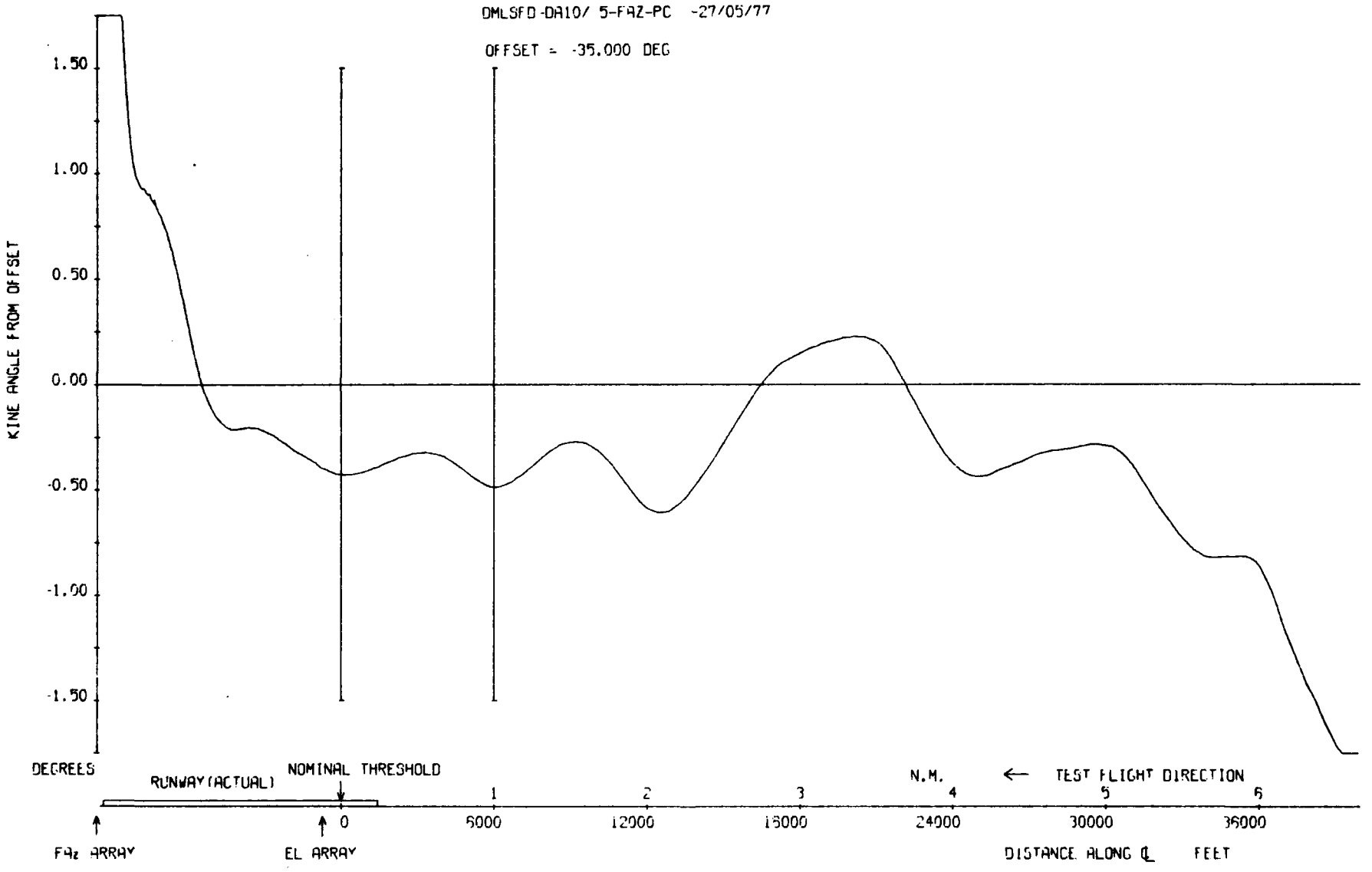

Fig 7.33a

Fig 7.33a Azimuth 54λ,constant height radial at 2000 ft and −35 degrees

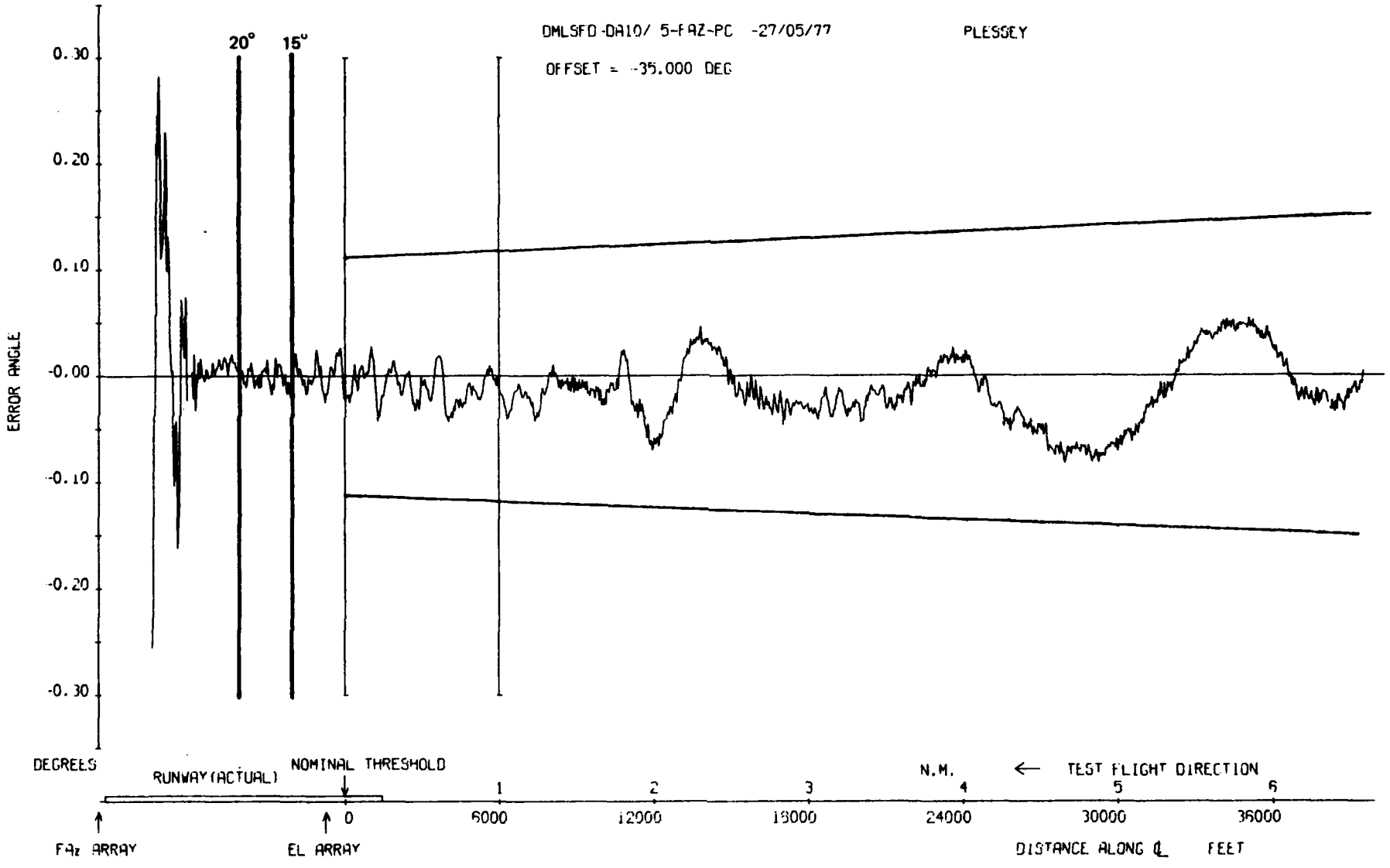

Fig 7.33b

Fig 7.33b Azimuth 54λ,constant height radial at 2000 ft and −35 degrees

TA 79052

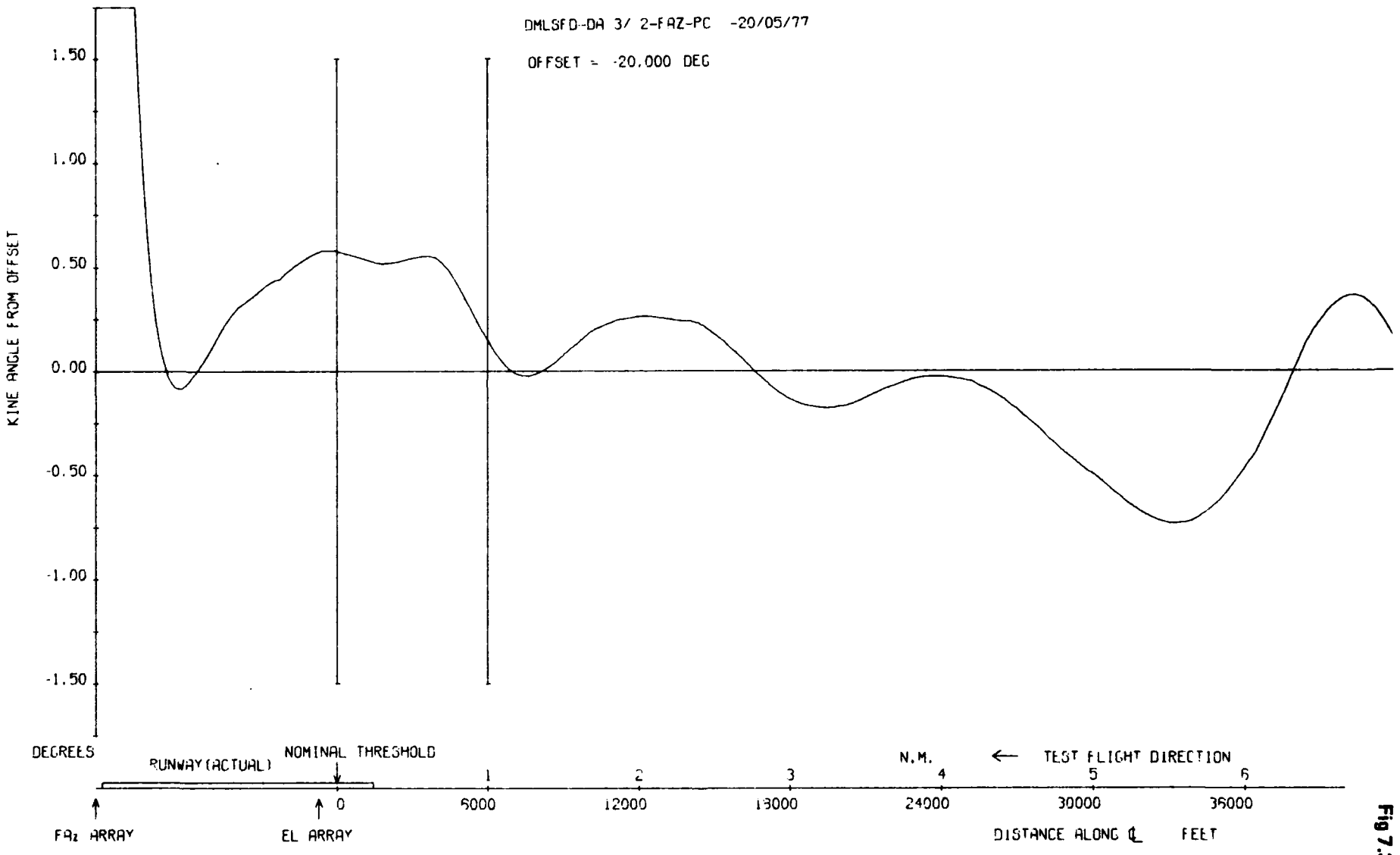

Fig 7.34a

Fig 7.34a Azimuth 54λ, constant height radial at 2000 ft and −20 degrees

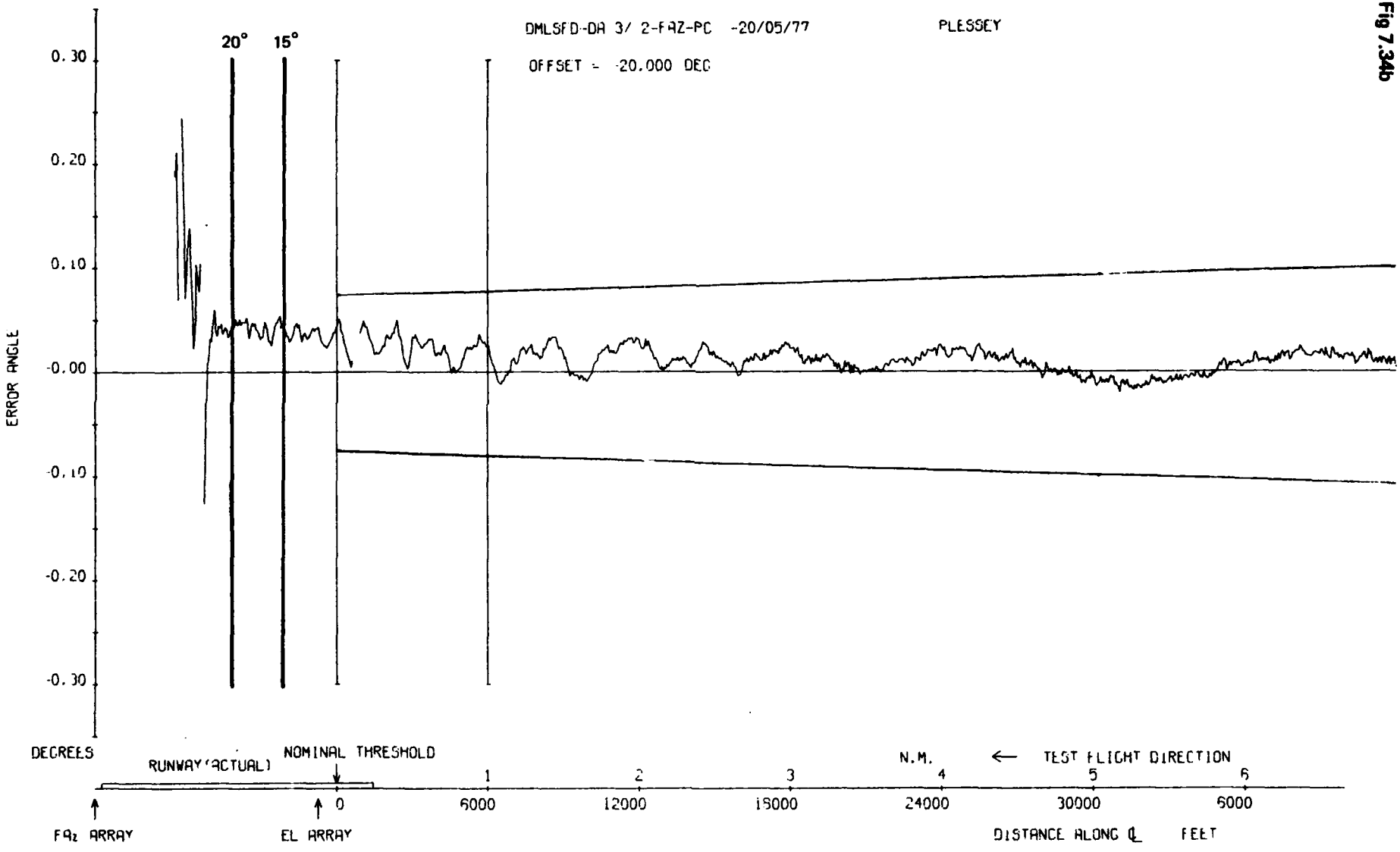

Fig 7.34b

Fig 7.34b Azimuth 54λ, constant height radial at 2000 ft and −20 degrees

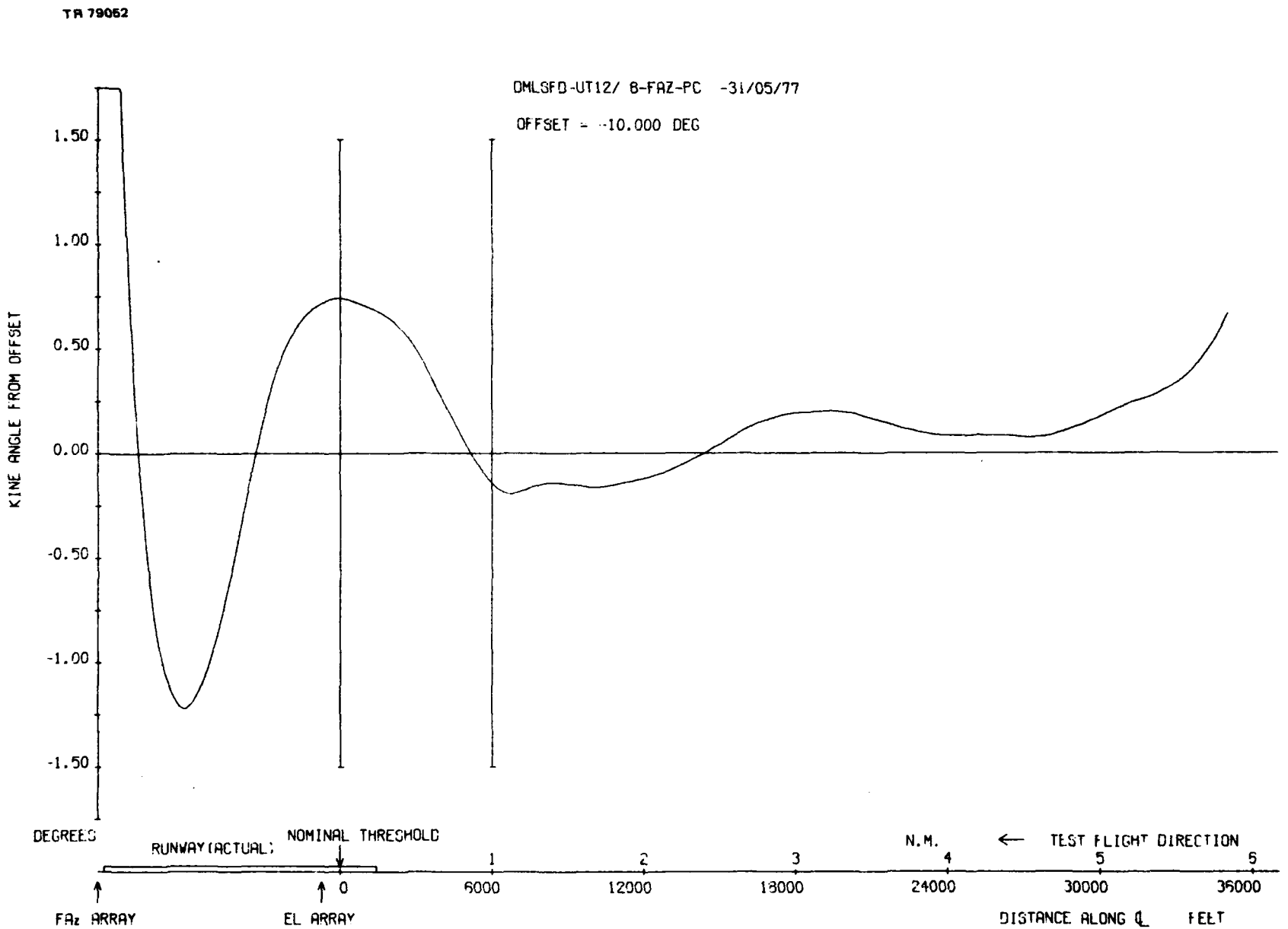

Fig 7.35a Azimuth 54λ, constant height radial at 2000 ft and −10 degrees

Fig 7.35a

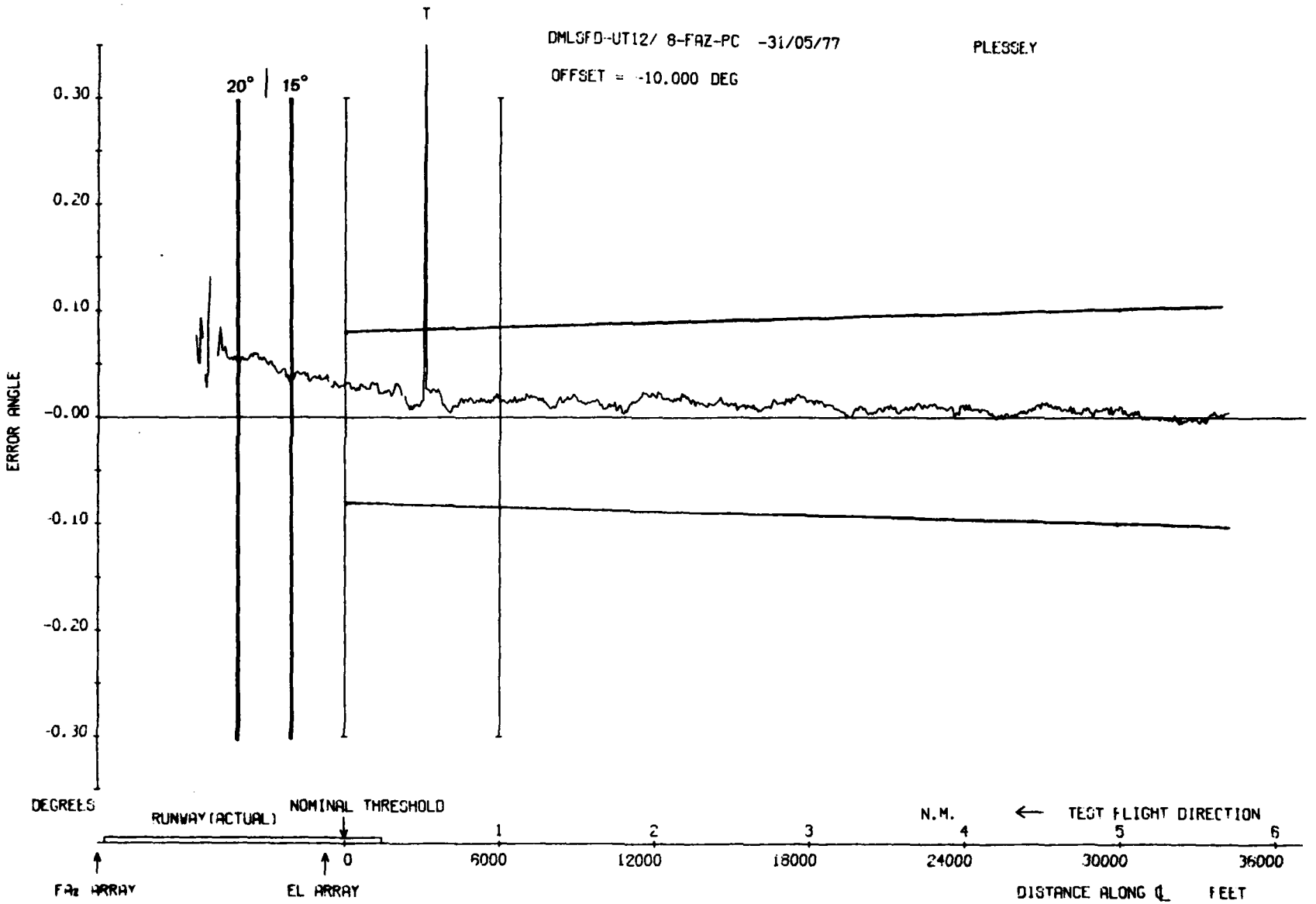

Fig 7.35b Azimuth 54λ, constant height radial at 2000 ft and −10 degrees

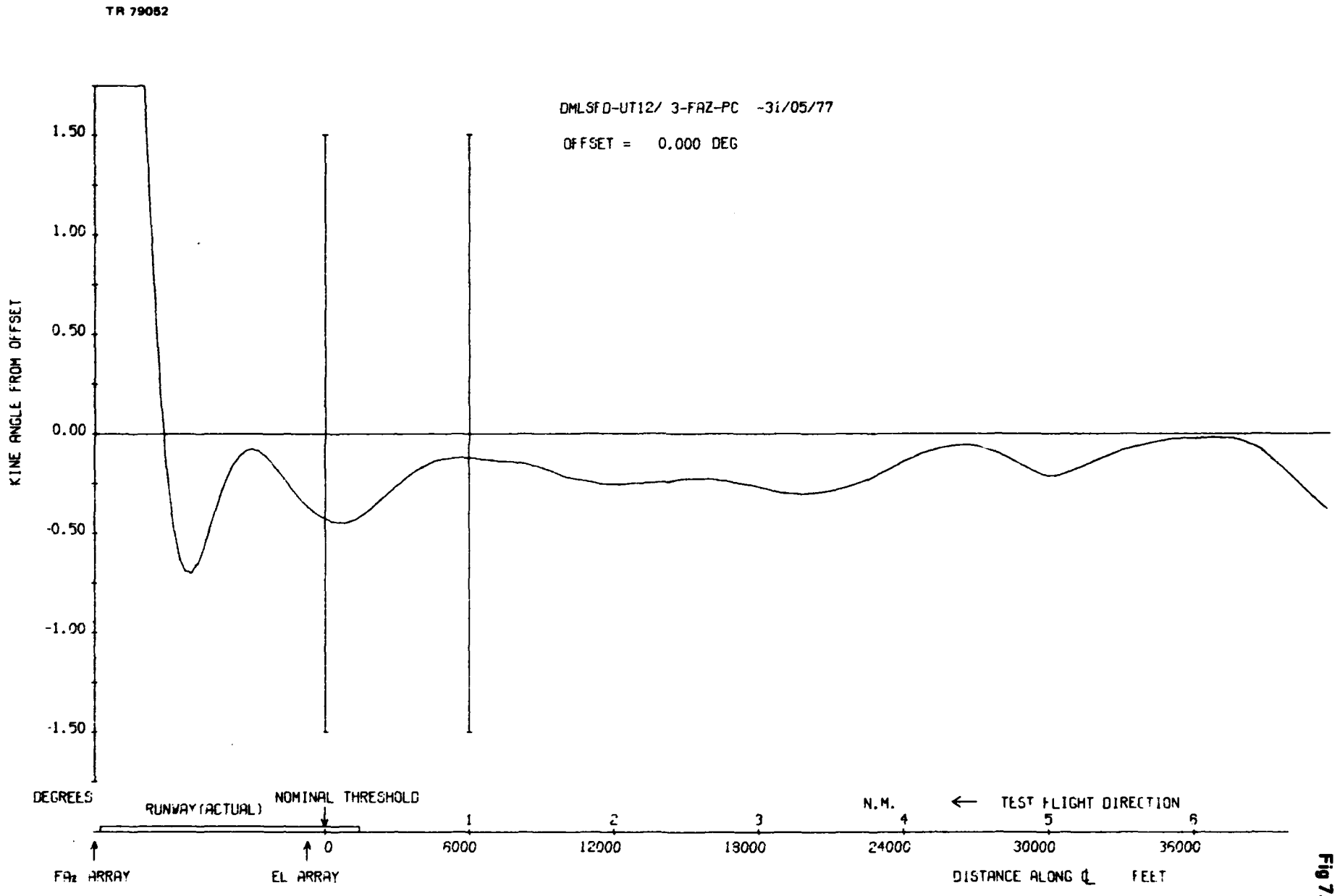

Fig 7.36a

Fig 7.36a Azimuth 54λ, constant height radial at 2000 ft on centre line

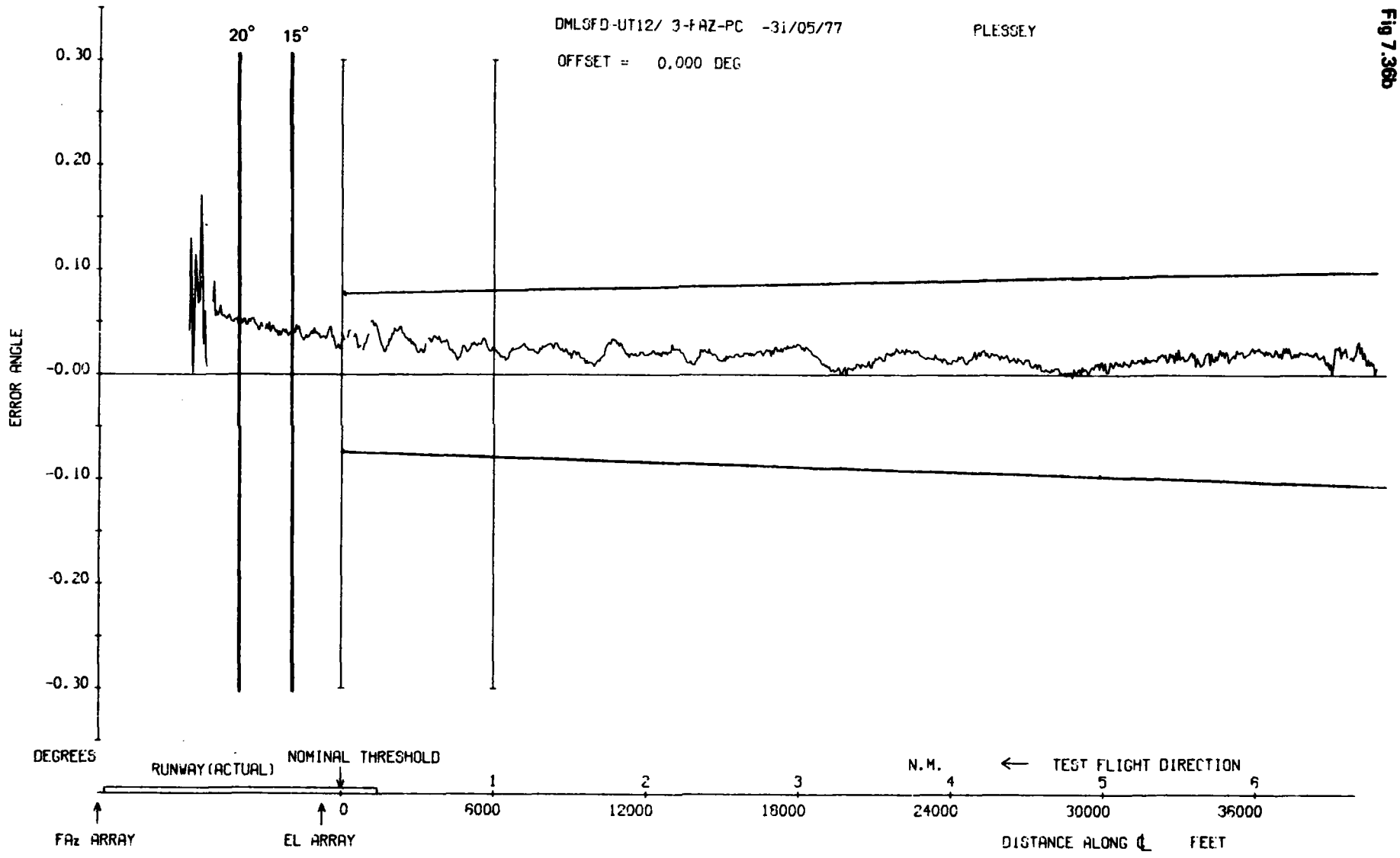

Fig 7.36b

Fig 7.36b Azimuth 54λ, constant height radial at 2000 ft on centre line

TR 79052

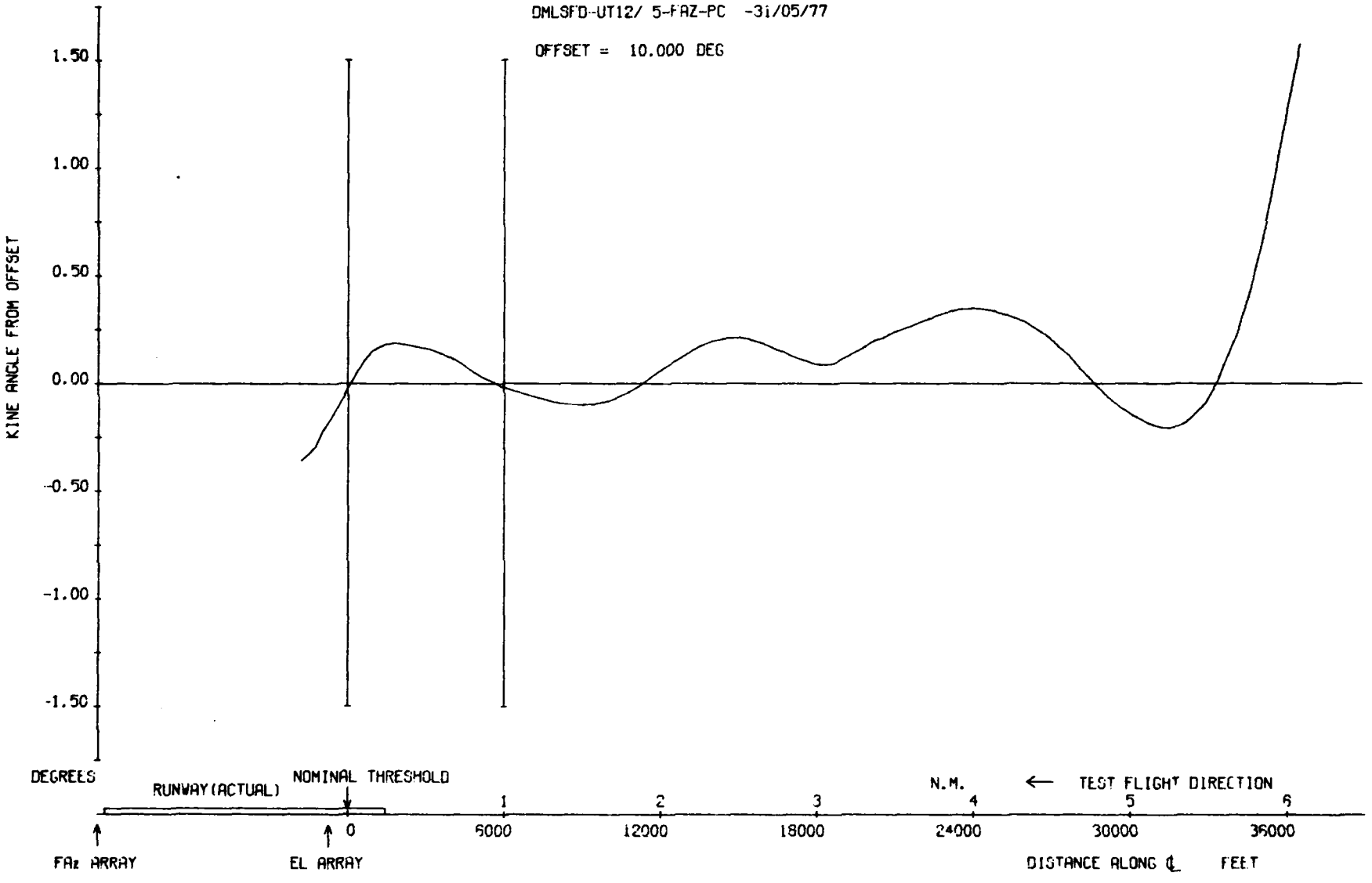

Fig 7.37a

Fig 7.37a Azimuth 54λ, constant height radial at 2000 ft and +10 degrees

Fig 7.37b

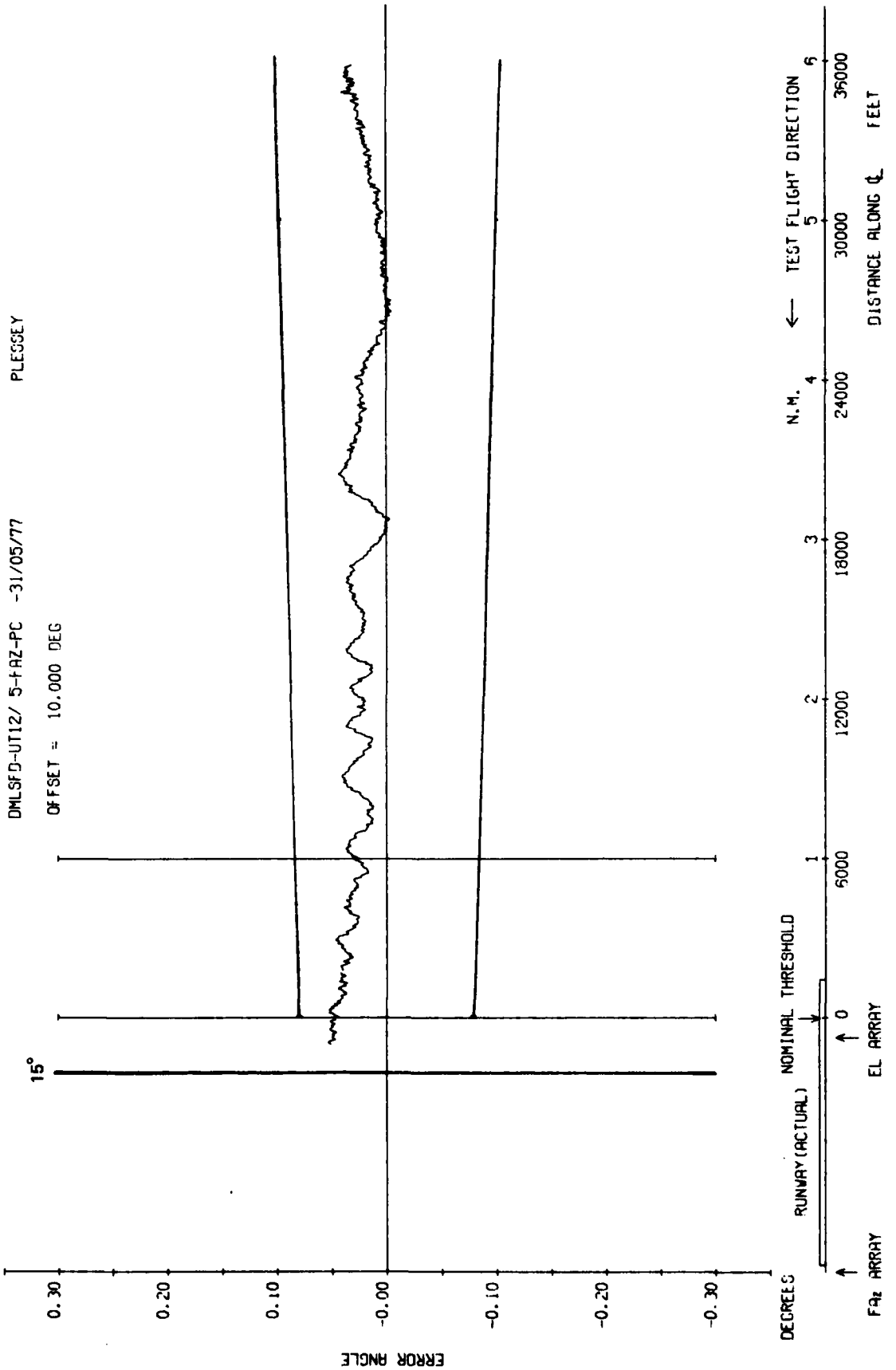

Fig 7.37b Azimuth 54λ, constant height radial at 2000 ft and +10 degrees

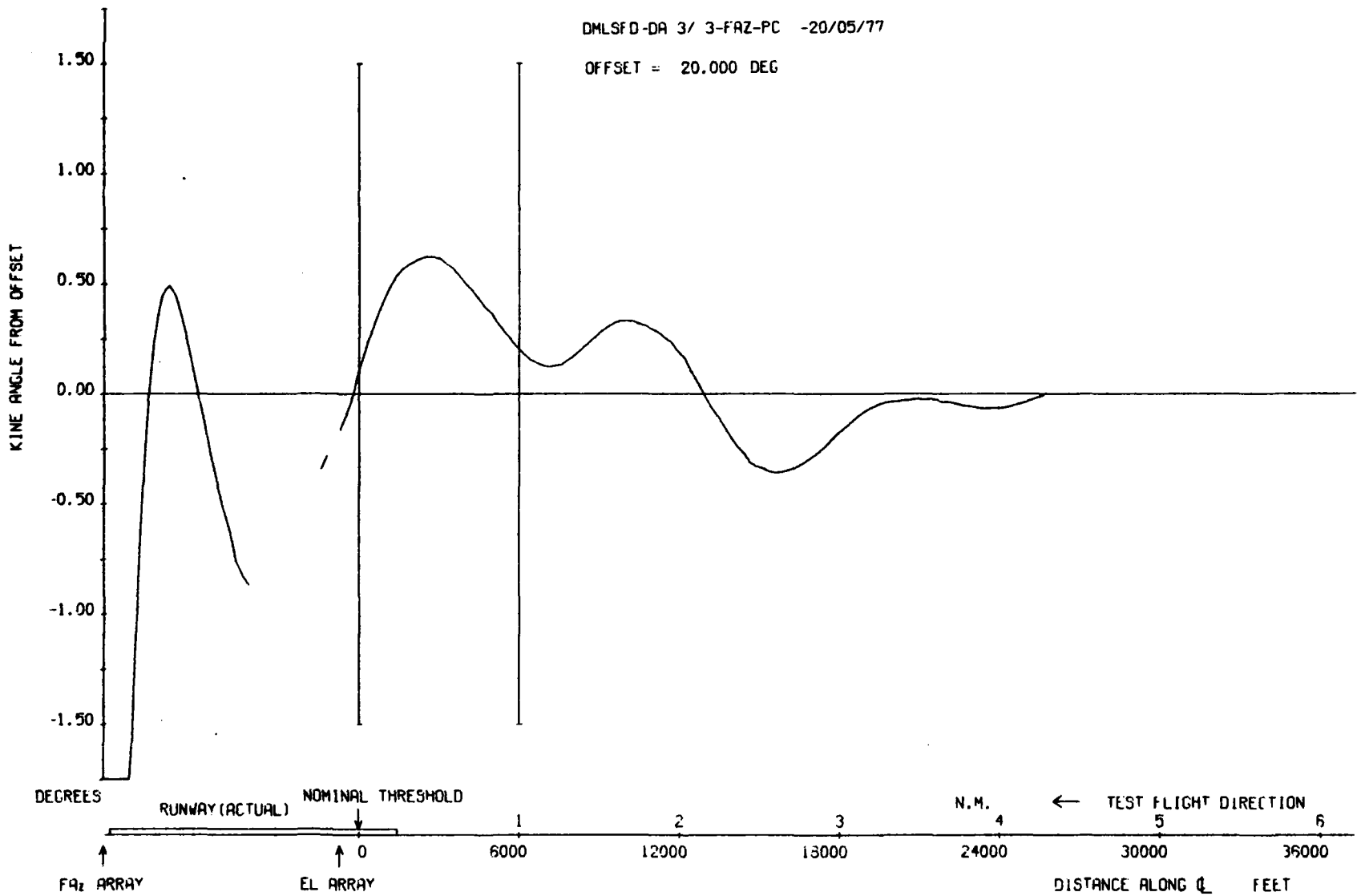

Fig 7.38a Azimuth 54λ, constant height radial at 2000 ft and +20 degrees

Fig 7.38a

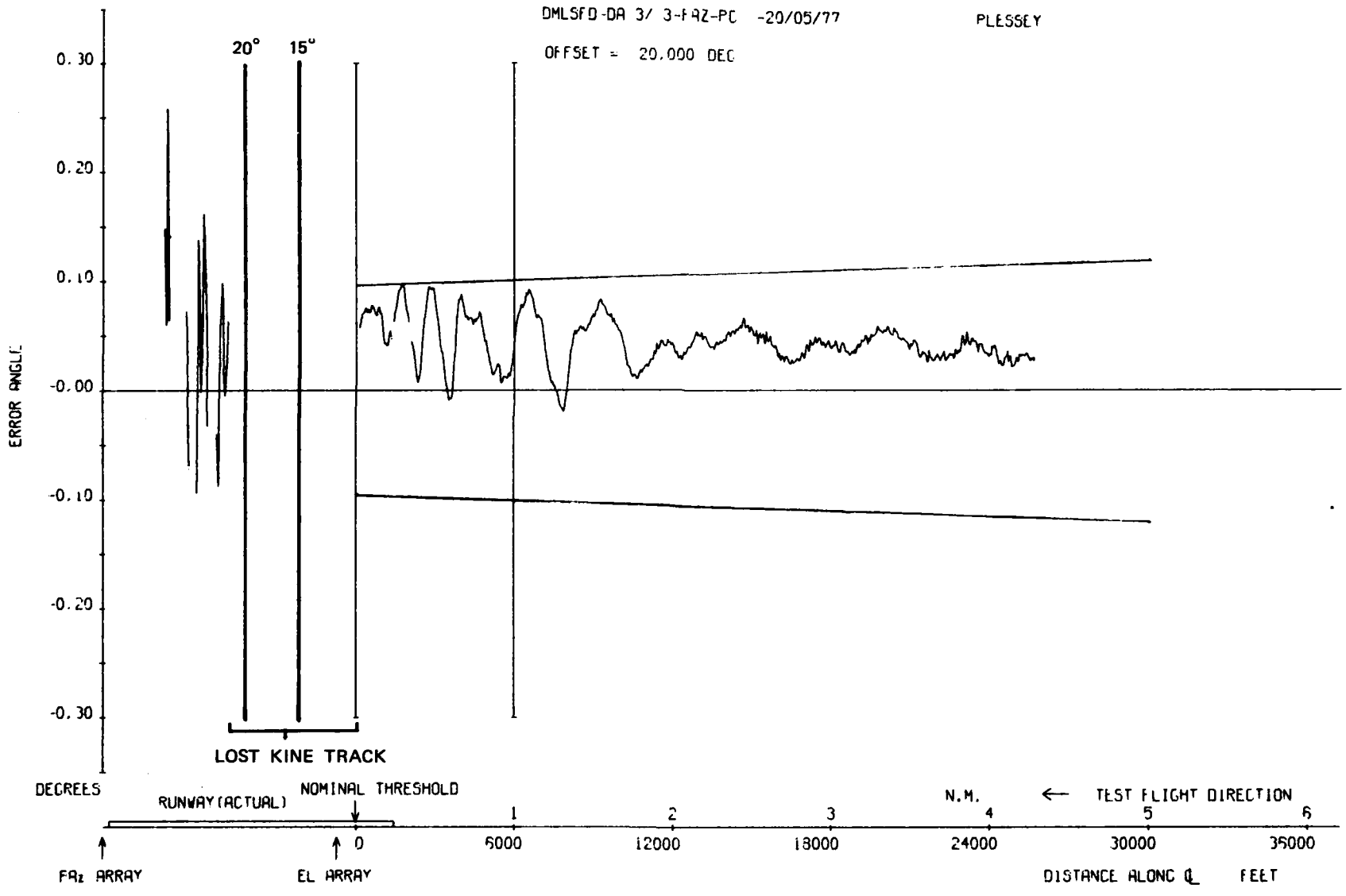

Fig 7.38b

Fig 7.38b Azimuth 54λ,constant height radial at 2000 ft and +20 degrees

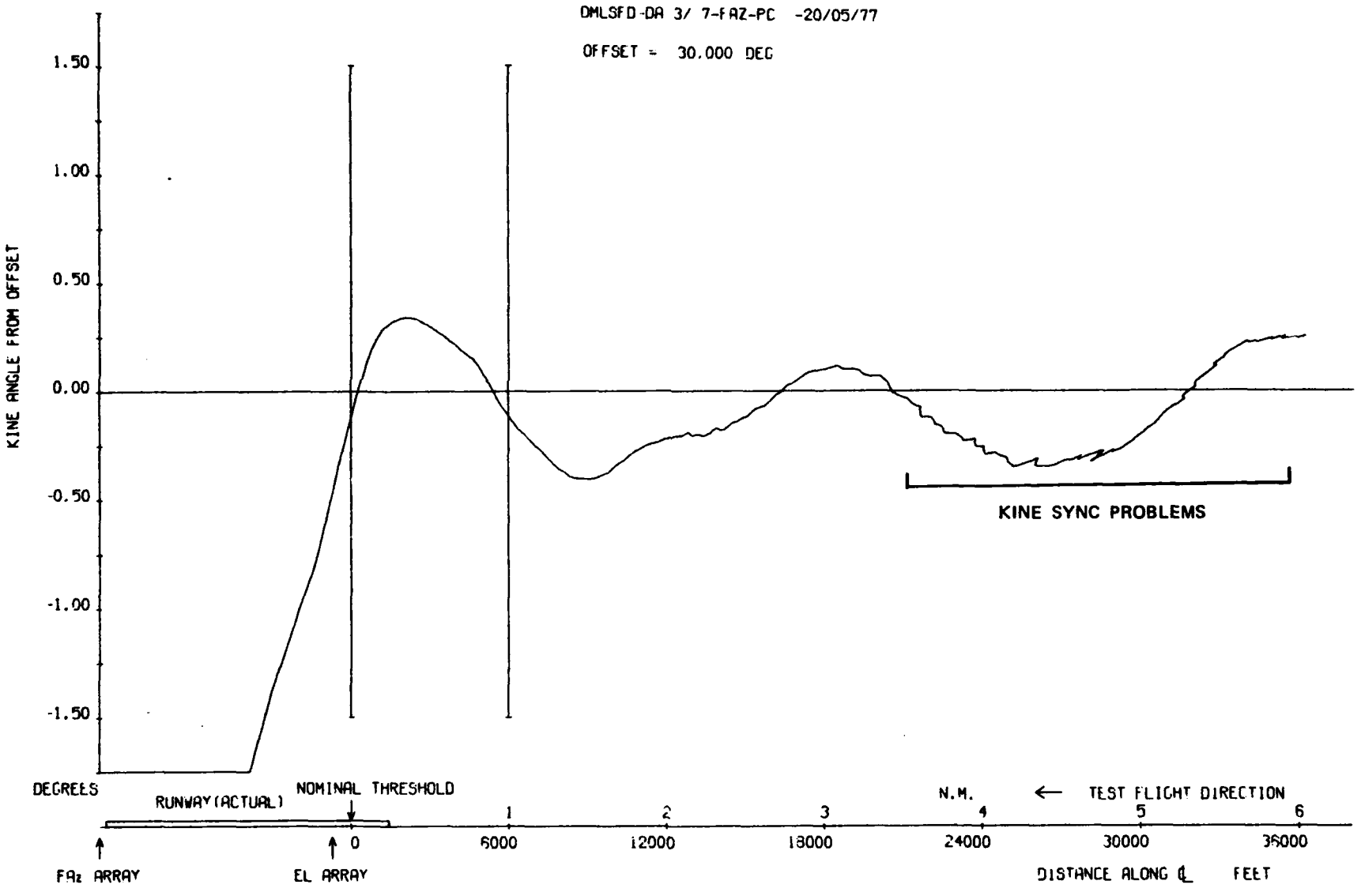

Fig 7.39a Azimuth 54λ, constant height radial at 2000 ft and +30 degrees

Fig 7.39a

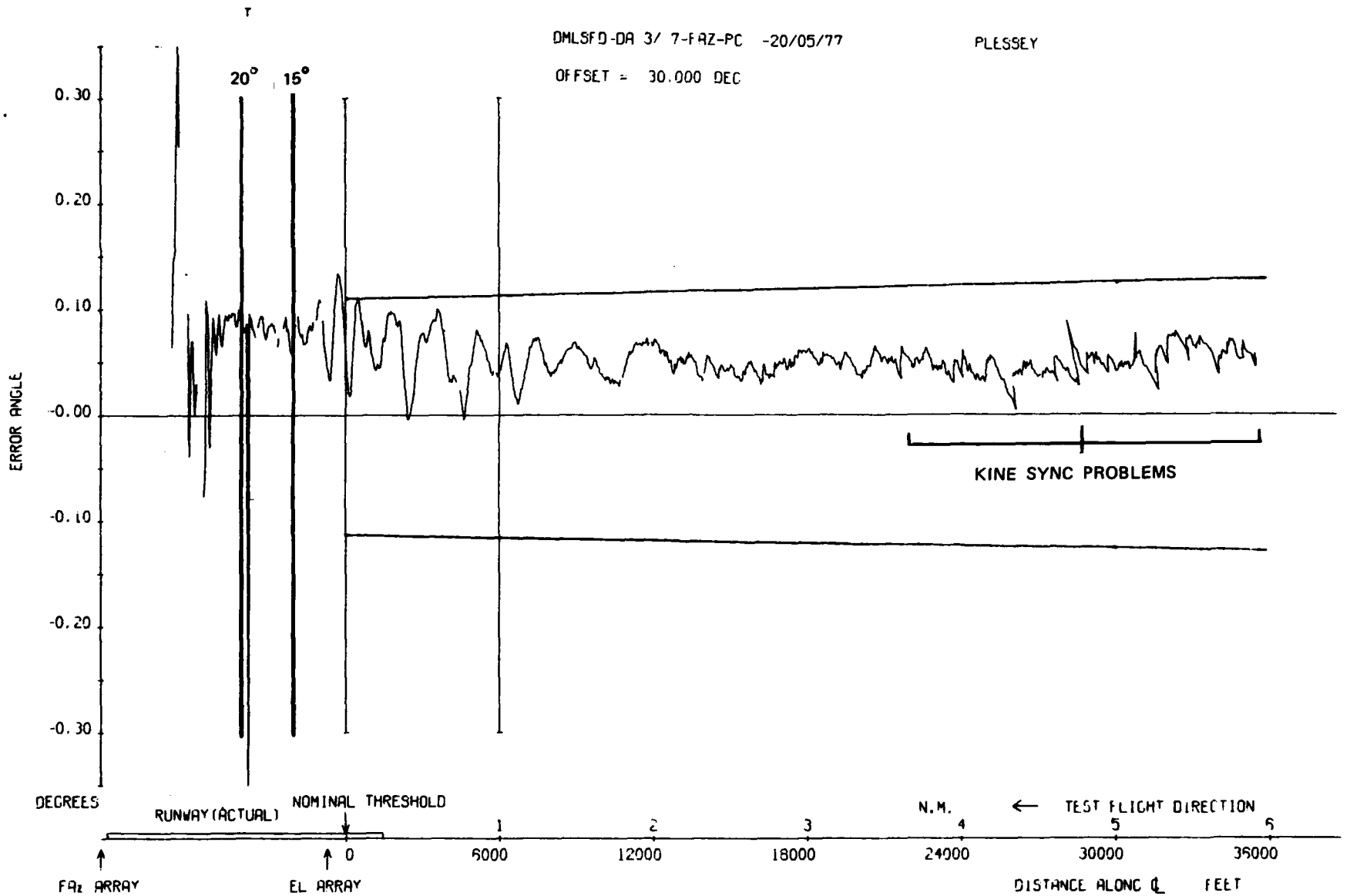

Fig 7.39b

Fig 7.39b Azimuth 54λ, constant height radial at 2000 ft and +30 degrees

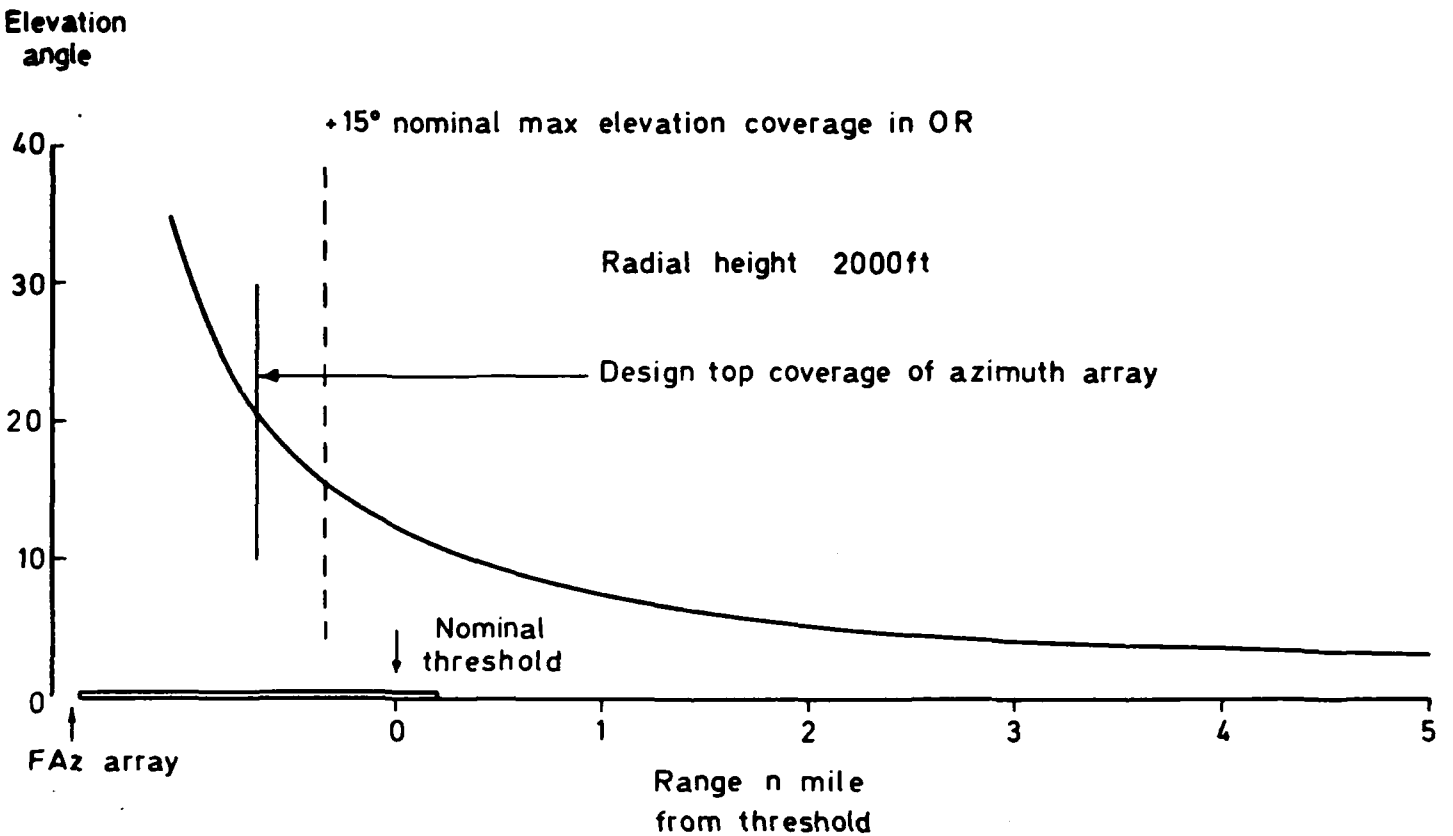

Fig 7.40 Elevation from azimuth array as function of range for radial flights

Fig 7.40

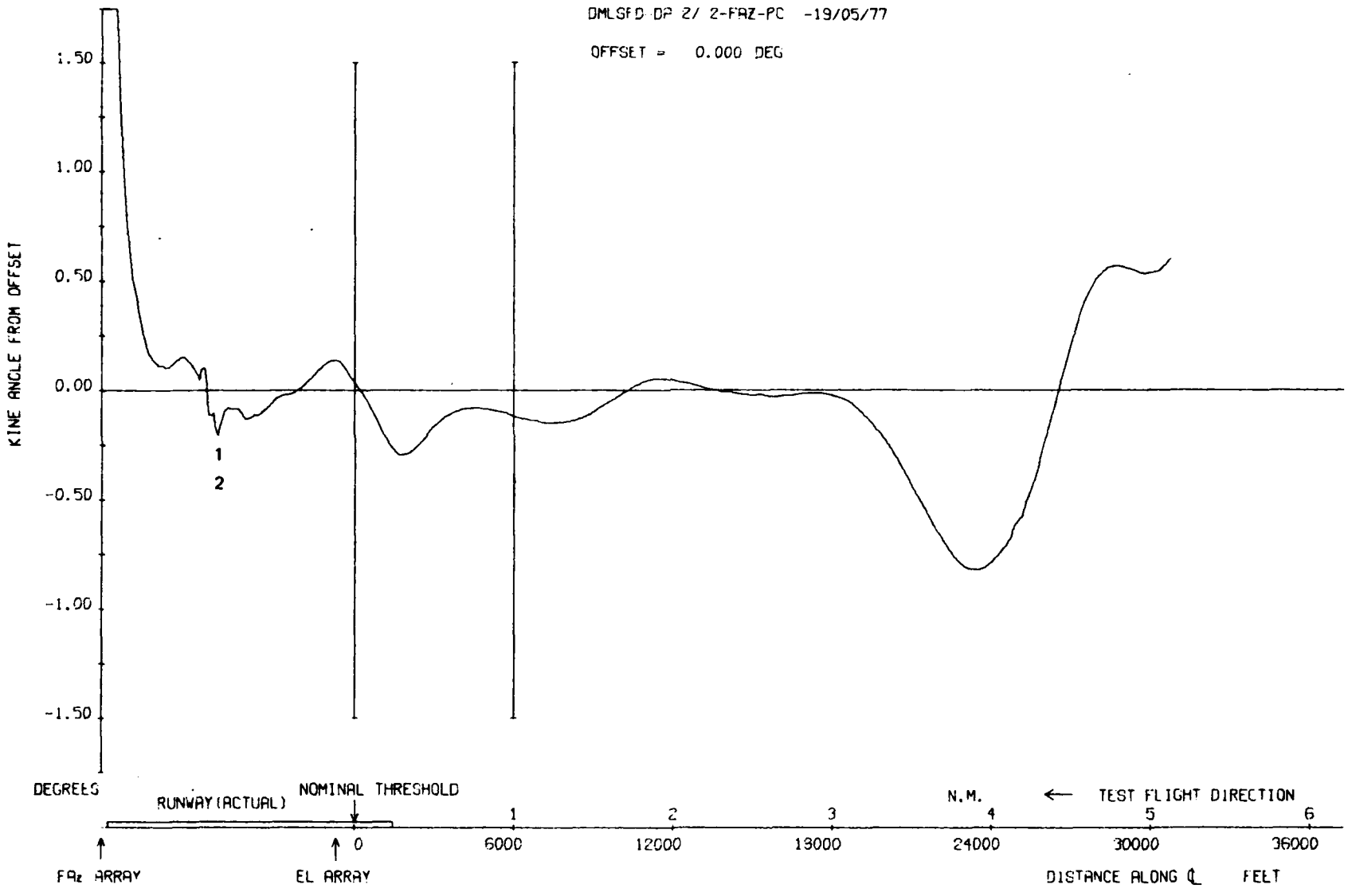

Fig 7.41a

Fig 7.41a Azimuth 54λ,3 degree approach to touch and go

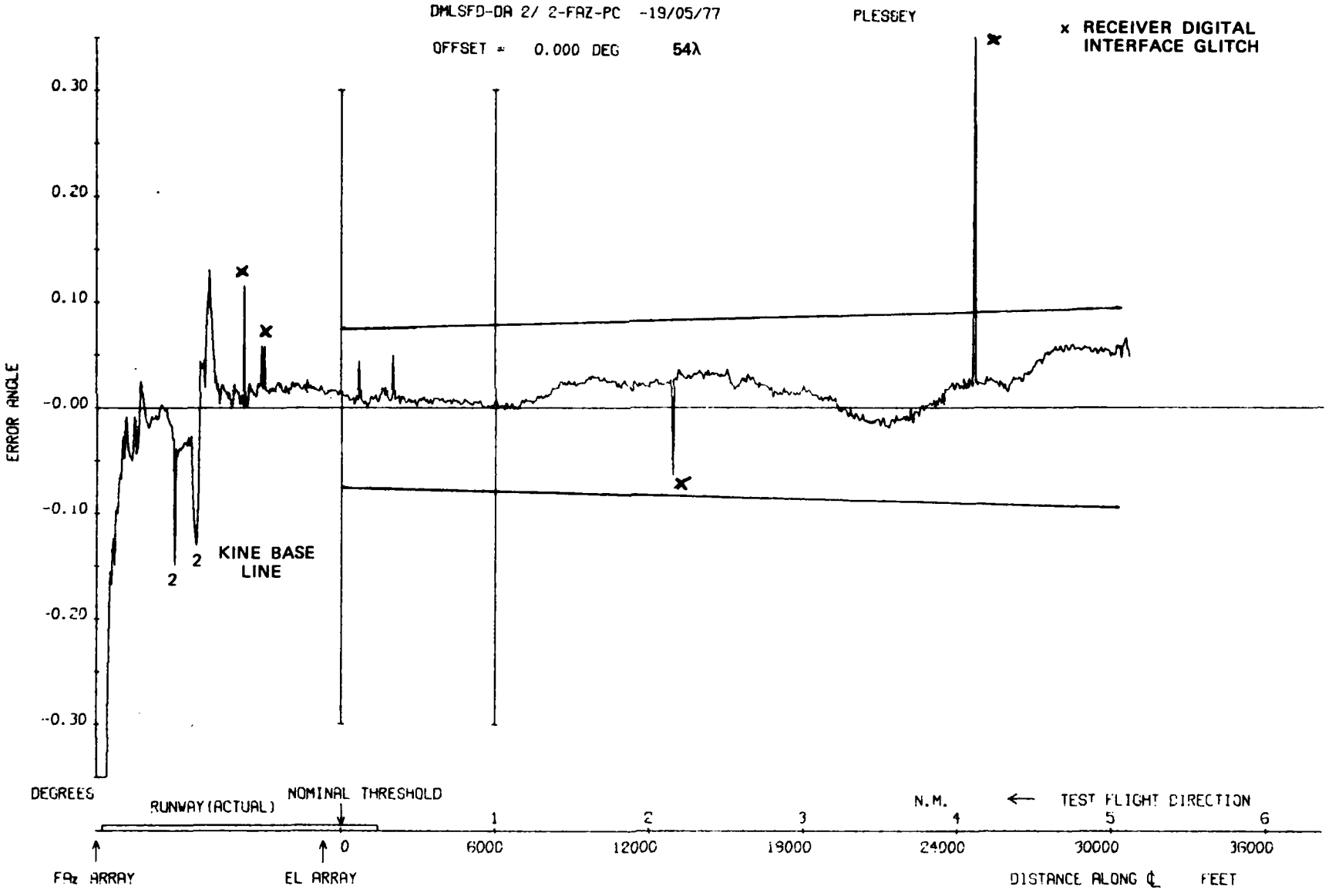

Fig 7.41c Azimuth 54λ,3 degree approach to touch and go

Fig 7.41c

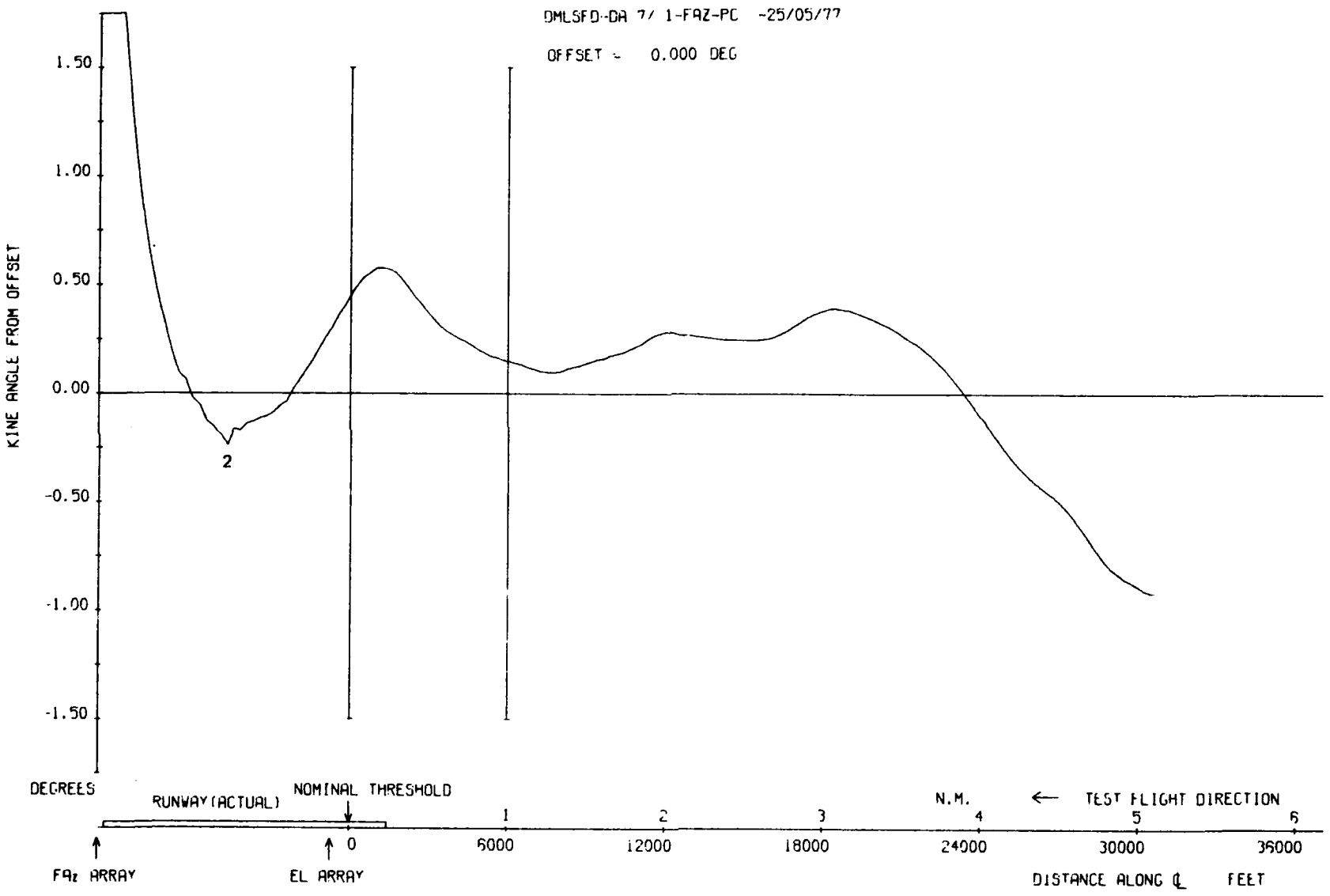

Fig 7.42a

Fig 7.42a Azimuth 54λ,3 degree approach to 300 ft overshoot

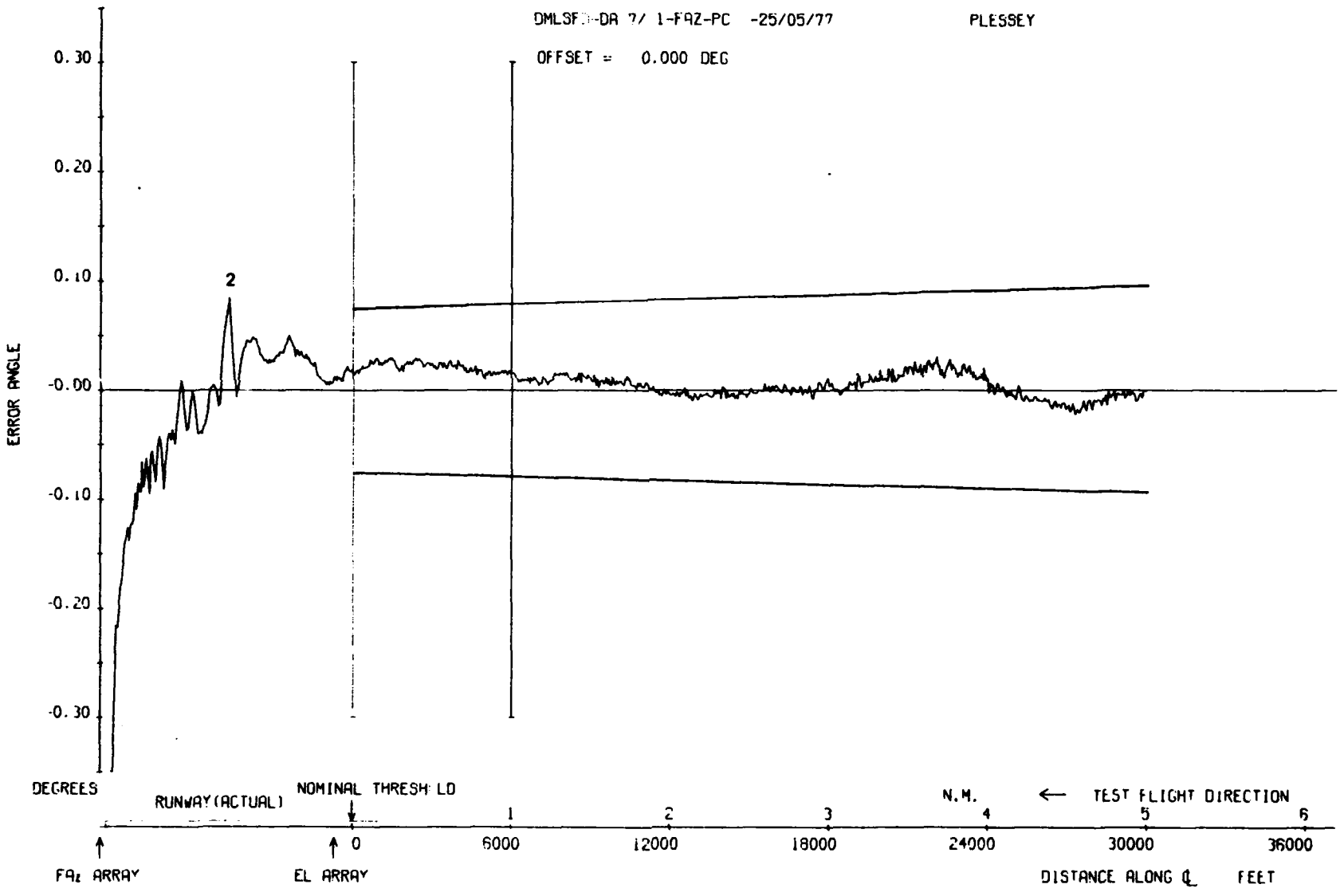

Fig 7.42c

Fig 7.42c Azimuth 54λ,3 degree approach to 300 ft overshoot

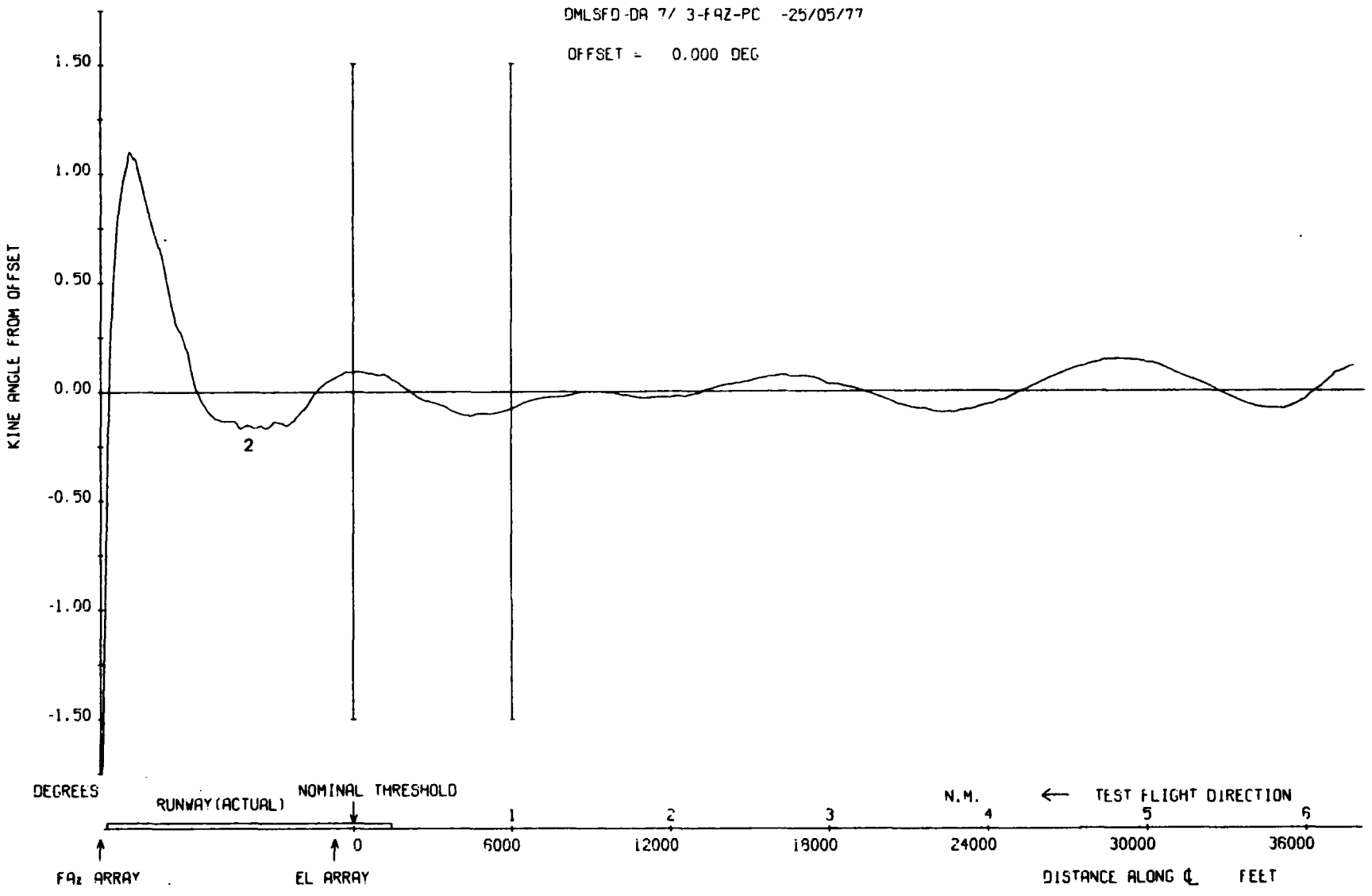

Fig 7.43a Azimuth 54λ, 1.5 degree approach to 300 ft overshoot

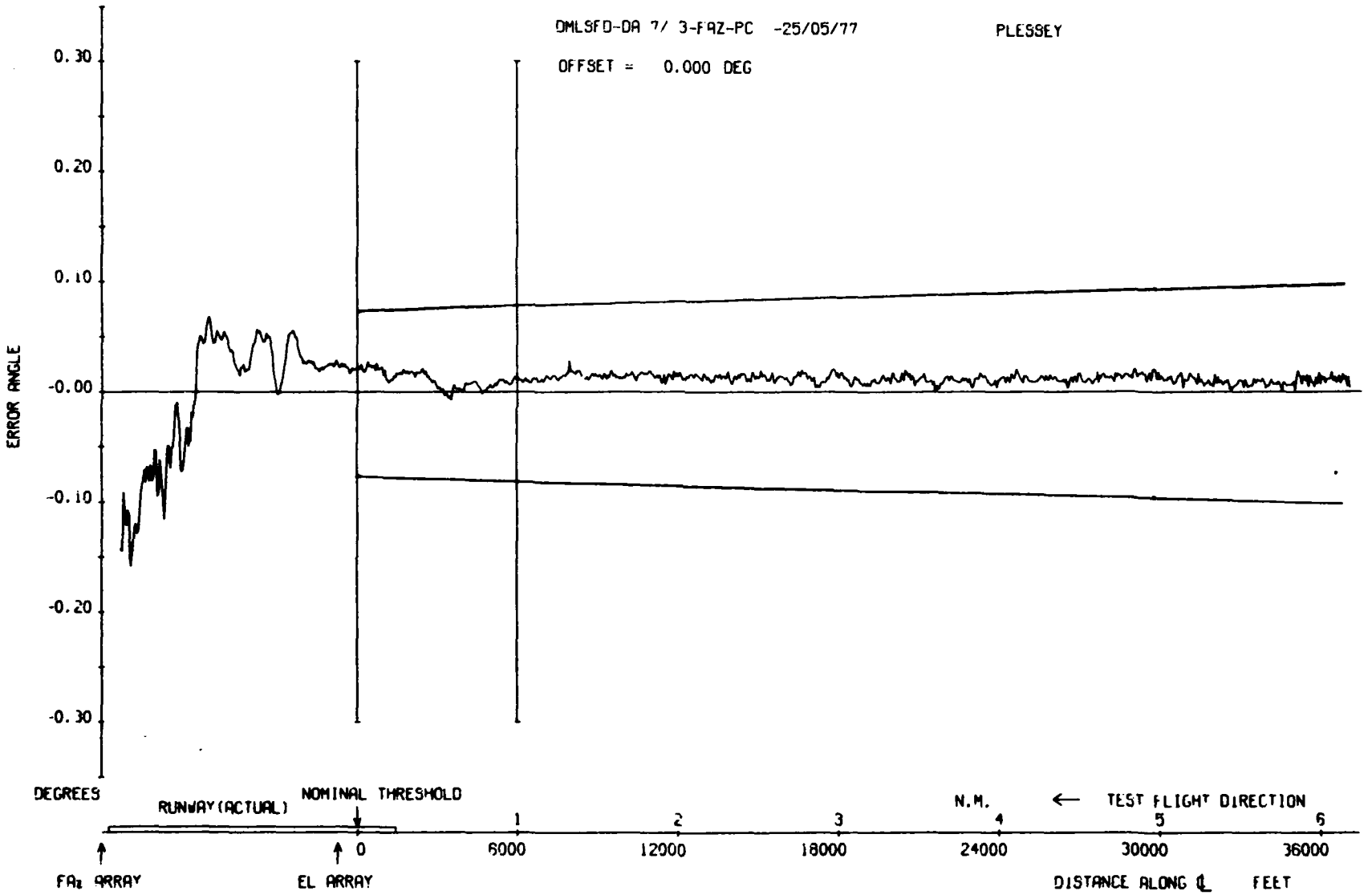

Fig 7.43c Azimuth 54λ, 1.5 degree approach to 300 ft overshoot

Fig 7.43c

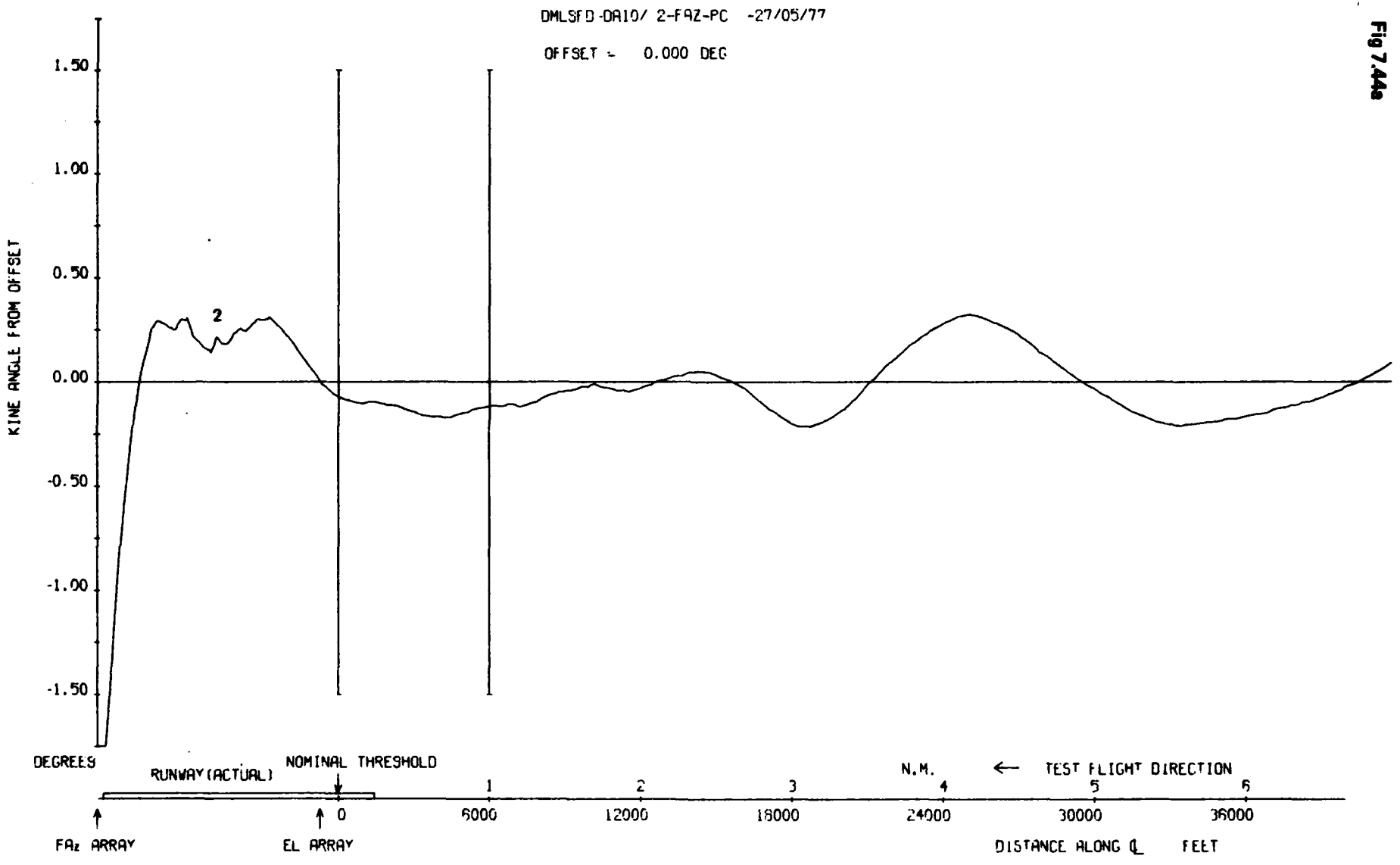

Fig 7.44a

Fig 7.44a Azimuth 54λ,3 degree approach to 300 ft overshoot

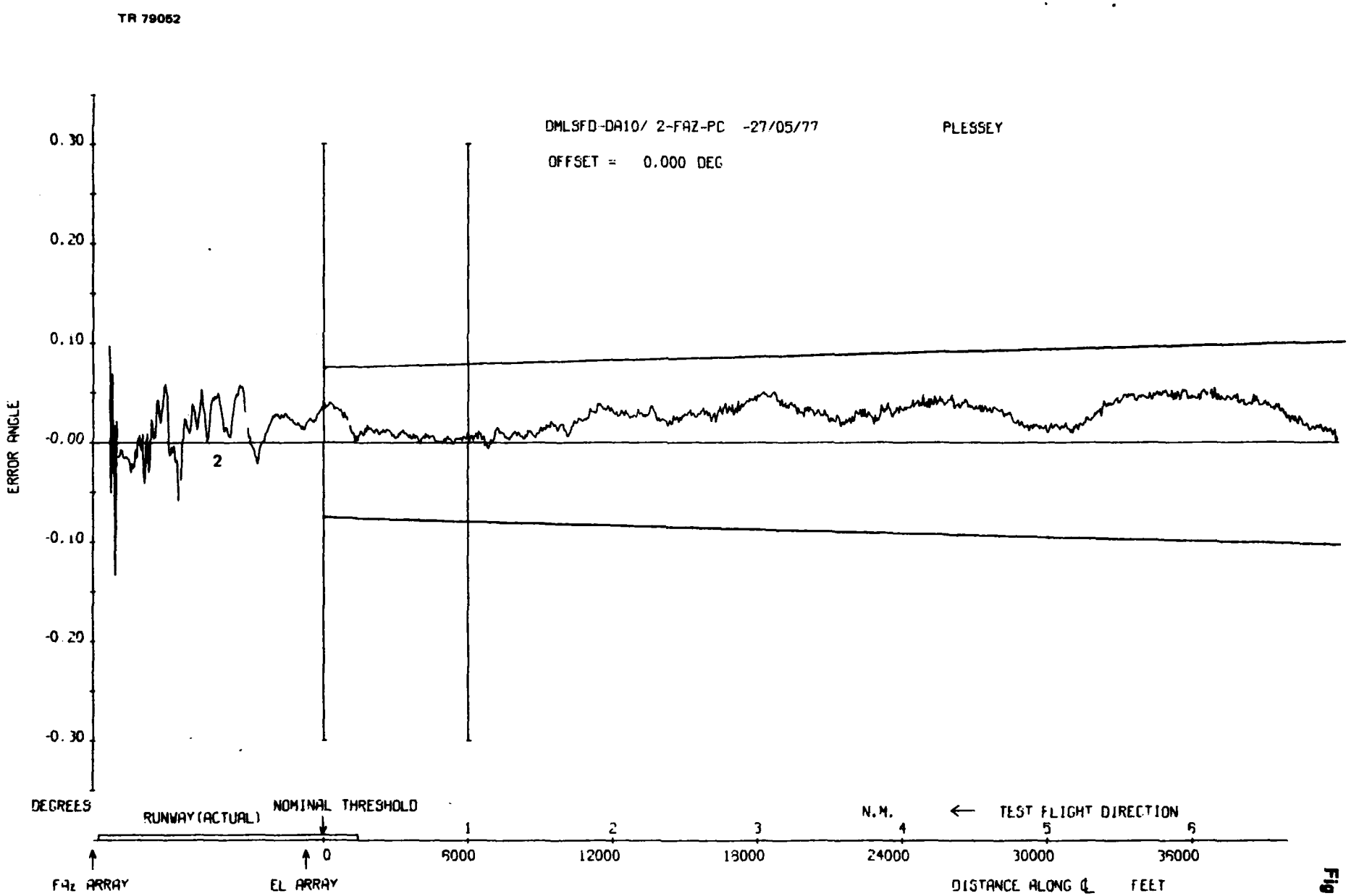

Fig 7.44c

Fig 7.44c Azimuth 54λ, 3 degree approach to 300 ft overshoot

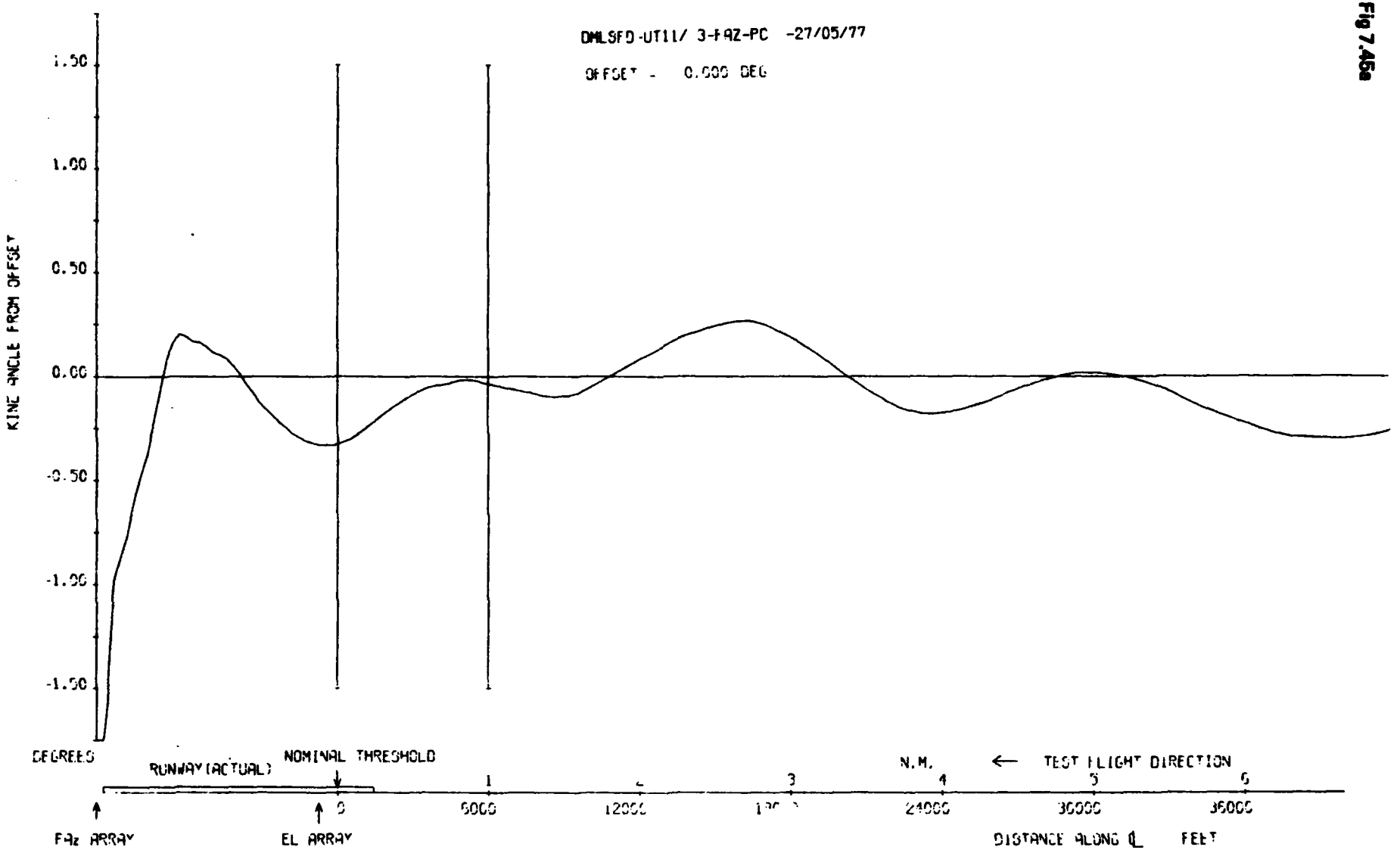

Fig 7.45a Azimuth 54λ,3 degree approach to 300 ft overshoot

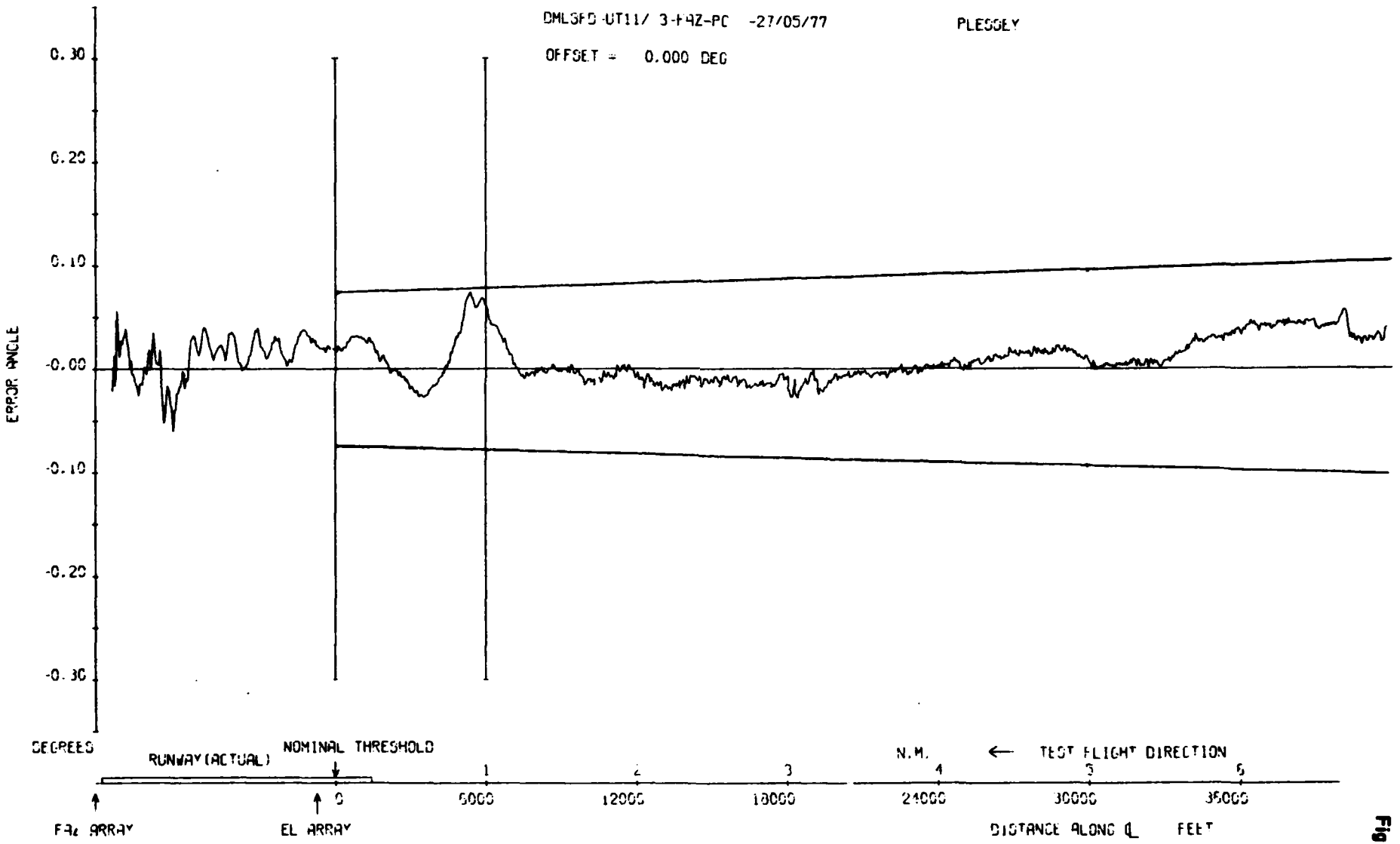

Fig 7.45c

Fig 7.45c Azimuth 54λ,3 degree approach to 300 ft overshoot

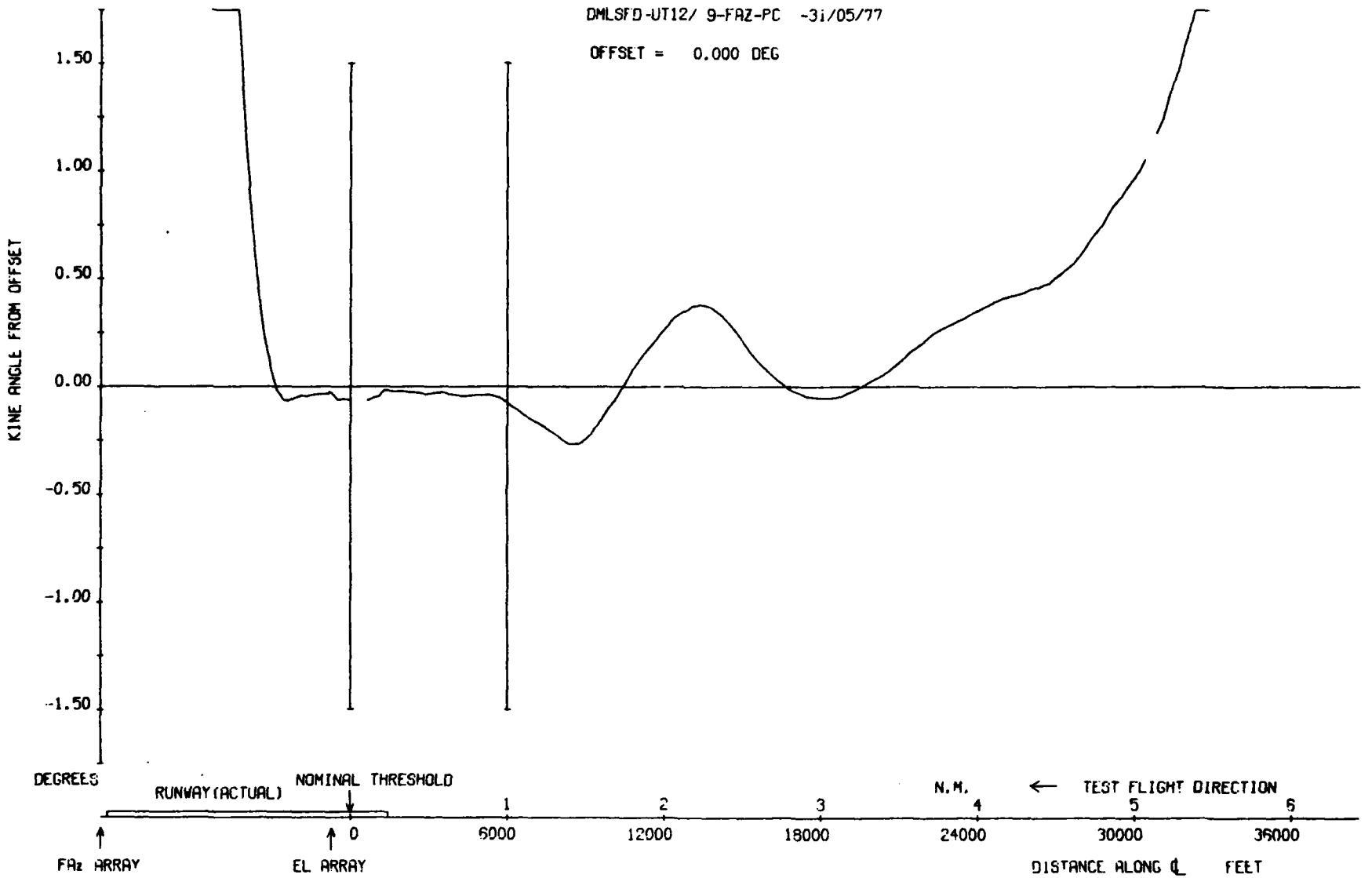

Fig 7.46a

Fig 7.46a Azimuth 54λ,3 degree approach to 50 ft overshoot

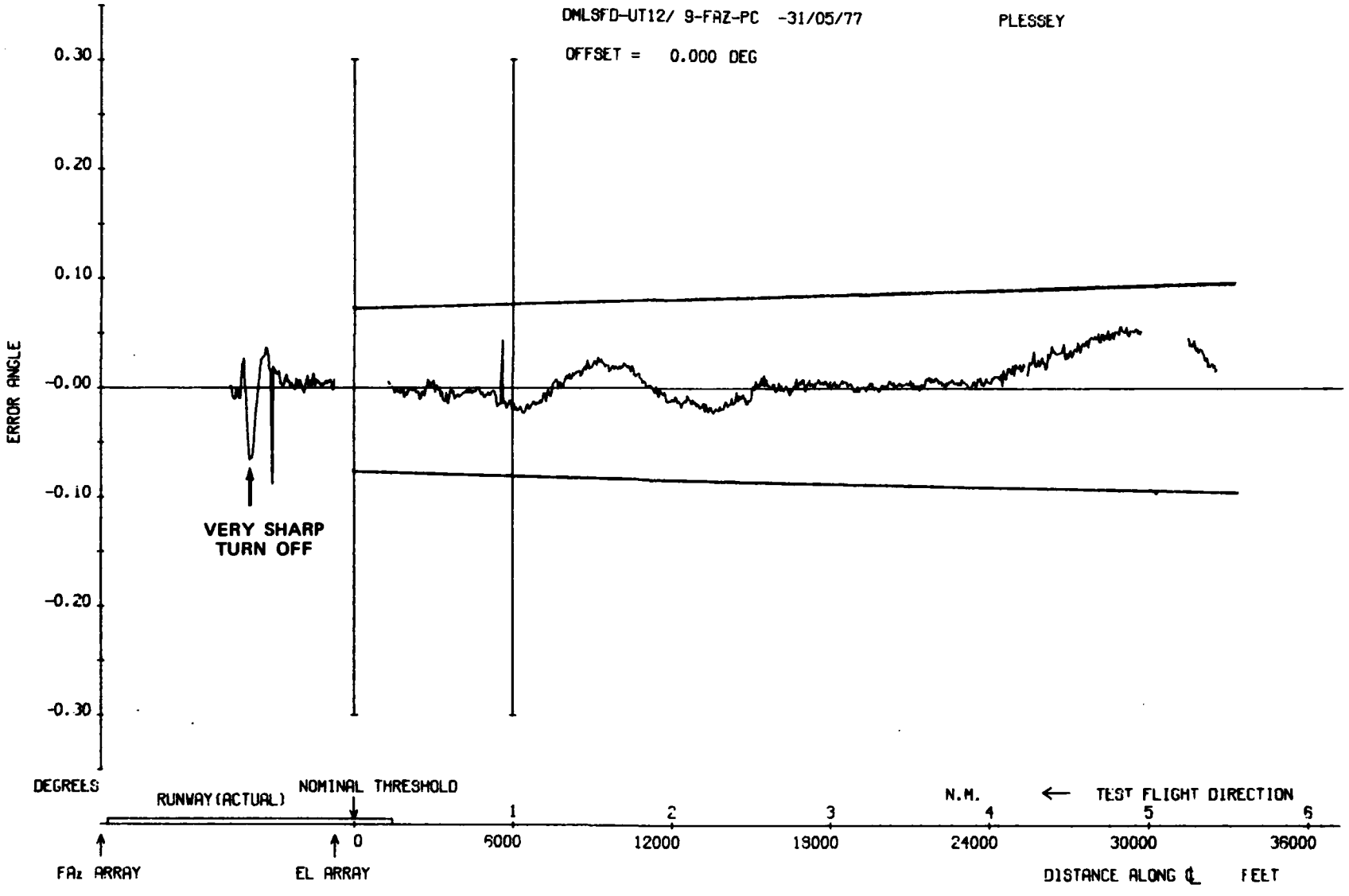

Fig 7.46c Azimuth 54λ, 3 degree approach to 50 ft overshoot

Fig 7.46c

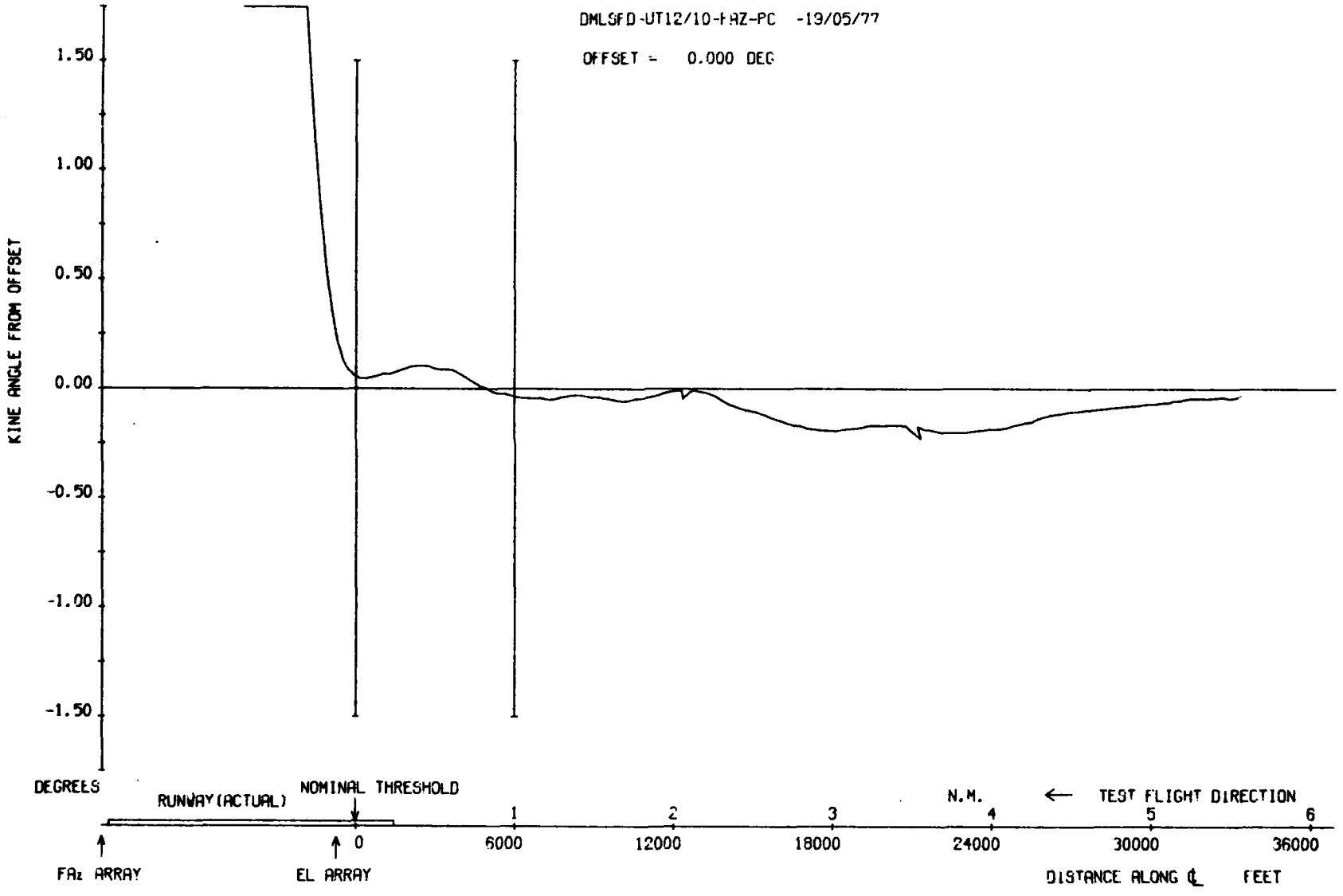

Fig 7.47a Azimuth 54λ, 3 degree approach to 50 ft overshoot

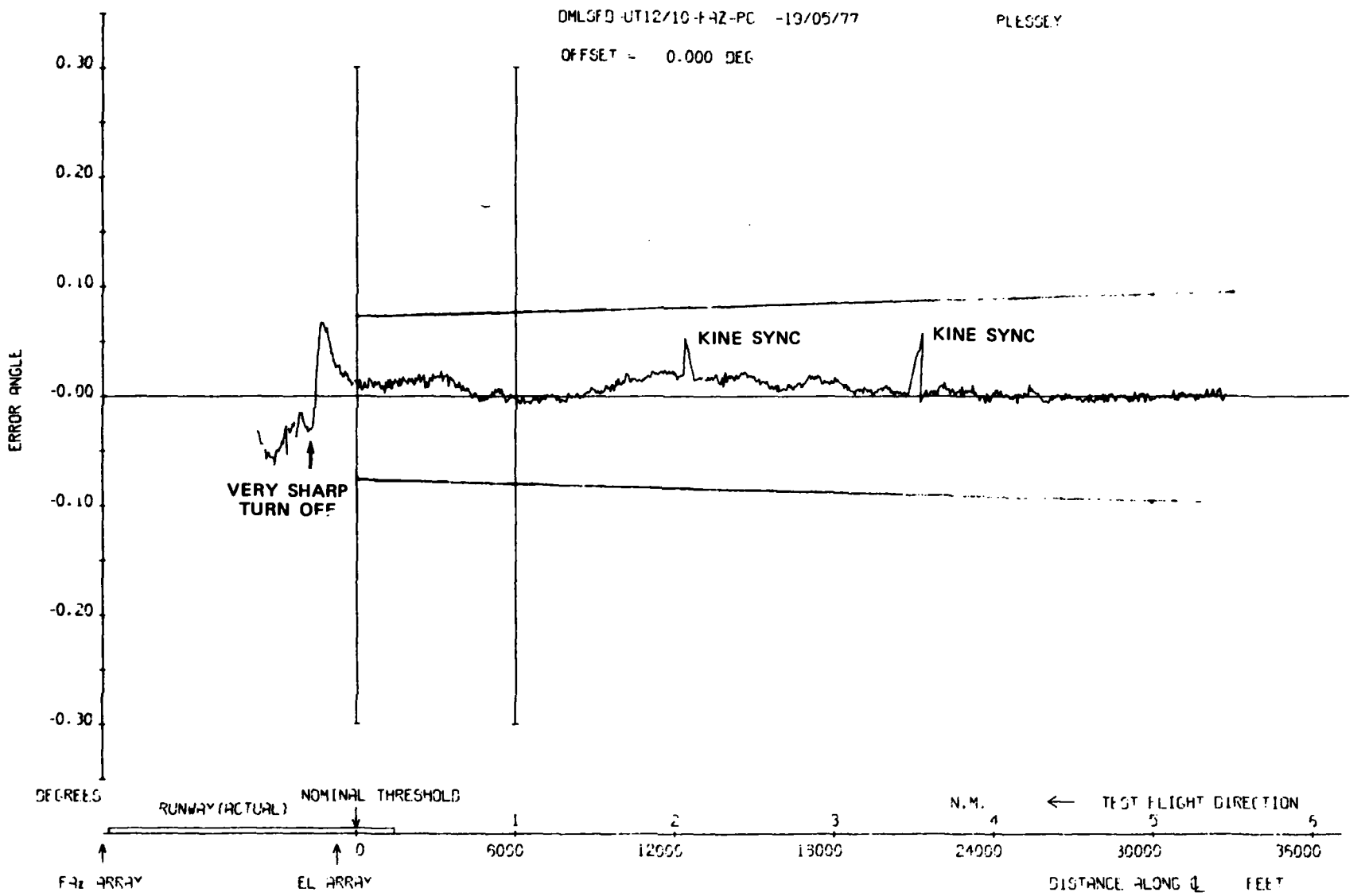

Fig 7.47c

Fig 7.47c Azimuth 54λ,3 degree approach to 50 ft overshoot

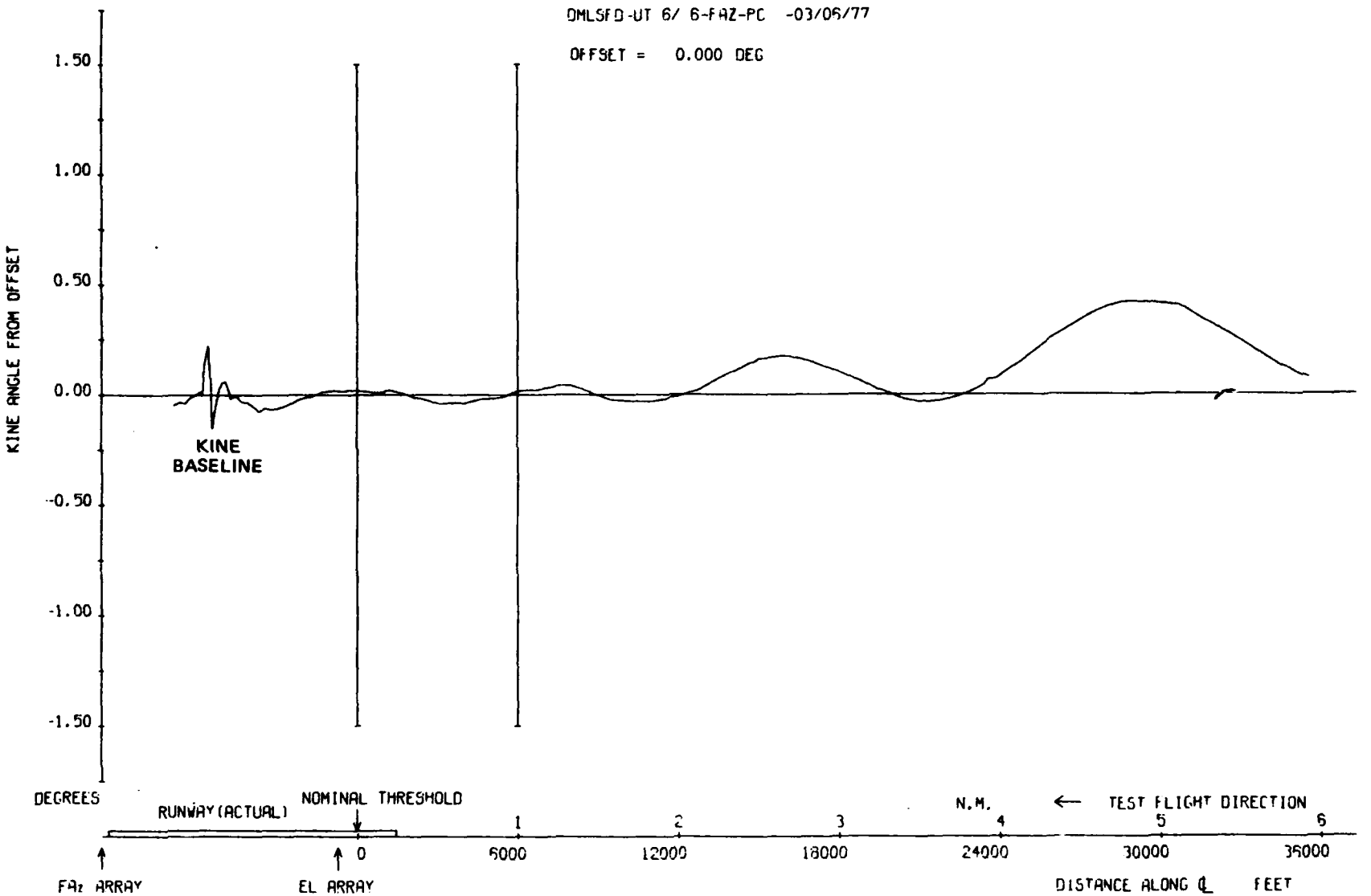

Fig 7.48a

Fig 7.48a Azimuth 54λ, 3 degree approach to 50 ft overshoot

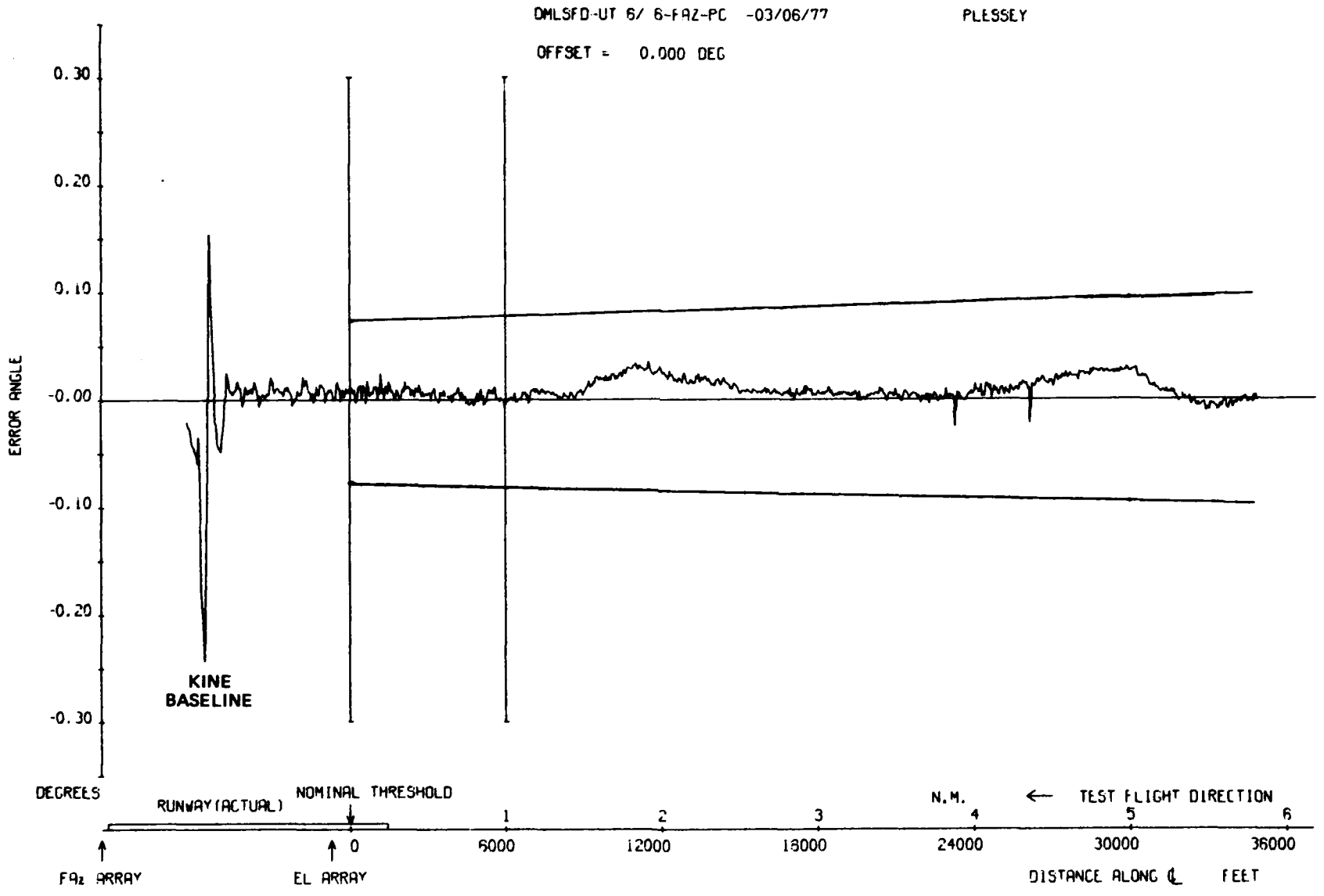

Fig 7.48c Azimuth 54λ,3 degree approach to 50 ft overshoot

Fig 7.48c

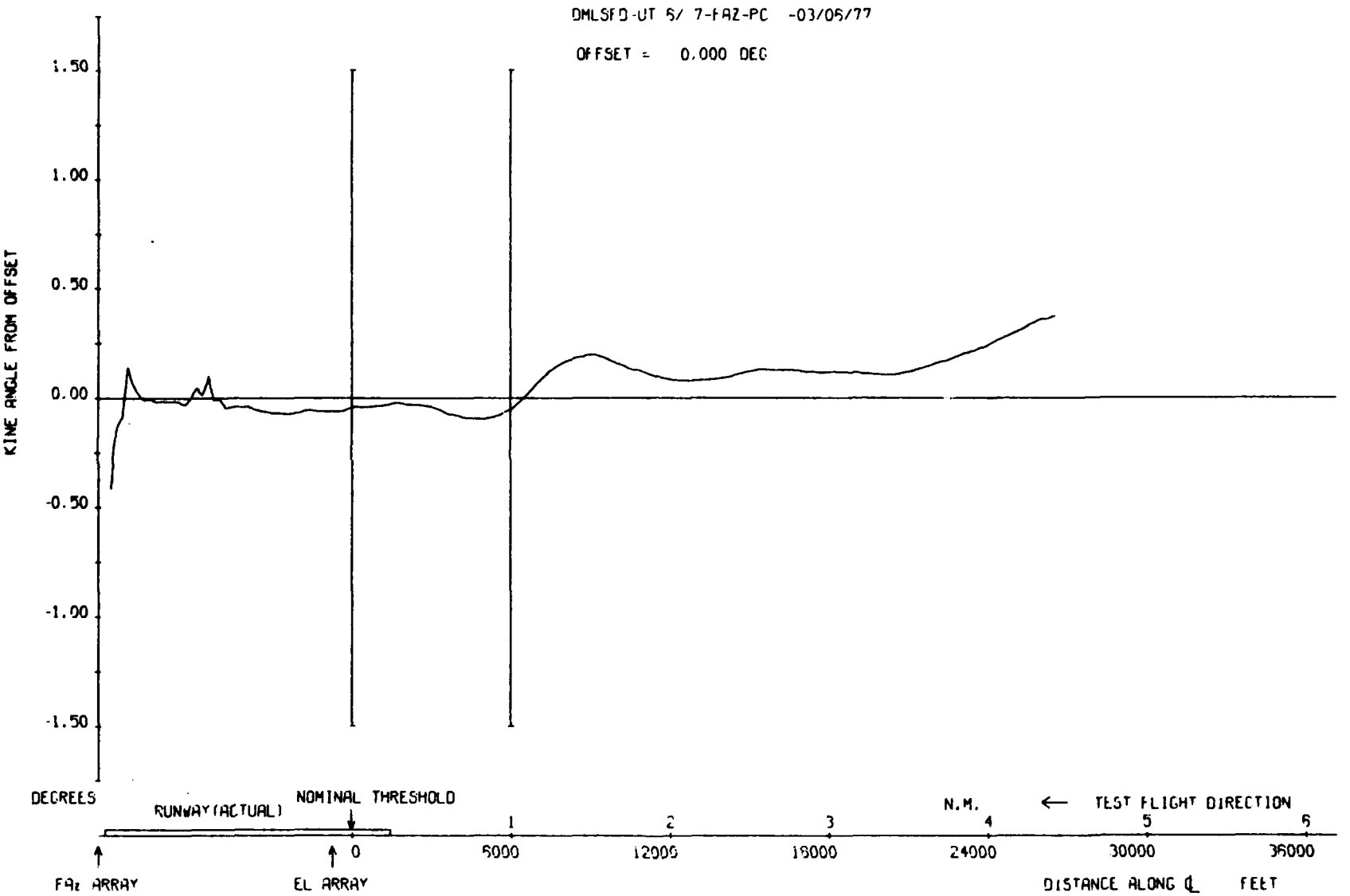

Fig 7.49a

Fig 7.49a Azimuth 54λ,3 degree approach to 50 ft overshoot

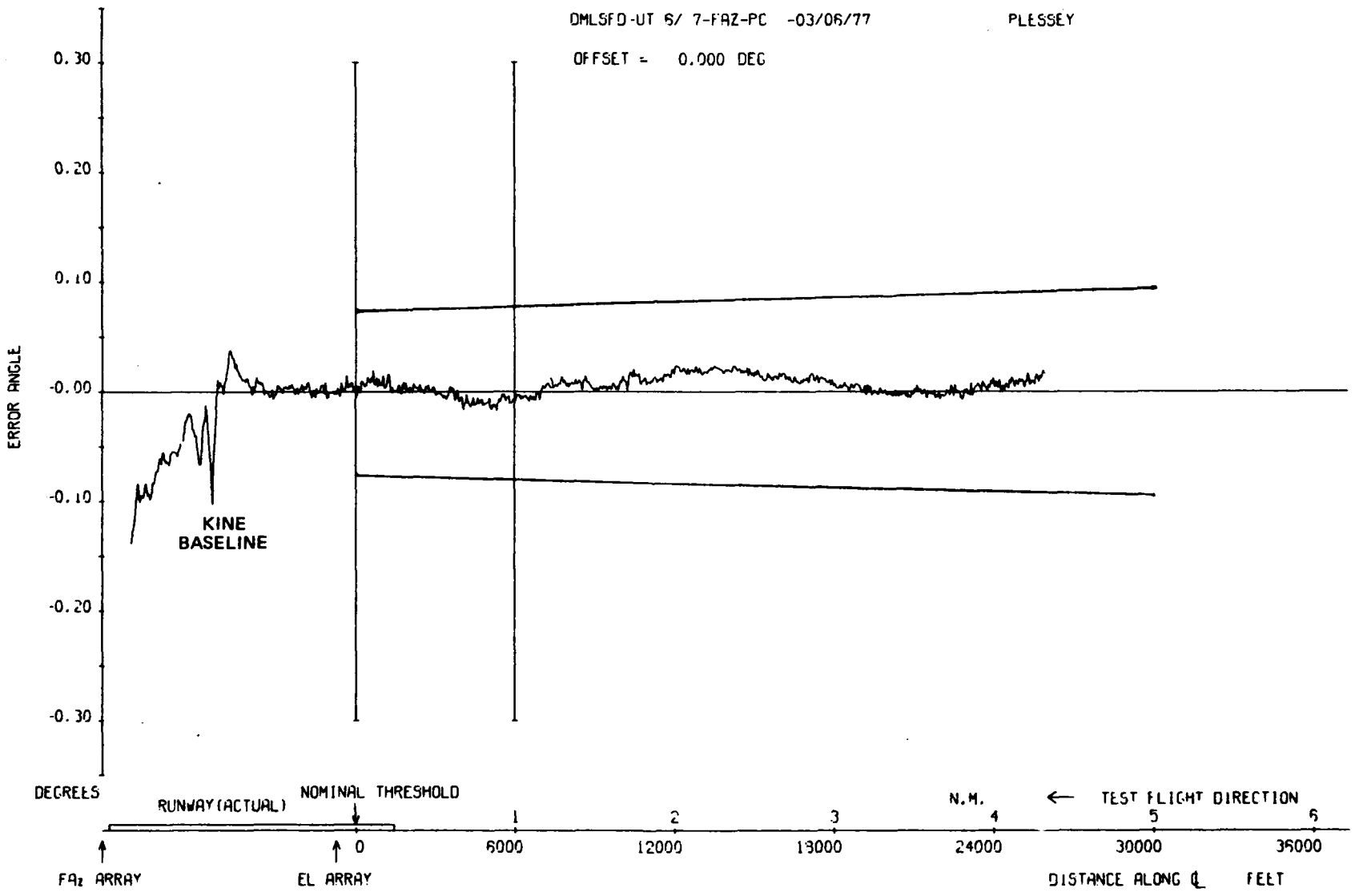

Fig 7.49c Azimuth 54λ,3 degree approach to 50 ft overshoot

Fig 7.49c

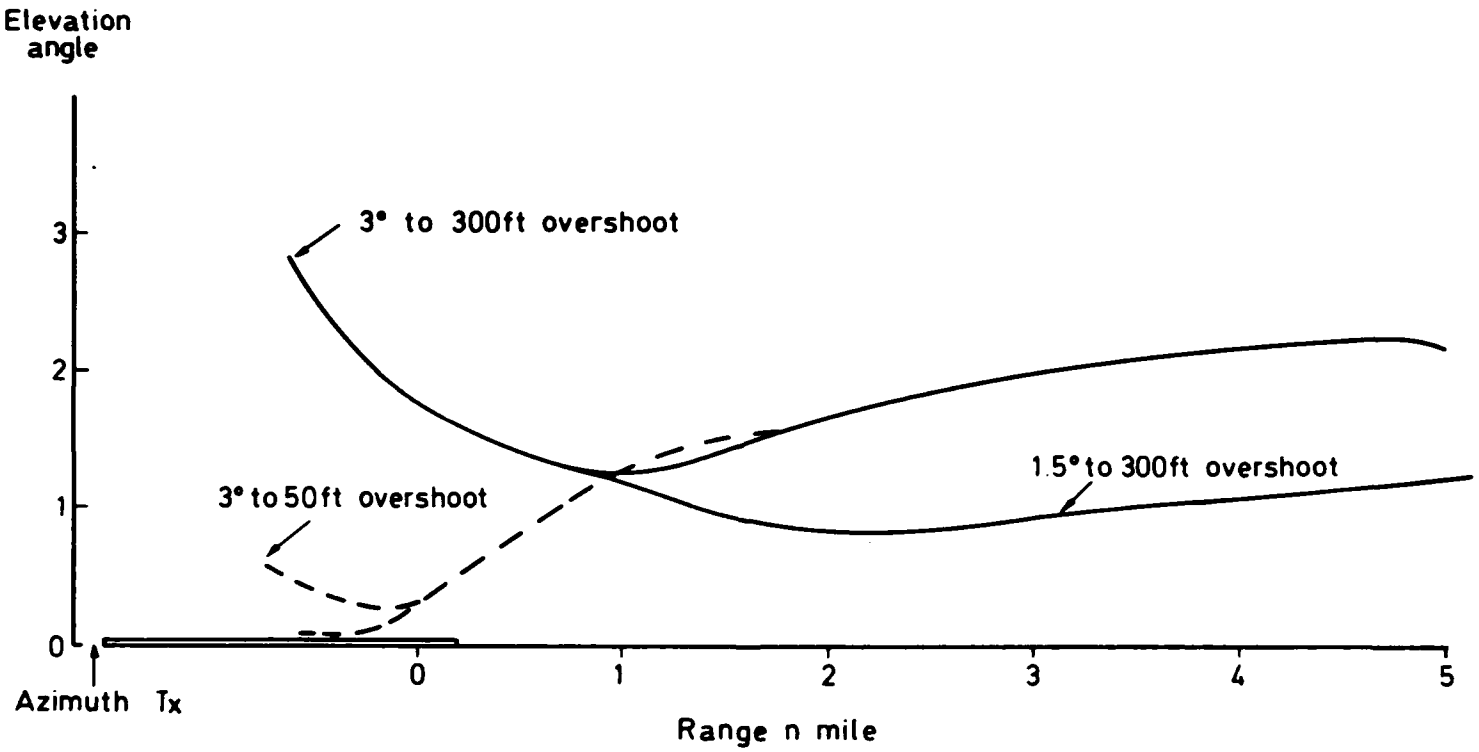

Fig 7.50 Elevation profiles referenced to azimuth site

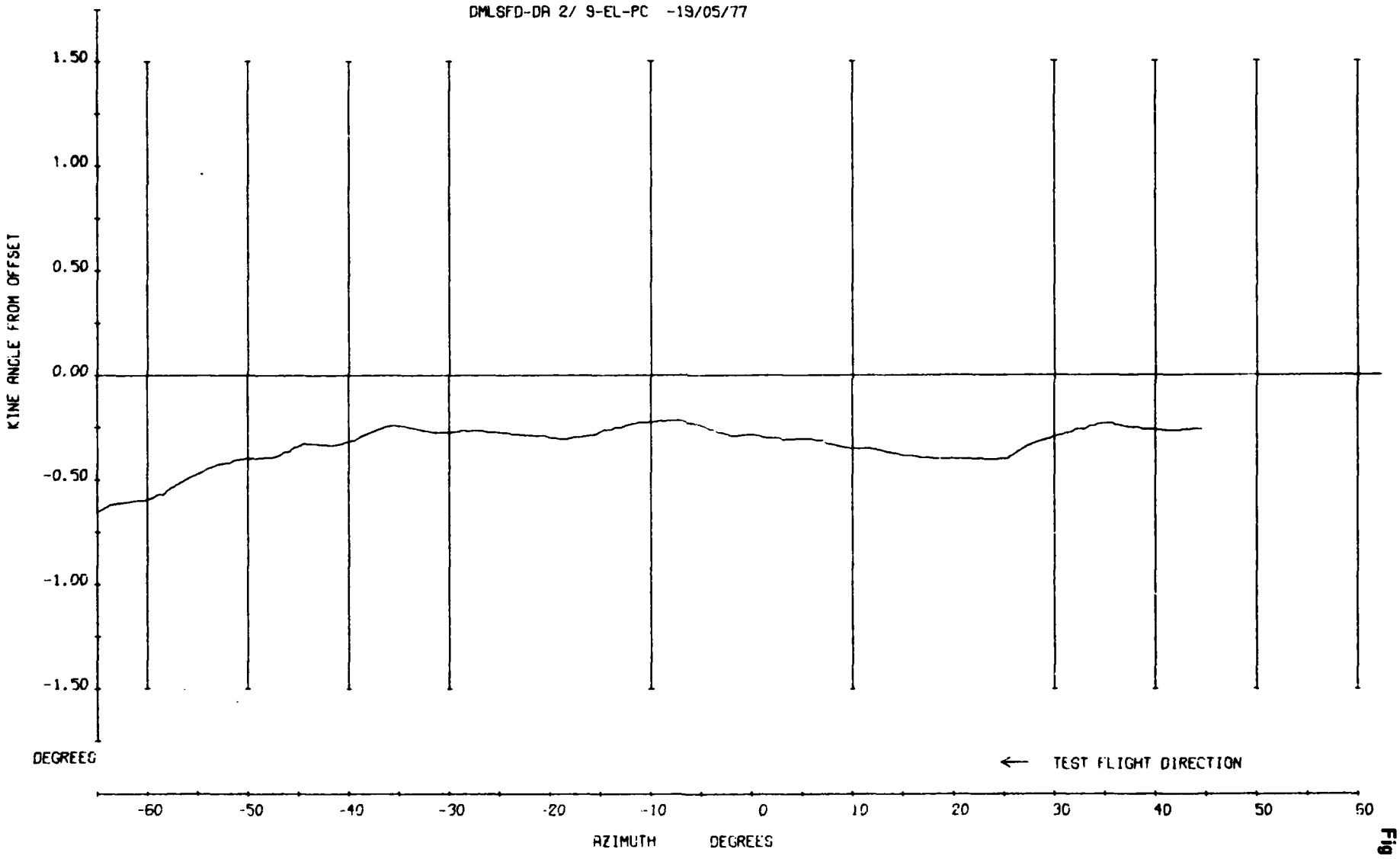

Fig 7.51a

Fig 7.51a Elevation 54λ,part orbit, 3 degrees nominal

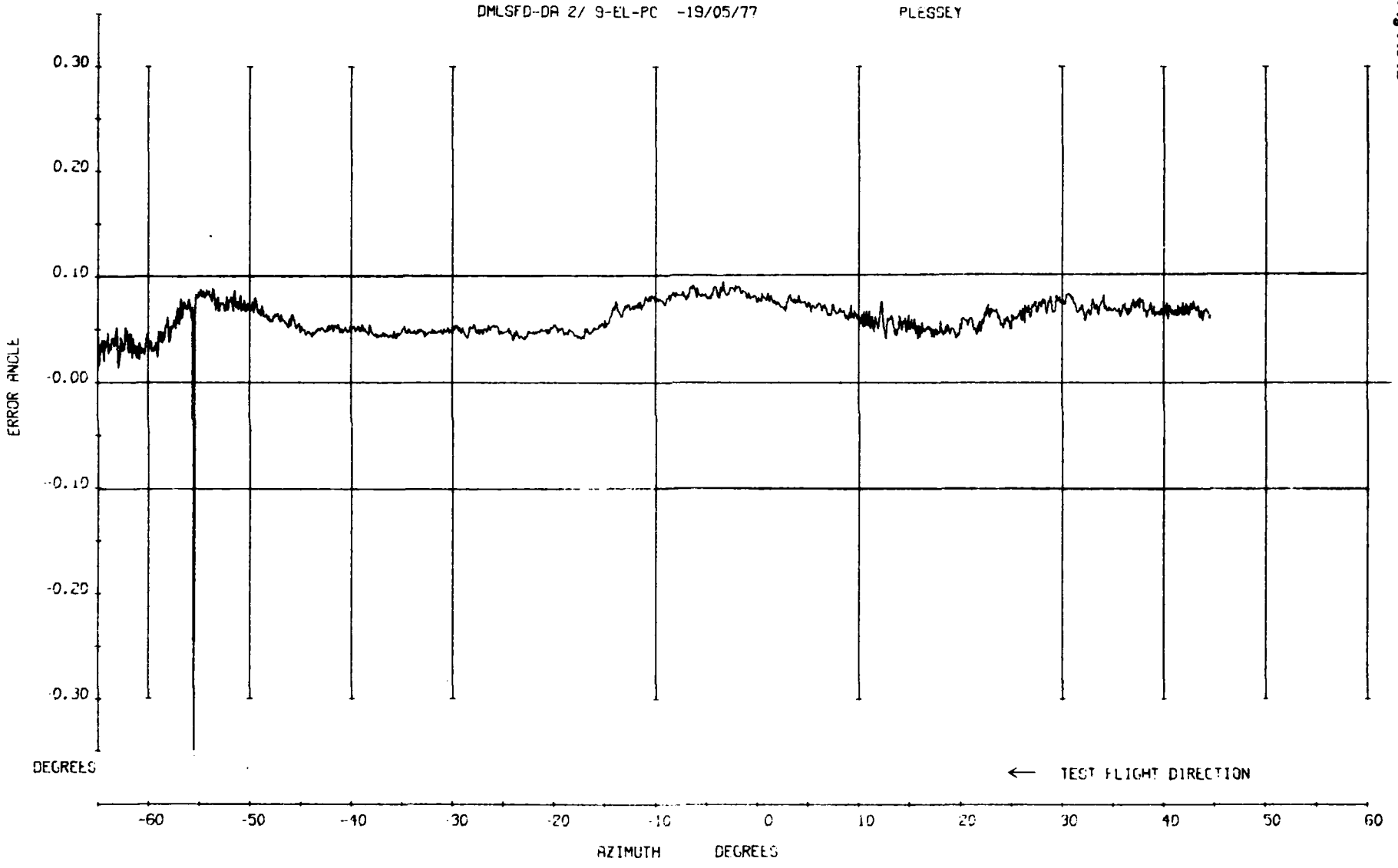

Fig 7.51b

Fig 7.51b Elevation 54λ,part orbit, 3 degrees nominal

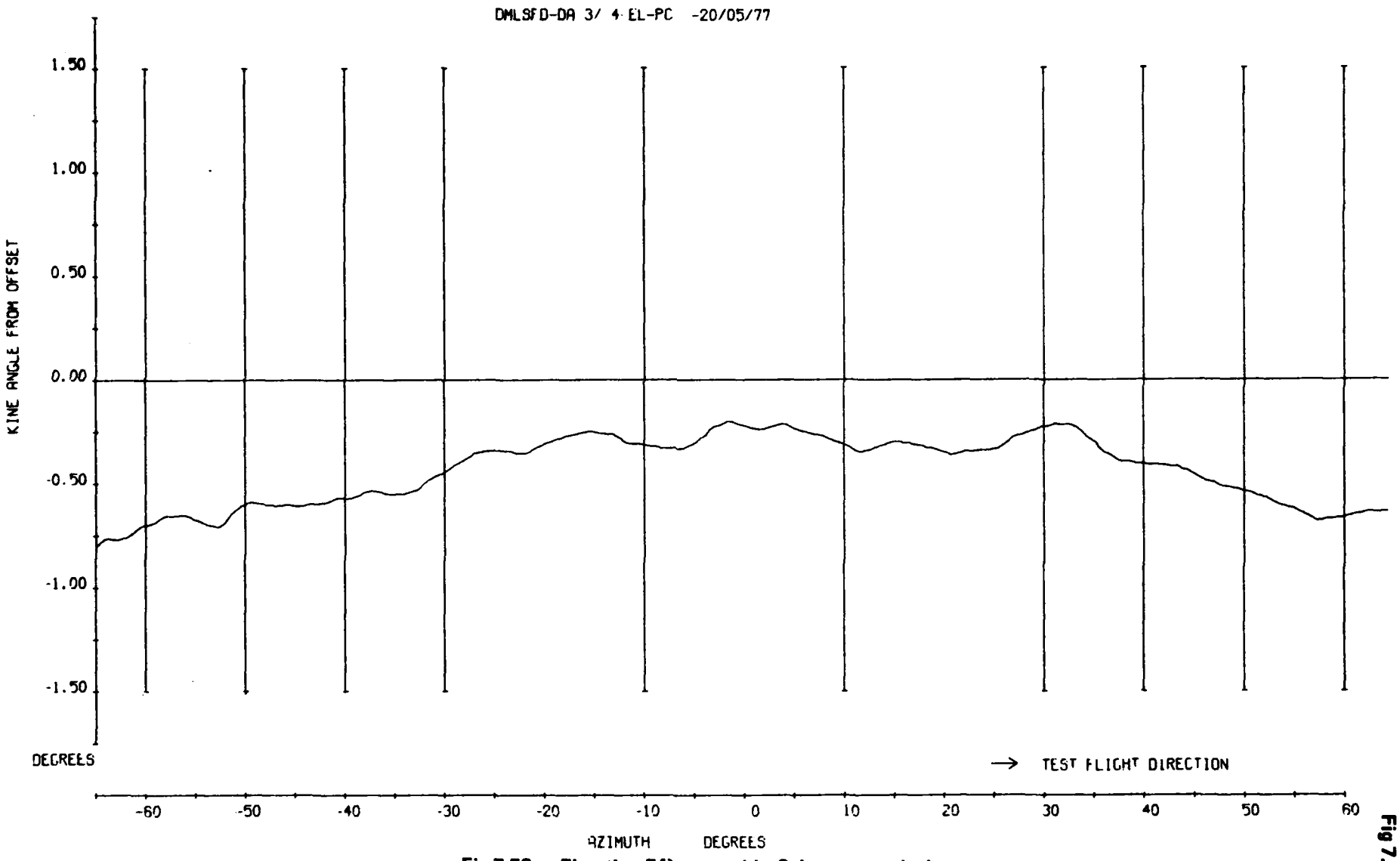

Fig 7.52a Elevation 54λ,part orbit, 3 degrees nominal

Fig 7.52a

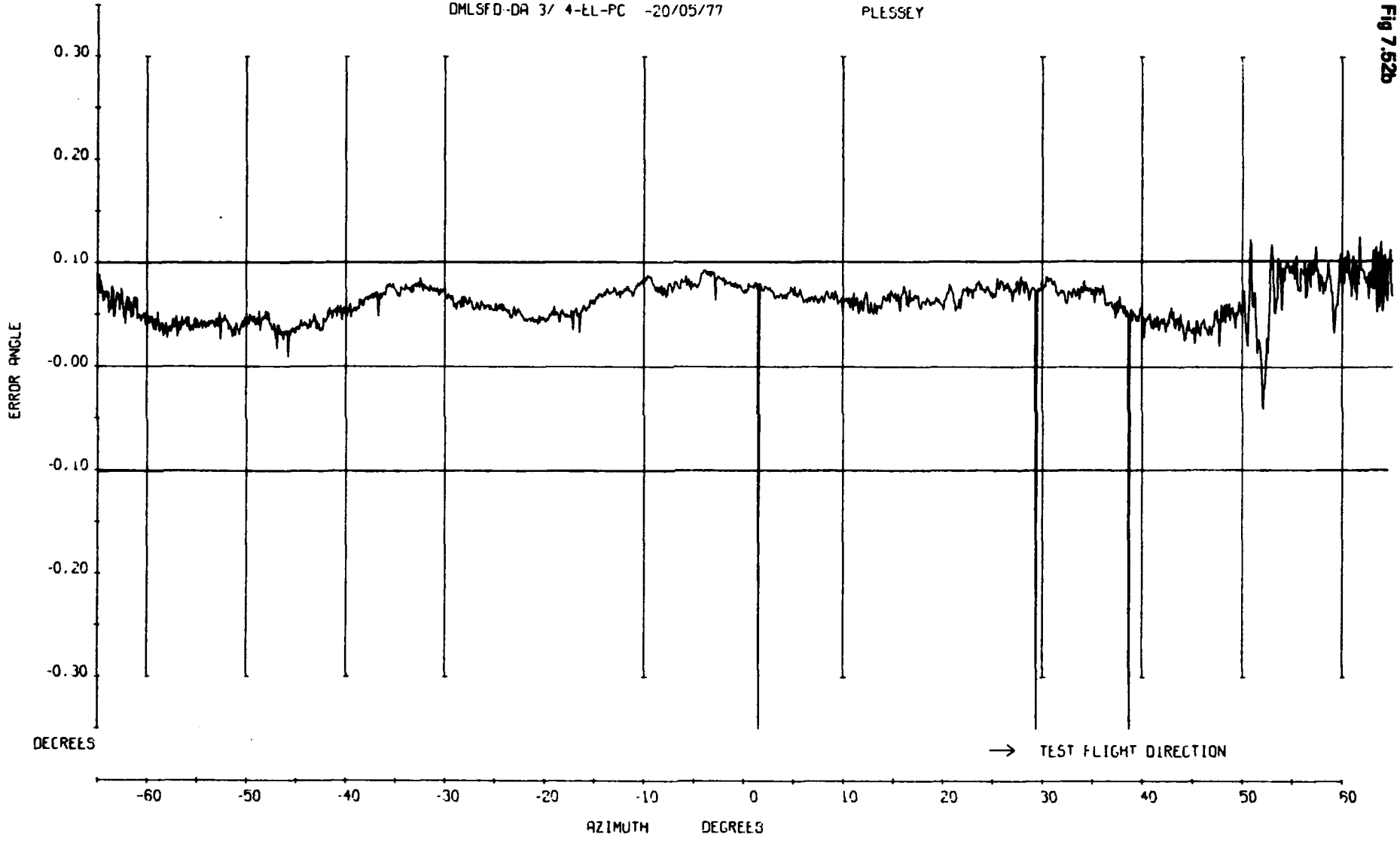

Fig 7.52b

Fig 7.52b Elevation 54λ,part orbit, 3 degrees nominal

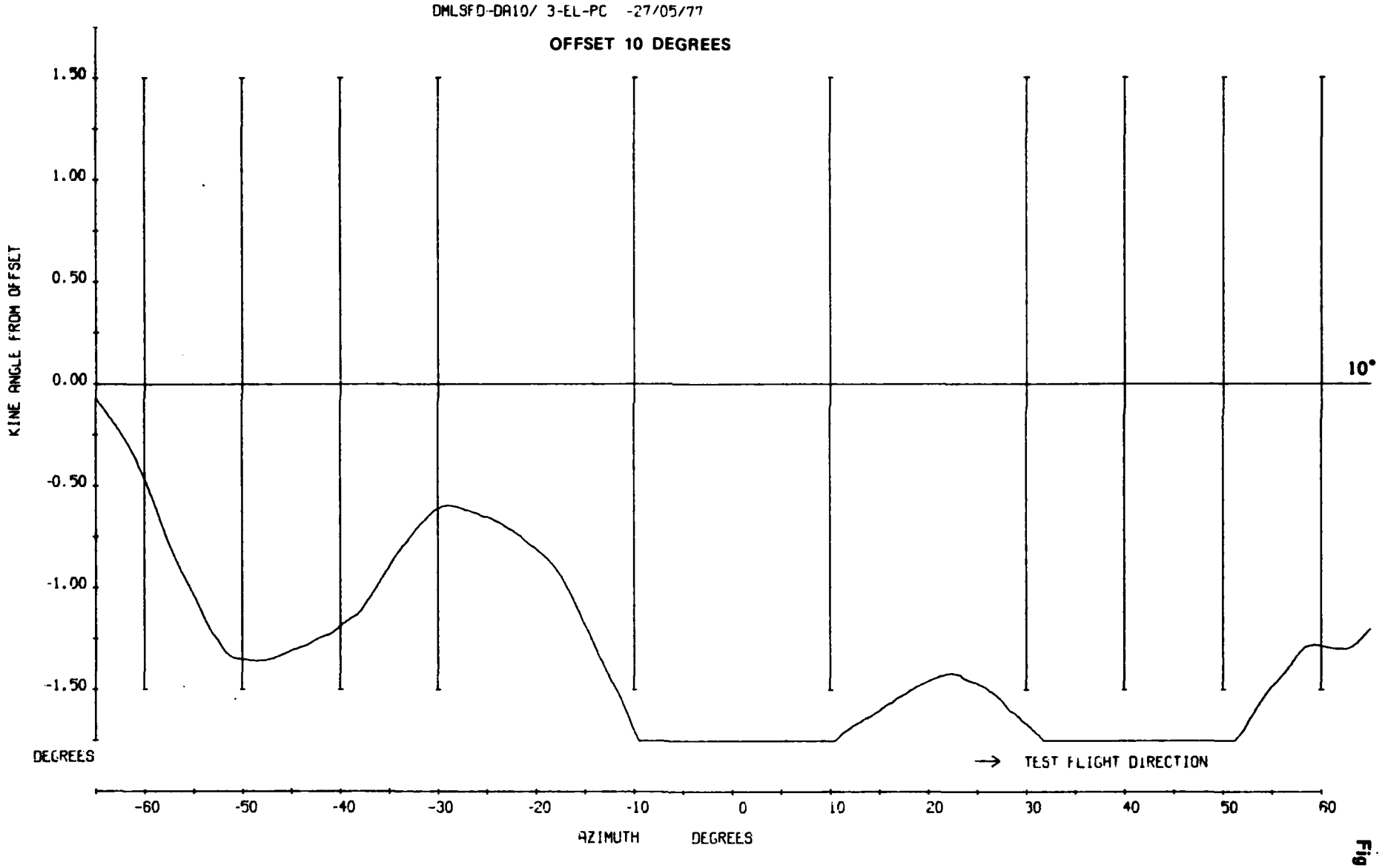

Fig 7.53a Elevation part orbit, 10 degrees nominal

Fig 7.53a

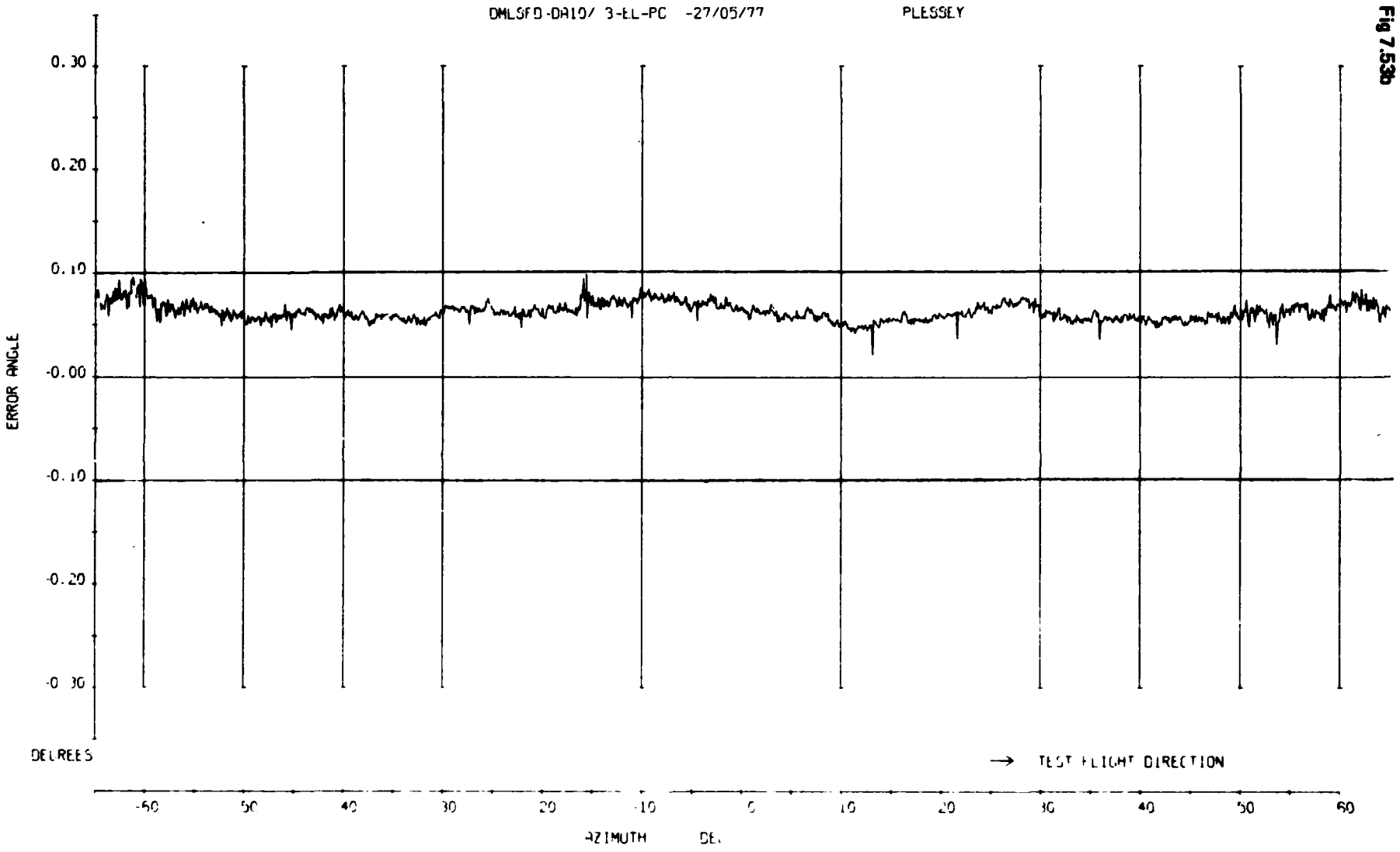

Fig 7.53b

Fig 7.53b Elevation part ( ) degrees nominal

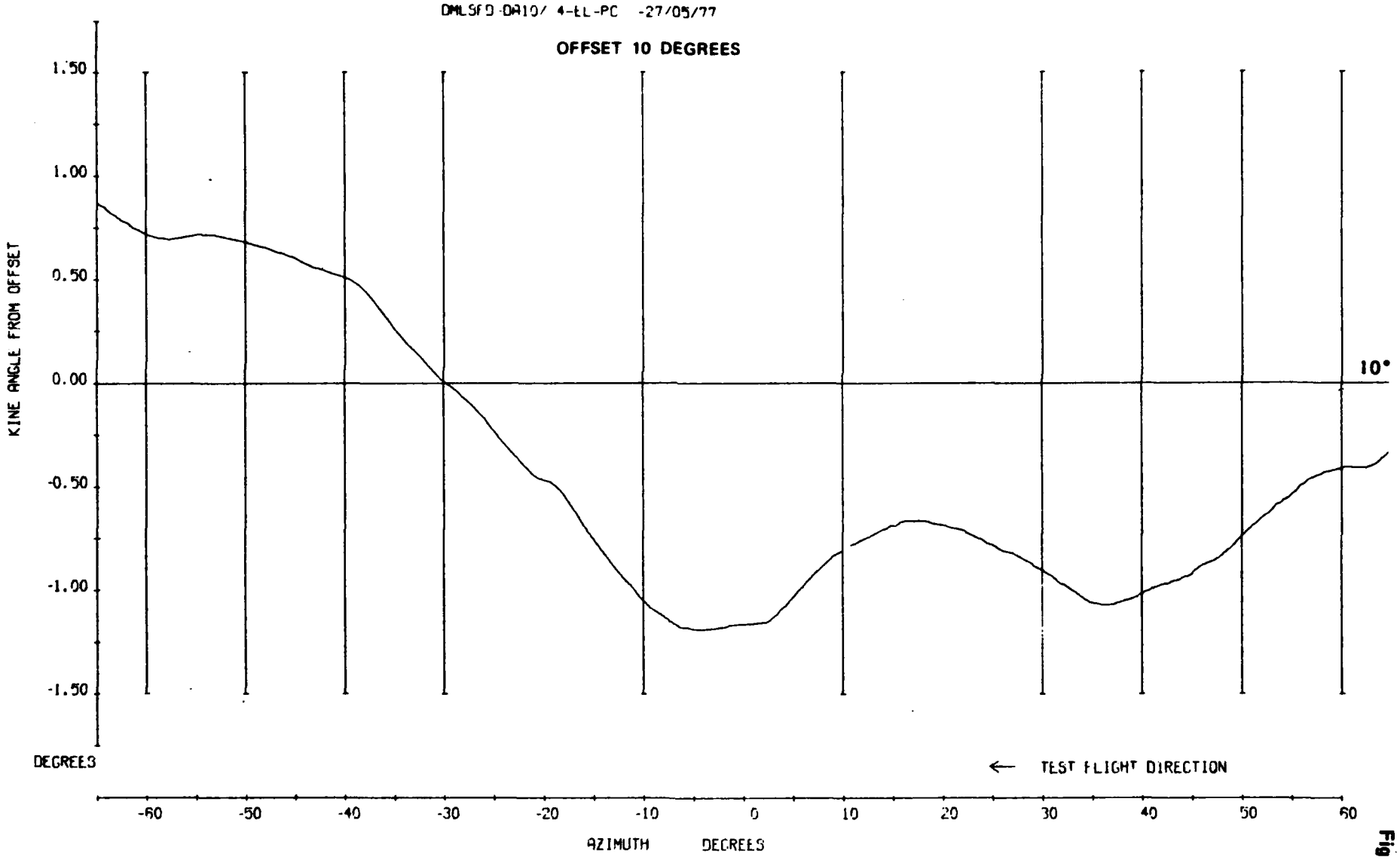

Fig 7.54a

Fig 7.54a Elevation part orbit, 10 degrees nominal

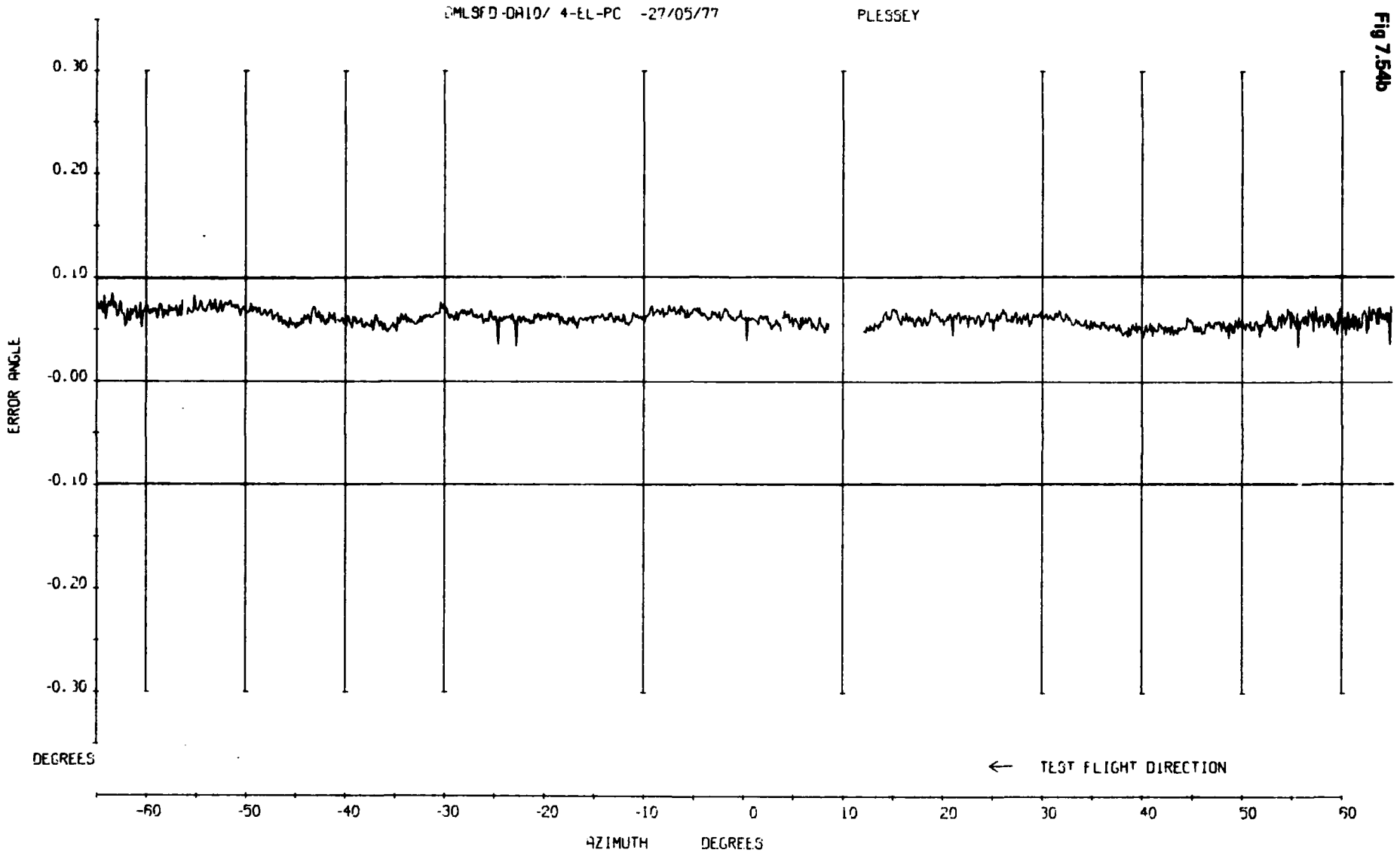

Fig 7.54b

Fig 7.54b Elevation part orbit, 10 degrees nominal

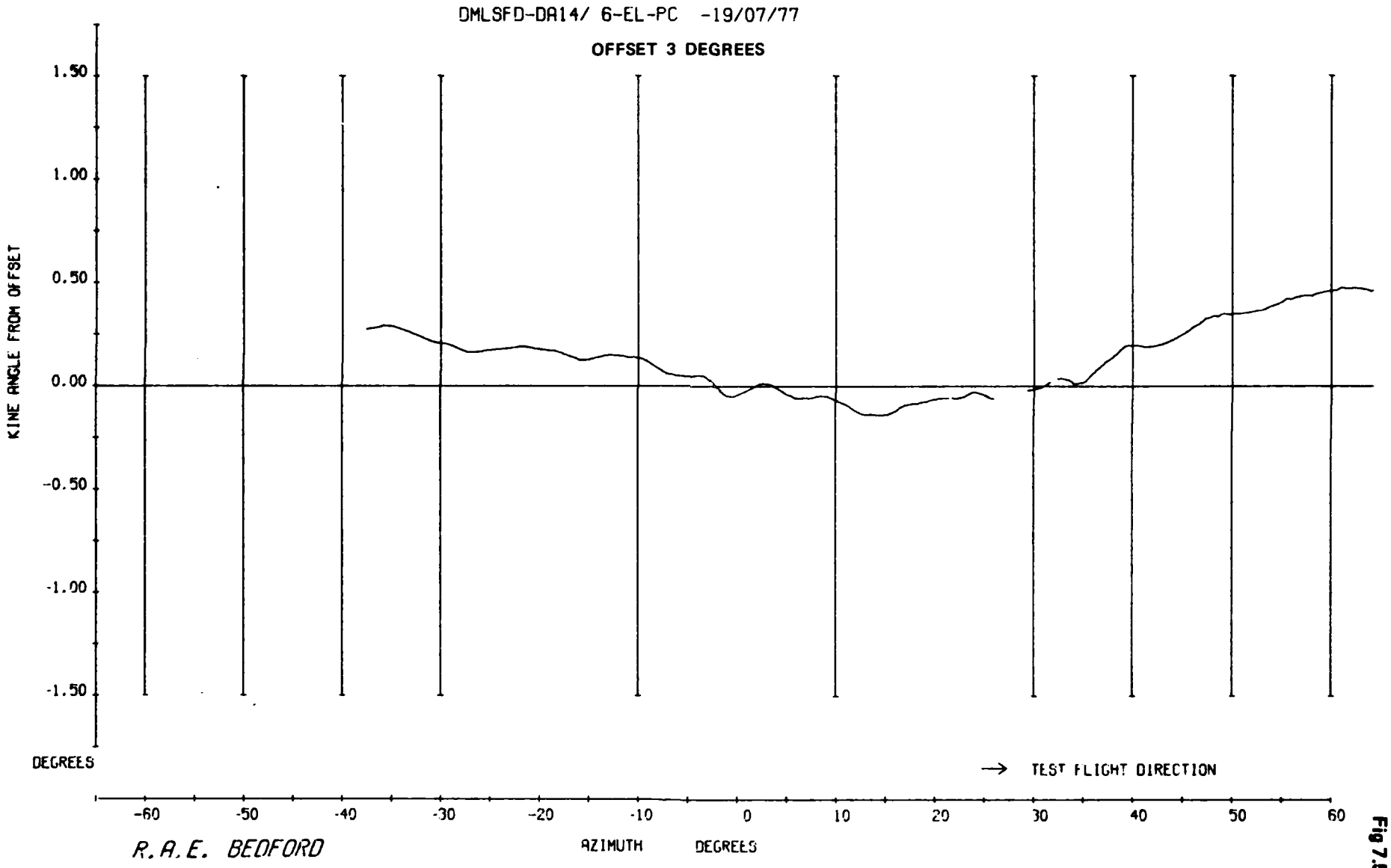

Fig 7.55a

Fig 7.55a Elevation part orbit, 3 degrees nominal. Range 4.6 n mile. Height 1550 ft

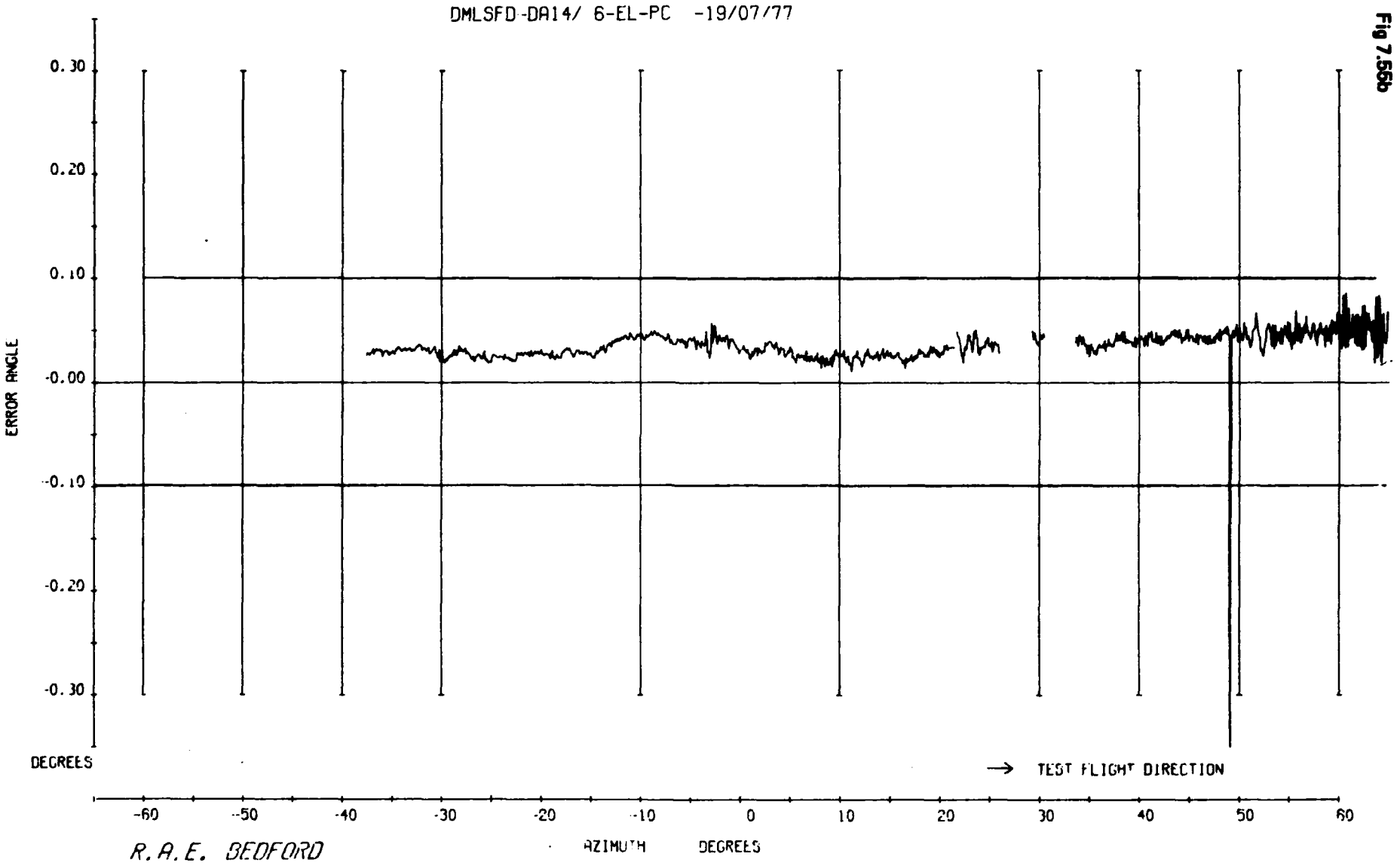

Fig 7.55b

Fig 7.55b Elevation part orbit, 3 degrees nominal

TR 79062

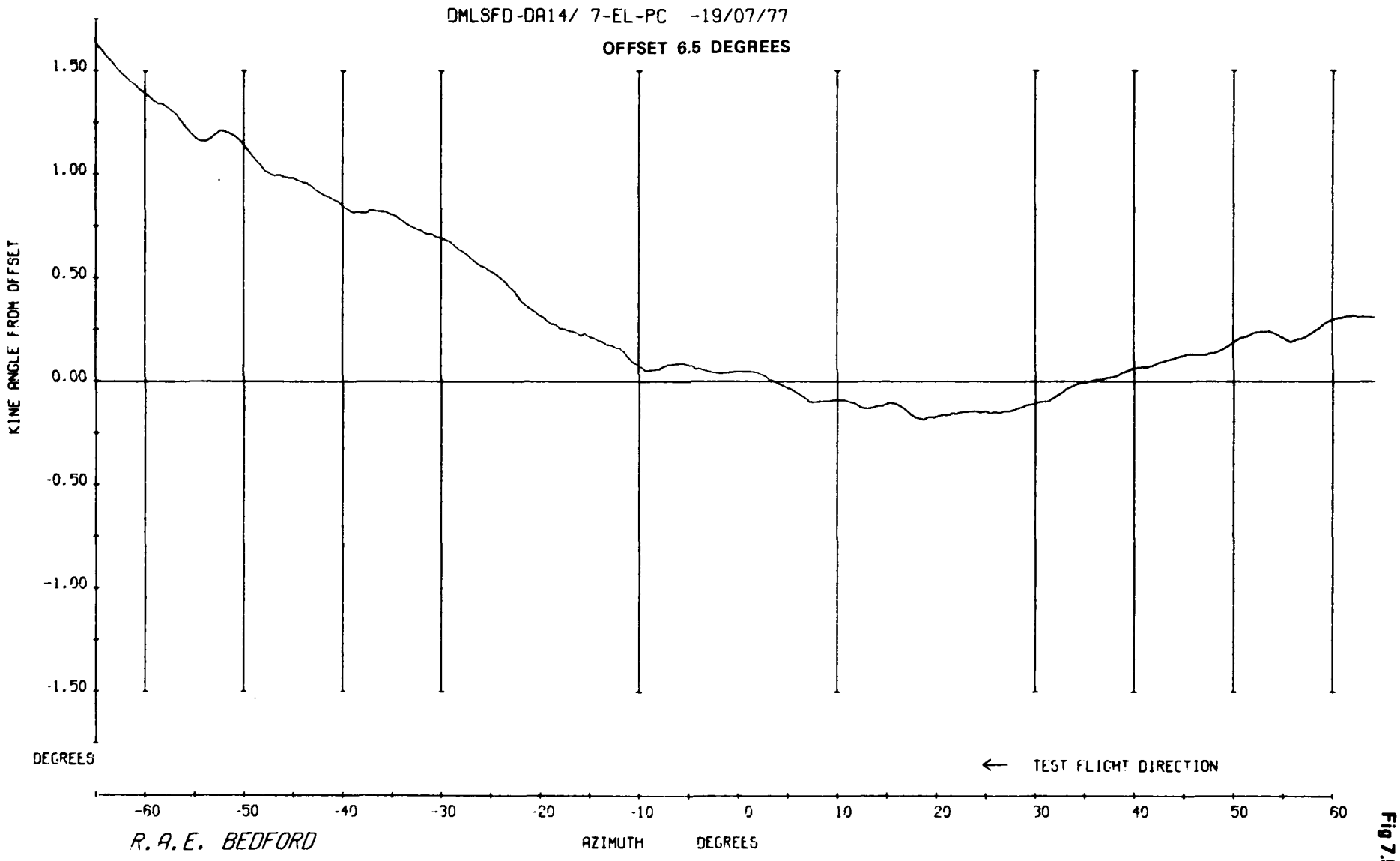

Fig 7.56a

Fig 7.56a Elevation part orbit. Range 4.5 n mile. Height 3060 ft

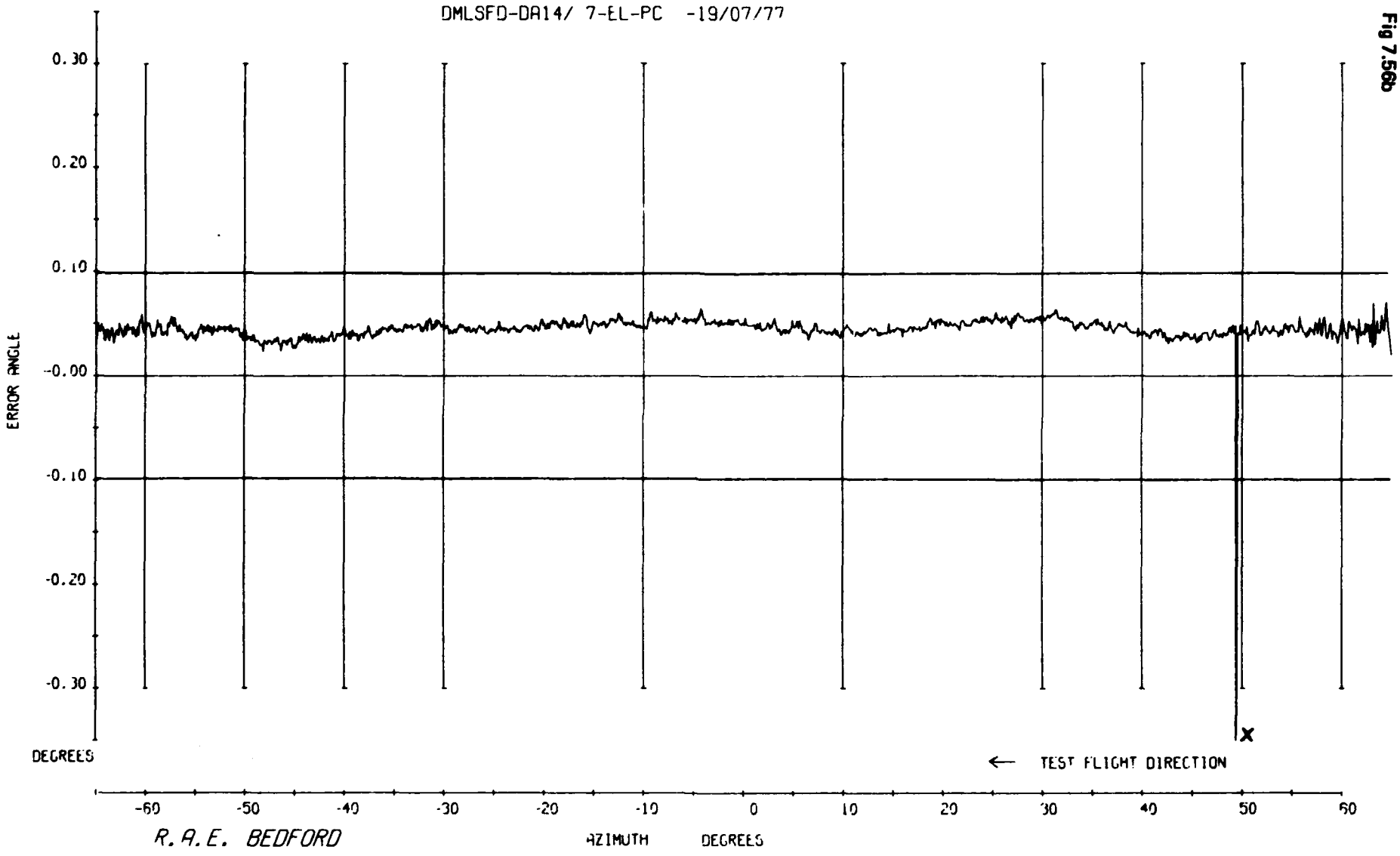

Fig 7.56b Elevation part orbit at 4.5 n mile and 3060 ft

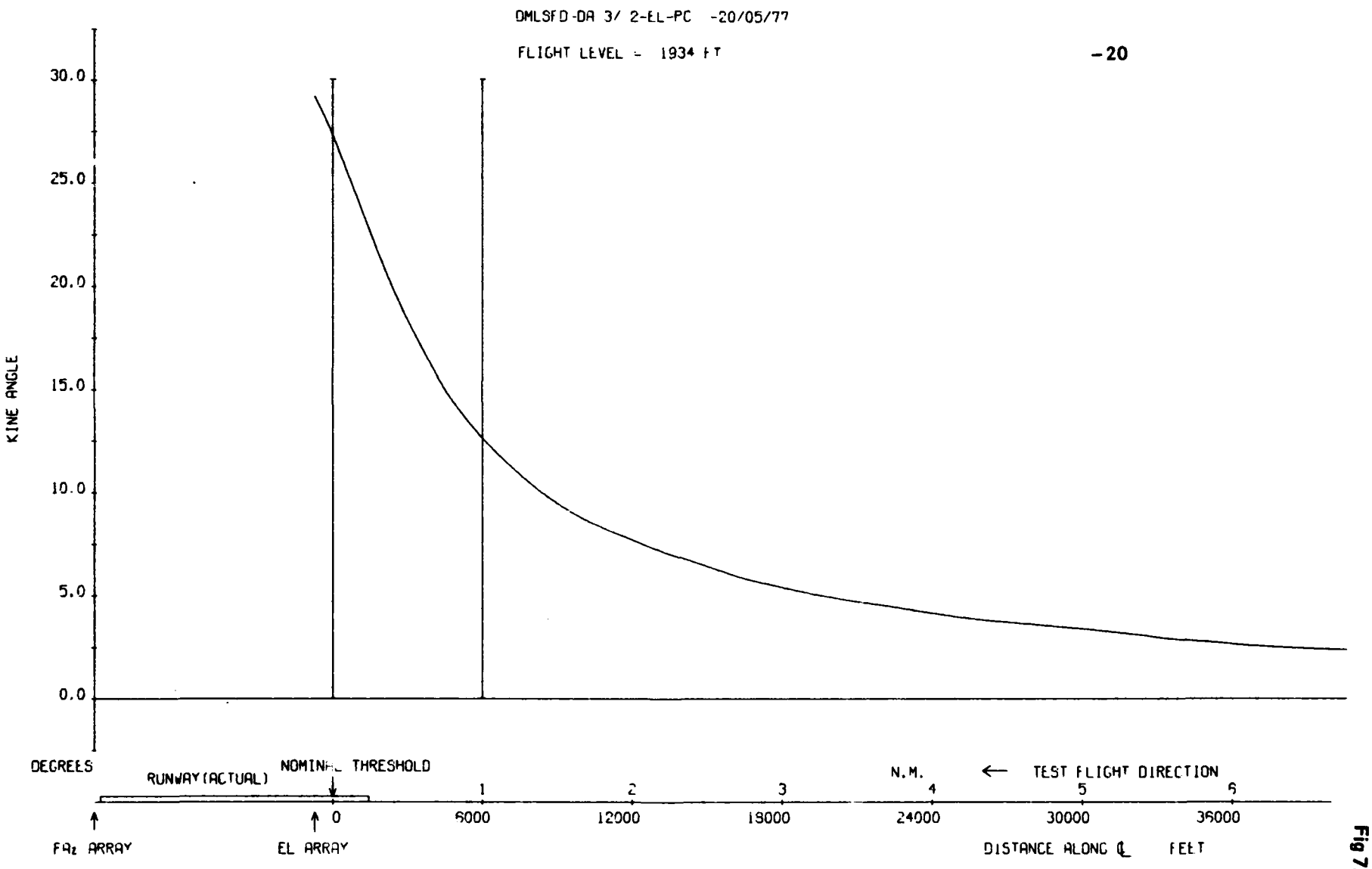

Fig 7.57a

Fig 7.57a Elevation 54λ, constant height radial 1934 ft, – 20 degrees azimuth

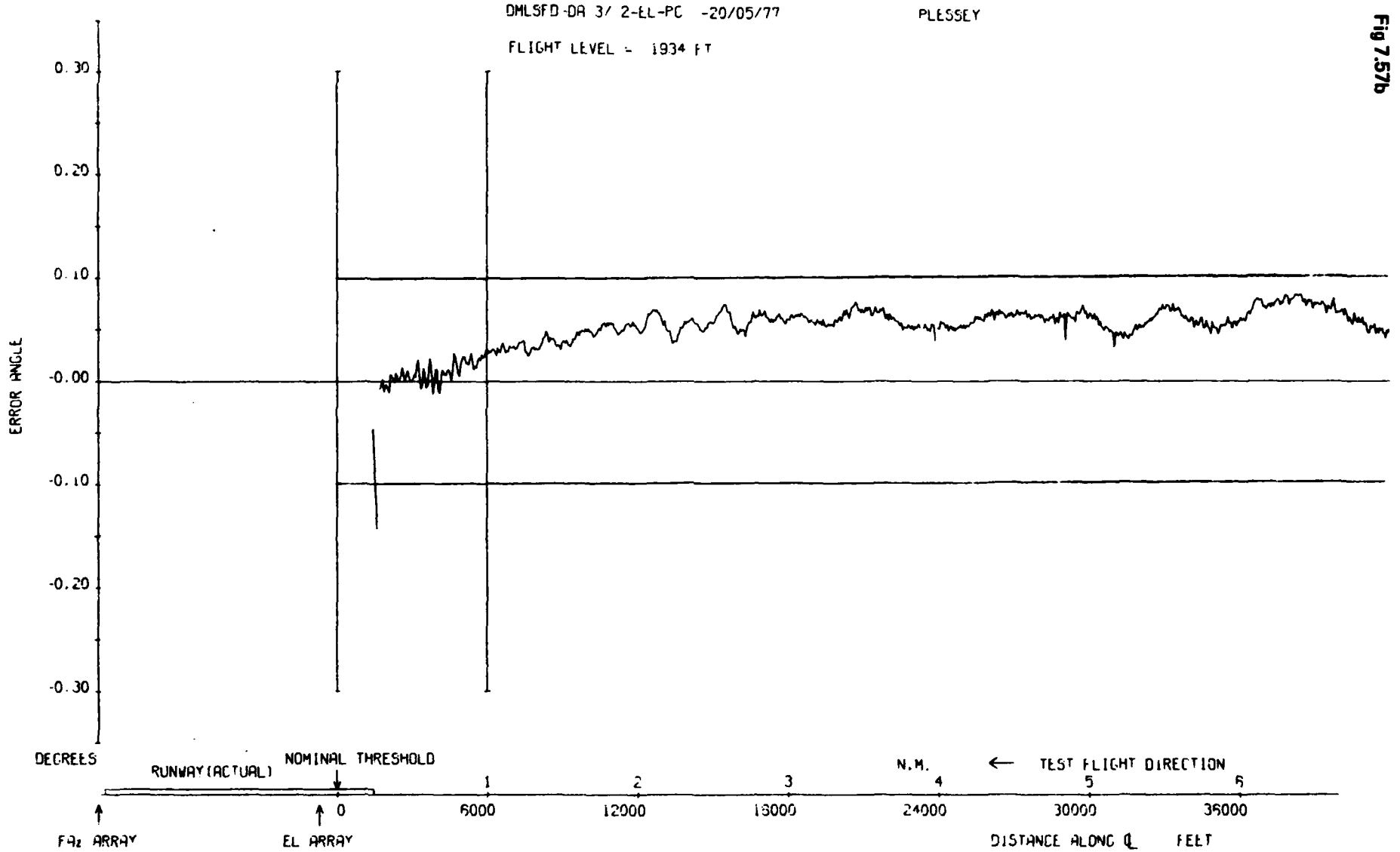

Fig 7.57b

Fig 7.57b Elevation 54λ, constant height radial 1934 ft, — 20 degrees azimuth

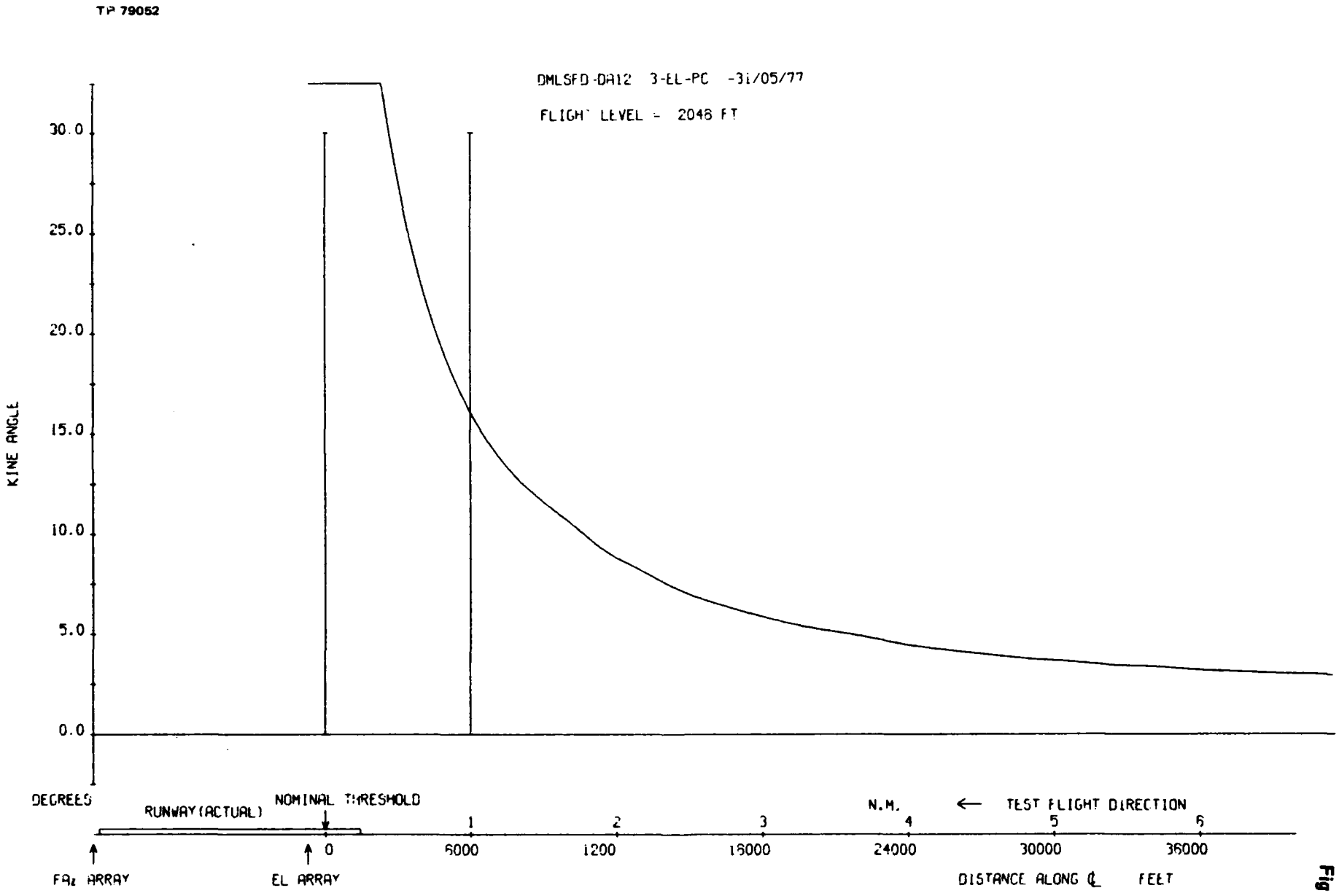

Fig 7.58a Elevation 54λ, constant height radial 2048 ft, 0 degree azimuth

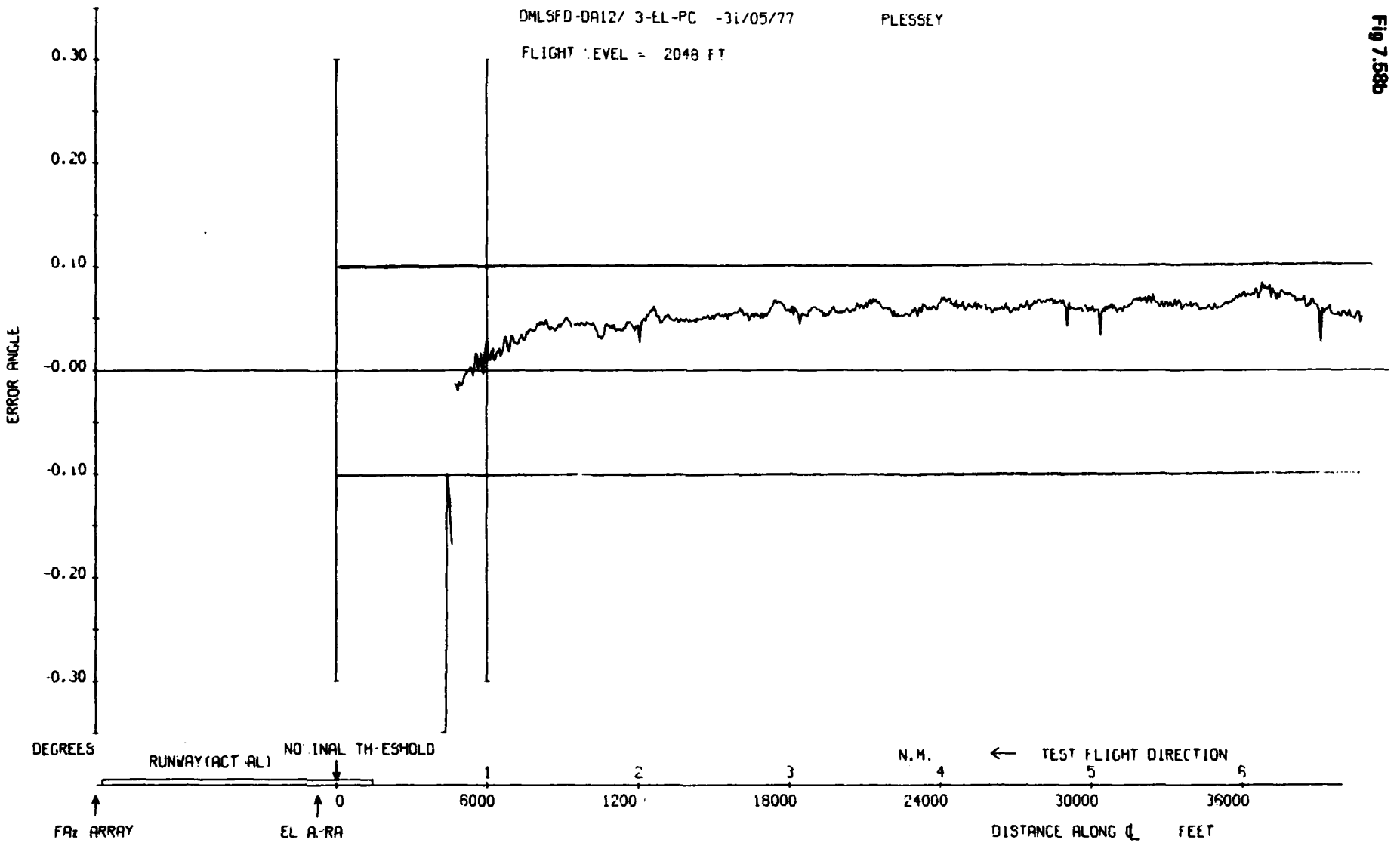

Fig 7.58b

Fig 7.58b Elevation 54λ, constant height radial 2048 ft, 0 degree azimuth

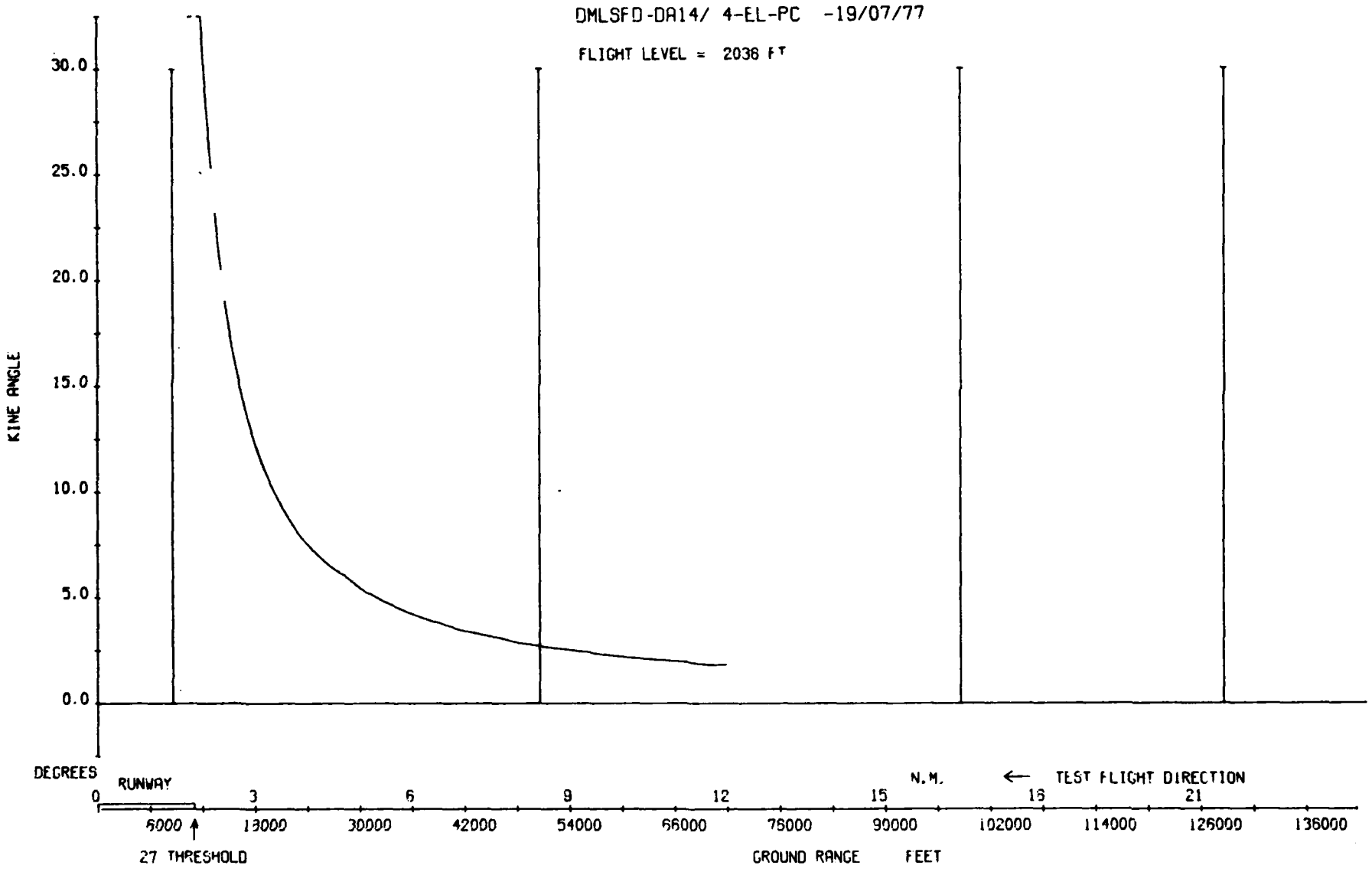

Fig 7.59a Elevation 54λ, constant height radial 2038 ft, 0° degree azimuth

Fig 7.59a

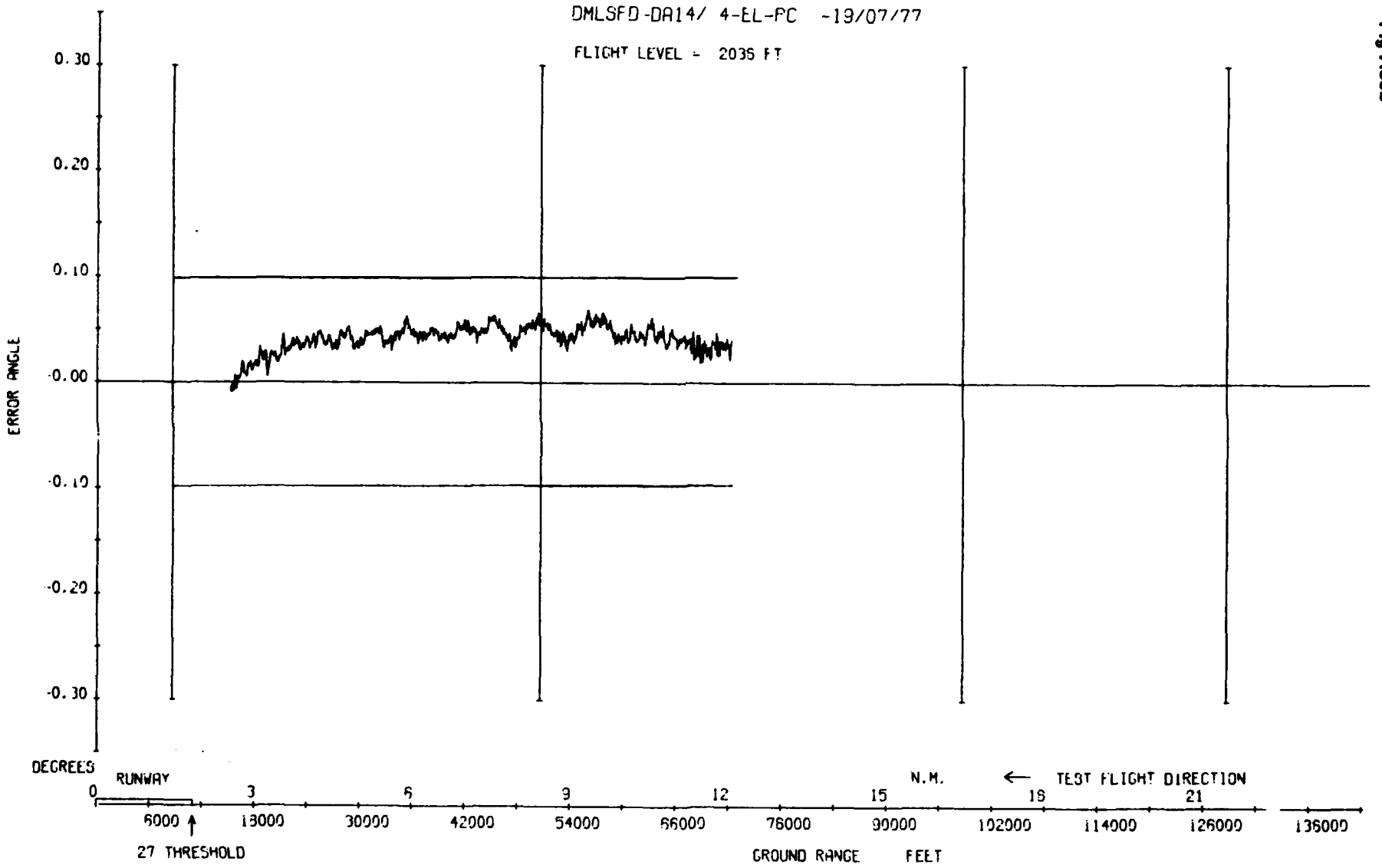

Fig 7.59b

R. A. E. BEDFORD

Fig 7.59b Elevation 54λ, constant height radial 2036 ft, 0 degree azimuth

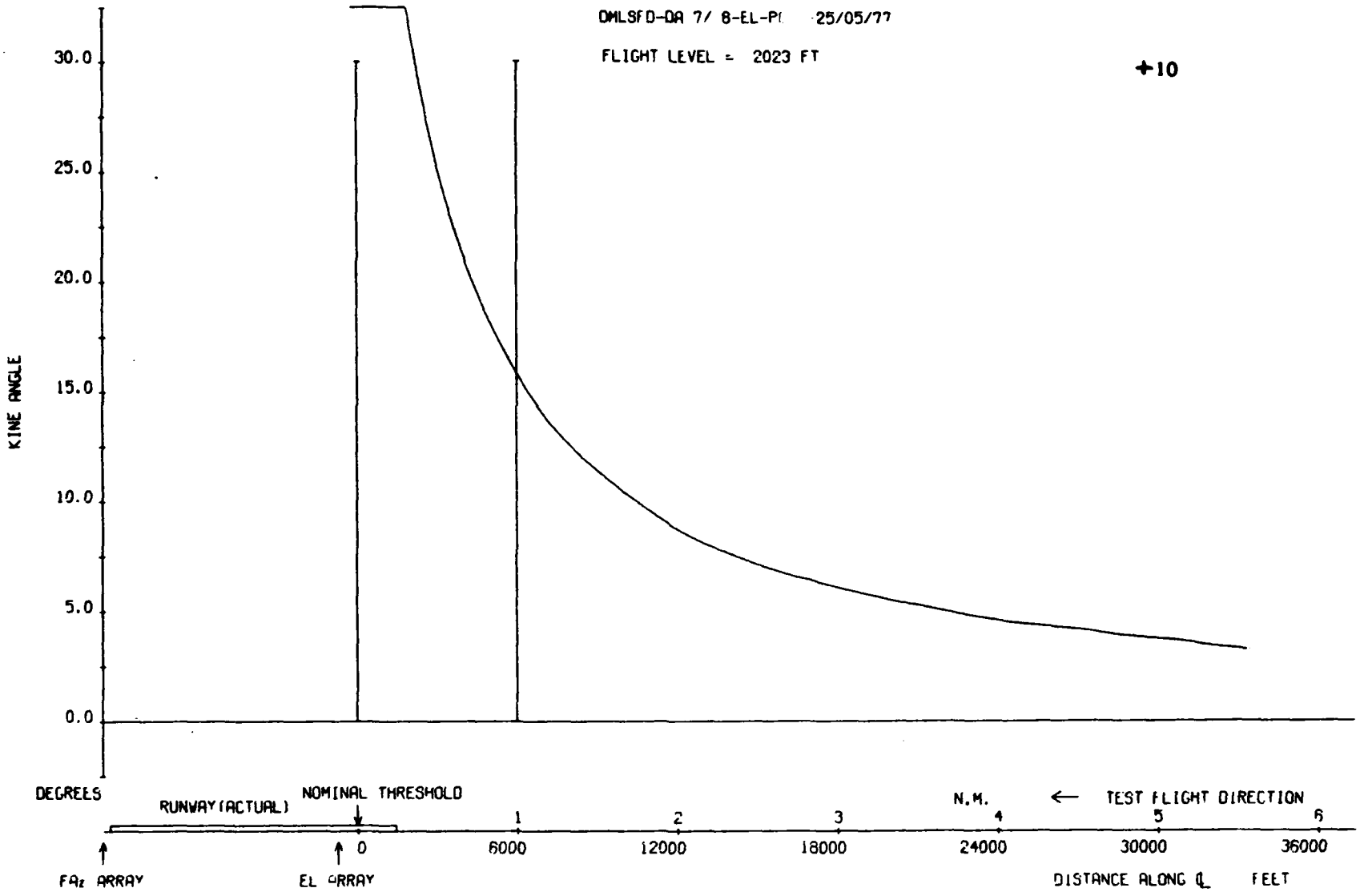

Fig 7.60a Elevation 54λ, constant height radial 2023 ft, +10 degrees azimuth

Fig 7.60a

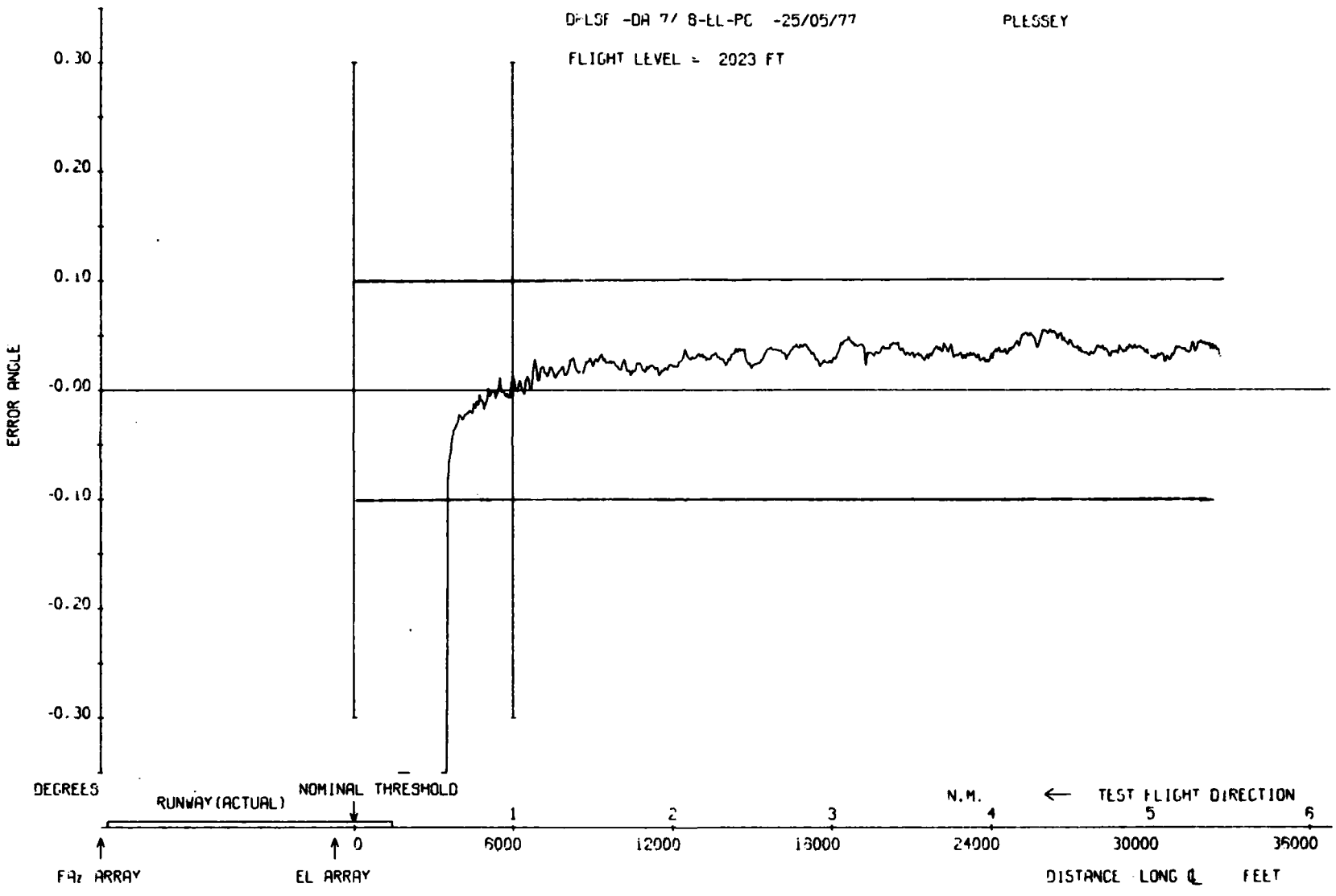

Fig 7.60b

Fig 7.60b Elevation 54λ, constant height radial 2023 ft, +10 degrees azimuth

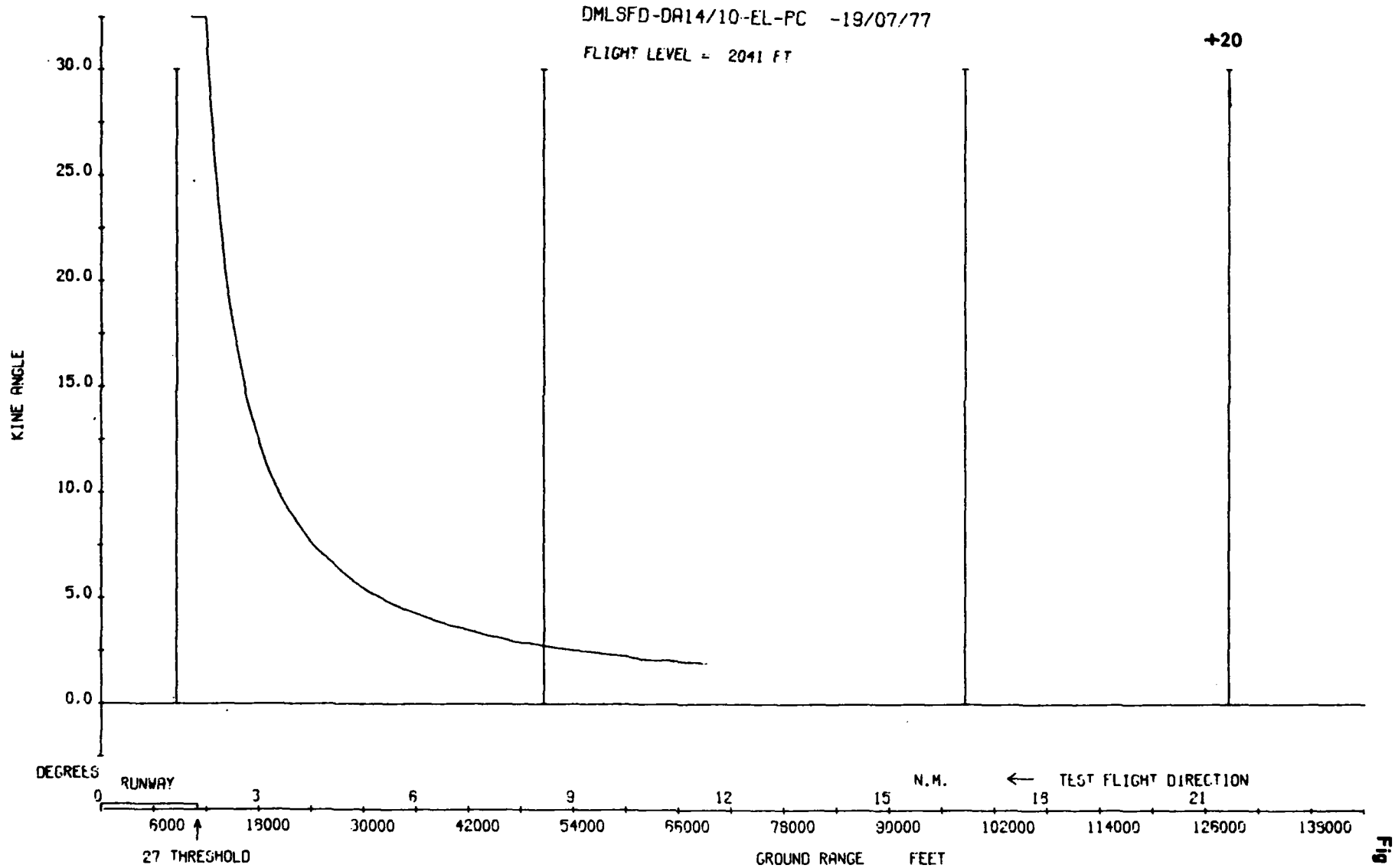

R. A. E. BEDFORD

Fig 7.61a Elevation 54λ, constant height radial 2041 ft, +20 degrees azimuth

Fig 7.61a

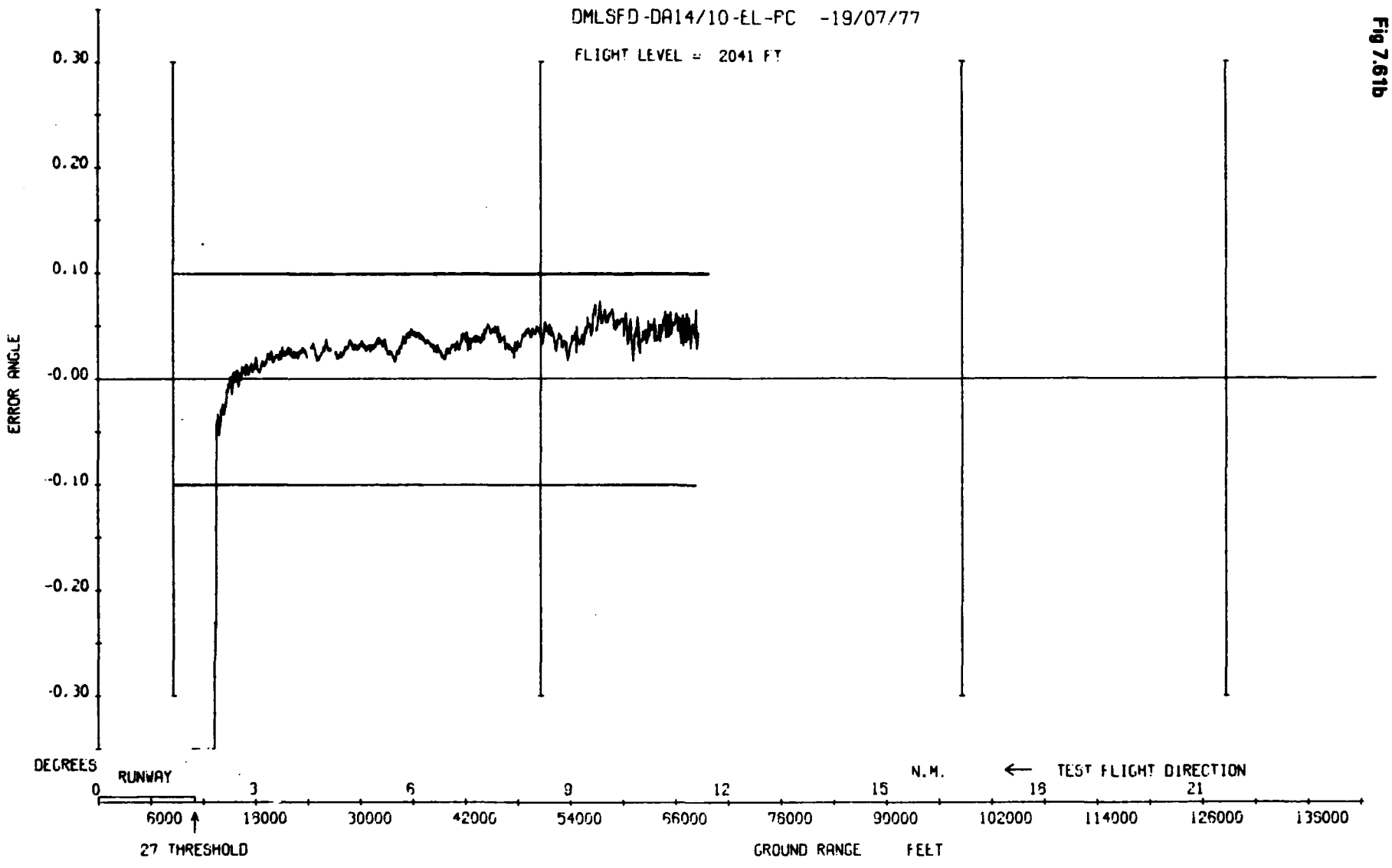

Fig 7.61b

R.A.E. BEDFORD **Fig 7.61b Elevation 54λ, constant height radial 2041 ft, +20 degrees azimuth**

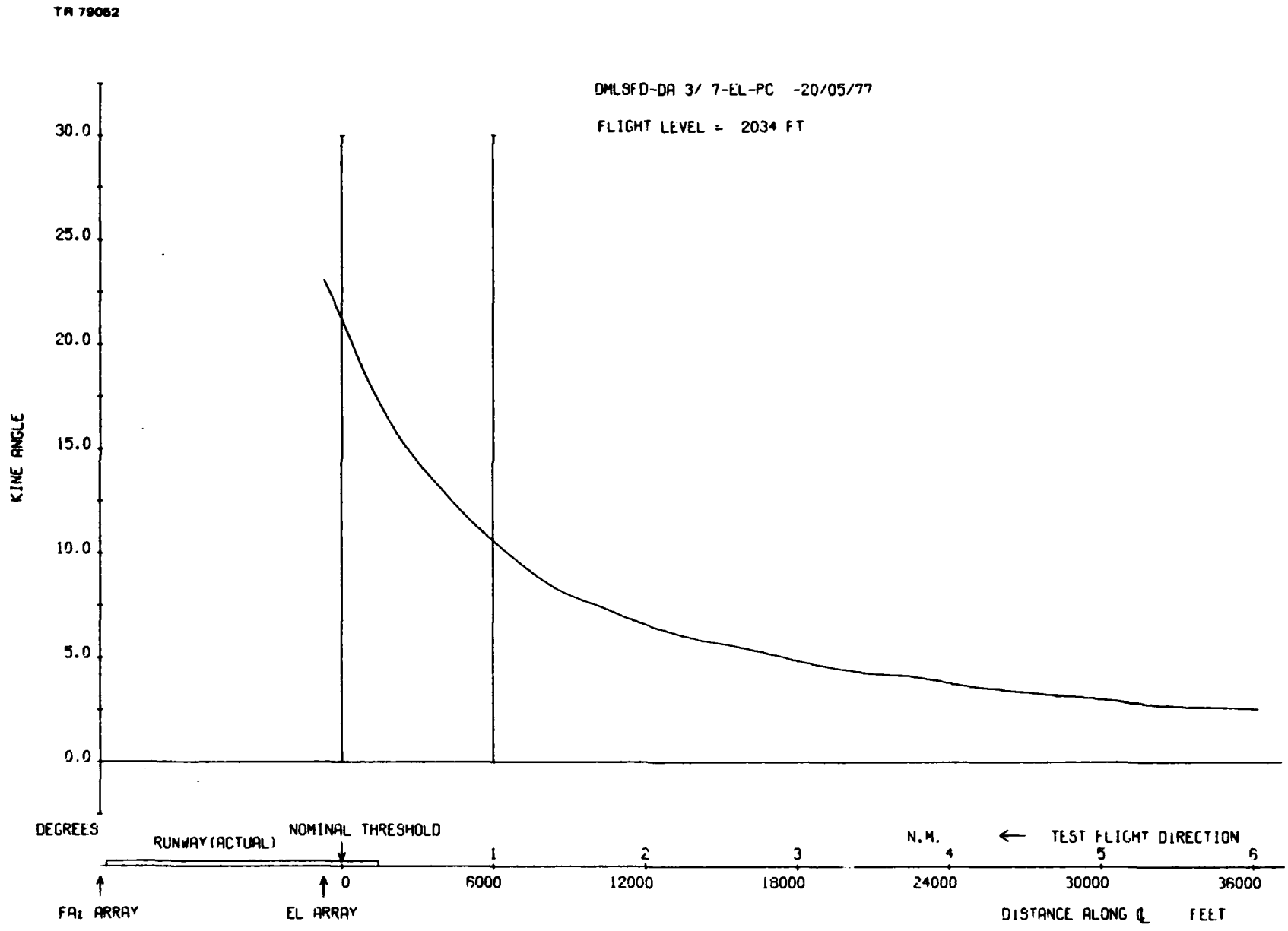

Fig 7.62a Elevation 54λ, constant height radial 2034 ft, +30 degrees azimuth

Fig 7.62a

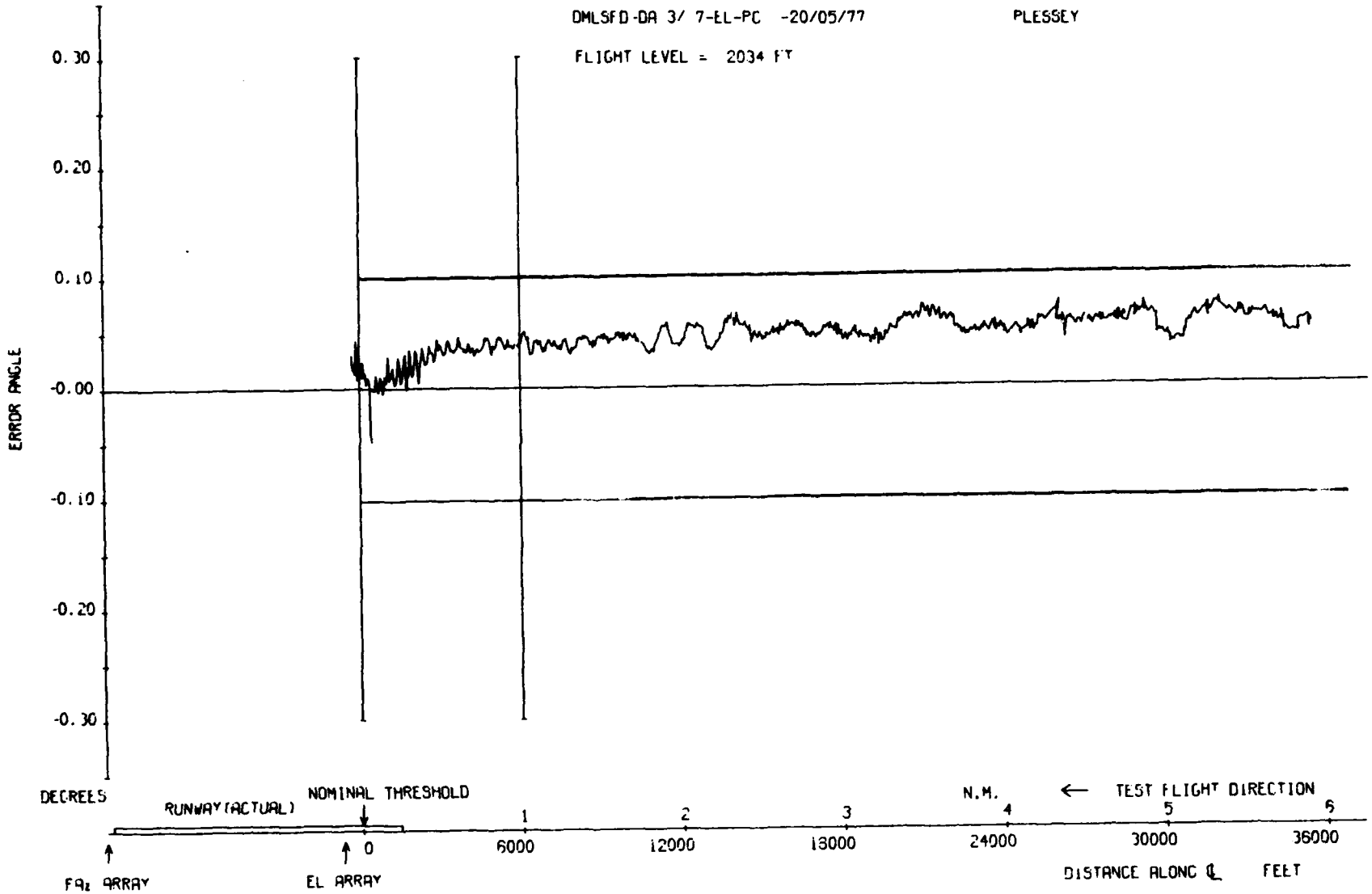

Fig 7.62b Elevation 54λ, constant height radial 2034 ft, +30 degrees azimuth

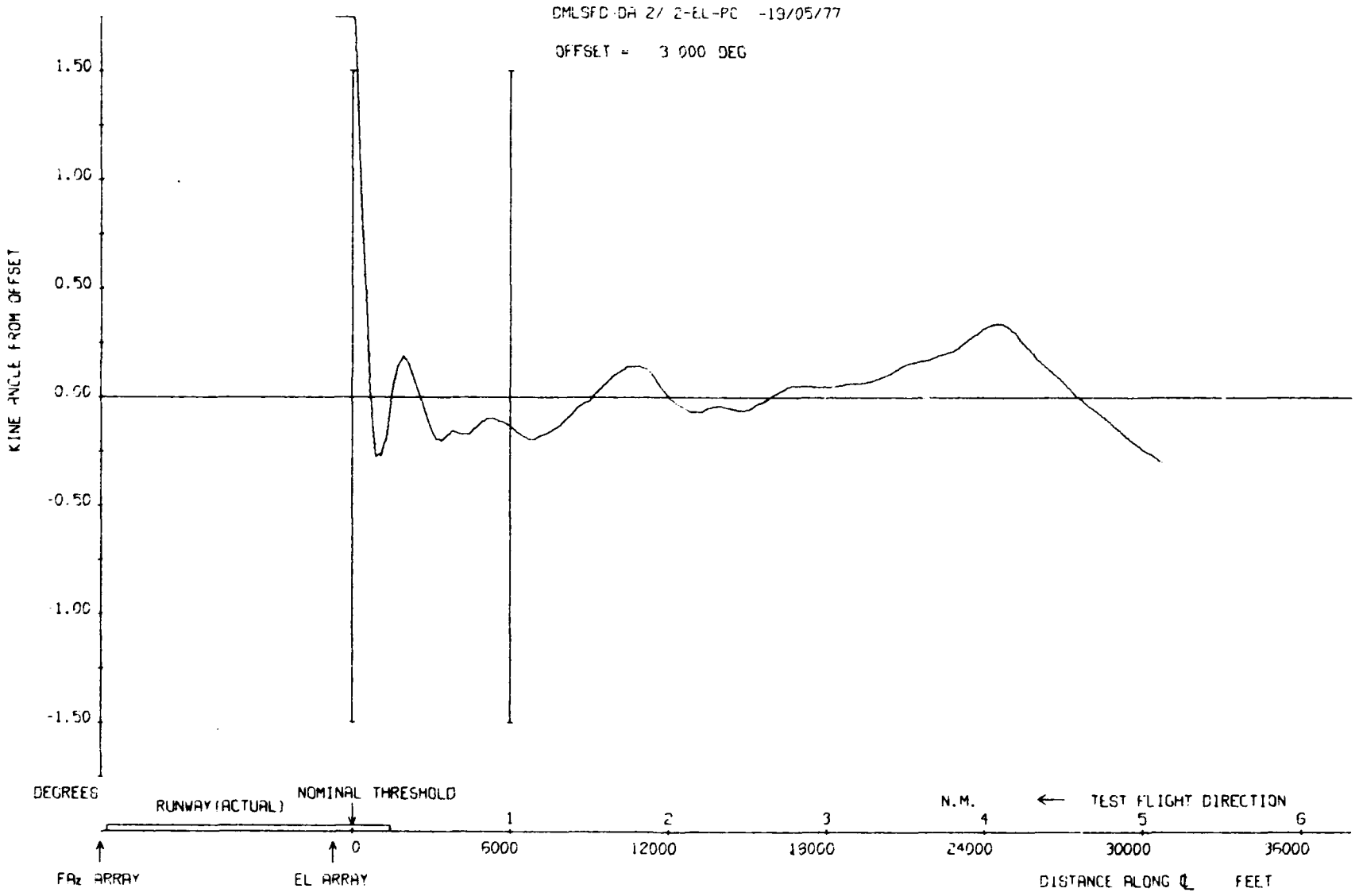

Fig 7.63a Elevation 54λ, 3 degree approach to touch and go

Fig 7.63a

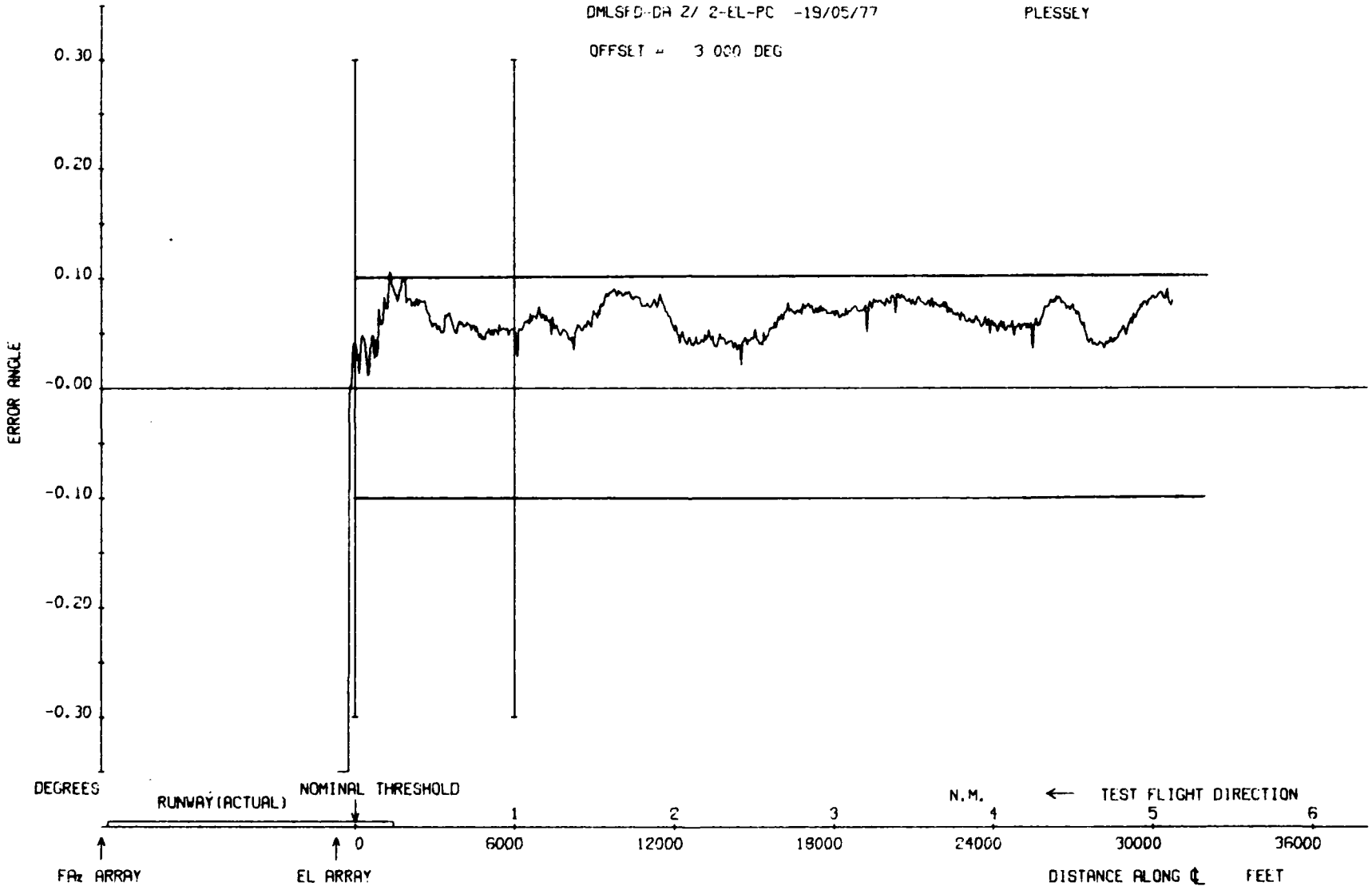

Fig 7.63b

Fig 7.63b Elevation 54λ, 3 degree approach to touch and go

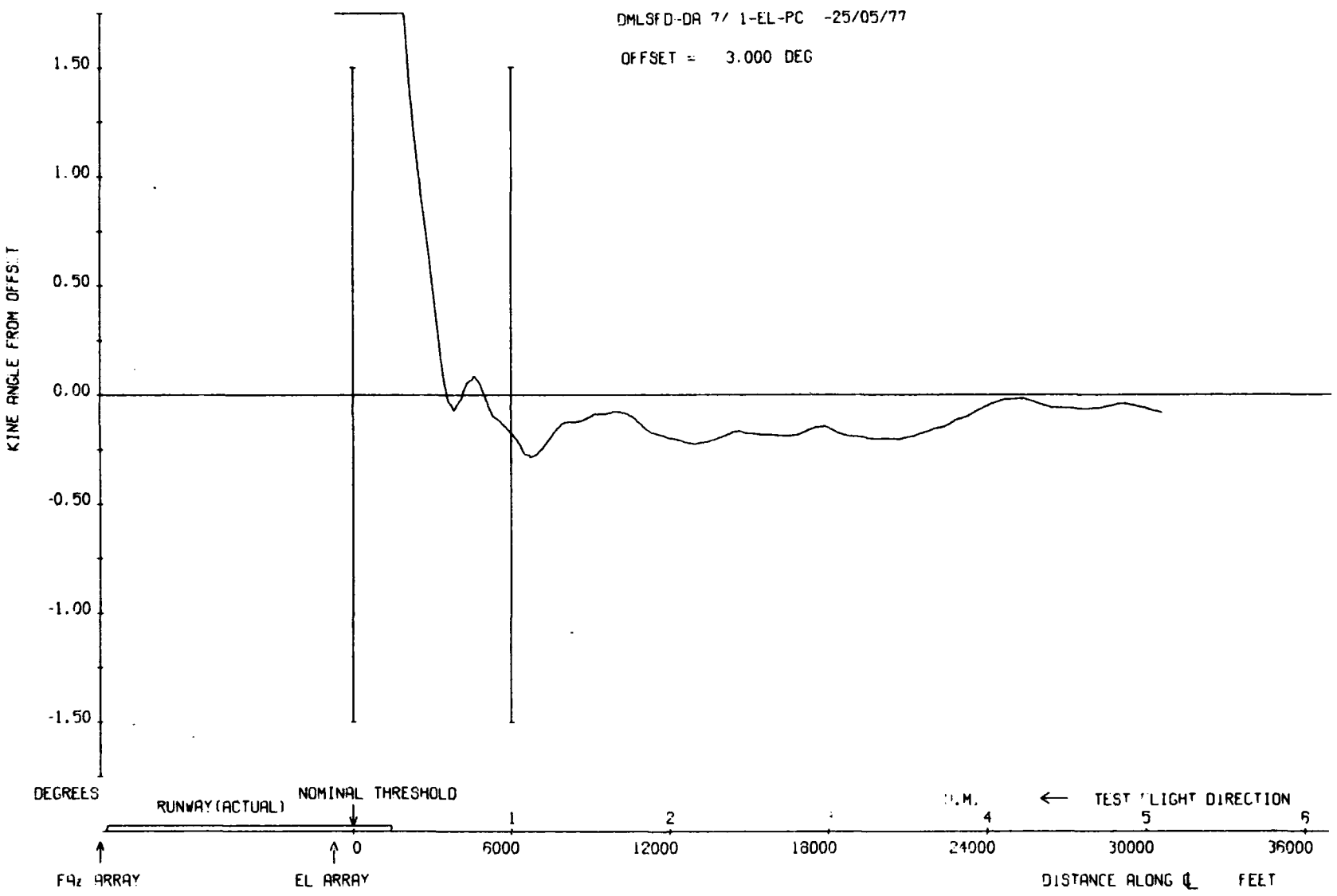

Fig 7.64a Elevation 54λ, 3 degree approach to 300 ft overshoot

Fig 7.64a

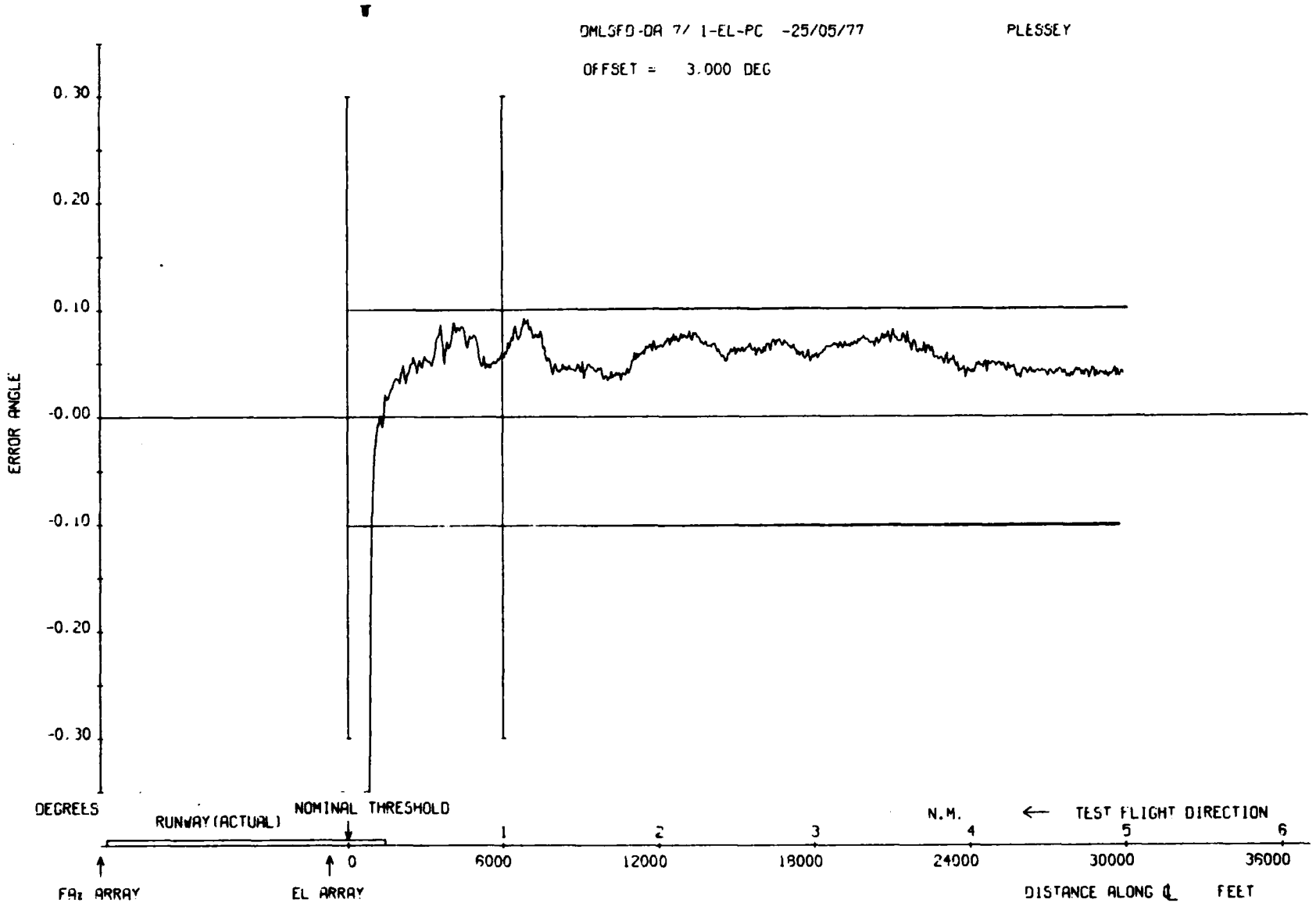

Fig 7.64b

Fig 7.64b Elevation 54λ, 3 degree approach to 300 ft overshoot

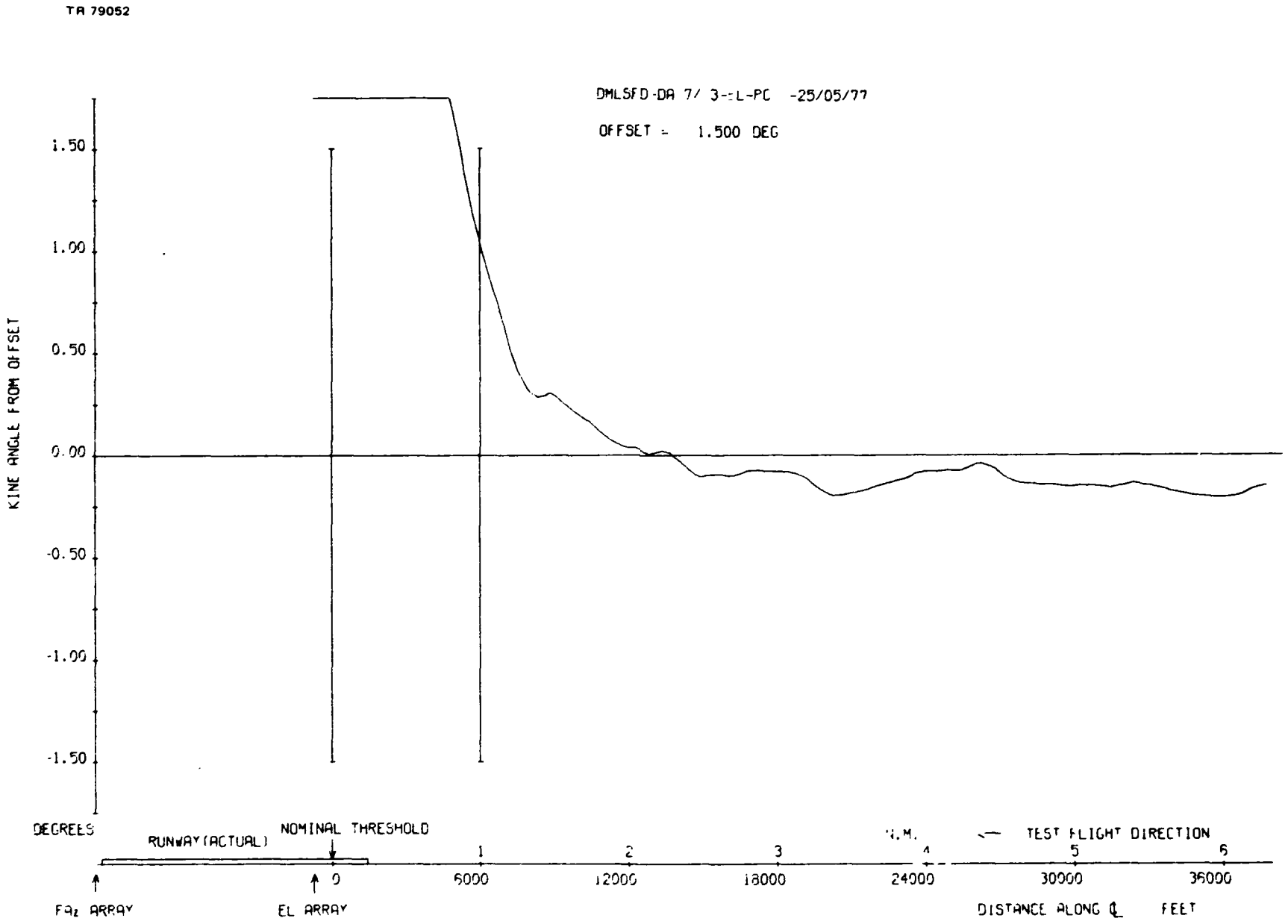

Fig 7.65a

Fig 7.65a Elevation 54λ, 1.5 degree approach to 300 ft overshoot

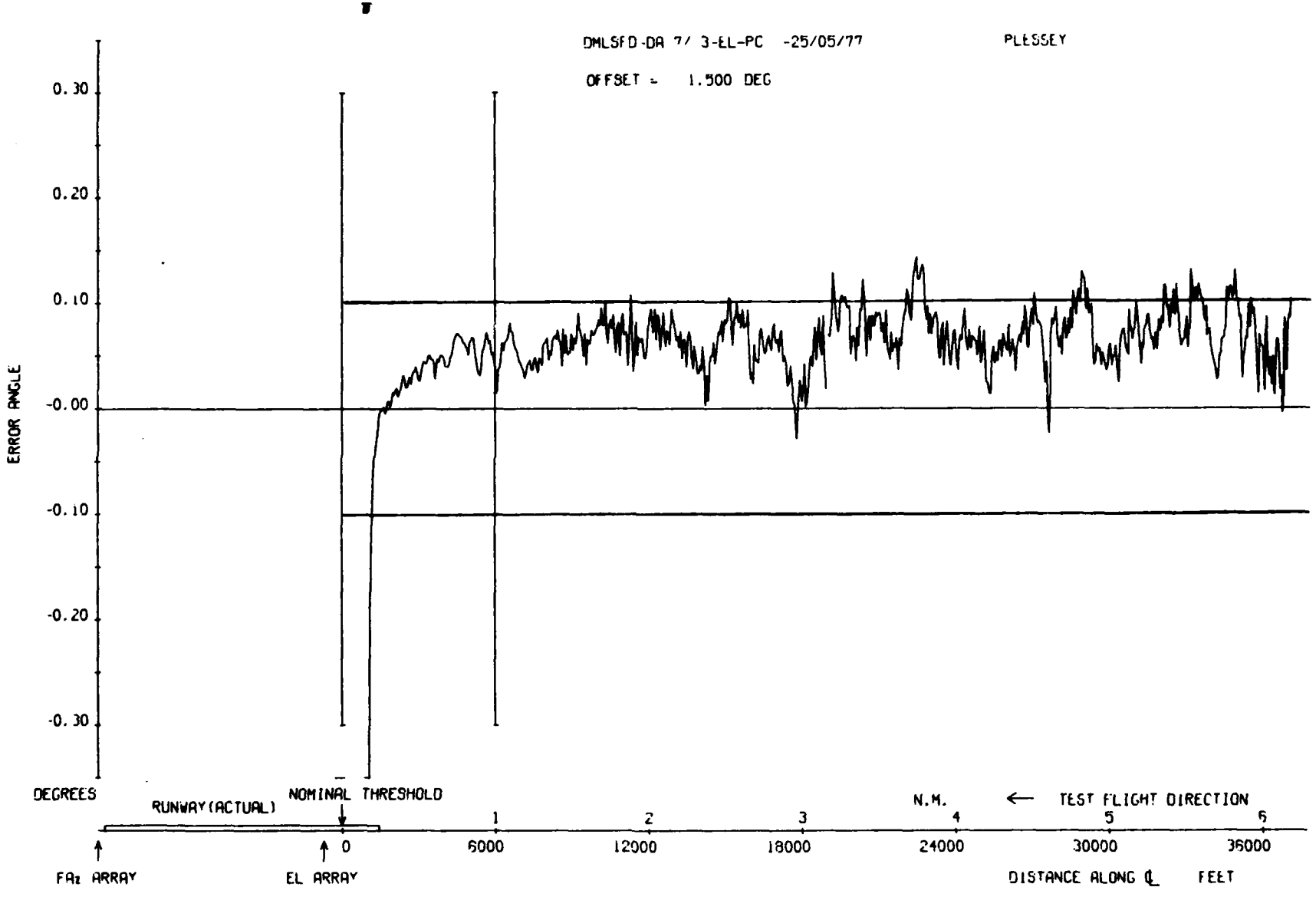

Fig 7.65b

Fig 7.65b Elevation 54λ, 1.5 degree approach to 300 ft overshoot

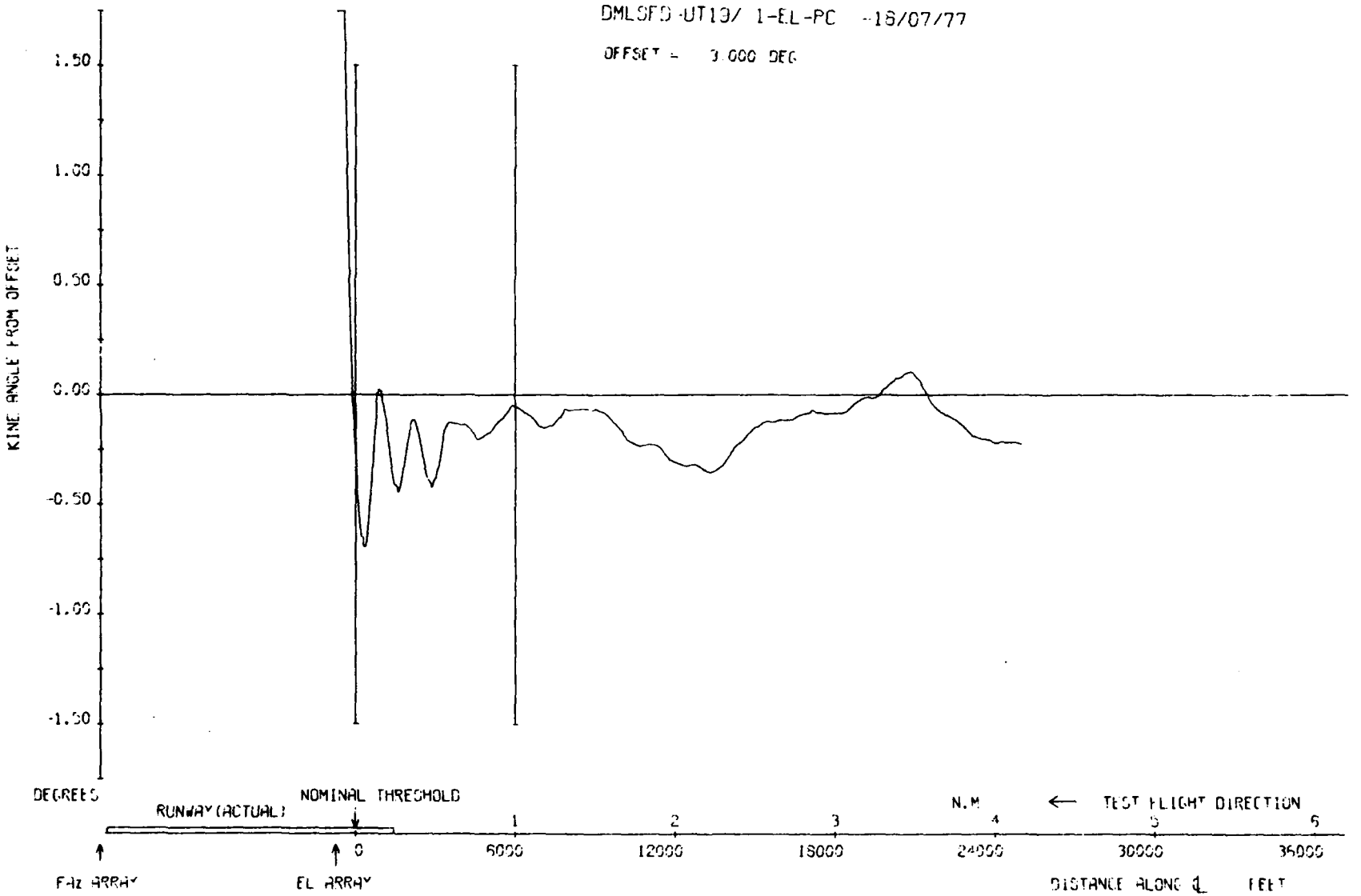

R. A. E. BEDFORD

Fig 7.66a Elevation 54λ, 3 degree approach to 50 ft overshoot

Fig 7.66a

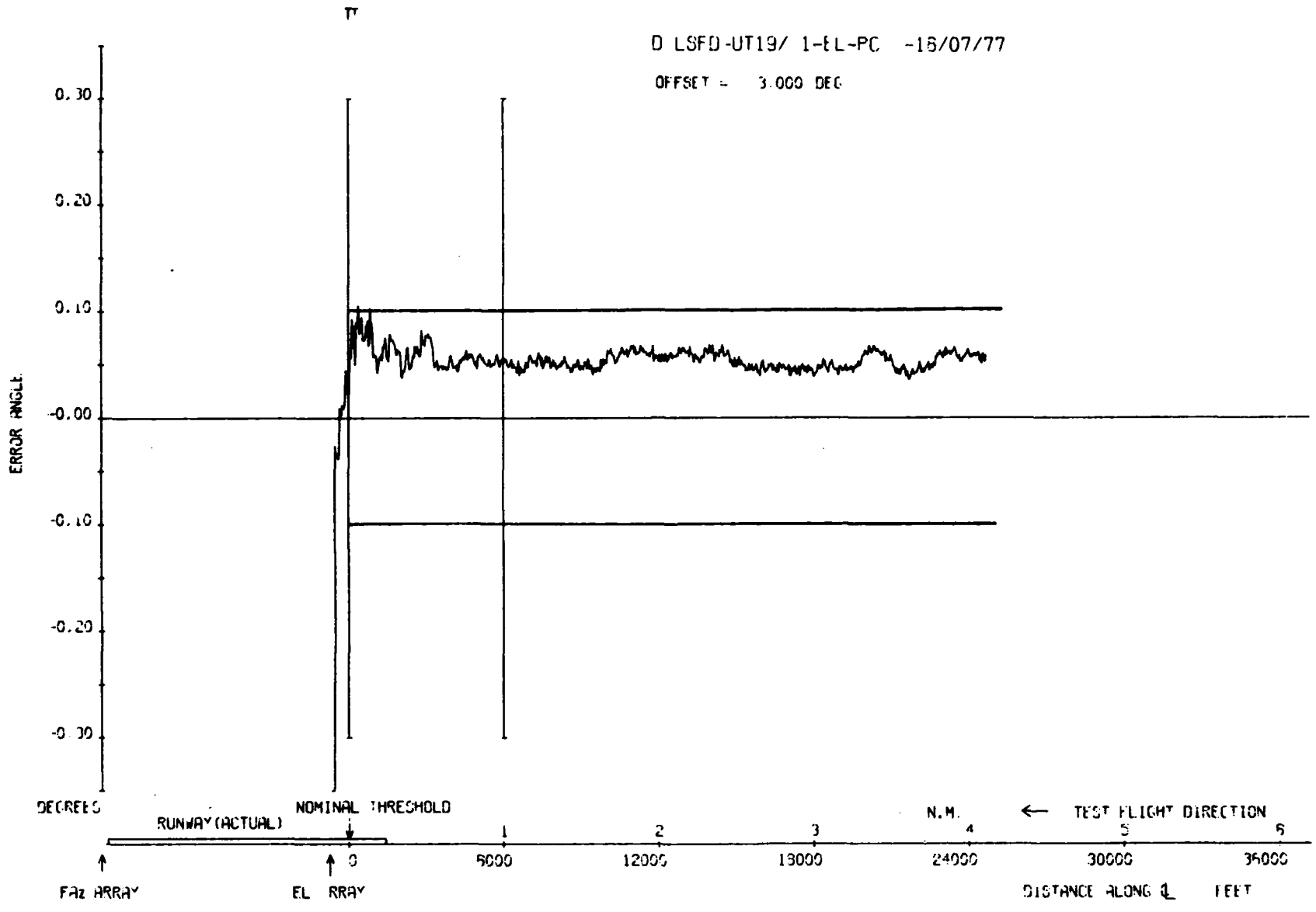

R. A. E. BEDFORD

Fig 7.66b Elevation 54λ, 3 degree approach to 50 ft overshoot

Fig 7.66b

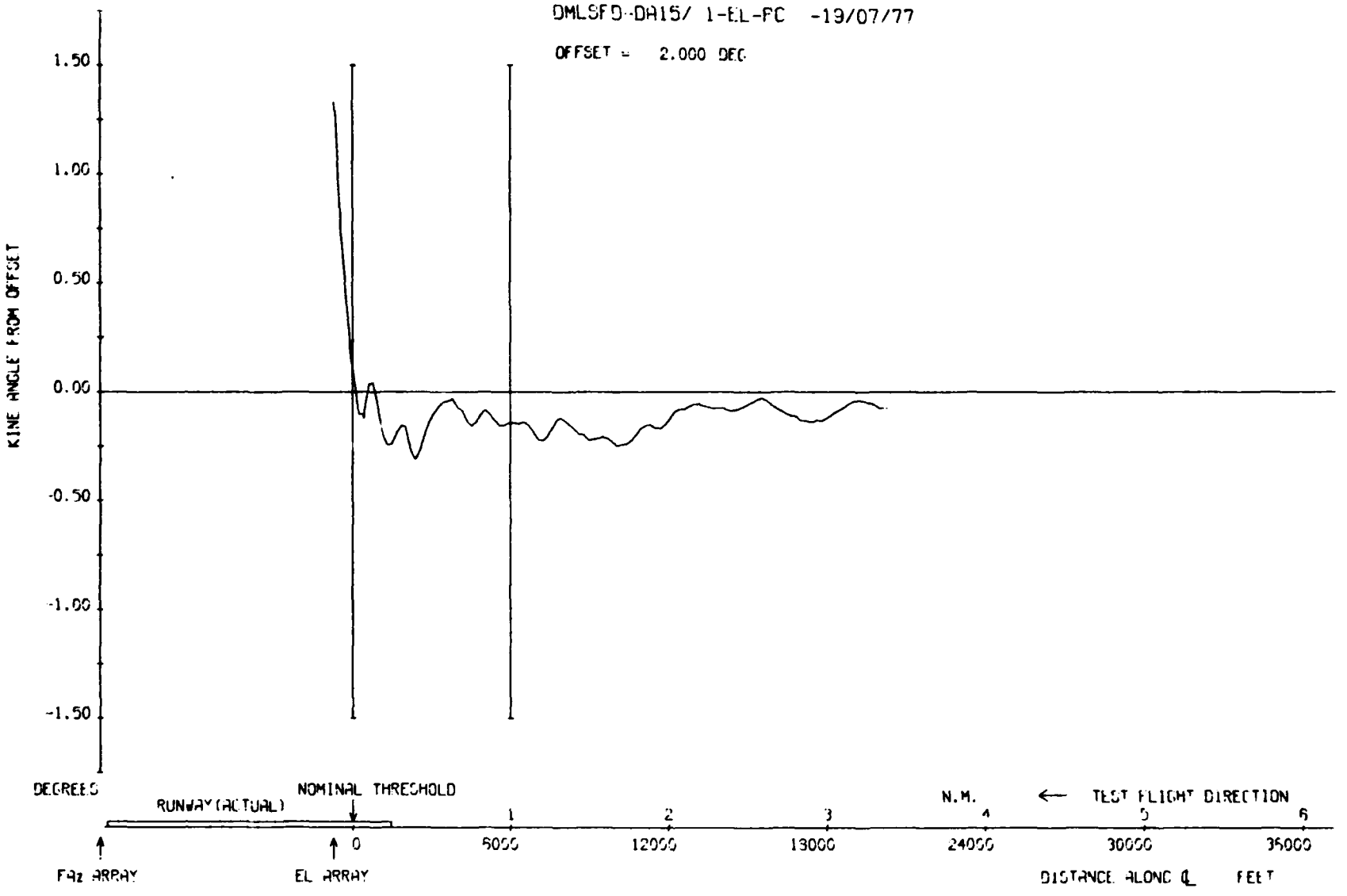

R. A. E. BEDFORD

Fig 7.67a Elevation 54λ, 2 degree approach to low overshoot

Fig 7.67a

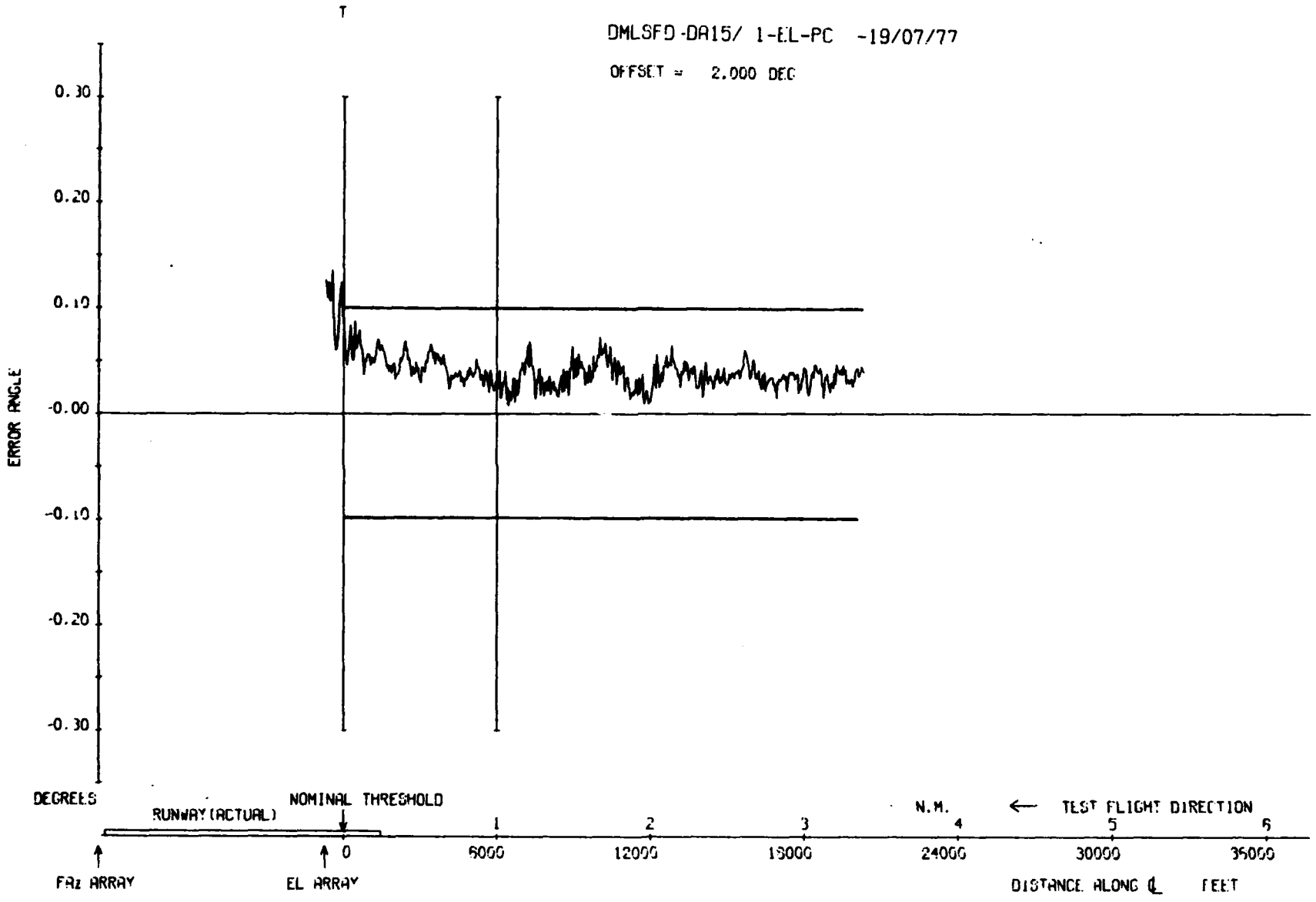

R. A. E. BEDFORD

Fig 7.67b Elevation 54λ, 2 degree approach to low overshoot

TR 79062

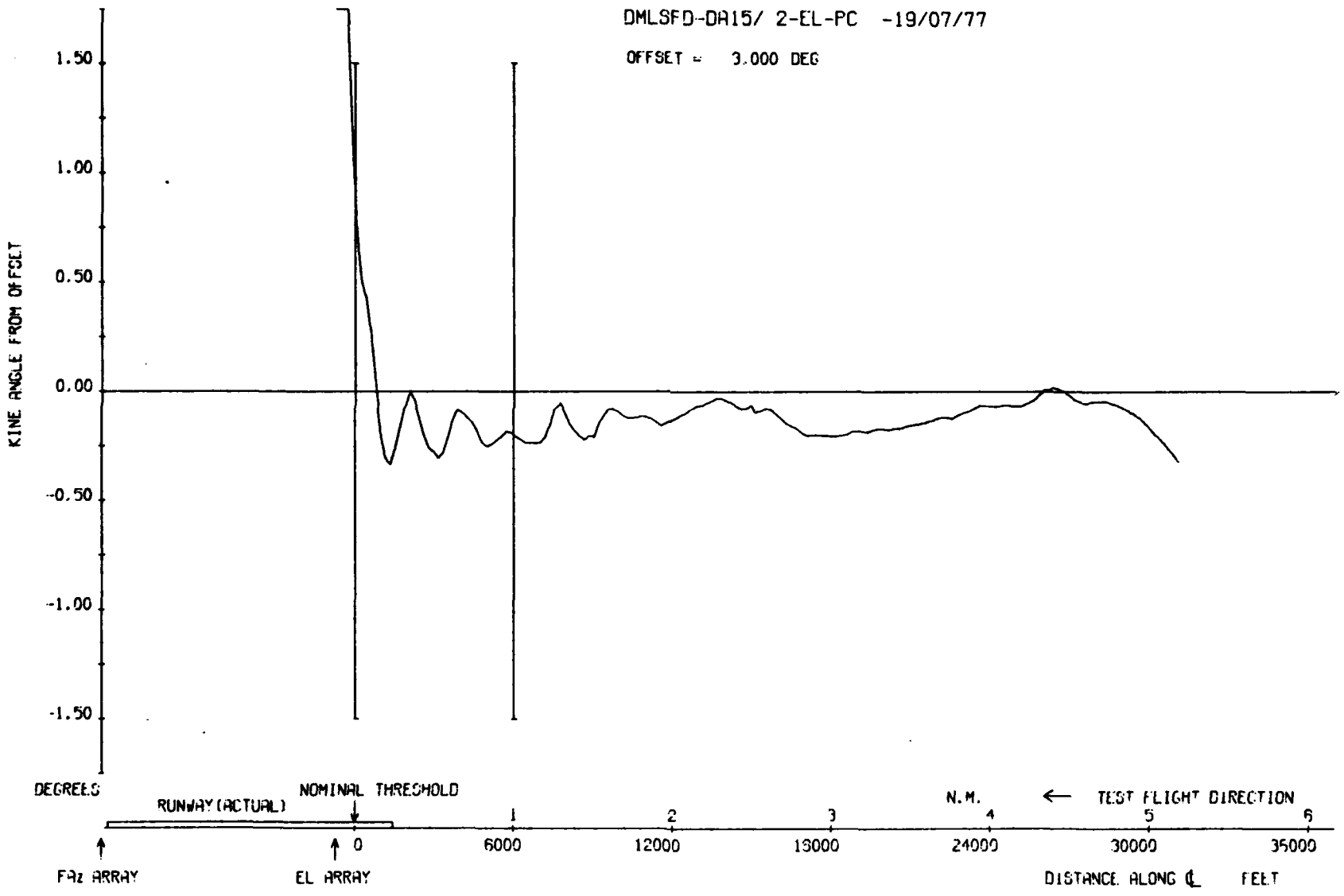

R. A. E. BEDFORD

Fig 7.68a Elevation 54λ, 3 degree approach to low overshoot

Fig 7.68a

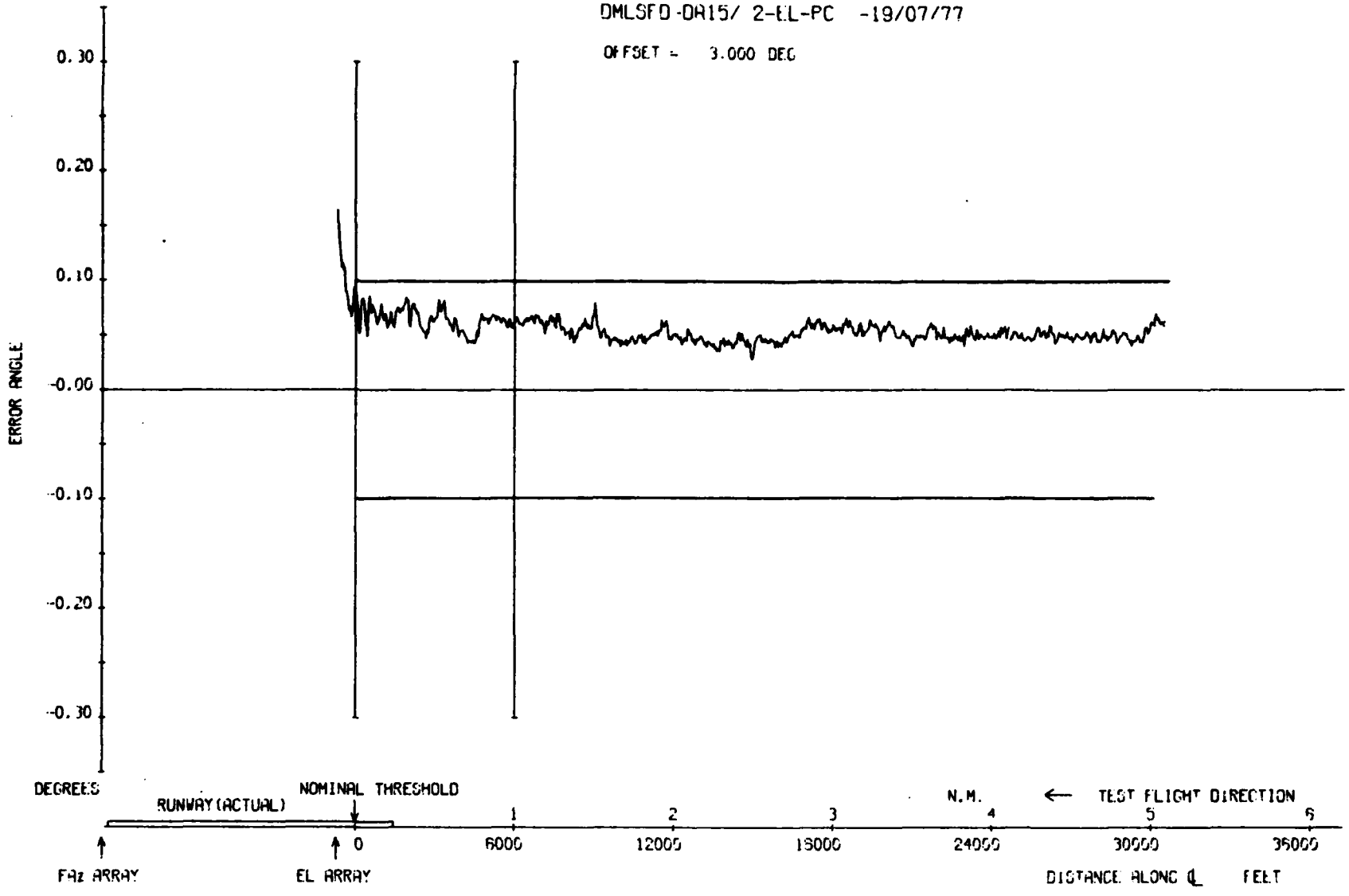

R. A. E. BEDFORD

Fig 7.68b Elevation 54λ, 3 degree approach to low overshoot

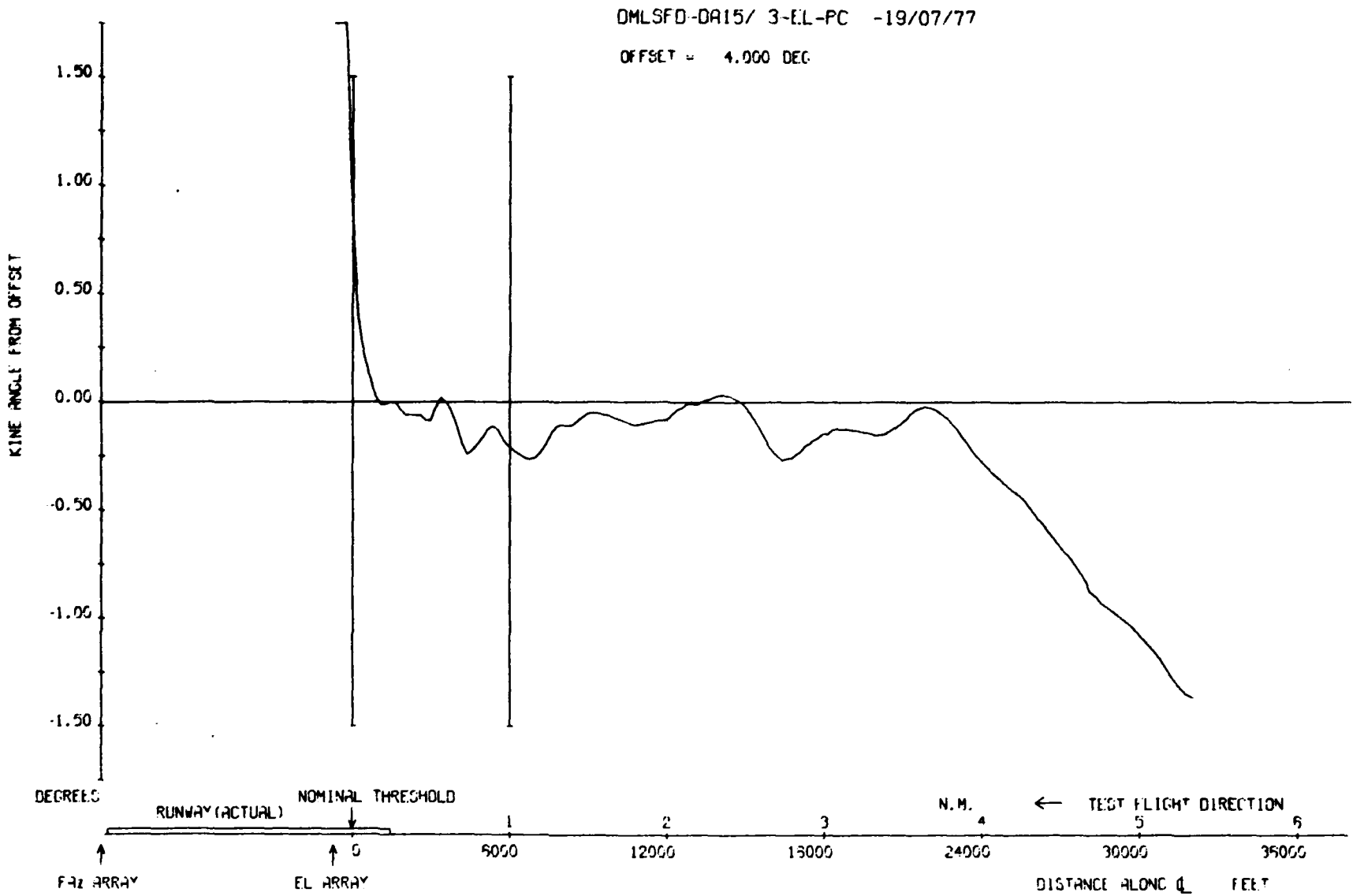

R. A. E. BEDFORD

Fig 7.69a Elevation 54λ, 4 degree approach to low overshoot

Fig 7.69a

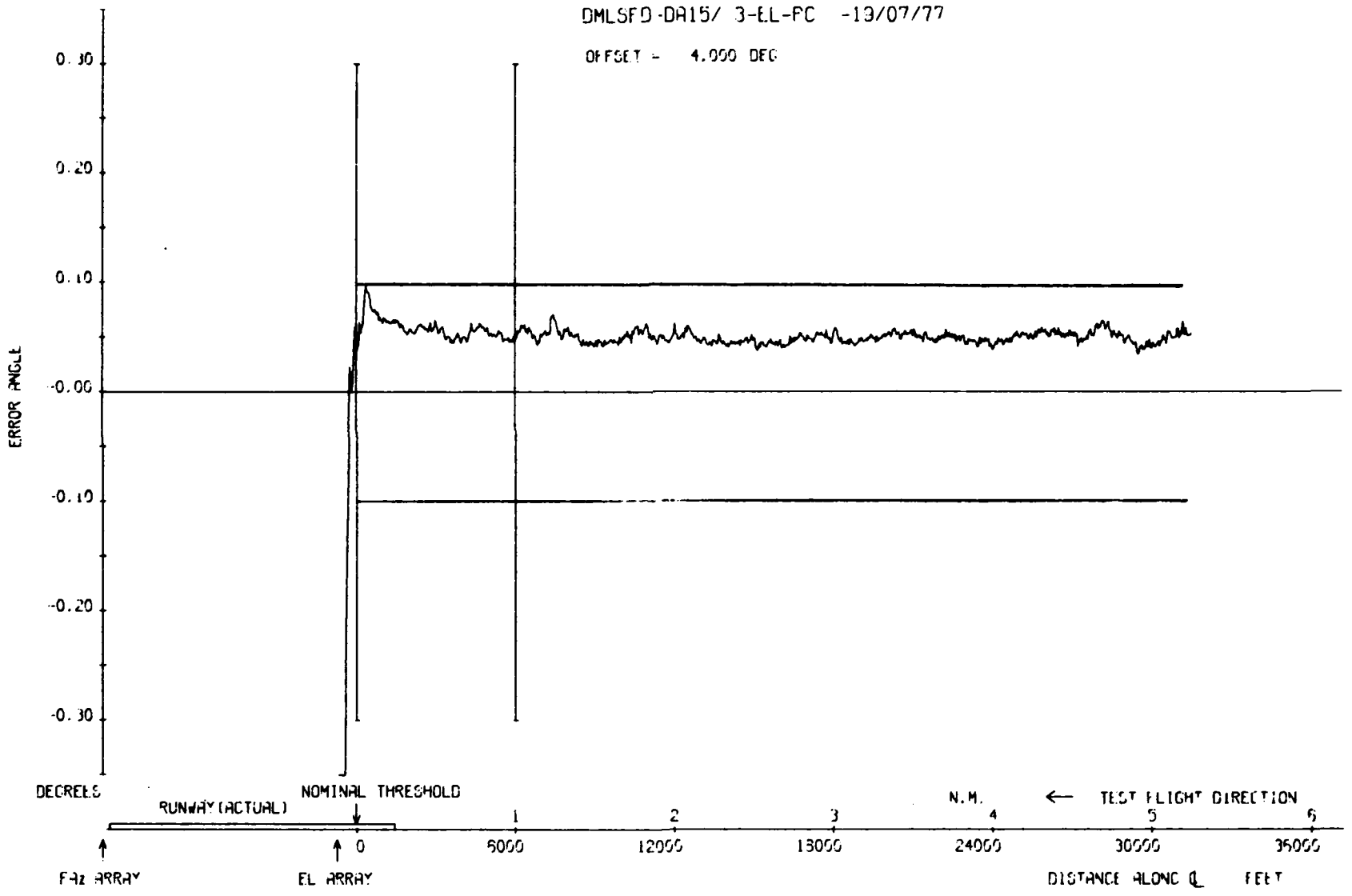

Fig 7.69b

R.A.E. BEDFORD

Fig 7.69b Elevation 54λ, 4 degree approach to low overshoot

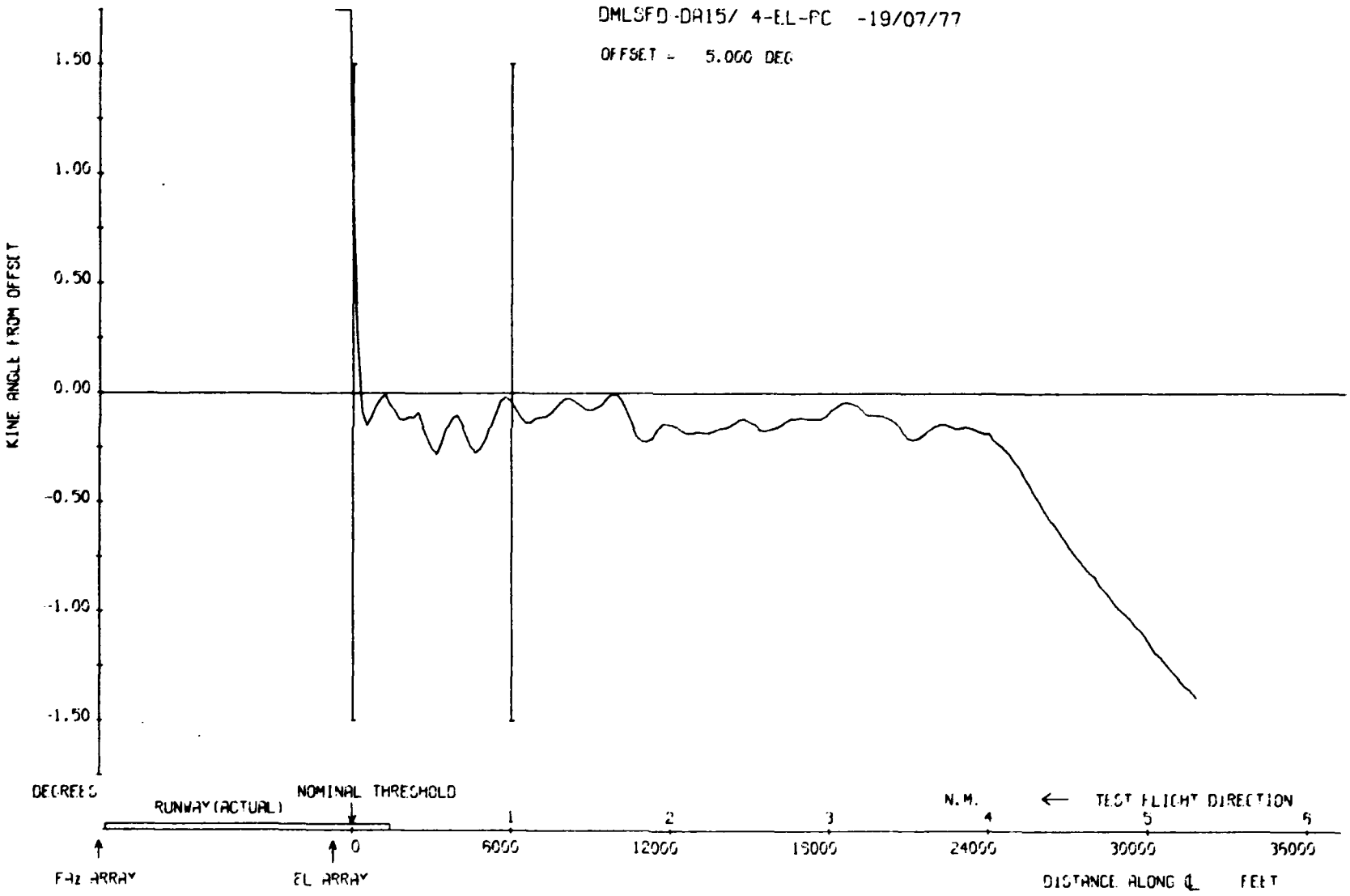

R. A. E. BEDFORD

Fig 7.70a Elevation 54λ, 5 degree approach to low overshoot

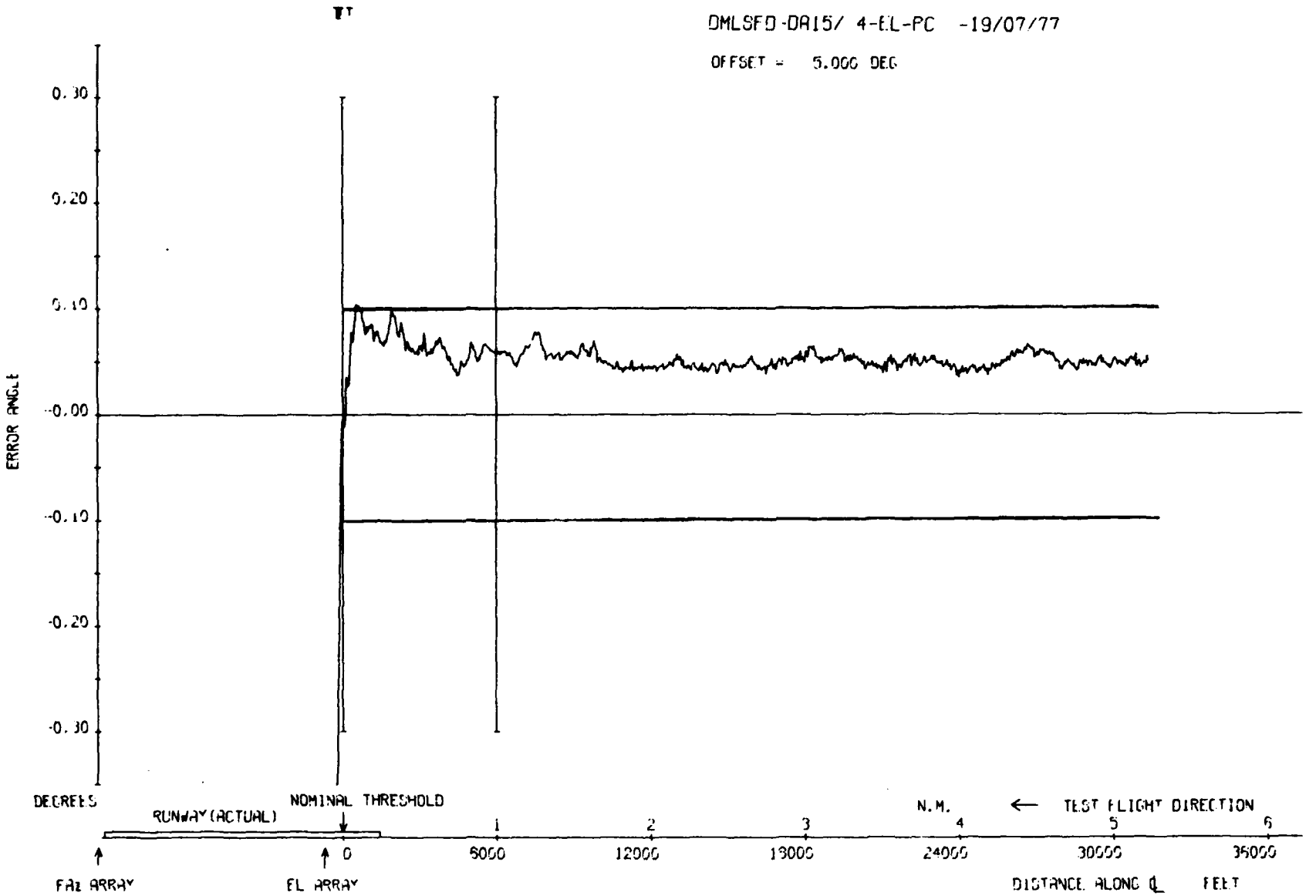

R. A. E. BEDFORD

Fig 7.70b Elevation 54λ, 5 degree approach to low overshoot

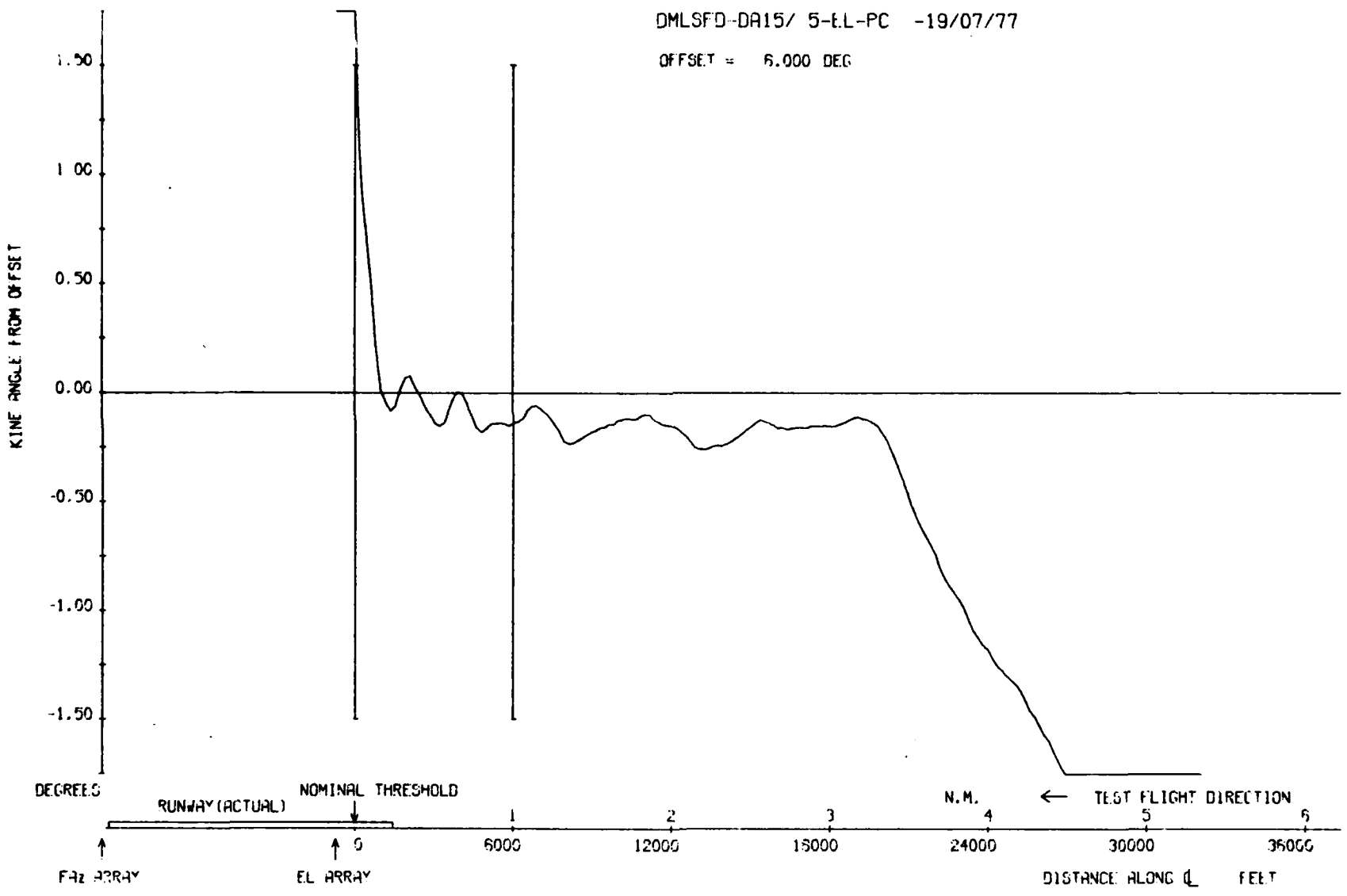

R. A. E. BEDFORD

Fig 7.71a Elevation 54λ, 6 degree approach to low overshoot

Fig 7.71a

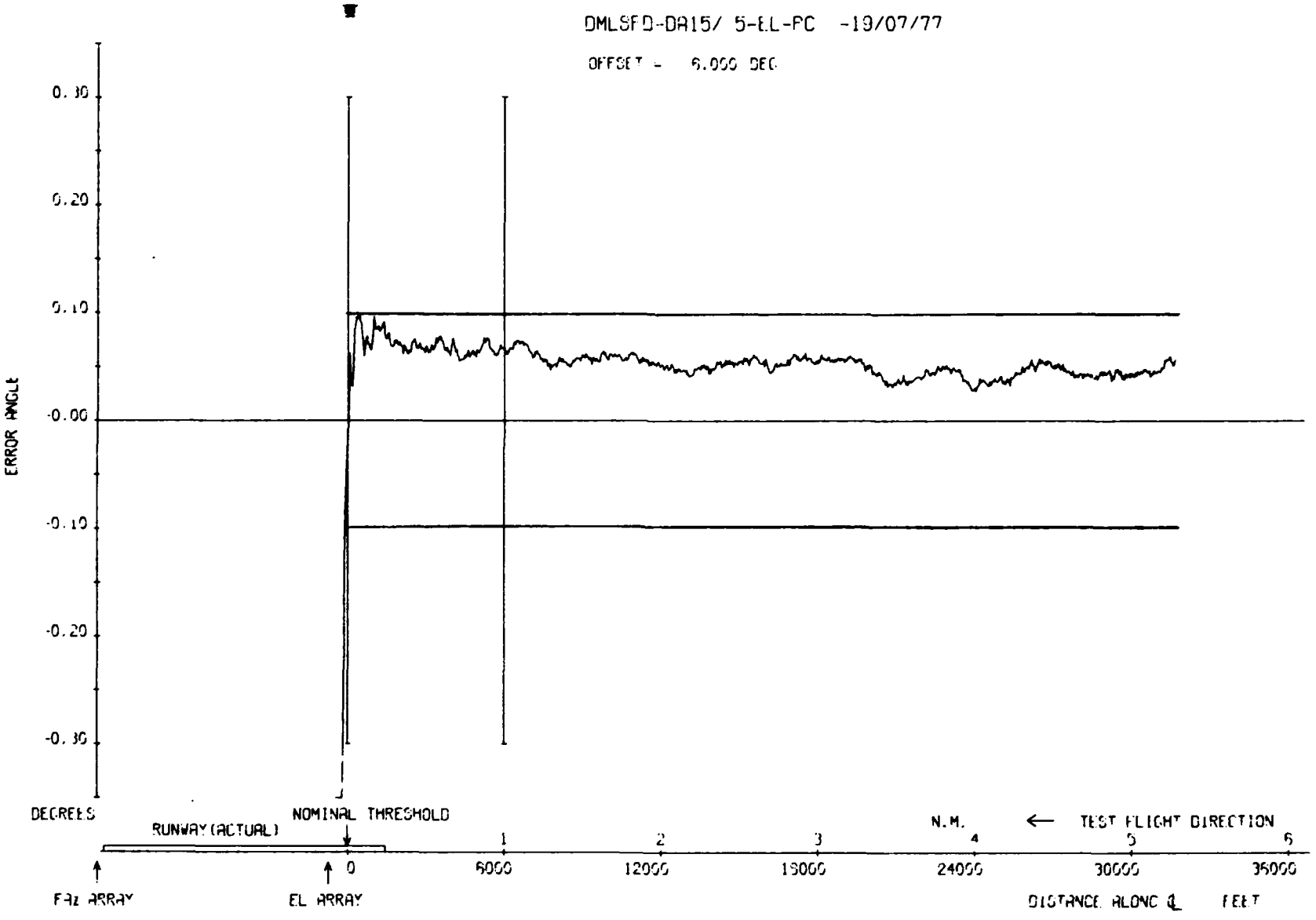

R. G. E. BEDFORD

Fig 7.71b Elevation 54λ, 6 degree approach to low overshoot

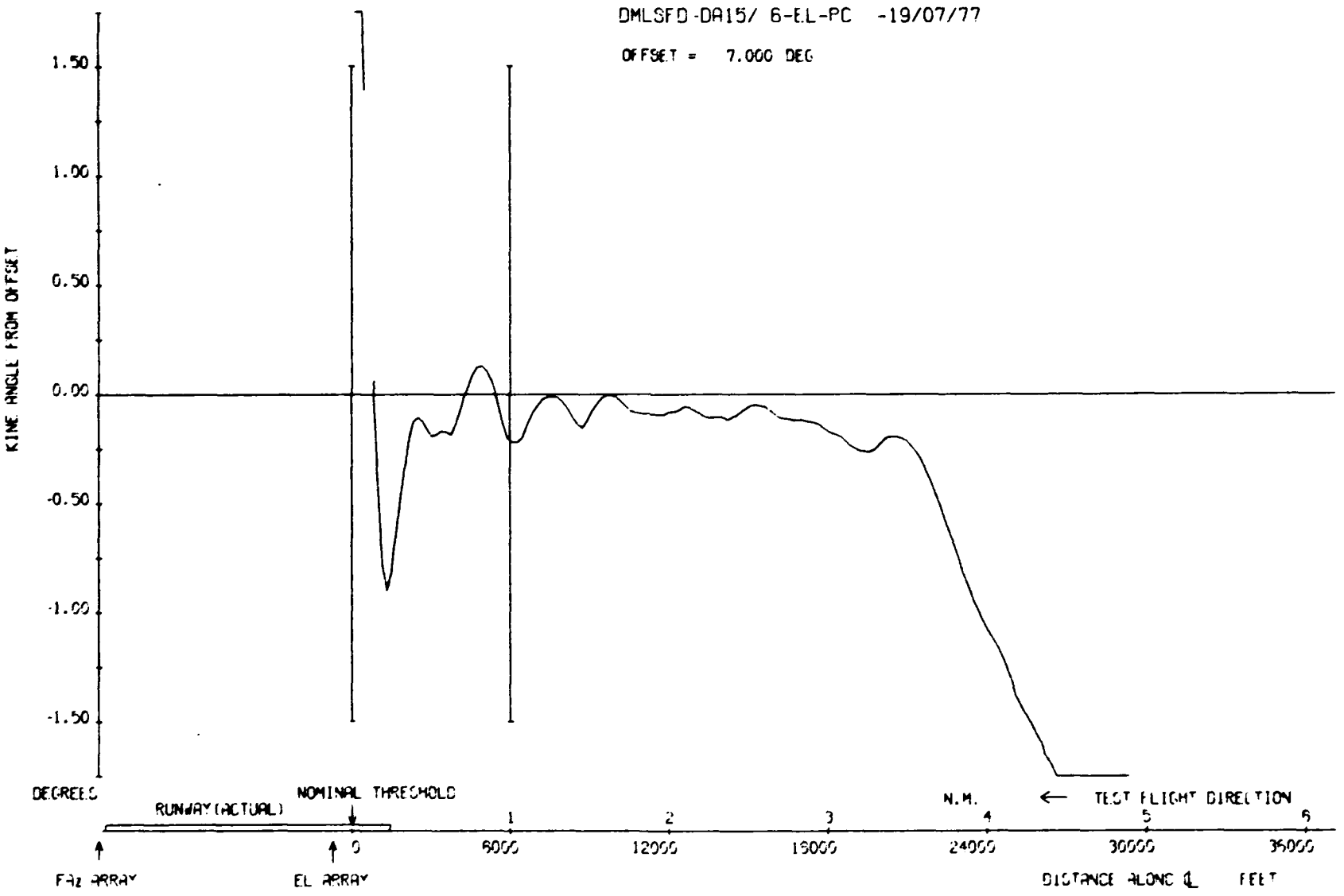

R. A. E. BEDFORD

Fig 7.72a Elevation 54λ, 7 degree approach to low overshoot

Fig 7.72a

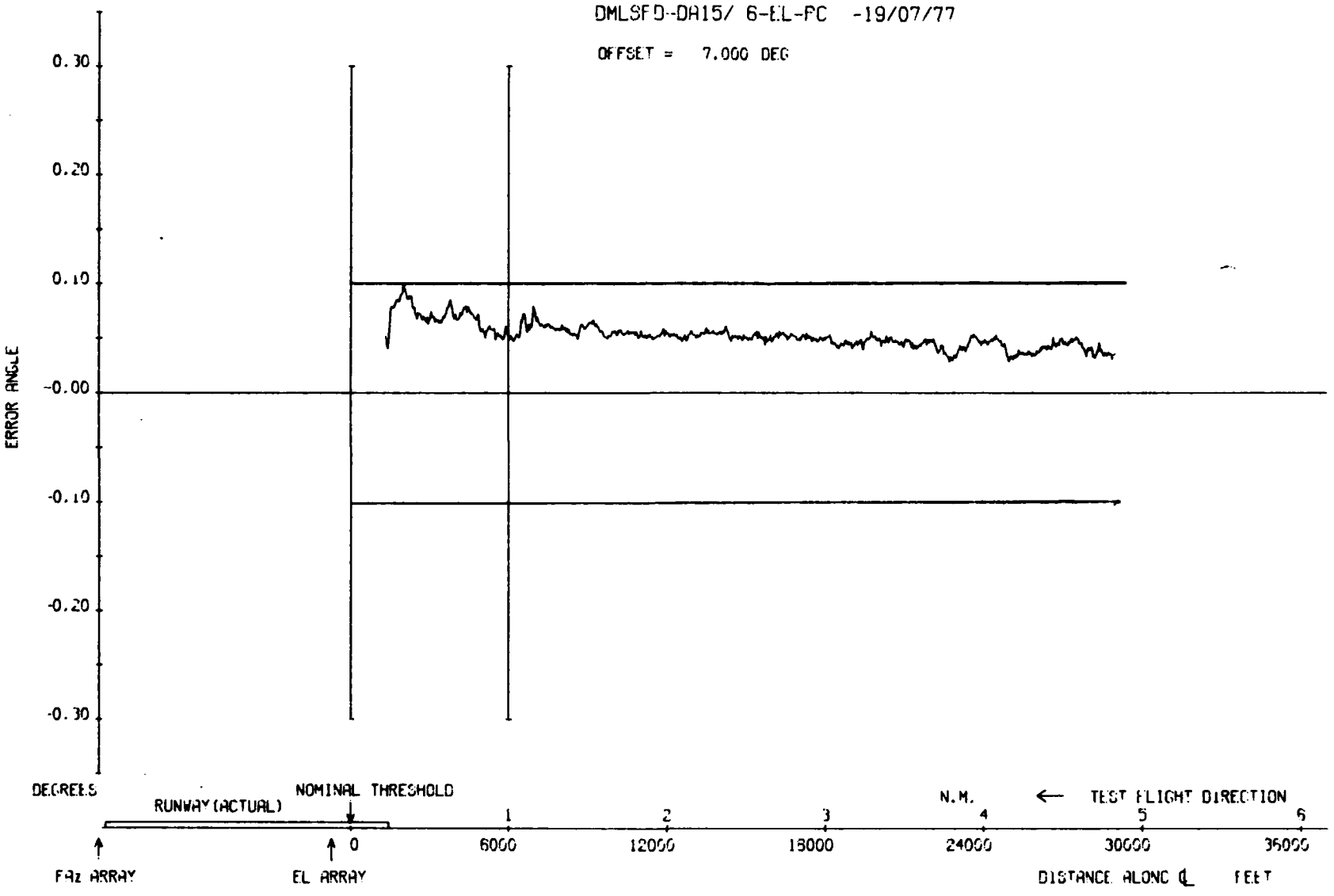

R. A. E. BEDFORD

Fig 7.72b Elevation 54λ, 7 degree approach to low overshoot

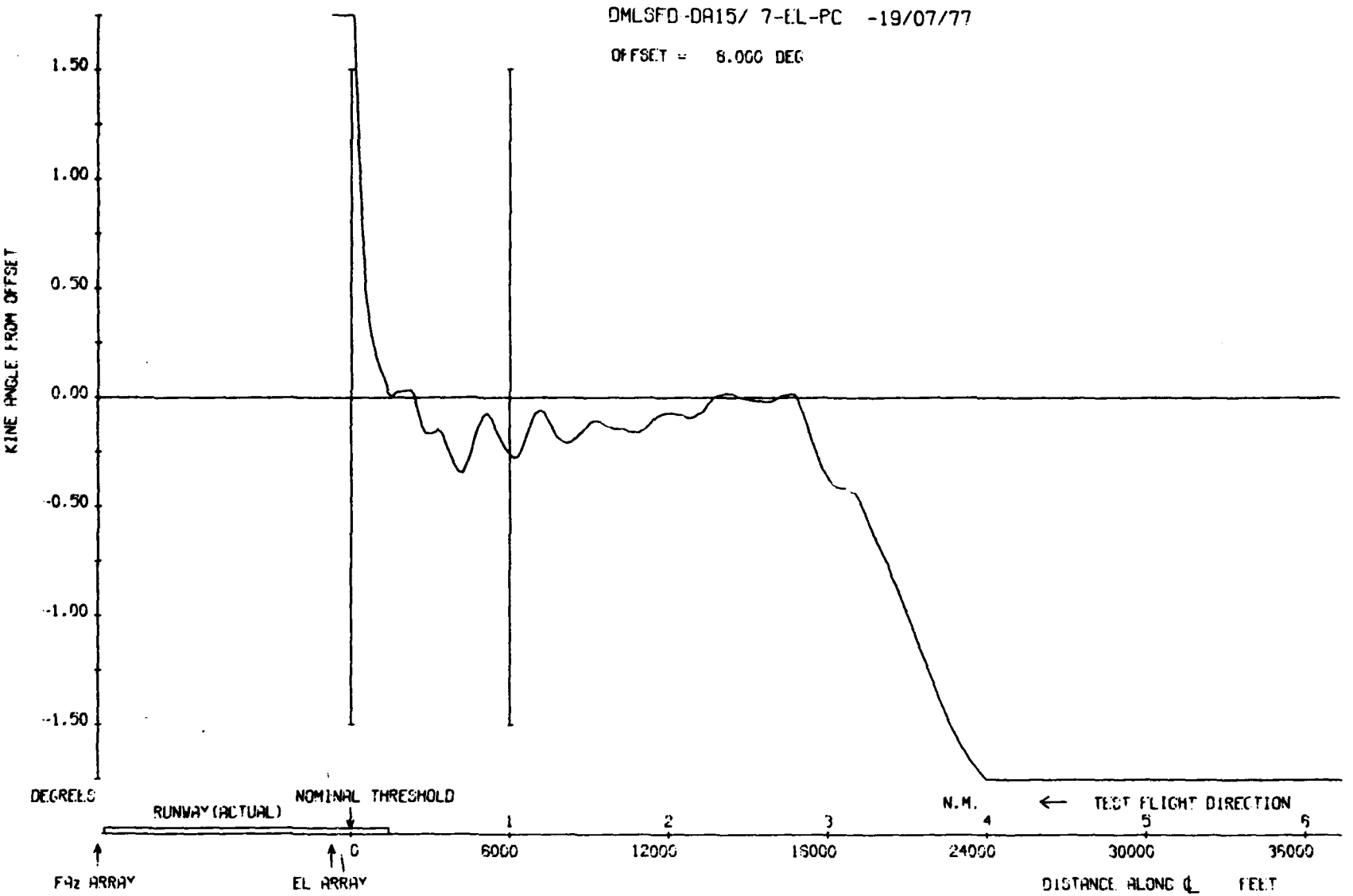

R. A. E. BEDFORD

Fig 7.73a Elevation 54λ, 8 degree approach to low overshoot

Fig 7.73a

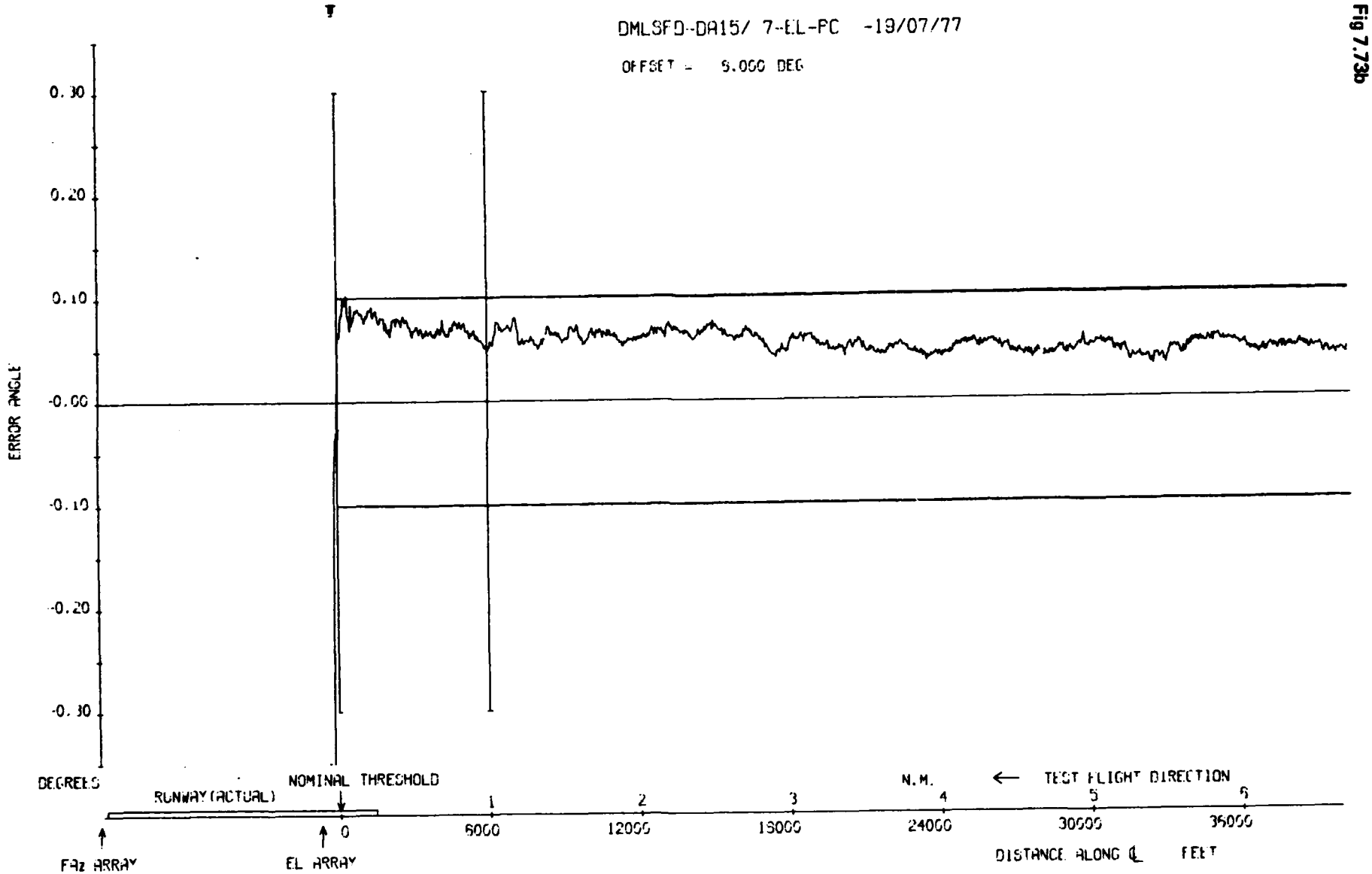

R. A. E. BEDFORD

Fig 7.73b Elevation 54λ, 8 degree approach to low overshoot

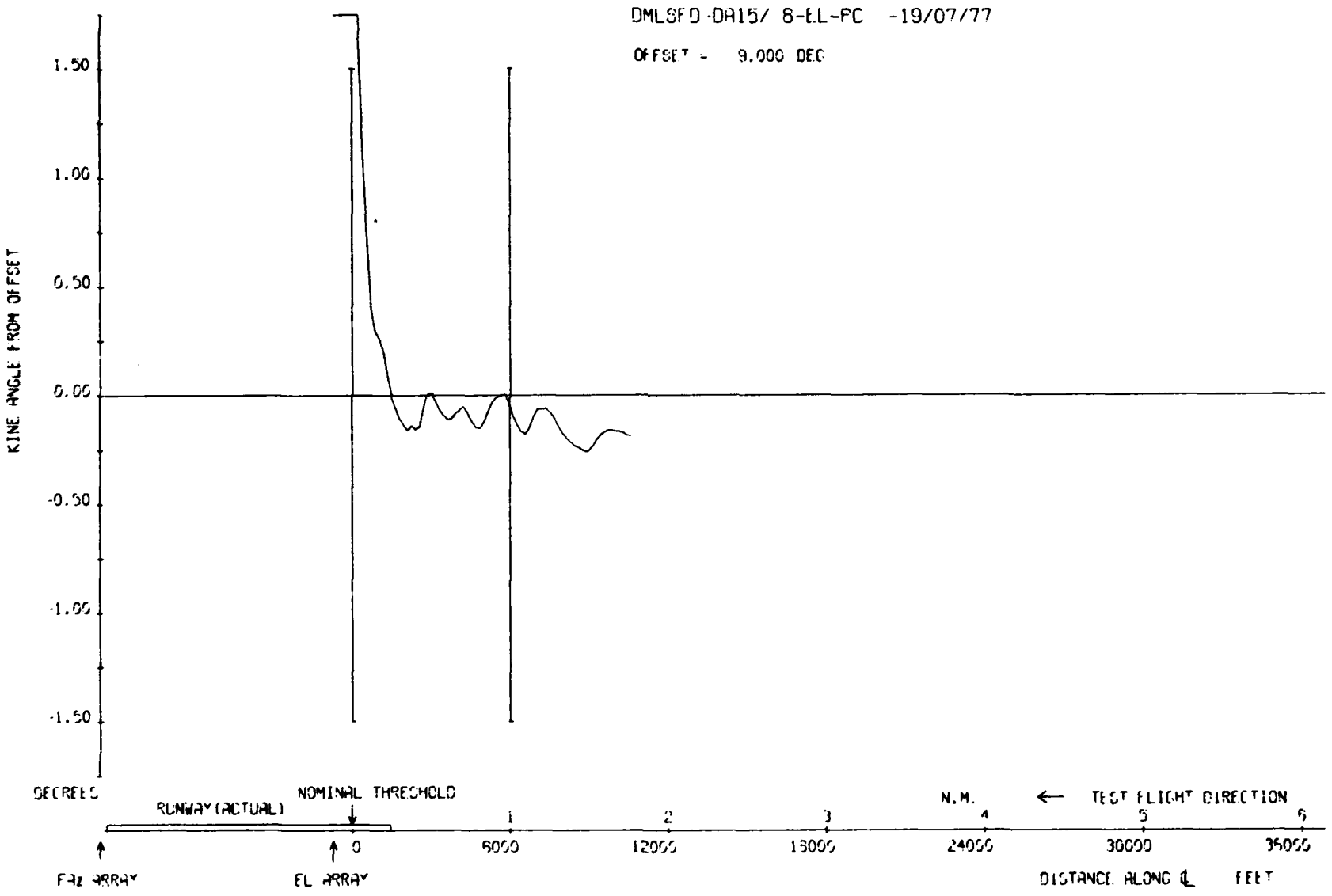

R.A.E. BEDFORD

Fig 7.74a Elevation 54λ, 9 degree approach to low overshoot

Fig 7.74a

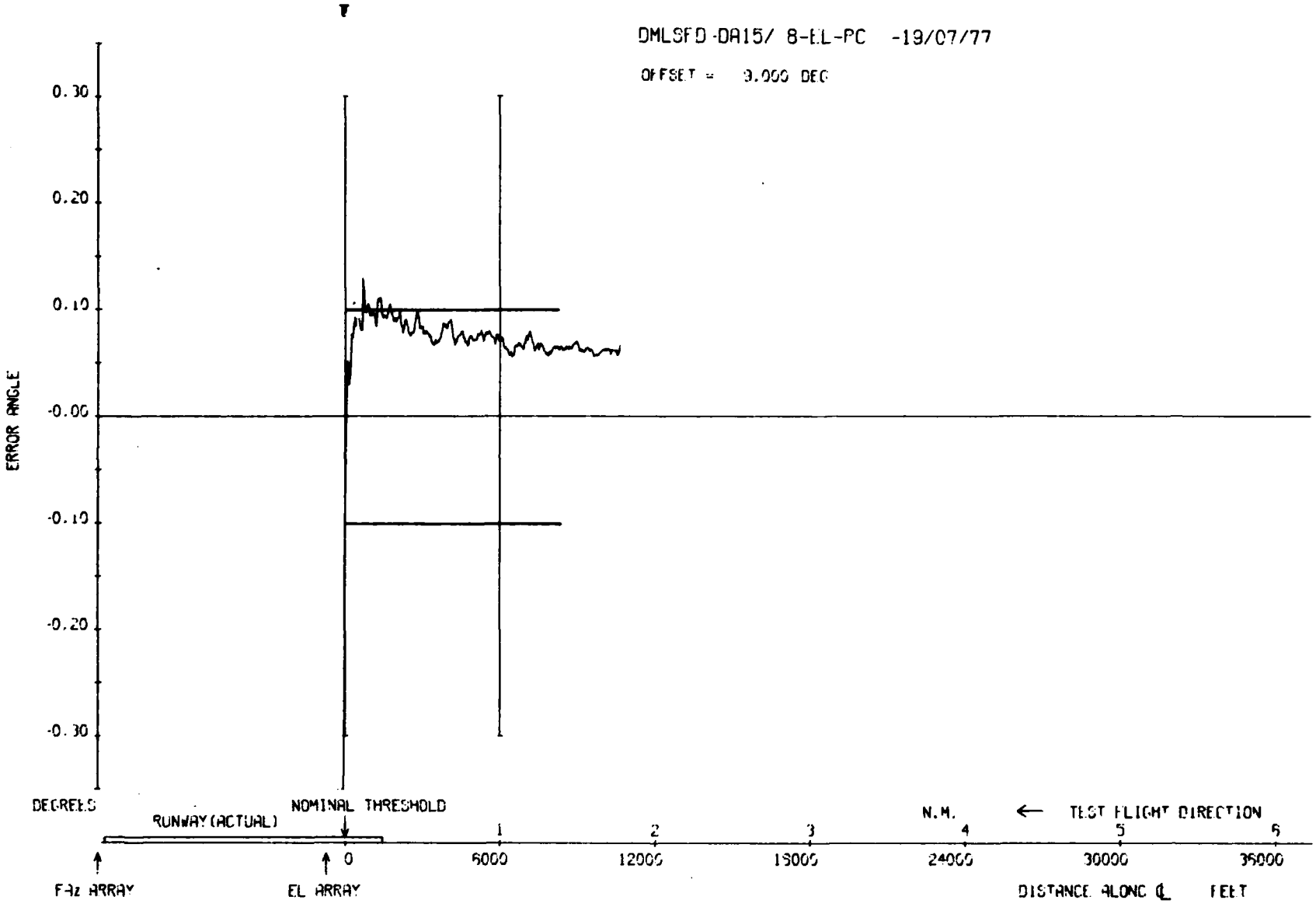

Fig 7.74b

R. A. E. BEDFORD

Fig 7.74b Elevation 54λ, 9 degree approach to low overshoot

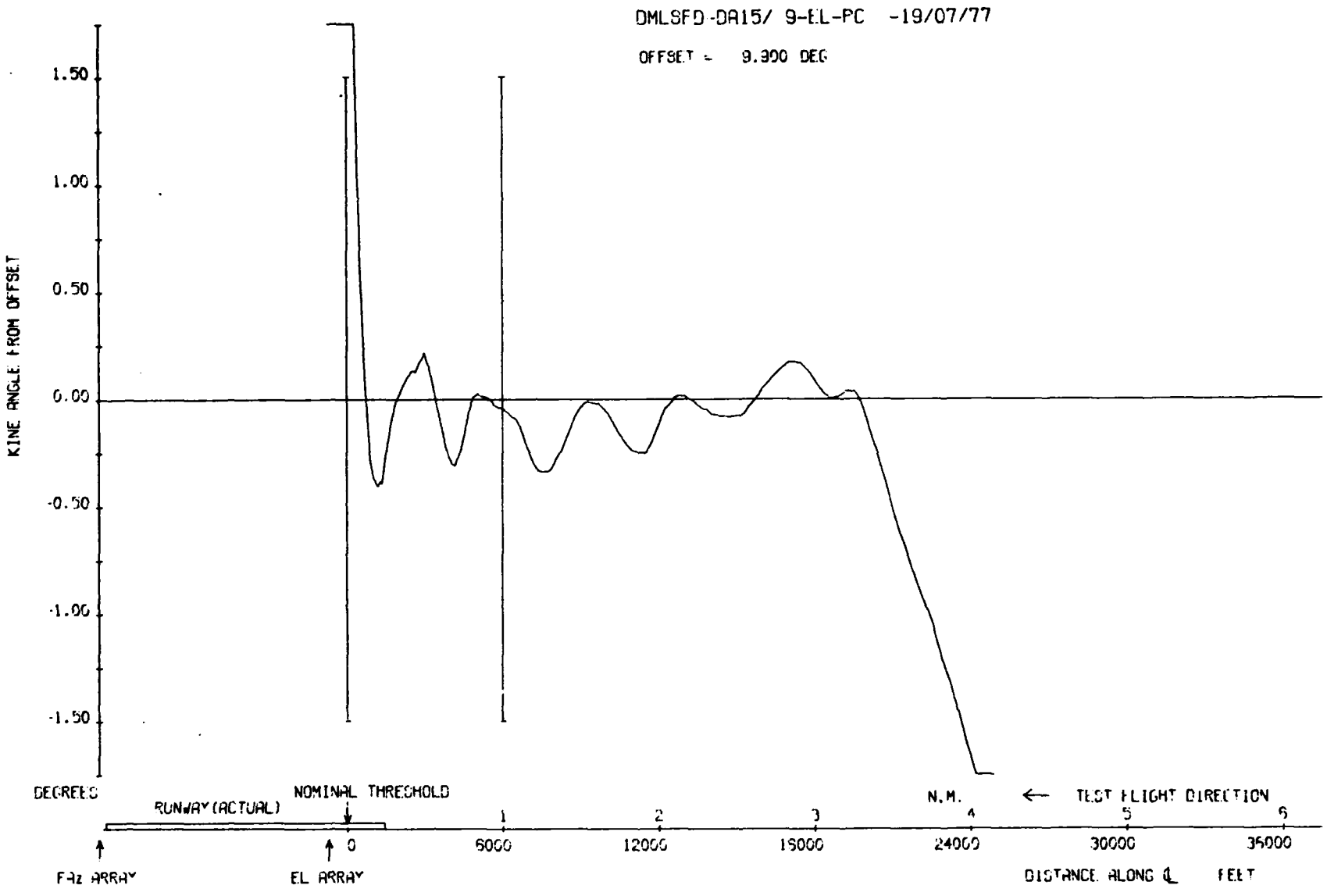

R. A. E. BEDFORD

Fig 7.75a Elevation 54λ, 9.9 degree approach to low overshoot

Fig 7.75a

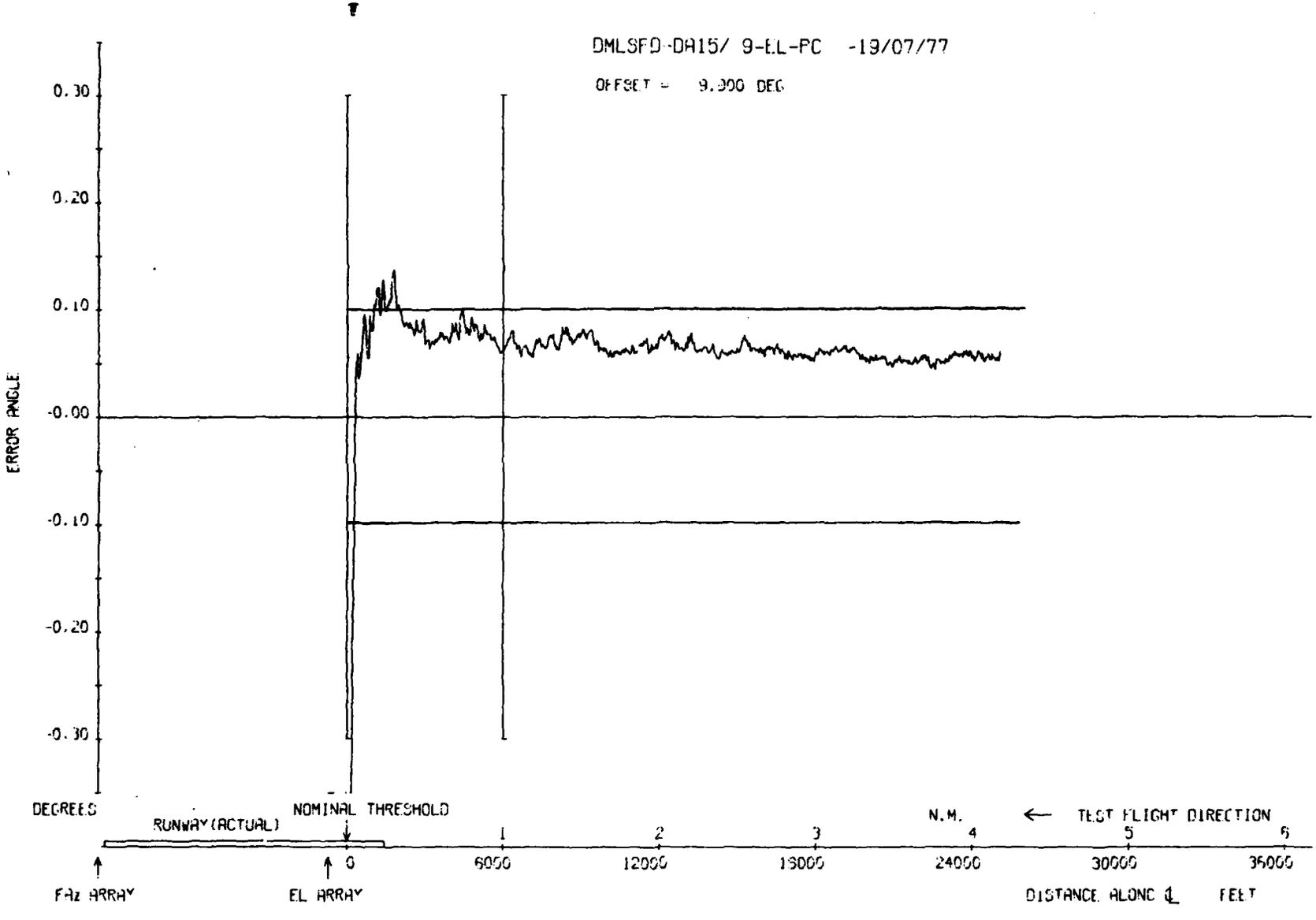

Fig 7.75b

Fig 7.75b Elevation 54λ, 9.9 degree approach to low overshoot

R. A. E. BEDFORD

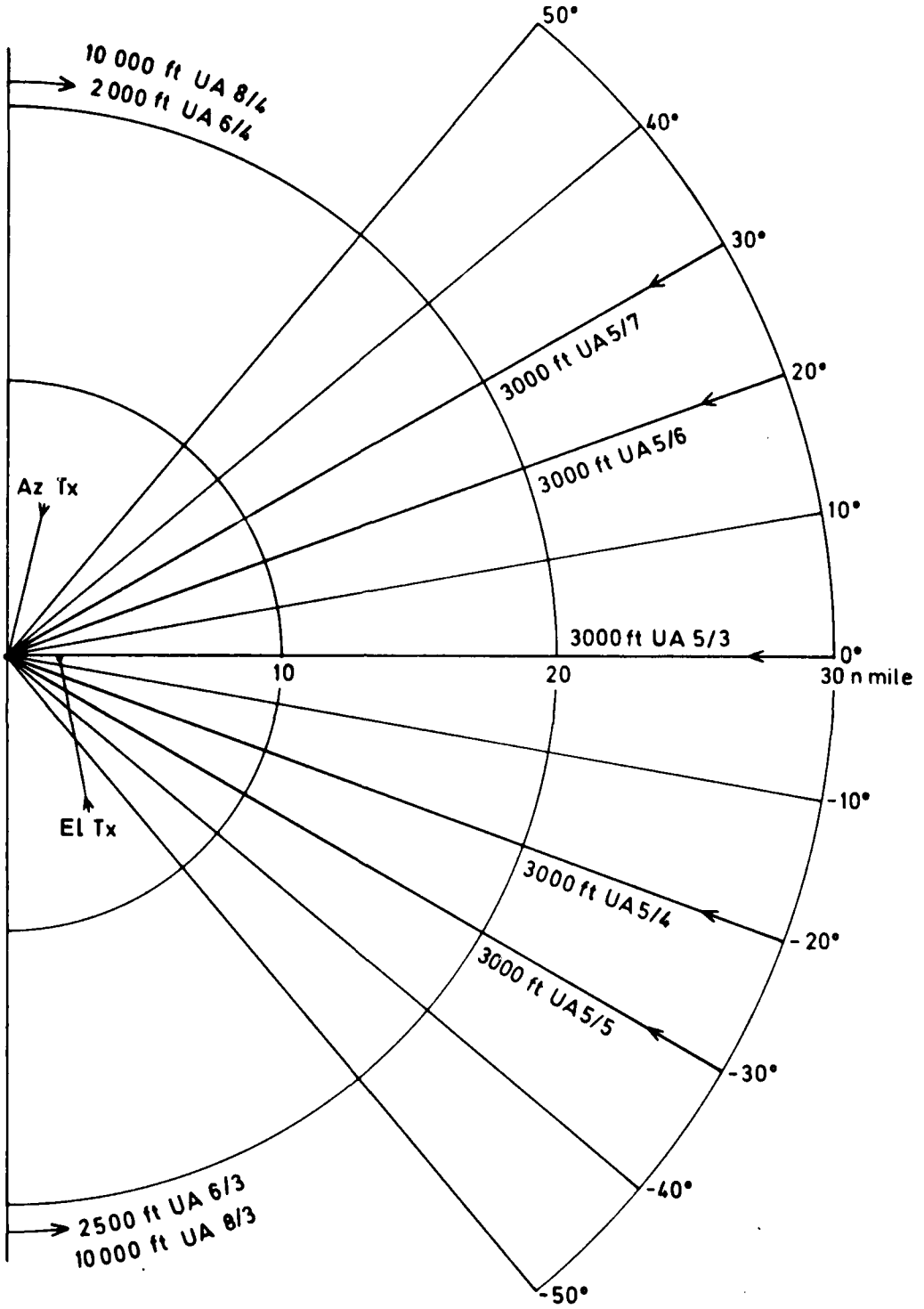

TR 79062

Fig 7.76 Coverage profiles

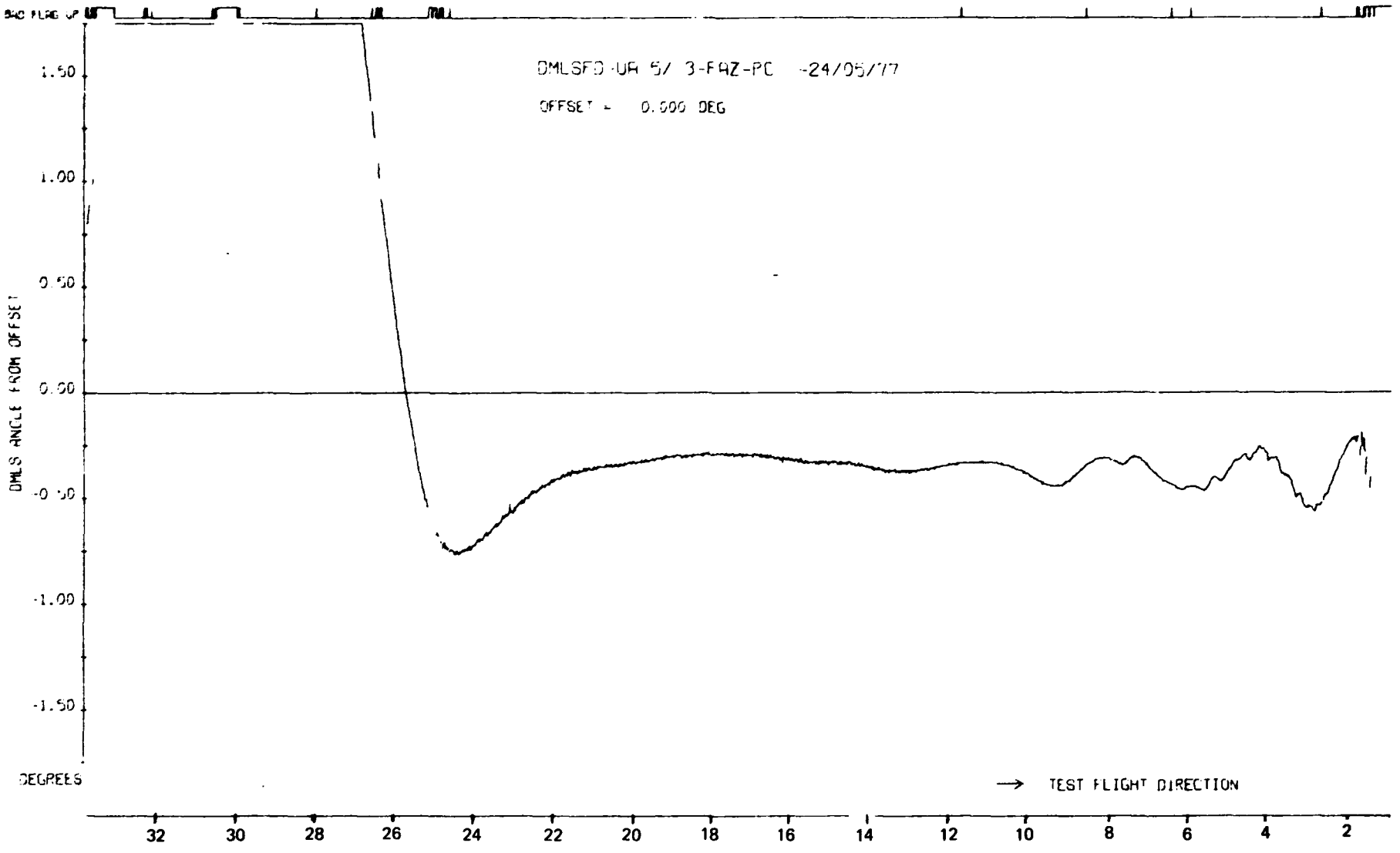

Fig 7.77a

R. A. E. BEDFORD

Fig 7.77a Azimuth radial on ℄ at 3000 ft height

TR 79052

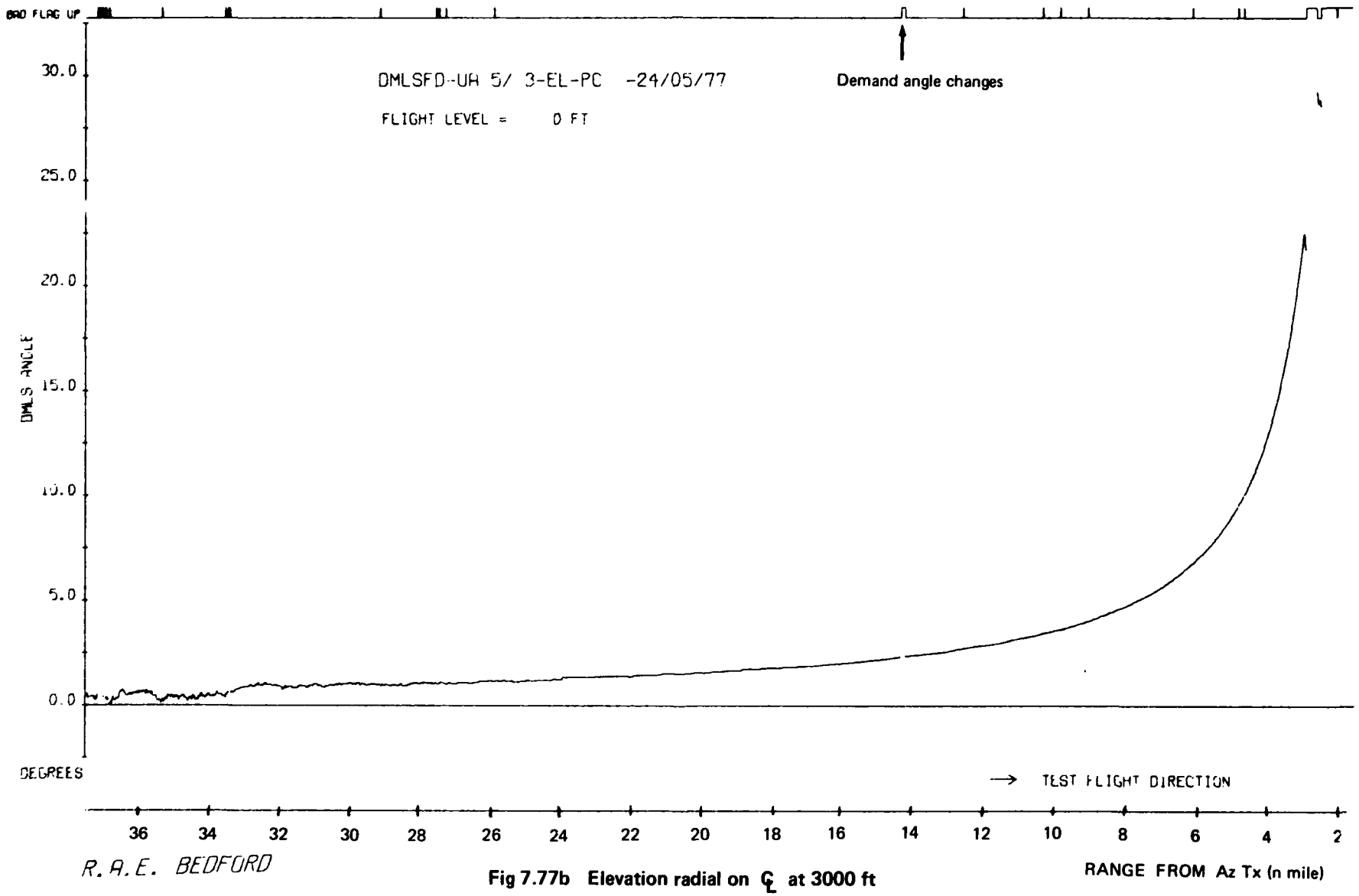

R. A. E. BEDFORD

Fig 7.77b Elevation radial on ℄ at 3000 ft

Fig 7.77b

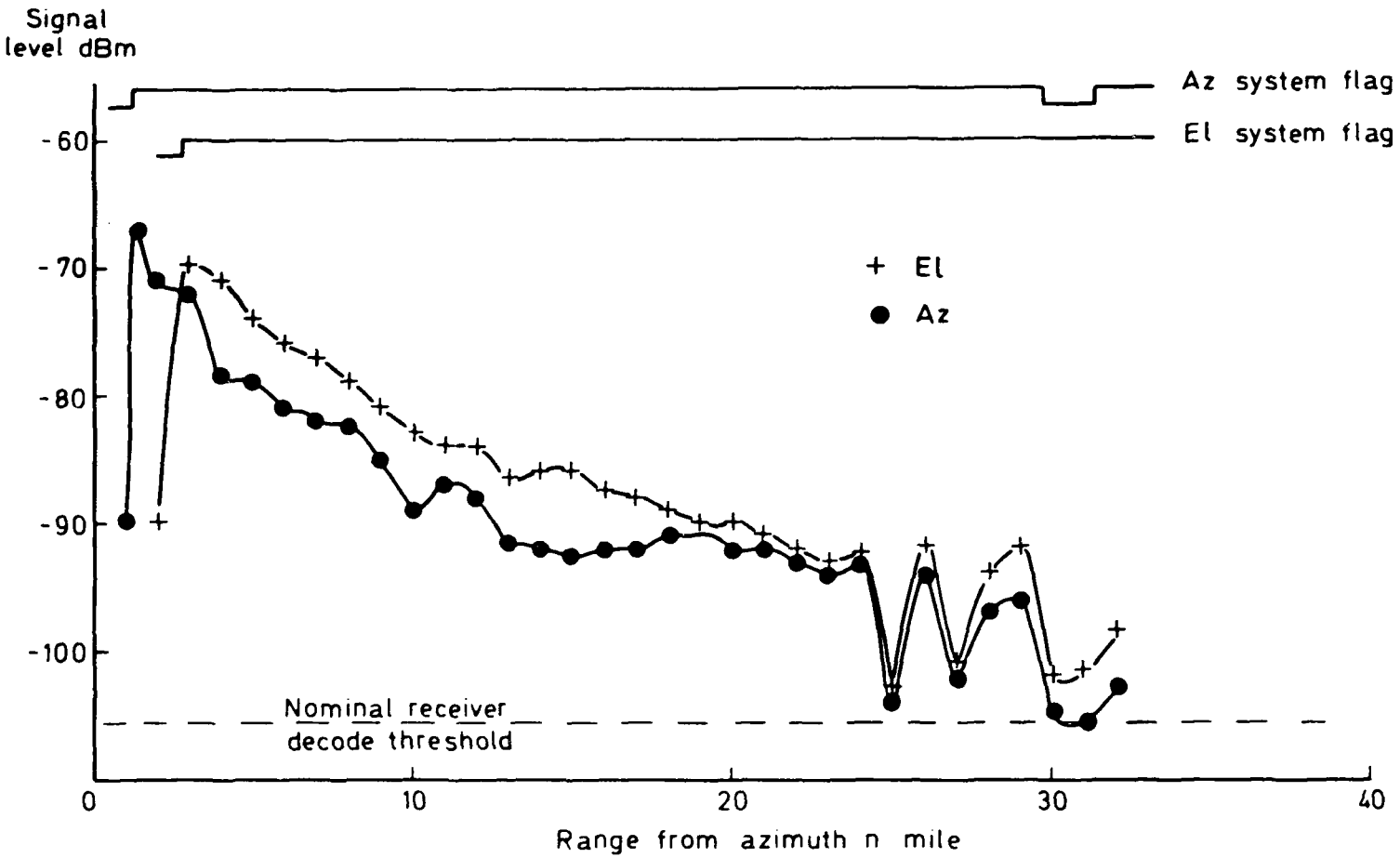

Fig 7.77c Received signal levels for UA05/3

AD-A085 480 ROYAL AIRCRAFT ESTABLISHMENT FARNBOROUGH (ENGLAND) F/6 17/7
CONTRIBUTIONS TO THE UK MICROWAVE LANDING SYSTEM RESEARCH AND D--ETC(U)
MAY 79 J M JONES
UNCLASSIFIED RAE-TR-79052-VOL-3 DRIC-BR-73763 NL

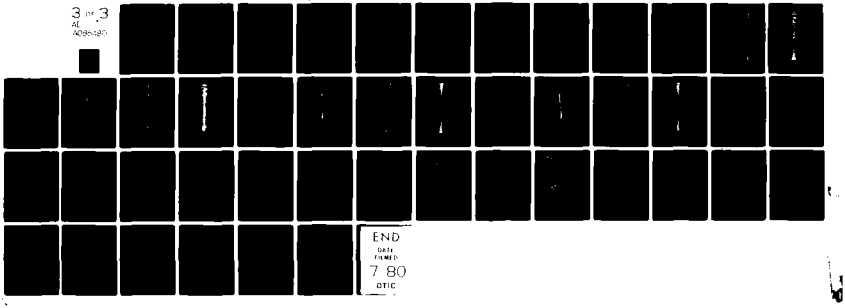

TR 79052

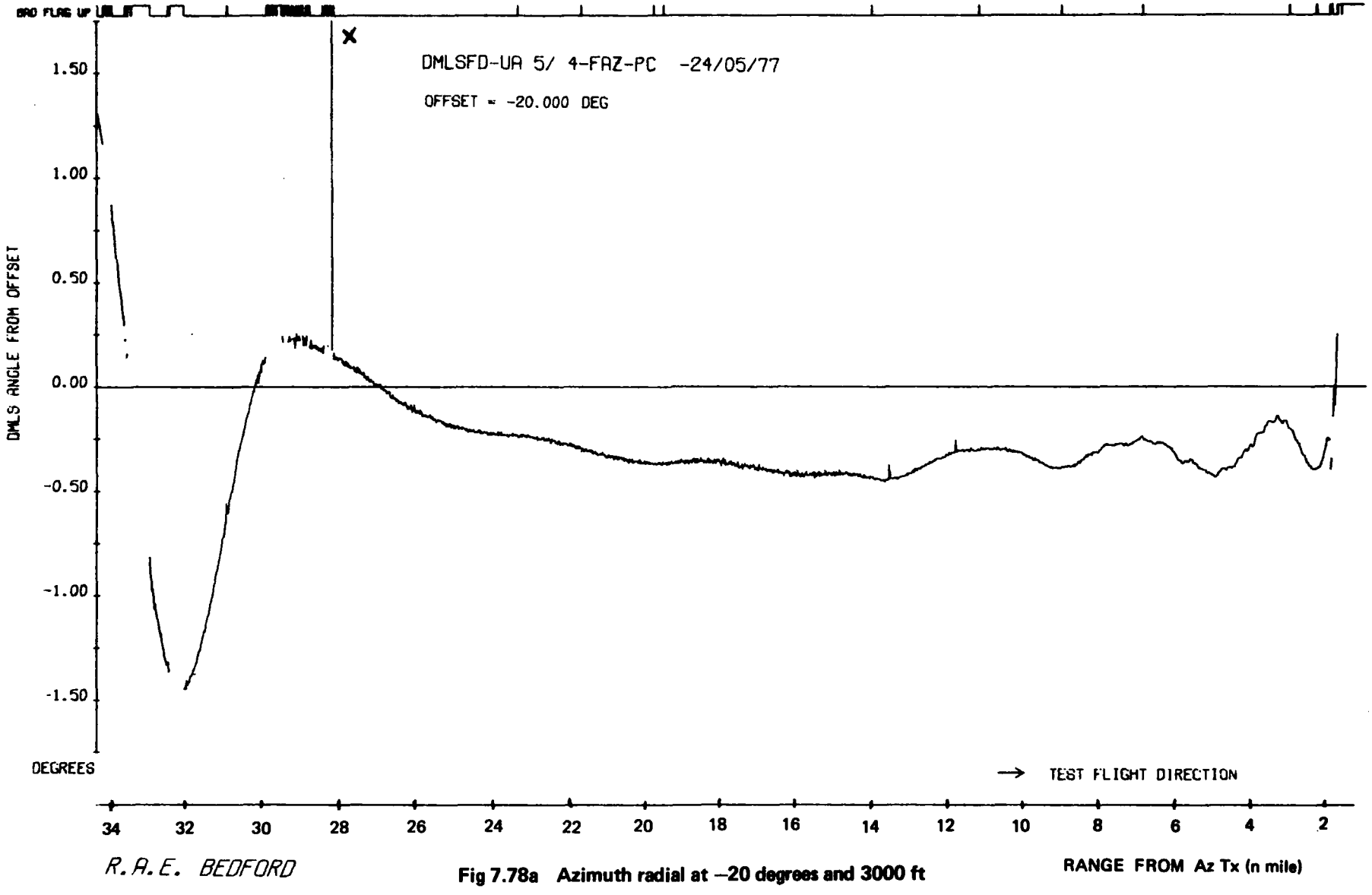

R.A.E. BEDFORD

Fig 7.78a Azimuth radial at –20 degrees and 3000 ft

Fig 7.78a

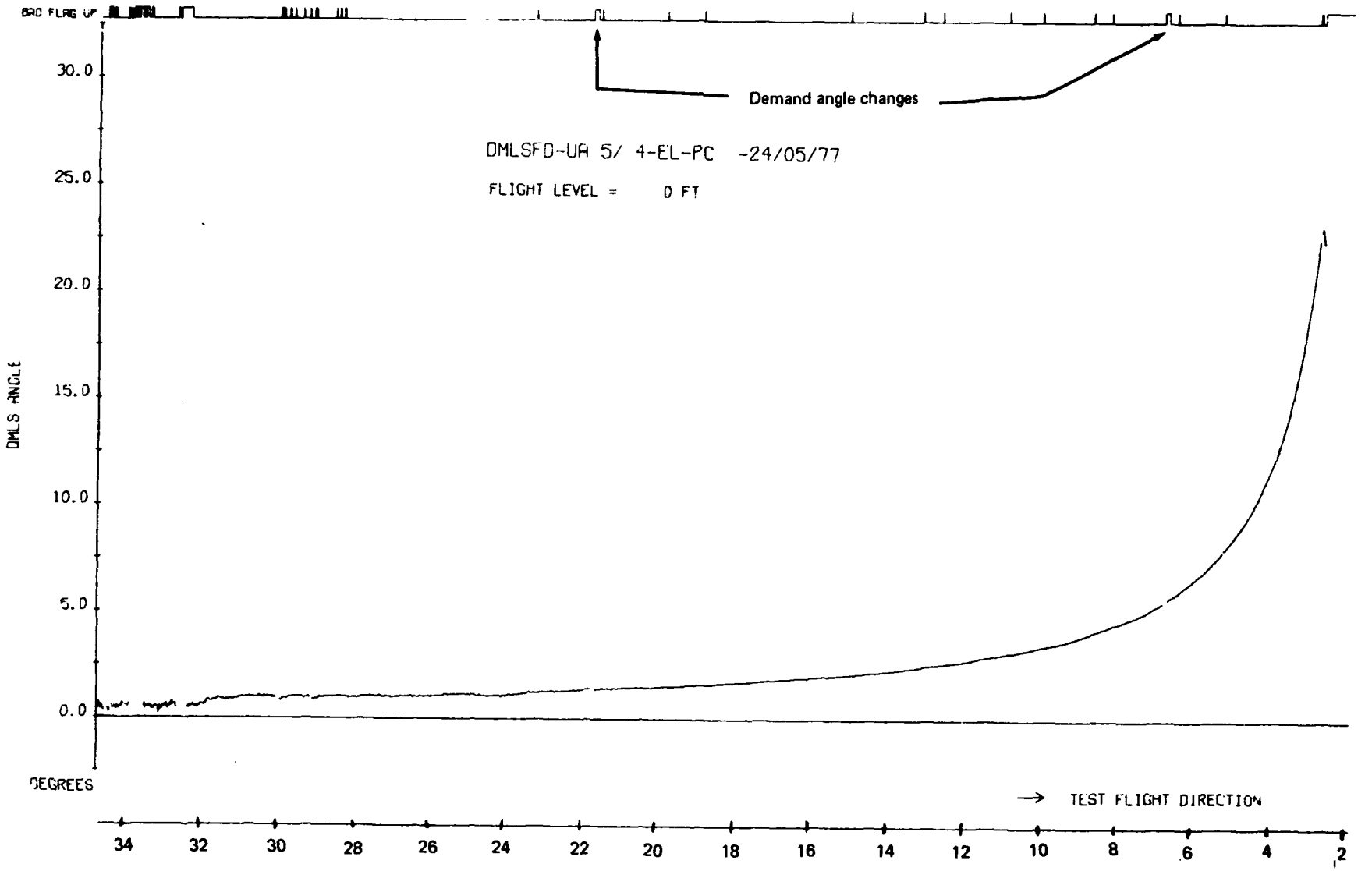

Fig 7.78b

R. A. E. BEDFORD

Fig 7.78b Elevation radial at –20 degrees and 3000 ft

TR 79062

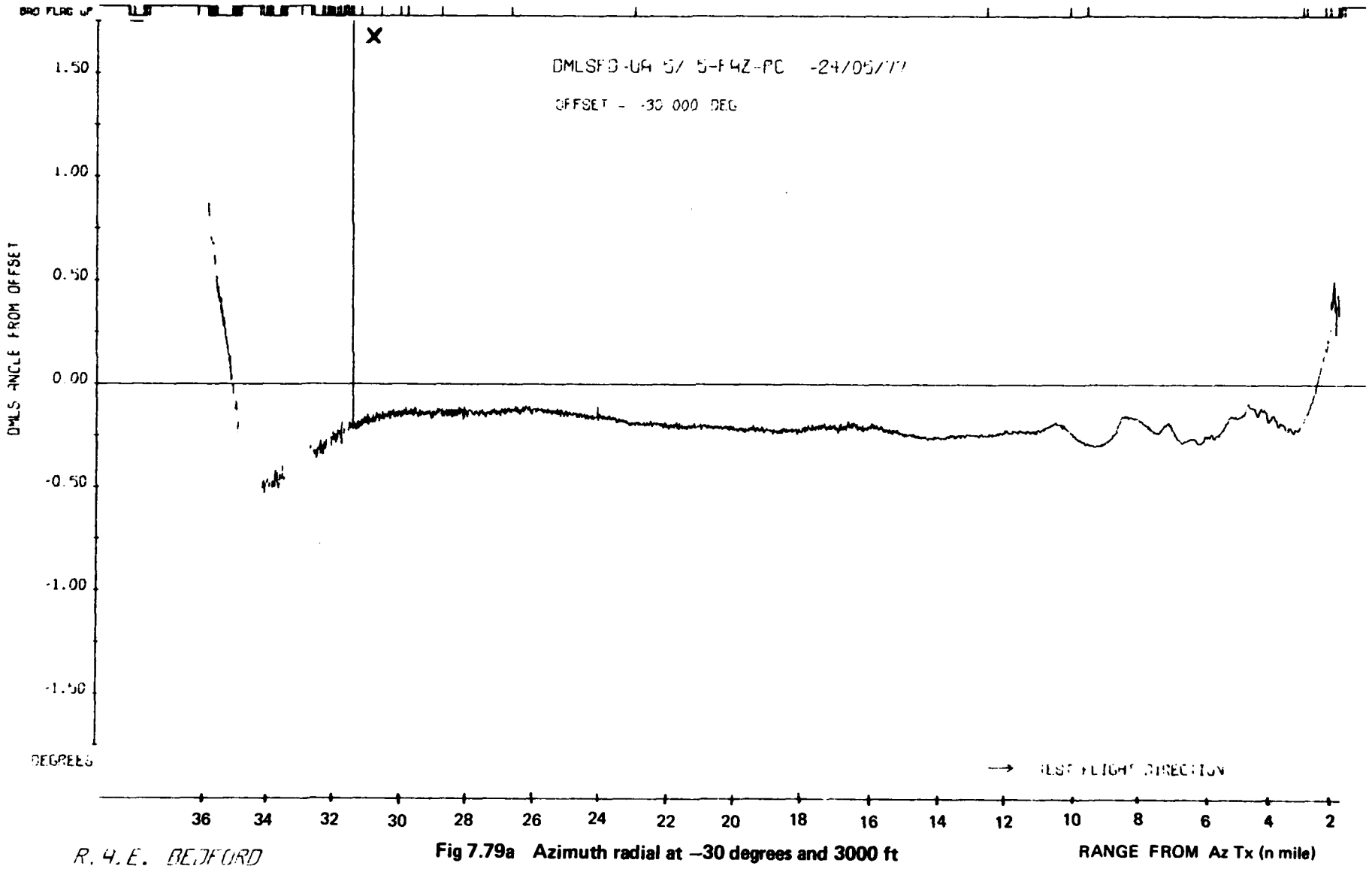

R. A. E. BEDFORD

Fig 7.79a Azimuth radial at –30 degrees and 3000 ft

Fig 7.79a

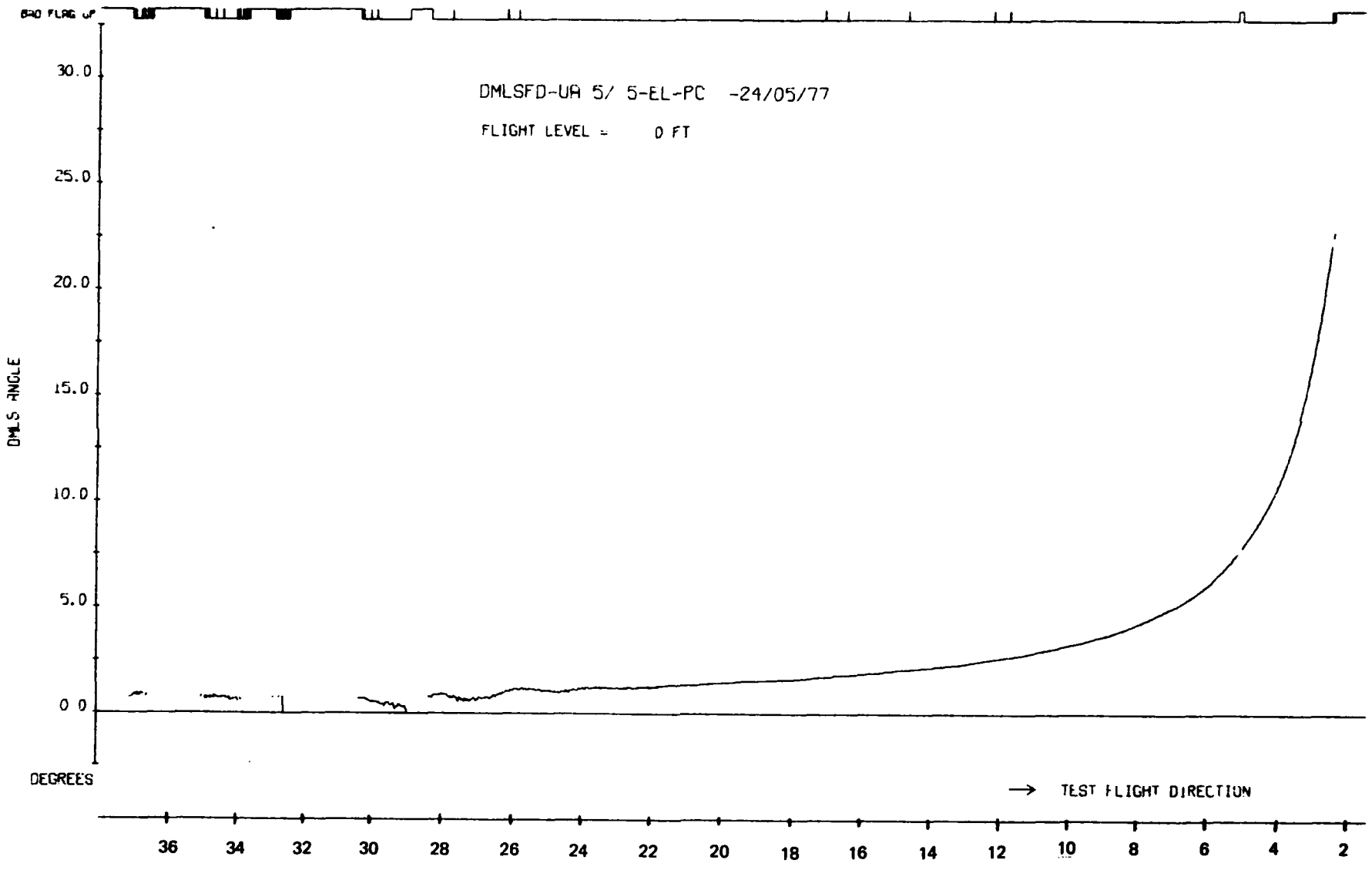

Fig 7.79b Elevation radial at −30 degrees and 3000 ft

TR 79062

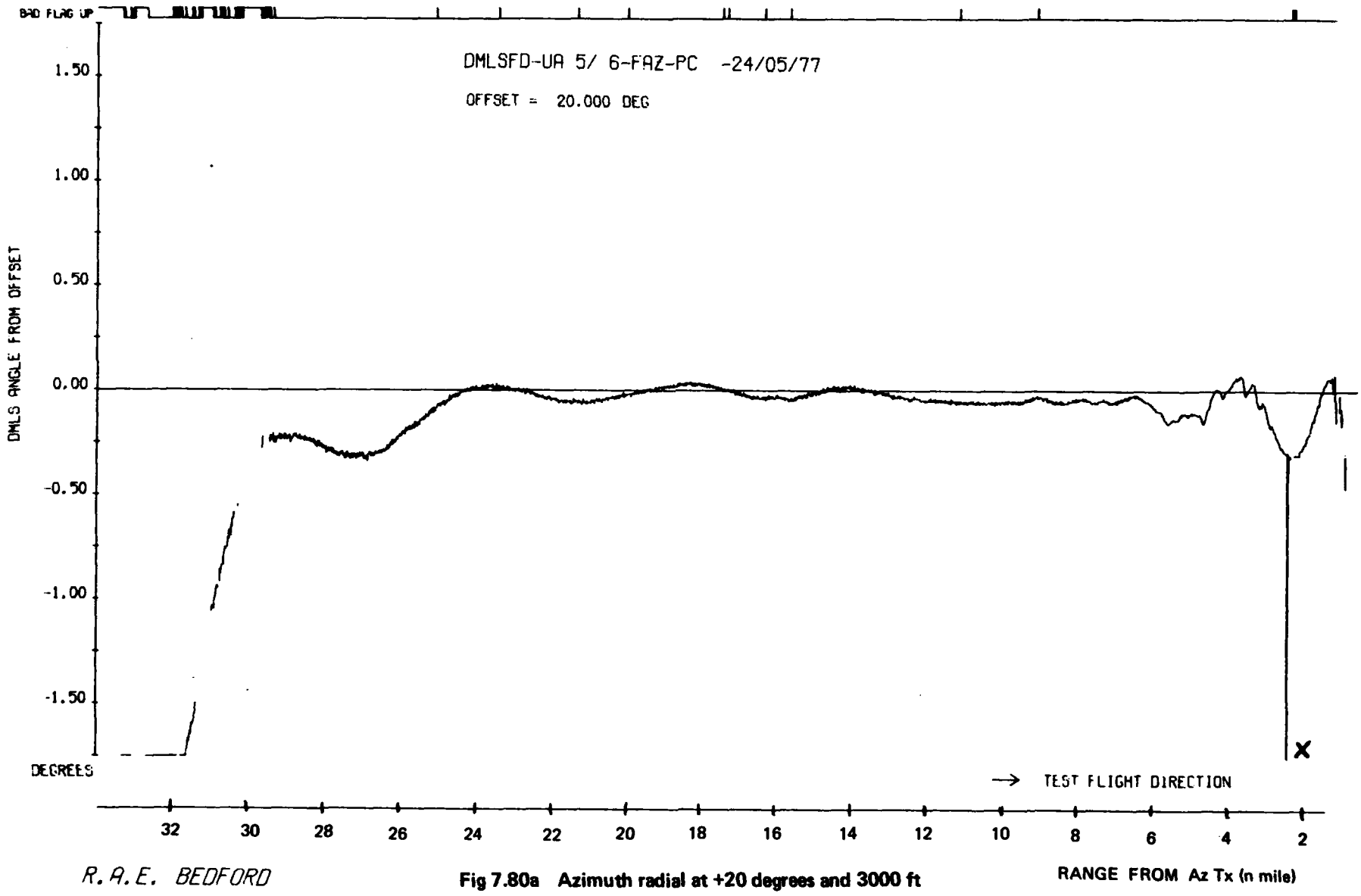

R.A.E. BEDFORD

Fig 7.80a Azimuth radial at +20 degrees and 3000 ft

Fig 7.80a

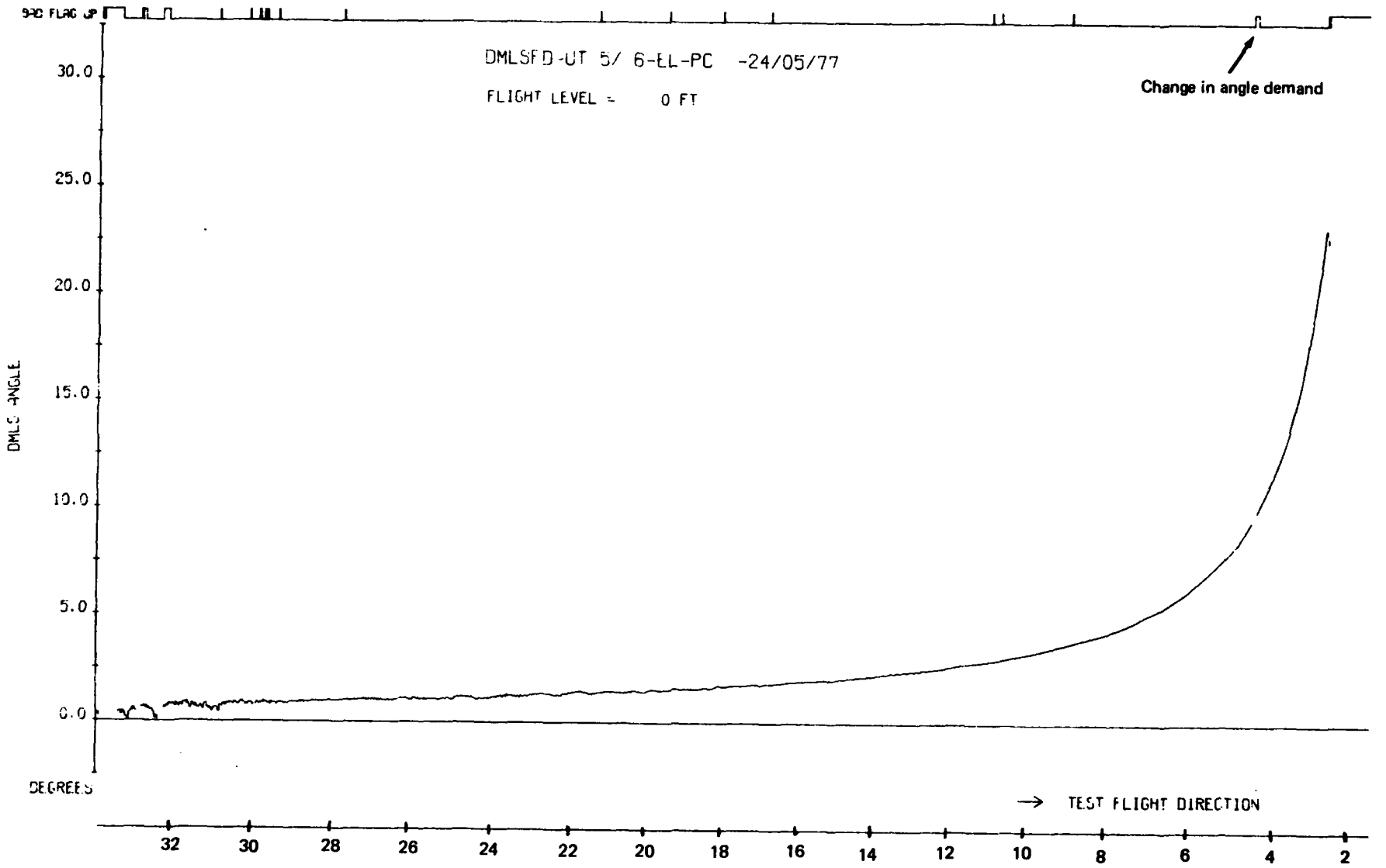

Fig 7.80b

R.A.E. BEDFORD

Fig 7.80b Elevation radial at +20 degrees and 3000 ft

TR 79052

TR 79052

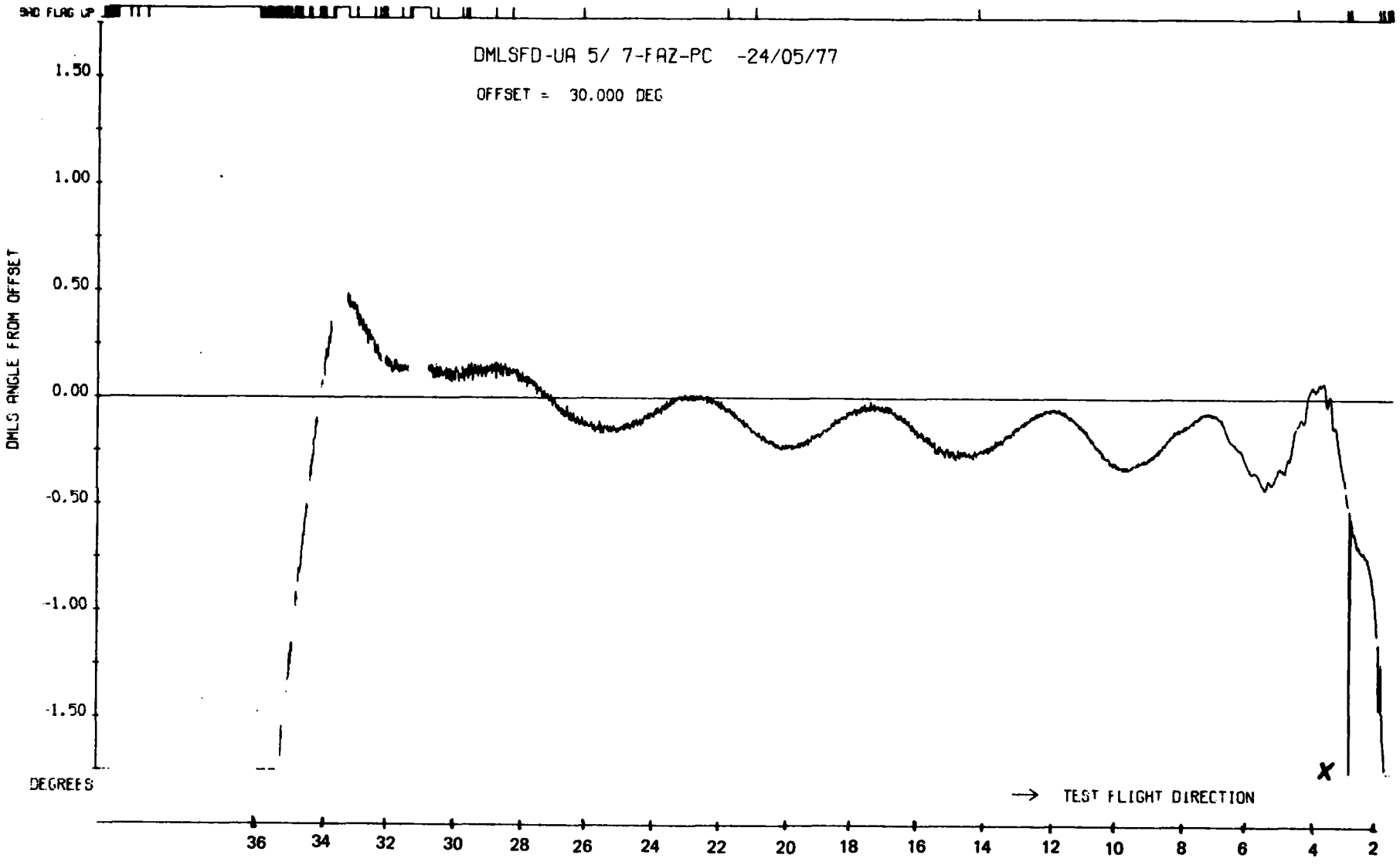

R. A. E. BEDFORD

Fig 7.81a Azimuth radial at +30 degrees and 3000 ft

Fig 7.81a

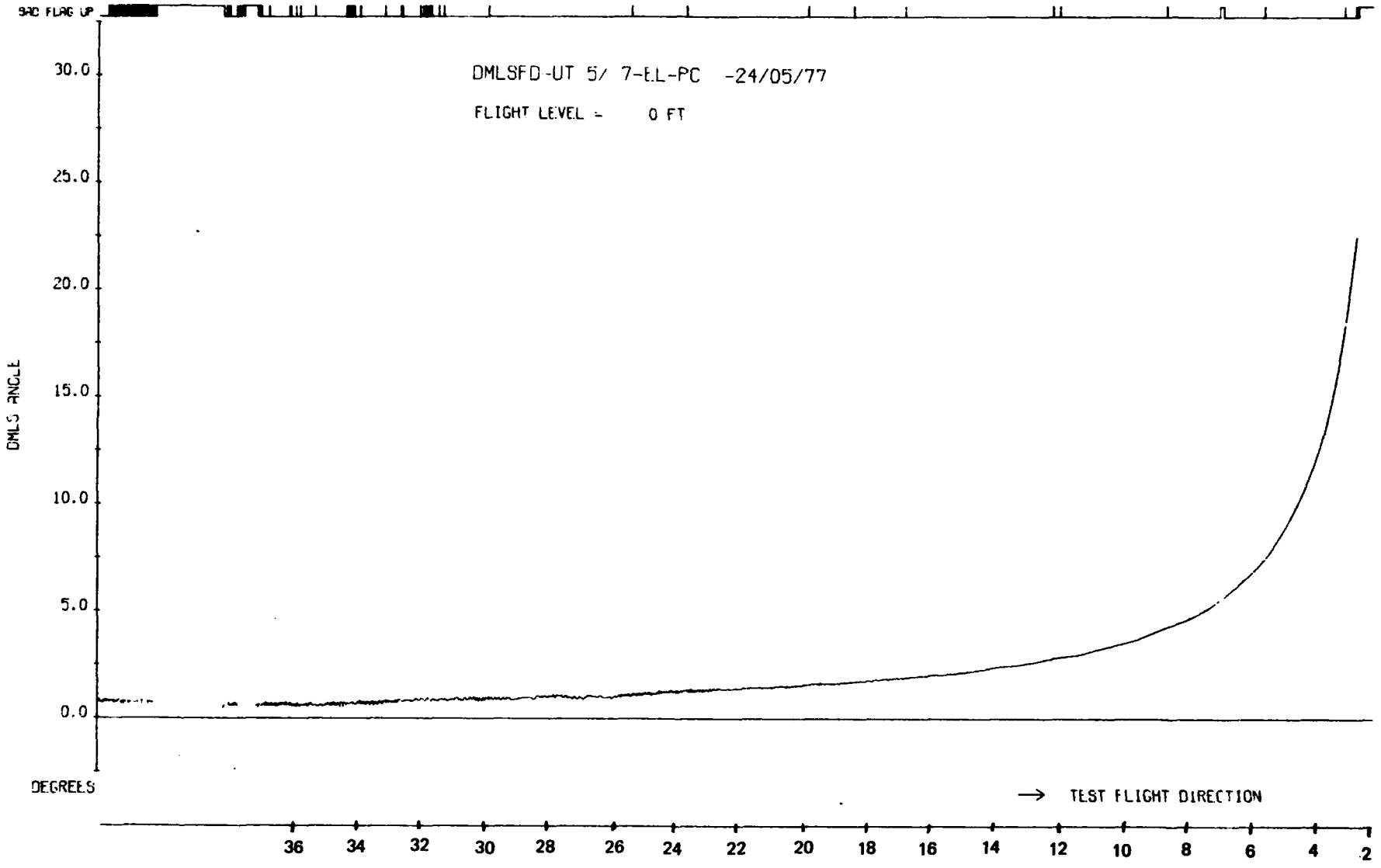

Fig 7.81b

R. A. E. BEDFORD

Fig 7.81b Elevation radial at +30 degrees and 3000 ft

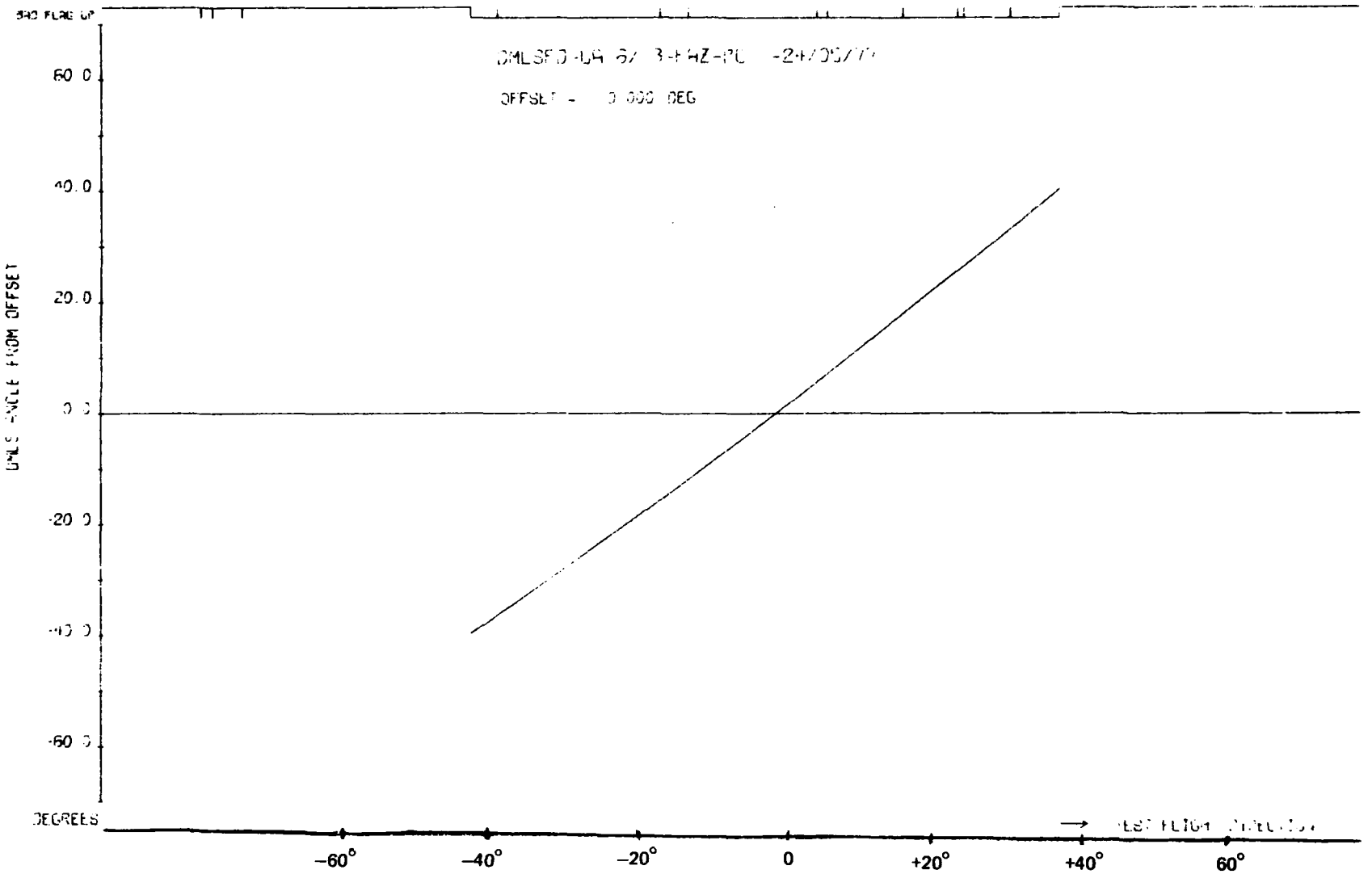

R. H. E. BEDFORD

Fig 7.82a Azimuth, orbit at 20 n mile and 2500 ft

Fig 7.82a

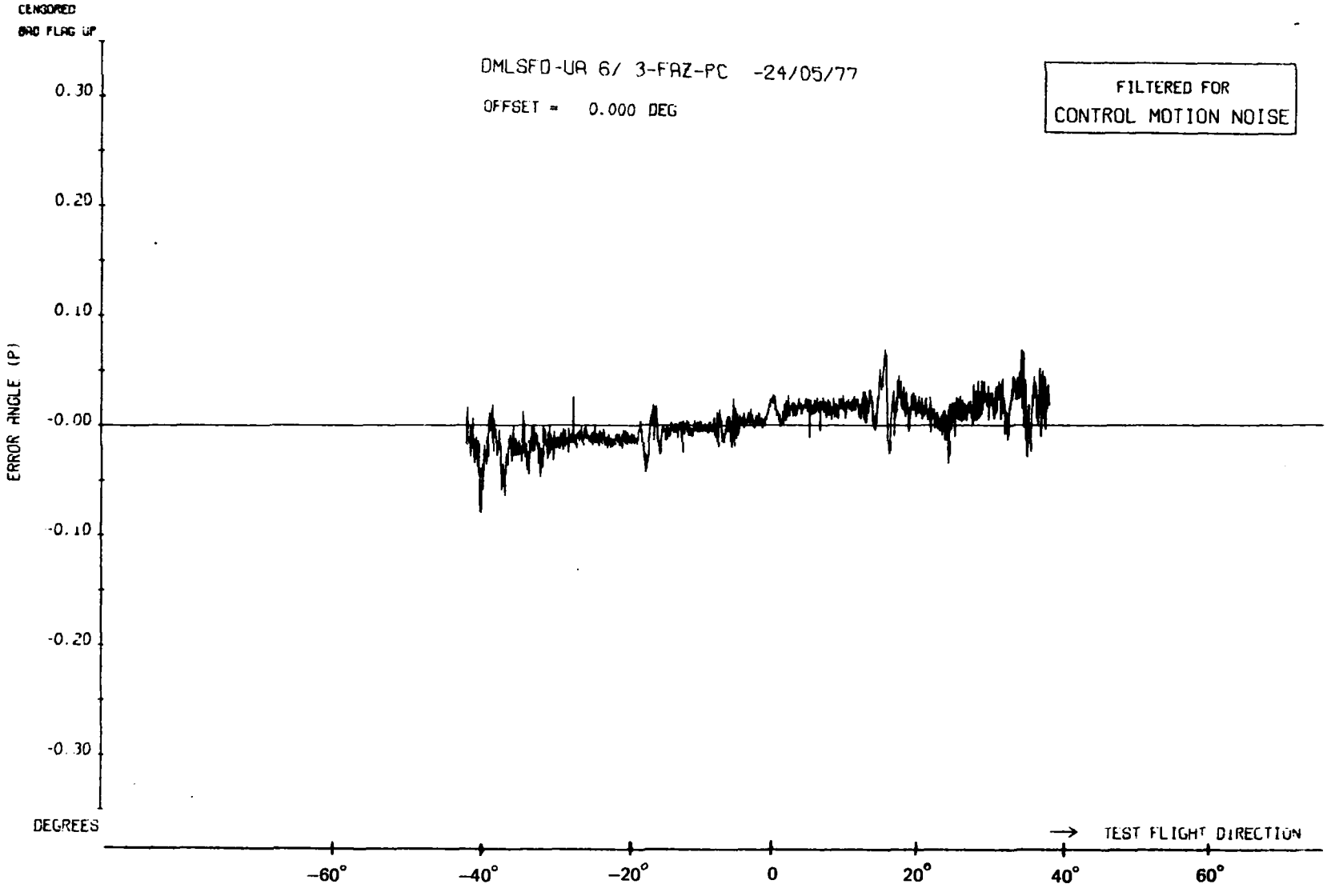

R. A. E. BEDFORD

Fig 7.82b Azimuth, orbit at 20 n mile and 2500 ft

TR 79052

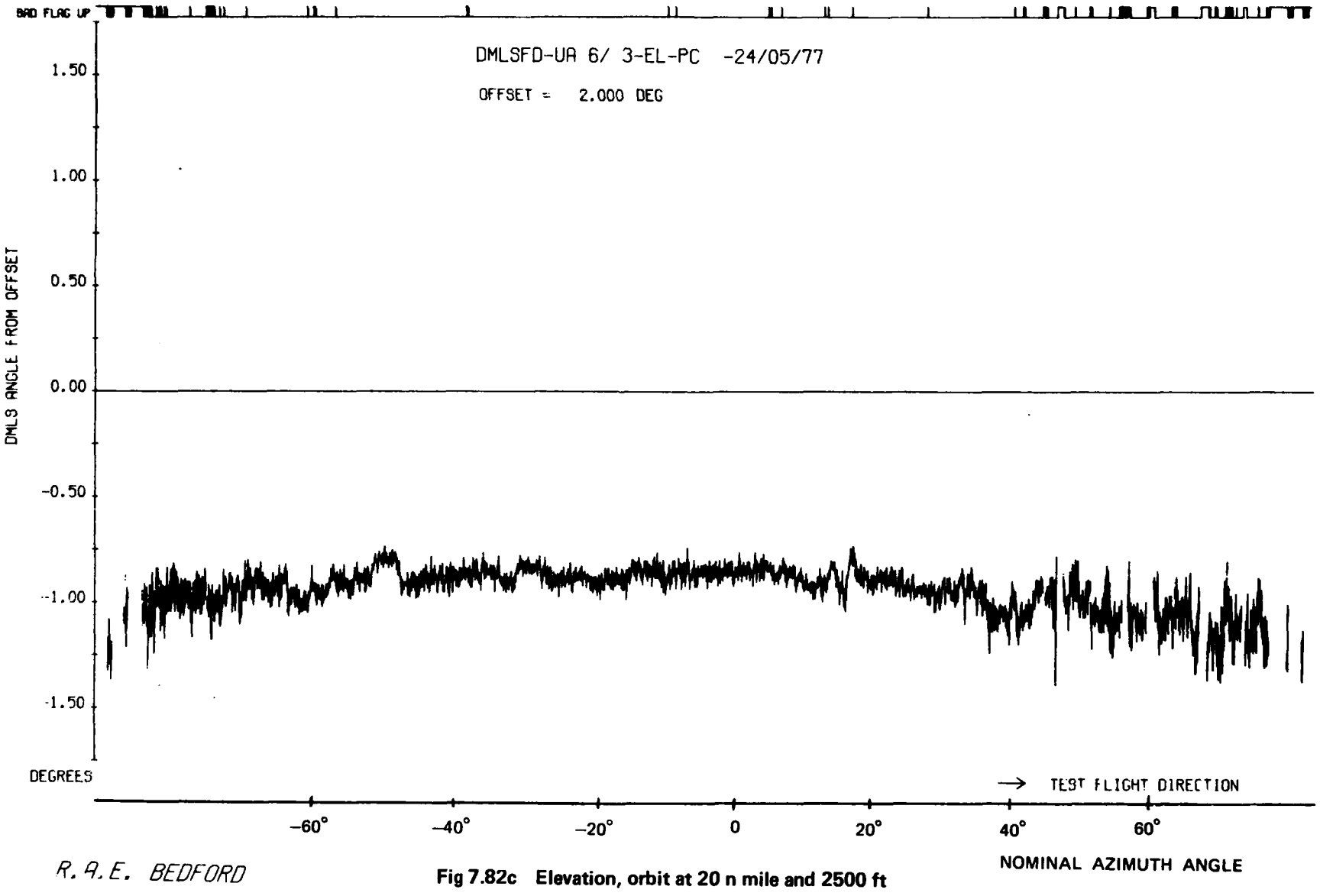

R. A. E. BEDFORD

Fig 7.82c Elevation, orbit at 20 n mile and 2500 ft

Fig 7.82c

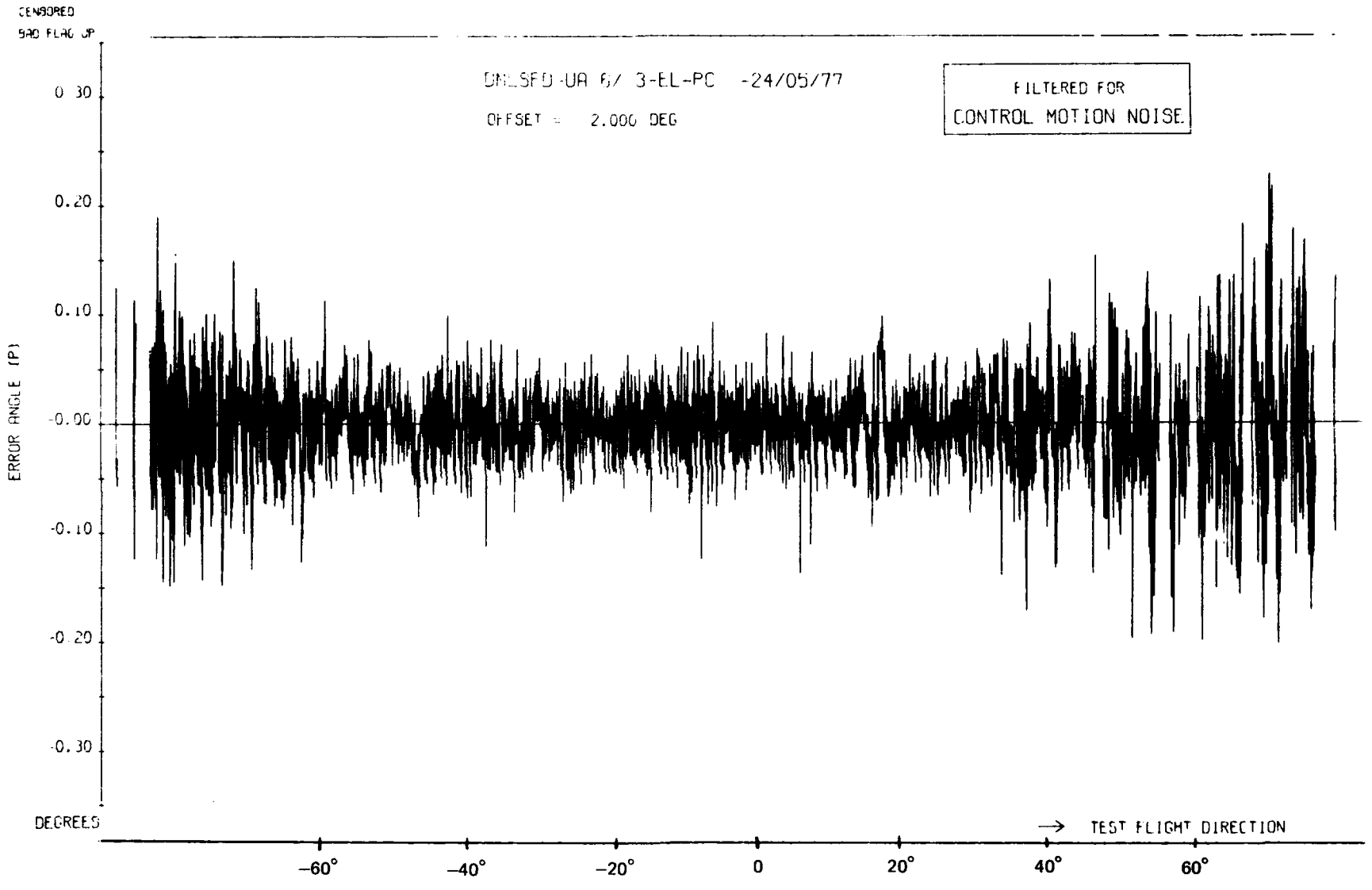

R. A. E. BEDFORD

Fig 7.82d Elevation, orbit at 20 n mile and 2500 ft

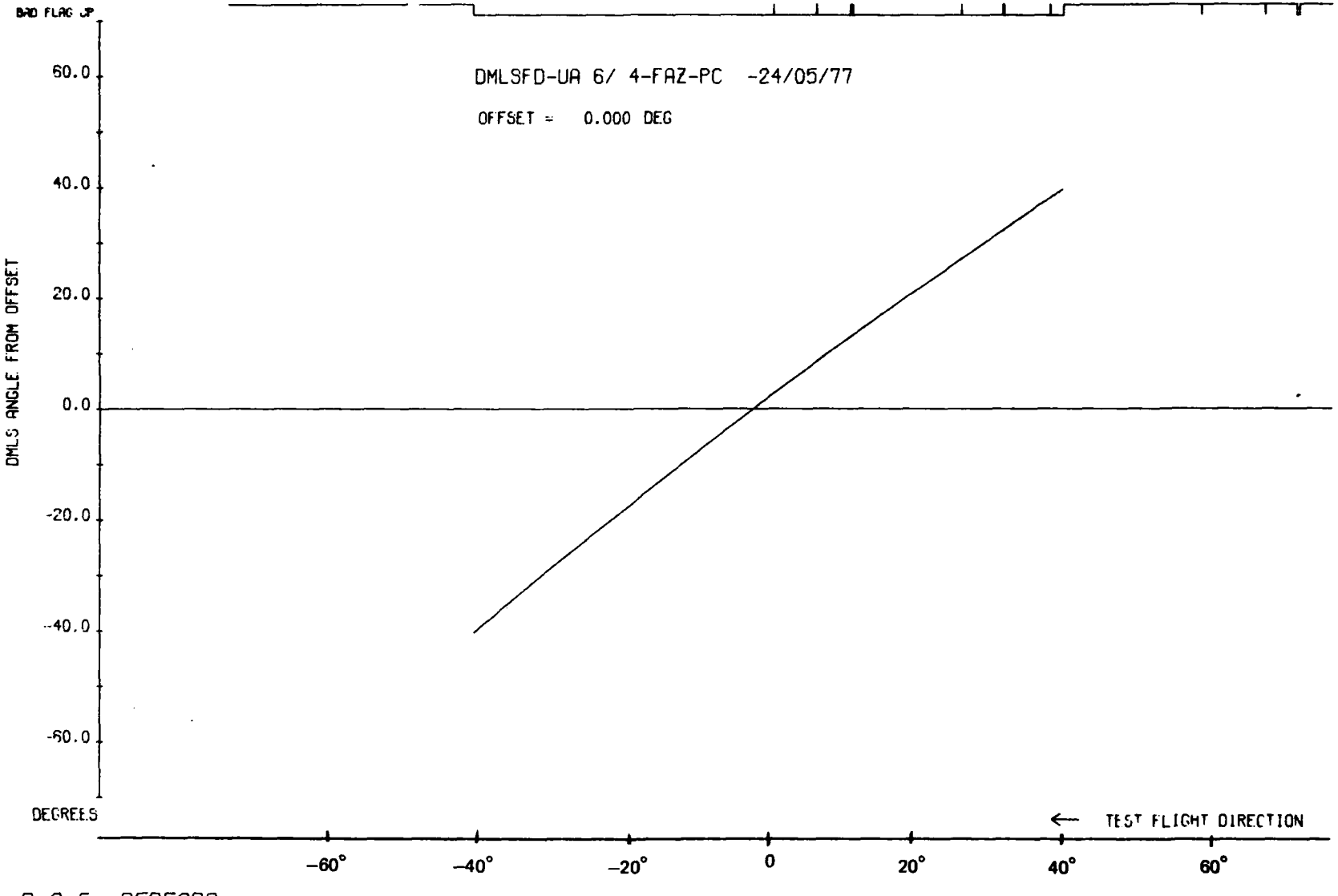

R. A. E. BEDFORD

Fig 7.83a Azimuth, orbit at 20 n mile and 2000 ft

Fig 7.83a

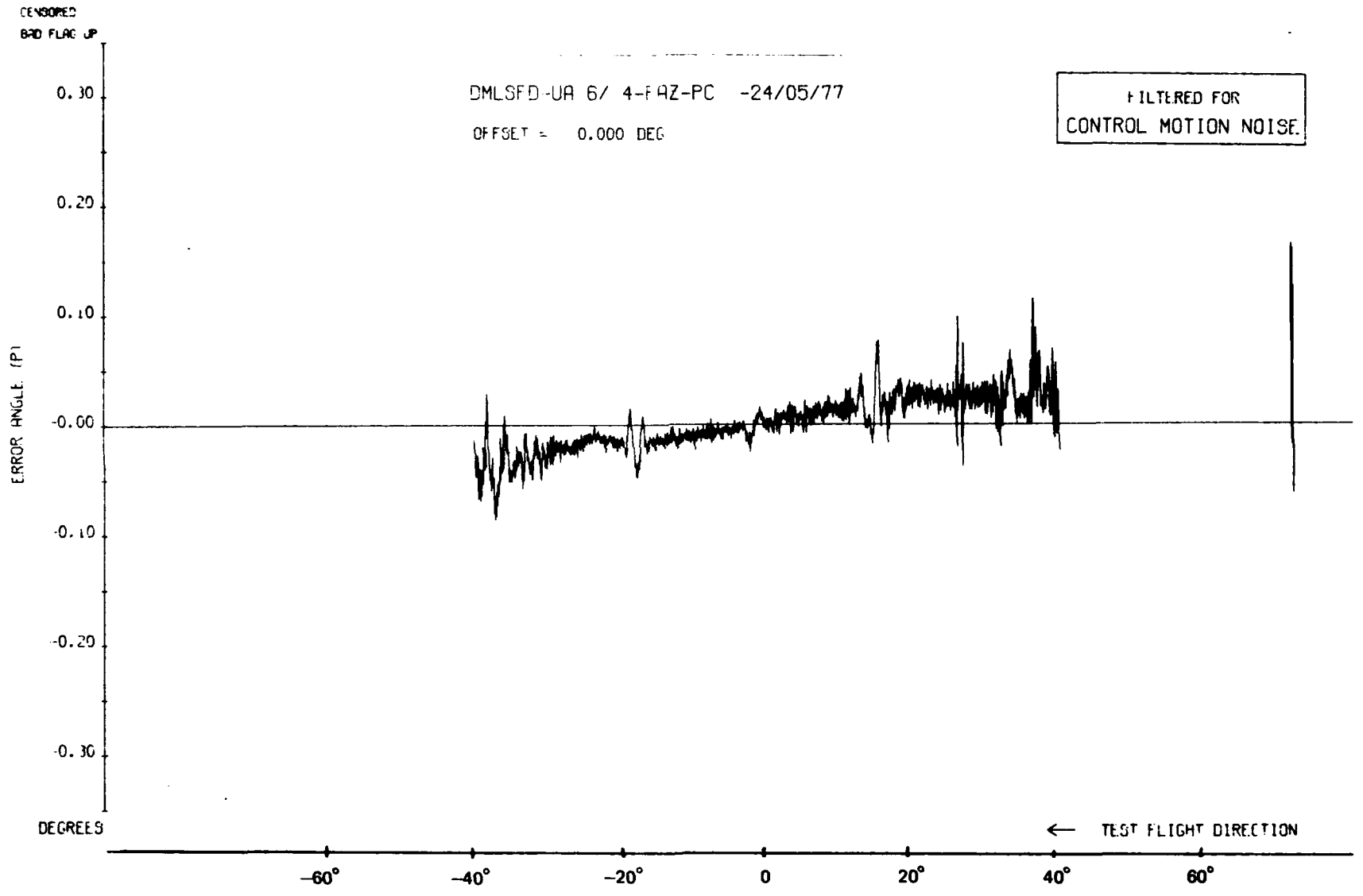

R.A.E. BEDFORD

Fig 7.83b Azimuth, orbit at 20 n mile and 2000 ft

TR 79052

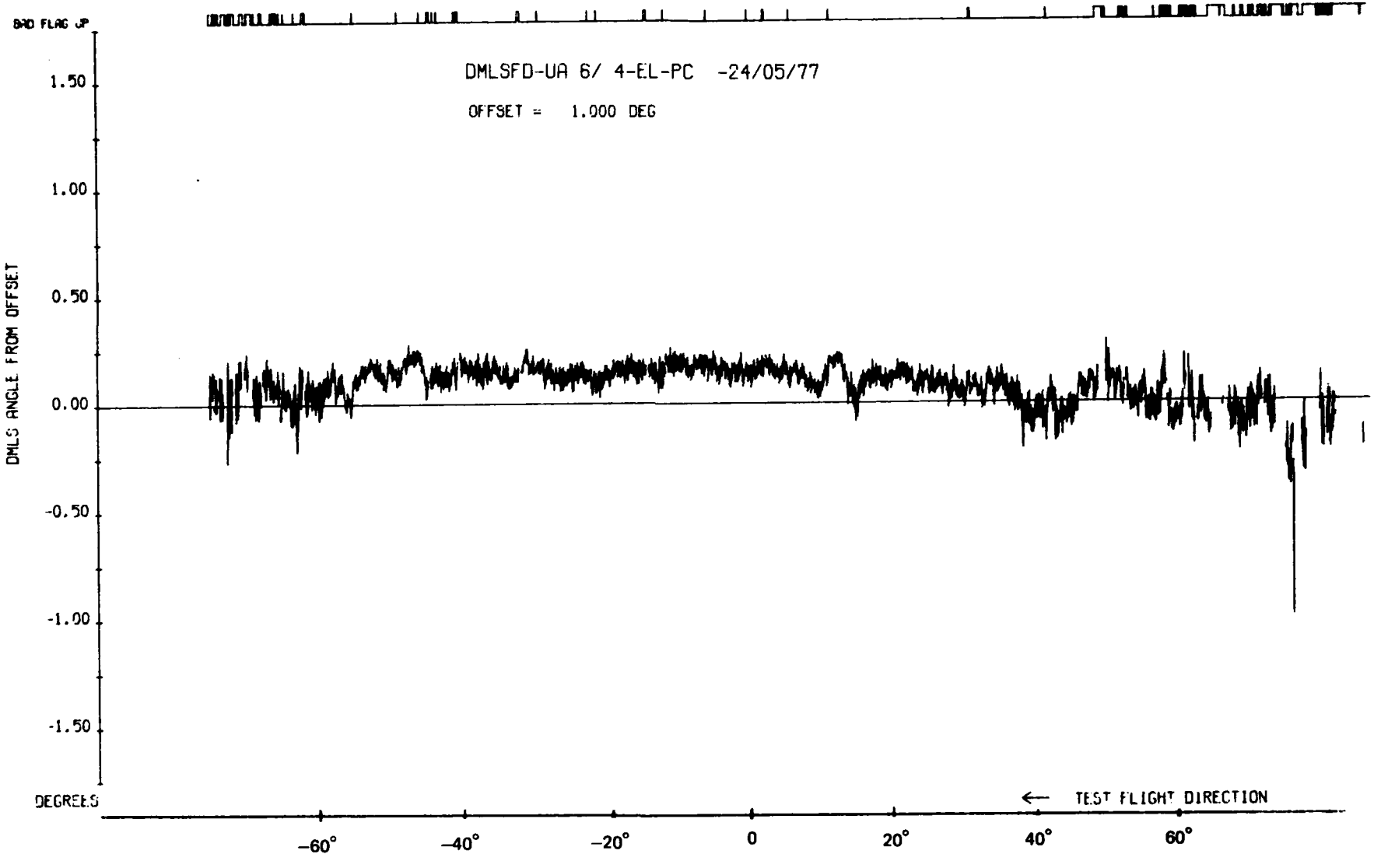

R. A. E. BEDFORD

Fig 7.83c Elevation, orbit at 20 n mile and 2000 ft

Fig 7.83c

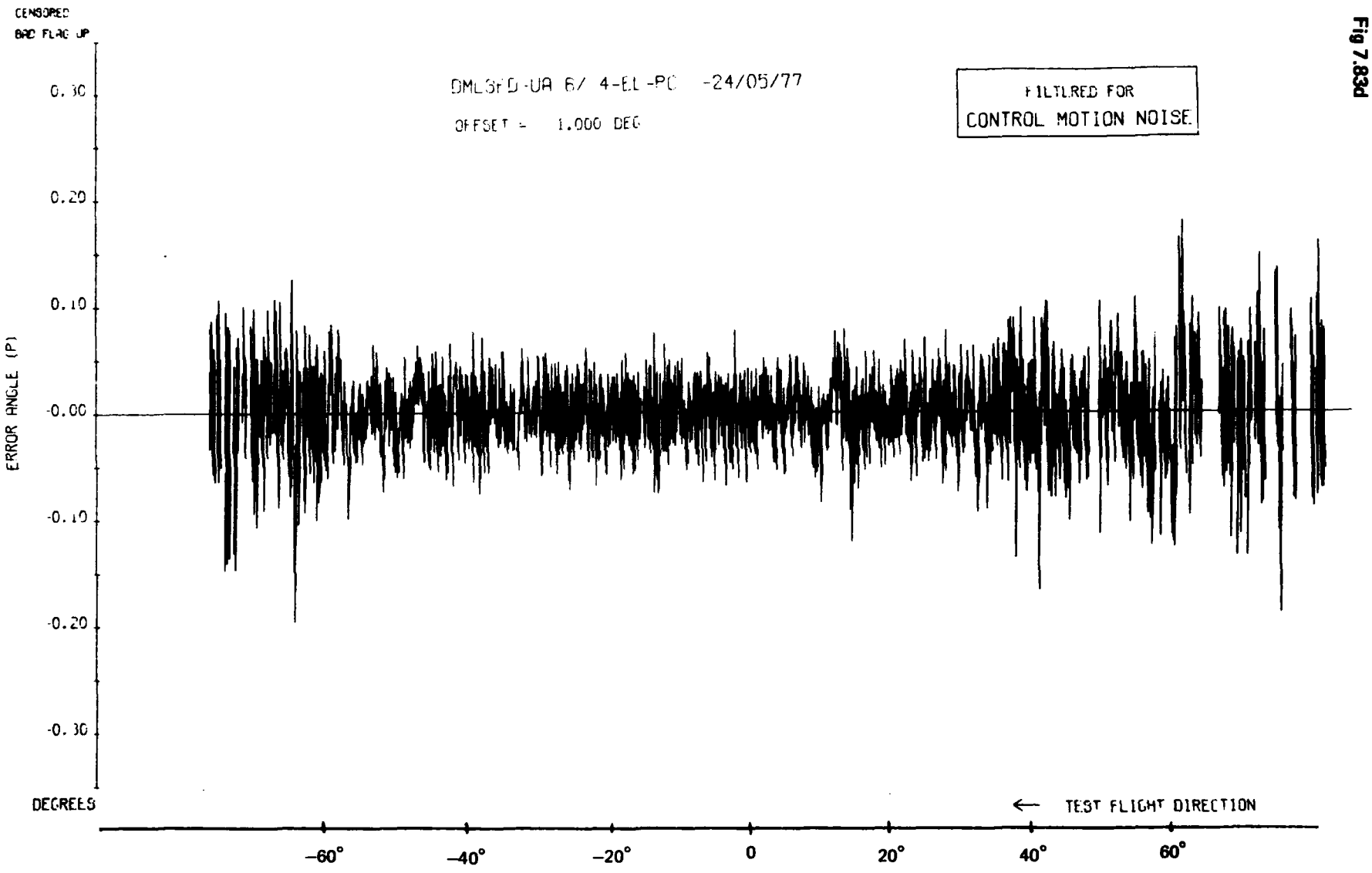

R.A.E. BEDFORD

Fig 7.83d Elevation, orbit at 20 n mile and 2000 ft

Fig 7.83d

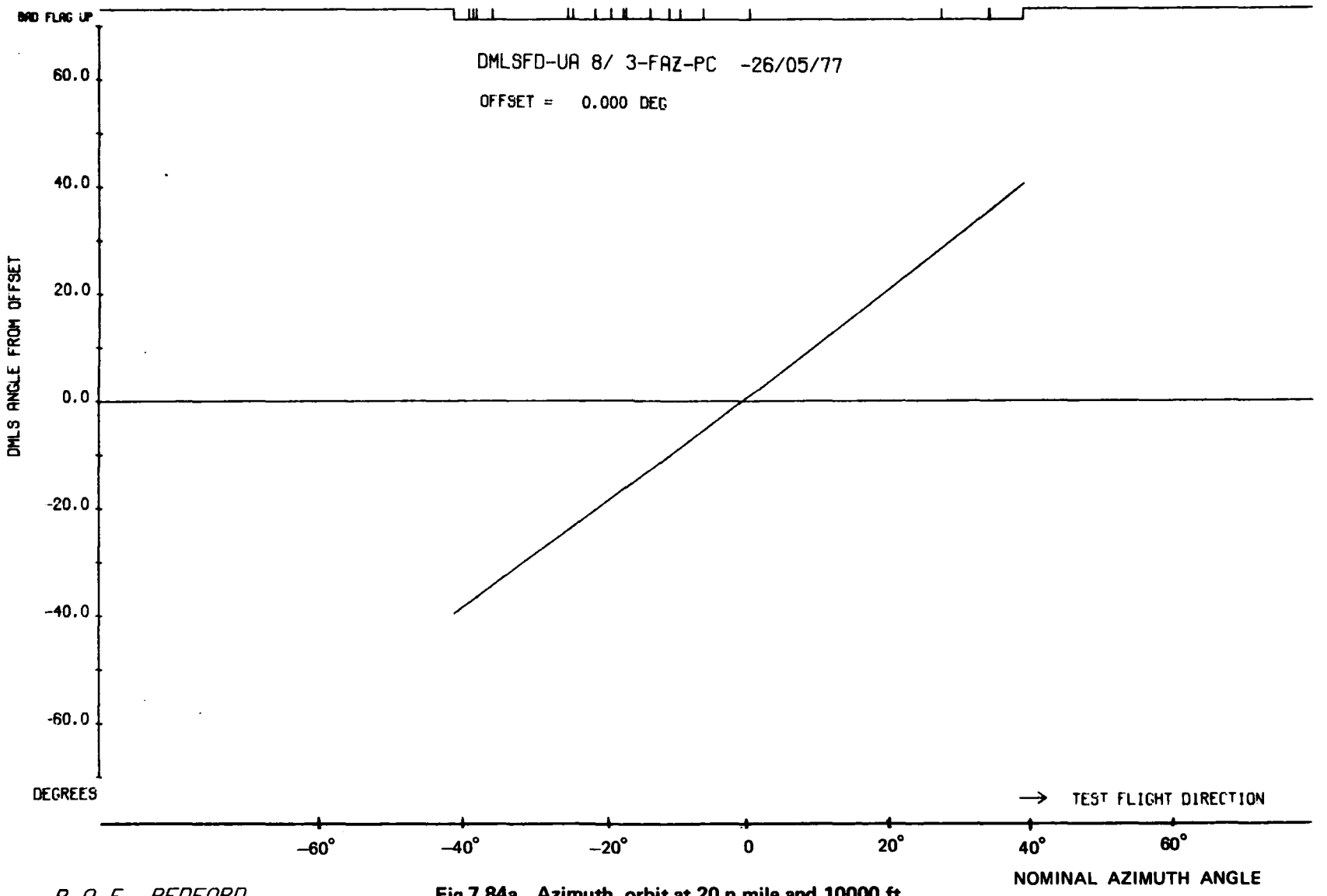

R.A.E. BEDFORD

Fig 7.84a Azimuth, orbit at 20 n mile and 10000 ft

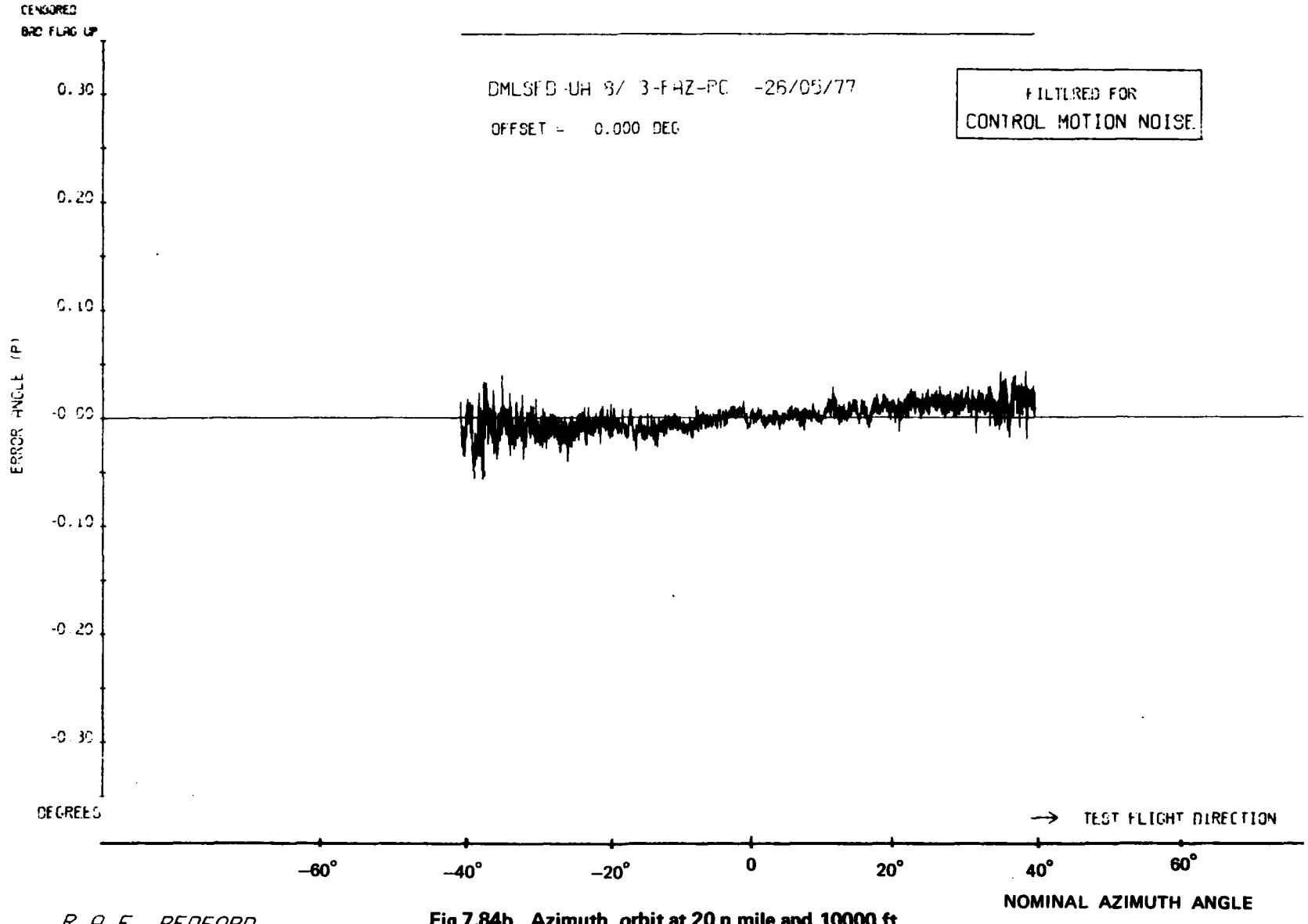

R. A. E. BEDFORD

Fig 7.84b Azimuth, orbit at 20 n mile and 10000 ft

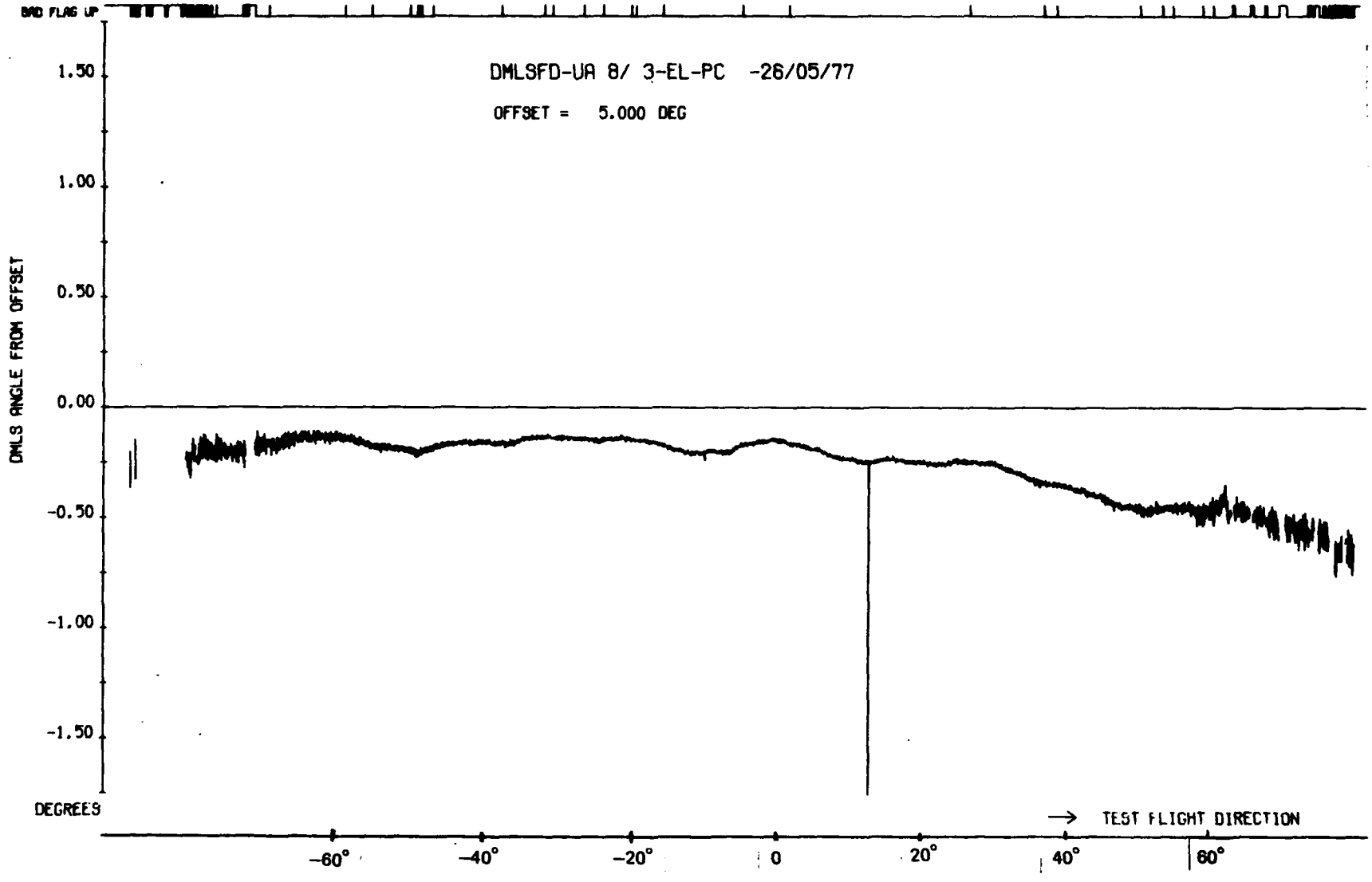

R.A.E. BEDFORD

Fig 7.84c Elevation, orbit at 20 n mile and 10000 ft

Fig 7.84c

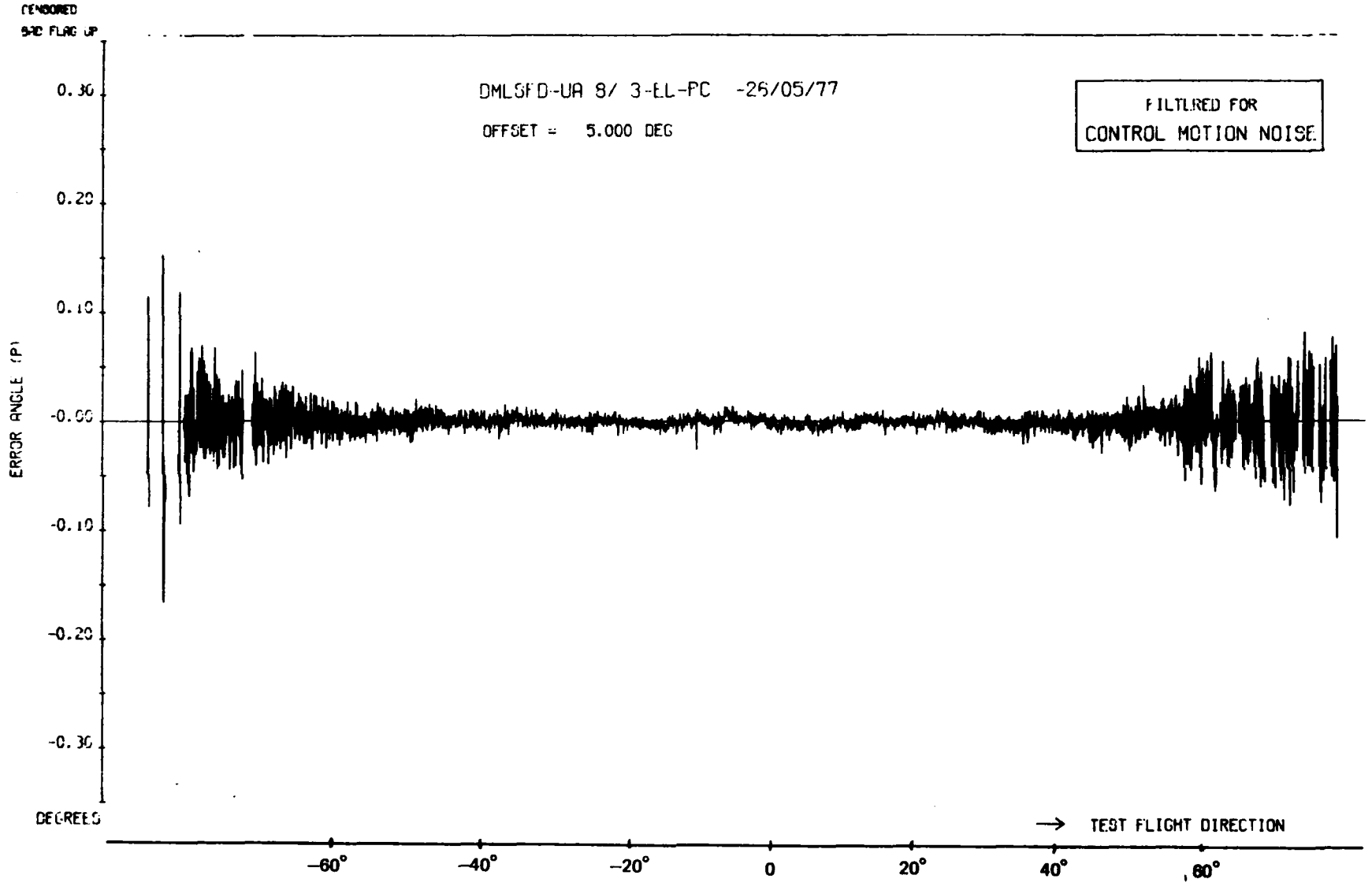

R. A. E. BEDFORD

Fig 7.84d Elevation, orbit at 20 n mile and 10000 ft

Fig 7.84d

TR 79062

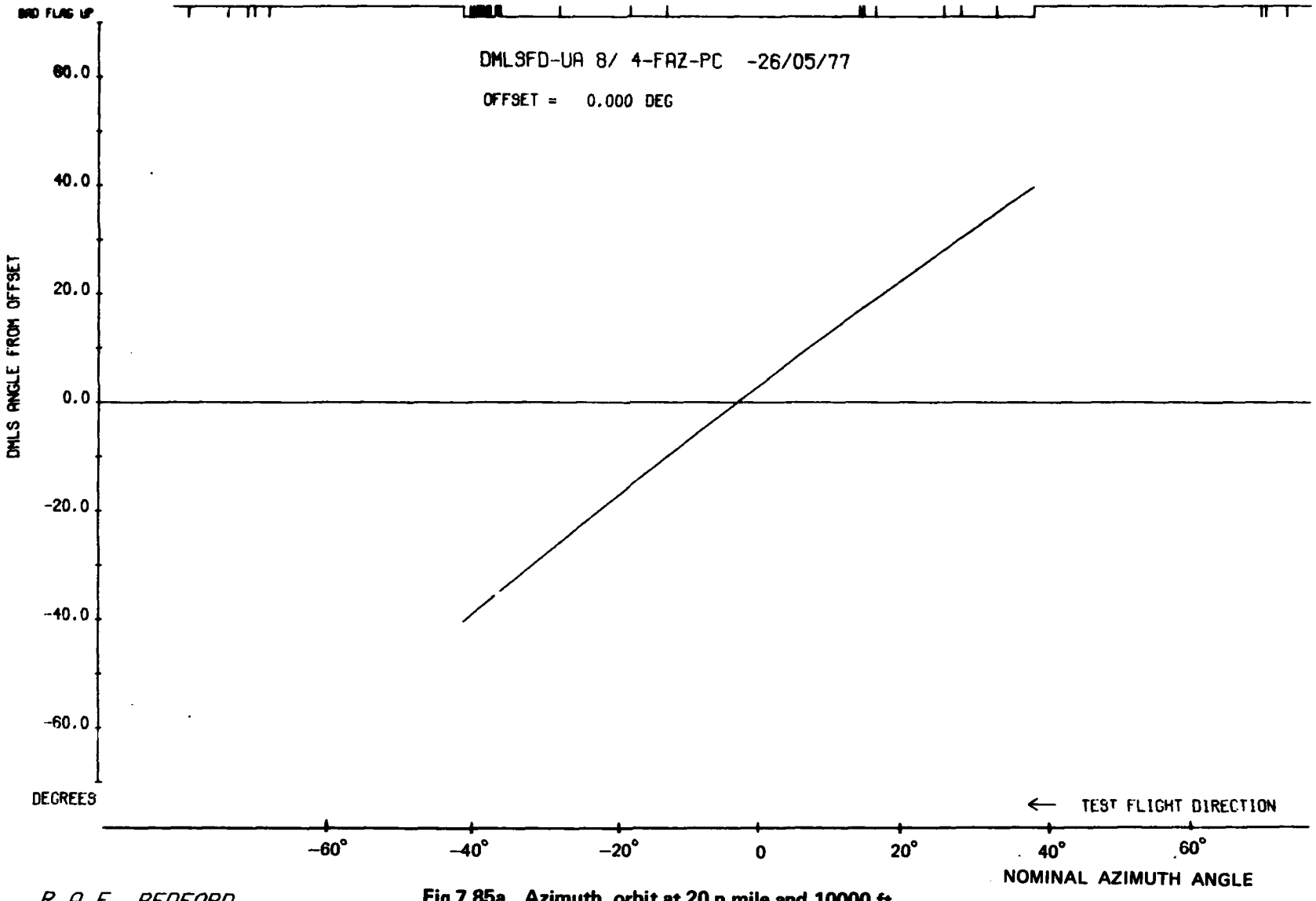

R. A. E. BEDFORD

Fig 7.85a Azimuth, orbit at 20 n mile and 10000 ft

Fig 7.85a

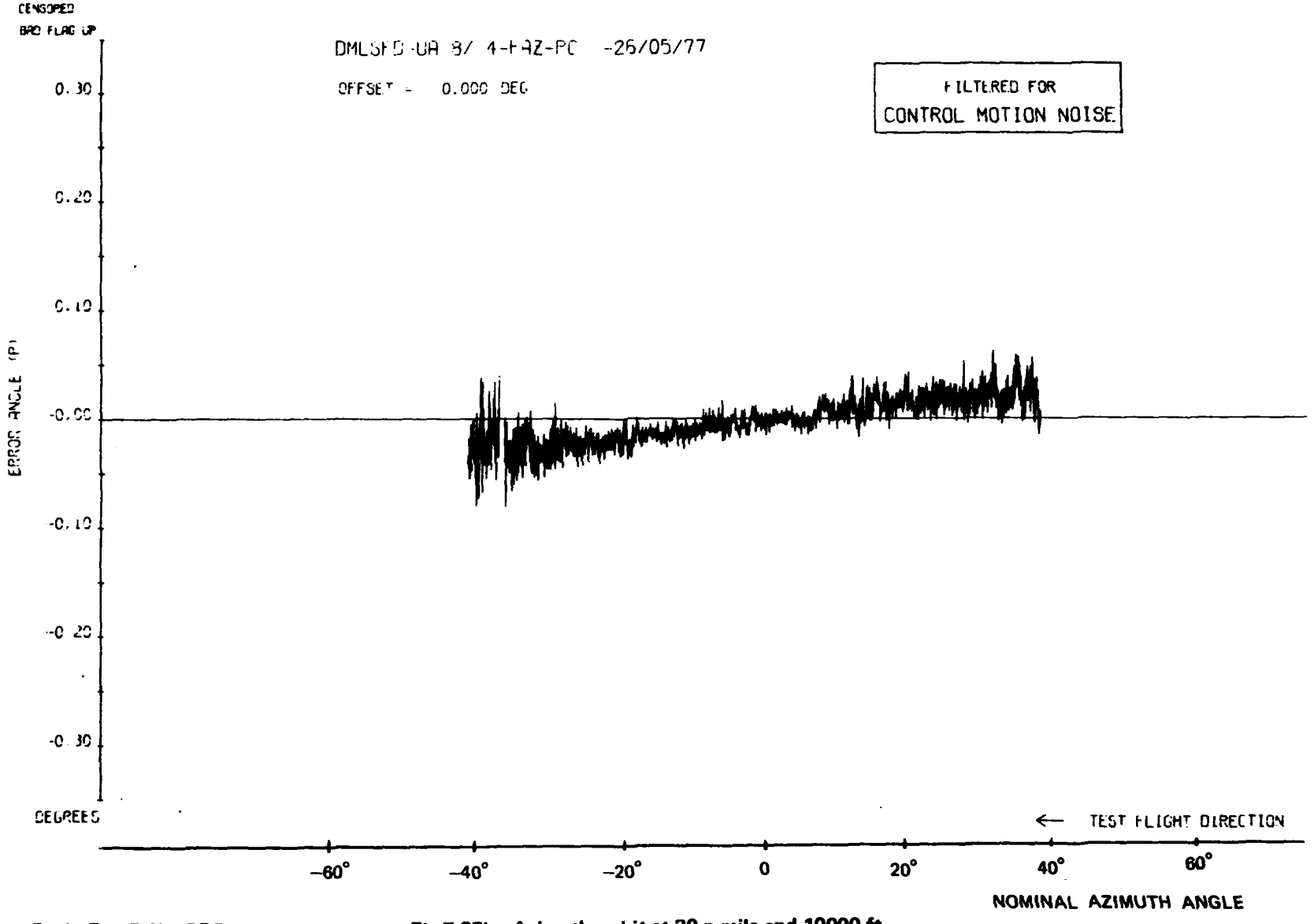

Fig 7.85b

R. A. E. BEDFORD

Fig 7.85b Azimuth, orbit at 20 n mile and 10000 ft

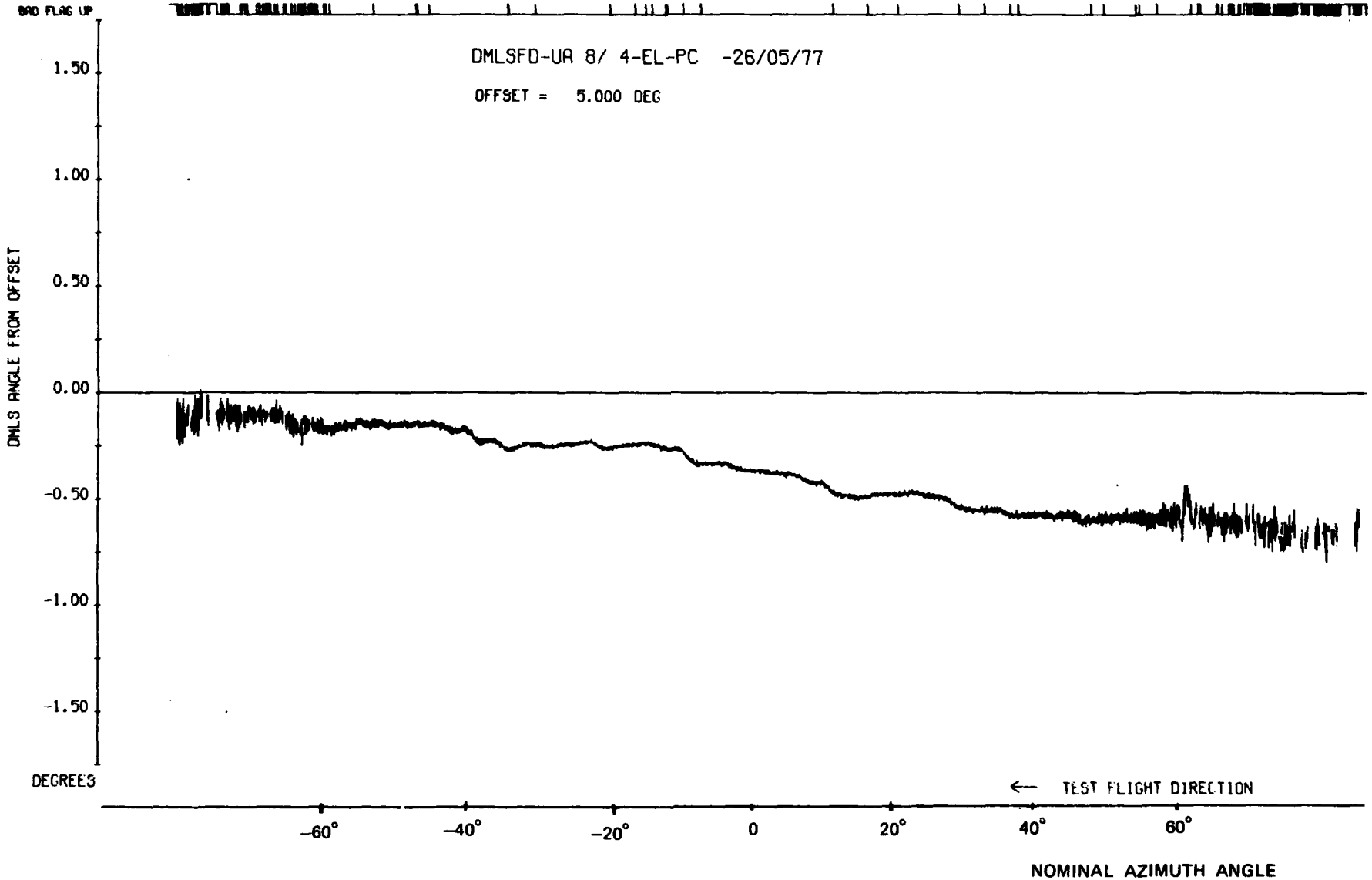

R. A. E. BEDFORD

Fig 7.85c Elevation, orbit at 20 n mile and 10000 ft

Fig 7.85c

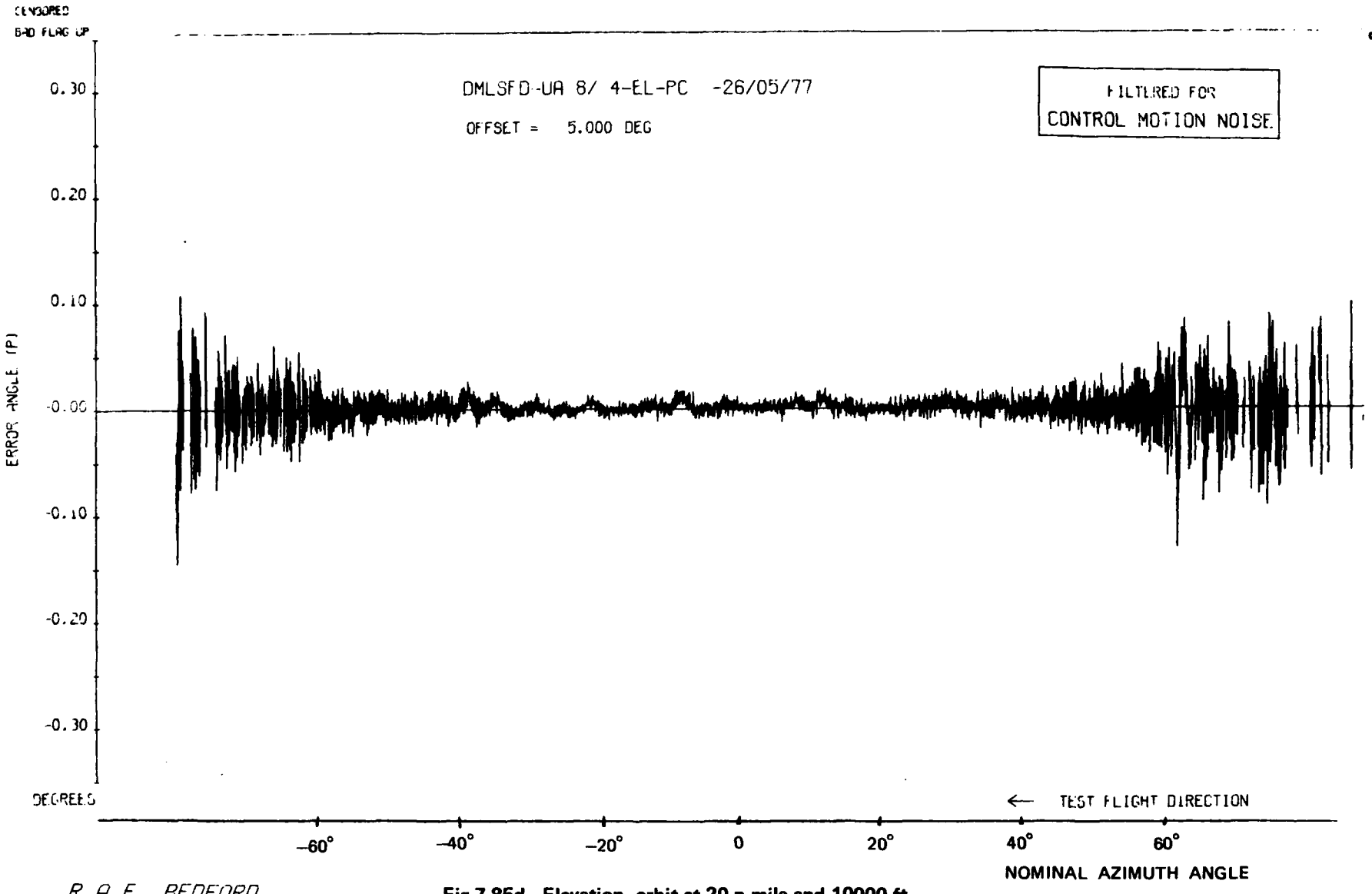

Fig 7.85d

R.A.E. BEDFORD

Fig 7.85d Elevation, orbit at 20 n mile and 10000 ft

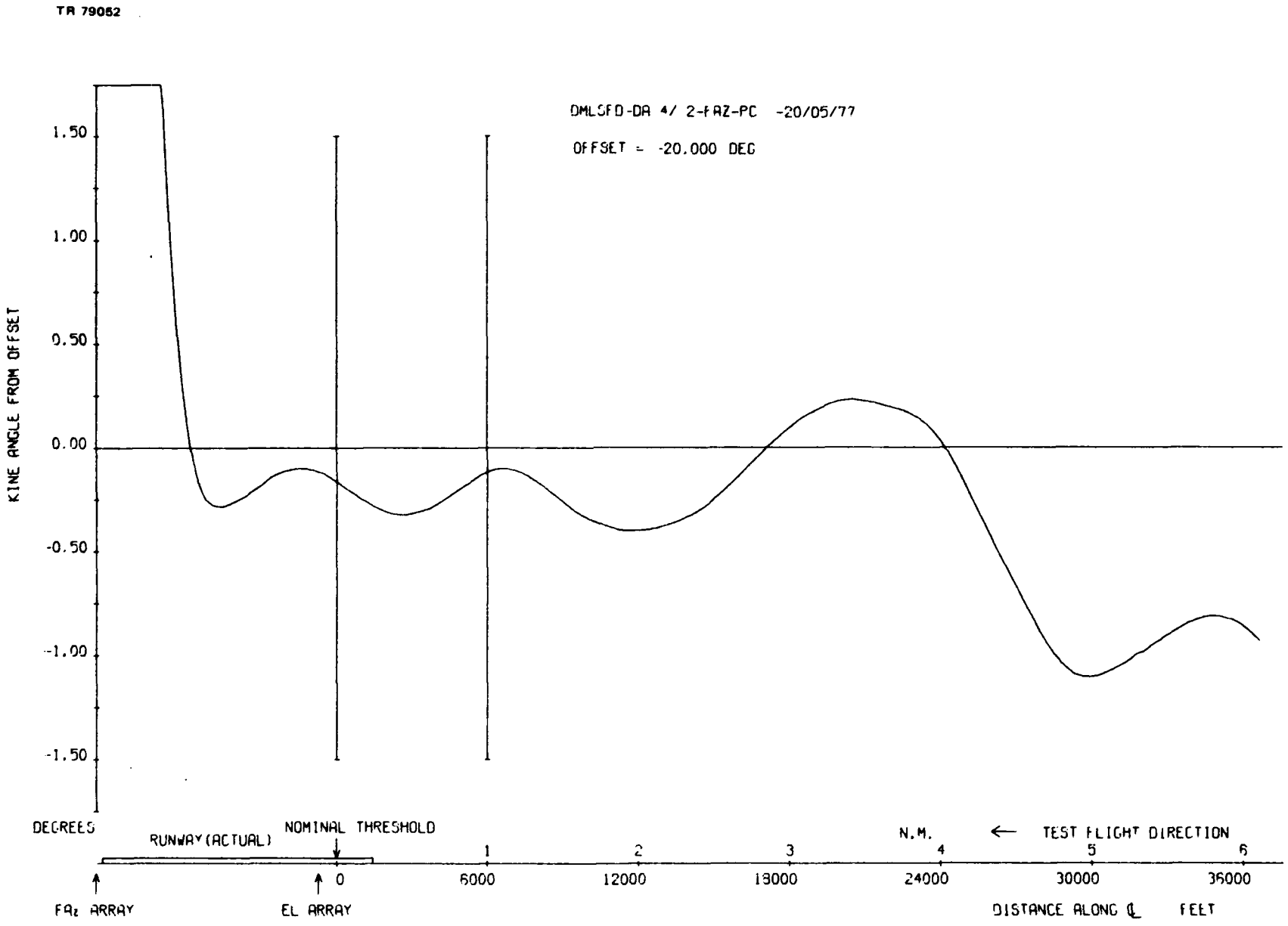

Fig 7.86a Azimuth 27λ, constant height radial at 2000 ft and −20 degrees

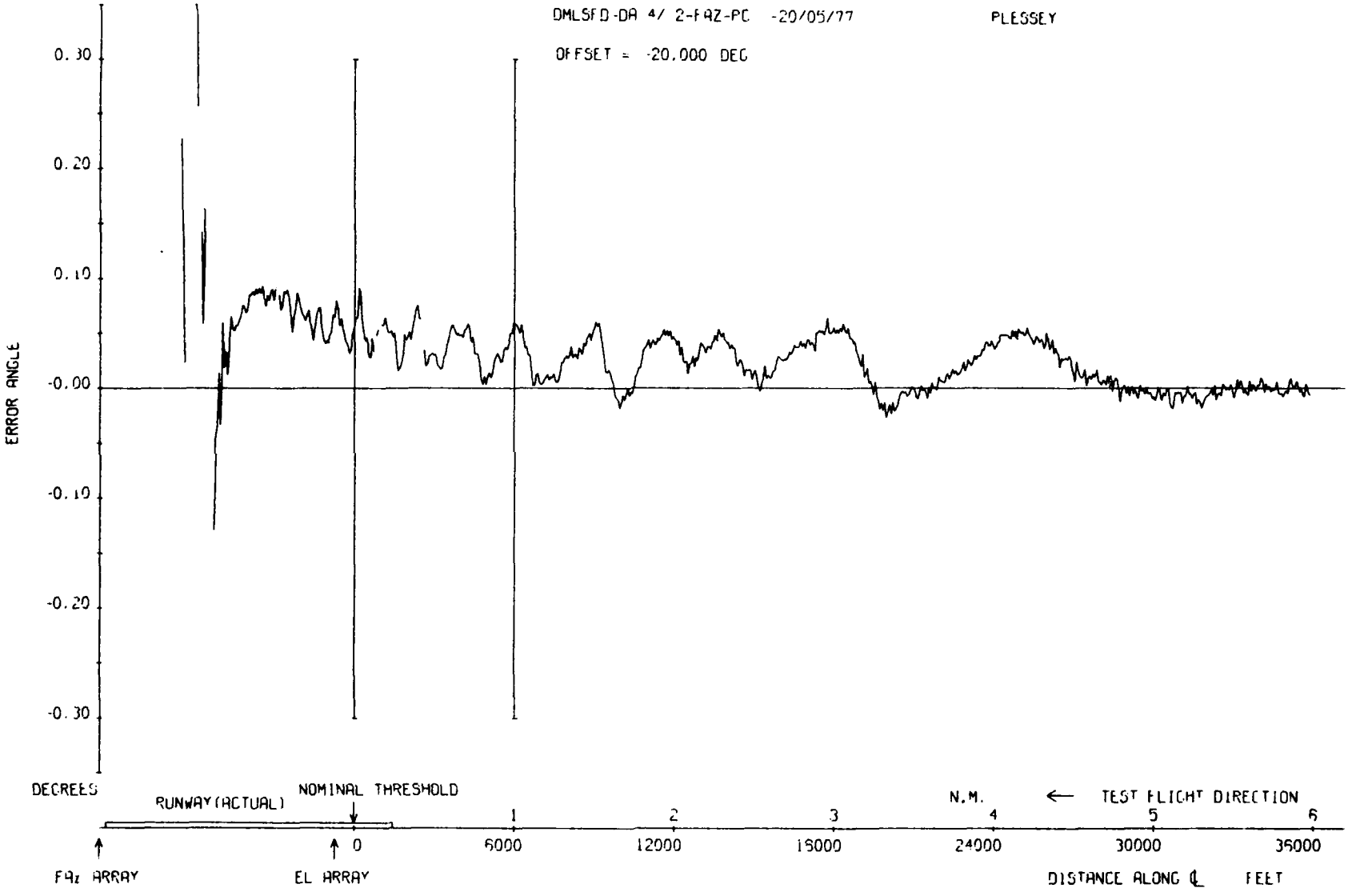

Fig 7.86b Azimuth 27λ, constant height radial at 2000 ft and −20 degrees

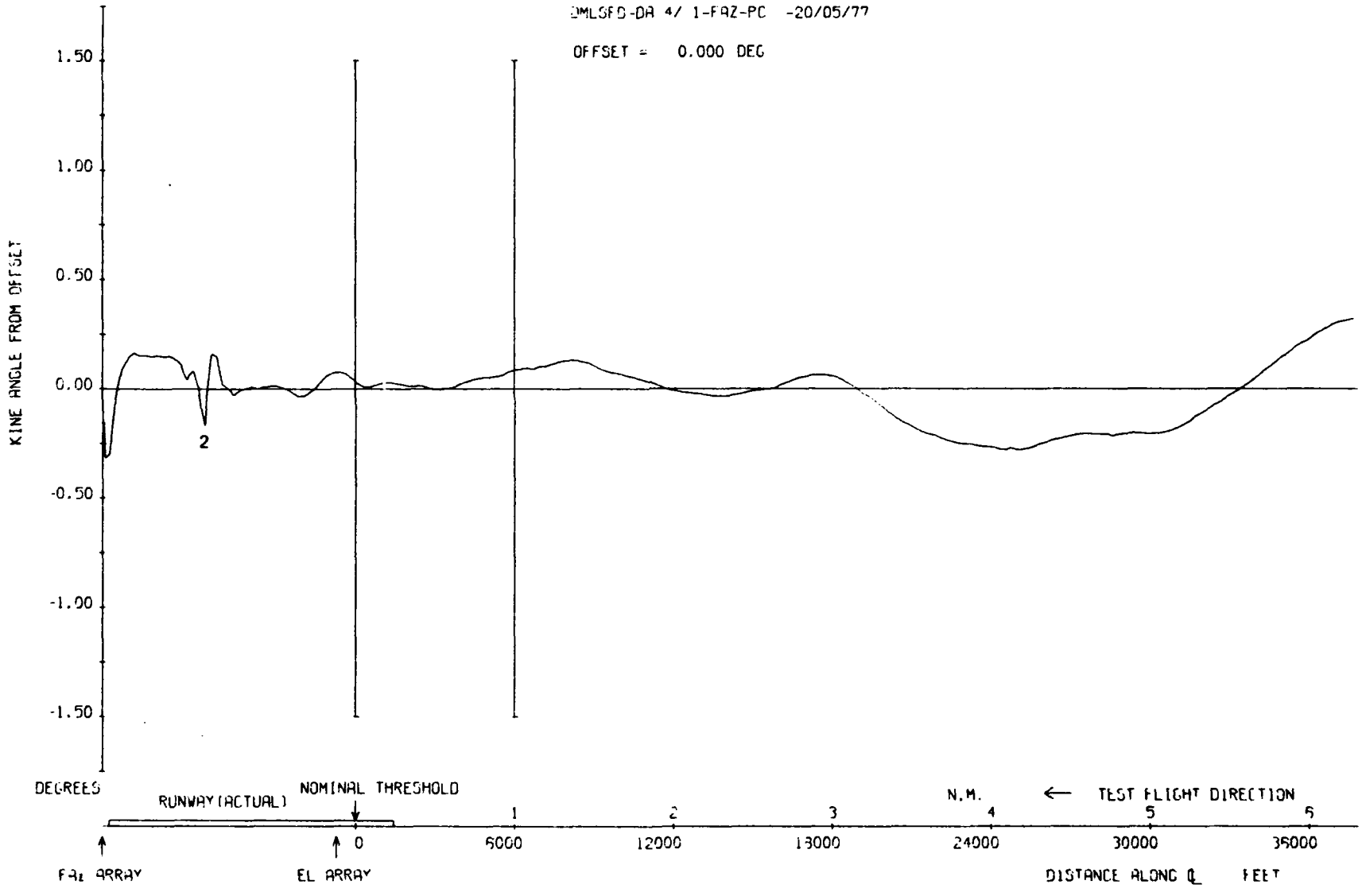

Fig 7.87a Azimuth 27λ, 3 degree approach to low overshoot

Fig 7.87a

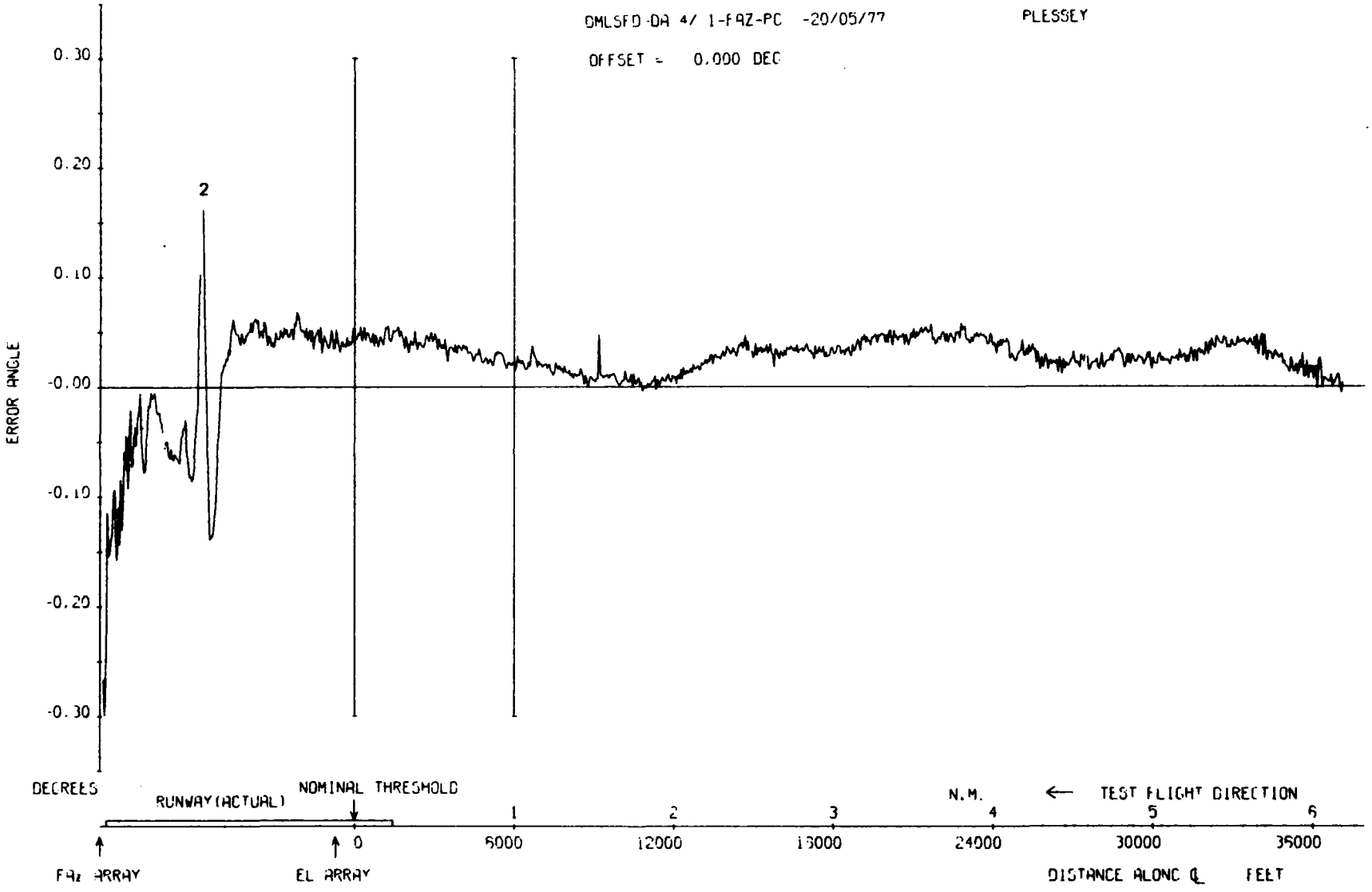

Fig 7.87b

Fig 7.87b Azimuth 27λ, 3 degree approach to low overshoot

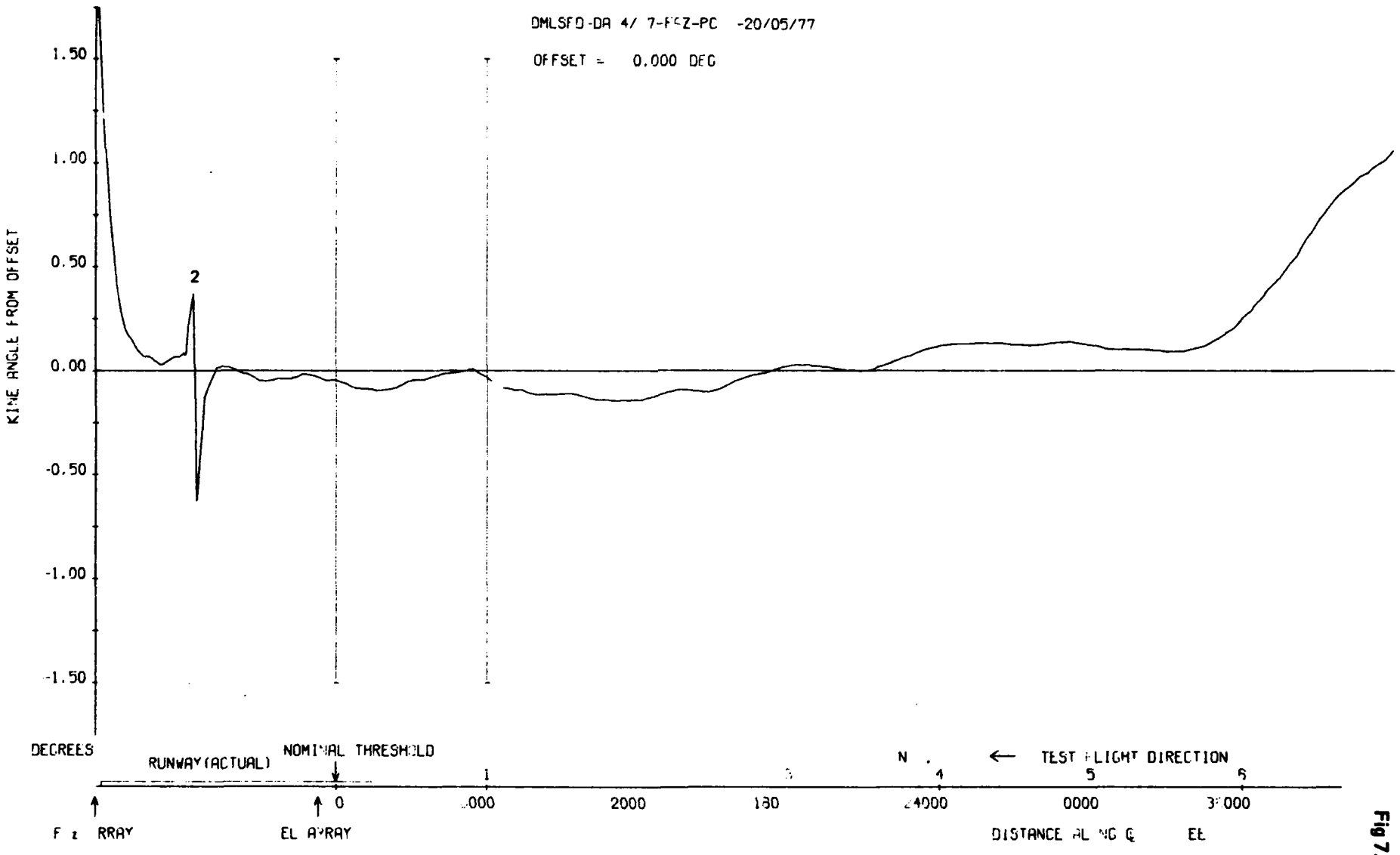

Fig 7.88a Azimuth 27λ, 2 degree approach to low overshoot

Fig 7.88a

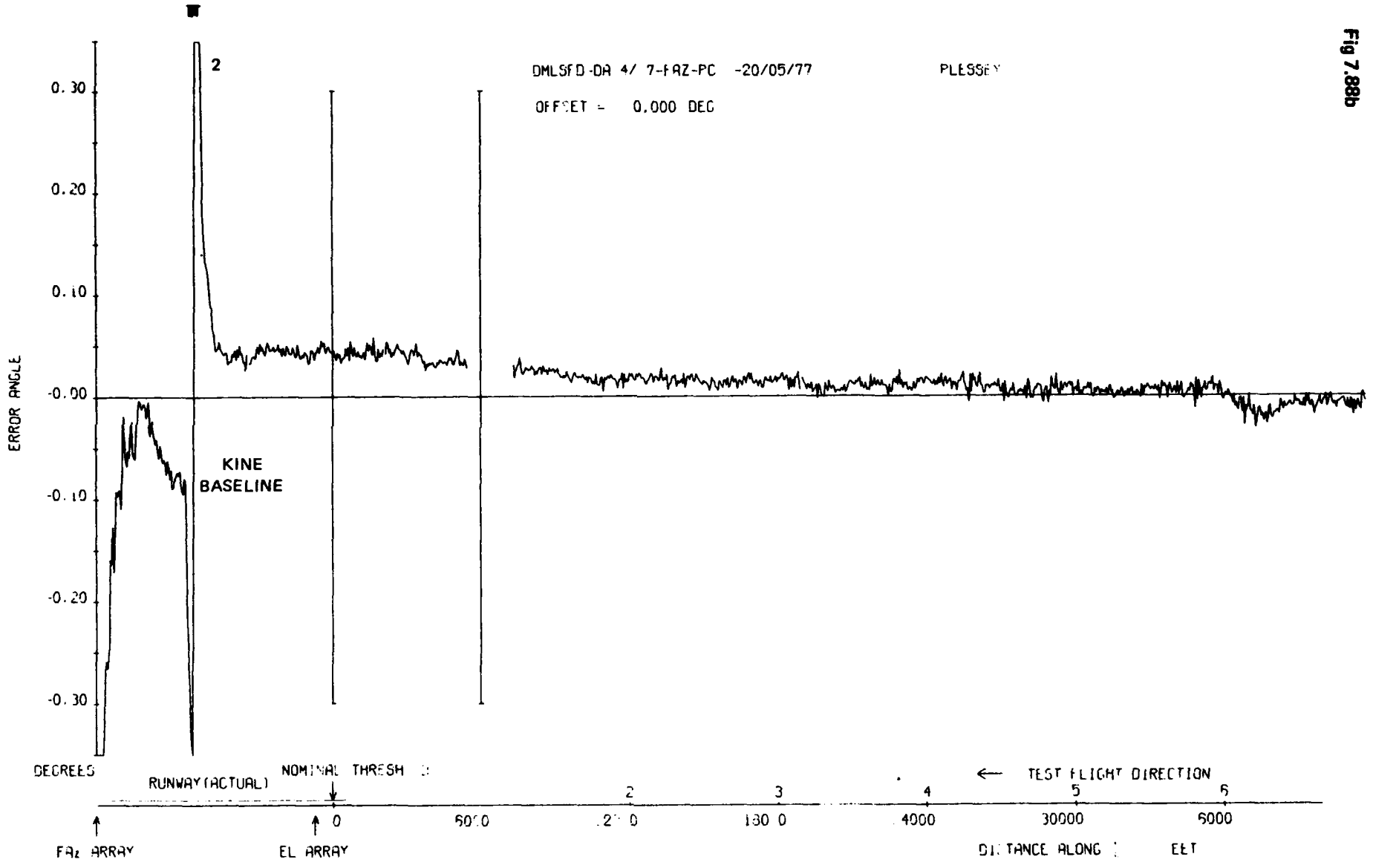

Fig 7.88b

Fig 7.88b Azimuth 27λ, 2 degree approach to low overshoot

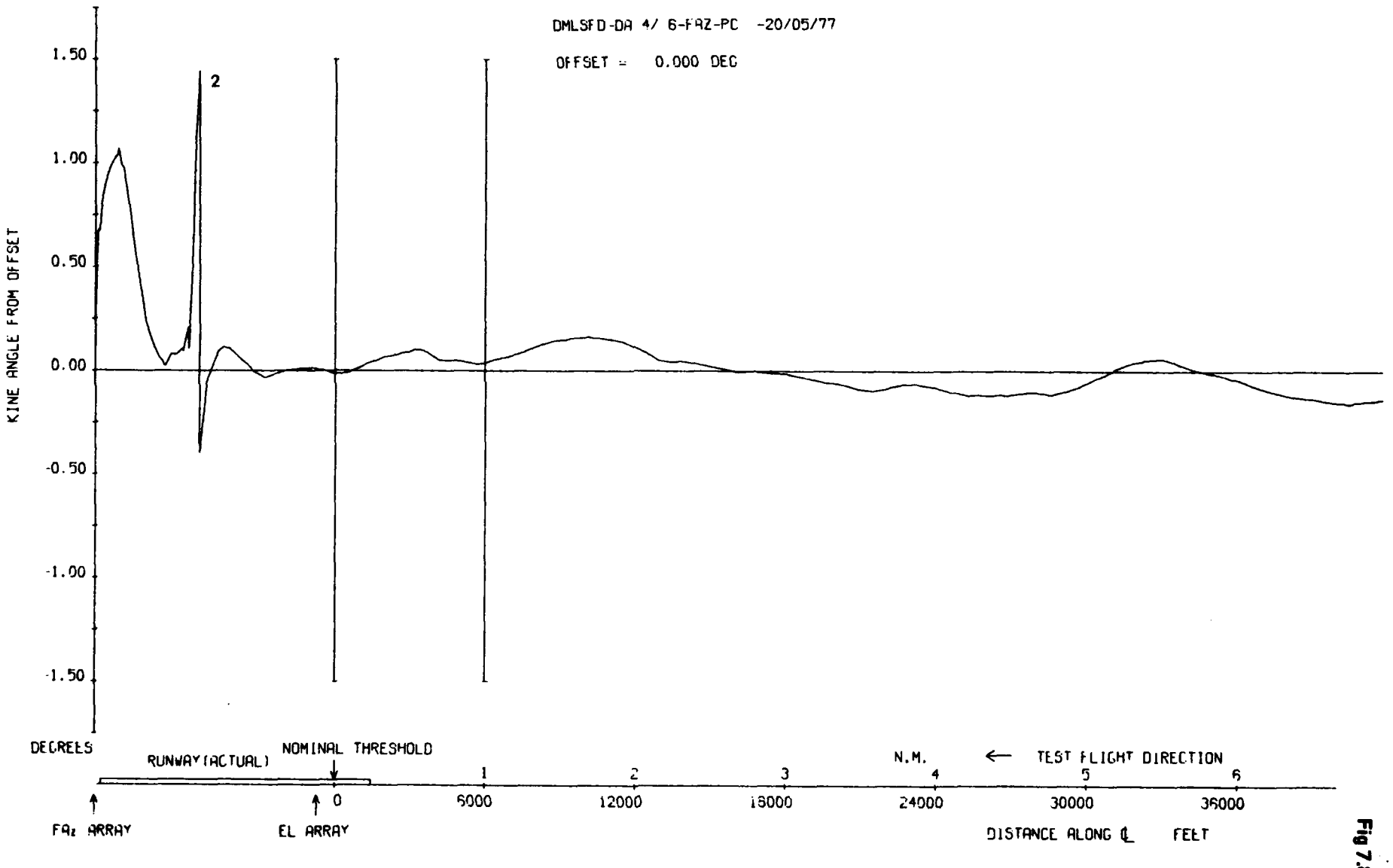

Fig 7.89a Azimuth 1.5 degree approach to low overshoot

Fig 7.89a

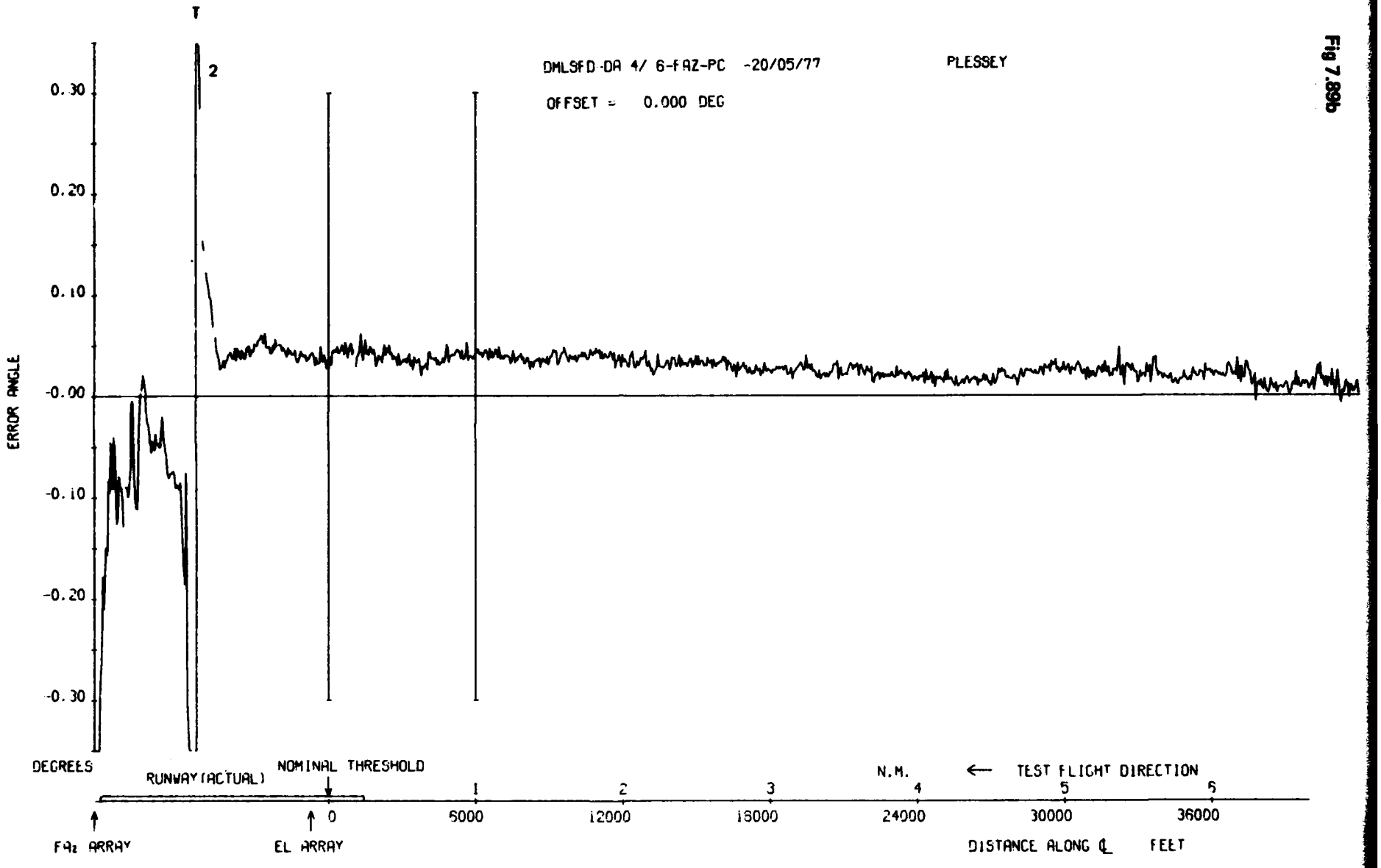

Fig 7.89b

Fig 7.89b Azimuth 1.5 degree approach to low overshoot

TR 79062

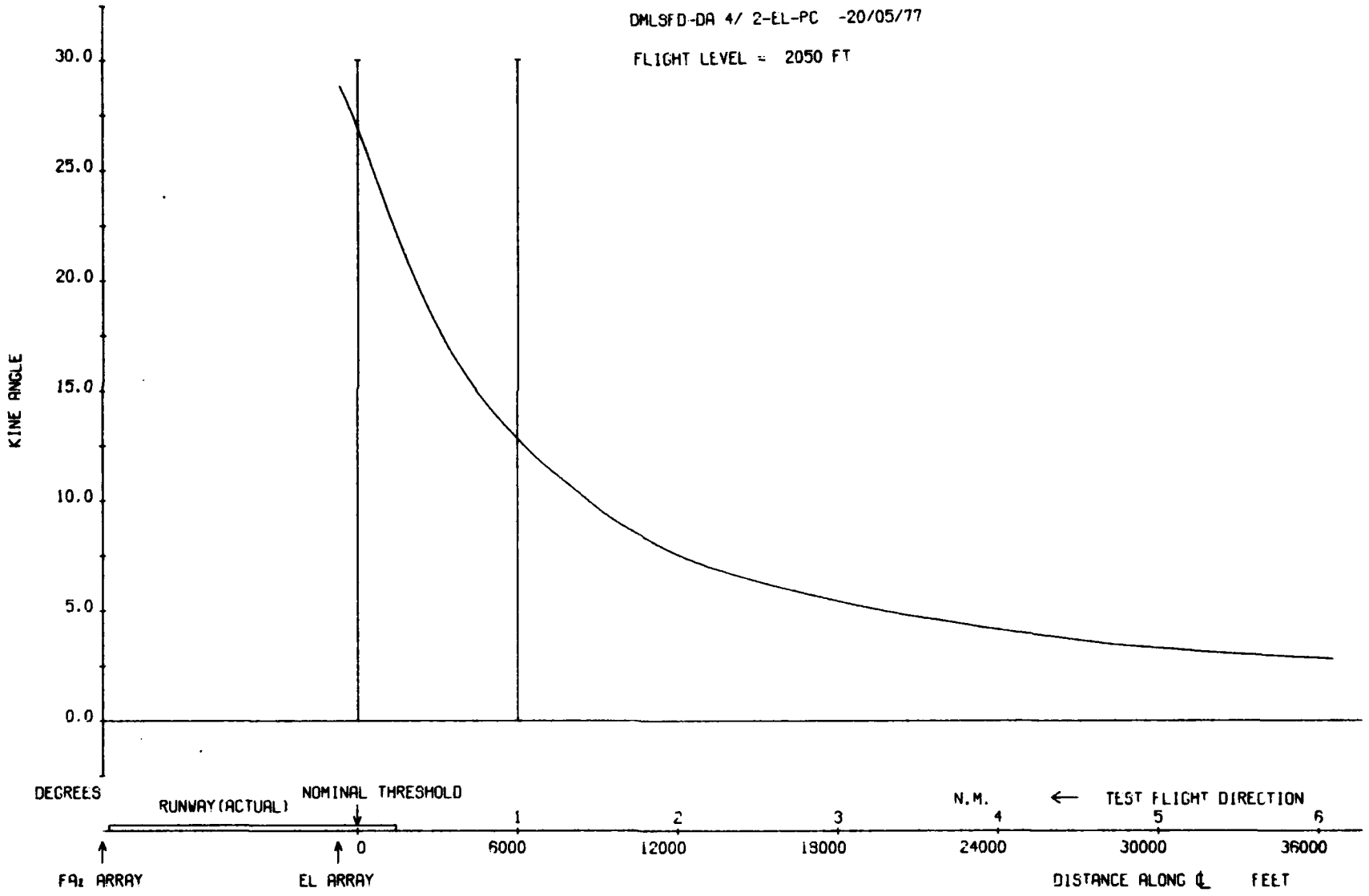

Fig 7.90a Elevation 27λ, constant height radial at 2000 ft and –20 degrees azimuth

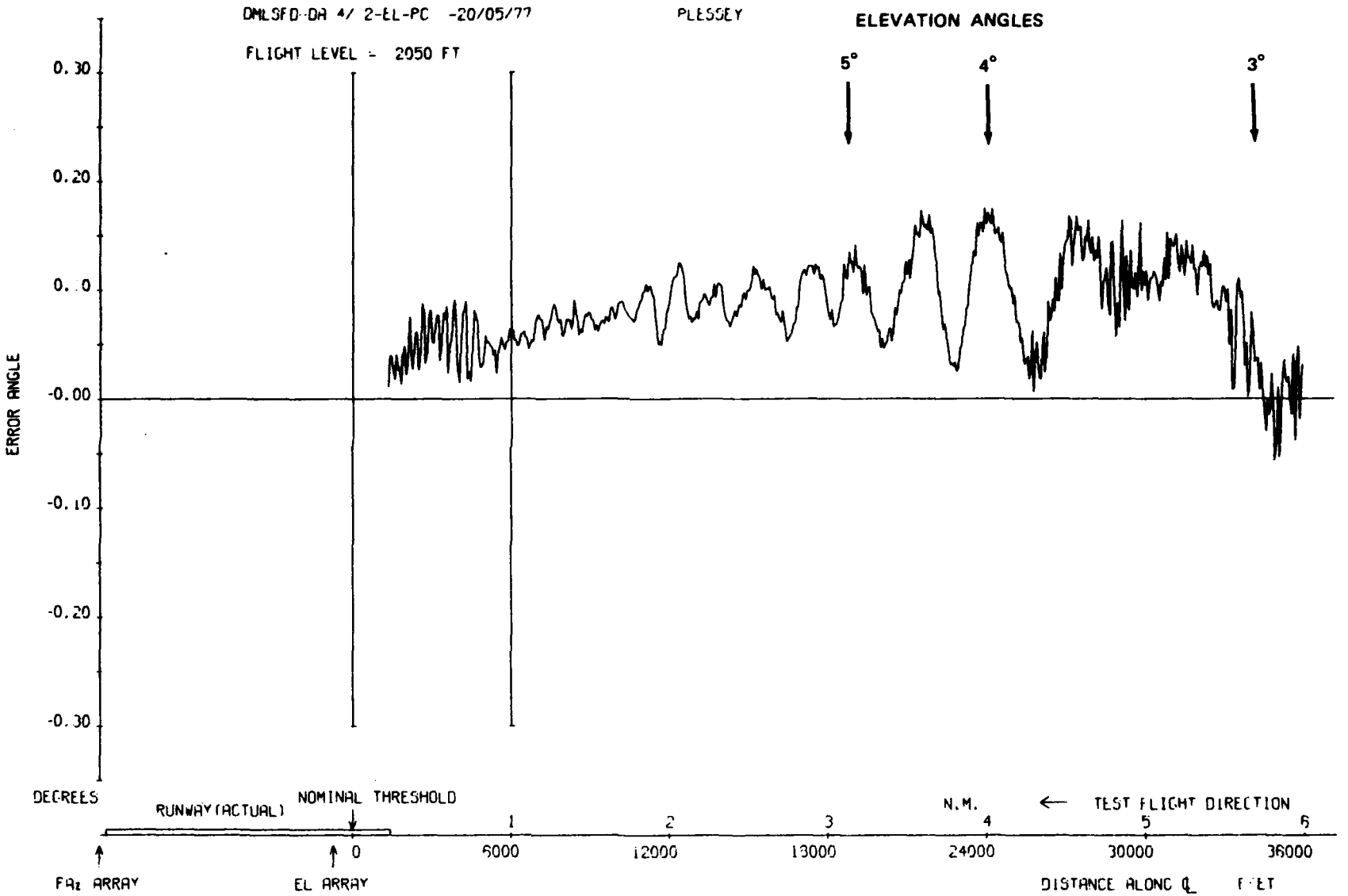

Fig 7.90b

Fig 7.90b Elevation 27λ, constant height radial at 2000 ft and –20 degrees azimuth

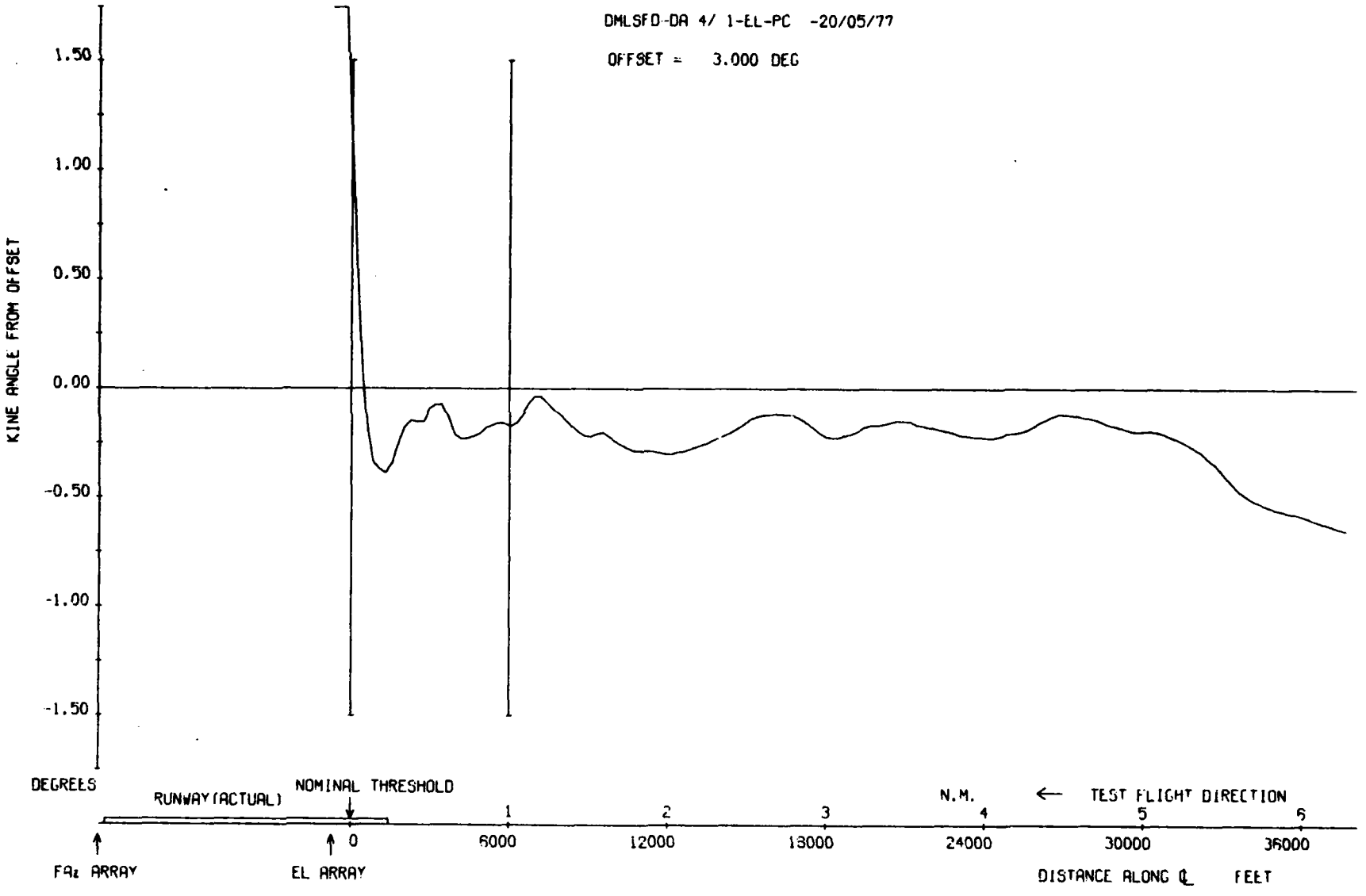

Fig 7.91a Elevation 27λ, 3 degree approach

Fig 7.91a

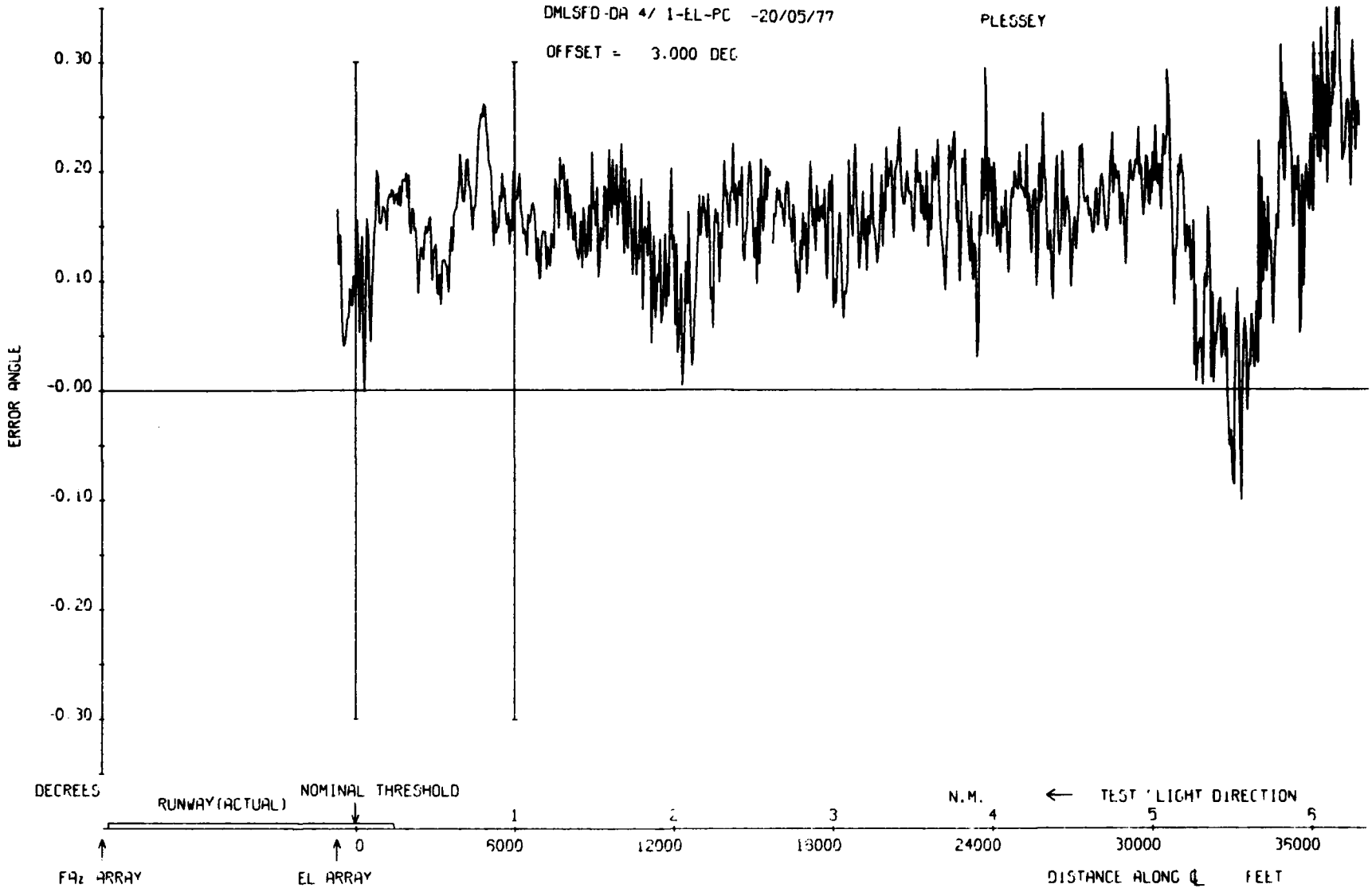

Fig 7.91b

Fig 7.91b Elevation 27λ, 3 degree approach

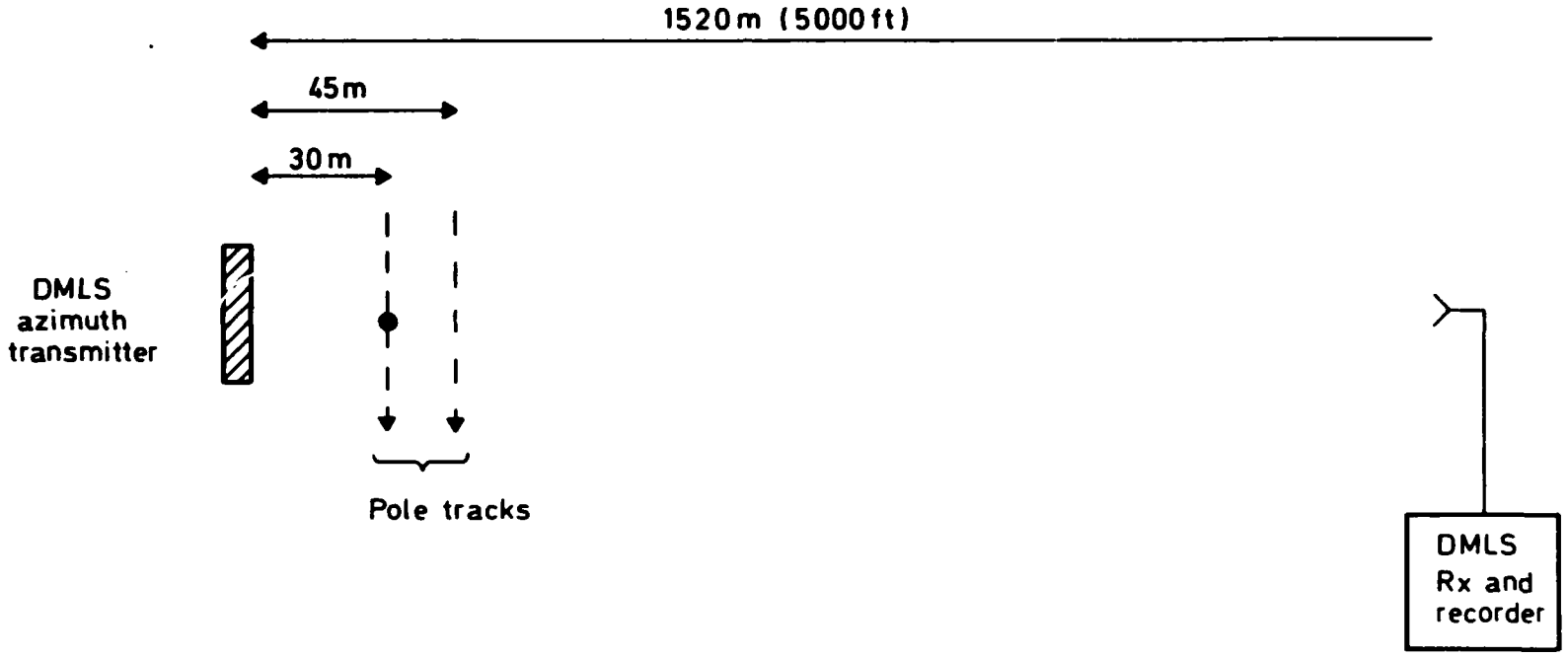

Fig 7.92 Effects of poles — test geometry

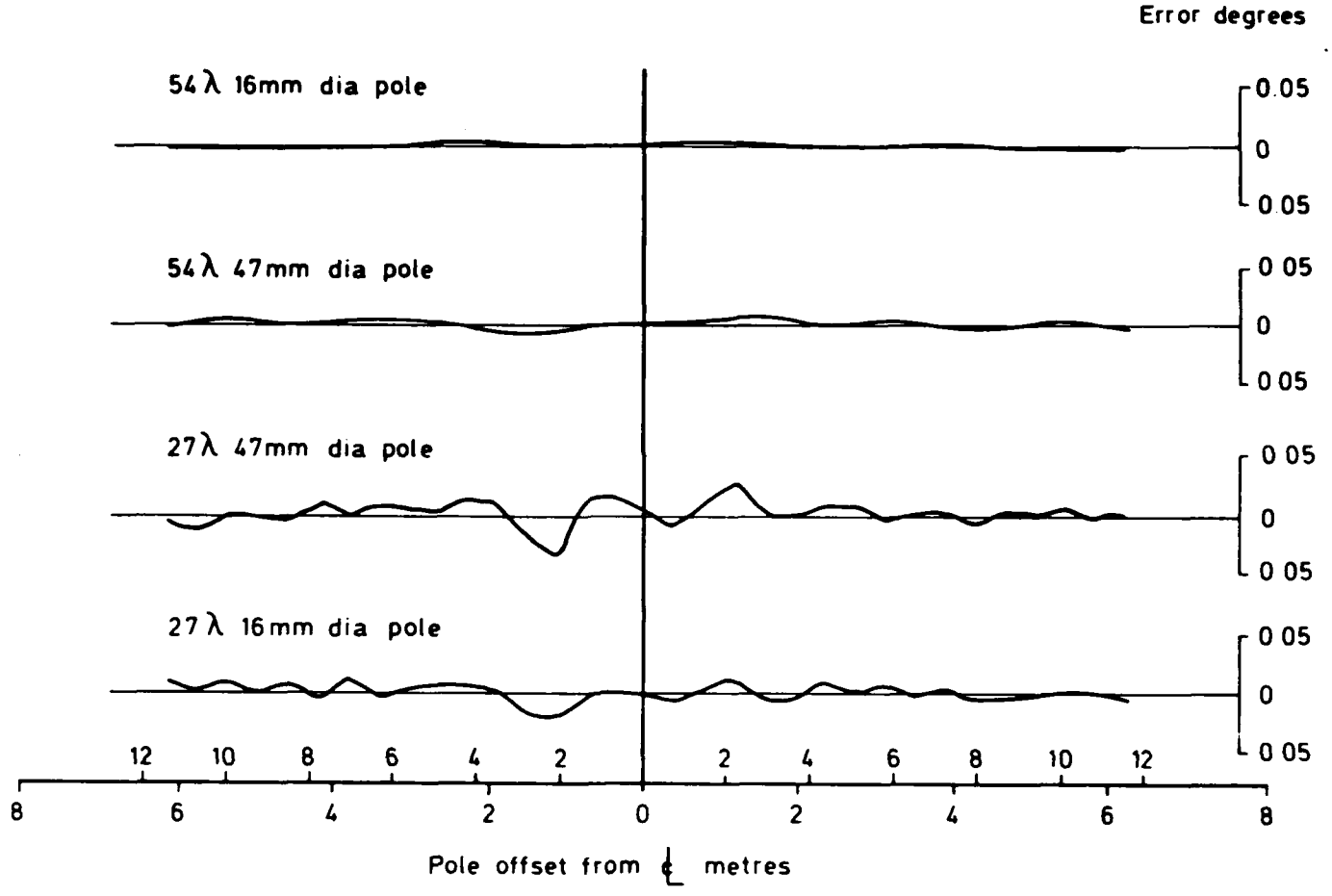

Fig 7.93a Effect of metal poles – range 30 m (100 ft)

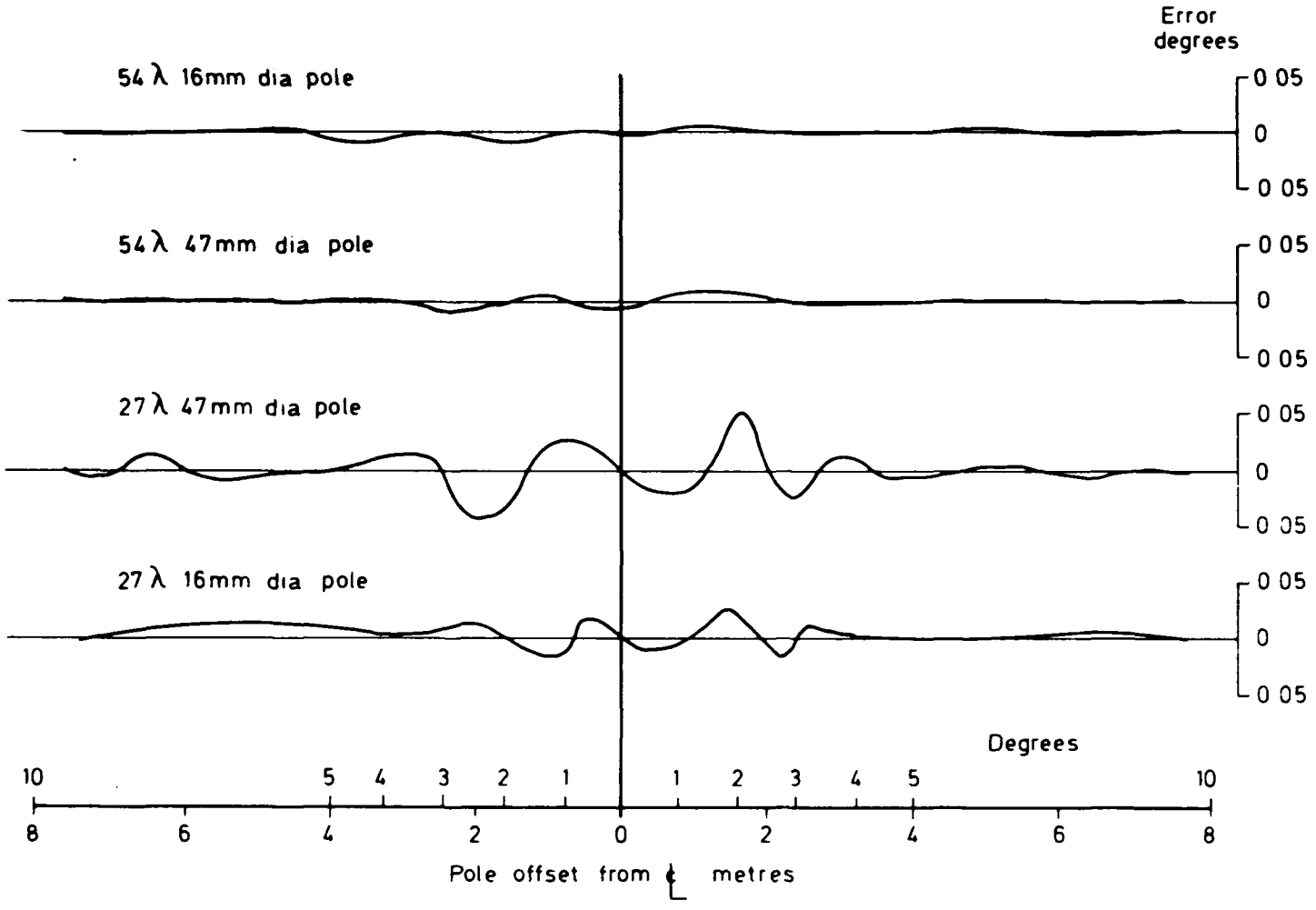

Fig 7.93b Effect of metal poles — range 45 m (150 ft)

Fig 7.93b

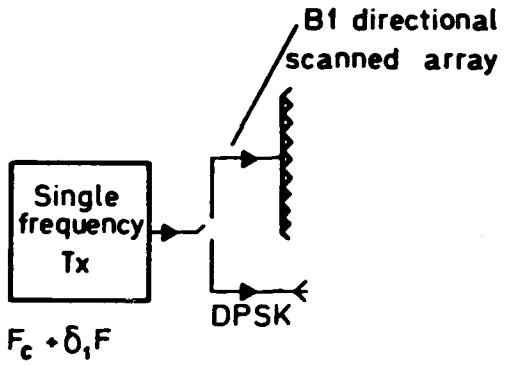

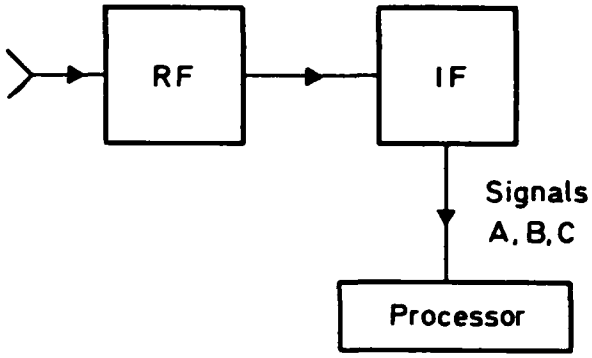

A = DPSK $F_C + \delta_1 F - F_{LO} + \delta_2 F + \delta_3 F$

B = odd scans $F_C + \delta_1 F - F_{LO} + \delta_2 F + \delta_3 F + F_D$

C = even scans $F_C + \delta_1 F - F_{LO} + \delta_2 F + \delta_3 F - F_D$

Angle output $B - C = 2F_D$

$\delta_1 F + \delta_2 F + \delta_3 F = \pm 25$KHz max

F_D = doppler code

F_C = basic transmitter frequency

$\delta_1 F$ = Tx drift

$\delta_2 F$ = Rx motion doppler shift

$\delta_3 F$ = Rx LO drift

Fig 9.1 Reference-less DMLS

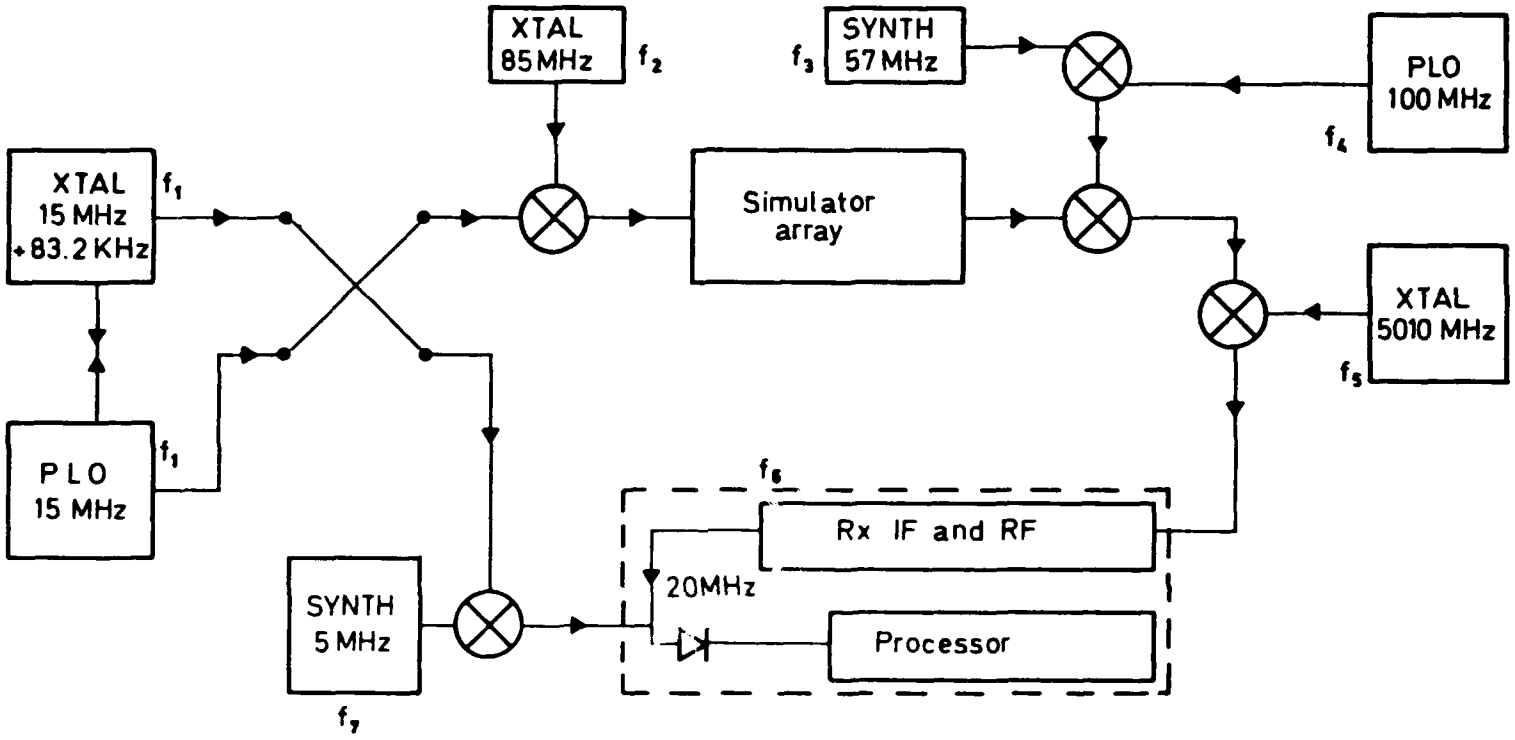

XTAL = crystal oscillator source

SYNTH = frequency synthesiser

f_1 to f_7 = frequency errors

Fig 9.2 Simulation of reference-less system

Fig 9.2

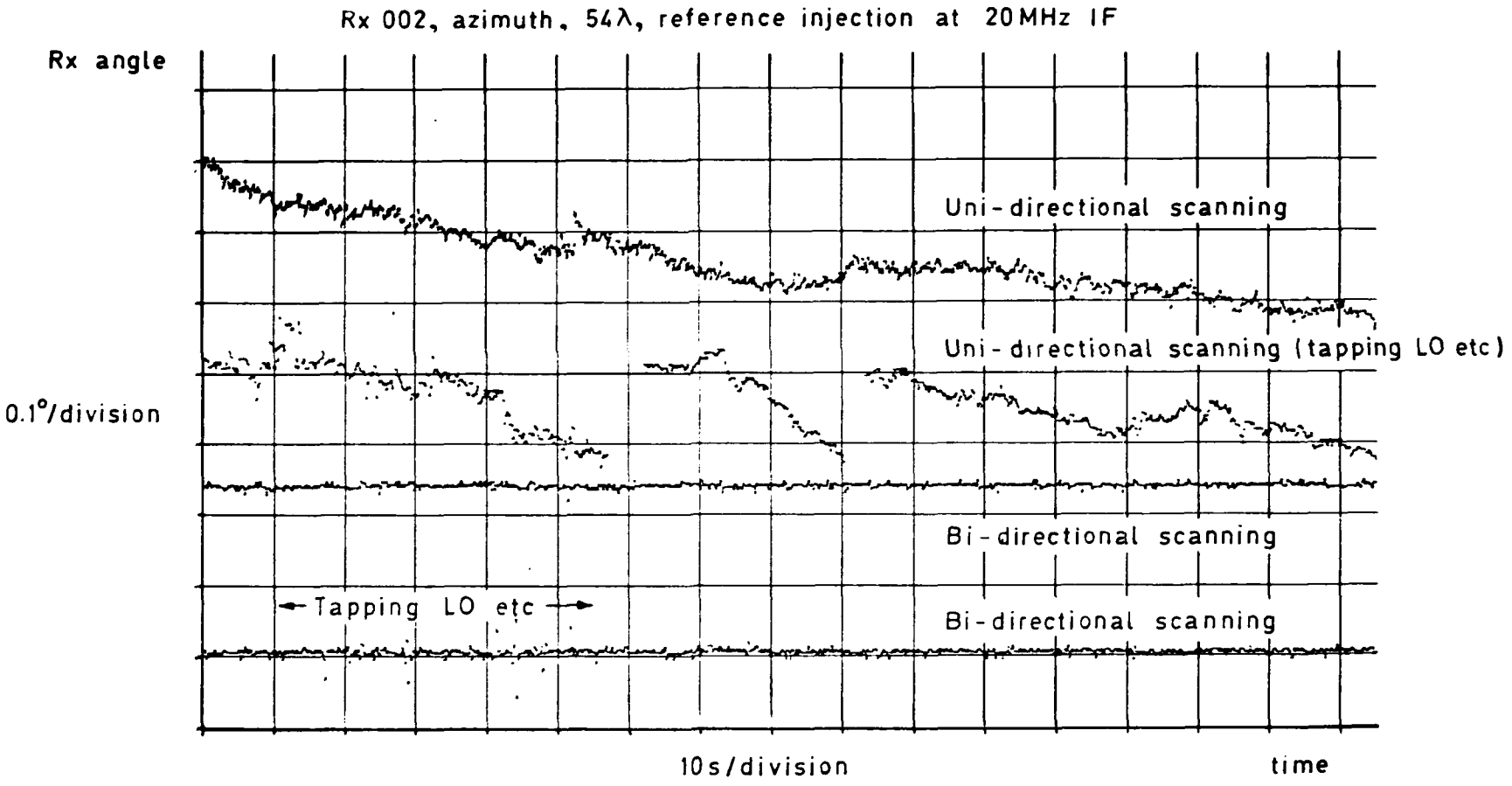

Fig 9.3 Basic angle noise with reference-less transmission

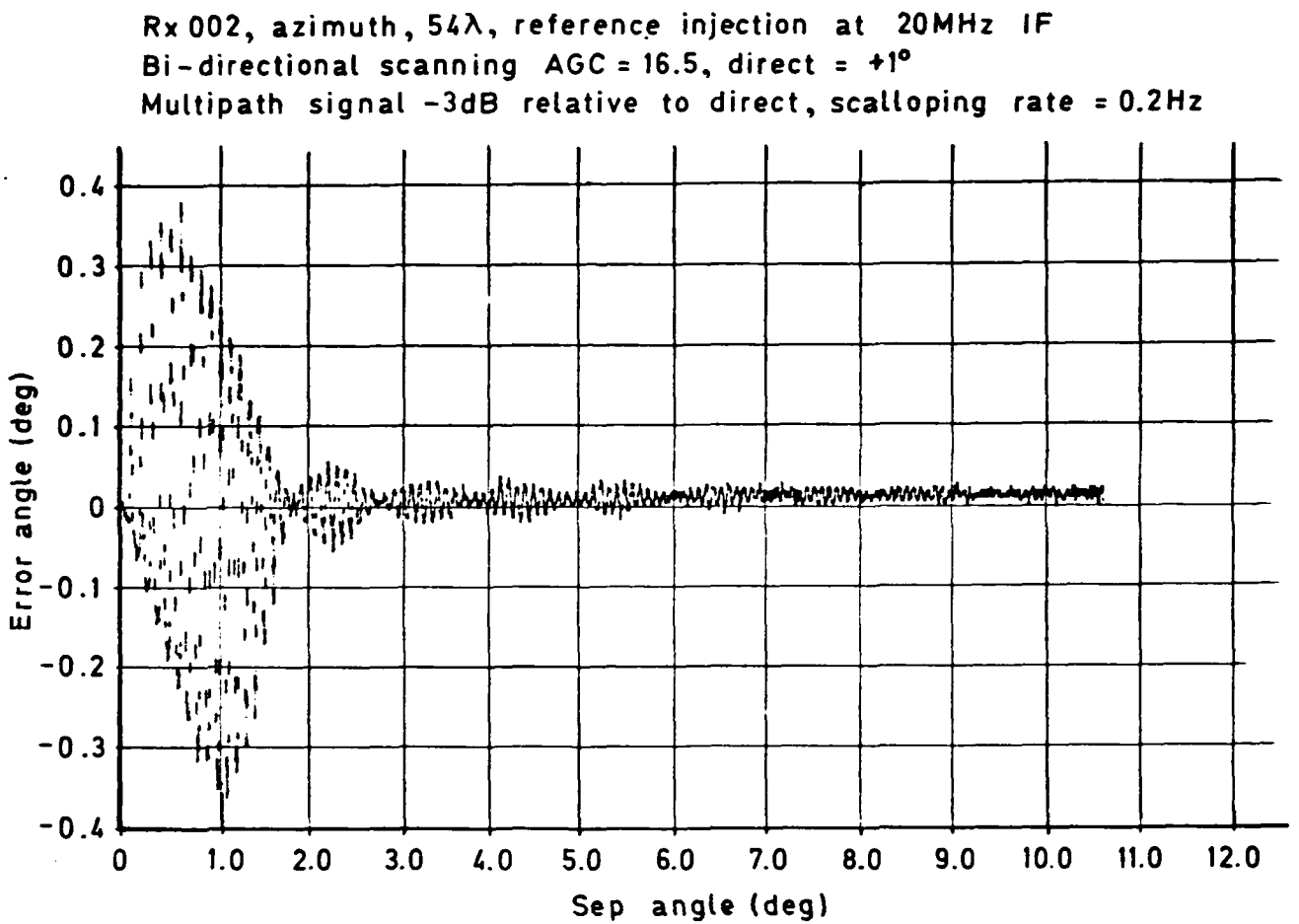

Fig 9.4 Receiver error v separation angle — reference-less transmission

Fig 9.5

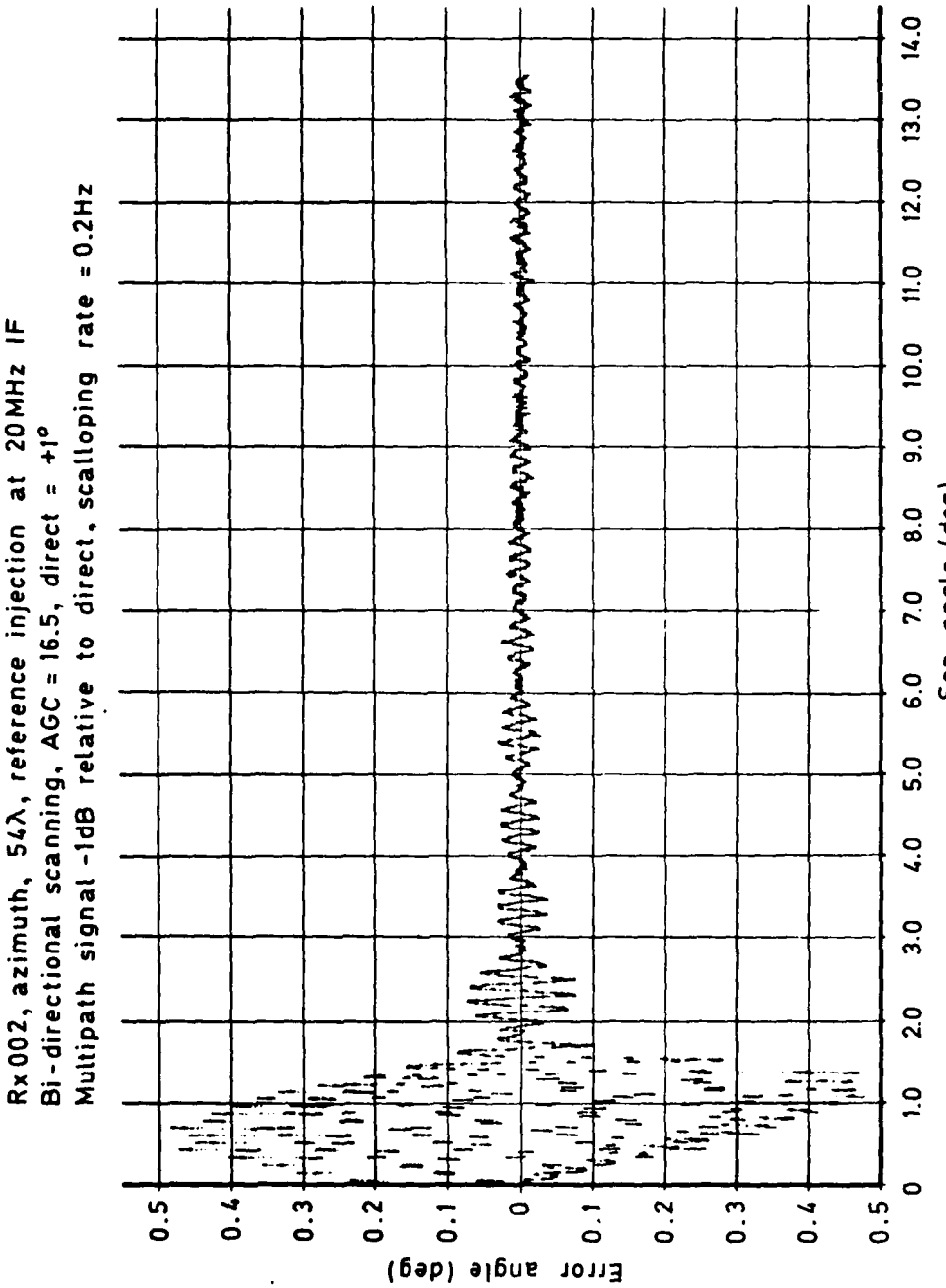

Fig 9.5 Receiver error v separation angle – reference-less transmission

TR 79052

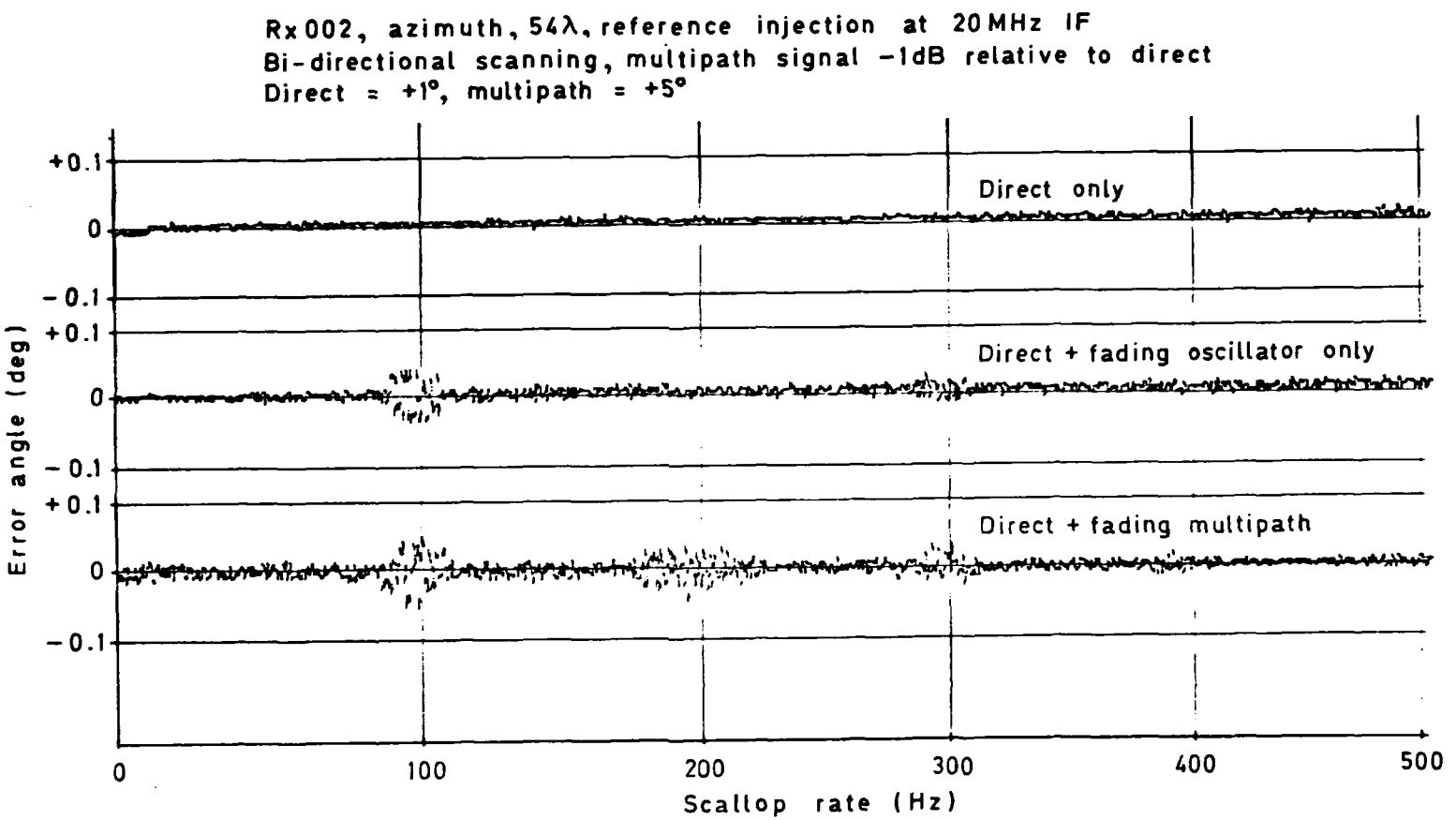

Fig 9.6 Receiver error v scalloping rate — reference-less transmission

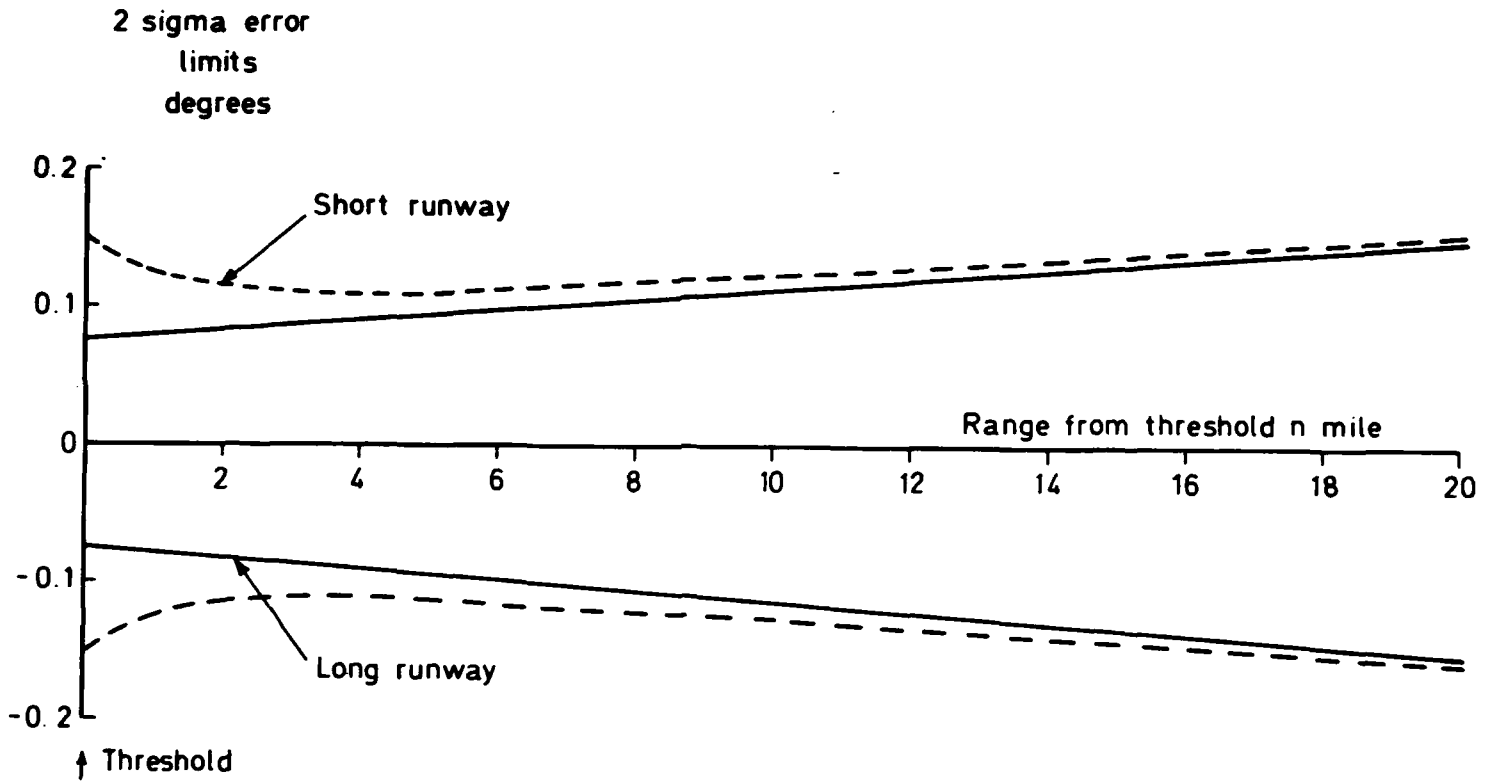

Fig 10.1 Angular error limits for long and short runways